

J. N. REDDY

*Distinguished Professor*

*Department of Mechanical Engineering*

*Texas A&M University, College Station*

*TX 77843-3123, USA*

---

# An Introduction to Nonlinear Finite Element Analysis



**OXFORD**  
UNIVERSITY PRESS

---

## About the Author

---

**J. N. Reddy** is Distinguished Professor and the Holder of Oscar S. Wyatt Endowed Chair in the Department of Mechanical Engineering at Texas A&M University, College Station, Texas. Prior to the current position, he was the Clifton C. Garvin Professor in the Department of Engineering Science and Mechanics at Virginia Polytechnic Institute and State University (VPI&SU), Blacksburg, Virginia.

Dr. Reddy is internationally known for his contributions to theoretical and applied mechanics and computational mechanics. He is the author of over 300 journal papers and dozen other books, including *Introduction to the Finite Element Method* (Second Edition), McGraw-Hill, 1993; *Theory and Analysis of Elastic Plates*, Taylor & Francis, 1999; *Energy Principles and Variational Methods in Applied Mechanics* (Second Edition), John Wiley, 2002; *Mechanics of Laminated Plates and Shells: Theory and Analysis*, (second Edition) CRC Press, 2004; *An Introduction to the Mathematical Theory of Finite Elements* (coauthored with J. T. Oden), John Wiley, 1976; *Variational Methods in Theoretical Mechanics* (coauthored with J. T. Oden), Springer-Verlag, 1976; *The Finite Element Method in Heat Transfer and Fluid Dynamics* (Second Edition; coauthored with D. K. Gartling), CRC Press, 2001; and

Professor Reddy is the recipient of the *Walter L. Huber Civil Engineering Research Prize* of the American Society of Civil Engineers (ASCE), the *Worcester Reed Warner Medal* and the *Charles Russ Richards Memorial Award* of the American Society of Mechanical Engineers (ASME), the 1997 *Archie Higdon Distinguished Educator Award* from the American Society of Engineering Education (ASEE), the 1998 *Nathan M. Newmark Medal* from the American Society of Civil Engineers, the 2000 *Excellence in the Field of Composites* from the American Society of Composites, the 2000 *Faculty Distinguished Achievement Award for Research* and the 2003 *Bush Excellence Award for Faculty in International Research* from Texas A&M University, and the 2003 *Computational Solid Mechanics Award* from the U.S. Association of Computational Mechanics (USACM).

Dr. Reddy is a Fellow of ASCE, ASME, the American Academy of Mechanics (AAM), the American Society of Composites, the U.S. Association of Computational Mechanics, the International Association of Computational Mechanics (IACM), and the Aeronautical Society of India (ASI). Professor Reddy is the Editor-in-Chief of *Mechanics of Advanced Materials and Structures*, *International Journal of Computational Engineering Science* and *International Journal of Structural Stability and Dynamics*, and he serves on the editorial boards of over two dozen other journals, including *International Journal for Numerical Methods in Engineering*, *Computer Methods in Applied Mechanics and Engineering*, and *International Journal of Non-Linear Mechanics*.

---

# Contents

---

<b>Preface</b>	xvii
<b>1 Introduction</b>	1
1.1 Mathematical Models	1
1.2 Numerical Simulations	3
1.3 The Finite Element Method	5
1.4 Nonlinear Analysis	7
1.4.1 Introduction	7
1.4.2 Classification of Nonlinearities	7
1.5 The Big Picture	11
References	12
<b>2 The Finite Element Method: A Review</b>	13
2.1 Introduction	13
2.2 One-Dimensional Problems	13
2.2.1 Governing Differential Equation	13
2.2.2 Finite Element Approximation	14
2.2.3 Derivation of the Weak Form	16
2.2.4 Interpolation Functions	18
2.2.5 Finite Element Model	22
2.3 Two-Dimensional Problems	24
2.3.1 Governing Differential Equation	24
2.3.2 Finite Element Approximation	24
2.3.3 Weak Formulation	26
2.3.4 Finite Element Model	27
2.3.5 Interpolation Functions	28
2.3.6 Assembly of Elements	33
2.4 Library of Two-Dimensional Finite Elements	36
2.4.1 Introduction	36
2.4.2 Triangular Elements	37
2.4.3 Rectangular Elements	38
2.5 Numerical Integration	40
2.5.1 Preliminary Comments	40
2.5.2 Coordinate Transformations	41
2.5.3 Integration Over a Master Rectangular Element	44
2.5.4 Integration Over a Master Triangular Element	45

---

2.6 Computer Implementation	46
2.6.1 General Comments	46
2.6.2 One-Dimensional Problems	48
2.6.3 Two-Dimensional Problems	52
2.7 Closure	53
Problems	57
References	59
<b>3 Heat Transfer and Other Field Problems in One Dimension</b>	<b>61</b>
3.1 Model Differential Equation	61
3.2 Weak Formulation	62
3.3 Finite Element Model	62
3.4 Solution Procedures	64
3.4.1 General Comments	64
3.4.2 Direct Iteration Procedure	65
3.4.3 Newton's Iteration Procedure	68
3.5 Computer Implementation	73
3.5.1 Introduction	73
3.5.2 Preprocessor Unit	73
3.5.3 Processor Unit	76
3.6 Closing Remarks	82
Problems	82
References	85
<b>4 Nonlinear Bending of Straight Beams</b>	<b>87</b>
4.1 Introduction	87
4.2 Euler-Bernoulli Beams	88
4.2.1 Basic Assumptions	88
4.2.2 Displacement Field and Strains	88
4.2.3 Weak Forms	89
4.2.4 Finite Element Model	95
4.2.5 Iterative Solutions of Nonlinear Equations	97
4.2.6 Load Increments	100
4.2.7 Membrane Locking	101
4.2.8 Computer Implementation	102
4.3 Timoshenko Beams	110
4.3.1 Displacement Field and Strains	110
4.3.2 Weak Forms	111
4.3.3 General Finite Element Model	113
4.3.4 Shear and Membrane Locking	115
4.3.5 Tangent Stiffness Matrix	117

Problems	124
References	126
<b>5 Heat Transfer and Other Fields Problems in Two Dimensions</b>	<b>127</b>
5.1 Model Equation	127
5.2 Weak Form	128
5.3 Finite Element Model	129
5.4 Solution Procedures	131
5.4.1 Direct Iteration	131
5.4.2 Newton-Raphson Iteration	131
5.5 Computer Implementation	132
5.5.1 Introduction	132
5.5.2 Numerical Integration	133
5.5.3 Element Calculations	135
Problems	139
References	140
<b>6 Nonlinear Bending of Elastic Plates</b>	<b>141</b>
6.1 Introduction	141
6.2 Classical Plate Theory	141
6.2.1 Assumptions of the Kinematics	141
6.2.2 Displacement Field and Strains	142
6.3 Variational Formulation of CPT	144
6.3.1 Virtual Work	144
6.3.2 Weak Forms	147
6.3.3 Equilibrium Equations	148
6.3.4 Boundary Conditions	149
6.3.5 Stress Resultant-Deflection Relations	152
6.4 Finite Element Models of CPT	153
6.4.1 General Formulation	153
6.4.2 Tangent Stiffness Coefficients	157
6.4.3 Some Plate Finite Elements	161
6.5 Computer Implementation Aspects and Numerical Results of CPT Elements	164
6.5.1 Computer Implementation	164
6.5.2 Results of Linear Analysis	166
6.5.3 Results of Nonlinear Analysis	168
6.6 First-Order Shear Deformation Plate Theory	173
6.6.1 Introduction	173
6.6.2 Displacement Field	173
6.6.3 Weak Formulation	174

6.7 Finite Element Models of FSDT	177
6.7.1 Virtual Work Statements	177
6.7.2 Finite Element Model	178
6.7.3 Tangent Stiffness Coefficients	182
6.7.4 Shear and Membrane Locking	184
6.8 Computer Implementation and Numerical Results of FSDT Elements	184
6.8.1 Computer Implementation	184
6.8.2 Results of Linear Analysis	185
6.8.3 Results of Nonlinear Analysis	189
6.9 Theory of Doubly-Curved Shells	196
6.9.1 Introduction	196
6.9.2 Geometric Description	197
6.9.3 Strain-Displacement Relations	201
6.9.4 Stress Resultants	202
6.9.5 Equations of Motion	205
6.10 Finite Element Analysis of Shells	206
6.10.1 Weak Forms	206
6.10.2 Finite Element Model	207
6.10.3 Linear Results	209
6.10.4 Nonlinear Results	217
Problems	222
References	225
<b>7 Flows of Viscous Incompressible Fluids</b>	<b>229</b>
7.1 Introduction	229
7.2 Governing Equations	230
7.2.1 Introduction	230
7.2.2 Conservation of Mass	231
7.2.3 Conservation of Momenta	232
7.2.4 Conservation of Energy	232
7.2.5 Constitutive Equations	233
7.2.6 Boundary Conditions	234
7.3 Governing Equations in Terms of Primitive Variables	235
7.3.1 Vector Form	235
7.3.2 Cartesian Component Form	236
7.4 Velocity-Pressure Finite Element Model	237
7.4.1 Weak Form	237
7.4.2 Finite Element Model	239
7.5 Penalty Finite Element Models	241
7.5.1 Introduction	241
7.5.2 Penalty Function Method	242

7.5.3 Reduced Integration Penalty Model	244
7.5.4 Consistent Penalty Model	245
7.6 Computational Aspects	246
7.6.1 Properties of the Matrix Equations	246
7.6.2 Choice of Elements	247
7.6.3 Evaluation of Element Matrices in Penalty Models	249
7.6.4 Post-Computation of Stresses	250
7.7 Computer Implementation	251
7.7.1 Mixed Model	251
7.7.2 Penalty Model	254
7.8 Numerical Examples	254
7.8.1 Preliminary Comments	254
7.8.2 Fluid Squeezed Between Parallel Plates	255
7.8.3 Flow of a Viscous Lubricant in a Slider Bearing	258
7.8.4 Wall-Driven Cavity Flow	261
7.8.5 Backward-Facing Step	267
7.9 Least-Squares Finite Element Models	269
7.9.1 Introduction	269
7.9.2 Finite Element Model	272
7.9.3 Computational Aspects	274
7.9.4 Numerical Examples	275
Problems	283
References	283
<b>8 Nonlinear Analysis of Time-Dependent Problems</b>	<b>287</b>
8.1 Introduction	287
8.2 Time Approximations	288
8.2.1 Introduction	288
8.2.2 Parabolic Equations	289
8.2.3 Hyperbolic Equations	292
8.3 Stability and Accuracy	295
8.3.1 Preliminary Comments	295
8.3.2 Stability Criteria	296
8.4 Transient Analysis of Nonlinear Problems	297
8.4.1 Introduction	297
8.4.2 Heat Transfer	297
8.4.3 Flows of Viscous Incompressible Fluids	298
8.4.4 Plate Bending (FSDT)	300
8.5 Computer Implementation	304

8.6 Numerical Examples	307
8.6.1 Linear Problems	307
8.6.2 Nonlinear Problems	314
Problems	323
References	325
<b>9 Finite Element Formulations of Solid Continua</b>	<b>327</b>
9.1 Introduction	327
9.1.1 Background	327
9.1.2 Descriptions of Motion	328
9.2 Strain and Stress Measures	329
9.2.1 Deformation Gradient Tensor	329
9.2.2 Green and Almansi Strain Tensors	331
9.2.3 Polar Decomposition	334
9.2.4 Stress Tensors	334
9.2.5 Energetically-Conjugate Stresses and Strains	335
9.3 Strain and Stress Measures Between Configurations	337
9.3.1 Notation	337
9.3.2 Conservation of Mass	339
9.3.3 Green Strain Tensors for Various Configurations	340
9.3.4 Euler Strain Tensor	342
9.3.5 Relationships Between Various Stress Tensors	343
9.4 Constitutive Equations	346
9.5 Total Lagrangian and Updated Lagrangian Formulations of Continua	347
9.5.1 Principle of Virtual Displacements	347
9.5.2 Total Lagrangian Formulation	348
9.5.3 Updated Lagrangian Formulation	350
9.6 Finite Element Models of Two-Dimensional Continua	353
9.6.1 Introduction	353
9.6.2 Total Lagrangian Formulation	353
9.6.3 Updated Lagrangian Formulation	360
9.6.4 Computer Implementation	361
9.6.5 Numerical Results	361
9.7 Shell Finite Elements	369
9.7.1 Introduction	369
9.7.2 Incremental Equations of Motion	369
9.7.3 Finite Element Models of a Continuum	370
9.7.4 Shell Finite Element	372
9.7.5 Numerical Examples	378
Problems	381
References	387



<b>10 Material Nonlinearities and Coupled Problems</b>	<b>389</b>
10.1 Introduction	389
10.2 Nonlinear Elastic Problems	390
10.3 Small Deformation Theory of Plasticity	391
10.3.1 Introduction	391
10.3.2 Ideal Plasticity	392
10.3.3 Strain Hardening Plasticity	393
10.3.4 Elastic-Plastic Analysis of a Bar	395
10.4 Non-Newtonian Fluids	404
10.4.1 Introduction	404
10.4.2 Governing Equations in Cylindrical Coordinates	405
10.4.3 Power-Law Fluids	407
10.4.4 White-Metzner Fluids	409
10.4.5 Numerical Examples	412
10.5 Coupled Fluid Flow and Heat Transfer	417
10.5.1 Finite Element Models	417
10.5.2 Numerical Examples	419
References	423
<b>Appendix A1: Solution Procedures for Linear Algebraic Equations</b>	<b>425</b>
A1.1 Introduction	425
A1.2 Direct Methods	427
A1.2.1 Preliminary Comments	427
A1.2.2 Symmetric Solver	428
A1.2.3 Unsymmetric Solver	430
A1.3 Iterative Methods	430
A1.3.1 General Comments	430
A1.3.2 Solution Algorithms	432
References	433
<b>Appendix A2: Solution Procedures for Nonlinear Algebraic Equations</b>	<b>439</b>
A2.1 Introduction	439
A2.2 Picard Iteration Method	440
A2.3 Newton-Raphson Iteration Method	444
A2.4 Riks and Modified Riks Schemes	448
References	457
<b>Subject Index</b>	<b>459</b>

---

## Preface

---

The objective of this book is to present the theory and computer implementation of the finite element method as applied to simple nonlinear problems of heat transfer and similar field problems, fluid mechanics, and solid mechanics. Both geometric as well as material nonlinearities are considered, and static and transient (i.e. time-dependent) responses are studied. The guiding principle in writing the book was to make the presentation suitable for (a) adoption as a text book for a first course on nonlinear finite element analysis (or for a second course following an introductory course on the finite element method), and (b) for use by engineers and scientists from various disciplines for self study and practice.

There exist a number of books on nonlinear finite elements. Most of these books contain a good coverage of the topics of structural mechanics, and few address topics of fluid dynamics and heat transfer. While these books serve as good references to engineers or scientists who are already familiar with the subject but wish to learn advanced topics or latest developments, they are not suitable as textbooks for a first course or for self study on nonlinear finite element analysis.

The motivation and encouragement that led to the writing of the present book have come from the users of the author's book, *An Introduction to the Finite Element Method* (McGraw-Hill, 1984; Second Edition, 1993; third edition scheduled for 2004), who have found the approach presented there to be most suitable for any one – irrespective of their scientific background – interested in learning the method, and also from the fact that there does not exist a book that is suitable as a textbook for a first course on nonlinear finite element analysis. The author has taught a course on nonlinear finite element analysis many times during the last twenty years, and the present book is an outcome of the lecture notes developed during this period. The same approach as that used in the aforementioned book, namely, the *differential equation approach*, is adopted in the present book to introduce the theory, formulation, and computer implementation of the finite element method as applied to nonlinear problems of science and engineering.

Beginning with a model (i.e. typical) second-order, nonlinear differential equation in one dimension, the book takes the reader through increasingly complex problems of nonlinear beam bending, nonlinear field problems in two dimensions, nonlinear plate bending, nonlinear formulations of solid continua, flows of viscous incompressible fluids in two dimensions (i.e. Navier-Stokes equations), time-approximation schemes, continuum formulations of shells, and material nonlinear problems of solid mechanics.

As stated earlier, the book is suitable as a textbook for a first course on nonlinear finite elements in civil, aerospace, mechanical, and mechanics departments as well as in applied sciences. It can be used as a reference by engineers and scientists working in industry, government laboratories and academia. Introductory courses on the finite element method, continuum mechanics, and numerical analysis should prove to be helpful.

The author has benefited in writing the book by the encouragement and support of many colleagues around the world who have used his book, *An Introduction to the Finite Element Method*, and students who have challenged him to explain and implement complicated concepts and formulations in simple ways. While it is not possible to name all of them, the author expresses his sincere appreciation. In particular, it is a pleasure to acknowledge the help of the author's students Juan P. Pontaza with the least-squares finite element analysis of fluid flow problems in Chapters 7 and 8, and Goy Teck Lim with the plasticity example in Chapter 10. The author expresses his deep sense of gratitude to his teacher, Professor J. T. Oden (University of Texas at Austin), to whom this book is dedicated and without whose advice, mentorship and support it would not have been possible for the author to modestly contribute to the field of applied mechanics in general and theory and application of the finite element method in particular, through author's teaching, research, and technical writings.

J. N. Reddy  
College Station, Texas

---

# Introduction

---

## 1.1 Mathematical Models

One of the most important thing engineers and scientists do is to model natural phenomena. They develop conceptual and mathematical models to simulate physical events, whether they are aerospace, biological, chemical, geological, or mechanical. The mathematical models are developed using laws of physics and they are often described in terms of algebraic, differential, and/or integral equations relating various quantities of interest.

A *mathematical model* can be broadly defined as a set of relationships among variables that express the essential features of a physical system or process in analytical terms. The relationships that govern the system take the form of algebraic, differential, and integral equations. Mathematical models of physical phenomena are often based on fundamental scientific laws of physics such as the principle of conservation of mass, the principle of conservation of linear momentum, and the principle of conservation of energy. Mathematical models of biological and other phenomena may be based on observations and accepted theories. Keeping the scope of the present study in mind, we limit our discussions to engineering systems that are governed by laws of continuum mechanics.

Mathematical models of engineering systems are often characterized by very complex equations posed on geometrically complicated regions. Consequently, many of the mathematical models, until the advent of electronic computation, were drastically simplified in the interest of analytically solving them. Over the last three decades, however, the computer has made it possible, with the help of mathematical models and numerical methods, to solve many practical problems of science and engineering. There now exists a new and growing body of knowledge connected with the use of numerical methods and computers to analyze mathematical models of physical systems, and this body is known as *computational mechanics*. Major established industries such as the automobile, aerospace, chemical, pharmaceutical, petroleum, electronics and communications, as well as emerging industries such as biotechnology, rely on computational mechanics-based capabilities to simulate complex systems

Here, we consider the familiar example of a simple pendulum to illustrate how a mathematical model of the motion of the pendulum can be constructed using the principle of conservation of linear momentum, that is, Newton's second law of motion. Numerical analysis of the problem will be considered in the sequel.

### Example 1.1.1

As an example of the mathematical model development, consider the problem of a simple pendulum. The system consists of a bob of mass  $m$  attached to one end of a rod of length  $l$  and the other end is pivoted to a fixed point  $O$ , as shown in Figure 1.1.1. The primary goal of the mathematical model to be derived here is to have a means to determine the motion (i.e. angular displacement as a function of time) of the bob. Keeping the goal of the analysis in mind, we make several assumptions. (1) The bob as well as the rod connecting the bob to the fixed point  $O$  are rigid; (2) the mass of the rod is negligible relative to the mass of the bob; and (3) there is no friction at the pivot. These assumptions may be removed to obtain a mathematical model that describes the system more accurately.

The equation governing the motion can be derived using the principle of conservation of linear momentum, also known as Newton's second law of motion, which states that the vector sum of externally applied forces is equal to the time rate of change of the linear momentum of the body:

$$\mathbf{F} = m\mathbf{a} \quad (1.1.1)$$

where  $\mathbf{F}$  is the vector sum of all forces acting on a system,  $m$  is the mass of the system, and  $\mathbf{a}$  is the acceleration of the system.

Applying Newton's second law in the  $x$  direction (see Figure 1.1.1), we have

$$F_x = -mg \sin \theta, \quad v = l \frac{d\theta}{dt} \quad (1.1.2)$$

where  $\theta$  is the angular displacement,  $v$  is the velocity along  $x$ , and  $t$  denotes time. Then, the equation for motion about the pivot becomes

$$-mg \sin \theta = ml \frac{d^2\theta}{dt^2} \quad \text{or} \quad \frac{d^2\theta}{dt^2} + \frac{g}{l} \sin \theta = 0 \quad (1.1.3)$$

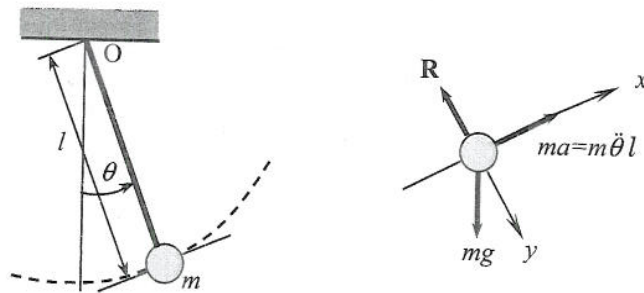


Figure 1.1.1 Simple pendulum.

Thus, the problem at hand involves solving the nonlinear differential equation

$$\frac{d^2\theta}{dt^2} + \frac{g}{l} \sin\theta = 0, \quad 0 < t \leq T \quad (1.1.4)$$

subjected to the initial (i.e. at time  $t = 0$ ) conditions

$$\theta(0) = \theta_0, \quad \frac{d\theta}{dt}(0) = v_0 \quad (1.1.5)$$

where  $\theta_0$  and  $v_0$  are the initial values of angular displacement and velocity, respectively. Mathematically, the problem is called an *initial-value problem*. If the amplitude  $\theta$  is not small, the restoring moment is proportional to  $\sin\theta$ , and Eq. (1.1.3) represents a nonlinear equation. For small  $\theta$ ,  $\sin\theta$  is approximately equal to the angle  $\theta$ , and the motion is described by the linear equation

$$\frac{d^2\theta}{dt^2} + \lambda^2\theta = 0, \quad \lambda^2 = \frac{g}{l} \quad (1.1.6)$$

which represents a simple harmonic motion.

The general analytical solution to the linear equation (1.1.6) is given by

$$\theta(t) = A \sin \lambda t + B \cos \lambda t, \quad \lambda = \sqrt{\frac{g}{l}} \quad (1.1.7)$$

where  $A$  and  $B$  are constants to be determined using the initial conditions in (1.1.5). We obtain

$$A = \frac{v_0}{\lambda}, \quad B = \theta_0 \quad (1.1.8)$$

and the solution to the linear problem is

$$\theta(t) = \frac{v_0}{\lambda} \sin \lambda t + \theta_0 \cos \lambda t \quad (1.1.9)$$

For zero initial velocity and non-zero initial position  $\theta_0$ , we have

$$\theta(t) = \theta_0 \cos \lambda t \quad (1.1.10)$$

## 1.2 Numerical Simulations

By a *numerical simulation* of a process, we mean the solution of the governing equations (or mathematical model) of the process using a numerical method and a computer. While the derivation of the governing equations for most problems is not unduly difficult, their solution by exact methods of analysis is a formidable task. In such cases, numerical methods of analysis provide an alternative means of finding solutions. Numerical methods typically transform differential equations to algebraic equations that are to be solved using computers. For example, the mathematical formulation of the simple pendulum resulted in the nonlinear differential equation (1.1.4), whose analytical solution cannot be obtained. Therefore, one must consider using a numerical method to solve it. Even linear problems may not admit exact solutions due to geometric and material complexities, but it is relatively easy

to obtain approximate solutions using numerical methods. These ideas are illustrated below using the simple pendulum problem of Example 1.1.1. The finite difference method is used as the numerical method.

### Example 1.2.1

Here we consider the numerical solution of Eq. (1.1.4) governing a simple pendulum using the finite difference method. In the finite difference method, the derivatives are approximated by difference quotients (or the function is expanded in a Taylor series) that involve the unknown value of the solution at time  $t_{i+1}$  and the known value of the solution at  $t_i$ . For example, consider the first-order equation

$$\frac{du}{dt} = f(t, u) \quad (1.2.1)$$

We approximate the derivative at  $t_i$  by

$$\left. \left( \frac{du}{dt} \right) \right|_{t=t_i} \approx \frac{u(t_{i+1}) - u(t_i)}{t_{i+1} - t_i} = f(u_i, t_i) \quad (1.2.2)$$

or

$$u_{i+1} = u_i + \Delta t f(u_i, t_i) \quad (1.2.3a)$$

where

$$u_i = u(t_i), \quad \Delta t = t_{i+1} - t_i \quad (1.2.3b)$$

Equation (1.2.3a) can be solved, starting from the known value  $u_0$  of  $u(t)$  at  $t = 0$ , for  $u_1 = u(t_1) = u(\Delta t)$ . This process can be repeated to determine the values of  $u$  at times  $t = \Delta t, 2\Delta t, \dots, n\Delta t$ . This is known as *Euler's explicit method*, also known as the *forward difference scheme*. Note that we are able to convert the ordinary differential equation (1.2.1) to an algebraic equation (1.2.3a) that needs to be evaluated at different times to construct the time history of  $u(t)$ .

Euler's explicit method can be applied to the nonlinear second-order equation (1.1.4). First we rewrite Eq. (1.1.4) as a pair of first-order equations

$$\frac{d\theta}{dt} = v, \quad \frac{dv}{dt} = -\lambda^2 \sin \theta \quad (1.2.4)$$

which are *coupled* (i.e. one cannot be solved without the other). Applying the scheme of Eq. (1.2.4) to the equations at hand, we obtain

$$\theta_{i+1} = \theta_i + \Delta t v_i; \quad v_{i+1} = v_i - \Delta t \lambda^2 \sin \theta_i \quad (1.2.5)$$

The expressions for  $\theta_{i+1}$  and  $v_{i+1}$  in Eq. (1.2.5) are repeatedly computed using the known solution  $(\theta_i, v_i)$  from the previous time step. At time  $t = 0$ , we use the known initial values  $(\theta_0, v_0)$ . Thus, one needs a computer and a computer language like Fortran (77 or 90) to write a computer program to compute numbers.

The numerical solutions of equation (1.2.5) for two different time steps,  $\Delta t = 0.05$  and  $\Delta t = 0.025$ , along with the exact linear solution (1.1.10) (with  $\theta_0 = \pi/4$ ) are presented in Figure 1.2.1. The numerical solutions of the nonlinear problem are dependent on the time step, and smaller the time step more accurate the solution is. This is because the approximation of the derivative in Eq. (1.2.2) tends to the exact derivative with  $\Delta t \rightarrow 0$ .

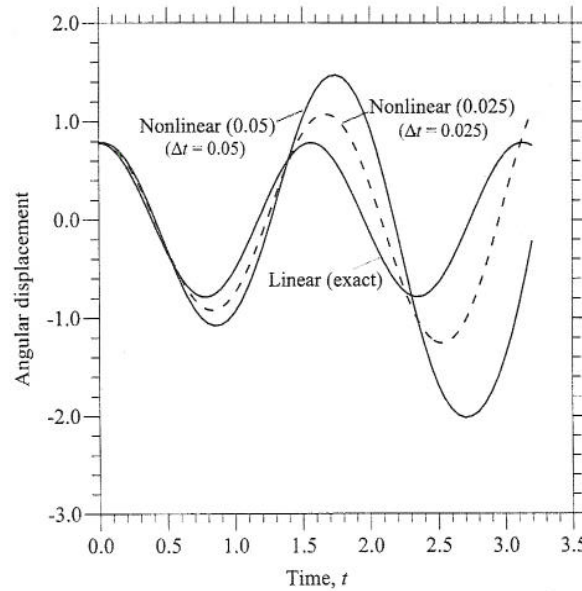


Figure 1.2.1 Analytical and numerical solutions of the simple pendulum.

### 1.3 The Finite Element Method

As illustrated in the previous section, numerical methods are extremely powerful tools for engineering analysis. With the advent of computers, there has been a tremendous explosion in the development and use of numerical methods. Of these, the finite difference methods and the finite element method and their variants are the most commonly used methods in the analysis of practical engineering problems. In finite difference methods, derivatives of various order are approximated using Taylor's series. The traditional finite difference methods suffer from two major drawbacks: (1) applying boundary conditions of the gradient type requires additional approximation; (2) finite difference formulas are traditionally developed for rectangular grids, making it difficult to use them for irregular domains. Advances have been made in recent years to overcome these drawbacks but the remedies are problem dependent. The finite element method is based on the idea that every system is physically composed of different parts and hence its solution may be represented in parts. In addition, the solution over each part is represented as a linear combination of undetermined parameters and known functions of position and possibly time. The parts can differ from each other in shape, material properties, and physical behavior. Even when the system is of one geometric shape and made of one material, it is simpler to represent its solution in a piecewise manner.



In recent years, generalizations of the finite element method have emerged (e.g. the generalized finite element method and element-free methods or meshless methods); however, in this study we limit our discussion to the traditional finite element method [9].

The traditional finite element method is endowed with three basic features. First, a domain of the system is represented as a collection of geometrically simple subdomains, called *finite elements*. Second, over each finite element, the unknown variables are approximated by a linear combination of algebraic polynomials and undetermined parameters, and algebraic relations among the parameters are obtained by satisfying the governing equations, often in a weighted-integral sense, over each element. The undetermined parameters represent the values of the unknown variables at a finite number of preselected points, called *nodes*, in the element. Third, the algebraic relations from all elements are assembled using continuity and "equilibrium" considerations.

There are several reasons why an engineer or scientist should study the finite element method; these are listed below.

1. The finite element method is the most powerful numerical method ever devised for the analysis of engineering problems. It is capable of handling geometrically complicated domains, a variety of boundary conditions, nonlinearities, and coupled phenomena that are common in practical problems. The knowledge of how the method works greatly enhances the analysis skill and provides a greater understanding of the problem being solved.
2. Commercial software packages or "canned" computer programs based on the finite element method are often used in industrial, research, and academic institutions for the solution of a variety of engineering and scientific problems. The intelligent use of these programs and a correct interpretation of the output is often predicated on knowledge of the basic theory underlying the method.
3. It is not uncommon to find mathematical models derived in personal research and development that cannot be evaluated using canned programs. In such cases, an understanding of the finite element method and knowledge of computer programming can help design programs to evaluate the mathematical models.

The basic ideas underlying the finite element method are reviewed in Chapter 2 using linear differential equations involving a single variable in one and two dimensions. The main objective there is to introduce the terminology and steps involved, e.g. weak formulation of differential equations over a element, derivation of the interpolation functions, and numerical evaluation of coefficients and so on. Readers who are familiar with the finite element method as applied to linear differential equations may skip Chapter 2 and go straight to Chapter 3.

## 1.4 Nonlinear Analysis

### 1.4.1 Introduction

Recall from the simple pendulum problem of Examples 1.1.1 and 1.2.1, that nonlinearity naturally arises in a true, rigorous mathematical formulation of physical problems. Based on assumptions of smallness of certain quantities of the formulation, the problem may be reduced to a linear problem. Linear solutions may be obtained with considerable ease and less computational cost when compared to nonlinear solutions. Further, linear solutions due to various boundary conditions and “load” cases may be scaled and superimposed. In many instances, assumptions of linearity lead to reasonable idealization of the behavior of the system. However, in some cases assumption of linearity may result in an unrealistic approximation of the response. The type of analysis, linear or nonlinear, depends on the goal of the analysis and errors in the system’s response that may be tolerated. In some cases, nonlinear analysis is the only option left for the analyst as well as the designer (e.g. high-speed flows of inviscid fluids around solid bodies).

Nonlinear analysis is a necessity, for example, in (a) designing high performance and efficient components of certain industries (e.g. aerospace, defense and nuclear), (b) assessing functionality (e.g., residual strength and stiffness of structural elements) of existing systems that exhibit some types of damage and failure, (c) establishing causes of system failure, (d) simulating true material behavior of processes, and (e) research to gain a realistic understanding of physical phenomena.

The following features of nonlinear analysis should be noted (see [1–7]):

- The principle of superposition does not hold.
- Analysis can be carried out for one “load” case at a time.
- The history (or sequence) of “loading” influences the response.
- The initial state of the system (e.g. prestress) may be important.

### 1.4.2 Classification of Nonlinearities

There are two common sources of nonlinearity: (1) geometric and (2) material. The geometric nonlinearity arises purely from geometric consideration (e.g. nonlinear strain–displacement relations), and the material nonlinearity is due to nonlinear constitutive behavior of the material of the system. A third type of nonlinearity may arise due to changing initial or boundary conditions. We will discuss various types of nonlinearities through simple examples [5].

The simple pendulum problem of Example 1.1.1 is an example of geometric nonlinearity. A common example of geometric nonlinearity is provided by (see Hinton [5]) a rigid link supported by a linear elastic torsional spring at one end and subjected to a vertical point load at the other end, as shown in Figure 1.4.1. Moment equilibrium (i.e. summing the moments about the hinge) and

the linear moment-rotation relationship give

$$M - Fl \cos \theta = 0, \quad M = k_T \theta \quad \text{or} \quad F = \frac{k_T \theta}{l \cos \theta} \quad (1.4.1)$$

where  $k_T$  is the torsional spring constant,  $l$  length of the link, and  $M$  is the moment experienced by the torsional spring due to the angular displacement  $\theta$ . If  $\theta$  is small,  $\cos \theta \rightarrow 1$  and the governing equation is reduced to a linear equation

$$F = \frac{k_T \theta}{l}, \quad \theta < \frac{\pi}{2} \quad (1.4.2)$$

The nonlinear and linear responses are shown in Figure 1.4.2. Clearly, the nonlinearity in the present case is due to the change of geometry, and the nonlinear deflection is less than the linear deflection as the load is increased. Such a nonlinearity is known as the *hardening* type.

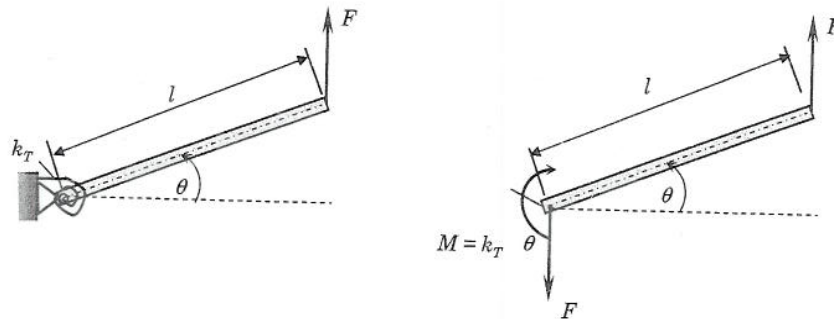


Figure 1.4.1 Rigid link-linear torsional spring cantilever.

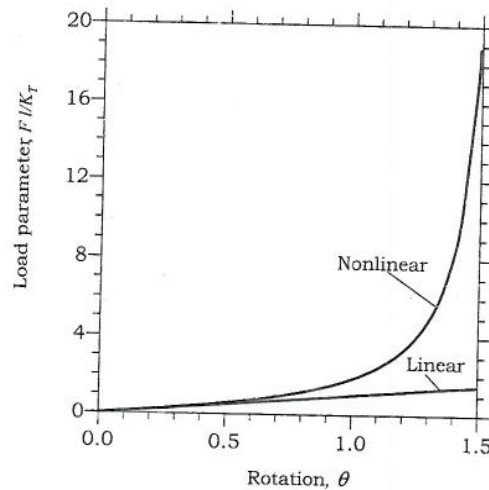


Figure 1.4.2 Geometric nonlinear response of a rigid link-linear torsional spring cantilever.

The material nonlinearity may be introduced into the problem if the moment-rotation relationship is nonlinear

$$M = k_T(\theta)\theta, \quad \text{say} \quad k_T = k_0 - k_1\theta \quad (1.4.3)$$

where  $k_0$  and  $k_1$  are material parameters that are determined through tests. If we use the relationship (1.4.3) in (1.4.1), we obtain a nonlinear equation that contains both geometric and material nonlinearities; if Eq. (1.4.3) is used in (1.4.2), the resulting nonlinearity is only due to the material behavior.

Figure 1.4.3 contains plots of load  $F$  versus rotation  $\theta$  for the materially nonlinear case. Note that the material nonlinearity in the present case is due to the change (reduction) in the torsional spring stiffness, and the nonlinear deflection is greater than the linear deflection as the load is increased. Such a nonlinearity is known as the *softening* type. In the present case, the geometric nonlinearity dominates if both nonlinearities are included.

An example of another type of nonlinearity is provided by (see Hinton [5]) the axial deformation of an isotropic, homogeneous, linear elastic rod with constrained end displacement, as shown in Figure 1.4.4. The rod is of length  $2L$ , uniform cross-sectional area of  $A$ , and loaded with an axial force  $P$  at its midpoint. The lower end of the rod is constrained so that it can at most have an axial displacement of  $u_0$  (which is assumed to be very small compared to the length  $L$ ).

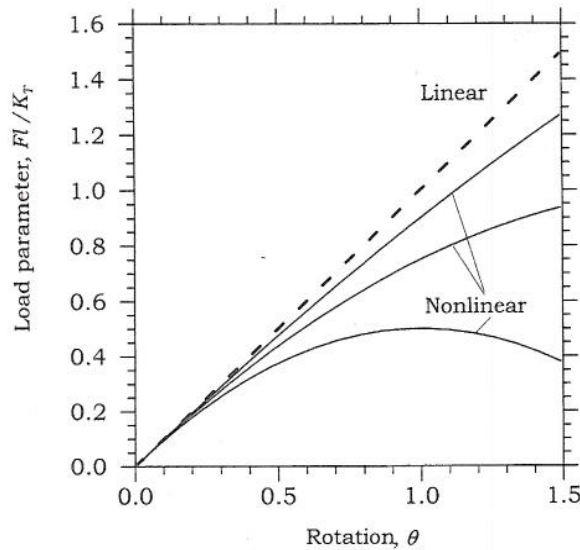


**Figure 1.4.3** Material nonlinear response of a rigid link-linear torsional spring cantilever.

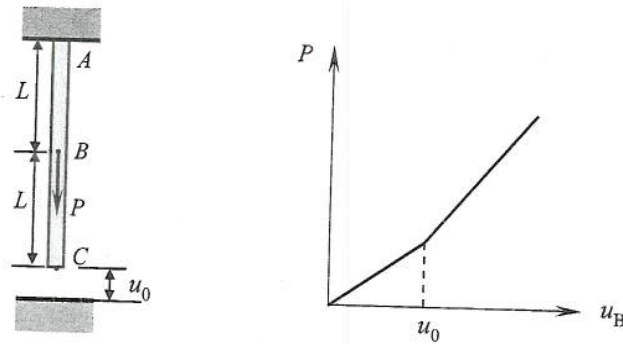


Figure 1.4.4 Axial deformation of a rod with constrained end displacement.

The governing equation and boundary condition at A are given by

$$EA \frac{d^2 u}{dx^2} = 0, \quad u(0) = 0 \quad (1.4.4)$$

The displacement at point B can be determined using the boundary condition at point C, which is dependent on whether the displacement of point C equals  $u_0$ . Thus, we have

$$\left( EA \frac{du}{dx} \right)_B - P = 0, \quad \text{if } u_B = u_C < u_0 \quad (1.4.5)$$

$$u_C = 0, \quad \text{if } u_B \geq u_0 \quad (1.4.6)$$

In the former case, the displacement is given by

$$u(x) = \frac{Px}{EA}, \quad u_B = \frac{PL}{EA}, \quad \text{if } u_C < u_0 \quad (1.4.7)$$

In the latter case (by solving the governing equation in the two intervals and using the continuity and boundary condition with  $L+u_0 \approx L$ ) the displacement is given by

$$u(x) = \begin{cases} \frac{Px}{2EA}, & 0 \leq x \leq L, \\ \frac{P(2L-x)}{2EA}, & L \leq x \leq 2L \end{cases} \quad (1.4.8a)$$

and

$$u_B = \frac{PL}{2EA} \quad (1.4.8b)$$

Thus the force–displacement relationship of the rod is bilinear. Such problems are called “contact” or “nonlinear boundary” problems [5].

## 1.5 The Big Picture

Engineers design and manufacture various types of systems. Engineering design is the process of altering dimensions, shapes, and materials to find the best (optimum) configuration of the system to carry out certain specific function. Analysis is an aid to design and it involves (1) mathematical model development, (2) data acquisition by measurements, (3) numerical simulation, and (4) evaluation of the results in light of known information and corrections to the mathematical model. The mathematical model is developed using laws of physics and assumptions concerning the process behavior. The data includes the actual system parameters (geometry, loading, and boundary conditions) and constitutive properties. The constitutive properties such as the modulus, conductivity, and so on are determined in laboratory experiments. The mathematical model, in most practical cases, does not admit analytical (or exact) solution due to the geometric complexity and/or nonlinearities. Nonlinearities in a mathematical model arise from changing geometry or material behavior. It is necessary to employ numerical methods to compute an approximate solution to the mathematical model. The finite element method is a powerful numerical method that can be used to analyze engineering problems [1–15].

A typical finite element analysis exercise begins with the actual physical system or part thereof to be analyzed [5]. Then we form a set of objectives for the analysis. If the analysis objective is to help develop a preliminary design of the system, the analysis can be very simple. On the other hand, if the analysis objective is to verify and certify the final design of a system, the analysis must be the most sophisticated that can be carried out. Thus, the objectives will dictate the type of idealization of the system to be adopted; for example, should we model as a two-dimensional or three-dimensional problem?, analyze as a linear or nonlinear problem and what type of nonlinearities to be considered?, what type constitutive model to be used?, how are the loads and boundary conditions of the actual system are idealized?, what coupling effects, if any, to be considered?, and so on.

Once the system idealization is complete (i.e. mathematical model is in place), one must decide on type of numerical approximation (and software to be used). This involves (1) choice of unknowns, which in turn dictates the type of finite element model, (2) type of elements, (3) type of mesh, and if nonlinear analysis is to be carried out, select (4) magnitude of “load” increments, (5) type of iterative method of solution, (6) error criterion, (7) error tolerance, and (8) maximum allowable number of iterations for termination of the program.

The final step in creating a computational model is verification of the code and validation of the mathematical model. *Verification* is the process of determining if the computational model is an accurate discrete analog of the mathematical model [15]. Thus, if the round-off errors introduced due to finite arithmetic in a computer are negligible, the computational model should

give the exact solution of the mathematical model. Thus verification involves comparing the numerical results with known exact and/or experimental results of benchmark problems. On the other hand, *validation* is the process of determining the degree to which the mathematical model (hence the computer code that is verified) represents the physical reality of the system from the perspective of the intended uses of the model. Obviously, the validation exercise can be defined only in relation to the intended uses of the model. For example, a mathematical model based on linear elasticity is adequate for determining linear elastic solutions of a solid but inadequate for determining its nonlinear response. The validation exercise allows one to modify the mathematical model to include the missing elements that make the computed response come closer to the physical response. In fact, a mathematical model can never be validated; it can only be invalidated. It is always a good idea, when developing new software, to undertake the verification exercise. Validation is a must when studying new and multi-physics problems.

## References

1. Bathe, K. J., *Finite Element Procedures*, Prentice-Hall, Englewood Cliffs, NJ (1996).
2. Belytschko, T., Liu, W. K., and Moran, B., *Nonlinear Finite Elements for Continua and Structures*, John Wiley, Chichester, UK (2000).
3. Crisfield, M. A., *Non-Linear Finite Element Analysis of Solids and Structures, Vol. 1: Essentials*, John Wiley, Chichester, UK (1991).
4. Crisfield, M. A., *Non-Linear Finite Element Analysis of Solids and Structures, Vol. 2: Advanced Topics*, John Wiley, Chichester, UK (1997).
5. Hinton, E. (ed.) *NAFEMS Introduction to Nonlinear Finite Element Analysis*, NAFEMS, Glasgow, UK (1992).
6. Oden, J. T., *Finite Elements of Nonlinear Continua*, McGraw-Hill, New York (1972).
7. Owen, D. R. J. and Hinton, E., *Finite Elements in Plasticity: Theory and Practice*, Pineridge Press, Swansea, UK (1991).
8. Reddy, J. N., *Energy and Variational Methods in Applied Mechanics*, John Wiley, New York (1984).
9. Reddy, J. N., *An Introduction to the Finite Element Method*, 2nd edn, McGraw-Hill, New York (1993).
10. Reddy, J. N., *Energy Principles and Variational Methods in Applied Mechanics*, 2nd edn, John Wiley, New York (2002).
11. Reddy, J. N. and Gartling, D. K., *The Finite Element Method in Heat Transfer and Fluid Dynamics*, 2nd edn, CRC Press, Boca Raton, FL (1999).
12. Yang, Y.-B. and Kuo, S.-R., *Theory & Analysis of Nonlinear Framed Structures*, Prentice-Hall, Singapore (1994).
13. Zienkiewicz, O. C. and Taylor, R. L., *The Finite Element Method*, Fourth Edition, Vol. 1: *Basic Formulation and Linear Problems*, McGraw-Hill, London, UK (1989).
14. Zienkiewicz, O. C. and Taylor, R. L., *The Finite Element Method*, 4th edn, Vol. 2: *Solid and Fluid Mechanics, Dynamics and Non-linearity*, McGraw-Hill, London, UK (1989).
15. Sargent, R. G., "An overview of verification and validation of simulation models," *Proceedings of the 1987 Winter Simulation Conference*, Society of Computer Simulation (1987).

---

# The Finite Element Method: A Review

---

## 2.1 Introduction

The main ideas of the finite element method were presented in Chapter 1. To summarize, the finite element method has the following three basic features:

1. Divide the whole (i.e. domain) into parts, called *finite elements*.
2. Over each representative element, develop the relations among the secondary and primary variables (e.g. “forces” and “displacements”, “heats” and “temperatures”, and so on).
3. Assemble the elements (i.e. combine the relations of all elements) to obtain the relations between the secondary and primary variables of the whole system.

In the present chapter, we review the basic steps of the finite element model development as applied to one- and two-dimensional problems described by typical second-order differential equations. The main objective is to familiarize the reader with the specific steps involved in the finite element formulation and its applications. Readers who are already familiar with the author’s approach to finite element modeling may skip this chapter.

## 2.2 One-Dimensional Problems

### 2.2.1 Governing Differential Equation

Consider the differential equation

$$-\frac{d}{dx} \left( a \frac{du}{dx} \right) + cu = f \quad \text{for} \quad 0 < x < L \quad (2.2.1)$$

where  $a = a(x)$ ,  $c = c(x)$ , and  $f = f(x)$  are the data (i.e. known quantities) of the problem, and  $u(x)$  is the solution to be determined. The data depends on the material properties, geometry, and “loads” or source. The equation arises in a number of fields, and it must be solved subject to appropriate boundary conditions. Table 2.2.1 contains a list of fields, by no means exhaustive, in which Eq. (2.2.1) arises.



### 2.2.2 Finite Element Approximation

The domain  $(0, L)$  of the problem consists of all points between  $x = 0$  and  $x = L$ . The points  $x = 0$  and  $x = L$  are the boundary points of the total domain. In the finite element method, the domain  $(0, L)$  is divided into a set of intervals. A typical interval, called a *finite element*, is of length  $h_e$  and located between points  $x = x_a$  and  $x = x_b$ , where  $x_a$  and  $x_b$  denote the coordinates of the end points of the finite element with respect to the coordinate  $x$ .

**Table 2.2.1** List of fields in which the model equation (2.2.1) arises, with meaning of various parameters and variables (see the bottom of the table for the meaning of some parameters\*).

Field of study	Primary variable $u$	Problem data			Secondary variable $Q$
		$a$	$c$	$f$	
Heat transfer	Temperature $T - T_\infty$	Thermal conductance $kA$	Surface convection $Ap\beta$	Heat generation $f$	Heat $Q$
Flow through porous medium	Fluid-head $\phi$	Permeability $\mu$	0	Infiltration $f$	Point source $Q$
Flow through pipes	Pressure $P$	Pipe resistance $1/R$	0	0	Point source $Q$
Flow of viscous fluids	Velocity $v_z$	Viscosity $\mu$	0	Pressure gradient $-dP/dx$	Shear stress $\sigma_{xz}$
Elastic cables	Displacement $u$	Tension $T$	0	Transverse force $f$	Point force $P$
Elastic bars	Displacement $u$	Axial stiffness $EA$	0	Axial force $f$	Point force $P$
Torsion of bars	Angle of twist $\theta$	Shear stiffness $GJ$	0	0	Torque $T$
Electrostatics	Electrical potential $\phi$	Dielectric constant $\epsilon$	0	Charge density $\rho$	Electric flux $E$

\* $k$  = thermal conductance;  $\beta$  = convective film conductance;  $p$  = perimeter;  $P$  = pressure or force;  $T_\infty$  = ambient temperature of the surrounding fluid medium;  $R = 128\mu h/(\pi d^4)$  with  $\mu$  being the viscosity;  $h$ , the length and  $d$  the diameter of the pipe;  $E$  = Young's modulus;  $A$  = area of cross-section;  $J$  = polar moment of inertia.

In the finite element method, we seek an approximate solution to Eq. (2.2.1) over each finite element; a typical finite element is shown in Figure 2.2.1. The finite element approximation  $u_h^e(x)$  is sought in the form

$$\begin{aligned} u(x) \approx u_h^e(x) &= c_1^e \varphi_1^e(x) + c_2^e \varphi_2^e(x) + \dots + c_n^e \varphi_n^e(x) \\ &= \sum_{j=1}^n c_j^e \varphi_j^e(x) \end{aligned} \quad (2.2.2)$$

where  $\varphi_j^e(x)$  are functions to be selected and  $c_j^e$  are constants to be determined such that Eq. (2.2.2) satisfies the differential equation (2.2.1) and appropriate end conditions over the element. Since there are  $n$  unknown parameters, we need  $n$  relations to determine them. Substituting the approximate solution (2.2.2) into the left-hand side of Eq. (2.2.1), we obtain an expression that, in general, will not be equal to the right-hand side of the equation,  $f(x)$ . The difference between the two sides of the equation is called the *residual*

$$-\frac{d}{dx} \left( a \frac{du_h^e}{dx} \right) + cu_h^e(x) - f(x) \equiv R^e(x, c_1^e, c_2^e, \dots, c_n^e) \neq 0 \quad (2.2.3)$$

We wish to determine  $c_j^e$  ( $j = 1, 2, \dots, n$ ) such that the residual is zero, in some sense, over the element.

One way of making the residual zero is in weighted-integral sense

$$\int_{x_a}^{x_b} w_i^e(x) R^e(x, c_1, c_2, \dots) dx = 0, \quad i = 1, 2, \dots, n \quad (2.2.4)$$

where  $w_i^e$  ( $i = 1, 2, \dots, n$ ) are weight functions. Equation (2.2.4) provides a set of  $n$  algebraic relations among the parameters  $c_j^e$  ( $j = 1, 2, \dots, n$ ). The set  $\{w_1^e(x), w_2^e(x), \dots, w_n^e(x)\}$  must be linearly independent so that the algebraic equations (2.2.4) are also linearly independent and invertible.

There are other choices of  $w_i^e$  that may be used. In the present study we take  $w_i^e(x)$  to be the same as the approximation functions  $\varphi_i^e(x)$ . This particular choice is known as the *Galerkin method*. Different choice of the weight functions will result in a different set of algebraic equations or different finite element models of the same differential equation.

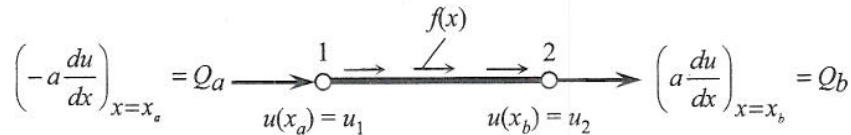


Figure 2.2.1 A typical finite element in one dimension.

### 2.2.3 Derivation of the Weak Form

To weaken the continuity required of  $u_h^e(x)$ , we must trade some of the differentiation in (2.2.4) from  $u_h^e$  to  $w_i^e$  such that both  $u_h^e$  and  $w_i^e$  are differentiated equally, once each in the present case. The resulting integral form is termed the *weak form* of Eq. (2.2.1) because it allows approximation functions with less (or weaker) continuity (or differentiability).

A three-step procedure of constructing the weak form of Eq. (2.2.1) is presented next.

**Step 1.** The first step is to write the weighted-residual statement as in Eq. (2.2.4)

$$0 = \int_{x_a}^{x_b} w_i^e \left[ -\frac{d}{dx} \left( a \frac{du_h^e}{dx} \right) + cu_h^e - f \right] dx \quad (2.2.5)$$

**Step 2.** The second step is to trade differentiation from  $u_h^e$  to  $w_i^e$ , using integration by parts. We obtain

$$0 = \int_{x_a}^{x_b} \left( a \frac{dw_i^e}{dx} \frac{du_h^e}{dx} + cw_i^e u_h^e - w_i^e f \right) dx - \left[ w_i^e \cdot a \frac{du_h^e}{dx} \right]_{x_a}^{x_b} \quad (2.2.6)$$

**Step 3.** Examining the boundary term appearing in the weak form (2.2.6), namely, the expression

$$\left[ w_i^e \cdot a \frac{du}{dx} \right]_{x_a}^{x_b}$$

The coefficient of the weight function  $w_i^e$  in the boundary expression,  $a(du/dx)$ , is called the *secondary variable*, and its specification constitutes the *natural* or *Neumann boundary condition*. The *primary variable* is the dependent unknown of the differential equation,  $u$ , in the same form as the weight function in the boundary expression (i.e. replace  $w_i^e$  with  $u$ ). The specification of a primary variable on the boundary constitutes the *essential* or *Dirichlet boundary condition*. For the model equation at hand, the primary and secondary variables are

$$\text{Primary variable: } u \quad \text{Secondary variable: } a \frac{du}{dx} \equiv Q \quad (2.2.7)$$

In writing the final weak form, we denote the secondary variables at the ends of the element as

$$Q_a^e = - \left( a \frac{du}{dx} \right)_{x_a}, \quad Q_b^e = \left( a \frac{du}{dx} \right)_{x_b} \quad (2.2.8)$$

The primary and secondary variables at the nodes are shown on the typical element in Figure 2.2.1. Students of engineering who have taken a course in

mechanics of deformable bodies (or strength of materials) recognize that this figure shows the *free-body diagram* of a typical but arbitrary portion of a bar, with  $Q_a^e$  and  $Q_b^e$  denoting the axial forces;  $Q_a^e$  is a compressive force while  $Q_b^e$  is a tensile force (algebraically, both are in the positive  $x$  direction, as shown in Figure 2.2.1). For heat conduction problems,  $Q_a^e$  denotes the heat input at the left end and  $Q_b^e$  the heat output from the right end of the element. With the notation in (2.2.8), the final expression for the weak form is given by

$$0 = \int_{x_a}^{x_b} \left( a \frac{dw_i^e}{dx} \frac{du_h^e}{dx} + cw_i^e u_h^e - w_i^e f \right) dx - w_i^e(x_a) Q_a^e - w_i^e(x_b) Q_b^e \quad (2.2.9)$$

This completes the three-step procedure of constructing the weak form.

### Remarks

1. The weak form in (2.2.9) contains two types of expressions: those containing both  $w_i^e$  and  $u_h^e$ , and those containing only  $w_i^e$ . The expression containing both  $w_i^e$  and  $u_h^e$  is called the *bilinear form* (i.e. linear in  $w_i^e$  and linear in  $u_h^e$ ):

$$B(w_i^e, u_h^e) \equiv \int_{x_a}^{x_b} \left( a \frac{dw_i^e}{dx} \frac{du_h^e}{dx} + cw_i^e u_h^e \right) dx \quad (2.2.10)$$

Similarly, the expression containing only  $w_i^e$  (but not  $u_h^e$ ) is called the *linear form*:

$$\ell(w_i^e) = \int_{x_a}^{x_b} w_i^e f dx + w_i^e(x_a) Q_a^e + w_i^e(x_b) Q_b^e \quad (2.2.11)$$

More formally, we say that  $B(u, v)$  is linear in both  $u$  and  $v$ , and  $\ell(v)$  is linear in  $v$ , if and only if the following conditions hold:

$$\begin{aligned} B(c_1 u_1 + c_2 u_2, v) &= c_1 B(u_1, v) + c_2 B(u_2, v) \\ B(u, c_1 v_1 + c_2 v_2) &= c_1 B(u, v_1) + c_2 B(u, v_2) \end{aligned} \quad (2.2.12a)$$

$$\ell(c_1 v_1 + c_2 v_2) = c_1 \ell(v_1) + c_2 \ell(v_2) \quad (2.2.12b)$$

where  $c_1$  and  $c_2$  are constants and  $u, v, u_1, u_2, v_1$ , and  $v_2$  are dependent variables.

2. In view of the above definitions, the weak form (2.2.9) of Eq. (2.2.1) can now be expressed as

$$B(w_i^e, u_h^e) = \ell(w_i^e) \quad (2.2.13)$$

which is called the *variational problem* associated with Eq. (2.2.1). As will be seen later, the bilinear form  $B(w_i^e, u_h^e)$  results directly in the element coefficient matrix, and the linear form  $\ell(w_i^e)$  leads to the right-hand side column vector of the finite element equations.

3. Those who have a background in applied mathematics or solid and structural mechanics will appreciate the fact that the weak form (2.2.9) or the variational problem (2.2.13) is nothing but the statement of the principle of the minimum total potential energy  $\Pi(u_h^e)$  (applied to the bar element):

$$0 = \delta\Pi = B(\delta u_h^e, u_h^e) - \ell(\delta u_h^e)$$

where  $\delta$  is the variational symbol and  $\Pi(u_h^e)$  is the quadratic functional defined by

$$\Pi(u_h^e) = \frac{1}{2}B(u_h^e, u_h^e) - \ell(u_h^e) \quad (2.2.14)$$

$$= \int_{x_a}^{x_b} \left[ \frac{a}{2} \left( \frac{du_i^e}{dx} \right)^2 + \frac{c}{2} (u_h^e)^2 - u_h^e f \right] dx - u_h^e(x_a) Q_a^e - u_h^e(x_b) Q_b^e \quad (2.2.15)$$

Equation (2.2.14) holds only when the bilinear form  $B(w, u)$  is symmetric in  $u$  and  $w$ ,

$$B(w, u) = B(u, w) \quad (2.2.16)$$

and  $\ell(u)$  is linear in  $u$ . The expression  $\frac{1}{2}B(u_h^e, u_h^e)$  represents the elastic strain energy stored in the bar finite element and  $\ell(u_h^e)$  represents the work done by applied distributed force  $f(x)$  and point loads  $Q_a^e$  and  $Q_b^e$ .

### 2.2.4 Interpolation Functions

Recall that the weak form over an element is equivalent to the differential equation, and it contains the end conditions on the "forces"  $Q_i^e$  (see Figure 2.2.1). Therefore, the approximate solution  $u_h^e(x)$  should be selected such that the differentiability (or continuity) conditions implied by the weak form are met and the end conditions on the primary variables  $u(x_i) = u_i^e$  are satisfied. Since the weak form contains the first-order derivative of  $u_h^e$ , any function with a non-zero first derivative would be a candidate for  $u_h^e$ . Thus, the finite element approximation  $u_h^e$  of  $u(x)$  can be an interpolant, that is, must be equal to  $u_a^e$  at  $x_a$  and  $u_b^e$  at  $x_b$ . Thus, a linear polynomial (see Figure 2.2.2)

$$u_h^e(x) = c_1^e + c_2^e x \quad (2.2.17)$$

is admissible if we can select  $c_1^e$  and  $c_2^e$  such that

$$u_h^e(x_a) = c_1^e + c_2^e x_a = u_a^e, \quad u_h^e(x_b) = c_1^e + c_2^e x_b = u_b^e$$

or

$$\begin{bmatrix} 1 & x_a \\ 1 & x_b \end{bmatrix} \begin{Bmatrix} c_1^e \\ c_2^e \end{Bmatrix} = \begin{Bmatrix} u_a^e \\ u_b^e \end{Bmatrix} \rightarrow c_1^e = \frac{u_b^e x_b - u_a^e x_a}{x_b - x_a}, \quad c_2^e = \frac{u_b^e - u_a^e}{x_b - x_a} \quad (2.2.18)$$

Substitution of (2.2.18) for  $c_i^e$  into (2.2.17) yields

$$u_h^e(x) = L_1^e(x)u_1^e + L_2^e(x)u_2^e = \sum_{j=1}^2 L_j^e(x)u_j^e \quad (2.2.19)$$

where

$$L_1^e(x) = \frac{x_b - x}{x_b - x_a}, \quad L_2^e(x) = \frac{x - x_a}{x_b - x_a} \quad (2.2.20)$$

are the *linear Lagrange interpolation functions*, and

$$u_1^e = u_a^e, \quad u_2^e = u_b^e \quad (2.2.21)$$

are the nodal values of  $u_h^e(x)$  at  $x = x_a$  and  $x = x_b$ , respectively. Note that  $L_i^e(x)$  satisfy the *interpolation property*

$$L_i^e(x_j^e) = \begin{cases} 1, & \text{if } i = j \\ 0, & \text{if } i \neq j \end{cases} \quad (2.2.22)$$

where  $x_1^e = x_a$  and  $x_2^e = x_b$  (see Figure 2.2.2). In addition, the Lagrange interpolation functions satisfy the property, known as the “partition of unity”:

$$\sum_{j=1}^n L_j^e(x) = 1 \quad (2.2.23)$$

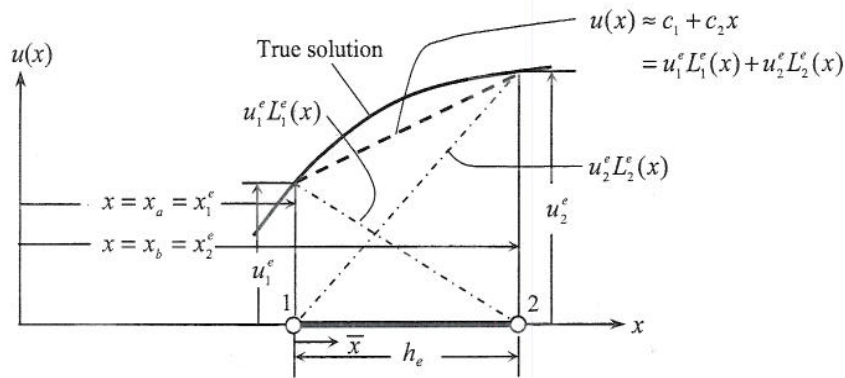


Figure 2.2.2 Linear finite element approximation over an element.

If we wish to approximate  $u(x)$  with a quadratic polynomial, we write

$$u_h^e(x) = c_1^e + c_2^e x + c_3^e x^2 \quad (2.2.24)$$

Since there are three parameters  $c_1^e$ ,  $c_2^e$ , and  $c_3^e$ , we must identify one more nodal point in the element to express all three  $c$ 's in terms of the values of  $u_h^e$  at three nodes. Of course, we can also carry the nodal values  $u_a^e$  and  $u_b^e$  (so that they can be used to join adjacent elements) and the parameter  $c_3^e$  as the unknowns of the approximation. Identifying the third node at the center of the element [see Figure 2.2.3(a)], we can write

$$\begin{aligned} u_h^e(x_1^e) &\equiv u_1^e = c_1^e + c_2^e x_1^e + c_3^e (x_1^e)^2 \\ u_h^e(x_2^e) &\equiv u_2^e = c_1^e + c_2^e x_2^e + c_3^e (x_2^e)^2 \\ u_h^e(x_3^e) &\equiv u_3^e = c_1^e + c_2^e x_3^e + c_3^e (x_3^e)^2 \end{aligned} \quad (2.2.25)$$

where

$$x_1^e = x_a, \quad x_2^e = x_a + \frac{h_e}{2}, \quad x_3^e = x_a + h_e = x_b \quad (2.2.26)$$

Solving Eqs. (2.2.33) for  $c_i^e$  in terms of  $u_i^e$ , we obtain

$$u_h^e(x) = L_1^e(x)u_1^e + L_2^e(x)u_2^e + L_3^e(x)u_3^e = \sum_{j=1}^3 L_j^e(x)u_j^e \quad (2.2.27)$$

where  $L_i^e(x)$  are the quadratic Lagrange interpolation functions [see Figure 2.2.3(b)]

$$\begin{aligned} L_1^e(x) &= \left( \frac{x - x_2^e}{x_1^e - x_2^e} \right) \left( \frac{x - x_3^e}{x_1^e - x_3^e} \right) \\ L_2^e(x) &= \left( \frac{x - x_1^e}{x_2^e - x_1^e} \right) \left( \frac{x - x_3^e}{x_2^e - x_3^e} \right) \\ L_3^e(x) &= \left( \frac{x - x_1^e}{x_3^e - x_1^e} \right) \left( \frac{x - x_2^e}{x_3^e - x_2^e} \right) \end{aligned} \quad (2.2.28)$$

Higher-order Lagrange interpolation of  $u(x)$  can be developed along the similar lines. Thus, an  $(n-1)$ st degree Lagrange interpolation of  $u(x)$  can be written as

$$u_h^e(x) = L_1^e(x)u_1^e + L_2^e(x)u_2^e + \dots + L_n^e(x)u_n^e = \sum_{j=1}^n L_j^e(x)u_j^e \quad (2.2.29)$$

where the Lagrange interpolation functions of degree  $n-1$  are given by

$$L_j^e(x) = \prod_{i=1, i \neq j}^n \left( \frac{x - x_i^e}{x_j^e - x_i^e} \right) \quad (2.2.30)$$

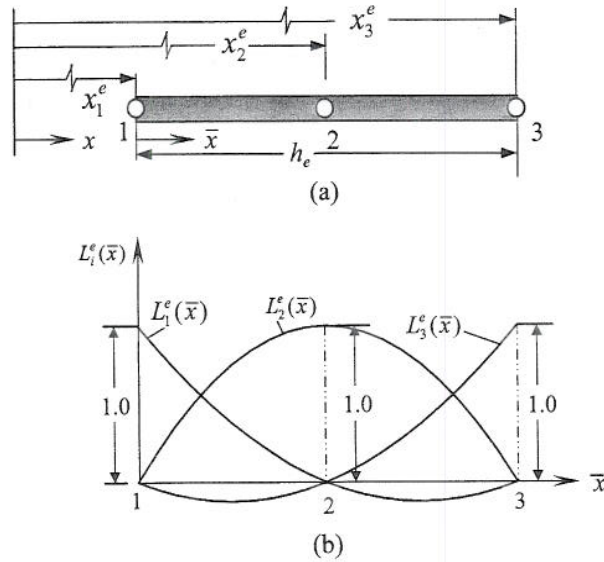


Figure 2.2.3 (a) Quadratic finite element. (b) Quadratic Lagrange interpolation functions.

The finite element solution  $u_h^e(x)$  must fulfill certain requirements in order that it be convergent to the actual solution  $u(x)$  as the number of elements ( $h$  refinement) or the degree of the polynomials ( $p$  refinement) is increased. These are:

1. The approximate solution should be continuous and differentiable as required by the weak form.
2. It should be a complete polynomial, that is, include all lower-order terms up to the highest order term used.
3. It should be an interpolant of the primary variables at the nodes of the finite element (at least interpolate the solution at the end points).

The reason for the first requirement is obvious; it ensures that every term of the governing equation has a non-zero contribution to the coefficient matrix. The second requirement is necessary in order to capture all possible states, that is, constant, linear and so on, of the actual solution. For example, if a linear polynomial without the constant term is used to represent the temperature distribution in a one-dimensional system, the approximate solution can never be able to represent a uniform state of temperature field in the element. The third requirement is necessary in order to enforce continuity of the primary variables at the end points where the element is connected to other elements.



### 2.2.5 Finite Element Model

Substitution of (2.2.29) into (2.2.9) will give the necessary algebraic equations among the nodal values  $u_i^e$  and  $Q_i^e$  of the element. In order to formulate the finite element model based on the weak form (2.2.9), it is not necessary to decide a priori the degree of approximation of  $u_h^e(x)$ . The model can be developed using an arbitrary degree of interpolation. For  $n > 2$ , the weak form in Eq. (2.2.9) must be modified to include non-zero secondary variables, if any, at interior nodes:

$$0 = \int_{x_a}^{x_b} \left( a \frac{dw}{dx} \frac{du_h^e}{dx} + cwu_h^e \right) dx - \int_{x_a}^{x_b} wf dx - \sum_{i=1}^n w(x_i^e) Q_i^e \quad (2.2.31)$$

where  $x_i^e$  is the global coordinate of the  $i$ th node of element  $\Omega^e$ . If nodes 1 and  $n$  denote the end points of the element, then  $Q_1^e$  and  $Q_n^e$  represent the *unknown* point sources, and all other  $Q_i^e$  are the point sources at nodes 2, 3, ...,  $n$ , which are always known.

Substituting Eq. (2.2.29) for  $u_h^e$  and  $w_1^e = L_1^e$ ,  $w_2^e = L_2^e, \dots, w_i^e = L_i^e, \dots, w_n^e = L_n^e$  into the weak form (2.2.31), we obtain  $n$  algebraic equations. The  $i$ th algebraic equation can be written as

$$\begin{aligned} 0 &= \int_{x_a}^{x_b} \left[ a \frac{dL_i^e}{dx} \left( \sum_{j=1}^n u_j^e \frac{dL_j^e}{dx} \right) + cL_i^e \left( \sum_{j=1}^n u_j^e L_j^e \right) - L_i^e f \right] dx \\ &\quad - \sum_{j=1}^n L_i^e(x_j^e) Q_j^e \\ &= \sum_{j=1}^n \left[ \int_{x_a}^{x_b} \left( a \frac{dL_i^e}{dx} \frac{dL_j^e}{dx} + cL_i^e L_j^e \right) dx \right] u_j^e - \int_{x_a}^{x_b} L_i^e f dx - Q_i^e \\ 0 &= \sum_{j=1}^n K_{ij}^e u_j^e - f_i^e - Q_i^e \end{aligned} \quad (2.2.32)$$

for  $i = 1, 2, \dots, n$ , where

$$K_{ij}^e = \int_{x_a}^{x_b} \left( a \frac{dL_i^e}{dx} \frac{dL_j^e}{dx} + cL_i^e L_j^e \right) dx = B(L_i^e, L_j^e), \quad f_i^e = \int_{x_a}^{x_b} f L_i^e dx \quad (2.2.33)$$

Note that the interpolation property (2.2.22) is used to write

$$\sum_{j=1}^n L_j^e(x_i^e) Q_j^e = Q_i^e \quad (2.2.34)$$

In matrix notation, these algebraic equations can be written as

$$[K^e] \{u^e\} = \{f^e\} + \{Q^e\} \quad (2.2.35)$$

The matrix  $[K^e]$  is called the *coefficient matrix*, or *stiffness matrix* in structural mechanics applications. The column vector  $\{f^e\}$  is the *source vector*, or *force vector* in structural mechanics problems.

Equation (2.2.35) has  $2n$  unknowns  $(u_1^e, u_2^e, \dots, u_n^e)$  and  $(Q_1^e, Q_2^e, \dots, Q_n^e)$ , called primary and secondary element *nodal degrees of freedom*; hence, it cannot be solved without having an additional  $n$  conditions. Some of these equations are provided by the boundary conditions of the problem and the remaining by the balance of the secondary variables  $Q_i^e$  at nodes common to elements. The balance of equations can be implemented by putting the elements together (i.e. assembling the element equations) to form the total system. Upon assembly and imposition of boundary conditions, we shall obtain exactly the same number of algebraic equations as the total number of unknown primary  $(u_i^e)$  and secondary  $(Q_i^e)$  degrees of freedom.

The coefficient matrix  $[K^e]$ , which is symmetric, and source vector  $\{f^e\}$  can be evaluated for a given interpolation and data  $(a, c, \text{ and } f)$ . When  $a, c,$  and  $f$  are functions of  $x$ , it may be necessary to evaluate  $[K^e]$  and  $\{f^e\}$  using numerical integration. We will discuss the numerical integration concepts in the sequel. Here we give the exact values of  $[K^e]$  and  $\{f^e\}$  for linear as well as quadratic interpolations for element-wise constant values of  $a, c,$  and  $f$ . Suppose that  $a_e, c_e,$  and  $f_e$  denote the element-wise constant values of  $a(x), c(x),$  and  $f(x)$ . Then the following matrices can be derived by evaluating the integrals exactly.

*Linear element*

$$L_1(\bar{x}) = 1 - \frac{\bar{x}}{h_e}, \quad L_2(\bar{x}) = \frac{\bar{x}}{h_e}$$

$$\left( \frac{a_e}{h_e} \begin{bmatrix} 1 & -1 \\ -1 & 1 \end{bmatrix} + \frac{c_e h_e}{6} \begin{bmatrix} 2 & 1 \\ 1 & 2 \end{bmatrix} \right) \begin{Bmatrix} u_1^e \\ u_2^e \end{Bmatrix} = \frac{f_e h_e}{2} \begin{Bmatrix} 1 \\ 1 \end{Bmatrix} + \begin{Bmatrix} Q_1^e \\ Q_2^e \end{Bmatrix} \quad (2.2.36)$$

*Quadratic element*

$$L_1(\bar{x}) = \left(1 - \frac{2\bar{x}}{h_e}\right) \left(1 - \frac{\bar{x}}{h_e}\right), \quad L_2(\bar{x}) = \frac{4\bar{x}}{h_e} \left(1 - \frac{\bar{x}}{h_e}\right), \quad L_3(\bar{x}) = -\frac{\bar{x}}{h_e} \left(1 - \frac{2\bar{x}}{h_e}\right)$$

$$\left( \frac{a_e}{3h_e} \begin{bmatrix} 7 & -8 & 1 \\ -8 & 16 & -8 \\ 1 & -8 & 7 \end{bmatrix} + \frac{c_e h_e}{30} \begin{bmatrix} 4 & 2 & -1 \\ 2 & 16 & 2 \\ -1 & 2 & 4 \end{bmatrix} \right) \begin{Bmatrix} u_1^e \\ u_2^e \\ u_3^e \end{Bmatrix}$$

$$= \frac{f_e h_e}{6} \begin{Bmatrix} 1 \\ 4 \\ 1 \end{Bmatrix} + \begin{Bmatrix} Q_1^e \\ Q_2^e \\ Q_3^e \end{Bmatrix} \quad (2.2.37)$$

Note that the contribution of uniform source to the nodes in a quadratic element is non-uniform, that is,  $f_i^e \neq f_e h_e/3$ .

## 2.3 Two-Dimensional Problems

### 2.3.1 Governing Differential Equation

Consider the problem of finding  $u(x, y)$  such that the following partial differential equation is satisfied

$$-\left[ \frac{\partial}{\partial x} \left( a_{xx} \frac{\partial u}{\partial x} \right) + \frac{\partial}{\partial y} \left( a_{yy} \frac{\partial u}{\partial y} \right) \right] = f(x, y) \quad \text{in } \Omega \quad (2.3.1)$$

where  $\Omega$  is a two-dimensional domain with boundary  $\Gamma$ . Here  $a_{xx}$  and  $a_{yy}$  are material coefficients in the  $x$  and  $y$  directions, respectively, and  $f(x, y)$  is the known source. For example, in a heat transfer problem,  $u$  denotes temperature  $T$ ,  $a_{xx}$  and  $a_{yy}$  denote the conductivities,  $k_{xx}$  and  $k_{yy}$ , and  $f$  is the internal heat generation. For an isotropic medium, we set  $k_{xx} = k_{yy} = k$ . Similarly, for a ground water flow problem  $u$  denotes the water head (i.e. velocity potential),  $a_{xx}$  and  $a_{yy}$  are the permeabilities in the  $x$  and  $y$  directions, respectively, and  $f(x, y)$  is distributed water source. Equation (2.3.1) also arises in other fields of science and engineering, and some of them are listed in Table 2.3.1.

Equation (2.3.1) must be solved in conjunction with specified boundary conditions of the problem. The following two types of boundary conditions are assumed:

$$u = \hat{u}(s) \quad \text{on } \Gamma_u \quad (2.3.2)$$

$$q_n = \left( a_{xx} \frac{\partial u}{\partial x} n_x + a_{yy} \frac{\partial u}{\partial y} n_y \right) + q_c = \hat{q}(s) \quad \text{on } \Gamma_q \quad (2.3.3)$$

where  $\Gamma_u$  and  $\Gamma_q$  are disjoint portions of the boundary  $\Gamma$  such that  $\Gamma = \Gamma_u \cup \Gamma_q$ ,  $q_c$  refers to the convective component of flux (e.g. in heat transfer problems)

$$q_c = h_c(u - u_c) \quad (2.3.4)$$

and  $(n_x, n_y)$  denote the direction cosines of the unit normal vector on the boundary. In Eq. (2.3.4),  $h_c$  denotes the convective heat transfer coefficient. The radiative heat transfer boundary condition (which is a nonlinear function of  $u$ ) is not considered here. However, radiation boundary condition will be considered in the nonlinear analysis.

### 2.3.2 Finite Element Approximation

In the finite element method, the domain  $\bar{\Omega} = \Omega \cup \Gamma$  is divided into a set of subdomains  $\bar{\Omega}^e = \Omega^e \cup \Gamma^e$ , called finite elements (see Figure 2.3.1). Any geometric shape for which the approximation functions can be derived uniquely qualifies as an element. We shall discuss simple geometric shapes and orders of approximation shortly. To keep the formulative steps very general (i.e. not confine the formulation to a specific geometric shape or order of the element), we have denoted the domain of a typical element by  $\Omega^e$  and its boundary by  $\Gamma^e$ .

The element  $\bar{\Omega}^e$  can be a triangle or quadrilateral in shape, and the degree of interpolation over it can be linear, quadratic, and so on. The non-overlapping sum of all elements  $\bar{\Omega}^e$  is denoted by  $\Omega^h$ , and it is called the *finite element mesh* of the domain  $\Omega$ . In general,  $\Omega^h$  may not equal  $\bar{\Omega}$  when the boundary  $\Gamma$  is curved. Of course, for polygonal domains, the finite element mesh exactly represents the actual domain.

**Table 2.3.1** List of fields in which the model equation (2.3.1) arises, with meaning of various parameters and variables (see the bottom of the table for the meaning of some parameters\*).

Field	Variable $u$	Data $a_{xx}$	Data $a_{yy}$	Data $f$	Variable $q_n$
Heat transfer	Temperature $T$	Thermal conductance $k_{xx}$	Thermal conductance $k_{yy}$	Heat generation $f$	Heat flux $q_n$
Flow through porous medium	Fluid-head $\phi$	Permeability $\mu_{xx}$	Permeability $\mu_{yy}$	Infiltration $f$	Flux $q_n$
Torsion of cylindrical members	Warping function $\phi$	1	1	0	$\frac{\partial \phi}{\partial n}$
Torsion of cylindrical members	Stress function $\psi$	1	1	$2G\theta$	$\frac{\partial \phi}{\partial n}$
Deflection of membranes	Displacement $u$	Tension $T$	Tension $T$	Transverse force $f$	$q_n$ $\frac{\partial u}{\partial n}$
Flows of inviscid flows	Velocity potential $\phi$	1	1	0	$q_n$ $\frac{\partial \phi}{\partial n}$
Flows of inviscid flows	Stream function $\psi$	1	1	0	$q_n$ $\frac{\partial \psi}{\partial n}$
Electrostatics	Electrical potential $\phi$	Dielectric constant $\epsilon$	Dielectric constant $\epsilon$	Charge density $\rho$	Electric flux $\frac{\partial \psi}{\partial n}$

\*  $k$  = thermal conductance;  $\beta$  = convective film conductance;  $T_\infty$  = ambient temperature of the surrounding fluid medium;  $G$  = shear modulus;  $\theta$  = angle of twist.

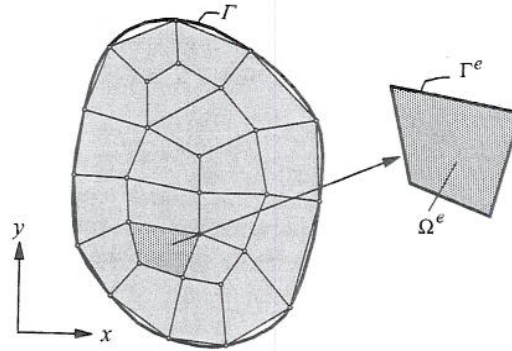


Figure 2.3.1 Finite element discretization of a domain.

Suppose that the dependent unknown  $u$  is approximated over a typical finite element  $\bar{\Omega}^e$  by the expression

$$u(x, y) \approx u_h^e(x, y) = \sum_{j=1}^n u_j^e L_j^e(x, y) \quad (2.3.5)$$

where  $u_h^e(x, y)$  represents an approximation of  $u(x, y)$  over the element  $\bar{\Omega}^e$ , parameters  $u_j^e$  denote the values of the function  $u_h^e(x, y)$  at a selected number of points, called element nodes, in the element  $\bar{\Omega}^e$ , and  $L_j^e$  are the Lagrange interpolation functions associated with the element. As we shall see shortly, the interpolation functions depend not only on the number of nodes in the element, but also on the shape of the element. The shape of the element must be such that its geometry is uniquely defined by a set of nodes. A triangle ( $n = 3$ ) is the simplest two-dimensional geometric shape in two dimensions.

### 2.3.3 Weak Formulation

The  $n$  parameters (or nodal values)  $u_j^e$  in Eq. (2.3.5) must be determined such that the approximate solution  $u^e(x, y)$  satisfies the governing Eq. (2.3.1) and boundary conditions of the problem. As in the case of a variational and weighted-residual method, we seek to satisfy the governing differential equation in a weighted-integral sense, as described in Section 2.2. The type of finite element model depends on the weighted-integral form used to generate the algebraic equations. Thus, if one uses the weak form, the resulting model will be different from those obtained with a weighted-residual statement in which the weight function can be any one of several choices. In the remainder of this chapter, we shall be primarily concerned with the weak form finite element models.

The weak form of a differential equation is a weighted-integral statement that is equivalent to both the governing differential equation as well as the associated natural boundary conditions. We shall develop the weak form of Eqs. (2.3.1) and (2.3.3) over the typical element  $\Omega^e$  using the three-step procedure. The first step is to take all non-zero expressions in Eq. (2.3.1) to one side of the equality, multiply the resulting equation with a weight function  $w$ , and integrate the equation over the element domain  $\Omega^e$ :

$$0 = \int_{\Omega^e} w \left[ -\frac{\partial}{\partial x} \left( a_{xx} \frac{\partial u_h^e}{\partial x} \right) - \frac{\partial}{\partial y} \left( a_{yy} \frac{\partial u_h^e}{\partial y} \right) - f(x, y) \right] dx dy \quad (2.3.6)$$

The expression in the square brackets of the above equation represents a residual of the approximation of the differential equation (2.3.1), because  $u_h^e(x, y)$  is only an approximation of  $u(x, y)$ . For  $n$  independent choices of  $w$ , we obtain a set of  $n$  linearly independent algebraic equations.

In the second step, we distribute the differentiation among  $u$  and  $w$  equally, so that both  $u$  and  $w$  are required to be differentiable only once with respect to  $x$  and  $y$ . To achieve this we use the component form of the gradient (or divergence) theorem,

$$\int_{\Omega^e} \frac{\partial}{\partial x} (wF_1) dx dy = \oint_{\Gamma^e} (wF_1)n_x ds \quad (2.3.7a)$$

$$\int_{\Omega^e} \frac{\partial}{\partial y} (wF_2) dx dy = \oint_{\Gamma^e} (wF_2)n_y ds \quad (2.3.7b)$$

where  $n_x$  and  $n_y$  are the components (i.e. the direction cosines) of the unit normal vector

$$\hat{\mathbf{n}} = n_x \hat{\mathbf{e}}_x + n_y \hat{\mathbf{e}}_y = \cos \alpha \hat{\mathbf{e}}_x + \sin \alpha \hat{\mathbf{e}}_y \quad (2.3.8)$$

on the boundary  $\Gamma^e$ , and  $ds$  is the arc length of an infinitesimal line element along the boundary. We obtain

$$0 = \int_{\Omega^e} \left[ a_{xx} \frac{\partial w}{\partial x} \frac{\partial u}{\partial x} + a_{yy} \frac{\partial w}{\partial y} \frac{\partial u}{\partial y} - wf \right] dx dy - \oint_{\Gamma^e} w \left[ a_{xx} \frac{\partial u}{\partial x} n_x + a_{yy} \frac{\partial u}{\partial y} n_y \right] ds \quad (2.3.9)$$

From an inspection of the boundary term in Eq. (2.3.9), we note that  $u$  is the primary variable, and specification of  $u$  constitutes the essential boundary condition. The coefficient of the weight function in the boundary expression, namely

$$q_n = a_{xx} \frac{\partial u}{\partial x} n_x + a_{yy} \frac{\partial u}{\partial y} n_y \quad (2.3.10)$$

is the secondary variable. Its specification constitutes the natural boundary condition. By definition  $q_n$  is positive outward from the surface as we move counterclockwise along the boundary  $\Gamma^e$ . The secondary variable  $q_n$  denotes the flux normal to the boundary of the element.

The third and last step of the formulation is to use the definition (2.3.10) in Eq. (2.3.9) and write it as

$$0 = \int_{\Omega^e} \left( a_{xx} \frac{\partial w}{\partial x} \frac{\partial u}{\partial x} + a_{yy} \frac{\partial w}{\partial y} \frac{\partial u}{\partial y} - wf \right) dx dy - \oint_{\Gamma^e} w q_n ds \quad (2.3.11)$$

or

$$0 = B(w, u) - \ell(w) \quad (2.3.12)$$

where the bilinear form  $B(\cdot, \cdot)$  and linear form  $\ell(\cdot)$  are defined by

$$B(w, u) = \int_{\Omega^e} \left( a_{xx} \frac{\partial w}{\partial x} \frac{\partial u}{\partial x} + a_{yy} \frac{\partial w}{\partial y} \frac{\partial u}{\partial y} \right) dx dy \quad (2.3.13a)$$

$$\ell(w) = \int_{\Omega^e} w f dx dy + \oint_{\Gamma^e} w q_n ds \quad (2.3.13b)$$

Note that the bilinear form is symmetric in its arguments ( $w, u$ )

$$B(w, u) = B(u, w)$$

and  $\ell(w)$  is linear in  $w$ . Therefore, it is possible to construct the associated quadratic functional from the formula

$$I(u) = \frac{1}{2} B(u, u) - \ell(u) \quad (2.3.14)$$

### 2.3.4 Finite Element Model

The weak form in Eq. (2.3.11) requires that the approximation chosen for  $u$  should be at least linear in both  $x$  and  $y$  so that there are no terms in (2.3.11) that become identically zero. Suppose that  $u$  is approximated over a typical finite element  $\Omega^e$  by the expression of the form (2.3.5). Substituting the finite element approximation (2.3.5) for  $u$  into the weak form (2.3.11), we obtain

$$0 = \sum_{j=1}^n \left\{ \int_{\Omega^e} \left[ \frac{\partial w}{\partial x} \left( a_{xx} \frac{\partial L_j^e}{\partial x} \right) + \frac{\partial w}{\partial y} \left( a_{yy} \frac{\partial L_j^e}{\partial y} \right) - wf \right] dx dy \right\} u_j^e - \oint_{\Gamma^e} w q_n ds \quad (2.3.15)$$

This equation must hold for any weight function  $w$ . Since we need  $n$  independent algebraic equations to solve for the  $n$  unknowns,  $u_1^e, u_2^e, \dots, u_n^e$ , we choose  $n$  independent functions for  $w$ :  $w = L_1^e, L_2^e, \dots, L_n^e$ . This particular choice of weight functions is a natural one when the weight function is viewed as a virtual variation of the dependent unknown (i.e.  $w = \delta u^e = \sum_{i=1}^n \delta u_i^e L_i^e$ ).

For each choice of  $w$  we obtain an algebraic relation among  $(u_1^e, u_2^e, \dots, u_n^e)$ . The  $i$ th algebraic equation is obtained by substituting  $w = L_i^e$  into Eq. (2.3.15):

$$\sum_{j=1}^n K_{ij}^e u_j^e = Q_i^e + q_i^e \quad (2.3.16)$$

where the coefficients  $K_{ij}^e$ ,  $Q_i^e$ , and  $q_i^e$  are defined by

$$K_{ij}^e = \int_{\Omega^e} \left( a_{xx} \frac{\partial L_i^e}{\partial x} \frac{\partial L_j^e}{\partial x} + a_{yy} \frac{\partial L_i^e}{\partial y} \frac{\partial L_j^e}{\partial y} \right) dx dy \quad (2.3.17a)$$

$$Q_i^e = \int_{\Omega^e} f L_i^e dx dy, \quad q_i^e = \oint_{\Gamma^e} q_n L_i^e ds \quad (2.3.17b)$$

We note that  $K_{ij}^e = K_{ji}^e$  (i.e.  $[K^e]$  is symmetric). The symmetry of the coefficient matrix is due to the symmetry of the bilinear form, which in turn is due to the weak form development. In matrix notation, Eq. (2.3.16) takes the form

$$[K^e]\{u^e\} = \{Q^e\} + \{q^e\} \equiv \{F^e\} \quad (2.3.18)$$

This completes the finite element model development. Before we discuss assembly of elements, it is informative to determine the interpolation functions  $L_i^e$  for certain basic two-dimensional finite elements.

### 2.3.5 Interpolation Functions

The finite element approximation  $u^e(x, y)$  of  $u(x, y)$  over an element  $\Omega^e$  must satisfy the following conditions in order for the approximate solution to converge to the true solution:

1.  $u^e(x, y)$  must be continuous as required in the weak form of the problem (i.e. all terms in the weak form are represented as non-zero values).
2. The polynomials used to represent  $u^e(x, y)$  must be complete (i.e. all terms, beginning with a constant term up to the highest order used in the polynomial should be included in the expression of  $u^e(x, y)$ ).
3. All terms in the polynomial should be linearly independent.

The number of linearly independent terms in the representation of  $u^e$  dictates the shape and number of degrees of freedom of the element. Here we review the interpolation functions of linear triangular and rectangular elements.

An examination of the variational form (2.3.11) and the finite element matrices in Eq. (2.3.17a) shows that the  $L_i^e$  should be at least linear functions of  $x$  and  $y$ . The polynomial

$$u^e(x, y) = c_1^e + c_2^e x + c_3^e y \quad (2.3.19)$$



is the lowest-order polynomial that meets the requirements. It contains three linearly independent terms, and it is linear in both  $x$  and  $y$ . The polynomial is complete because the lower-order term, namely, the constant term, is included. To write the three constants  $(c_1^e, c_2^e, c_3^e)$  in terms of the nodal values of  $u^e$ , we must identify three points or nodes in the element  $\Omega^e$ . The three nodes must be such that they uniquely define the geometry of the element and allow the imposition of inter-element continuity of the variable  $u^e(x, y)$ . Obviously, the geometric shape defined by three points in a two-dimensional domain is a triangle. Thus the polynomial in Eq. (2.3.19) is associated with a triangular element and the three nodes are identified as the vertices of the triangle.

On the other hand, the polynomial

$$u^e(x, y) = c_1^e + c_2^e x + c_3^e y + c_4^e xy \quad (2.3.20)$$

contains four linearly independent terms, and is linear in  $x$  and  $y$ , with a bilinear term in  $x$  and  $y$ . This polynomial requires an element with four nodes. It is a rectangle with nodes at the four corners of the rectangle.

The interpolation functions for linear triangular and rectangular elements are given below. Higher-order two-dimensional elements (i.e. element with higher-order interpolation polynomials) will be discussed in Section 2.4.

#### Linear triangular element

The linear interpolation functions for the three-node triangle [see Figure 2.3.2(a)] are (see Reddy [1, pp. 304-307])

$$L_i^e(x, y) = \frac{1}{2A_e}(\alpha_i^e + \beta_i^e x + \gamma_i^e y), \quad (i = 1, 2, 3) \quad (2.3.21)$$

where  $A_e$  is the area of the triangle, and  $\alpha_i^e$ ,  $\beta_i^e$ , and  $\gamma_i^e$  are geometric constants known in terms of the nodal coordinates  $(x_i, y_i)$ :

$$\alpha_i^e = x_j y_k - x_k y_j; \quad \beta_i^e = y_j - y_k; \quad \gamma_i^e = -(x_j - x_k) \quad (2.3.22)$$

for  $i \neq j \neq k$ , and  $i, j$ , and  $k$  permute in a natural order. Note that  $(x, y)$  are the *global coordinates* used in the governing equation (2.3.1) over the domain  $\Omega$ . The interpolation functions  $L_i^e$  ( $i = 1, 2, \dots, n$ ) satisfy the following interpolation properties:

$$(i) \quad L_i^e(x_j, y_j) = \delta_{ij}, \quad (i, j = 1, 2, 3); \quad (ii) \quad \sum_{i=1}^3 L_i^e(x, y) = 1 \quad (2.3.23)$$

and they are called the *Lagrange interpolation functions*. Note that use of the linear interpolation functions  $L_i^e$  of a triangle will result in the approximation of the curved surface  $u(x, y)$  by a planar function  $u_h^e(x, y) = \sum_{i=1}^3 u_i^e L_i^e(x, y)$ .

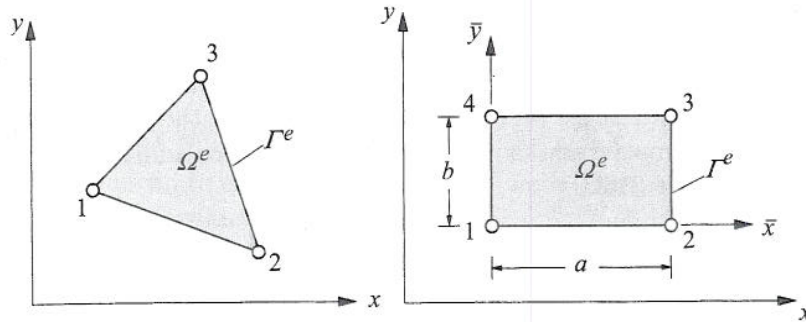


Figure 2.3.2 The linear (a) triangular and (b) rectangular finite elements.

The integrals in the definition of  $K_{ij}^e$  and  $Q_i^e$  can be evaluated for given data:  $a_{xx}$ ,  $a_{yy}$ , and  $f$ . For example, for element-wise constant values of the data, that is,  $a_{xx} = a_{xx}^e$ ,  $a_{yy} = a_{yy}^e$ , and  $f = f^e$ , we have (see Reddy [1, pp. 311–313]) the following results:

$$K_{ij}^e = \frac{1}{4A_e} (a_{xx}^e \beta_i^e \beta_j^e + a_{yy}^e \gamma_i^e \gamma_j^e); \quad Q_i^e = \frac{f_e A_e}{3} \quad (2.3.24)$$

where  $A_e$  is the area of the triangular element, and  $\beta_i^e$  and  $\gamma_i^e$  are known in terms of the global nodal coordinates of the element nodes, as given in Eq. (2.3.22). For a right-angled triangular element with base  $a$  and height  $b$ , and node 1 at the right angle (nodes are numbered counterclockwise),  $[K^e]$  takes the form (see Reddy [1, p. 387])

$$[K^e] = \frac{a_{xx}^e}{2} \begin{bmatrix} \alpha & -\alpha & 0 \\ -\alpha & \alpha & 0 \\ 0 & 0 & 0 \end{bmatrix} + \frac{a_{yy}^e}{2} \begin{bmatrix} \beta & 0 & -\beta \\ 0 & 0 & 0 \\ -\beta & 0 & \beta \end{bmatrix} \quad (2.3.25)$$

where  $\alpha = b/a$  and  $\beta = a/b$ . Of course, for cases in which the conductivities are functions of  $(x, y)$ , numerical integration can be used to evaluate the coefficients (see Section 2.5.3).

The evaluation of boundary integrals of the type

$$q_i^e = \oint_{\Gamma^e} q_n^e L_i^e(s) ds \quad (2.3.26)$$

where  $q_n^e$  is a known function of the distance  $s$  along the boundary  $\Gamma^e$ , involves evaluation of line integrals. It is necessary to compute such integrals only when

$\Gamma^e$ , or a portion of it, coincides with the boundary  $\Gamma_q$  of the total domain  $\Omega$  on which the flux is specified. On portions of  $\Gamma^e$  that are in the interior of the domain  $\Omega$ ,  $q_n^e$  on side  $(i, j)$  of element  $\Omega^e$  cancels with  $q_n^f$  on side  $(p, q)$  of element  $\Omega^f$  when sides  $(i, j)$  of element  $\Omega^e$  and  $(p, q)$  of element  $\Omega^f$  are the same (i.e. at the interface of elements  $\Omega^e$  and  $\Omega^f$ ). This can be viewed as the balance of the internal flux. When  $\Gamma^e$  falls on the boundary  $\Gamma_u$  of the domain  $\Omega$ ,  $q_n^e$  is not known there and can be determined in the post-computation. Note that the primary variable  $u$  is specified on  $\Gamma_u$ . For additional details, see Reddy [1, pp. 313–318].

### Linear rectangular element

For a linear rectangular element, we have

$$u(\bar{x}, \bar{y}) = \sum_{i=1}^4 u_i^e L_i^e(\bar{x}, \bar{y}) \quad (2.3.27)$$

where  $L_i$  are the Lagrange interpolation functions expressed in terms of the element coordinates  $(\bar{x}, \bar{y})$  (see Reddy [1, pp. 308–311])

$$\begin{aligned} L_1^e &= \left(1 - \frac{\bar{x}}{a}\right)\left(1 - \frac{\bar{y}}{b}\right), & L_2^e &= \frac{\bar{x}}{a}\left(1 - \frac{\bar{y}}{b}\right) \\ L_3^e &= \frac{\bar{x}\bar{y}}{ab}, & L_4^e &= \left(1 - \frac{\bar{x}}{a}\right)\frac{\bar{y}}{b} \end{aligned} \quad (2.3.28)$$

and  $(\bar{x}, \bar{y})$  denote the local coordinates with origin located at node 1 of the element, and  $(a, b)$  denote the horizontal and vertical dimensions of the rectangle [see Figure 2.3.2(b)].

The integrals in the definition of  $K_{ij}^e$  and  $Q_i^e$  can be easily evaluated over a rectangular element of sides  $a$  and  $b$ . For example, for element-wise constant values of the data, that is,  $a_{xx} = a_{xx}^e$ ,  $a_{yy} = a_{yy}^e$ , and  $f = f^e$ , we have (see Reddy [1, p. 313; p. 387]) the following results:

$$[K^e] = a_{xx}^e [S^{11}] + a_{yy}^e [S^{22}], \quad Q_i^e = \frac{f_e ab}{4} \quad (2.3.29)$$

where

$$[S^{11}] = \frac{1}{6} \begin{bmatrix} 2\alpha & -2\alpha & -\alpha & \alpha \\ -2\alpha & 2\alpha & \alpha & -\alpha \\ -\alpha & \alpha & 2\alpha & -2\alpha \\ \alpha & -\alpha & -2\alpha & 2\alpha \end{bmatrix} \quad (2.3.30a)$$

$$[S^{22}] = \frac{1}{6} \begin{bmatrix} 2\beta & \beta & -\beta & -2\beta \\ \beta & 2\beta & -2\beta & -\beta \\ -\beta & -2\beta & 2\beta & \beta \\ -2\beta & -\beta & \beta & 2\beta \end{bmatrix} \quad (2.3.30b)$$

and  $\alpha = b/a$  and  $\beta = a/b$ . Again, for cases in which the conductivities are functions of  $(x, y)$ , numerical integration is used to evaluate the coefficients, as discussed in Section 2.5.4. When the element is non-rectangular, that is, a quadrilateral, we use coordinate transformations to represent the integrals over a square geometry and then use numerical integration to evaluate them.

### 2.3.6 Assembly of Elements

The assembly of finite elements to obtain the equations of the entire domain is based on the following two rules:

1. Continuity of the primary variable (i.e. temperature)
2. Balance of secondary variables (i.e. heat flux)

We illustrate the assembly procedure by considering a finite element mesh consisting of a triangular element and a quadrilateral element (see Figure 2.3.3).

Let  $K_{ij}^1$  ( $i, j = 1, 2, 3$ ) denote the coefficient matrix corresponding to the triangular element, and let  $K_{ij}^2$  ( $i, j = 1, 2, 3, 4$ ) denote the coefficient matrix corresponding to the quadrilateral element. The nodes of the finite element mesh are called *global nodes*. From the mesh shown in Figure 2.3.3, it is clear that the following correspondence between global and element nodes exists: nodes 1, 2, and 3 of element 1 correspond to global nodes 1, 2, and 3, respectively. Nodes 1, 2, 3, and 4 of element 2 correspond to global nodes 2, 4, 5, and 3, respectively. Hence, the correspondence between the local and global nodal values of temperature is

$$u_1^1 = u_1, \quad u_2^1 = u_2^2 = u_2, \quad u_3^1 = u_4^2 = u_3, \quad u_2^2 = u_4, \quad u_3^2 = u_5 \quad (2.3.31)$$

which amounts to imposing the continuity of the primary variables at the nodes common to elements 1 and 2. Note that the continuity of the primary variables at the inter-element nodes guarantees the continuity of the primary variable along the entire inter-element boundary.

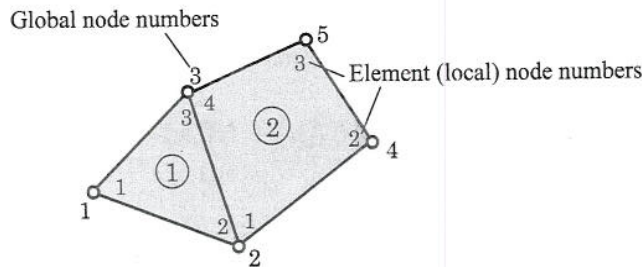


Figure 2.3.3 Global-local correspondence of nodes for assembly of elements.

Next, we consider the balance of secondary variables at the interelement boundaries. At the interface between the two elements, the flux from the two elements should be equal in magnitude and opposite in sign. For the two elements shown in Figure 2.3.3, the interface is along the side connecting global nodes 2 and 3. Hence, the internal flux  $q_n^1$  on side 2-3 of element 1 should balance the flux  $q_n^2$  on side 4-1 of element 2 (recall the sign convention on  $q_n^e$ ):

$$(q_n^1)_{2-3} = (q_n^2)_{4-1} \quad \text{or} \quad (q_n^1)_{2-3} = (-q_n^2)_{1-4} \quad (2.3.32)$$

In the finite element method, the above relation is imposed in a weighted-integral sense:

$$\int_{h_{23}^1} q_n^1 L_2^1 ds = - \int_{h_{14}^2} q_n^2 L_1^2 ds, \quad \int_{h_{23}^1} q_n^1 L_3^1 ds = - \int_{h_{14}^2} q_n^2 L_4^2 ds \quad (2.3.33)$$

where  $h_{pq}^e$  denotes length of the side connecting node  $p$  to node  $q$  of element  $\Omega^e$ .

Now we are ready to assemble the element equations for the two-element mesh. The element equations of the two elements are written separately first. For the triangular element, the element equations are of the form

$$\begin{aligned} K_{11}^1 u_1^1 + K_{12}^1 u_2^1 + K_{13}^1 u_3^1 &= Q_1^1 + q_1^1 \\ K_{21}^1 u_1^1 + K_{22}^1 u_2^1 + K_{23}^1 u_3^1 &= Q_2^1 + q_2^1 \\ K_{31}^1 u_1^1 + K_{32}^1 u_2^1 + K_{33}^1 u_3^1 &= Q_3^1 + q_3^1 \end{aligned} \quad (2.3.34a)$$

For the rectangular element the element equations are given by

$$\begin{aligned} K_{11}^2 u_1^2 + K_{12}^2 u_2^2 + K_{13}^2 u_3^2 + K_{14}^2 u_4^2 &= Q_1^2 + q_1^2 \\ K_{21}^2 u_1^2 + K_{22}^2 u_2^2 + K_{23}^2 u_3^2 + K_{24}^2 u_4^2 &= Q_2^2 + q_2^2 \\ K_{31}^2 u_1^2 + K_{32}^2 u_2^2 + K_{33}^2 u_3^2 + K_{34}^2 u_4^2 &= Q_3^2 + q_3^2 \\ K_{41}^2 u_1^2 + K_{42}^2 u_2^2 + K_{43}^2 u_3^2 + K_{44}^2 u_4^2 &= Q_4^2 + q_4^2 \end{aligned} \quad (2.3.34b)$$

In order to impose the balance condition in (2.3.32), it is necessary to add the second equation of element 1 to the first equation of element 2, and also add the third equation of element 1 to the fourth equation of element 2:

$$\begin{aligned} (K_{21}^1 u_1^1 + K_{22}^1 u_2^1 + K_{23}^1 u_3^1) + (K_{11}^2 u_1^2 + K_{12}^2 u_2^2 + K_{13}^2 u_3^2 + K_{14}^2 u_4^2) \\ = (Q_2^1 + q_2^1) + (Q_1^2 + q_1^2) \end{aligned}$$

$$\begin{aligned} (K_{31}^1 u_1^1 + K_{32}^1 u_2^1 + K_{33}^1 u_3^1) + (K_{41}^2 u_1^2 + K_{42}^2 u_2^2 + K_{43}^2 u_3^2 + K_{44}^2 u_4^2) \\ = (Q_3^1 + q_3^1) + (Q_4^2 + q_4^2) \end{aligned}$$

Using the local-global nodal variable correspondence in Eq. (2.3.1), we can rewrite the above equations as

$$\begin{aligned} K_{21}^1 u_1 + (K_{22}^1 + K_{11}^2) u_2 + (K_{23}^1 + K_{14}^2) u_3 + K_{12}^2 u_4 + K_{13}^2 u_5 \\ = Q_2^1 + Q_1^2 + (q_2^1 + q_1^2) \end{aligned}$$

$$\begin{aligned} K_{31}^1 u_1 + (K_{32}^1 + K_{41}^2) u_2 + (K_{33}^1 + K_{44}^2) u_3 + K_{42}^2 u_4 + K_{43}^2 u_5 \\ = Q_3^1 + Q_4^2 + (q_3^1 + q_4^2) \end{aligned}$$

Now we can impose the conditions in Eq. (2.3.33) by setting appropriate portions of the expressions in parenthesis on the right-hand side of the above equations to zero (or a specified non-zero value). In general, when several elements are connected, the assembly of the elements is carried out by putting element coefficients  $K_{ij}^e$ ,  $Q_i^e$ , and  $q_i^e$  into proper locations of the global coefficient matrix and right-hand column vectors. This is done by means of the connectivity relations, that is, correspondence of the local node number to the global node number.

The assembly procedure described above can be used to assemble elements of any shape and type. The procedure can be implemented in a computer with the help of the local-global nodal correspondence.

For heat conduction problems that involve convection heat transfer at the boundary, that is, when heat is transferred from one medium to the surrounding medium (often, a fluid) by convection, the finite element model developed earlier requires some modification. For a convection boundary, the natural boundary condition is a balance of energy transfer across the boundary due to conduction and/or convection (i.e. Newton's law of cooling):

$$\left( a_{xx} \frac{\partial u}{\partial x} n_x + a_{yy} \frac{\partial u}{\partial y} n_y \right) + h_c (u - u_c) = q_n \quad (2.3.35)$$

where  $h_c$  is the convective conductance (or the convective heat transfer coefficient),  $u_c$  is the (ambient) temperature of the surrounding fluid medium, and  $q_n$  is the specified heat flux. The first term accounts for heat transfer by conduction, the second by convection, and the third accounts for the specified heat flux, if any. It is the presence of the term  $h_c(u - u_c)$  that requires some modification of the weak form in Eq. (2.3.11). To include the convective boundary condition (2.3.35), the boundary integral in Eq. (2.3.9) should be modified. Instead of replacing the coefficient of  $w$  in the boundary integral with  $q_n$ , we use Eq. (2.3.35):

$$\begin{aligned} 0 &= \int_{\Omega^e} \left[ a_{xx} \frac{\partial w}{\partial x} \frac{\partial u}{\partial x} + a_{yy} \frac{\partial w}{\partial y} \frac{\partial u}{\partial y} - w f \right] dx dy - \oint_{\Gamma^e} w \left[ a_{xx} \frac{\partial u}{\partial x} n_x + a_{yy} \frac{\partial u}{\partial y} n_y \right] ds \\ &= \int_{\Omega^e} \left( a_{xx} \frac{\partial w}{\partial x} \frac{\partial u}{\partial x} + a_{yy} \frac{\partial w}{\partial y} \frac{\partial u}{\partial y} - w f \right) dx dy - \oint_{\Gamma^e} w [q_n - h_c(u - u_c)] ds \end{aligned} \quad (2.3.36)$$

or

$$0 = B(w, u) - \ell(w) \quad (2.3.37)$$

where  $w$  is the weight function, and  $B(\cdot, \cdot)$  and  $\ell(\cdot)$  are the bilinear and linear forms

$$B(w, u) = \int_{\Omega^e} \left( a_{xx} \frac{\partial w}{\partial x} \frac{\partial u}{\partial x} + a_{yy} \frac{\partial w}{\partial y} \frac{\partial u}{\partial y} \right) dx dy + \oint_{\Gamma^e} h_c w u ds \quad (2.3.38a)$$

$$\ell(w) = \int_{\Omega^e} f w dx dy + \oint_{\Gamma^e} h_c u_c w ds + \oint_{\Gamma^e} q_n w ds \quad (2.3.38b)$$

Note that the unknown surface temperature in the convective boundary condition has been made part of the bilinear form  $B(\cdot, \cdot)$  while all the known quantities remain part of the linear form  $\ell(\cdot)$ . The finite element model of Eq. (2.3.36) is (see Reddy [1], pp. 341–346) given by

$$[K^e] \{u^e\} = \{F^e\} \quad (2.3.39)$$

where

$$K_{ij}^e = \int_{\Omega^e} \left( a_{xx} \frac{\partial L_i}{\partial x} \frac{\partial L_j}{\partial x} + a_{yy} \frac{\partial L_i}{\partial y} \frac{\partial L_j}{\partial y} \right) dx dy + \oint_{\Gamma^e} h_c L_i L_j ds \quad (2.3.40a)$$

$$F_i = \int_{\Omega^e} f L_i dx dy + \oint_{\Gamma^e} h_c u_c L_i ds + \oint_{\Gamma^e} q_n L_i ds \quad (2.3.40b)$$

The finite element model (2.3.39) is valid for both conductive and convective heat transfer boundary conditions. For problems with no convective boundary conditions, the convective contributions to the element coefficients are omitted. Indeed, these contributions have to be included only for those elements whose sides fall on the boundary with specified convection heat transfer. The contribution due to convective boundaries to the element coefficient matrix and source vector can be computed by evaluating line integrals, as discussed in Reddy [1], pp. 342–345.

## 2.4 Library of Two-Dimensional Finite Elements

### 2.4.1 Introduction

The objective of this section is to present a library of two-dimensional triangular and rectangular elements of the Lagrange family, that is, elements over which only the function – not its derivatives – are interpolated. Once we have elements of different shapes and order at our disposal, we can choose appropriate elements and associated interpolation functions for a given problem. The interpolation functions are developed here for regularly shaped elements, called *master elements*. These elements can be used for numerical

evaluation of integrals defined on irregularly shaped elements. This requires a transformation of the geometry from the actual element shape to its associated master element. We will discuss the numerical evaluation of integrals in Section 2.6.

### 2.4.2 Triangular Elements

The three-node triangular element was developed in Section 2.3.5. Higher-order triangular elements (i.e. triangular elements with interpolation functions of higher degree) can be systematically developed with the help of the so-called *area coordinates*. For triangular elements, it is possible to construct three non-dimensional coordinates  $\hat{L}_i$  ( $i = 1, 2, 3$ ), which vary in a direction normal to the sides directly opposite each node (see Figure 2.4.1). The coordinates are defined such that

$$\hat{L}_i = \frac{A_i}{A}, \quad A = \sum_{i=1}^3 A_i \quad (2.4.1)$$

where  $A_i$  is the area of the triangle formed by nodes  $j$  and  $k$  and an arbitrary point  $P$  in the element, and  $A$  is the total area of the element. For example,  $A_1$  is the area of the shaded triangle which is formed by nodes 2 and 3 and point  $P$ . The point  $P$  is at a perpendicular distance of  $s$  from the side connecting nodes 2 and 3. We have  $A_1 = bs/2$  and  $A = bh/2$ . Hence

$$\hat{L}_1 = \frac{A_1}{A} = \frac{s}{h} \quad (2.4.2)$$

Clearly,  $\hat{L}_1$  is zero on side 2-3 (hence, zero at nodes 2 and 3) and has a value of unity at node 1. Thus,  $\hat{L}_1$  is the interpolation function associated with node 1. Similarly,  $\hat{L}_2$  and  $\hat{L}_3$  are the interpolation functions associated with nodes 2 and 3, respectively. In summary, we have

$$L_i = \hat{L}_i \quad (2.4.3)$$

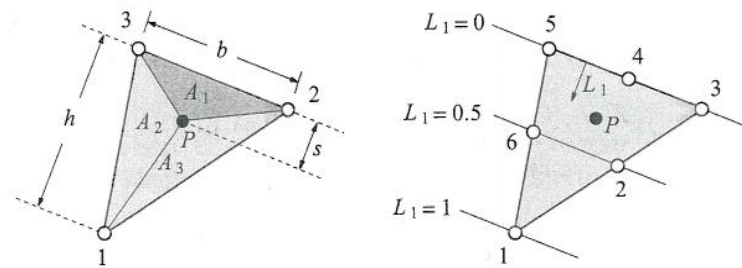


Figure 2.4.1 Definition of area coordinates  $\hat{L}_i$  for triangular elements.



The area coordinates  $\hat{L}_i$  can be used to construct interpolation functions for higher-order triangular elements. For example, a higher-order element with  $k$  nodes per side (equally spaced on each side) has a total of  $n$  nodes

$$n = \sum_{i=0}^{k-1} (k-i) = k + (k-1) + \cdots + 1 = \frac{k}{2}(k+1) \quad (2.4.4)$$

and its degree is equal to  $k-1$ . The explicit forms of the interpolation functions for the linear and quadratic elements are recorded below:

$$\{\mathbf{L}^e\} = \begin{Bmatrix} \hat{L}_1 \\ \hat{L}_2 \\ \hat{L}_3 \end{Bmatrix}; \quad \{\mathbf{L}^e\} = \begin{Bmatrix} \hat{L}_1(2\hat{L}_1 - 1) \\ \hat{L}_2(2\hat{L}_2 - 1) \\ \hat{L}_3(2\hat{L}_3 - 1) \\ 4\hat{L}_1\hat{L}_2 \\ 4\hat{L}_2\hat{L}_3 \\ 4\hat{L}_3\hat{L}_1 \end{Bmatrix} \quad (2.4.5)$$

Note that the order of the interpolation functions in the above arrays corresponds to the node numbers shown in Figure 2.4.2(a). Thus, the first three rows of the vectors in Eq. (2.4.5) correspond to the first three nodes of the linear and quadratic elements, which correspond to the three vertices of the triangular element. The last three rows of the second vector in Eq. (2.4.5) associated with the quadratic element correspond to the mid-side nodes of the triangular element. A similar node-numbering scheme is used for rectangular elements, which are discussed next.

### 2.4.3 Rectangular Elements

The Lagrange interpolation functions associated with rectangular elements can be obtained from the tensor product of corresponding one-dimensional Lagrange interpolation functions. We take a local coordinate system  $(\xi, \eta)$  such that  $-1 \leq (\xi, \eta) \leq 1$ . This choice of local coordinate system is dictated by the Gauss quadrature rule used in the numerical evaluation of integrals over the element (see Section 2.5).

The linear and quadratic interpolation functions are given in Eqs. (2.4.6) and (2.4.7), respectively (see Figure 2.4.2(b) for the node numbers).

$$\{\mathbf{L}^e\} = \frac{1}{4} \begin{Bmatrix} (1-\xi)(1-\eta) \\ (1+\xi)(1-\eta) \\ (1+\xi)(1+\eta) \\ (1-\xi)(1+\eta) \end{Bmatrix} \quad (2.4.6)$$

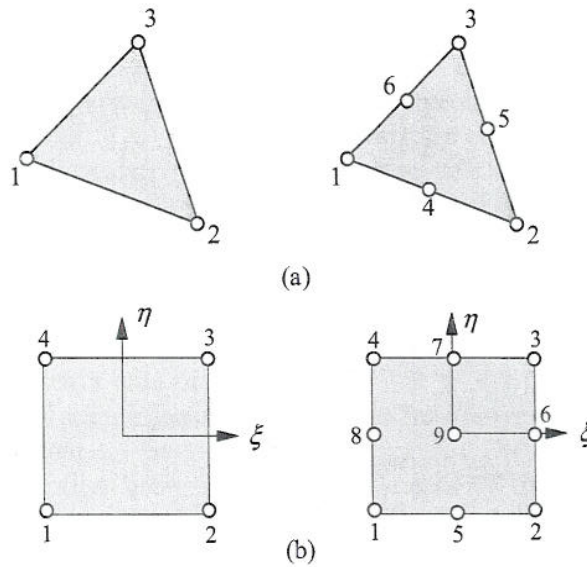


Figure 2.4.2 Linear and quadratic (a) triangular and (b) rectangular elements.

$$\{\mathbf{L}^e\} = \frac{1}{4} \left\{ \begin{array}{l} (1 - \xi)(1 - \eta)(-\xi - \eta - 1) + (1 - \xi^2)(1 - \eta^2) \\ (1 + \xi)(1 - \eta)(\xi - \eta - 1) + (1 - \xi^2)(1 - \eta^2) \\ (1 + \xi)(1 + \eta)(\xi + \eta - 1) + (1 - \xi^2)(1 - \eta^2) \\ (1 - \xi)(1 + \eta)(-\xi + \eta - 1) + (1 - \xi^2)(1 - \eta^2) \\ 2(1 - \xi^2)(1 - \eta) - (1 - \xi^2)(1 - \eta^2) \\ 2(1 + \xi)(1 - \eta^2) - (1 - \xi^2)(1 - \eta^2) \\ 2(1 - \xi^2)(1 + \eta) - (1 - \xi^2)(1 - \eta^2) \\ 2(1 - \xi)(1 - \eta^2) - (1 - \xi^2)(1 - \eta^2) \\ 4(1 - \xi^2)(1 - \eta^2) \end{array} \right\} \quad (2.4.7)$$

The *serendipity elements* are those rectangular elements that have no interior nodes. These elements have fewer nodes compared with the higher-order Lagrange elements. The interpolation functions of the serendipity elements are not complete, and they cannot be obtained using tensor products of one-dimensional Lagrange interpolation functions. Instead, an alternative procedure must be employed, as discussed in Reddy [1]. The interpolation functions for the two-dimensional quadratic serendipity element are given by

(see Figure 2.4.3)

$$\{\mathbf{L}^e\} = \frac{1}{4} \begin{Bmatrix} (1-\xi)(1-\eta)(-\xi-\eta-1) \\ (1+\xi)(1-\eta)(\xi-\eta-1) \\ (1+\xi)(1+\eta)(\xi+\eta-1) \\ (1-\xi)(1+\eta)(-\xi+\eta-1) \\ 2(1-\xi^2)(1-\eta) \\ 2(1+\xi)(1-\eta^2) \\ 2(1-\xi^2)(1+\eta) \\ 2(1-\xi)(1-\eta^2) \end{Bmatrix} \quad (2.4.8)$$

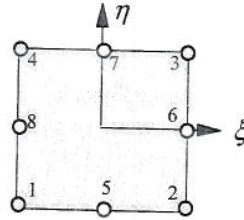


Figure 2.4.3 Quadratic rectangular serendipity element.

## 2.5 Numerical Integration

### 2.5.1 Preliminary Comments

An accurate representation of irregular domains (i.e. domains with curved boundaries) can be accomplished by the use of refined meshes and/or irregularly shaped curvilinear elements. For example, a non-rectangular region cannot be represented using rectangular elements; however, it can be represented by quadrilateral elements. Since the interpolation functions are easily derivable for a rectangular element and it is easier to evaluate integrals over rectangular geometries, we transform the finite element integral statements defined over quadrilaterals to a rectangle. The transformation results in complicated expressions for the integrands in terms of the coordinates used for the rectangular element. Therefore, numerical integration is used to evaluate such complicated integrals. The numerical integration schemes, such as the Gauss-Legendre numerical integration scheme, require the integral to be evaluated on a specific domain or with respect to a specific coordinate system.

### 2.5.2 Coordinate Transformations

Gauss quadrature requires the integral to be expressed over a square region  $\hat{\Omega}$  of dimension  $2 \times 2$  with respect to the coordinate system,  $(\xi, \eta)$  to be such that  $-1 \leq (\xi, \eta) \leq 1$ . The transformation of the geometry and the variable coefficients of the differential equation from the problem coordinates  $(x, y)$  to the local coordinates  $(\xi, \eta)$  results in algebraically complex expressions, and they preclude analytical (i.e. exact) evaluation of the integrals. Thus, the transformation of a given integral expression, defined over element  $\Omega^e$ , to one on the domain  $\hat{\Omega}$  facilitates the numerical integration. Each element of the finite element mesh is transformed to  $\hat{\Omega}$ , only for the purpose of numerically evaluating the integrals (see Figure 2.5.1). The element  $\hat{\Omega}$  is called a *master element*. For example, every quadrilateral element can be transformed to a square element with a side of length 2 and  $-1 \leq (\xi, \eta) \leq 1$  that facilitates the use of Gauss-Legendre quadrature to evaluate integrals defined over the quadrilateral element.

The transformation between a typical element  $\Omega^e$  in the mesh and the master element  $\hat{\Omega}$  [or equivalently, between  $(x, y)$  and  $(\xi, \eta)$ ] is accomplished by a coordinate transformation of the form

$$x = \sum_{j=1}^m x_j^e \phi_j^e(\xi, \eta), \quad y = \sum_{j=1}^m y_j^e \phi_j^e(\xi, \eta) \quad (2.5.1)$$

where  $\phi_j$  denote the finite element interpolation functions of the master element  $\hat{\Omega}$ . The coordinates in the master element are chosen to be the natural coordinates  $(\xi, \eta)$  such that  $-1 \leq (\xi, \eta) \leq 1$ . This choice is dictated by the limits of integration in the Gauss quadrature rule used to evaluate the integrals. For this case, the  $\phi_j^e$  denote the interpolation functions of the four-node rectangular element shown in Figure 2.4.2(b) (i.e.  $m = 4$ ).

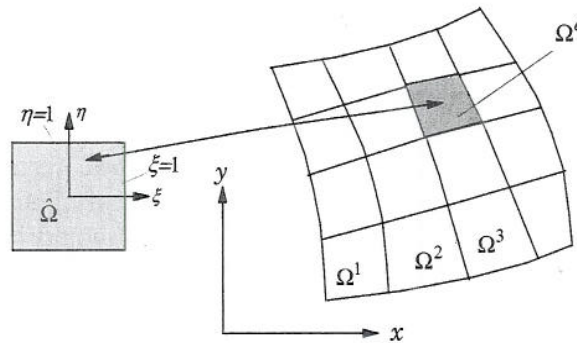


**Figure 2.5.1** Transformation of quadrilateral elements to the master rectangular element for numerical evaluation of integrals.

The transformation (2.5.1) maps, for example, the line  $\xi = 1$  in  $\hat{\Omega}$  to the line defined parametrically by  $x = x(1, \eta)$  and  $y = y(1, \eta)$  in the  $xy$ -plane. In other words, the master element  $\hat{\Omega}$  is transformed, under the linear transformation, into a quadrilateral element (i.e. a four-sided element whose sides are not parallel) in the  $xy$ -plane. Conversely, every quadrilateral element of a mesh can be transformed to the same four-noded square (master) element  $\hat{\Omega}$  in the  $(\xi, \eta)$ -plane.

In general, the dependent variable(s) of the problem are approximated by expressions of the form

$$u(x, y) = \sum_{j=1}^n u_j^e L_j^e(x, y) \quad (2.5.2)$$

The interpolation functions  $L_j^e$  used for the approximation of the dependent variable, in general, are different from  $\phi_j^e$  used in the approximation of the geometry. Depending on the relative degree of approximations used for the geometry [see Eq. (2.5.1)] and the dependent variable(s) [see Eq. (2.5.2)], the finite element formulations are classified into three categories:

1. *Superparametric* ( $m > n$ ). The approximation used for the geometry is higher order than that used for the dependent variable.
2. *Isoparametric* ( $m = n$ ). Equal degree of approximation is used for both geometry and dependent variables.
3. *Subparametric* ( $m < n$ ). Higher-order approximation of the dependent variable is used.

It should be noted that the transformation of a quadrilateral element of a mesh to the master element  $\hat{\Omega}$  is solely for the purpose of numerically evaluating the integrals (see Figure 2.5.1). *No transformation of the physical domain or elements is involved in the finite element analysis.* The resulting algebraic equations of the finite element formulation are always in terms of the nodal values of the physical domain. Different elements of the finite element mesh can be generated from the same master element by assigning appropriate global coordinates to each of the elements. Master elements of a different order define different transformations and hence different collections of finite elements within the mesh. For example, a quadratic rectangular master element can be used to generate a mesh of quadratic curvilinear quadrilateral elements. The transformations of a master element should be such that no spurious gaps exist between elements, and no element overlaps occur. For example, consider the element coefficients

$$K_{ij}^e = \int_{\Omega^e} \left[ a_{xx}(x, y) \frac{\partial L_i^e}{\partial x} \frac{\partial L_j^e}{\partial x} + a_{yy}(x, y) \frac{\partial L_i^e}{\partial y} \frac{\partial L_j^e}{\partial y} \right] dx dy \quad (2.5.3)$$

The integrand (i.e. the expression in the square brackets under the integral) is a function of the global coordinates  $x$  and  $y$ . We must rewrite it in terms of  $\xi$  and  $\eta$  using the transformation (2.5.1). Note that the integrand contains not only functions but also derivatives with respect to the global coordinates  $(x, y)$ . Therefore, we must relate  $(\frac{\partial L_i^e}{\partial x}, \frac{\partial L_i^e}{\partial y})$  to  $(\frac{\partial L_i^e}{\partial \xi}, \frac{\partial L_i^e}{\partial \eta})$  using the transformation (2.5.1).

The functions  $L_i^e(x, y)$  can be expressed in terms of the local coordinates  $(\xi, \eta)$  by means of the transformation (2.5.1). Hence, by the chain rule of partial differentiation, we have

$$\frac{\partial L_i^e}{\partial \xi} = \frac{\partial L_i^e}{\partial x} \frac{\partial x}{\partial \xi} + \frac{\partial L_i^e}{\partial y} \frac{\partial y}{\partial \xi}; \quad \frac{\partial L_i^e}{\partial \eta} = \frac{\partial L_i^e}{\partial x} \frac{\partial x}{\partial \eta} + \frac{\partial L_i^e}{\partial y} \frac{\partial y}{\partial \eta}$$

or, in matrix notation,

$$\begin{Bmatrix} \frac{\partial L_i^e}{\partial \xi} \\ \frac{\partial L_i^e}{\partial \eta} \end{Bmatrix} = \begin{bmatrix} \frac{\partial x}{\partial \xi} & \frac{\partial y}{\partial \xi} \\ \frac{\partial x}{\partial \eta} & \frac{\partial y}{\partial \eta} \end{bmatrix} \begin{Bmatrix} \frac{\partial L_i^e}{\partial x} \\ \frac{\partial L_i^e}{\partial y} \end{Bmatrix} \quad (2.5.4)$$

which gives the relation between the derivatives of  $L_i^e$  with respect to the global and local coordinates. The matrix in Eq. (2.5.4) is called the *Jacobian matrix* of the transformation (2.5.1):

$$[J^e] = \begin{bmatrix} \frac{\partial x}{\partial \xi} & \frac{\partial y}{\partial \xi} \\ \frac{\partial x}{\partial \eta} & \frac{\partial y}{\partial \eta} \end{bmatrix} \quad (2.5.5)$$

Note from the expression given for  $K_{ij}^e$  in Eq. (2.5.3) that we must relate  $(\frac{\partial L_i^e}{\partial x}, \frac{\partial L_i^e}{\partial y})$  to  $(\frac{\partial L_i^e}{\partial \xi}, \frac{\partial L_i^e}{\partial \eta})$ , whereas Eq. (2.5.4) provides the inverse relations. Therefore, Eq. (2.5.4) must be inverted. We have

$$\begin{Bmatrix} \frac{\partial L_i^e}{\partial x} \\ \frac{\partial L_i^e}{\partial y} \end{Bmatrix} = [J^e]^{-1} \begin{Bmatrix} \frac{\partial L_i^e}{\partial \xi} \\ \frac{\partial L_i^e}{\partial \eta} \end{Bmatrix} \quad (2.5.6)$$

This requires that the Jacobian matrix  $[J^e]$  be non-singular.

Using the transformation (2.5.1), we can write

$$\frac{\partial x}{\partial \xi} = \sum_{j=1}^m x_j \frac{\partial \phi_j^e}{\partial \xi}, \quad \frac{\partial y}{\partial \xi} = \sum_{j=1}^m y_j \frac{\partial \phi_j^e}{\partial \xi} \quad (2.5.7a)$$

$$\frac{\partial x}{\partial \eta} = \sum_{j=1}^m x_j \frac{\partial \phi_j^e}{\partial \eta}, \quad \frac{\partial y}{\partial \eta} = \sum_{j=1}^m y_j \frac{\partial \phi_j^e}{\partial \eta} \quad (2.5.7b)$$

and by means of Eq. (2.5.5) one can compute the Jacobian matrix and then its inverse. Thus, given the global coordinates  $(x_j, y_j)$  of element nodes and

the interpolation functions  $\phi_j^e$  used for geometry, the Jacobian matrix can be evaluated using Eq. (2.5.5). A necessary and sufficient condition for  $[J]^{-1}$  to exist is that the determinant  $J$ , called the Jacobian, be non-zero at every point  $(\xi, \eta)$  in  $\hat{\Omega}$ :

$$J_e \equiv \det[J^e] = \frac{\partial x}{\partial \xi} \frac{\partial y}{\partial \eta} - \frac{\partial x}{\partial \eta} \frac{\partial y}{\partial \xi} \neq 0. \quad (2.5.8)$$

From Eq. (2.5.8) it is clear that the functions  $\xi(x, y)$  and  $\eta(x, y)$  must be continuous, differentiable, and invertible. Moreover, the transformation should be algebraically simple so that the Jacobian matrix can be easily evaluated. Transformations of the form in Eq. (2.5.1) satisfy these requirements and the requirement that no spurious gaps between elements or overlapping of elements occur.

Returning to numerical evaluation of integrals, we have from Eq. (2.5.6),

$$\begin{Bmatrix} \frac{\partial L_i^e}{\partial x} \\ \frac{\partial L_i^e}{\partial y} \end{Bmatrix} = [J]^{-1} \begin{Bmatrix} \frac{\partial L_i^e}{\partial \xi} \\ \frac{\partial L_i^e}{\partial \eta} \end{Bmatrix} \equiv [J^*] \begin{Bmatrix} \frac{\partial L_i^e}{\partial \xi} \\ \frac{\partial L_i^e}{\partial \eta} \end{Bmatrix} \quad (2.5.9)$$

where  $J_{ij}^*$  is the element in position  $(i, j)$  of the inverse of the Jacobian matrix  $[J^e]$ . The element area  $dA = dx dy$  in element  $\Omega^e$  is transformed to

$$dA = |[J^e]| d\xi d\eta \quad (2.5.10)$$

in the master element  $\hat{\Omega}$ .

Equations (2.5.7)-(2.5.10) provide the necessary relations to transform integral expressions on any element  $\Omega^e$  to an associated master element  $\hat{\Omega}$ . For instance, consider the integral expression in Eq. (2.5.3), where  $a_{xx}$  and  $a_{yy}$  are functions of  $x$  and  $y$ . Suppose that the finite element  $\Omega^e$  can be generated by the master element  $\hat{\Omega}^e$ . Under the transformation (2.5.1) we can write

$$\begin{aligned} K_{ij}^e &= \int_{\Omega^e} \left[ a_{xx}(x, y) \frac{\partial L_i^e}{\partial x} \frac{\partial L_j^e}{\partial x} + a_{yy}(x, y) \frac{\partial L_i^e}{\partial y} \frac{\partial L_j^e}{\partial y} \right] dx dy \\ &= \int_{\hat{\Omega}^e} F_{ij}(\xi, \eta) d\xi d\eta \end{aligned} \quad (2.5.11)$$

The discussion presented above is valid for master elements of both rectangular and triangular geometry.

### 2.5.3 Integration Over a Master Rectangular Element

Integrals defined over a rectangular master element  $\hat{\Omega}_R$  can be numerically evaluated using the Gauss-Legendre quadrature formulas

$$\int_{\hat{\Omega}_R} F(\xi, \eta) d\xi d\eta = \int_{-1}^1 \int_{-1}^1 F(\xi, \eta) d\xi d\eta \approx \sum_{I=1}^M \sum_{J=1}^N F(\xi_I, \eta_J) W_I W_J \quad (2.5.12)$$

where  $M$  and  $N$  denote the number of Gauss quadrature points,  $(\xi_I, \eta_J)$  denote the Gauss point coordinates, and  $W_I$  and  $W_J$  denote the corresponding Gauss weights as shown in Table 2.5.1 (from Table 7.2 in Reddy [1]).

**Table 2.5.1** Gauss quadrature points and weights for rectangular elements.

$$\int_{-1}^1 F(\xi) d\xi = \sum_{I=1}^N F(\xi_I) W_I$$

$N$	Points, $\xi_I$	Weights, $W_I$
1	0.0000000000	2.0000000000
2	$\pm 0.5773502692$	1.0000000000
3	0.0000000000 $\pm 0.7745966692$	0.8888888889 0.5555555555
4	$\pm 0.3399810435$ $\pm 0.8611363116$	0.6521451548 0.3478548451
5	0.0000000000 $\pm 0.5384693101$ $\pm 0.9061798459$	0.5688888889 0.4786286705 0.2369268850
6	$\pm 0.2386191861$ $\pm 0.6612093865$ $\pm 0.9324695142$	0.4679139346 0.3607615730 0.1713244924

The selection of the number of Gauss points is based on the formula  $N = \text{int}[(p+1)/2] + 1$ , where  $p$  is the polynomial degree to which the integrand is approximated. In most cases, the interpolation functions are of the same degree in both  $\xi$  and  $\eta$ , and therefore one has  $M = N$ . When the integrand is of a different degree in  $\xi$  and  $\eta$ , we use  $\max(M, N)$ . The minimum allowable quadrature rule is one that yields the area or volume of the element exactly. The maximum degree of the polynomial refers to the degree of the highest polynomial in  $\xi$  or  $\eta$  that is present in the integrands of the element matrices of the type in Eq. (2.5.3). Note that the polynomial degree of coefficients as well as  $J_{ij}^e$  should be accounted for in determining the total polynomial degree of the integrand. Of course, the coefficients  $a_{xx}$ ,  $a_{yy}$ , and  $J_{ij}^e$ , in general, may not be polynomials. In those cases, their functional variations must be approximated by a suitable polynomial (e.g. by a binomial series) in order to determine the polynomial degree of the integrand.

#### 2.5.4 Integration Over a Master Triangular Element

In the preceding section, we discussed numerical integration on quadrilateral elements which can be used to represent very general geometries as well as field variables in a variety of problems. Here we discuss numerical integration



on triangular elements. Since quadrilateral elements can be geometrically distorted, it is possible to distort a quadrilateral element to obtain a required triangular element by moving the position of the corner nodes, and the fourth corner in the quadrilateral is merged with one of the neighboring nodes. In actual computation, this is achieved by assigning the same global node number to two corner nodes of the quadrilateral element. Thus, master triangular elements can be obtained in a natural way from associated master rectangular elements. Here we discuss the transformations from a master triangular element to an arbitrary triangular element.

We choose the unit right isosceles triangle (see Table 2.5.2) as the master element. An arbitrary triangular element  $\Omega^e$  can be generated from the master triangular element  $\hat{\Omega}_T$  by transformation of the form (2.6.1). The derivatives of  $L_i^e$  with respect to the global coordinates can be computed from Eq. (2.5.6), which take the form

$$\begin{Bmatrix} \frac{\partial L_i^e}{\partial x} \\ \frac{\partial L_i^e}{\partial y} \end{Bmatrix} = [J^e]^{-1} \begin{Bmatrix} \frac{\partial L_i^e}{\partial \hat{L}_1} \\ \frac{\partial L_i^e}{\partial \hat{L}_2} \end{Bmatrix}, \quad [J^e] = \begin{bmatrix} \frac{\partial x}{\partial \hat{L}_1} & \frac{\partial y}{\partial \hat{L}_1} \\ \frac{\partial x}{\partial \hat{L}_2} & \frac{\partial y}{\partial \hat{L}_2} \end{bmatrix} \quad (2.5.13)$$

Note that only  $\hat{L}_1$  and  $\hat{L}_2$  are treated as linearly independent coordinates because  $\hat{L}_3 = 1 - \hat{L}_1 - \hat{L}_2$ .

After transformation, integrals on  $\hat{\Omega}_T$  have the form

$$\int_{\Omega^e} G(\xi, \eta) d\xi d\eta = \int_{\Omega^e} G(\hat{L}_1, \hat{L}_2, \hat{L}_3) d\hat{L}_1 d\hat{L}_2 \quad (2.5.14)$$

which can be approximated by the quadrature formula

$$\int_{\Omega^e} G(\hat{L}_1, \hat{L}_2, \hat{L}_3) d\hat{L}_1 d\hat{L}_2 \approx \sum_{I=1}^N G(\mathbf{S}_I) W_I \quad (2.5.15)$$

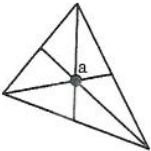
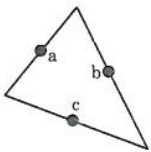
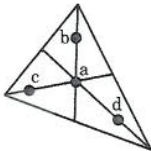
where  $W_I$  and  $\mathbf{S}_I$  denote the weights and integration points of the quadrature rule. Table 2.5.2 contains the location of integration points and weights for one-, three-, and four-point quadrature rules over triangular elements.

## 2.6 Computer Implementation

### 2.6.1 General Comments

In this section, computer implementation of finite element calculations is presented to illustrate the ease with which theoretical ideas can be transformed into practice. The material presented here is based on a more detailed account presented by Reddy [1] and Reddy and Gartling [4]. We begin with some general comments on a typical finite element program.

Table 2.5.2 Quadrature weights and points for triangular elements.

Number of integration points	Degree of polynomial Order of the residual	Location of integration points					
		$\hat{L}_1$	$\hat{L}_2$	$\hat{L}_3$	$W$	Geometric locations	
1	1 $O(h^2)$	1/3	1/3	1/3	1	a	
3	2 $O(h^3)$	1/2	0	1/2	1/3	a	
		1/2	1/2	0		b	
		0	1/2	1/2		c	
4	3 $O(h^4)$	1/3	1/3	1/3	-27/48	a	
		0.6	0.2	0.2	25/48	b	
		0.2	0.6	0.2	25/48	c	
		0.2	0.2	0.6	25/48	d	

A typical computer program consists of three basic parts:

1. Preprocessor
2. Processor
3. Postprocessor

In the preprocessor part of a program, the input data of the problem are read in and/or generated. This includes the geometry of the domain, analysis option (e.g. static, eigenvalue, or transient analysis), the data of the problem (e.g. definition of the coefficients appearing in the differential equation), boundary conditions, finite element analysis information (e.g. element type, number of elements, geometric information required to generate the finite element mesh and element connectivity), and indicators for various postprocessing options (e.g. print, no print, types of quantities to be calculated, and so on). In the postprocessor part of the program, the solution is computed by interpolation at points other than the nodes, secondary variables that are derivable from the solution are also computed, and the output data are

processed in a desired format for printout and/or plotting. The preprocessor and postprocessor computer modules may contain a few Fortran statements to read and print pertinent information, simple subroutines (e.g. subroutines to generate mesh and compute the gradient of the solution), or complex programs linked to other units via disk and tape files.

The processor module, where typically large amounts of computing time are spent, may consist of several subroutines, each having a special purpose. The main modules include:

1. Generation of the element matrices using numerical integration.
2. Assembly of element equations.
3. Imposition of the boundary conditions.
4. Solution of the algebraic equations for the nodal values of the primary variables (see Appendix 1).

The degree of sophistication and the complexity of a finite element program depend on the general class of problems being programmed, the generality of the data in the equation, and the intended user of the program. Figure 2.6.1 contains the flow chart of a typical finite element computer program. A typical but simple finite element programs are included in the book by Reddy [1] and interested reader may wish to study Chapters 7 and 13 of [1], where details of the implementation of one- and two-dimensional problems of heat transfer, fluid mechanics, and solid mechanics are discussed.

### 2.6.2 One-Dimensional Problems

Here we discuss the main ideas behind the calculation of element coefficient matrices,  $[K^e]$ ,  $[M^e]$ , and  $\{f^e\}$  for the model problem discussed in Sections 2.2 and 2.3 (see Chapter 8 for transient problems). Recall that the coefficient matrices are of the form

$$\begin{aligned} K_{ij}^e &= \int_{x_a}^{x_b} \left[ a(x) \frac{dL_i^e}{dx} \frac{dL_j^e}{dx} + c(x) L_i^e L_j^e \right] dx \\ M_{ij}^e &= \int_{x_a}^{x_b} c_t(x) L_i^e L_j^e dx, \quad f_i^e = \int_{x_a}^{x_b} f(x) L_i^e(x) dx \end{aligned} \quad (2.6.1)$$

We use the coordinate transformation of the form [see Eq. (2.5.1)]

$$x = \sum_{j=1}^M x_j^e \phi_j^e(\xi) \quad (2.6.2)$$

to express the integrals posed over a typical element  $\Omega^e = (x_a, x_b)$  as those over the interval,  $-1 \leq \xi \leq 1$ , so that we can use the Gauss quadrature to

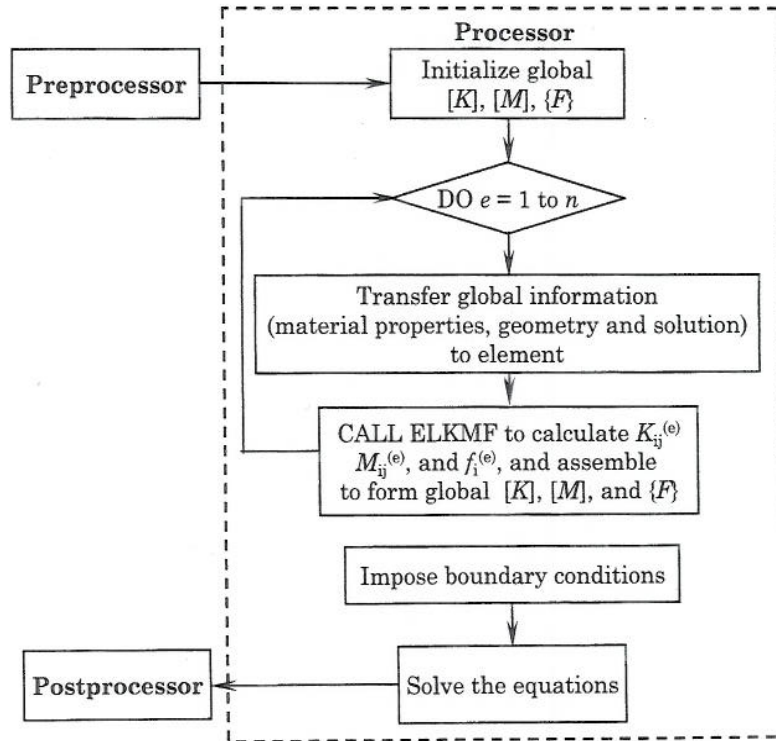


Figure 2.6.1 The flow chart of a typical finite element program.

evaluate them numerically. In Eq. (2.6.2),  $x_j^e$  denote the global coordinates of node  $j$  of element  $\omega^e = (x_a, x_b)$ , and  $\phi_j^e$  are the approximation functions used to approximate the geometry. For example, if we use linear interpolation functions  $\phi_j^e(\xi) = L_j^e(\xi)$  to represent the geometry of the element, we have  $x_1^e = x_a$ ,  $x_2^e = x_b$  and Eq. (2.6.2) becomes

$$x = x_a L_1^e(\xi) + x_b L_2^e(\xi) = \frac{x_a + x_b}{2} + \frac{x_b - x_a}{2} \xi = x_a + \frac{h_e}{2} \xi \quad (2.6.3)$$

The Jacobian of transformation is given by

$$J_e \equiv \frac{dx}{d\xi} = \frac{h_e}{2} \quad (2.6.4)$$

The above transformation is exact for all (straight) line elements.

The derivatives of  $L_i^e(x)$  with respect to the global coordinate  $x$  is given by

$$\frac{dL_i^e}{dx} = \frac{dL_i^e}{d\xi} \frac{d\xi}{dx} = \frac{dL_i^e}{d\xi} J_e^{-1}$$

Then the integrals in Eq. (2.6.1) become

$$\begin{aligned}
 K_{ij}^e &= \int_{x_a}^{x_b} \left[ a(x) \frac{dL_i^e}{dx} \frac{dL_j^e}{dx} + c(x) L_i^e L_j^e \right] dx \\
 &= \int_{-1}^1 \left[ \hat{a}(\xi) \left( \frac{dL_i^e}{d\xi} J_e^{-1} \right) \left( \frac{dL_j^e}{d\xi} J_e^{-1} \right) + \hat{c}(\xi) L_i^e L_j^e \right] J_e d\xi \\
 M_{ij}^e &= \int_{x_a}^{x_b} c_t(x) L_i^e L_j^e dx = \int_{-1}^1 (\hat{c}_t(\xi) L_i^e L_j^e) J_e d\xi \\
 f_i^e &= \int_{x_a}^{x_b} f(x) L_i^e(x) dx = \int_{-1}^1 \hat{f}(\xi) L_i^e L_j^e J_e d\xi
 \end{aligned} \tag{2.6.5}$$

where  $\hat{a}(\xi) = a(x(\xi))$  and so on. Each of the integral expressions above can be evaluated using the Gauss quadrature

$$\int_{-1}^1 F(\xi) J_e d\xi = \sum_{NI=1}^{NGP} F(\xi_{NI}) J_e W_{NI} \tag{2.6.6}$$

where  $NGP$  is the number of Gauss points,  $\xi_{NI}$  is the  $NI$ th Gauss point, and  $W_{NI}$  is the  $NI$ th Gauss weight.

To implement the above development into a computer subroutine for arbitrary degree of  $L_i^e$ , we must first create a subroutine of all interpolations functions and their derivatives with respect to  $\xi$  that we intend to use in our analysis. For the present discussion, we limit them to the linear and quadratic Lagrange family of functions. These functions and their derivatives are given below.

*Linear*

$$L_1(\xi) = \frac{1}{2}(1 - \xi), \quad \frac{dL_1}{d\xi} = -0.5; \quad L_2(\xi) = \frac{1}{2}(1 + \xi), \quad \frac{dL_2}{d\xi} = 0.5 \tag{2.6.7}$$

*Quadratic*

$$\begin{aligned}
 L_1(\xi) &= -\frac{1}{2}\xi(1 - \xi), & \frac{dL_1}{d\xi} &= 0.5(2\xi - 1) \\
 L_2(\xi) &= (1 - \xi^2), & \frac{dL_2}{d\xi} &= -2\xi \\
 L_3(\xi) &= \frac{1}{2}\xi(1 + \xi), & \frac{dL_3}{d\xi} &= 0.5(1 + 2\xi)
 \end{aligned} \tag{2.6.8}$$

The following variables names are used in the subroutine (see INTRPL1D in Box 2.6.1):

$$\text{SFL}(i) = L_i, \quad \text{DSFL}(i) = \frac{dL_i}{d\xi}, \quad \text{GDSFL}(i) = \frac{dL_i}{dx}$$

## Box 2.6.1 Listing of subroutine INTRPL1D.

```

SUBROUTINE INTRPL1D(ELX,GJ,IEL,NPE,XI)
C
C
C The subroutine computes shape functions and their derivatives for
C Hermite cubic and Lagrange linear, quadratic, and cubic elements
C
C X..... Global (i.e. problem) coordinate
C XI ..... Local (i.e. element) coordinate
C H..... Element length
C {SFL}..... Interpolation (or shape) functions
C {DSFL}..... First derivative of SF with respect to XI
C {GDSFL}.. First derivative of SF with respect to X
C GJ..... Jacobian of the transformation
C
C
C
C IMPLICIT REAL*8(A-H,O-Z)
COMMON /SHP/SFL(4),GDSFL(4)
DIMENSION DSFL(4),ELX(3)
C
C SHAPE FUNCTIONS AND THEIR DERIVATIVES
C
C Linear functions
C
IF(IEL.EQ.1)THEN
  SFL(1)=0.5*(1.0-XI)
  SFL(2)=0.5*(1+XI)
  DSFL(1)=-0.5
  DSFL(2)=0.5
ENDIF
C
C Quadratic functions
C
IF(IEL.EQ.2)THEN
  SFL(1)=0.5*(XI-1.0)*XI
  SFL(2)=1.0-XI*XI
  SFL(3)=0.5*(XI+1.0)*XI
  DSFL(1)=XI-0.5
  DSFL(2)=-2.0*XI
  DSFL(3)=XI+0.5
ENDIF
GJ=0.0
DO 10 I=1,NPE
10  GJ=GJ+DSFL(I)*ELX(I)
   DO 30 I=1,NPE
     GDSFL(I)=DSFL(I)/GJ
30  CONTINUE
C
RETURN
END

```

The notation should be transparent to the reader: *SFL* = Shape Functions of the Lagrange family; *DSFL* = Derivative of *SFL* with respect to  $\xi$ ; and *GDSFL* = Global Derivative (i.e. derivative with respect to  $x$ ) of *SFL*. All of them are  $n \times 1$  arrays, where  $n$  is the Nodes Per Element, NPE (i.e.  $n = \text{NPE}$ ). In addition, *GJ* is used for the Jacobian  $J$  and *XI* for  $\xi$ .

Next, we implement the steps to evaluate the matrix coefficients  $K_{ij}$ ,  $M_{ij}$ , and  $f_i$  ( $i = 1$  to  $NPE$ ) into a subroutine called `ELEKMF1D`. To this end, we must assume some form of the data,  $a(x)$ ,  $c(x)$ ,  $c_t(x)$  and  $f(x)$ . Although we can use any integrable functions, we restrict in the present discussion our choice of these coefficients to linear polynomials for the entire domain of the problem:

$$a(x) = a_0 + a_1x, \quad c(x) = c_0 + c_1x, \quad c_t(x) = c_{t0} + c_{t1}x, \quad f(x) = f_0 + f_1x \quad (2.6.9)$$

Obviously, the coefficients of the polynomials must be read in the preprocessor and transferred to the subroutine `ELEKMF1D` through a common block (or the argument list).

Since the evaluation of the matrix coefficients involves summation on the number of Gauss points, the arrays used for  $[K]$ ,  $[M]$ , and  $\{f\}$  must be initialized outside the do-loop on  $NGP$ , the Number of Gauss Points. The following notation is used:

$$ELK(i,j) = K_{ij}^e, \quad ELM(i,j) = M_{ij}^e, \quad ELF(i) = f_i^e, \quad i = 1, 2, \dots, NPE \quad (2.6.11)$$

The Gauss points are arranged in a matrix form so that the  $J$ th column corresponds to the  $J$ th order Gauss rule. The same notation is used for the Gauss weights:  $GAUSPT(NI, NJ) = \xi_{NI}$ ,  $NI$ th Gauss point of the  $NJ$ -point Gauss rule;  $GAUSWT(NI, NJ) = W_{NI}$ ,  $NI$ th Gauss weight of the  $NJ$  weight Gauss rule. Inside the do-loop on  $NI = 1$  to  $NGP$ , we must call Subroutine `INTRPL1D` to compute  $SFL(i)$  and  $GDSFL(i)$  at the  $NI$ th Gauss point and then compute all necessary quantities. Box 2.6.2 contains a listing of Subroutine `ELEKMF1D`.

### 2.6.3 Two-Dimensional Problems

The ideas presented in Section 2.6.2 for one-dimensional problems extend in a straightforward way to two-dimensional problems. The main differences are: (a) numerical integration over two-dimensional elements; (b) the Jacobian  $J_e$  is the determinant of the Jacobian matrix  $[J^e]$  defined in Eq. (2.5.5); and (c) global derivatives of the interpolation functions are determined using Eq. (2.5.9).

The Fortran statements of generating element coefficient matrices  $[K^e]$ ,  $[M^e]$ , and  $\{Q^e\}$  are provided in the form of subroutine `ELEKMF2D` in Box 2.6.3, along with the subroutine `INTRPL2D` for interpolation functions of rectangular elements and subroutine `TEMPORAL` for generating the coefficient matrices  $[\hat{K}^e]$  and  $\{\hat{F}^e\}$  defined in Eq. (8.2.10) for transient problems.

## Box 2.6.2 Listing of subroutine ELEKMF1D.

```

SUBROUTINE ELEKMF1D(MODEL,NDF,NGP,NPE)
C
C
C IEL..... Element TYPE (1, Linear; 2, Quadratic)
C H..... Element length
C X..... Global (i.e. problem) coordinate
C XI ..... Local (i.e. element) coordinate
C [GAUSPT].. 4x4 matrix of Gauss points: Nth column corresponds
C            to the N-point Gauss rule
C [GAUSWT].. 4x4 matrix of Gauss weights (see the comment above)
C [ELK]..... Element coefficient matrix [K]
C {ELF}..... Element source vector {f}
C {ELX}..... Vector of the global coordinates of element nodes
C
IMPLICIT REAL*8(A-H,O-Z)
COMMON/STF1/ELK(9,9),ELF(9),ELX(4)
COMMON/STF2/AX0,AX1,CX0,CX1,FX0,FX1
COMMON/SHP/SF(4),GDSF(4)
DIMENSION GAUSPT(5,5),GAUSWT(5,5)
C
  DATA GAUSPT/5*0.0D0,-0.57735027D0,0.57735027D0,3*0.0D0,-0.77459667D0,
* 0.0D0,0.77459667D0,2*0.0D0,-0.86113631D0,-0.33998104D0,0.33998104D0,
* 0.86113631D0,0.0D0,-0.906180D0,-0.538469D0,0.0D0,0.538469D0,0.906180D0/
  DATA GAUSWT/2.0D0,4*0.0D0,2*1.0D0,3*0.0D0,0.5555555D0,0.88888888D0,
* 0.5555555D0,2*0.0D0,0.34785485D0,2*0.65214515D0,0.34785485D0,0.0D0,
* 0.236927D0,0.478629D0,0.568889D0,0.478629D0,0.236927D0/
C
  H = ELX(NPE) - ELX(1)
  IEL = NPE-1
C Initialize the arrays   DO 10 J=1,NPE
  ELF(J) = 0.0
  DO 10 I=1,NPE
10   ELK(I,J)=0.0
C DO-LOOP on number of Gauss points begins here
  DO 40 NI=1,NGP
  XI=GAUSS(NI,NGP)
  CALL INTRPL1D(ELX,GJ,IEL,NPE,XI)
  CNST=GJ*WT(NI,NGP)
  X=ELX(1)+0.5*(1.0+XI)*H
  AX=AX0+AX1*X
  CX=CX0+CX1*X
  FX=FX0+FX1*X
C Calculate element coefficients
  DO 20 I=1,NPE
  ELF(I)=ELF(I)+FX*SFL(I)*CNST
  DO 20 J=1,NPE
  S00=SFL(I)*SFL(J)*CNST
  S11=GDSFL(I)*GDSFL(J)*CNST
  ELK(I,J)=ELK(I,J)+AX*S11+CX*S00
20  CONTINUE
40  CONTINUE
  RETURN
  END

```

## 2.7 Closure

The present chapter was devoted to a study of (1) the finite element models of one- and two-dimensional problems involving Poisson's equation, (2) a derivation of interpolation functions for basic one- and two-dimensional elements, (3) numerical evaluation of integrals, and (4) computer implementation ideas. An understanding of the topics presented in this chapter is a prerequisite for the subsequent chapters of this book.





```

IF(ITEM.NE.0) THEN
C
C Compute the coefficient matrices of the final algebraic equations
C (i.e. after time approximation) in the transient analysis: _____
C
      CALL TEMPORAL(NN)
      ENDIF
      RETURN
      END

SUBROUTINE INTRPL2D(NPE,XI,ETA,DET,ELXY,NDF)
C
C The subroutine evaluates the interpolation functions (SF(I)) and
C their derivatives with respect to global coordinates (GDSF(I,J))
C for Lagrange linear & quadratic rectangular elements, using the
C isoparametric formulation. The subroutine also evaluates Hermite
C interpolation functions and their global derivatives using the
C subparametric formulation.
C
C SF(I).....Interpolation function for node I of the element
C DSF(J,I).....Derivative of SF(I) with respect to XI if J=1 and
C              and ETA if J=2
C GDSF(J,I).....Derivative of SF(I) with respect to X if J=1 and
C              and Y if J=2
C XNODE(I,J)...J-TH (J=1,2) Coordinate of node I of the element
C NP(I).....Array of element nodes (used to define SF and DSF)
C GJ(I,J).....Jacobian matrix
C GJINV(I,J)....Inverse of the jacobian matrix
C
C IMPLICIT REAL*8 (A-H,O-Z)
C DIMENSION ELXY(9,2),XNODE(9,2),NP(9),DSF(2,9),GJ(2,2),GJINV(2,2)
C COMMON/SHP/SF(9),GDSF(2,9)
C COMMON/IO/IN,ITT
C DATA XNODE/-1.0D0, 2*1.0D0, -1.0D0, 0.0D0, 1.0D0, 0.0D0, -1.0D0,
C *          0.0D0, 2*-1.0D0, 2*1.0D0, -1.0D0, 0.0D0, 1.0D0, 2*0.0D0/
C DATA NP/1,2,3,4,5,7,6,8,9/
C
C FNC(A,B) = A*B
C IF(NPE.EQ.4) THEN
C
C LINEAR Lagrange interpolation functions for FOUR-NODE element
C
      DO 10 I = 1, NPE
      XP = XNODE(I,1)
      YP = XNODE(I,2)
      XI0 = 1.0+XI*XP
      ETA0 = 1.0+ETA*YP
      SF(I) = 0.25*FNC(XI0,ETA0)
      DSF(1,I) = 0.25*FNC(XP,ETA0)
10    DSF(2,I) = 0.25*FNC(YP,XI0)
      ELSE
      IF(NPE.EQ.8) THEN
C
C QUADRATIC Lagrange interpolation functions for EIGHT-NODE element
C
      DO 20 I = 1, NPE
      NI = NP(I)
      XP = XNODE(NI,1)
      YP = XNODE(NI,2)
      XI0 = 1.0+XI*XP
      ETA0 = 1.0+ETA*YP
      XI1 = 1.0-XI*XI
      ETA1 = 1.0-ETA*ETA
      IF(I.LE.4) THEN
      SF(NI) = 0.25*FNC(XI0,ETA0)*(XI*XP+ETA*YP-1.0)
      DSF(1,NI) = 0.25*FNC(ETA0,XP)*(2.0*XI*XP+ETA*YP)
      DSF(2,NI) = 0.25*FNC(XI0,YP)*(2.0*ETA*YP+XI*XP)
      ELSE
      IF(I.LE.6) THEN
      SF(NI) = 0.5*FNC(XI1,ETA0)
      DSF(1,NI) = -FNC(XI,ETA0)
      DSF(2,NI) = 0.5*FNC(YP,XI1)
      ELSE
      SF(NI) = 0.5*FNC(ETA1,XI0)
      DSF(1,NI) = 0.5*FNC(XP,ETA1)
      DSF(2,NI) = -FNC(ETA,XI0)
      ENDIF
      ENDIF
20    CONTINUE
      ELSE

```

```

C
C QUADRATIC Lagrange interpolation functions for NINE-NODE element
C
DO 30 I=1,NPE
NI = NP(I)
XP = XNODE(NI,1)
YP = XNODE(NI,2)
XI0 = 1.0+XI*XP
ETA0 = 1.0+ETA*YP
XI1 = 1.0-XI*XI
ETA1 = 1.0-ETA*ETA
XI2 = XP*XI
ETA2 = YP*ETA
IF(I.LE.4) THEN
SF(NI) = 0.25*FNC(XI0,ETA0)*XI2*ETA2
DSF(1,NI) = 0.25*XP*FNC(ETA2,ETA0)*(1.0+2.0*XI2)
DSF(2,NI) = 0.25*YP*FNC(XI2,XI0)*(1.0+2.0*ETA2)
ELSE
IF(I.LE.6) THEN
SF(NI) = 0.5*FNC(XI1,ETA0)*ETA2
DSF(1,NI) = -XI*FNC(ETA2,ETA0)
DSF(2,NI) = 0.5*FNC(XI1,YP)*(1.0+2.0*ETA2)
ELSE
IF(I.LE.8) THEN
SF(NI) = 0.5*FNC(ETA1,XI0)*XI2
DSF(2,NI) = -ETA*FNC(XI2,XI0)
DSF(1,NI) = 0.5*FNC(ETA1,XP)*(1.0+2.0*XI2)
ELSE
SF(NI) = FNC(XI1,ETA1)
DSF(1,NI) = -2.0*XI*ETA1
DSF(2,NI) = -2.0*ETA*XI1
ENDIF
ENDIF
ENDIF
30 CONTINUE
ENDIF
C
C Compute the Jacobian matrix [GJ] and its inverse [GJINV], and [GDSF]
C
DO 40 I = 1,2
DO 40 J = 1,2
GJ(I,J) = 0.0
DO 40 K = 1,NPE
40 GJ(I,J) = GJ(I,J) + DSF(I,K)*ELXY(K,J)
C
DET = GJ(1,1)*GJ(2,2)-GJ(1,2)*GJ(2,1)
GJINV(1,1) = GJ(2,2)/DET
GJINV(2,2) = GJ(1,1)/DET
GJINV(1,2) = -GJ(1,2)/DET
GJINV(2,1) = -GJ(2,1)/DET
DO 50 I = 1,2
DO 50 J = 1,NPE
GDSF(I,J) = 0.0
DO 50 K = 1,2
50 GDSF(I,J) = GDSF(I,J) + GJINV(I,K)*DSF(K,J)
RETURN
END
SUBROUTINE TEMPORAL(NN)
C
C The subroutine computes the algebraic equations associated with the parabolic differential equations
C by using the  $\alpha$ -family of approximations. A constant source is assumed.
C
C
C IMPLICIT REAL*8(A-H,O-Z)
COMMON/STF/ELF(18),ELK(18,18),ELM(18,18),ELXY(9,2),ELU(18),A1,A2
C
C The  $\alpha$ -family of time approximation for parabolic equations
C
DO 20 I=1,NN
SUM=0.0
DO 10 J=1,NN
SUM=SUM+(ELM(I,J)-A2*ELK(I,J))*ELU(J)
10 ELK(I,J)=ELM(I,J)+A1*ELK(I,J)
20 ELF(I)=(A1+A2)*ELF(I)+SUM
RETURN
END

```

## Problems

- 2.1 (*Least-Squares Method*). In the least-squares method, the residual  $R^e$  [see Eq. (2.2.3)] is minimized in the following sense:

$$\delta \int_{x_a}^{x_b} [R^e]^2 dx = 0 \quad \text{or} \quad \frac{\partial}{\partial c_i} \int_{x_a}^{x_b} [R^e(x, c_1, c_2, \dots, c_n)]^2 dx = 0, \quad i = 1, 2, \dots, n$$

- (a) Identify the weight function  $w_i^e$  if the least-squares method is to be deduced from Eq. (2.2.4), (b) develop the least-squares finite element model, and (c) discuss the type of finite element approximation of  $u$  that may be used.
- 2.2 Consider the differential equation

$$-\frac{d}{dx} \left( a \frac{du}{dx} \right) + \frac{d^2}{dx^2} \left( b \frac{d^2 u}{dx^2} \right) + cu = f$$

- where  $a$ ,  $b$ ,  $c$ , and  $f$  are known functions of position  $x$ . (a) Develop the weak form over a typical element  $\Omega^e = (x_a, x_b)$  such that the bilinear form is symmetric, (b) identify the bilinear and linear forms and construct the quadratic functional, (c) develop the finite element model of the equation, and (d) discuss the type of finite element approximation of  $u$  that may be used.
- 2.3 Derive the Lagrange cubic interpolation functions for a four-node (one-dimensional) element (with equally spaced nodes) using the alternative procedure based on interpolation properties (2.2.22). Use the local coordinate  $\bar{x}$  for simplicity.
- 2.4 Derive the finite element model of the differential equation

$$-\frac{d}{dx} \left( a(x) \frac{du}{dx} \right) = f(x) \quad \text{for} \quad 0 < x < L$$

for the boundary conditions

$$u(0) = u_0, \quad \left[ \left( a(x) \frac{du}{dx} \right) + ku \right]_{x=L} = P$$

- 2.5 The following differential equation arises in connection with heat transfer in an insulated rod:

$$-\frac{d}{dx} \left( k \frac{dT}{dx} \right) = q \quad \text{for} \quad 0 < x < L$$

$$T(0) = T_0, \quad \left[ k \frac{dT}{dx} + \beta(T - T_\infty) + \hat{q} \right]_{x=L} = 0$$

where  $T$  is the temperature,  $k$  the thermal conductivity, and  $q$  the heat generation. Take the following values for the data:  $q = 0$ ,  $\hat{q} = 0$ ,  $L = 0.1$  m,  $k = 0.01$  W m<sup>-1</sup> °C<sup>-1</sup>,  $\beta = 25$  W m<sup>-2</sup> °C<sup>-1</sup>,  $T_0 = 50$ °C, and  $T_\infty = 5$ °C. Solve the problem using two linear finite elements for temperature values at  $x = \frac{1}{2}L$  and  $L$ . *Answer:*  $U_2 = 27.59$ °C,  $U_3 = 5.179$ °C,  $Q_1^{(1)} = 4.482$  W m<sup>-2</sup> =  $-Q_2^{(2)}$ .

- 2.6 An insulating wall is constructed of three homogeneous layers with conductivities  $k_1$ ,  $k_2$ , and  $k_3$  in intimate contact (see Figure P2.6). Under steady-state conditions, the temperatures at the boundaries of the layers are characterized by the external surface temperatures  $T_1$  and  $T_4$  and the interface temperatures  $T_2$  and  $T_3$ . Formulate the problem to determine the temperatures  $T_i$  ( $i = 1, \dots, 4$ ) when the ambient temperatures  $T_0$  and  $T_5$  and the (surface) film coefficients  $\beta_0$  and  $\beta_5$  are known.

Assume that there is no internal heat generation and that the heat flow is one-dimensional ( $\partial T / \partial y = 0$ ). Answer:  $U_1 = 84.489^\circ\text{C}$ ,  $U_2 = 68.977^\circ\text{C}$ ,  $U_3 = 50.881^\circ\text{C}$ ,  $U_4 = 45.341^\circ\text{C}$ ,  $(Q_1^1)_{\text{def}} = 217.16 \text{ W}\cdot\text{m}^{-2}$ ,  $(Q_2^3)_{\text{def}} = -155.11 \text{ W}\cdot\text{m}^{-2}$ .

- $k_1 = 90 \text{ W}/(\text{m}\cdot^\circ\text{C})$
- $k_2 = 75 \text{ W}/(\text{m}\cdot^\circ\text{C})$
- $k_3 = 50 \text{ W}/(\text{m}\cdot^\circ\text{C})$
- $h_1 = 0.03 \text{ m}$
- $h_2 = 0.04 \text{ m}$
- $h_3 = 0.05 \text{ m}$
- $\beta = 500 \text{ W}/(\text{m}^2\cdot^\circ\text{C})$
- $T_\infty = 20^\circ\text{C}$

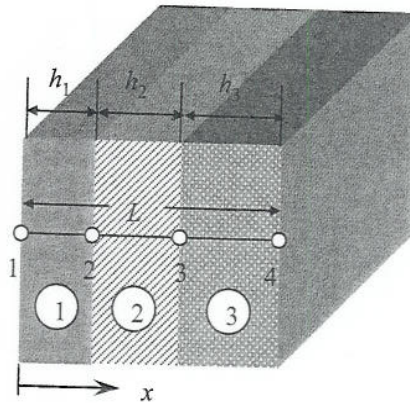


Figure P2.6

- 2.7 Consider the steady laminar flow of a viscous fluid through a long circular cylindrical tube. The governing equation is

$$-\frac{1}{r} \frac{d}{dr} \left( r \mu \frac{dw}{dr} \right) = \frac{P_0 - P_L}{L} \equiv f_0, \quad 0 < r < R_0$$

where  $w$  is the axial (i.e.  $z$ ) component of velocity,  $\mu$  is the viscosity, and  $f_0$  is the gradient of pressure (which includes the combined effect of static pressure and gravitational force). The boundary conditions are

$$\left( r \frac{dw}{dr} \right) \Big|_{r=0} = 0, \quad w(R_0) = 0$$

Using the symmetry and (a) two linear elements, (b) one quadratic element, determine the velocity field and compare with the exact solution at the nodes:

$$w_e(r) = \frac{f_0 R_0^2}{4\mu} \left[ 1 - \left( \frac{r}{R_0} \right)^2 \right]$$

- 2.8. In the problem of the flow of a viscous fluid through a circular cylinder (see Problem 2.7), assume that the fluid slips at the cylinder wall; that is, instead of assuming that  $w = 0$  at  $r = R_0$ , use the boundary condition that

$$kw = -\mu \frac{dw}{dr} \quad \text{at} \quad r = R_0$$

in which  $k$  is the “coefficient of sliding friction.” Solve the problem with two linear elements.

- 2.9 The two members in Figure P2.9 are fastened together and to rigid walls. If the members are stress free before they are loaded, what will be the stresses and deformations in each after the two 50,000 lbs. loads are applied? Use  $E_s = 30 \times 10^6$  psi and  $E_a = 10^7$  psi; the aluminum rod is 2 in. in diameter and the steel rod is 1.5 in. in diameter. Answer:  $U_2 = 0.0134$  in.,  $P_2^{(1)} = -21,052.6$  lb, and  $\sigma^{(1)} = 6701.25$  psi.

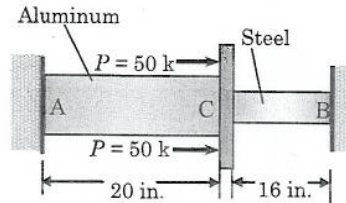


Figure P2.9

- 2.10 Evaluate the coefficients  $K_{ij}^e$  and  $F_i^e$  of Eqs. (2.3.40a,b) for a linear triangular element.  
 2.11 Repeat Problem 2.10 for a linear rectangular element.  
 2.12 Consider the partial differential equation governing heat transfer in an axisymmetric geometry

$$-\frac{1}{r} \frac{\partial}{\partial r} \left( r k_{rr} \frac{\partial T}{\partial r} \right) - \frac{\partial}{\partial z} \left( k_{zz} \frac{\partial T}{\partial z} \right) = f(r, z) \quad (1)$$

where  $(k_{rr}, k_{zz})$  and  $f$  are the conductivities and internal heat generation per unit volume, respectively. In developing the weak form, we integrate over the elemental volume of the axisymmetric geometry:  $r dr d\theta dz$ . Develop the weak form and associated finite element model over an element.

## References

1. Reddy, J. N., *An Introduction to the Finite Element Method*, 2nd edn, McGraw-Hill, New York (1993).
2. Reddy, J. N. and Gartling, D. K., *The Finite Element Method in Heat Transfer and Fluid Dynamics*, 2nd edn, CRC Press, Boca Raton, FL (2001).

## Heat Transfer and Other Field Problems in One Dimension

### 3.1 Model Differential Equation

We shall consider a model nonlinear differential equation governing one-dimensional problems involving a single unknown to illustrate the finite element model development and discuss solution methods to solve the resulting nonlinear algebraic equations. As we shall see, the weak form and finite element model developed in Section 2.2 for a linear model equation are also valid for the nonlinear case. The main difference is that the finite element equations are nonlinear, and therefore iterative methods must be used to solve the nonlinear finite element equations.

Consider the differential equation (see Table 2.2.1 for fields of study)

$$-\frac{d}{dx} \left[ a(x, u) \frac{du}{dx} \right] + b(x, u) \frac{du}{dx} + c(x, u)u = f(x), \quad 0 < x < L \quad (3.1.1)$$

subjected to boundary conditions of the form

$$n_x a \frac{du}{dx} + \beta(x, u)(u - u_\infty) = Q, \quad \text{or} \quad u = \hat{u} \quad (3.1.2)$$

at a boundary point. Here  $u(x)$  denotes the dependent variable to be determined,  $a$ ,  $b$ , and  $c$  are known functions of  $x$  and  $u$  (and possibly derivatives of  $u$ ),  $f$  is a known function of  $x$ ,  $u_\infty$  and  $\hat{u}$  are known parameters,  $Q$  the secondary variable, and  $n_x$  is the cosine of the angle between the positive  $x$ -axis and the outward normal to the edge at the node (note that  $n_x = -1$  at  $x = x_a$  and  $n_x = 1$  at  $x = x_b$ ). The second boundary condition is a special case of the first (with  $\hat{u} = u_\infty$ ) in the limit  $\beta \rightarrow \infty$ . We wish to solve this nonlinear differential equation using the finite element method.

Clearly, the source of nonlinearity is in  $a$ ,  $b$  and/or  $c$ , which in most engineering systems include geometric and material parameters that may be functions of the dependent variable  $u$ . For example, for heat conduction in a rod with convective heat transfer through the surface, one has  $a = kA$ ,  $b = 0$ ,

and  $c = P\beta$ , where  $k$  denotes conductivity,  $\beta$  the convective heat transfer coefficient,  $A$  the cross-sectional area, and  $P$  the perimeter of the rod. Then the nonlinearity arises from the conductivity and heat transfer coefficients being functions of temperature  $u$ .

### 3.2 Weak Formulation

Suppose that the domain  $\Omega = (0, L)$  is divided into  $N$  elements. A typical element is denoted as  $\Omega^e = (x_a, x_b)$ , where  $x_a$  and  $x_b$  denote the global coordinates of the end nodes of the element. The weak form of Eq. (3.1.1) over the element is given by

$$\begin{aligned} 0 &= \int_{x_a}^{x_b} \left[ a \frac{dw}{dx} \frac{du}{dx} + bw \frac{du}{dx} + cwu - wf \right] dx - \left[ w \left( a \frac{du}{dx} \right) \right]_{x_a}^{x_b} \\ &= \int_{x_a}^{x_b} \left[ a(x, u) \frac{dw}{dx} \frac{du}{dx} + b(x, u)w \frac{du}{dx} + c(x, u)wu - wf(x) \right] dx \\ &\quad - [Q_1^e - \beta_a (u(x_a) - u_\infty^a)] w(x_a) - [Q_2^e - \beta_b (u(x_b) - u_\infty^b)] w(x_b) \end{aligned} \quad (3.2.1)$$

where  $w(x)$  is a weight function, and [see Eq. (3.1.2)]

$$\begin{aligned} - \left[ a \frac{du}{dx} \right]_{x=x_a} &= Q_1^e - \beta_a [u(x_a) - u_\infty^a] \\ \left[ a \frac{du}{dx} \right]_{x=x_b} &= Q_2^e - \beta_b [u(x_b) - u_\infty^b] \end{aligned} \quad (3.2.2)$$

Here  $(u_\infty^a, u_\infty^b)$  denote the reference values and  $(\beta_a, \beta_b)$  denote the film coefficients at the left and right ends of the element, respectively. The weak form (3.2.1) suggests that  $u$  is the primary variable and  $Q$  is the secondary variable of the formulation. Recall that specifying a primary variable is called the essential (or geometric) boundary condition and specifying a secondary variable is termed the natural (or force) boundary condition. The first boundary condition in Eq. (3.1.2) is of the natural type and it is nonlinear; the second boundary condition in Eq. (3.1.2) one is of the essential type.

### 3.3 Finite Element Model

Suppose that the dependent unknown  $u(x)$  is approximated over element  $\Omega^e$  by the finite element approximation of the form

$$u(x) \approx u_h^e(x) = \sum_{j=1}^n u_j^e L_j^e(x) \quad (3.3.1)$$

Substituting the approximation (3.3.1) for  $u$  and  $w = L_i^e$  into the weak form (3.2.1), we obtain the finite element model

$$[K^e] \{u^e\} = \{f^e\} + \{Q^e\} \quad (3.3.2)$$



where

$$K_{ij}^e = \int_{x_a}^{x_b} \left[ a(x, u_h) \frac{dL_i^e}{dx} \frac{dL_j^e}{dx} + b(x, u_h) L_i^e \frac{dL_j^e}{dx} + c(x, u_h) L_i L_j \right] dx \\ + \beta_a L_i^e(x_a) L_j^e(x_a) + \beta_b L_i^e(x_b) L_j^e(x_b) \quad (3.3.3a)$$

$$f_i^e = \int_{x_a}^{x_b} f(x) L_i^e dx + \beta_a u_\infty^a L_i^e(x_a) + \beta_b u_\infty^b L_i^e(x_b) \quad (3.3.3b)$$

Note that the coefficient matrix is a nonlinear function of the unknown nodal values  $u_j^e$ , and it is an unsymmetric matrix when  $b \neq 0$ ; when  $b = 0$ ,  $K_{ij}^e$  is a symmetric matrix. Also, the coefficients involving  $\beta$  are only present at the boundary nodes where convection type boundary condition is specified.

### Example 3.3.1

To gain more insight into the make up of the coefficient matrix, suppose that  $a(x) = a_0 u(x)$ ,  $b = c = 0$  and  $\beta = 0$ , where  $a_0$  may be a function of  $x$  only. Then we have

$$K_{ij}^e = \int_{x_a}^{x_b} a_0^e \left( \sum_{k=1}^n u_k^e L_k^e \right) \frac{dL_i^e}{dx} \frac{dL_j^e}{dx} dx \\ = \sum_{k=1}^n u_k^e \int_{x_a}^{x_b} a_0 L_k^e \frac{dL_i^e}{dx} \frac{dL_j^e}{dx} dx \quad (i)$$

Now consider, as an example, linear approximation ( $n = 2$ ) of  $u(x)$ , and  $a_0$  is a constant within an element, say  $a_0^e$ . Then we have

$$K_{ij}^e = \sum_{k=1}^n a_0^e u_k^e \int_{x_a}^{x_b} L_k^e \frac{dL_i^e}{dx} \frac{dL_j^e}{dx} dx \\ = \sum_{k=1}^n a_0^e u_k^e (-1)^{i+j} \frac{1}{h_e^2} \int_{x_a}^{x_b} L_k^e dx \\ = (-1)^{i+j} \frac{a_0^e}{2h_e} \left( \sum_{k=1}^n u_k^e \right) = (-1)^{i+j} \frac{a_0^e}{2h_e} (u_1^e + u_2^e) \quad (ii)$$

or

$$[K^e] = \frac{a_0^e (u_1^e + u_2^e)}{2h_e} \begin{bmatrix} 1 & -1 \\ -1 & 1 \end{bmatrix} \quad (iii)$$

The assembly of element equations follows the same procedure as in linear finite element analysis. If we denote the global nodal vector by  $\{U\}$ , the assembled system of equations can be written as

$$[K(\{U\})]\{U\} = \{F\} \quad (3.3.4)$$

where  $[K]$  and  $\{F\}$  denote the global coefficient matrix and the right-hand side vector, respectively. In the example above,  $[K]$  is a linear function of

the nodal values  $U_i$  and it is a symmetric matrix. Consequently, the resulting finite element equations are nonlinear; in the present case, they are quadratic in  $U_i$ . Example 3.3.2 illustrates these ideas.

### Example 3.3.2

The assembled equations (3.3.4) associated with a mesh of two linear elements of equal length, and with the data used in Example 3.3.1, are

$$\frac{1}{2h} \begin{bmatrix} (U_1 + U_2) & -(U_1 + U_2) & 0 \\ -(U_1 + U_2) & (U_1 + 2U_2 + U_3) & -(U_2 + U_3) \\ 0 & -(U_2 + U_3) & (U_2 + U_3) \end{bmatrix} \begin{Bmatrix} U_1 \\ U_2 \\ U_3 \end{Bmatrix} = \begin{Bmatrix} f_1^{(1)} \\ f_2^{(1)} + f_1^{(2)} \\ f_2^{(2)} \end{Bmatrix} + \begin{Bmatrix} Q_1^{(1)} \\ Q_2^{(1)} + Q_1^{(2)} \\ Q_2^{(2)} \end{Bmatrix} \quad (\text{i})$$

Now suppose that the assembled system of equations is subjected to the boundary conditions

$$u(0) = u_0, \quad \left[ a \frac{du}{dx} + \beta(u - u_\infty) \right]_{x=L} = \hat{Q} \quad (\text{ii})$$

with

$$\beta = \beta_0 + \beta_1 u \quad (\text{iii})$$

These conditions for the present mesh of two linear elements imply

$$U_1 = u_0, \quad Q_2^{(2)} = \hat{Q} - (\beta_0 + \beta_1 U_3)(U_3 - u_\infty) \quad (\text{iv})$$

Hence, after imposing the boundary conditions and balance of the secondary variables  $Q_2^{(1)} + Q_1^{(2)} = 0$ , the assembled equations in (i) become

$$\frac{1}{2h} \begin{bmatrix} (U_1 + U_2) & -(U_1 + U_2) & 0 \\ -(U_1 + U_2) & (U_1 + 2U_2 + U_3) & -(U_2 + U_3) \\ 0 & -(U_2 + U_3) & (U_2 + U_3) + 2h(\beta_0 + \beta_1 U_3) \end{bmatrix} \begin{Bmatrix} u_0 \\ U_2 \\ U_3 \end{Bmatrix} = \begin{Bmatrix} f_1^{(1)} \\ f_2^{(1)} + f_1^{(2)} \\ f_2^{(2)} \end{Bmatrix} + \begin{Bmatrix} Q_1^{(1)} \\ Q_2^{(1)} + Q_1^{(2)} \\ \hat{Q} + (\beta_0 + \beta_1 U_3)u_\infty \end{Bmatrix} \quad (\text{v})$$

## 3.4 Solution Procedures

### 3.4.1 General Comments

The numerical procedures used to solve nonlinear algebraic equations (3.3.4) are iterative in nature. Two iterative procedures are outlined here for the problem at hand. Some general features of iterative methods used for nonlinear equations are discussed before getting into the details of each method (see Appendix 2 for additional discussion).

Suppose that we wish to solve the nonlinear matrix equation

$$[A(\{U\})]\{U\} = \{F\}$$

We begin by assuming that the solution  $\{U\}^{(r-1)}$  at the  $(r-1)$ st iteration is known, and we wish to seek the solution  $\{U\}^{(r)}$  at the  $r$ th iteration. At the beginning of the iteration, that is, when  $r = 1$ , the solution  $\{U\}^{(0)}$  is assumed or "guessed" consistent with the problem data. Using the solution from the  $(r-1)$ st iteration, we compute the coefficient matrix  $[A(\{U\}^{(r-1)})]$ . Since  $[A]$  is evaluated using estimated vector  $\{U\}$ , in general,  $[A(\{U\}^{(r-1)})]\{U\}^{(r)} \neq \{F\}$ . Hence, we are left with a residual

$$\{R\} \equiv [A(\{U\}^{(r-1)})]\{U\}^{(r)} - \{F\} \quad (3.4.1)$$

The objective of the iteration process is to reduce this residual to a very small, negligible value,  $\epsilon$ :

$$\sqrt{\sum_{I=1}^N R_I^2} \leq \epsilon \quad (3.4.2)$$

Alternatively, the iteration may proceed until the difference between solutions from two consecutive iterations, measured with the Euclidean norm, is less than the tolerance  $\epsilon$ :

$$\sqrt{\frac{\sum_{I=1}^N |U_I^{(r)} - U_I^{(r-1)}|^2}{\sum_{I=1}^N |U_I^{(r)}|^2}} \leq \epsilon \quad (3.4.3)$$

### 3.4.2 Direct Iteration Procedure

The direct iteration technique, also known as the *Picard iteration method of successive substitution*, is the simplest of the two methods discussed here. In the direct iteration procedure, the solution at the  $r$ th iteration is determined from the equation

$$[K(\{U\}^{(r-1)})]\{U\}^{(r)} = \{F\} \quad (3.4.4)$$

where the coefficient matrix  $[K]$  is evaluated using the known solution from the  $(r-1)$ st iteration. It is assumed that the coefficient matrix  $[K]$  is invertible after the imposition of boundary conditions. Thus, the initial "guess" vector  $\{U\}^0$  should be such that (a) it satisfies the specified essential boundary conditions and (b)  $[K]$  is invertible. This means, in the present case, that  $U_I \neq 0$  for at least one value of  $I$ .

Figure 3.4.1 depicts the general idea of the direct iteration procedure for a single degree-of-freedom system. Here  $K$  denotes the slope of the line joining the origin to the point  $K(U)$  on the curve  $F = K(U)U \equiv f(U)$ . Note that  $K(U)$  is not the slope of the tangent to the curve at  $U$ . The direct iteration converges if the nonlinearity is mild and it diverges if the nonlinearity is severe. Divergence is more likely for hardening type nonlinearity. Acceleration of convergence for some types of nonlinearities may be achieved by using a

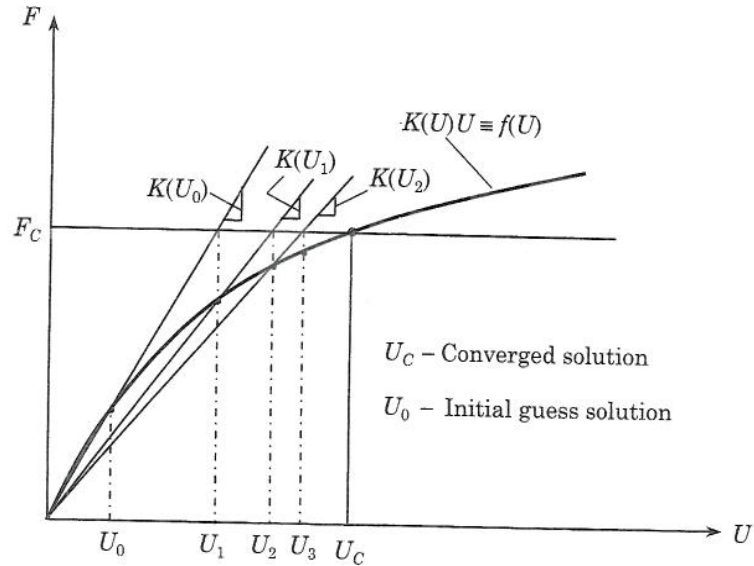


Figure 3.4.1 Convergence of the direct iteration procedure (calculation of  $U$  for a specified source value  $F$ ).

weighted-average of solutions from the last two iterations rather than the solution from the last iteration:

$$\{\bar{U}\} \equiv \rho\{U\}^{(r-2)} + (1 - \rho)\{U\}^{(r-1)}, \quad 0 \leq \rho \leq 1 \quad (3.4.5)$$

where  $\rho$  is called the *acceleration parameter* and  $r$  is the current iteration number (i.e. when we seek solution  $\{U\}^{(r)}$ ). The value of  $\rho$  depends on the nature of nonlinearity.

**Example 3.4.1**

We wish to solve the nonlinear differential equation

$$-\frac{d}{dx} \left( u \frac{du}{dx} \right) = f_0, \quad 0 < x < 1 \quad (i)$$

subjected to the boundary conditions

$$\left[ u \frac{du}{dx} \right]_{x=0} = \hat{Q}, \quad u(1) = \hat{u} \quad (ii)$$

For a mesh of two linear elements with  $h_1 = h_2 = h$ , the assembled equations are given by Eq. (i) of Example 3.3.2. After imposing the boundary conditions  $Q_1^{(1)} = \hat{Q}$ ,  $Q_2^{(1)} + Q_1^{(2)} = 0$

and  $U_3 = \hat{u}$ , Eq. (i) of Example 3.3.2 becomes

$$\begin{aligned} \frac{1}{2h} \begin{bmatrix} (\bar{U}_1 + \bar{U}_2) & -(\bar{U}_1 + \bar{U}_2) & 0 \\ -(\bar{U}_1 + \bar{U}_2) & (\bar{U}_1 + 2\bar{U}_2 + \bar{U}_3) & -(\bar{U}_2 + \bar{U}_3) \\ 0 & -(\bar{U}_2 + \bar{U}_3) & (\bar{U}_2 + \bar{U}_3) \end{bmatrix} \begin{Bmatrix} U_1 \\ U_2 \\ \hat{u} \end{Bmatrix}^{(r)} \\ = \begin{Bmatrix} f_1^{(1)} \\ f_2^{(1)} + f_1^{(2)} \\ f_2^{(2)} \end{Bmatrix} + \begin{Bmatrix} \hat{Q} \\ 0 \\ Q_2^{(2)} \end{Bmatrix} \end{aligned} \quad (\text{iii})$$

or, omitting the last equation, we obtain the following condensed set of equations:

$$\begin{aligned} \frac{1}{2h} \begin{bmatrix} (\bar{U}_1 + \bar{U}_2) & -(\bar{U}_1 + \bar{U}_2) \\ -(\bar{U}_1 + \bar{U}_2) & (\bar{U}_1 + 2\bar{U}_2 + \bar{U}_3) \end{bmatrix} \begin{Bmatrix} U_1 \\ U_2 \end{Bmatrix}^{(r)} \\ = \begin{Bmatrix} f_1^{(1)} \\ f_2^{(1)} + f_1^{(2)} \end{Bmatrix} + \begin{Bmatrix} \hat{Q} \\ \frac{(\bar{U}_2 + \bar{U}_3)}{2h} \hat{u} \end{Bmatrix} \end{aligned} \quad (\text{iv})$$

where  $\bar{U}_I = U_I^{(r-1)}$  ( $I = 1, 2, 3$ ) denote the nodal values from the previous iteration.

As a specific problem, we use the following data

$$\hat{Q} = 0, \quad \hat{u} = \sqrt{2} = 1.4142, \quad f_0 = -1, \quad h = L/2 = 0.5 \quad (\text{v})$$

and select the initial guess vector, which must be consistent with specified essential boundary conditions (i.e.  $U_3 = \hat{u} = \sqrt{2}$ ), to be

$$U_1^{(0)} = 1.0, \quad U_2^{(0)} = 1.0, \quad U_3^{(0)} = \sqrt{2} = 1.4142 \quad (\text{vi})$$

Then Eq. (iii) becomes ( $f_i^e = -h/2$ )

$$\begin{bmatrix} 2 & -2 & 0 \\ -2 & 4.4142 & -2.4142 \\ 0 & -2.4142 & 2.4142 \end{bmatrix} \begin{Bmatrix} U_1 \\ U_2 \\ \sqrt{2} \end{Bmatrix}^{(1)} = - \begin{Bmatrix} 0.25 \\ 0.5 \\ 0.25 \end{Bmatrix} + \begin{Bmatrix} 0 \\ 0 \\ Q_2^{(2)} \end{Bmatrix} \quad (\text{vii})$$

and eliminating the third equation, we obtain the following global set of equations at the beginning of the first iteration [see Eq. (iv)]:

$$\begin{bmatrix} 2 & -2 \\ -2 & 4.4142 \end{bmatrix} \begin{Bmatrix} U_1 \\ U_2 \end{Bmatrix}^{(1)} = - \begin{Bmatrix} 0.25 \\ 0.5 \end{Bmatrix} + \begin{Bmatrix} 0 \\ 2.4142\sqrt{2} \end{Bmatrix} = \begin{Bmatrix} -0.25 \\ 2.9142 \end{Bmatrix} \quad (\text{viii})$$

The solution at the end of first iteration is

$$U_1^{(1)} = 0.9785, \quad U_2^{(1)} = 1.1035, \quad U_3^{(1)} = 1.4142 \quad (\text{ix})$$

For the second iteration, the equations solved are ( $\rho = 0$ )

$$\begin{bmatrix} 2.0821 & -2.0821 \\ -2.0821 & 4.5998 \end{bmatrix} \begin{Bmatrix} U_1 \\ U_2 \end{Bmatrix}^{(2)} = - \begin{Bmatrix} 0.25 \\ 0.5 \end{Bmatrix} + \begin{Bmatrix} 0 \\ 3.5607 \end{Bmatrix} \quad (\text{x})$$

and the solution becomes

$$U_1^{(2)} = 0.9962, \quad U_2^{(2)} = 1.1163, \quad U_3^{(2)} = 1.4142 \quad (\text{xi})$$

The root-mean-square error in the solution (with respect to solution obtained in the iteration) [see Eq. (3.4.1)] is 0.0106.

The exact solution to this problem, with the data given in Eq. (ii), is (one can verify by direct substitution)

$$u(x) = \sqrt{1+x^2}$$

The convergence tolerance is taken to be  $\epsilon = 10^{-3}$ , and the maximum number of iterations prescribed to be 10. The finite element solutions obtained with the linear (L) and quadratic (Q) elements are compared with the exact solution in Table 3.4.1. The finite element solution converges to the exact solution in four iterations.

**Table 3.4.1** Comparison of finite element solutions with the exact solution of the problem in Example 3.4.1 (direct iteration).

$x$	Iteration	2L	4L	1Q	2Q	Exact
0.00	1	0.9785	0.9517	0.9699	0.9415	1.0000
	2	0.9962	0.9903	0.9954	0.9881	
	3	0.9995	0.9988	0.9995	0.9986	
	4	0.9999	0.9999	0.9999	0.9999	
0.25	1	—	0.9830	—	0.9727	1.0308
	2	—	1.0226	—	1.0208	
	3	—	1.0299	—	1.0298	
	4	—	1.0307	—	1.0308	
0.50	1	1.1036	1.0767	1.1013	1.0665	1.1180
	2	1.1163	1.1136	1.1168	1.1127	
	3	1.1178	1.1176	1.1118	1.1176	
	4	1.1180	1.1180	1.1187	1.1180	
0.75	1	—	1.2330	—	1.2285	1.2500
	2	—	1.2489	—	1.2488	
	3	—	1.2499	—	1.2500	
	4	—	1.2500	—	1.2500	
1.00		1.4142	1.4142	1.4142	1.4142	1.4142

### 3.4.3 Newton's Iteration Procedure

In Newton's method, also referred to as the Newton-Raphson method, Eq. (3.4.4) is written as

$$\{R\} \equiv [K]\{U\} - \{F\} = \{0\} \quad (3.4.6)$$

where  $\{R\}$  is the residual vector. We expand  $\{R\}$  in Taylor's series about the (known) solution at the  $i$ th iteration:

$$\{R(\{U\})\} = \{R(\{U\}^{(r-1)})\} + \left(\frac{\partial\{R\}}{\partial\{U\}}\right)^{(r-1)} \cdot \{\delta U\} + \dots \quad (3.4.7)$$

first  
by  
(xii)  
ns is  
atic  
tion

Omitting the terms of order 2 and higher, we obtain

$$\left(\frac{\partial\{R\}}{\partial\{U\}}\right)^{(r-1)} \cdot \{\delta U\} = -\{R(\{U\}^{(r-1)})\} \tag{3.4.8a}$$

$$[T(\{U\}^{(r-1)})]\{\delta U\} = -\{R(\{U\}^{(r-1)})\} \tag{3.4.8b}$$

where  $[T]$  is called the *tangent matrix*

$$[T(\{U\}^{(r-1)})] \equiv \left(\frac{\partial\{R\}}{\partial\{U\}}\right)^{(r-1)} \tag{3.4.9}$$

ion  
—  
—

The component definition of the tangent matrix at the element level is

$$\begin{aligned} T_{ij}^e &\equiv \frac{\partial R_i^e}{\partial u_j^e} = \frac{\partial}{\partial u_j^e} \left( \sum_{m=1}^n K_{im}^e u_m^e - F_i^e \right) \\ &= \sum_{m=1}^n \left( \frac{\partial K_{im}^e}{\partial u_j^e} u_m^e + K_{im}^e \frac{\partial u_m^e}{\partial u_j^e} \right) = \sum_{m=1}^n \frac{\partial K_{im}^e}{\partial u_j^e} u_m^e + K_{ij}^e \end{aligned} \tag{3.4.10}$$

The residual vector after the  $(r - 1)$ st iteration is given by

$$-\{R(\{U\}^{(r-1)})\} = \{F\} - [K(\{U\}^{(r-1)})]\{U\}^{(r-1)} \tag{3.4.11}$$

The solution at the  $r$ th iteration is then given by

$$\{U\}^r = \{U\}^{(r-1)} + \{\delta U\} \tag{3.4.12}$$

—  
1.  
)  
3

The symmetry or unsymmetry of the direct matrix or the tangent matrix depends on the original differential equation as well as the weak form used to develop the finite element equations; the symmetry or unsymmetry of the tangent matrix depends on the direct matrix as well as on the nature of nonlinearity included in  $a(x, u)$  and  $c(x, u)$ .

Figure 3.4.2 shows the convergence of the Newton–Raphson iteration procedure for a single degree-of-freedom system. Here  $T(U)$  denotes the slope of the tangent to the curve  $F = K(U)U$  at  $U$ . The Newton–Raphson iteration converges for hardening as well as softening type nonlinearities. For hardening type, convergence may be accelerated using the underrelaxation in Eq. (3.4.5). The method may diverge for a saddle point behavior. Several comments regarding the Newton–Raphson procedure are in order.

- At the end of each iteration, the procedure gives an increment of the solution as opposed to the total solution in the direct iteration procedure.

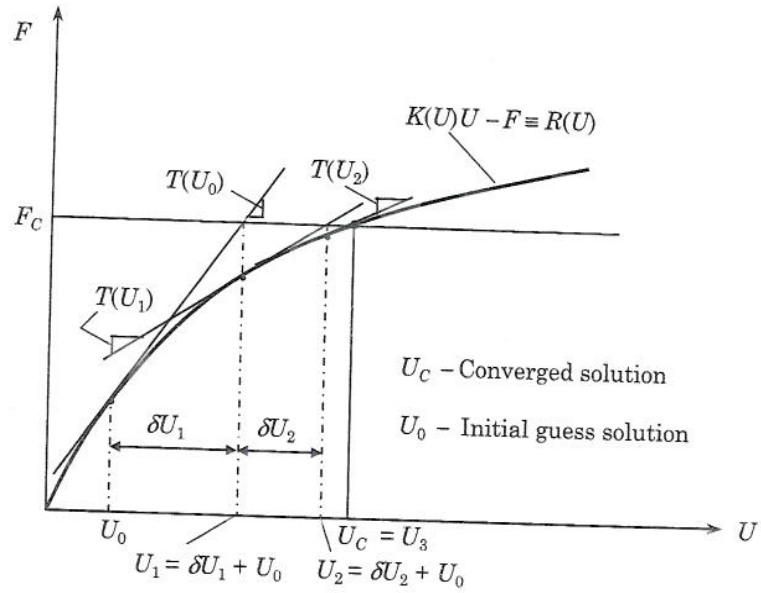


Figure 3.4.2 Convergence of the Newton iteration procedure (calculation of  $\delta U$  for a specified residual value  $R$ ).

- Since the actual specified essential boundary conditions are included in the initial guess vector, the incremental vector  $\{\delta U\}$  is subjected to only the homogeneous form of the specified essential boundary conditions.
- The tangent matrix does not have to be exact; an approximate  $[T]$  can also provide the solution but it may take more iterations. In any case, the residual vector will be computed using the definition  $\{R\} = \{F\} - [K]\{U\}$ .
- When the tangent matrix is updated only once in a certain number of iterations (to save computational time), the procedure is known as the *modified Newton-Raphson method*. Generally, the modified Newton-Raphson iteration method takes more iterations to converge than the full Newton's iteration, and it may even diverge if the nonlinearity is severe.

**Example 3.4.2**

Consider the element coefficient matrix in Eq. (3.3.3a). Assume that  $a(x, u) = a^e(x)$ ,  $b = 0$ ,  $c(x, u) = c_0(x) + c_1(x)u + c_2(x)u^2$ ,  $\beta_a = 0$ ,  $\beta_b = \beta_0 + \beta_1 u_n^e$ . Then we have

$$K_{ij}^e = \int_{x_a}^{x_b} \left\{ a^e(x) \frac{dL_i^e}{dx} \frac{dL_j^e}{dx} + [c_0(x) + c_1(x)u_n(x) + c_2(x)u_n^2(x)] L_i^e L_j^e \right\} dx + [\beta_0 + \beta_1 u_n(x_b)] L_i^e(x_b) L_j^e(x_b) \tag{i}$$

Note that in this case  $[K^e]$  is symmetric. We wish to compute the element tangent coefficient



matrix. We have

$$\begin{aligned}
 T_{ij}^e &= \sum_{m=1}^n \frac{\partial K_{im}^e}{\partial u_j^e} u_m^e + K_{ij}^e \\
 &= \sum_{m=1}^n \frac{\partial}{\partial u_j^e} \left\{ \int_{x_a}^{x_b} [c_0(x) + c_1(x)u_h + c_2(x)u_h^2] L_i^e L_m^e dx \right. \\
 &\quad \left. + [\beta_0 + \beta_1 u_h(x_b)] L_i^e(x_b) L_m^e(x_b) \right\} u_m^e + K_{ij}^e \\
 &= \sum_{m=1}^n u_m^e \left[ \int_{x_a}^{x_b} (c_1 L_j^e + 2c_2 u_h L_j^e) L_i^e L_m^e dx + \beta_1 L_j^e(x_b) L_i^e(x_b) L_m^e(x_b) \right] + K_{ij}^e \\
 &= \int_{x_a}^{x_b} (c_1 u_h + 2c_2 u_h^2) L_i^e L_j^e dx + \beta_1 u_h(x_b) L_i^e(x_b) L_j^e(x_b) + K_{ij}^e \tag{ii}
 \end{aligned}$$

where the identities

$$\frac{\partial u_h}{\partial u_j^e} = L_j^e, \quad \sum_{m=1}^n u_m^e L_m^e = u_h(x)$$

are used in arriving at the last line. Note that the tangent matrix  $[T^e]$  is also symmetric.

**Example 3.4.3**

Here we wish to solve the nonlinear finite element equations of Example 3.4.1 using the Newton-Raphson iterative technique. First, we compute the tangent matrix at the element level and then assemble the equations. For an element, we have

$$\begin{aligned}
 T_{ij}^e &= \sum_{m=1}^n \frac{\partial K_{im}^e}{\partial u_j^e} u_m^e + K_{ij}^e \\
 &= \sum_{m=1}^n \frac{\partial}{\partial u_j^e} \left( \int_{x_a}^{x_b} u_h \frac{dL_i^e}{dx} \frac{dL_m^e}{dx} dx \right) u_m^e + K_{ij}^e \\
 &= \int_{x_a}^{x_b} \frac{\partial u_h}{\partial u_j^e} \frac{dL_i^e}{dx} \left( \sum_{m=1}^n u_m^e \frac{dL_m^e}{dx} \right) dx + K_{ij}^e \\
 &= \int_{x_a}^{x_b} \frac{du_h}{dx} \frac{dL_i^e}{dx} L_j^e dx + K_{ij}^e \equiv \hat{K}_{ij}^e + K_{ij}^e \tag{i}
 \end{aligned}$$

where the identity

$$\sum_{m=1}^n u_m^e \frac{dL_m^e}{dx} = \frac{du_h}{dx}$$

is used in arriving at the last line. We have,

$$\hat{K}_{ij}^e = \int_{x_a}^{x_b} \frac{du_h}{dx} \frac{dL_i^e}{dx} L_j^e dx = \frac{u_2^e - u_1^e}{2} \int_{x_a}^{x_b} \frac{dL_i^e}{dx} L_j^e dx$$

or

$$[\hat{K}^e] = \frac{u_2^e - u_1^e}{2h_e} \begin{bmatrix} -1 & -1 \\ 1 & 1 \end{bmatrix}$$

Thus, the tangent matrix becomes

$$[T^e] = [K^e] + [\hat{K}^e] = \frac{(\bar{u}_1^e + \bar{u}_2^e)}{2h_e} \begin{bmatrix} 1 & -1 \\ -1 & 1 \end{bmatrix} + \frac{(\bar{u}_2^e - \bar{u}_1^e)}{2h_e} \begin{bmatrix} -1 & -1 \\ 1 & 1 \end{bmatrix}$$

where  $\bar{u}_i^e$  denote the nodal values known from the previous iteration. Alternatively,

$$\begin{aligned} [T^e] &= [K^e] + \left[ \begin{array}{cc} \frac{\partial K_{11}^e}{\partial u_1^e} u_1^e + \frac{\partial K_{12}^e}{\partial u_1^e} u_2^e & \frac{\partial K_{11}^e}{\partial u_2^e} u_1^e + \frac{\partial K_{12}^e}{\partial u_2^e} u_2^e \\ \frac{\partial K_{21}^e}{\partial u_1^e} u_1^e + \frac{\partial K_{22}^e}{\partial u_1^e} u_2^e & \frac{\partial K_{21}^e}{\partial u_2^e} u_1^e + \frac{\partial K_{22}^e}{\partial u_2^e} u_2^e \end{array} \right]_{u_i^e = \bar{u}_i^e} \\ &= \frac{(\bar{u}_1^e + \bar{u}_2^e)}{2h_e} \begin{bmatrix} 1 & -1 \\ -1 & 1 \end{bmatrix} + \frac{1}{2h_e} \begin{bmatrix} \bar{u}_1^e - \bar{u}_2^e & \bar{u}_1^e - \bar{u}_2^e \\ -\bar{u}_1^e + \bar{u}_2^e & -\bar{u}_1^e + \bar{u}_2^e \end{bmatrix} \\ &= \frac{(\bar{u}_1^e + \bar{u}_2^e)}{2h_e} \begin{bmatrix} 1 & -1 \\ -1 & 1 \end{bmatrix} + \frac{(\bar{u}_2^e - \bar{u}_1^e)}{2h_e} \begin{bmatrix} -1 & -1 \\ 1 & 1 \end{bmatrix} \end{aligned} \quad (\text{ii})$$

Note that the tangent coefficient matrix is not symmetric.

With the data in Eqs. (ii) and (iii) of Example 3.4.1, at the beginning of the first iteration we have (after assembly and imposition of the boundary conditions)

$$\begin{aligned} \begin{bmatrix} 2 & -2 \\ -2 & 4 \end{bmatrix} \begin{Bmatrix} \delta U_1 \\ \delta U_2 \end{Bmatrix} &= - \begin{Bmatrix} 0.25 \\ 0.50 \end{Bmatrix} - \begin{Bmatrix} 2 - 2 \\ -2 + 4.4142 - 3.4142 \end{Bmatrix} \\ &= \begin{Bmatrix} -0.25 \\ 0.50 \end{Bmatrix} \end{aligned} \quad (\text{iii})$$

The solution to these equations is

$$\delta U_1 = 0.0, \quad \delta U_2 = 0.125, \quad \delta U_3 = 0.0 \quad (\text{iv})$$

and the complete solution becomes

$$U_1^{(1)} = 1.0000, \quad U_2^{(1)} = 1.1250, \quad U_3^{(1)} = 1.4142 \quad (\text{v})$$

The solution at the second iteration is obtained using

$$\begin{bmatrix} 2 & -2.25 \\ -2 & 4.50 \end{bmatrix} \begin{Bmatrix} \delta U_1 \\ \delta U_2 \end{Bmatrix} = \begin{Bmatrix} 0.0156 \\ -0.0312 \end{Bmatrix} \quad (\text{vi})$$

The solution to these equations is

$$\delta U_1 = 0.0, \quad \delta U_2 = -0.0007, \quad \delta U_3 = 0.0 \quad (\text{vii})$$

and the complete solution becomes

$$U_1^{(2)} = 1.0000, \quad U_2^{(2)} = 1.1180, \quad U_3^{(2)} = 1.4142 \quad (\text{viii})$$

The root-mean-square error in the solution (with respect to the solution obtained in the first iteration) [see Eq. (3.4.2)] is 0.0034.

Table 3.4.2 contains the numerical results obtained with the Newton–Raphson iteration method. The Newton–Raphson method gives converged solution in only three iterations as opposed to four iterations taken by the direct iteration method. For the mesh of 1 quadratic element, the error criterion is met while the solution did not actually coincide with the exact solution.

**Table 3.4.2** Comparison of finite element solutions with the exact solution of the problem in Example 3.4.3 (Newton–Raphson iteration).

$x$	Iteration	2L	4L	1Q	2Q	Exact
0.00	1	1.0000	1.0000	1.0000	1.0000	
	2	1.0000	1.0000	1.0000	1.0000	
	3	1.0000	1.0000	1.0000	1.0000	1.0000
0.25	1	–	1.0312	–	1.0312	
	2	–	1.0308	–	1.0308	
	3	–	1.0308	–	1.0308	1.0308
0.50	1	1.1250	1.1250	1.1241	1.1250	
	2	1.1180	1.1180	1.1187	1.1180	
	3	1.1180	1.1180	1.1187	1.1180	1.1180
0.75	1	–	1.2812	–	1.2766	
	2	–	1.2504	–	1.2502	
	3	–	1.2500	–	1.2500	1.2500

## 3.5 Computer Implementation

### 3.5.1 Introduction

The nonlinear formulations and solution procedures described above can be implemented on a computer using Fortran language. Fortran is chosen here mainly because of its transparent nature (i.e. one can see how the statements correspond to the theory) compared to  $C^{++}$  language. Of course, once the logic of implementation is understood, it is easier to carry out the actual computations in any suitable computational languages. The logical statements for each of the iterative methods are described here. It is necessary for the reader to familiarize with programs FEM1DV2 and FEM2DV2 described in Appendix 1 of the finite element book by Reddy [1] to fully understand the logic and variable names used here. The listing of FEM1DV2 contains Fortran statements for assembly, imposition of boundary conditions, and solution of equations (banded symmetric and unsymmetric equation solvers are listed in Appendix 1 of this book). A general flow chart of the nonlinear analysis program is given in Figure 3.5.1.

### 3.5.2 Preprocessor Unit

The following information is read in the preprocessor.

1. Read or define the model equation data

(a) Define the coefficients  $a(x, u)$ ,  $b(x, u)$ , and  $c(x, u)$  and source  $f(x)$  in the model differential equation (3.1.1) (they are assumed to be polynomials of certain degree); for example, assume

$$a(x, u) = a_{x0} + a_{x1}x + a_{u1}u + a_{u2}u^2 + a_{ux1}\frac{du}{dx} + a_{ux2}\left(\frac{du}{dx}\right)^2$$

$$b(x, u) = b_{x0} + b_{x1}x + b_{u1}u + b_{u2}u^2 + b_{ux1}\frac{du}{dx} + b_{ux2}\left(\frac{du}{dx}\right)^2$$

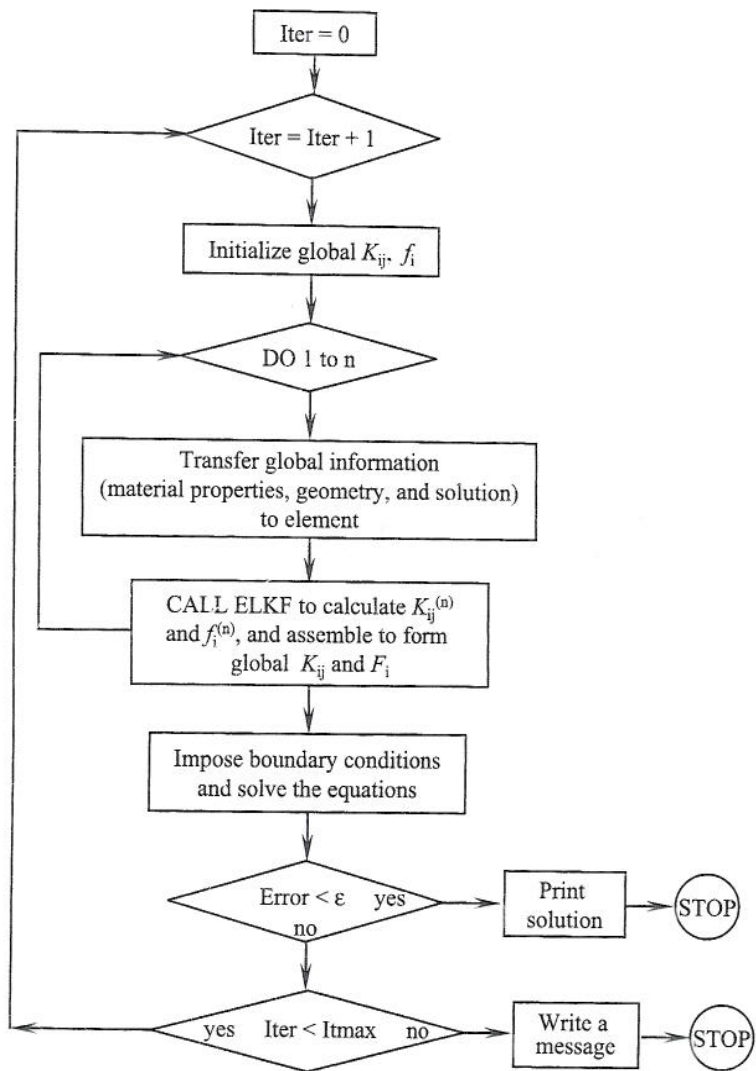


Figure 3.5.1 A flow chart of the nonlinear analysis program for the solution of the model equation (3.1.1).

$$\begin{aligned}
 c(x, u) &= c_{x0} + c_{x1}x + c_{u1}u + c_{u2}u^2 + c_{ux1}\frac{du}{dx} + c_{ux2}\left(\frac{du}{dx}\right)^2 \\
 f(x) &= f_{x0} + f_{x1}x + f_{x2}x^2
 \end{aligned}
 \tag{3.5.1}$$

so that a large class of nonlinear one-dimensional problems may be solved with the program. The choice in Eq. (3.5.1) requires us to read the following parameters (assuming continuous data for the whole domain)

*AX0, AX1, AU1, AU2, AUX1, AUX2; BX0, BX1, BU1, etc.*

(b) Read geometric and analysis data

*X0* = global coordinate of the first node of the domain (assumed to be a straight line),

*AL* = domain size (length),

*IEL* = element type (= 1, linear; = 2, quadratic),

*NEM* = number of elements in the mesh,

*NONLIN* = flag for type of analysis (= 0, linear; > 0, nonlinear)

*EPS* = allowable error tolerance  $\epsilon$  for the convergence test,

*ITMAX* = maximum allowable number of iterations for convergence.

(c) Read specified boundary and initial data: *NSPV, NSSV, NSMB, ISPV(I, J), VSPV(I), ISSV(I, J), VSSV(I), ISMB(I, J), BETA0(I), BETAU(I), UREF(I), and GU0(I)*, where

*NSPV* = number of specified primary degrees of freedom (*U*),

*NSSV* = number of specified secondary degrees of freedom ( $Q \equiv n_x a \frac{du}{dx}$ ),

*NSMB* = number of specified mixed boundary conditions

$$[Q + (\beta_0 + \beta_u U)(U - U_{\text{ref}})],$$

*ISPV(I, J)* = array of specified primary degrees of freedom ( $I = 1, 2, \dots, NSPV$  and  $J = 1, 2$ ); *ISPV(I, 1)* = global node number at which the primary variable is specified, and *ISPV(I, 2)* is the degree of freedom number at that node which is specified (in the class of problems discussed in this chapter, *NDF* = 1 and therefore *ISPV(I, 2)* = 1 for all cases).

*VSPV(I)* = array of specified values of primary variable DOF in *ISPV(I, J)* [*VSPV(I)* should be in the same sequence as the specified degrees of freedom in *ISPV(I)*],

*ISSV(I, J)* = similar to *ISPV(I, J)*, except for secondary variables,

*VSSV(I)* = similar to *VSPV(I)*, except for secondary variables,

*ISMB(I, J)* = array of specified mixed boundary conditions ( $I = 1, 2, \dots, NSSV$ ) and has meaning similar to arrays *ISPV(I, J)* and *ISSV(I, J)*,

*BETA0(I)* = array of specified values of  $\beta_0$ ,

$BETA1(I)$  = array of specified values of  $\beta_u$ ,  
 $UREF(I)$  = array of specified values of  $U_{ref}$ ,  
 $GU0(I)$  = initial (guess) solution vector ( $I = 1, 2, \dots, NEQ$ );  
 $NEQ$  = number of total primary degrees of freedom in the mesh.

2. Write out the input data and necessary warning messages.

### 3.5.3 Processor Unit

Here we discuss mainly the calculation of element coefficients, imposition of various types of boundary conditions, and iterative algorithm. The number of Gauss points needed to evaluate the coefficients is determined by the highest polynomial degree,  $p$  [ $NGP = (p + 1)/2$ ]. In the present case, the expression that dictates the degree of the polynomial is the integral involving  $c(x, u)$ . If we assume  $c$  to be a linear function of  $u$ , and if  $u$  is approximated using linear polynomials, the integrand of the above integral expression is cubic ( $p = 3$ ). Hence, a two-point integration is needed to evaluate it; for quadratic interpolation of  $u$ , the integrand is a fifth degree polynomial ( $p = 5$ ), and hence it requires three-point Gauss quadrature. Of course, the polynomial degrees goes up if  $a$  is a higher degree polynomial of  $x$ .

The element coefficients are evaluated using the Gauss rule. Based on the discussion presented in Section 2.7, the element coefficients in (3.3.3a), for  $\beta = 0$ , can be expressed as

$$\begin{aligned}
 ELK(I, J) = & ELK(I, J) + (AX * GDSFL(I) * GDSFL(J) \\
 & + BX * SFL(I) * GDSFL(J) + CX * SFL(I) * SFL(J)) * \\
 & GJ * GAUSWT(NI, NGP)
 \end{aligned}$$

which is evaluated inside a loop on  $NI = 1, 2, \dots, NGP$  and inner loops on  $I, J = 1, 2, \dots, NPE$ . Boxes 3.5.1 and 3.5.2 show the Fortran subroutines for the calculation of  $[K^e]$  and  $\{f^e\}$ .

The imposition of boundary conditions on a banded system of non-symmetric equations is discussed next. The assembled coefficient matrix  $[GLK]$  is stored a full band width ( $NBW$ ) form, and it is of the order  $NEQ \times NBW$ , the last column  $GLK(I, NBW)$  being reserved for the source vector. Note that  $GLK(I, NHBW)$  is the main diagonal of the assembled matrix.

#### Essential boundary conditions

Now suppose that  $U_I$  is specified to be  $\hat{U}_I$ . Then the  $I$ th equation of the system is replaced with the equation  $U_I = \hat{U}_I$ . This is done as follows:

$$\begin{aligned}
 GLK(I, J) = 0.0 \quad & \text{for all } J = 1, 2, \dots, NBW \quad \text{and } J \neq I \\
 GLK(I, NHBW) = 1.0, \quad & GLK(I, NBW) = \hat{U}_I
 \end{aligned} \tag{3.5.2}$$

This is repeated for all  $NSPV$  conditions.

**Box 3.5.1** Subroutine for the generation of the coefficient matrices in the *direct iteration method*.

```

SUBROUTINE COEFF (IEL,NPE,F0)
IMPLICIT REAL*8(A-H,O-Z)
DIMENSION GAUSS(5,5),WT(5,5)
COMMON /SHP/ SFL(4),GDSFL(4)
COMMON /STF/ STIF(3,3),ELF(3),ELX(3),ELU(3),AX0,AX1,AU
C
DATA GAUSS/5*0.0D0,-0.57735027D0,0.57735027D0,3*0.0D0,
1 -0.77459667D0,0.0D0,0.77459667D0,2*0.0D0,-0.86113631D0,
2 -0.33998104D0,0.33998104D0,0.86113631D0,0.0D0,
3 -0.906180D0,-0.538469D0,0.0D0,0.538469D0,0.906180D0/

DATA WT /2.0D0,4*0.0D0,2*1.0D0,3*0.0D0,0.55555555D0,
1 0.88888888D0,0.55555555D0,2*0.0D0,0.34785485D0,
2 2*0.65214515D0,0.34785485D0,0.0D0,0.2369227D0,
3 0.478629D0,0.568889D0,0.478629D0,0.236927D0/
C
NGP=IEL+1
EL=ELX(IEL+1)-ELX(1)
DO 10 I=1,NPE
  ELF(I)=0.0
  DO 10 J=1,NPE
10   ELK(I,J)=0.0
C
DO 80 NI=1,NGP
  XI=GAUSS(NI,NGP)
  CALL SHAPE (EL,ELX,GJ,IEL,NPE,XI)
  CNST=GJ*WT(NI,NGP)
  X=0.0
  U=0.0
  DO 20 I=1,NPE
    X=X+SFL(I)*ELX(I)
    U=U+SFL(I)*ELU(I)
20  CONTINUE
C
  AX=AX0+AX1*X+AU*U
  DO 40 I=1,NPE
    ELF(I)=ELF(I)+F0*SFL(I)*CNST
    DO 40 J=1,NPE
      S00=GDSFL(I)*GDSFL(J)*CNST
      ELK(I,J)=ELK(I,J)+AX*S00
40  CONTINUE
80  CONTINUE
  RETURN
  END

```

**Box 3.5.2** Subroutine for the generation of the coefficient matrices in the Newton-Raphson iteration method.

```

SUBROUTINE COEFF (IEL,NPE,F0)
IMPLICIT REAL*8(A-H,O-Z)
DIMENSION GAUSS(5,5),WT(5,5),TANG(3,3)
COMMON /SHP/ SFL(4),GDSFL(4)
COMMON /STF/ STIF(3,3),ELF(3),ELX(3),ELU(3),AX0,AX1,AU
C
DATA GAUSS/5*0.0D0,-0.57735027D0,0.57735027D0,3*0.0D0,
1 -0.77459667D0,0.0D0,0.77459667D0,2*0.0D0,-0.86113631D0,
2 -0.33998104D0,0.33998104D0,0.86113631D0,0.0D0,
3 -0.906180D0,-0.538469D0,0.0D0,0.538469D0,0.906180D0/

DATA WT /2.0D0,4*0.0D0,2*1.0D0,3*0.0D0,0.55555555D0,
1 0.88888888D0,0.55555555D0,2*0.0D0,0.34785485D0,
2 2*0.65214515D0,0.34785485D0,0.0D0,0.2369227D0,
3 0.478629D0,0.568889D0,0.478629D0,0.236927D0/
C
NGP=IEL+1
EL=ELX(IEL+1)-ELX(1)
DO 10 I=1,NPE
  ELF(I)=0.0
  DO 10 J=1,NPE
    TANG(I,J)= 0.0
10  ELK(I,J) = 0.0
DO 80 NI=1,NGP
  XI=GAUSS(NI,NGP)
  CALL SHAPE (EL,ELX,GJ,IEL,NPE,XI)
  CNST=GJ*WT(NI,NGP)
  X=0.0
  U=0.0
  DU=0.0
  DO 20 I=1,NPE
    X=X+SFL(I)*ELX(I)
    U=U+SFL(I)*ELU(I)
    DU=DU+GDSFL(I)*ELU(I)
20  CONTINUE
  AX=AX0+AX1*X+AU*U
  DO 40 I=1,NPE
    ELF(I)=ELF(I)+F0*SFL(I)*CNST
    DO 40 J=1,NPE
      S00=GDSFL(I)*GDSFL(J)*CNST
      S10=GDSFL(I)*SFL(J)*CNST
      ELK(I,J)=ELK(I,J)+AX*S00
      TANG(I,J)=TANG(I,J)+AU*DU*S10
40  CONTINUE
80  CONTINUE
C
C Compute the residual vector and tangent matrix
C
DO 100 I=1,NPE
  DO 100 J=1,NPE
100  ELF(I)=ELF(I)-ELK(I,J)*ELU(J)
  DO 120 I=1,NPE
    DO 120 J=1,NPE
120  ELK(I,J)=ELK(I,J)+TANG(I,J)
C
RETURN
END

```



*Natural boundary conditions*

Next, suppose that  $Q_I$  is specified to be  $\hat{Q}_I$ . Then the force in the  $I$ th equation is augmented with  $\hat{Q}_I$ :

$$GLK(I, NBW) = GLK(I, NBW) + \hat{Q}_I \quad (3.5.3)$$

This is repeated for all  $NSSV$  conditions.

*Mixed boundary conditions*

Finally, we consider mixed boundary conditions of the form

$$Q_I + \beta_I (U_I - U_{\text{ref}}) = 0 \quad (3.5.4)$$

where  $\beta_I$  is a function of  $u$ , say  $\beta_I = \beta_I^0 + \beta_I^1 U_I$ . The boundary condition may be implemented as follows:

$$\begin{aligned} GLK(I, NHBW) &= GLK(I, NHBW) + (\beta_I^0 + \beta_I^1 U_I) \\ GLK(I, NBW) &= GLK(I, NBW) + (\beta_I^0 + \beta_I^1 U_I) U_{\text{ref}} \end{aligned} \quad (3.5.5)$$

The above statement modifies the assembled direct stiffness matrix and source vector in direct iteration procedure. In the case of Newton-Raphson iteration, the assembled tangent matrix is modified as follows:

$$\begin{aligned} GLK(I, NHBW) &= GLK(I, NHBW) + (\beta_I^0 + 2\beta_I^1 U_I) - \beta_I^1 U_{\text{ref}} \\ GLK(I, NBW) &= GLK(I, NBW) - (\beta_I^0 + \beta_I^1 U_I) U_I + (\beta_I^0 + \beta_I^1 U_I) U_{\text{ref}} \end{aligned} \quad (3.5.6)$$

Box 3.5.3 contains a listing of the subroutine that imposes various types of boundary conditions on an banded, unsymmetric system of equations.

The major steps of the two iterative algorithms are summarized below.

1. Read in the convergence tolerance  $TOLR$ , maximum allowable number of iterations  $ITMAX$ , and the initial guess vector  $GUC(I)$ .
2. Initialize the previous solution vector  $\{GUP\} = \{0\}$ .
3. Set the iteration counter,  $ITER = 0$ .
4. Begin the iteration counter on  $ITER = ITER + 1$ .
5. Initialize the global coefficient matrix  $[GLK]$  (and source vector  $\{GLF\}$  if used); when unsymmetric banded solver is used, the last column of  $[GLK]$  takes the place of  $\{GLF\}$ .
6. Calculate the element coefficient matrices  $[ELK]$  using the last iteration solution  $\{GUC\}$  (or a weighted-average of  $\{GUC\}$  and  $\{GUP\}$  when underrelaxation is used) and element source vectors  $\{ELF\}$  and assemble to obtain  $[GLK]$  (and  $\{GLF\}$ ).

**Box 3.5.3** Subroutine for the implementation of various types of boundary conditions.

```

SUBROUTINE BNDYUNSYM(ITYPE,MXNEQ,MXFBW,MXEBC,MXNBC,NDF,NHBW,
1  GLK, GLU,NSPV,NSSV,NSMB,ISPV,ISSV,ISMB,VSPV,VSSV,BETA0,BETAU,UREF)
C
C
C   The subroutine is used to implement specified boundary conditions
C   on BANDED UNSYMMETRIC system of finite element equations
C
C
C   IMPLICIT REAL*8 (A-H,O-Z)
C   DIMENSION ISPV(MXEBC,2),ISSV(MXNBC,2),JSMB(MXNBC,2),VSPV(MXEBC),
1   VSSV(MXEBC),UREF(MXNBC),BETA0(MXNBC),BETAU(MXNBC),
2   GLU(MXNEQ),GLK(MXNEQ,MXFBW)
C
C   NBW=2*NHBW
C
C   Include specified PRIMARY degrees of freedom
C
C   IF(NSPV.NE.0)THEN
C     DO 120 NP=1,NSPV
C       NB=(ISPV(NP,1)-1)*NDF+ISPV(NP,2)
C       DO 110 J=1,NBW
110      GLK(NB,J)=0.0D0
C       GLK(NB,NHBW)=1.0D0
120      GLK(NB,NBW)=VSPV(NP)
C     ENDF
C
C   Modify the source vector to include specified non-zero SECONDARY VARIABLES
C
C   IF(NSSV.NE.0)THEN
C     DO 130 NS=1,NSSV
C       NB=(ISSV(NS,1)-1)*NDF+ISSV(NS,2)
130      GLK(NB,NBW)=GLK(NB,NBW)+VSSV(NS)
C     ENDF
C
C   Implement the specified MIXED BOUNDARY CONDITIONS
C
C   IF(NSMB.NE.0)THEN
C     DO 150 MB=1,NSMB
C       NB=(ISMB(MB,1)-1)*NDF+ISMB(MB,2)
C       IF(ITYPE.LE.1)THEN
C         GLK(NB,NHBW)=GLK(NB,NHBW)+BETA0(MB)+BETAU(MB)*GLU(NB)
C         GLK(NB,NBW)=GLK(NB,NBW)+UREF(MB)*(BETA0(MB)+BETAU(MB)*GLU(NB))
C       ELSE
C         GLK(NB,NHBW)=GLK(NB,NHBW)+BETA0(MB)+2.0*BETAU(MB)*GLU(NB)
*         -UREF(MB)*BETAU(MB)
C         GLK(NB,NBW)=GLK(NB,NBW)+UREF(MB)*(BETA0(MB)+BETAU(MB)*GLU(NB))
*         -(BETA0(MB)+BETAU(MB)*GLU(NB))*GLU(NB)
C       ENDF
150      CONTINUE
C     ENDF
C     RETURN
C     END

```

7. Impose the boundary conditions (the essential boundary conditions must be homogeneous).
8. Solve the equations (solution is returned in the last column of  $[GLK]$ ).
- 9a. In direct iteration, update the current and previous solution vectors  $\{GUP\} = \{GUC\}$  and  $\{GUC\} = \{GLF\}$  ( $\{GLF\} = [GLK]_{\text{last}}$ ).
- 9b. In Newton-Raphson iteration, update the current and previous solution vectors  $\{GUP\} = \{GUC\}$  and  $\{GUC\} = \{GUC\} + \{GLF\}$ .
10. Calculate the residual or solution error,  $ERROR$  [see Eqs. (3.4.2)–(3.4.3)].
11. If  $ERROR \leq TOLR$  print  $ITER, ERROR$ , and  $\{GUC\}$  and stop. If  $ERROR > TOLR$ , continue.
12. If  $ITER > ITMAX$ , stop; otherwise, repeat steps 4 through 11.

**Example 3.5.1**

Consider heat transfer in an isotropic bar of length  $L = 0.18$  m. The surface of the bar is insulated so that there is no convection from the surface. The governing equation of the problem is the same as Eq. (3.1.1) with  $b = c = 0$ ,  $u = T$ , the temperature. The conductivity  $a(x, T) = k$  is assumed to vary according to the relation

$$k = k_0 (1 + \beta T) \tag{3.5.7}$$

where  $k_0$  is the constant thermal conductivity [ $k_0 = 0.2$  W/(m °K)] and  $\beta$  the temperature coefficient of thermal conductivity [ $\beta = 2 \times 10^{-3}$  (°C<sup>-1</sup>)]. Suppose that there is no internal heat generation (i.e.  $f = 0$ ) and the boundary conditions are

$$T(0) = 500^\circ\text{K}, \quad T(L) = 300^\circ\text{K} \tag{3.5.8}$$

Table 3.5.1 shows the linear and nonlinear solutions  $T(x)$ . The results obtained with the direct iteration method and Newton-Raphson method with  $\epsilon = 0.001$  are tabulated in Table 3.5.1. In both methods, the convergent solution was obtained for three iterations. Both methods and both meshes give the same solution.

**Table 3.5.1** Finite element solutions of a nonlinear heat conduction equation.

$x$	DI/NR	Direct Iteration		Newton-Raphson	
	Linear	8L	4Q	8L	4Q
0.0000	500.00	500.00	500.00	500.00	500.00
0.0225	475.00	477.24	477.24	477.24	477.24
0.0450	450.00	453.94	453.94	453.94	453.94
0.0675	425.00	430.06	430.06	430.05	430.05
0.0900	400.00	405.54	405.54	405.54	405.54
0.1125	375.00	380.35	380.35	380.34	380.34
0.1350	350.00	354.40	354.40	354.40	354.40
0.1575	325.00	327.65	327.65	327.65	327.65
0.1800	300.00	300.00	300.00	300.00	300.00

### 3.6 Closing Remarks

In this chapter, finite element formulations of nonlinear boundary-value problems in one dimension are discussed, iterative methods of solving the nonlinear algebraic equations are studied, and computer implementation of the nonlinear finite element analysis is outlined. The simple class of problems discussed herein should give the reader a clear understanding of the workings of nonlinear finite element analysis steps. In the next chapter we will consider multi-variable, one-dimensional, nonlinear equations governing bending and stretching of straight beams.

### Problems

3.1 Consider the second-order differential equation

$$-\frac{d}{dx} \left( \mu \frac{du}{dx} \right) = f(x), \quad \mu = \mu_0 \left( \frac{du}{dx} \right)^{n-1} \quad (\text{a})$$

where  $u(x)$  is the dependent unknown,  $f(x)$  is a known function of position  $x$ , and  $\mu$  is a function of the dependent variable, as given in Eq. (a). Write the finite element model and derive the tangent stiffness matrix coefficients.

3.2 Compute the tangent matrix for the case  $a(x, u) = a_0^e(x) \frac{du}{dx}$ ,  $c(x, u) = 0$ , and  $\beta = 0$  (see Example 3.4.2).

3.3 Consider the nonlinear differential equation

$$-\frac{d}{dx} \left[ (u + \sqrt{2}) \frac{du}{dx} \right] = 1, \quad 0 < x < 1 \quad (\text{a})$$

$$\frac{du}{dx}(0) = 0, \quad u(1) = 0 \quad (\text{b})$$

Analyze the nonlinear problem using the finite element method with direct iteration procedure. Tabulate the nodal values of  $u(x)$  for 4 and 8 linear elements and 2 and 4 quadratic elements.

3.4 Formulate Problem 3.2 with Newton-Raphson iteration procedure, and compute the tangent coefficient matrix. Tabulate the nodal values of  $u(x)$  for 4 and 8 linear elements and 2 and 4 quadratic elements.

3.5 Formulate the nonlinear differential equation

$$-\frac{d^2 u}{dx^2} + 2u^3 = 0, \quad 1 < x < 2 \quad (\text{a})$$

$$u(1) = 1, \quad \left[ \frac{du}{dx} + u^2 \right]_{x=2} = 0 \quad (\text{b})$$

using the finite element method, and solve the problem using direct iteration procedure. Tabulate the nodal values of  $u(x)$  for 4 and 8 linear elements and 2 and 4 quadratic elements. The exact solution is given by  $u(x) = 1/x$ .

3.6 Compute the tangent stiffness matrix associated with Problem 3.5, and solve it with Newton-Raphson iteration procedure. Tabulate the nodal values of  $u(x)$  for 4 and 8 linear elements and 2 and 4 quadratic elements.

3.7 Formulate the nonlinear differential equation

$$-\frac{d^2u}{dx^2} - 2u \frac{du}{dx} = 0, \quad 0 < x < 1 \quad (\text{a})$$

$$u(0) = 1, \quad u(1) = 0.5 \quad (\text{b})$$

using the finite element method, and solve the problem using direct iteration procedure. Tabulate the nodal values of  $u(x)$  for 4 and 8 linear elements and 2 and 4 quadratic elements. The exact solution is given by  $u(x) = 1/(1+x)$ .

3.8 Compute the tangent stiffness matrix associated with Problem 3.7, and solve it with Newton-Raphson iteration procedure. Tabulate the nodal values of  $u(x)$  for 4 and 8 linear elements and 2 and 4 quadratic elements.

3.9 Formulate the nonlinear differential equation in Problem 3.7 subject to the boundary conditions

$$u(0) = 1, \quad \left[ \frac{du}{dx} + u^2 \right]_{x=1} = 0 \quad (\text{a})$$

using the finite element method, and solve the problem using direct iteration procedure. Tabulate the nodal values of  $u(x)$  for 4 and 8 linear elements and 2 and 4 quadratic elements. The exact solution is given by  $u(x) = 1/(1+x)$ .

3.10 Compute the tangent stiffness matrix associated with Problem 3.9, and solve it with Newton-Raphson iteration procedure. Tabulate the nodal values of  $u(x)$  for 4 and 8 linear elements and 2 and 4 quadratic elements.

3.11 Formulate the nonlinear differential equation in Problem 3.7 subject to the boundary conditions

$$\left[ \frac{du}{dx} + 2u \right]_{x=0} = 1, \quad \left[ \frac{du}{dx} + u^2 \right]_{x=1} = 0 \quad (\text{a})$$

using the finite element method, and solve the problem using direct iteration procedure. Tabulate the nodal values of  $u(x)$  for 4 and 8 linear elements and 2 and 4 quadratic elements. The exact solution is given by  $u(x) = 1/(1+x)$ .

3.12 Compute the tangent stiffness matrix associated with Problem 3.11, and solve it with Newton-Raphson iteration procedure. Tabulate the nodal values of  $u(x)$  for 4 and 8 linear elements and 2 and 4 quadratic elements.

3.13 Formulate the nonlinear differential equation

$$-\frac{d^2u}{dx^2} - \left( \frac{du}{dx} \right)^3 = 0, \quad 0 < x < 1 \quad (\text{a})$$

$$\left[ \frac{du}{dx} + u \right]_{x=0} = \frac{3}{\sqrt{2}}, \quad \left[ \frac{du}{dx} \right]_{x=1} = 0.5 \quad (\text{b})$$

using the finite element method, and solve the problem using direct iteration procedure. Tabulate the nodal values of  $u(x)$  for 4 and 8 linear elements and 2 and 4 quadratic elements. The exact solution is given by  $u(x) = \sqrt{2(1+x)}$ .

3.14 Consider simultaneous steady-state conduction and radiation in a plate. The mathematical formulation of the problem in non-dimensional form is given by

$$-\frac{d}{d\xi} \left( k(\theta) \frac{d\theta}{d\xi} \right) = 0, \quad 0 < \xi < \xi_0 \quad (\text{a})$$

$$\theta(0) = \theta_0, \quad \theta(\xi_0) = 1.0 \quad (\text{b})$$

where  $\xi$  is the non-dimensional thickness coordinate,  $\theta$  is the non-dimensional temperature, and  $k$  is the conductivity

$$k(\theta) = k_0 \left( 1 + \frac{4}{3N} \theta^3 \right) \quad (c)$$

and  $N$  is called the conduction-to-radiation parameter. Develop the finite element model of the problem and compute the element tangent matrix.

- 3.15 Analyze the nonlinear problem in Problem 3.14 using the finite element method with Newton-Raphson iteration procedure. Take  $k_0 = 1$ ,  $N = 0.01$ ,  $\xi_0 = 1$ , and  $\theta_0 = 0.5$ . Tabulate and plot the nodal values of  $\theta(\xi)$  for 8 linear elements and 4 quadratic elements.
- 3.16 The explosion of a solid explosive material in the form of an infinite cylinder may be described by [3]

$$-\frac{1}{r} \frac{d}{dr} \left( r \frac{du}{dr} \right) = 2e^u, \quad 0 < r < 1$$

subject to the boundary conditions

$$\text{At } r = 0: \frac{du}{dr} = 0; \quad \text{At } r = 1: u = 0$$

The exact solution of the nonlinear equation is

$$u(r) = \ln \frac{4}{(1+r^2)^2}$$

Analyze the nonlinear problem using the finite element method with (a) Newton-Raphson and (b) direct iteration procedure. Tabulate and plot the nodal values of  $u(r)$  for 8 linear elements and 4 quadratic elements and compare with the exact solution.

- 3.17 Redo Problem 3.16 when the right-hand side is replaced by  $e^u$ . This problem has two solutions

$$u_i(r) = \ln \frac{8\lambda_i}{(1+\lambda_i r^2)^2}, \quad i = 1, 2$$

where  $\lambda_i$  are the roots of the equation

$$\frac{8\lambda}{(1+\lambda)^2} = 1$$

- 3.18 Heat and mass transfer within a porous catalyst particle is described by [3]

$$\frac{d^2u}{dr^2} + \frac{a}{r} \frac{du}{dr} = b^2u \exp \left[ \frac{c(1-u)}{1+d(1-u)} \right], \quad 0 < r < 1$$

subject to the boundary conditions

$$\text{At } r = 0: \frac{du}{dr} = 0; \quad \text{At } r = 1: u = 1$$

Here  $a$ ,  $b$ ,  $c$ , and  $d$  are the problem parameters. Analyze the nonlinear problem using the finite element method with the direct iteration procedure. Take  $a = 0$ ,  $b = 1$ ,  $c = 2$  and  $d = 0.1$ , and tabulate and plot the solutions  $u(r)$  for meshes of 8 linear elements and 4 quadratic elements.

- 3.19 Repeat Problem 3.18 with the data  $a = 2$ ,  $b = 2$ ,  $c = 4$  and  $d = 0.2$ .

**3.20** Repeat Problem 3.18 with the data  $a = 0$ ,  $b = 0.16$ ,  $c = 14$  and  $d = 0.7$ . The problem has three possible numerical solutions.

**3.21** Axial mixing in an isothermal tubular reactor where a second-order reaction occurs is described by [3]

$$-\frac{1}{\text{Pe}} \frac{d^2 u}{dx^2} + \frac{du}{dx} + \text{Da} u^2 = 0, \quad 0 < x < 1$$

subject to the boundary conditions

$$\text{At } x = 0: u = 1 + \frac{1}{\text{Pe}} \frac{du}{dx}; \quad \text{At } x = 1: \frac{du}{dx} = 0$$

where Pe and Da are the problem parameters. Analyze the nonlinear problem using the finite element method with the direct iteration procedure. Take Pe=5 and Da=1, and tabulate and plot the solution  $u(x)$  for 8 linear elements.

**3.22** Consider the pair of nonlinear differential equations

$$\frac{d^3 u}{dx^3} + \frac{1}{6} \left( \frac{d^2 u}{dx^2} \right)^2 v \frac{dv}{dx} = 0, \quad \frac{d^2 v}{dx^2} + \frac{1}{2} \frac{du}{dx} \left( \frac{dv}{dx} \right)^3 = 0$$

subject to the boundary conditions

$$u(0) = v(0) = 1, \quad u(1) = 16, \quad \frac{dv}{dx}(0) = -1, \quad v(1) = 0.5$$

Formulate the finite element model of the equations and compute the tangent coefficient matrix.

**3.23** Consider the pair of nonlinear differential equations

$$\begin{aligned} -\frac{1}{\text{Pe}} \frac{d^2 u}{dx^2} + \frac{du}{dx} + \beta(u - u_c) &= \alpha \text{Da} (1 - v) \exp\left(\frac{u}{1 + u/\gamma}\right), \\ -\frac{1}{\text{Pe}} \frac{d^2 v}{dx^2} + \frac{dv}{dx} &= \text{Da} (1 - v) \exp\left(\frac{u}{1 + u/\gamma}\right) \end{aligned}$$

in  $(0,1)$  and subject to the boundary conditions

$$\begin{aligned} \text{At } x = 0: \text{Pe } u &= \frac{du}{dx}, \quad \text{Pe } v = \frac{dv}{dx} \\ \text{At } x = 1: \frac{du}{dx} &= 0, \quad \frac{dv}{dx} = 0 \end{aligned}$$

Formulate the finite element model of the equations and compute the tangent coefficient matrix.

## References

1. Reddy, J. N., *An Introduction to the Finite Element Method*, 2nd edn, McGraw-Hill, New York (1993).
2. Sachdev, P. L., *A Compendium on Nonlinear Ordinary Differential Equations*, John Wiley, New York (1997).
3. Kubicek, M. and Hlavacek, V., *Numerical Solution of Nonlinear Boundary Value Problems with Applications*, Prentice-Hall, Englewood Cliffs, NJ (1983).

---

# Nonlinear Bending of Straight Beams

---

## 4.1 Introduction

In this chapter, we consider a slightly more complicated one-dimensional nonlinear problem than that was discussed in Chapter 1. A *beam* is a structural member whose length to cross-sectional dimensions is very large and it undergoes not only stretching along its length but also bending about an axis transverse to the length. When the applied loads on the beam are large, the linear load–deflection relationship ceases to be valid because the beam develops internal forces that resist deformation, and the magnitude of internal forces increases with the loading as well as the deformation. This nonlinear load–deflection response of straight beams is the topic of this section.

In developing a general nonlinear formulation of beams, straight or curved, one must define the measures of stress and strain consistent with the deformations accounted for in the formulation. Such a formulation, called a *continuum formulation*, will be discussed in Chapter 9. The present nonlinear formulation of straight beams is based on assumptions of large transverse displacements, small strains and small to moderate rotations. These assumptions allow us to use the stress measure of force per unit undeformed area and strain measure of change in length to the original length (and in the case of shear strain, change in the angle from  $\pi/2$ ). The changes in the geometry are small so that no distinction between the Piola–Kirchoff and Cauchy stresses (to be discussed in detail later) will be made. The nonlinearity in the formulation comes solely from the inclusion of the inplane forces that are proportional to the square of the rotation of the transverse normal to the beam axis.

Two different theories to model the kinematic behavior of beams are considered here: (1) the Euler–Bernoulli beam theory (EBT) that neglects the transverse shear strain, and (2) the Timoshenko beam theory (TBT), which accounts for the transverse shear strain in the simplest way. In each



case, we begin with an assumed displacement field and compute strains that are consistent with the kinematic assumptions of the theory. Then we develop the weak forms using the principle of virtual displacements and the associated displacement finite element model. We also discuss certain computational aspects (e.g. membrane and shear locking) and iterative methods for the problems at hand. Computer implementation issues are also presented. Discussion of other linear finite element models of the Timoshenko beam theory are also presented for completeness.

## 4.2 Euler–Bernoulli Beams

### 4.2.1 Basic Assumptions

For the sake of completeness, the governing equations of the nonlinear bending of beams are developed from basic considerations. The classical beam theory is based on the Euler–Bernoulli hypothesis that plane sections perpendicular to the axis of the beam before deformation remain (a) plane, (b) rigid (not deform), and (c) rotate such that they remain perpendicular to the (deformed) axis after deformation. The assumptions amount to neglecting the Poisson effect and transverse strains. A refined theory is that due to Timoshenko, and it will be discussed in the sequel. The principle of virtual displacements will be used to formulate the variational problem and associated finite element model.

### 4.2.2 Displacement Field and Strains

The bending of beams with moderately large rotations but with small strains can be derived using the displacement field

$$u_1 = u_0(x) - z \frac{dw_0}{dx}, \quad u_2 = 0, \quad u_3 = w_0(x) \quad (4.2.1)$$

where  $(u_1, u_2, u_3)$  are the total displacements along the coordinate directions  $(x, y, z)$ , and  $u_0$  and  $w_0$  denote the axial and transverse displacements of a point on the neutral axis.

Using the nonlinear strain-displacement relations (sum on repeated subscripts is implied; see Chapter 9)

$$\varepsilon_{ij} = \frac{1}{2} \left( \frac{\partial u_i}{\partial x_j} + \frac{\partial u_j}{\partial x_i} \right) + \frac{1}{2} \left( \frac{\partial u_m}{\partial x_i} \frac{\partial u_m}{\partial x_j} \right) \quad (4.2.2)$$

and omitting the large strain terms but retaining only the square of  $du_3/dx$  (which represents the rotation of a transverse normal line in the beam), we obtain

$$\begin{aligned}
 \varepsilon_{11} = \varepsilon_{xx} &= \frac{du_0}{dx} - z \frac{d^2 w_0}{dx^2} + \frac{1}{2} \left( \frac{dw_0}{dx} \right)^2 \\
 &= \left[ \frac{du_0}{dx} + \frac{1}{2} \left( \frac{dw_0}{dx} \right)^2 \right] - z \left( \frac{d^2 w_0}{dx^2} \right) \\
 &\equiv \varepsilon_{xx}^0 + z \varepsilon_{xx}^1
 \end{aligned} \tag{4.2.3a}$$

$$\varepsilon_{xx}^0 = \frac{du_0}{dx} + \frac{1}{2} \left( \frac{dw_0}{dx} \right)^2, \quad \varepsilon_{xx}^1 = - \frac{d^2 w_0}{dx^2} \tag{4.2.3b}$$

and all other strains are zero. Note that the notation  $x_1 = x$ ,  $x_2 = y$ , and  $x_3 = z$  is used. These strains are known as the *von Kármán strains*.

### 4.2.3 Weak Forms

The weak form of structural problems can be directly derived (i.e. without knowing the governing differential equations) using the principle of virtual displacements. The principle states that *if a body is in equilibrium, the total virtual work done by actual internal as well as external forces in moving through their respective virtual displacements is zero*. The virtual displacements are arbitrary except that they are zero where displacements are prescribed. The analytical form of the principle over a typical element  $\Omega^e = (x_a, x_b)$  (see Figure 4.2.1) is given by (see Reddy [2])

$$\delta W^e \equiv \delta W_I^e - \delta W_E^e = 0 \tag{4.2.4}$$

where  $\delta W_I^e$  is the virtual strain energy stored in the element due to actual stresses  $\sigma_{ij}$  in moving through the virtual strains  $\delta \varepsilon_{ij}$ , and  $\delta W_E^e$  is the work done by externally applied loads in moving through their respective virtual displacements. Here  $\sigma_{ij}$  and  $\varepsilon_{ij}$  denote the Cartesian components of the stress and the Green strain tensors, respectively. Due to the assumption of small strains, no distinction will be made here between the Cauchy and second Piola-Kirchhoff stress tensors (see Chapter 9).

For the beam element, we have

$$\begin{aligned}
 \delta W_I^e &= \int_{V^e} \delta \varepsilon_{ij} \sigma_{ij} dV \\
 \delta W_E^e &= \int_{x_a}^{x_b} q \delta w_0 dx + \int_{x_a}^{x_b} f \delta u_0 dx + \sum_{i=1}^6 Q_i^e \delta \Delta_i^e
 \end{aligned} \tag{4.2.5}$$

where  $V^e$  denotes the element volume,  $q(x)$  is the distributed transverse load (measured per unit length),  $f(x)$  is the distributed axial load (measured per unit length),  $Q_i^e$  are the generalized nodal forces, and  $\delta \Delta_i^e$  are the virtual

generalized nodal displacements of the element (see Figure 4.2.1) defined by

$$\begin{aligned} \Delta_1^e &= u_0(x_a), & \Delta_2^e &= w_0(x_a), & \Delta_3^e &= \left[ -\frac{dw_0}{dx} \right]_{x_a} \equiv \theta(x_a) \\ \Delta_4^e &= u_0(x_b), & \Delta_5^e &= w_0(x_b), & \Delta_6^e &= \left[ -\frac{dw_0}{dx} \right]_{x_b} \equiv \theta(x_b) \end{aligned} \quad (4.2.6a)$$

$$\begin{aligned} Q_1^e &= -N_{xx}(x_a), & Q_4^e &= N_{xx}(x_b) \\ Q_2^e &= -\left[ \frac{dw_0}{dx} N_{xx} + \frac{dM_{xx}}{dx} \right]_{x_a}, & Q_5^e &= \left[ \frac{dw_0}{dx} N_{xx} + \frac{dM_{xx}}{dx} \right]_{x_b} \\ Q_3^e &= -M_{xx}(x_a), & Q_6^e &= M_{xx}(x_b) \end{aligned} \quad (4.2.6b)$$

In view of the explicit nature of the assumed displacement field (4.2.5) in the thickness coordinate  $z$  and its independence of coordinate  $y$ , the volume integral can be expressed as a product of integrals over the length and area of the element:

$$\int_{V^e} (\cdot) dV = \int_{x_a}^{x_b} \int_{A^e} (\cdot) dA dx$$

Therefore, the expression for the virtual strain energy can be simplified as follows (only non-zero components of strain and stress are  $\varepsilon_{11} \equiv \varepsilon_{xx}$  and  $\sigma_{11} \equiv \sigma_{xx}$ )

$$\begin{aligned} \delta W_I^e &= \int_{x_a}^{x_b} \int_{A^e} \delta \varepsilon_{xx} \sigma_{xx} dA dx = \int_{x_a}^{x_b} \int_{A^e} (\delta \varepsilon_{xx}^0 + z \delta \varepsilon_{xx}^1) \sigma_{xx} dA dx \\ &= \int_{x_a}^{x_b} \int_{A^e} \left[ \left( \frac{d\delta u_0}{dx} + \frac{dw_0}{dx} \frac{d\delta w_0}{dx} \right) - z \frac{d^2 \delta w_0}{dx^2} \right] \sigma_{xx} dA dx \\ &= \int_{x_a}^{x_b} \left[ \left( \frac{d\delta u_0}{dx} + \frac{dw_0}{dx} \frac{d\delta w_0}{dx} \right) N_{xx} - \frac{d^2 \delta w_0}{dx^2} M_{xx} \right] dx \end{aligned} \quad (4.2.7)$$

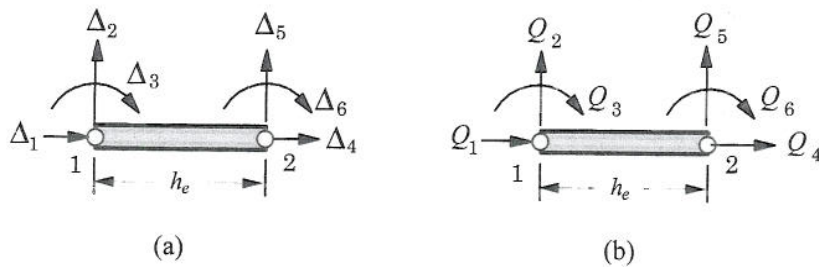


Figure 4.2.1 The Euler-Bernoulli beam finite element with generalized displacement and force degrees of freedom. (a) Nodal displacements. (b) Nodal forces.

where  $N_{xx}$  is the axial force (measured per unit length) and  $M_{xx}$  is the moment (measured per unit length)

$$N_{xx} = \int_{A^e} \sigma_{xx} dA, \quad M_{xx} = \int_{A^e} \sigma_{xx} z dA \quad (4.2.8)$$

The virtual work statement in Eq. (4.2.7) becomes

$$\begin{aligned} 0 = & \int_{x_a}^{x_b} \left[ \left( \frac{d\delta u_0}{dx} + \frac{dw_0}{dx} \frac{d\delta w_0}{dx} \right) N_{xx} - \frac{d^2 \delta w_0}{dx^2} M_{xx} \right] dx \\ & - \int_{x_a}^{x_b} q(x) \delta w_0(x) dx - \int_{x_a}^{x_b} f(x) \delta u_0(x) dx - \sum_{i=1}^6 Q_i^e \delta \Delta_i^e \end{aligned} \quad (4.2.9)$$

The above weak form is equivalent to the following two statements, which are obtained by collecting terms involving  $\delta u_0$  and  $\delta w_0$  separately [see the definitions in Eqs. (4.2.6a,b)]:

$$0 = \int_{x_a}^{x_b} \left( \frac{d\delta u_0}{dx} N_{xx} - \delta u_0 f(x) \right) dx - Q_1^e \delta \Delta_1^e - Q_4^e \delta \Delta_4^e \quad (4.2.10a)$$

$$\begin{aligned} 0 = & \int_{x_a}^{x_b} \left[ \frac{d\delta w_0}{dx} \left( \frac{dw_0}{dx} N_{xx} \right) - \frac{d^2 \delta w_0}{dx^2} M_{xx} - \delta w_0 q(x) \right] dx \\ & - Q_2^e \delta \Delta_2^e - Q_3^e \delta \Delta_3^e - Q_5^e \delta \Delta_5^e - Q_6^e \delta \Delta_6^e \end{aligned} \quad (4.2.10b)$$

The differential equations governing nonlinear bending of straight beams can be obtained, although not needed for finite element model development, from the virtual work statement in (4.2.9), equivalently, the weak forms (4.2.10a,b), or from a vector approach in which forces and moments are summed over a typical beam element.

Integration by parts of the expressions in (4.2.9) to relieve  $\delta u_0$  and  $\delta w_0$  of any differentiation results in

$$\begin{aligned} 0 = & \int_{x_a}^{x_b} \left\{ \left( -\frac{dN_{xx}}{dx} - f \right) \delta u_0 - \left[ \frac{d}{dx} \left( \frac{dw_0}{dx} N_{xx} \right) + \frac{d^2 M_{xx}}{dx^2} + q \right] \delta w_0 \right\} dx \\ & + \left[ N_{xx} \delta u_0 + \left( \frac{dw_0}{dx} N_{xx} + \frac{dM_{xx}}{dx} \right) \delta w_0 - M_{xx} \frac{d\delta w_0}{dx} \right]_{x_a}^{x_b} - \sum_{i=1}^6 Q_i^e \delta \Delta_i^e \end{aligned}$$

Since  $\delta u_0$  and  $\delta w_0$  are arbitrary and independent of each other in  $x_a < x < x_b$  as well as at  $x = x_a$  and  $x = x_b$  (independently), it follows that the governing equations of equilibrium, known as the Euler equations, are

$$\delta u_0 : \quad -\frac{dN_{xx}}{dx} = f(x) \quad (4.2.11a)$$

$$\delta w_0 : \quad -\frac{d}{dx} \left( \frac{dw_0}{dx} N_{xx} \right) - \frac{d^2 M_{xx}}{dx^2} = q(x) \quad (4.2.11b)$$

In view of the definitions (4.2.6a), definitions (4.2.6b) are obtained as the natural (or force) boundary conditions

$$\begin{aligned}
 Q_1^e + N_{xx}(x_a) &= 0, & Q_4^e - N_{xx}(x_b) &= 0 \\
 Q_2^e + \left[ \frac{dw_0}{dx} N_{xx} + \frac{dM_{xx}}{dx} \right]_{x_a} &= 0, & Q_5^e - \left[ \frac{dw_0}{dx} N_{xx} + \frac{dM_{xx}}{dx} \right]_{x_b} &= 0 \\
 Q_3^e + M_{xx}(x_a) &= 0, & Q_6^e - M_{xx}(x_b) &= 0
 \end{aligned}
 \tag{4.2.12}$$

The vector approach involves identifying a typical beam element of length  $\Delta x$  with all its forces and moments, summing them, and taking the limit  $\Delta x \rightarrow 0$ . Consider the beam element shown in Figure 4.2.2, where  $N_{xx}$  is the internal axial force,  $V(x)$  is the internal vertical shear force,  $M_{xx}$  is the internal bending moment,  $f(x)$  is the external axial force, and  $q(x)$  is external distributed transverse load. Summing the forces in the  $x$  and  $z$  coordinate directions, and moments about the  $y$  axis, we obtain

$$\begin{aligned}
 \sum F_x = 0: & \quad -N_{xx} + (N_{xx} + \Delta N_{xx}) + f(x)\Delta x = 0 \\
 \sum F_z = 0: & \quad -V + (V + \Delta V) + q(x)\Delta x = 0 \\
 \sum M_y = 0: & \quad -M_{xx} + (M_{xx} + \Delta M_{xx}) - V\Delta x + N_{xx}\Delta x \frac{dw_0}{dx} \\
 & \quad + q(x)\Delta x(c\Delta x) = 0
 \end{aligned}$$

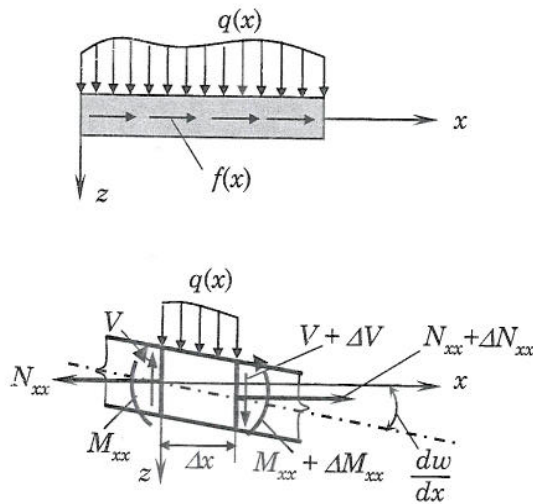


Figure 4.2.2 A typical beam element with forces and moments to derive equations of equilibrium using the vector approach.

Taking the limit  $\Delta x \rightarrow 0$ , we obtain the following three equations:

$$\begin{aligned}\frac{dN_{xx}}{dx} + f(x) &= 0 \\ \frac{dV}{dx} + q(x) &= 0 \\ \frac{dM_{xx}}{dx} - V + N_{xx} \frac{dw_0}{dx} &= 0\end{aligned}$$

which are equivalent to the two equations in (4.2.11a,b). Note that  $V$  is the shear force on a section perpendicular to the  $x$ -axis, and it is not equal to the shear force  $Q(x)$  acting on the section perpendicular to the deformed beam. In fact, one can show that  $V = Q + N_{xx}(dw_0/dx)$ .

If one starts with the governing equations (4.2.11a,b), their weak forms can be developed using the usual three-step procedure:

$$\begin{aligned}0 &= \int_{x_a}^{x_b} v_1 \left( -\frac{dN_{xx}}{dx} - f \right) dx \\ &= \int_{x_a}^{x_b} \left( \frac{dv_1}{dx} N_{xx} - v_1 f \right) dx - [v_1 N_{xx}]_{x_a}^{x_b} \\ &= \int_{x_a}^{x_b} \left( \frac{dv_1}{dx} N_{xx} - v_1 f \right) dx - v_1(x_a)[-N_{xx}(x_a)] - v_1(x_b)N_{xx}(x_b) \quad (4.2.13a) \\ 0 &= \int_{x_a}^{x_b} v_2 \left[ -\frac{d}{dx} \left( \frac{dw_0}{dx} N_{xx} \right) - \frac{d^2 M_{xx}}{dx^2} - q \right] dx \\ &= \int_{x_a}^{x_b} \left[ \frac{dv_2}{dx} \left( \frac{dw_0}{dx} N_{xx} \right) - \frac{d^2 v_2}{dx^2} M_{xx} - v_2 q \right] dx \\ &\quad - \left[ v_2 \left( \frac{dw_0}{dx} N_{xx} + \frac{dM_{xx}}{dx} \right) \right]_{x_a}^{x_b} - \left[ \left( -\frac{dv_2}{dx} \right) M_{xx} \right]_{x_a}^{x_b} \\ &= \int_{x_a}^{x_b} \left[ \frac{dv_2}{dx} \left( \frac{dw_0}{dx} N_{xx} \right) - \frac{d^2 v_2}{dx^2} M_{xx} - v_2 q \right] dx \\ &\quad - v_2(x_a) \left[ -\left( \frac{dw_0}{dx} N_{xx} - \frac{dM_{xx}}{dx} \right) \right]_{x_a} - v_2(x_b) \left[ \frac{dw_0}{dx} N_{xx} + \frac{dM_{xx}}{dx} \right]_{x_b} \\ &\quad - \left[ -\frac{dv_2}{dx} \right]_{x_a} [-M_{xx}(x_a)] - \left[ -\frac{dv_2}{dx} \right]_{x_b} M_{xx}(x_b) \quad (4.2.13b)\end{aligned}$$

where  $v_1$  and  $v_2$  are the weight functions, whose meaning is obvious if the expressions  $f v_1 dx$  and  $q v_2 dx$  are to represent the work done by external forces. We see that  $v_1 \sim \delta u_0$  and  $v_2 \sim \delta w_0$ . Clearly, Eqs. (4.2.13a,b) are the same, with the definitions (4.2.6b) or (4.2.12), as those in Eqs. (4.2.10a,b).

The resultant force  $N_{xx}$  and moment  $M_{xx}$  can be expressed in terms of the displacements once the constitutive behavior is assumed. Suppose that the

beam is made of a *linear elastic material*. Then the total stress is related to the total strain by Hooke's law

$$\sigma_{xx} = E^e \varepsilon_{xx} \quad (4.2.14)$$

Then we have

$$\begin{aligned} N_{xx} &= \int_{A^e} \sigma_{xx} dA = \int_{A^e} E^e \varepsilon_{xx} dA \\ &= \int_{A^e} E^e \left[ \frac{du_0}{dx} + \frac{1}{2} \left( \frac{dw_0}{dx} \right)^2 - z \frac{d^2 w_0}{dx^2} \right] dA \\ &= A_{xx}^e \left[ \frac{du_0}{dx} + \frac{1}{2} \left( \frac{dw_0}{dx} \right)^2 \right] - B_{xx}^e \frac{d^2 w_0}{dx^2} \end{aligned} \quad (4.2.15a)$$

$$\begin{aligned} M_{xx} &= \int_{A^e} \sigma_{xx} z dA = \int_{A^e} E^e \varepsilon_{xx} z dA \\ &= \int_{A^e} E^e \left[ \frac{du_0}{dx} + \frac{1}{2} \left( \frac{dw_0}{dx} \right)^2 - z \frac{d^2 w_0}{dx^2} \right] z dA \\ &= B_{xx}^e \left[ \frac{du_0}{dx} + \frac{1}{2} \left( \frac{dw_0}{dx} \right)^2 \right] - D_{xx}^e \frac{d^2 w_0}{dx^2} \end{aligned} \quad (4.2.15b)$$

where  $A_{xx}^e$ ,  $B_{xx}^e$ , and  $D_{xx}^e$  are the extensional, extensional-bending, and bending stiffnesses of the beam element

$$(A_{xx}^e, B_{xx}^e, D_{xx}^e) = \int_{A^e} E^e (1, z, z^2) dA \quad (4.2.16)$$

For beams made of an isotropic material, the extensional-bending stiffness  $B_{xx}^e$  is zero when the  $x$ -axis is taken along the geometric centroidal axis. We have  $B_{xx}^e = 0$ ,  $A_{xx}^e = E^e A^e$ , and  $D_{xx}^e = E^e I^e$ , where  $A^e$  and  $I^e$  are the cross-sectional area and second moment of inertia (about the  $y$ -axis) of the beam element. For simplicity, we shall omit the element label  $e$  on the variables. In general,  $A_{xx}$ ,  $B_{xx}$ , and  $D_{xx}$  are functions of  $x$  whenever the modulus  $E$  and/or the cross-sectional area is a function of  $x$ .

The virtual work statements (4.2.10a,b) can be expressed in terms of the generalized displacements ( $u_0, w_0$ ) by using Eqs. (4.2.15a,b). We have

$$\begin{aligned} 0 &= \int_{x_a}^{x_b} A_{xx} \frac{d\delta u_0}{dx} \left[ \frac{du_0}{dx} + \frac{1}{2} \left( \frac{dw_0}{dx} \right)^2 \right] dx - \int_{x_a}^{x_b} f(x) \delta u_0 dx \\ &\quad - Q_1 \delta u_0(x_a) - Q_4 \delta u_0(x_b) \end{aligned} \quad (4.2.17a)$$

$$\begin{aligned} 0 &= \int_{x_a}^{x_b} \left\{ A_{xx} \frac{d\delta w_0}{dx} \frac{dw_0}{dx} \left[ \frac{du_0}{dx} + \frac{1}{2} \left( \frac{dw_0}{dx} \right)^2 \right] + D_{xx} \frac{d\delta^2 w_0}{dx^2} \frac{d^2 w_0}{dx^2} \right\} dx \\ &\quad - \int_{x_a}^{x_b} q \delta w_0 dx - Q_2 \delta w_0(x_a) - Q_3 \delta \theta(x_a) - Q_5 \delta w_0(x_b) - Q_6 \delta \theta(x_b) \end{aligned} \quad (4.2.17b)$$

where it is assumed that the coupling coefficient  $B_{xx}$  is zero because of the choice of the coordinate system; that is, the  $x$ -axis is assumed to coincide with the geometric centroidal axis  $\int_A z dA = 0$ .

#### 4.2.4 Finite Element Model

Let the axial displacement  $u_0(x)$  and transverse deflection  $w_0(x)$  are interpolated as  $[\theta = -(dw_0/dx)]$

$$u_0(x) = \sum_{j=1}^2 u_j \psi_j(x), \quad w_0(x) = \sum_{j=1}^4 \bar{\Delta}_j \phi_j(x) \quad (4.2.18)$$

$$\bar{\Delta}_1 \equiv w_0(x_a), \quad \bar{\Delta}_2 \equiv \theta(x_a), \quad \bar{\Delta}_3 \equiv w_0(x_b), \quad \bar{\Delta}_4 \equiv \theta(x_b) \quad (4.2.19)$$

and  $\psi_j$  are the linear Lagrange interpolation functions, and  $\phi_j$  are the Hermite cubic interpolation functions. For a linear problem, this element gives exact nodal displacements  $u_i$  and  $\bar{\Delta}_i$  for any  $f(x)$  and  $q(x)$  when  $A_{xx}$  and  $D_{xx}$  are element-wise constants. Then the element is said to be a *superconvergent* element.

Substituting Eq. (4.2.18) for  $u_0(x)$ , (4.2.19) for  $w_0(x)$ , and  $\delta u_0(x) = \psi_i(x)$  and  $\delta w_0(x) = \phi_i(x)$  (to obtain the  $i$ th algebraic equation of the model) into the weak forms (4.2.17a,b), we obtain

$$0 = \sum_{j=1}^2 K_{ij}^{11} u_j + \sum_{J=1}^4 K_{iJ}^{12} \bar{\Delta}_J - F_i^1 \quad (i = 1, 2) \quad (4.2.20a)$$

$$0 = \sum_{j=1}^2 K_{Ij}^{21} u_j + \sum_{J=1}^4 K_{IJ}^{22} \bar{\Delta}_J - F_I^2 \quad (I = 1, 2, 3, 4) \quad (4.2.20b)$$

where

$$\begin{aligned} K_{ij}^{11} &= \int_{x_a}^{x_b} A_{xx} \frac{d\psi_i}{dx} \frac{d\psi_j}{dx} dx, \quad K_{iJ}^{12} = \frac{1}{2} \int_{x_a}^{x_b} \left( A_{xx} \frac{dw_0}{dx} \right) \frac{d\psi_i}{dx} \frac{d\phi_J}{dx} dx \\ K_{Ij}^{21} &= \int_{x_a}^{x_b} A_{xx} \frac{dw_0}{dx} \frac{d\phi_I}{dx} \frac{d\psi_j}{dx} dx, \quad K_{IJ}^{21} = 2K_{jI}^{12} \\ K_{IJ}^{22} &= \int_{x_a}^{x_b} D_{xx} \frac{d^2\phi_I}{dx^2} \frac{d^2\phi_J}{dx^2} dx + \frac{1}{2} \int_{x_a}^{x_b} \left[ A_{xx} \left( \frac{dw_0}{dx} \right)^2 \right] \frac{d\phi_I}{dx} \frac{d\phi_J}{dx} dx \\ F_i^1 &= \int_{x_a}^{x_b} f \psi_i dx + \hat{Q}_i, \quad F_I^2 = \int_{x_a}^{x_b} q \phi_I dx + \bar{Q}_I \end{aligned} \quad (4.2.21)$$

for  $(i, j = 1, 2)$  and  $(I, J = 1, 2, 3, 4)$ , where  $\hat{Q}_1 = Q_1$ ,  $\hat{Q}_2 = Q_4$ ,  $\bar{Q}_1 = Q_2$ ,  $\bar{Q}_2 = Q_3$ ,  $\bar{Q}_3 = Q_5$ , and  $\bar{Q}_4 = Q_6$ . See Eq. (4.2.6b) for the definitions of  $Q_i$ . Note that the coefficient matrices  $[K^{12}]$ ,  $[K^{21}]$  and  $[K^{22}]$  are functions of the



unknown  $w_0(x)$ . Also, note that  $[K^{12}]^T \neq [K^{21}]$ ; hence, the element direct stiffness matrix is unsymmetric.

The above definition of coefficients  $K_{ij}^{\alpha\beta}$  is based on a particular linearization of Eqs. (4.2.17a,b), which is probably the most natural. Other forms of linearization are possible. For example, if consider Eq. (4.2.17a), the coefficient of  $d\delta u_0/dx$  contains a linear term and a nonlinear term. To preserve the linear bar stiffness, the linear term should be kept as a part of the stiffness matrix. The nonlinear term can be either included in the stiffness coefficient, as is done in the definition given in Eq. (4.2.21), or the whole nonlinear term may be assumed to be known from the previous iteration. In the latter case, the term ends up in the load vector  $\{F^1\}$ . This choice of linearization is known to slow down the convergence. In the case of Eq. (4.2.17b), we know that the term  $dw_0/dx$  outside the square brackets is due to the nonlinear strain. Hence, it was linearized (i.e. calculated using the solution from the previous iteration) in defining  $K_{ij}^{21}$  of Eq. (4.2.21). One may linearize Eq. (4.2.17b) such that  $du_0/dx + 0.5(dw_0/dx)^2$  is calculated using the solution from the previous iteration. In that case  $K_{ij}^{21} = 0$  and  $K_{ij}^{22}$  will have additional contribution. Thus, it is possible to computationally decouple the equations for  $\{u\}$  and  $\{\bar{\Delta}\}$  and solve the two equations iteratively, feeding the solution from one equation to the other. However, such a strategy often results in nonconvergence.

Equations (4.2.20a,b) can be written compactly as

$$\sum_{\gamma=1}^2 \sum_{p=1}^2 K_{ip}^{\alpha\gamma} \Delta_p^\gamma = F_i^\alpha, \quad \text{or} \quad \sum_{p=1}^2 K_{ip}^{\alpha 1} u_p + \sum_{P=1}^4 K_{iP}^{\alpha 2} \bar{\Delta}_P = F_i^\alpha \quad (4.2.22)$$

In matrix form, we have

$$\begin{bmatrix} [K^{11}] & [K^{12}] \\ [K^{21}] & [K^{22}] \end{bmatrix} \begin{Bmatrix} \{\Delta^1\} \\ \{\Delta^2\} \end{Bmatrix} = \begin{Bmatrix} \{F^1\} \\ \{F^2\} \end{Bmatrix} \quad (4.2.23)$$

where

$$\Delta_i^1 = u_i, \quad i = 1, 2; \quad \Delta_i^2 = \bar{\Delta}_i, \quad i = 1, 2, 3, 4 \quad (4.2.24)$$

Note that the direct stiffness matrix is unsymmetric only due to the fact that  $[K^{12}]$  contains the factor 1/2 whereas  $[K^{21}]$  does not. One way to make  $[K^{21}]^T = [K^{12}]$  is to split the linear strain  $du_0/dx$  in Eq. (4.2.17) into two equal parts and take one of the two parts as known from a previous iteration:

$$\begin{aligned} & \int_{x_a}^{x_b} \left\{ A_{xx}^e \frac{d\delta w_0}{dx} \frac{dw_0}{dx} \left[ \frac{du_0}{dx} + \frac{1}{2} \left( \frac{dw_0}{dx} \right)^2 \right] \right\} dx \\ &= \frac{1}{2} \int_{x_a}^{x_b} A_{xx}^e \left\{ \frac{dw_0}{dx} \frac{d\delta w_0}{dx} \frac{du_0}{dx} + \left[ \frac{du_0}{dx} + \left( \frac{dw_0}{dx} \right)^2 \right] \frac{d\delta w_0}{dx} \frac{dw_0}{dx} \right\} dx \end{aligned} \quad (4.2.25)$$

The first term of the above equation constitutes  $[K^{21}]$  and the second one constitutes a part of  $[K^{22}]$ . The symmetrized equations are

$$\begin{bmatrix} [\bar{K}^{11}] & [\bar{K}^{12}] \\ [\bar{K}^{21}] & [\bar{K}^{22}] \end{bmatrix} \begin{Bmatrix} \{u\} \\ \{\Delta\} \end{Bmatrix} = \begin{Bmatrix} \{F^1\} \\ \{F^2\} \end{Bmatrix} \quad (4.2.26)$$

where

$$\begin{aligned} \bar{K}_{ij}^{11} &= K_{ij}^{11} = \int_{x_a}^{x_b} A_{xx}^e \frac{d\psi_i}{dx} \frac{d\psi_j}{dx} dx \\ \bar{K}_{iJ}^{12} &= K_{iJ}^{12} = \frac{1}{2} \int_{x_a}^{x_b} \left( A_{xx}^e \frac{dw_0}{dx} \right) \frac{d\psi_i}{dx} \frac{d\phi_J}{dx} dx \\ \bar{K}_{Ij}^{21} &= \frac{1}{2} \int_{x_a}^{x_b} \left( A_{xx}^e \frac{dw_0}{dx} \right) \frac{d\phi_I}{dx} \frac{d\psi_j}{dx} dx, \quad \bar{K}_{Ij}^{21} = \bar{K}_{jI}^{12} \\ \bar{K}_{IJ}^{22} &= \int_{x_a}^{x_b} D_{xx}^e \frac{d^2\phi_I}{dx^2} \frac{d^2\phi_J}{dx^2} dx \\ &\quad + \frac{1}{2} \int_{x_a}^{x_b} A_{xx}^e \left[ \frac{du_0}{dx} + \left( \frac{dw_0}{dx} \right)^2 \right] \frac{d\phi_I}{dx} \frac{d\phi_J}{dx} dx \end{aligned} \quad (4.2.27)$$

Note that in the symmetrized case, we must assume that  $u_0(x)$  is also known from a previous iteration.

#### 4.2.5 Iterative Solutions of Nonlinear Equations

The direct iteration and Newton-Raphson methods introduced in Chapter 3 are revisited here in connection with the nonlinear finite element equations of the EBT. Consider the nonlinear equations (4.2.23), which can be written as

$$[K^e(\{\Delta^e\})]\{\Delta^e\} = \{F^e\} \quad (4.2.28)$$

where

$$\Delta_1^e = u_1, \Delta_2^e = \bar{\Delta}_1^e, \Delta_3^e = \bar{\Delta}_2^e, \Delta_4^e = u_2, \Delta_5^e = \bar{\Delta}_3^e, \Delta_6^e = \bar{\Delta}_4^e \quad (4.2.29a)$$

$$F_1^e = F_1^1, F_2^e = F_1^2, F_3^e = F_2^2, F_4^e = F_2^1, F_5^e = F_3^2, F_6^e = F_4^2 \quad (4.2.29b)$$

The system (4.2.28) of nonlinear algebraic equations can be linearized using the direct iteration and Newton-Raphson iterative methods of Section 3.4. These are presented next. Note that the linearized equations may be symmetric or unsymmetric, depending on the formulation, and therefore an appropriate equation solver must be used. On the other hand, an unsymmetric banded equations solver may be used in all cases.

*Direct iteration procedure*

In the direct iteration procedure, the solution at the  $r$ th iteration is determined from the assembled set of equations

$$[K(\{\Delta\}^{(r-1)})]\{\Delta\}^r = \{F\} \quad \text{or} \quad [\bar{K}(\{\Delta\}^{(r-1)})]\{\Delta\}^r = \{F\} \quad (4.2.30)$$

where the direct stiffness matrix  $[K^e]$  is evaluated at the element level using the known solution  $\{\Delta^e\}^{(r-1)}$  at the  $(r-1)$ st iteration.

*Newton-Raphson iteration procedure*

In the Newton-Raphson procedure, the linearized element equation is of the form

$$[T(\{\Delta\}^{(r-1)})]\{\Delta\}^r = -\{R(\{\Delta\}^{(r-1)})\} = \{F\} - ([K^e]\{\Delta^e\})^{(r-1)} \quad (4.2.31)$$

where the tangent stiffness matrix  $[T^e]$  associated with the Euler-Bernoulli beam element is calculated using the definition

$$[T] \equiv \left( \frac{\partial \{R\}}{\partial \{\Delta\}} \right)^{(r-1)}, \quad \text{or} \quad T_{ij}^e \equiv \left( \frac{\partial R_i^e}{\partial \Delta_j^e} \right)^{(r-1)} \quad (4.2.32)$$

The solution at the  $r$ th iteration is then given by

$$\{\Delta\}^r = \{\Delta\}^{(r-1)} + \{\delta\Delta\} \quad (4.2.33)$$

Although the direct stiffness matrix  $[K^e]$  is unsymmetric, it can be shown that the tangent stiffness matrix  $[T^e]$  is symmetric. Further, it can be shown that the tangent stiffness matrix is the same whether one uses  $[K^e]$  or  $[\bar{K}^e]$  [see Eqs. (4.2.23) and (4.2.26)].

The coefficients of the element tangent stiffness matrix  $[T^e]$  can be computed using the definition in (4.2.32). In terms of the components defined in Eq. (4.2.22), we can write

$$T_{ij}^{\alpha\beta} = \left( \frac{\partial R_i^\alpha}{\partial \Delta_j^\beta} \right)^{(r-1)} \quad (4.2.34)$$

for  $\alpha, \beta = 1, 2$ . The components of the residual vector can be expressed as

$$\begin{aligned} R_i^\alpha &= \sum_{\gamma=1}^2 \sum_{p=1}^2 K_{ip}^{\alpha\gamma} \Delta_p^\gamma - F_i^\alpha \\ &= \sum_{p=1}^2 K_{ip}^{\alpha 1} \Delta_p^1 + \sum_{P=1}^4 K_{iP}^{\alpha 2} \Delta_P^2 - F_i^\alpha \\ &= \sum_{p=1}^2 K_{ip}^{\alpha 1} u_p + \sum_{P=1}^4 K_{iP}^{\alpha 2} \bar{\Delta}_P - F_i^\alpha \end{aligned} \quad (4.2.35)$$

Note that the range of  $p$  is dictated by the size of the matrix  $[K^{\alpha\beta}]$ . We have

$$\begin{aligned}
 T_{ij}^{\alpha\beta} &= \left( \frac{\partial R_i^\alpha}{\partial \Delta_j^\beta} \right) = \frac{\partial}{\partial \Delta_j^\beta} \left( \sum_{\gamma=1}^2 \sum_{p=1}^2 K_{ip}^{\alpha\gamma} \Delta_p^\gamma - F_i^\alpha \right) \\
 &= \sum_{\gamma=1}^2 \sum_{p=1}^2 \left( K_{ip}^{\alpha\gamma} \frac{\partial \Delta_p^\gamma}{\partial \Delta_j^\beta} + \frac{\partial K_{ip}^{\alpha\gamma}}{\partial \Delta_j^\beta} \Delta_p^\gamma \right) \\
 &= K_{ij}^{\alpha\beta} + \sum_{p=1}^2 \frac{\partial}{\partial \Delta_j^\beta} (K_{ip}^{\alpha 1}) u_p + \sum_{P=1}^4 \frac{\partial}{\partial \Delta_j^\beta} (K_{iP}^{\alpha 2}) \bar{\Delta}_P \quad (4.2.36)
 \end{aligned}$$

We compute the tangent stiffness matrix coefficients  $T_{ij}^{\alpha\beta}$  explicitly as shown below:

$$\begin{aligned}
 T_{ij}^{11} &= K_{ij}^{11} + \sum_{p=1}^2 \frac{\partial K_{ip}^{11}}{\partial u_j} u_p + \sum_{P=1}^4 \frac{\partial K_{iP}^{12}}{\partial u_j} \bar{\Delta}_P \\
 &= K_{ij}^{11} + \sum_{p=1}^2 0 \cdot u_p + \sum_{P=1}^4 0 \cdot \bar{\Delta}_P \quad (4.2.37)
 \end{aligned}$$

Since

$$\frac{\partial K_{ij}^{\alpha\beta}}{\partial u_k} = 0 \text{ for all } \alpha, \beta, i, j \text{ and } k \quad (4.2.38)$$

the coefficients  $[T^{11}]$  and  $[T^{21}]$  of the tangent stiffness matrix are the same as those of the direct stiffness matrix:

$$[T^{11}] = [K^{11}] \quad , \quad [T^{21}] = [K^{21}] \quad (4.2.39)$$

Next consider

$$\begin{aligned}
 T_{iJ}^{12} &= K_{iJ}^{12} + \sum_{p=1}^2 \left( \frac{\partial K_{ip}^{11}}{\partial \bar{\Delta}_J} \right) u_p + \sum_{P=1}^4 \left( \frac{\partial K_{iP}^{12}}{\partial \bar{\Delta}_J} \right) \bar{\Delta}_P \\
 &= K_{iJ}^{12} + 0 + \sum_{P=1}^4 \left[ \int_{x_a}^{x_b} \frac{1}{2} A_{xx} \frac{\partial}{\partial \bar{\Delta}_J} \left( \frac{dw_0}{dx} \right) \frac{d\psi_i}{dx} \frac{d\phi_P}{dx} dx \right] \bar{\Delta}_P \\
 &= K_{iJ}^{12} + \sum_{P=1}^4 \left[ \int_{x_a}^{x_b} \frac{1}{2} A_{xx} \frac{\partial}{\partial \bar{\Delta}_J} \left( \sum_K^4 \bar{\Delta}_K \frac{d\phi_K}{dx} \right) \frac{d\psi_i}{dx} \frac{d\phi_P}{dx} dx \right] \bar{\Delta}_P \\
 &= K_{iJ}^{12} + \sum_{P=1}^4 \left[ \int_{x_a}^{x_b} \frac{1}{2} A_{xx} \frac{d\phi_J}{dx} \frac{d\psi_i}{dx} \frac{d\phi_P}{dx} dx \right] \bar{\Delta}_P \\
 &= K_{iJ}^{12} + \int_{x_a}^{x_b} \frac{1}{2} A_{xx} \frac{d\psi_i}{dx} \frac{d\phi_J}{dx} \left( \sum_{P=1}^4 \frac{d\phi_P}{dx} \bar{\Delta}_P \right) dx
 \end{aligned}$$

$$\begin{aligned}
&= K_{iJ}^{12} + \int_{x_a}^{x_b} \left( \frac{1}{2} A_{xx} \frac{dw_0}{dx} \right) \frac{d\psi_i}{dx} \frac{d\phi_J}{dx} dx \\
&= K_{iJ}^{12} + K_{iJ}^{12} = 2K_{iJ}^{12} = K_{ji}^{21}
\end{aligned} \tag{4.2.40}$$

$$\begin{aligned}
T_{IJ}^{22} &= K_{IJ}^{22} + \sum_{p=1}^2 \left( \frac{\partial K_{IP}^{21}}{\partial \bar{\Delta}_J} \right) u_p + \sum_{P=1}^4 \left( \frac{\partial K_{IP}^{22}}{\partial \bar{\Delta}_J} \right) \bar{\Delta}_P \\
&= K_{IJ}^{22} + \sum_{p=1}^2 \left[ \int_{x_a}^{x_b} A_{xx} \frac{\partial}{\partial \bar{\Delta}_J} \left( \sum_K^4 \bar{\Delta}_K \frac{d\phi_K}{dx} \right) \frac{d\phi_I}{dx} \frac{d\psi_p}{dx} dx \right] u_p \\
&\quad + \sum_{P=1}^4 \left[ \int_{x_a}^{x_b} \frac{1}{2} A_{xx} \frac{\partial}{\partial \bar{\Delta}_J} \left( \frac{dw_0}{dx} \right)^2 \frac{d\phi_I}{dx} \frac{d\phi_P}{dx} dx \right] \bar{\Delta}_P \\
&= K_{IJ}^{22} + \int_{x_a}^{x_b} A_{xx} \frac{d\phi_I}{dx} \frac{d\phi_J}{dx} \left( \sum_{p=1}^2 \frac{d\psi_p}{dx} u_p \right) dx \\
&\quad + \int_{x_a}^{x_b} A_{xx} \left( \frac{dw_0}{dx} \right) \frac{d\phi_I}{dx} \frac{d\phi_J}{dx} \left( \sum_{P=1}^4 \bar{\Delta}_P \frac{d\phi_P}{dx} \right) dx \\
&= K_{IJ}^{22} + \int_{x_a}^{x_b} A_{xx} \left( \frac{du_0}{dx} + \frac{dw_0}{dx} \frac{dw_0}{dx} \right) \frac{d\phi_I}{dx} \frac{d\phi_J}{dx} dx
\end{aligned} \tag{4.2.41}$$

#### 4.2.6 Load Increments

Examining the expression (4.2.15a) for the internal axial force  $N_{xx}$ , it is clear that the rotation of a transverse normal contributes to tensile component of  $N_{xx}$  irrespective of the sign of the load. As a result, the beam becomes increasingly stiff with an increase in load. Hence, for large loads the nonlinearity may be too large for the numerical scheme to yield convergent solution. Therefore, it is necessary to divide the total load  $F$  into several smaller load increments  $\delta F_1, \delta F_2, \dots, \delta F_N$  such that

$$F = \sum_{i=1}^N \delta F_i \tag{4.2.42}$$

For the first load step, the iterative procedure outlined earlier can be used to determine the deflection. If it does not converge within a reasonable number of iterations, it may be necessary to further reduce the load increment  $F_1 = \delta F_1$ . Once the solution for the first load increment is obtained, it is used as the initial "guess" vector for the next load  $F_2 = \delta F_1 + \delta F_2$ . This is continued until the total load is reached.

Another way to accelerate the convergence is to use a weighted average of the solutions from the last two iterations in evaluating the stiffness matrix at

the  $r$ th iteration:

$$\{\Delta^*\}_{r-1} = \gamma\{\Delta\}_{r-2} + (1-\gamma)\{\Delta\}_{r-1}, \quad 0 \leq \gamma \leq 1 \quad (4.2.43)$$

where  $\gamma$  is called the acceleration parameter. A value of  $\gamma = 0.5$  is suggested when the iterative scheme experiences convergence difficulty. Otherwise, one should use  $\gamma = 0$ .

#### 4.2.7 Membrane Locking

For the linear case, the axial displacement  $u_0$  is uncoupled from the bending deflection  $w_0$ , and they can be determined independently from the finite element models [see Eqs. (4.2.20a,b)]

$$[K^{11}]\{u\} = \{F^1\}, \quad K_{ij}^{11} = \int_{x_a}^{x_b} A_{xx}^e \frac{d\psi_i}{dx} \frac{d\psi_j}{dx} dx \quad (4.2.44)$$

$$[K^{22(L)}]\{\bar{\Delta}\} = \{F^2\}, \quad K_{IJ}^{22(L)} = \int_{x_a}^{x_b} D_{xx}^e \frac{d^2\phi_I}{dx^2} \frac{d^2\phi_J}{dx^2} dx \quad (4.2.45)$$

respectively. Here the superscript  $L$  signifies the linear stiffness coefficients. Under the assumptions of linearity, if a beam is subjected to only bending forces and no axial loads, then  $u_0(x) = 0$  when  $u_0$  is specified to be zero at (at least) one point. In other words, a hinged-hinged beam and a pinned-pinned beam (see Figures 4.2.3(a) and (b), respectively) will have the same deflection  $w_0(x)$  under the same loads and  $u_0(x) = 0$  for all  $x$ . However, this is not the case when the beam undergoes nonlinear bending. The coupling between  $u_0$  and  $w_0$  will cause the beam to undergo axial displacement even when there are no axial forces, and the solution  $(u_0, w_0)$  will be different for the two cases shown in Figure 4.2.3.

First, we note that the hinged-hinged beam does not have any end constraints on  $u_0$ . If the geometry, boundary conditions, and loading are symmetric about the center, then  $u_0 = 0$  there. Consequently, the beam does not experience any axial strain, that is,  $\varepsilon_{xx}^0 = 0$  (because the beam is free to slide on the rollers to accommodate transverse deflection). On the other hand, the pinned-pinned beam is constrained from axial movement at  $x = 0$  and  $x = L$ . As a result, it will develop axial strain to accommodate the transverse deflection. The former beam will have larger transverse deflection than the latter, as the latter offers axial stiffness to stretching, and the axial stiffness increases with the load.

Thus, for a hinged-hinged beam, the element should experience no stretching:

$$\varepsilon_{xx}^0 \equiv \frac{du_0}{dx} + \frac{1}{2} \left( \frac{dw_0}{dx} \right)^2 = 0 \quad (\text{membrane strain}) \quad (4.2.46)$$

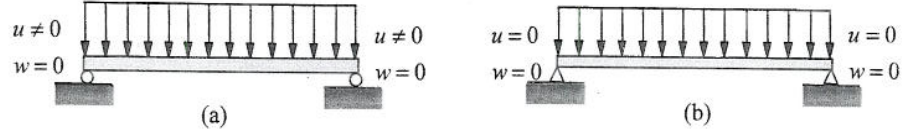


Figure 4.2.3 Nonlinear bending of (a) hinged-hinged and (b) pinned-pinned beams.

In order to satisfy the constraint in (4.2.46), we must have

$$\frac{du_0}{dx} \sim \left( \frac{dw_0}{dx} \right)^2 \quad (4.2.47)$$

The similarity is in the sense of having the same degree of polynomial variation of  $du_0/dx$  and  $(dw_0/dx)^2$ . For example, when  $u_0$  is interpolated using linear functions and  $w_0$  with cubic, the constraint in Eq. (4.2.47) is clearly *not* met and the resulting element stiffness matrix is excessively stiff (hence, results in zero displacement field), and the element is said to lock. This phenomenon is known as the *membrane locking*. In fact, unless a very higher-order interpolation of  $u_0$  is used, the element will not satisfy the constraint.

A practical way to satisfy the constraint in Eq. (4.2.47) is to use the minimum interpolation of  $u_0$  and  $w_0$  (i.e. linear interpolation of  $u_0$  and Hermite cubic interpolation of  $w_0$ ) but treat  $\varepsilon_{xx}^0$  as a constant. Since  $du_0/dx$  is constant, it is necessary to treat  $(dw_0/dx)^2$  as a constant in numerically evaluating the element stiffness coefficients. Thus, if  $A_{xx}$  is a constant, all nonlinear stiffness coefficients should be evaluated using one-point Gauss quadrature, that is, use the *reduced integration*. These coefficients include  $K_{ij}^{12}$ ,  $K_{ij}^{21}$ ,  $T_{ij}^{12}$ ,  $T_{ij}^{21}$ , and the nonlinear parts of  $K^{22}$  and  $T_{ij}^{22}$ . All other terms may be evaluated exactly using two-point quadrature for constant values of  $A_{xx}$  and  $D_{xx}$ .

#### 4.2.8 Computer Implementation

The flow chart for nonlinear bending of beams is shown in Figure 4.2.4. Note that there is an outer loop on load increments ( $NLS$ =number of load steps). Except for the definition of the stiffness coefficients, much of the logic remains the same as that shown in Box 3.5.1.

The element stiffness matrix in Eq. (4.2.22) is defined by submatrices  $[K^{11}]$ ,  $[K^{12}]$ , and  $[K^{22}]$ , and the solution vector  $\{\Delta\}$  is partitioned into the axial displacement vector  $\{u\}$  and vector  $\{\bar{\Delta}\}$  of transverse displacements.

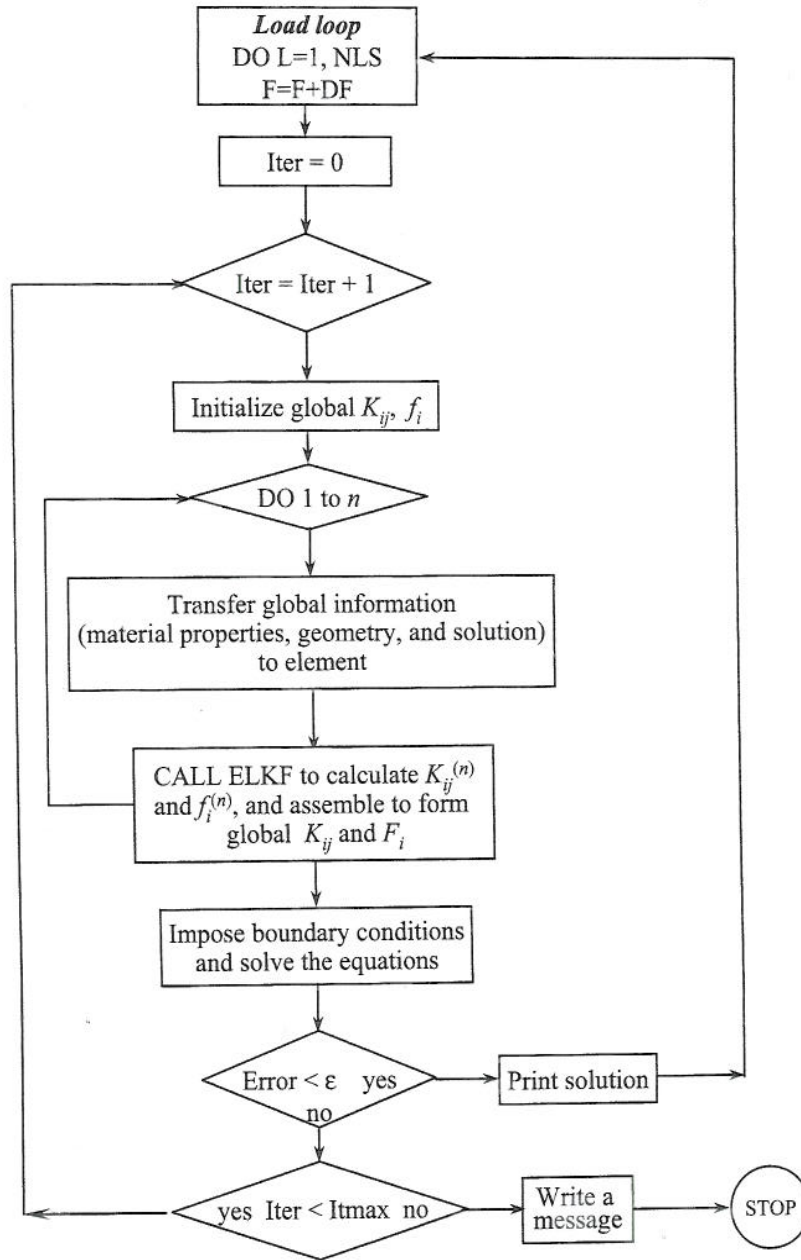


Figure 4.2.4 A computer flow chart for the nonlinear finite element analysis of beams.



In practice, it is desirable to rearrange the solution vector as

$$\{\Delta\} = \{u_1, w_1 = \bar{\Delta}_1, \theta_1 = \bar{\Delta}_2, u_2, w_2 = \bar{\Delta}_3, \theta_2 = \bar{\Delta}_4\}^T \quad (4.2.48)$$

This in turn requires rearrangement of the stiffness coefficients such that the original symmetry, if any, is preserved. For linear interpolation of  $u_0(x)$  and Hermite cubic interpolation of  $w_0(x)$ , the submatrix  $[K^{11}]$  is of the order  $2 \times 2$ ,  $[K^{12}]$  is  $2 \times 4$ , and  $[K^{22}]$  is  $4 \times 4$ . Therefore, the total size of the stiffness matrix is  $6 \times 6$ . Thus Eq. (4.2.23) has the specific matrix form

$$\begin{bmatrix} K_{11}^{11} & K_{12}^{11} & K_{11}^{12} & K_{12}^{12} & K_{13}^{12} & K_{14}^{12} \\ K_{21}^{11} & K_{22}^{11} & K_{21}^{12} & K_{22}^{12} & K_{23}^{12} & K_{24}^{12} \\ K_{11}^{21} & K_{12}^{21} & K_{11}^{22} & K_{12}^{22} & K_{13}^{22} & K_{14}^{22} \\ K_{21}^{21} & K_{22}^{21} & K_{21}^{22} & K_{22}^{22} & K_{23}^{22} & K_{24}^{22} \\ K_{31}^{21} & K_{32}^{21} & K_{31}^{22} & K_{32}^{22} & K_{33}^{22} & K_{34}^{22} \\ K_{41}^{21} & K_{42}^{21} & K_{41}^{22} & K_{42}^{22} & K_{43}^{22} & K_{44}^{22} \end{bmatrix} \begin{Bmatrix} u_1^e \\ u_2^e \\ \bar{\Delta}_1^e \\ \bar{\Delta}_2^e \\ \bar{\Delta}_3^e \\ \bar{\Delta}_4^e \end{Bmatrix} = \begin{Bmatrix} F_1^1 \\ F_2^1 \\ F_1^2 \\ F_2^2 \\ F_3^2 \\ F_4^2 \end{Bmatrix} \quad (4.2.49)$$

Rearranging the equations according to the displacement vector in Eq. (4.2.48), we obtain

$$\begin{bmatrix} K_{11}^{11} & K_{12}^{11} & K_{12}^{12} & K_{11}^{12} & K_{13}^{12} & K_{14}^{12} \\ K_{11}^{21} & K_{12}^{21} & K_{12}^{22} & K_{11}^{22} & K_{13}^{22} & K_{14}^{22} \\ K_{21}^{21} & K_{22}^{21} & K_{22}^{22} & K_{21}^{22} & K_{23}^{22} & K_{24}^{22} \\ K_{21}^{11} & K_{22}^{11} & K_{22}^{12} & K_{21}^{12} & K_{23}^{12} & K_{24}^{12} \\ K_{31}^{21} & K_{32}^{21} & K_{32}^{22} & K_{31}^{22} & K_{33}^{22} & K_{34}^{22} \\ K_{41}^{21} & K_{42}^{21} & K_{42}^{22} & K_{41}^{22} & K_{43}^{22} & K_{44}^{22} \end{bmatrix} \begin{Bmatrix} u_1^e \\ \bar{\Delta}_1^e \\ \bar{\Delta}_2^e \\ u_2^e \\ \bar{\Delta}_3^e \\ \bar{\Delta}_4^e \end{Bmatrix} = \begin{Bmatrix} F_1^1 \\ F_1^2 \\ F_2^2 \\ F_2^1 \\ F_3^2 \\ F_4^2 \end{Bmatrix} \quad (4.2.50)$$

The computer implementation of such rearrangement of element coefficients is presented in Box 4.2.1, where  $NDF$  denotes the degrees of freedom per node ( $=3$ ) and  $NPE$  the nodes per element ( $=2$ ). This rearrangement is carried out after the element coefficients  $[K^{11}]$ ,  $[K^{12}]$ ,  $[K^{22}]$ ,  $\{F^1\} = \{0\}$ , and  $\{F^2\}$  are computed inside loops on Gauss quadrature. There are two loops, one for full integration and another for reduced integration.

The number of full Gauss points (NGP) is determined by the highest polynomial degree  $p$  of all integrands of the linear stiffness coefficients (recall that reduced integration is to be used for the nonlinear terms):  $NGP = (p+1)/2$ . For example, if linear interpolation of  $u_0$  and Hermite cubic interpolation of  $w_0$  is used, the integrands of the stiffness coefficients defined in Eq. (4.2.21) have the following polynomial degrees (assuming that the nonlinear terms are treated as if they are constant):

$$\begin{aligned} K_{ij}^{11} &= \text{degree of } A_{xx}, & K_{iJ}^{12} &= \text{degree of } A_{xx}, \\ K_{IJ}^{22(1)} &= \text{degree of } D_{xx}^e + 2, & K_{IJ}^{22(2)} &= \text{degree of } A_{xx}^e + 0 \\ F_i^1 &= \text{degree of } f(x) + 1, & F_J^2 &= \text{degree of } q(x) + 3 \end{aligned}$$

## Box 4.2.1 Fortran statements to rearrange stiffness coefficients.

```

C
C Rearranging of the element matrix coefficients for
C the EULER-BERNOULLI beam element (EBE)
C
      II=1
      DO 200 I=1,NPE
        I0=2*I-1
        ELF(II+1)=ELF2(I0)
        ELF(II+2)=ELF2(I0+1)
        JJ=1
        DO 100 J=1,NPE
          J0=2*J-1
          ELK(II,JJ) = ELK11(I,J)
          ELK(II,JJ+1) = ELK12(I,J0)
          ELK(II,JJ+2) = ELK12(I,J0+1)
          ELK(II+1,JJ) = ELK21(I0,J)
          ELK(II+2,JJ) = ELK21(I0+1,J)
          ELK(II+1,JJ+1) = ELK22(I0,J0)
          ELK(II+1,JJ+2) = ELK22(I0,J0+1)
          ELK(II+2,JJ+1) = ELK22(I0+1,J0)
          ELK(II+2,JJ+2) = ELK22(I0+1,J0+1)
100      JJ=NDF*J+1
200      II=NDF*I+1

```

In particular, for constant values of  $AXX = A_{xx}^e$ ,  $DXX = D_{xx}^e$ ,  $FX = f$ , and  $QX = q$ , we have  $NGP = (3 + 1)/2 = 2$  (dictated by  $F_1^2$ ) and the number of reduced integration points is  $LGP = 1$ . The full Gauss quadrature is used to evaluate  $[K^{11}]$ ,  $[K^{22(1)}]$ ,  $\{F^1\}$ , and  $\{F^2\}$ , whereas the reduced integration is used to evaluate  $[K^{12}]$  and  $[K^{22(2)}]$ .

The computation of the direct stiffness coefficients and force vectors defined in Eq. (4.2.21) is straightforward. For example, we have

$$\begin{aligned}
 ELF1(i) &= ELF1(i) + FX * SFL(i) * CNST \\
 ELF2(I) &= ELF2(I) + QX * SFH(I) * CNST \\
 ELK11(i, j) &= ELK11(i, j) \\
 &\quad + AXX * GDSFL(i) * GDSFL(j) * CNST \\
 ELK22(I, J) &= ELK22(I, J) \\
 &\quad + DXX * GDDSFH(I) * GDDSFH(J) * CNST
 \end{aligned}$$

in the full integration loop, and

$$\begin{aligned}
 ELK12(i, J) &= ELK12(i, J) + 0.5 * AXX * DW \\
 &\quad * GDSFL(i) * GDSFH(J) * CNST
 \end{aligned}$$

$$\begin{aligned}
 ELK21(I, j) &= ELK21(I, j) + AXX * DW \\
 &\quad * GDSFH(I) * GDSFL(j) * CNST \\
 ELK22(I, J) &= ELK22(I, J) + 0.5 * AXX * DW * DW \\
 &\quad * GDSFH(I) * GDSFH(J) * CNST
 \end{aligned}$$

in the reduced integration loop. Here,  $SFL(i) = \psi_i$ ,  $SFH(I) = \phi_I$ ,  $GDSFH(I) = \frac{d\phi_I}{dx}$ ,  $GDDSFH(I) = \frac{d^2\phi_I}{dx^2}$ ,  $GDSFL(i) = \frac{d\psi_i}{dx}$ , and  $DW = (dw_0/dx)$  for  $i, j = 1, 2$  and  $I, J = 1, 2, 3, 4$ . Similarly, the extra terms that need to be added to the direct stiffnesses can be computed in the reduced integration loop as [see Eq. (4.2.41)]

$$\begin{aligned}
 TANG12(i, J) &= TANG12(i, J) + 0.5 * AXX * DW \\
 &\quad * GDSFL(i) * GDSFH(J) * CNST \\
 TANG22(I, J) &= TANG22(I, J) + AXX * (DU + DW * DW) \\
 &\quad * GDSFH(I) * GDSFH(J) * CNST
 \end{aligned}$$

where  $DU = (du_0/dx)$ .

#### Example 4.2.1

Consider a beam of length  $L = 100$  in., 1 in.  $\times$  1 in. cross-sectional dimensions, hinged at both ends, made of steel ( $E = 30$  msi), and subjected to uniformly distributed load of intensity  $q_0$  lb/in. Using the symmetry about  $x = L/2$ , one-half of the domain is used as the computational domain. The geometric boundary conditions for the computational domain are

$$w_0(0) = u_0(L/2) = \left(\frac{dw_0}{dx}\right)_{x=L/2} = 0 \quad (4.2.51)$$

The load is divided into load increments of equal size  $\Delta q_0 = 1$  lb/in. A tolerance of  $\epsilon = 10^{-3}$  and maximum allowable iterations of 30 (per load step) are used in the analysis. The initial solution vector is chosen to be the zero vector, so that the first iteration solution corresponds to the linear solution

$$u_0(x) = 0, \quad w_0(x) = \frac{q_0 L^4}{24D_{xx}} \left( \frac{x}{L} - 2\frac{x^3}{L^3} + \frac{x^4}{L^4} \right) \quad (4.2.52)$$

In particular, the center deflection is (for  $q_0 = 1$ )

$$w_0\left(\frac{L}{2}\right) = \frac{5q_0 L^4}{384D_{xx}} = 0.5208 \text{ in.} \quad (4.2.53)$$

For the four element mesh, the linear stiffness matrix, force vector, and the global linear solution vector are given by (with the specified boundary conditions  $\Delta_2 = 0$ ,  $\Delta_{13} = 0$  and  $\Delta_{15} = 0$ )

$$[K^e] = 10^5 \begin{bmatrix} 24 & 0.0000 & 0.00 & -24 & 0.0000 & 0.00 \\ 0 & 0.1536 & -0.96 & 0 & -0.1536 & -0.96 \\ 0 & -0.9600 & 8.00 & 0 & 0.9600 & 4.00 \\ -24 & 0.0000 & 0.00 & 24 & 0.0000 & 0.00 \\ 0 & -0.1536 & 0.96 & 0 & 0.1536 & 0.96 \\ 0 & -0.9600 & 4.00 & 0 & 0.9600 & 8.00 \end{bmatrix}$$

$$\{F^e\} = \begin{Bmatrix} 0.000 \\ 6.250 \\ -13.021 \\ 0.000 \\ 6.250 \\ 13.021 \end{Bmatrix}, \quad \begin{Bmatrix} \Delta_3 \\ \Delta_5 \\ \Delta_6 \\ \Delta_8 \\ \Delta_9 \\ \Delta_{11} \\ \Delta_{12} \\ \Delta_{14} \end{Bmatrix} = \begin{Bmatrix} -0.01666 \\ 0.20223 \\ -0.01523 \\ 0.37109 \\ -0.01146 \\ 0.48218 \\ -0.00612 \\ 0.52083 \end{Bmatrix}$$

Table 4.2.1 contains the results of the nonlinear analysis obtained with the direct iteration procedure as well as the Newton-Raphson iteration (acceleration parameter,  $\gamma = 0$ ). The Gauss rule  $M \times N$  has the meaning that  $M$  Gauss points are used for the evaluation of linear stiffness coefficients as well as the force components, and  $N$  Gauss points are used to evaluate the nonlinear stiffness coefficients. As discussed earlier, the problem should not exhibit any nonlinearity. The correct solution (4.2.53) is predicted by the use of  $2 \times 1$  Gauss rule (see the last column of Table 4.2.1). Both 4 and 8 element meshes and direct and Newton-Raphson methods predicted the same result. The  $2 \times 2$  Gauss rule not only yields incorrect results, but it takes more iterations to converge.

**Table 4.2.1** Finite element results for the deflections of a *hinged-hinged* beam under uniformly distributed load.

Load $q_0$	Direct iteration (DI)		Newton-Raphson (NR)		DI-NR 2 x 1
	(2 x 2)		(2 x 2)		
	4 elem.	8 elem.	4 elem.	8 elem.	
1.0	0.5108 (3)*	0.5182 (3)	0.5108 (4)	0.5182 (4)	0.5208 (3)
2.0	0.9739 (5)	1.0213 (3)	0.9739 (4)	1.0213 (4)	1.0417 (3)
3.0	1.3763 (6)	1.4986 (4)	1.3764 (4)	1.4986 (4)	1.5625 (3)
4.0	1.7269 (7)	1.9451 (4)	1.7265 (4)	1.9453 (4)	2.0833 (3)
5.0	2.0356 (9)	2.3609 (5)	2.0351 (4)	2.3607 (4)	2.6042 (3)
6.0	2.3122 (11)	2.7471 (5)	2.3116 (3)	2.7467 (3)	3.1250 (3)
7.0	2.5617 (14)	3.1054 (6)	2.5630 (2)	3.1074 (2)	3.6458 (3)
8.0	2.7936 (17)	3.4418 (7)	2.7930 (2)	3.4422 (2)	4.1667 (3)
9.0	3.0049 (22)	3.7570 (7)	3.0060 (3)	3.7564 (2)	4.6875 (3)
10.0	3.2063 (29)	4.5013 (8)	3.2051 (3)	4.0523 (2)	5.2083 (3)

\* Number of iterations taken to converge.

**Example 4.2.2**

Next, we consider the straight beam of Example 4.2.1 with (a) *pinned* ends, and (b) *clamped* ends, and under uniformly distributed transverse load. Noting the symmetry of the solution about  $x = L/2$ , one-half of the domain is used as the computational domain. The geometric boundary conditions for the computational domain of the two problems are

$$\text{pinned: } u_0(0) = w_0(0) = u_0\left(\frac{L}{2}\right) = \frac{dw_0}{dx}\Big|_{x=\frac{L}{2}} = 0 \tag{4.2.54}$$

$$\text{clamped: } u_0(0) = w_0(0) = \frac{dw_0}{dx}\Big|_{x=0} = u_0\left(\frac{L}{2}\right) = \frac{dw_0}{dx}\Big|_{x=\frac{L}{2}} = 0 \tag{4.2.55}$$

The load increments of  $\Delta q_0 = 1.0$  lb/in., a tolerance of  $\epsilon = 10^{-3}$ , and maximum allowable iterations of 25 (per load step) are used in the analysis. The initial solution vector is chosen to be the zero vector. Solutions to the linear problems are

$$\text{pinned: } u_0(x) = 0, \quad w_0(x) = \frac{q_0 L^4}{24 D_{xx}} \frac{x^2}{L^2} \left(1 - \frac{x}{L}\right)^2 \quad (4.2.56)$$

$$\text{clamped: } u_0(x) = 0, \quad w_0(x) = \frac{q_0 L^4}{24 D_{xx}} \left(\frac{x}{L} - 2\frac{x^3}{L^3} + \frac{x^4}{L^4}\right) \quad (4.2.57)$$

and the maximum deflections occurs at  $L/2$ . For  $q_0 = 1$  lb/in.,  $L = 100$  in., and  $E = 30 \times 10^6$  psi, they are given by ( $D_{xx} = EH^3/12$ ,  $H = 1$ )

$$\text{pinned: } w_0\left(\frac{L}{2}\right) = \frac{5q_0 L^4}{384 D_{xx}} = 0.5208 \text{ in.} \quad (4.2.58)$$

$$\text{clamped: } w_0\left(\frac{L}{2}\right) = \frac{q_0 L^4}{384 D_{xx}} = 0.1042 \text{ in.} \quad (4.2.59)$$

The linear nodal displacements obtained using four elements in half beam are

$$\begin{matrix} \left\{ \begin{matrix} \Delta_3 \\ \Delta_5 \\ \Delta_6 \\ \Delta_8 \\ \Delta_9 \\ \Delta_{11} \\ \Delta_{12} \\ \Delta_{14} \end{matrix} \right\} \\ \text{pinned} \end{matrix} = \begin{matrix} \left\{ \begin{matrix} -0.01666 \\ 0.20223 \\ -0.01523 \\ 0.37109 \\ -0.11458 \\ 0.48218 \\ -0.00612 \\ 0.52083 \end{matrix} \right\}, \end{matrix} \begin{matrix} \left\{ \begin{matrix} \Delta_5 \\ \Delta_6 \\ \Delta_8 \\ \Delta_9 \\ \Delta_{11} \\ \Delta_{12} \\ \Delta_{14} \end{matrix} \right\} \\ \text{clamped} \end{matrix} = \begin{matrix} \left\{ \begin{matrix} 0.01994 \\ -0.00273 \\ 0.05859 \\ -0.00313 \\ 0.09155 \\ -0.00195 \\ 0.10417 \end{matrix} \right\}$$

Tables 4.2.2 and 4.2.3 contain the results of the nonlinear analysis of pinned-pinned and clamped-clamped beams, respectively; the results were obtained with the Newton-Raphson iteration method. The direct iteration method did not converge even for 100 iterations per load step when  $\Delta q = 1.0$ . It is possible to find a value of  $\Delta q$  and *ITMAX* for which one can obtain converged solutions.

**Table 4.2.2** Finite element results for the deflections of a *pinned-pinned beam* under uniform load (N-R).

Load $q_0$	$2 \times 2$		$2 \times 1$	
	4 elements	8 elements	4 elements	8 elements
1.0	0.3669 (5)*	0.3680 (5)	0.3687 (5)	0.3685 (5)
2.0	0.5424 (4)	0.5446 (4)	0.5466 (4)	0.5457 (4)
3.0	0.6601 (3)	0.6629 (3)	0.6663 (4)	0.6645 (4)
4.0	0.7510 (3)	0.7543 (3)	0.7591 (4)	0.7564 (4)
5.0	0.8263 (3)	0.8299 (3)	0.8361 (4)	0.8324 (4)
6.0	0.8912 (3)	0.8950 (3)	0.9027 (4)	0.8979 (4)
7.0	0.9485 (3)	0.9525 (3)	0.9617 (4)	0.9558 (4)
8.0	1.0002 (3)	1.0043 (3)	1.0150 (4)	1.0080 (4)
9.0	1.0473 (3)	1.0516 (3)	1.0638 (4)	1.0557 (4)
10.0	1.0908 (3)	1.0952 (3)	1.1089 (4)	1.0997 (4)

\* Number of iterations taken to converge.

There is no significant difference between the solutions obtained with the two integration rules for this problem. Figure 4.2.5 shows the load-deflection curves for the two beams. If the axial displacement degrees of freedom are suppressed (i.e. equivalent to setting  $u_0 = 0$  at every point of the beam) in the nonlinear analysis of beams, the beam will behave very stiff, and the deflections experienced will be less than those shown in Tables 4.2.2 and 4.2.3 and Figure 4.2.5.

**Table 4.2.3** Finite element results for the deflections of a *clamped-clamped* beam under uniform load (N-R and  $2 \times 1$  Gauss rule).

Load $q_0$	Direct iteration		Newton-Raphson iteration	
	4 elements	8 elements	4 elements	8 elements
1.0	0.1033 (3)*	0.1034 (3)	0.1034 (3)	0.1034 (3)
2.0	0.2022 (4)	0.2023 (4)	0.2022 (3)	0.2023 (3)
3.0	0.2938 (4)	0.2939 (4)	0.2939 (3)	0.2939 (3)
4.0	0.3773 (5)	0.3774 (5)	0.3773 (3)	0.3774 (3)
5.0	0.4529 (5)	0.4531 (5)	0.4528 (3)	0.4530 (3)
6.0	0.5213 (6)	0.5215 (6)	0.5214 (3)	0.5216 (3)
7.0	0.5840 (7)	0.5842 (7)	0.5839 (3)	0.5841 (3)
8.0	0.6412 (8)	0.6412 (8)	0.6413 (3)	0.6414 (3)
9.0	0.6945 (9)	0.6944 (9)	0.6943 (3)	0.6943 (3)
10.0	0.7433 (10)	0.7431 (10)	0.7435 (3)	0.7433 (3)

\* Number of iterations taken to converge.

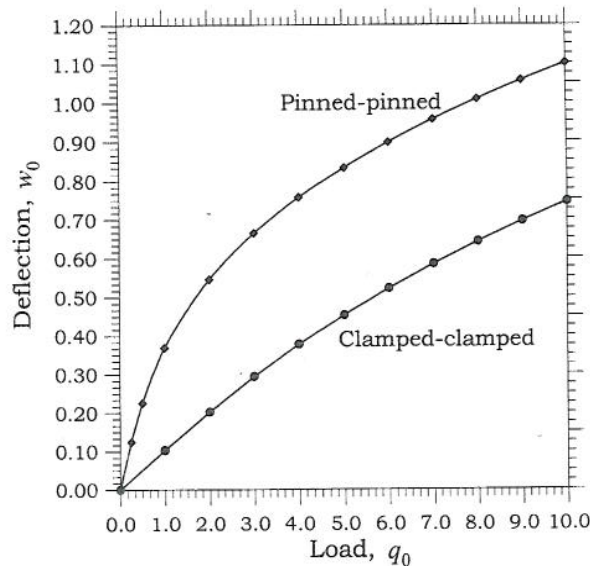


**Figure 4.2.5** Load versus deflection curves.

### 4.3 Timoshenko Beams

#### 4.3.1 Displacement Field and Strains

The EBT is based on the assumption that a straight line transverse to the axis of the beam before deformation remains (i) straight, (ii) inextensible, and (iii) normal to the mid-plane after deformation. In the TBT, the first two assumptions are kept but the normality condition is relaxed by assuming that the rotation is independent of the slope ( $w_{0,x}$ ) of the beam.

The displacement field of the beam in the TBT can be expressed as

$$u_1 = u_0(x) + z\phi_x(x), \quad u_2 = 0, \quad u_3 = w_0(x) \quad (4.3.1)$$

where  $(u_1, u_2, u_3)$  are the displacements of a point along the  $(x, y, z)$  coordinates,  $(u_0, w_0)$  are the displacements of a point on the mid-plane of an undeformed beam, and  $\phi_x$  is the rotation (about the  $y$ -axis) of a transverse straight line (see Figure 4.3.1).

The only non-zero strains are

$$\varepsilon_{xx} = \frac{\partial u_1}{\partial x} + \frac{1}{2} \left( \frac{dw_0}{dx} \right)^2 = \frac{du_0}{dx} + \frac{1}{2} \left( \frac{dw_0}{dx} \right)^2 + z \frac{d\phi_x}{dx} \equiv \varepsilon_{xx}^0 + z\varepsilon_{xx}^1 \quad (4.3.2)$$

$$\gamma_{xz} = \frac{\partial u_1}{\partial z} + \frac{\partial u_3}{\partial x} = \phi_x + \frac{dw_0}{dx} \equiv \gamma_{xz}^0 \quad (4.3.3)$$

The virtual strains are

$$\delta\varepsilon_{xx}^0 = \frac{d\delta u_0}{dx} + \frac{dw_0}{dx} \frac{d\delta w_0}{dx}, \quad \delta\varepsilon_{xx}^1 = \frac{d\delta\phi_x}{dx}, \quad \delta\gamma_{xz}^0 = \delta\phi_x + \frac{d\delta w_0}{dx} \quad (4.3.4)$$

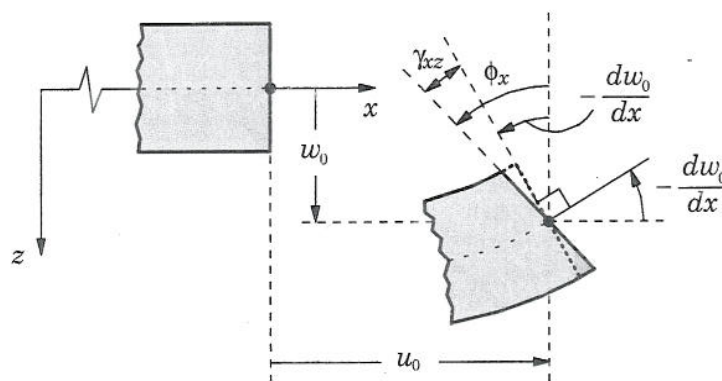


Figure 4.3.1 Kinematics of a beam in the TBT.

### 4.3.2 Weak Forms

Next, we use the principle of virtual displacements to develop the necessary weak statements of the TBT. We have

$$0 = \delta W^e \equiv \delta W_I^e + \delta W_E^e \quad (4.3.5)$$

$$\begin{aligned} \delta W_I^e &= \int_{x_a}^{x_b} \int_{A^e} (\sigma_{xx} \delta \varepsilon_{xx} + \sigma_{xz} \delta \gamma_{xz}) dA dx \\ &= \int_{x_a}^{x_b} \int_{A^e} [\sigma_{xx} (\delta \varepsilon_{xx}^0 + z \delta \varepsilon_{xx}^1) + \sigma_{xz} \delta \gamma_{xz}^0] dA dx \\ &= \int_{x_a}^{x_b} (N_{xx} \delta \varepsilon_{xx}^0 + M_{xx} \delta \varepsilon_{xx}^1 + Q_x \delta \gamma_{xz}^0) dx \end{aligned} \quad (4.3.6a)$$

$$\delta W_E^e = - \left[ \int_{x_a}^{x_b} q \delta w_0 dx + \int_{x_a}^{x_b} f \delta u_0 dx + \sum_{i=1}^6 Q_i^e \delta \Delta_i^e \right] \quad (4.3.6b)$$

where  $q$  is the distributed transverse load,  $Q_i^e$  are the element generalized forces,  $\Delta_i^e$  element generalized displacements, and

$$N_{xx} = \int_A \sigma_{xx} dA, \quad M_{xx} = \int_A \sigma_{xx} z dA, \quad Q_x = K_s \int_A \sigma_{xz} dA \quad (4.3.7)$$

and  $K_s$  is the *shear correction coefficient* introduced to account for the difference between the shear energy calculated using equilibrium stresses and that predicted by the Timoshenko beam theory on account of constant state of shear stress through the beam height.

For example, consider a homogeneous beam with rectangular cross-section, with width  $b$  and height  $h$ . The actual shear stress distribution through the thickness of the beam is given by

$$\sigma_{xz}^c = \frac{3Q_0}{2bh} \left[ 1 - \left( \frac{2z}{h} \right)^2 \right], \quad -\frac{h}{2} \leq z \leq \frac{h}{2}$$

where  $Q_0$  is the transverse load. The transverse shear stress in the first-order theory is a constant,  $\sigma_{xz}^f = Q_0/bh$ . The strain energies due to transverse shear stresses in the two theories are

$$U_s^c = \frac{1}{2G_{13}} \int_A (\sigma_{xz}^c)^2 dA = \frac{3Q_0^2}{5G_{13}bh}, \quad U_s^f = \frac{1}{2G_{13}} \int_A (\sigma_{xz}^f)^2 dA = \frac{Q_0^2}{2G_{13}bh}$$

The shear correction factor is the ratio of  $U_s^f$  to  $U_s^c$ , which gives  $K_s = 5/6$ . The shear correction factor, in general, depends on the geometry and material properties.



The Euler-Lagrange equations are given by

$$\delta u_0 : \quad -\frac{dN_{xx}}{dx} = f(x) \quad (4.3.8)$$

$$\delta \phi : \quad -\frac{dM_{xx}}{dx} + Q_x = 0 \quad (4.3.9)$$

$$\delta w_0 : \quad -\frac{dQ_x}{dx} - \frac{d}{dx} \left( N_{xx} \frac{dw_0}{dx} \right) = q(x) \quad (4.3.10)$$

It is clear that  $(u_0, w_0, \phi_x)$  are the primary variables and

$$N_{xx}, Q_x, \text{ and } M_{xx} \quad (4.3.11)$$

are the secondary variables. Thus the pairing of the primary and secondary variables is as follows:

$$(u_0, N_{xx}), \quad (w_0, Q_x), \quad (\phi_x, M_{xx}) \quad (4.3.12)$$

Only one member of each pair may be specified at a point in the beam.

If we assume linear elastic behavior

$$\sigma_{xx} = E\varepsilon_{xx}, \quad \sigma_{xz} = G\gamma_{xz} \quad (4.3.13a)$$

the axial force  $N_{xx}$ , the shear force  $Q_x$ , and bending moment  $M_{xx}$  can be expressed in terms of the generalized displacements  $(u_0, w_0, \phi_x)$  using the definitions (4.3.7). We obtain

$$\begin{aligned} N_{xx} &= A_{xx} \left[ \frac{du_0}{dx} + \frac{1}{2} \left( \frac{dw_0}{dx} \right)^2 \right] + B_{xx} \frac{d\phi_x}{dx} \\ M_{xx} &= B_{xx} \left[ \frac{du_0}{dx} + \frac{1}{2} \left( \frac{dw_0}{dx} \right)^2 \right] + D_{xx} \frac{d\phi_x}{dx} \\ Q_x &= S_{xx} \left( \frac{dw_0}{dx} + \phi_x \right) \end{aligned} \quad (4.3.13b)$$

where  $A_{xx}$ ,  $B_{xx}$ , and  $D_{xx}$  are defined in Eq. (4.2.16), and  $S_{xx}$  is the shear stiffness

$$S_{xx} = K_s \int_A G dA = K_s GA \quad (4.3.13c)$$

$G$  being the shear modulus,  $K_s$  the shear correction coefficient, and  $A$  the area of cross-section. As discussed earlier, the stiffnesses  $A_{xx}$ ,  $B_{xx}$ , and  $D_{xx}$  are functions of  $x$  whenever the modulus  $E$  and/or cross-sectional area is a function of  $x$ .

The equations of equilibrium of the TBT for the isotropic case can be expressed in terms of the generalized displacements as

$$-\frac{d}{dx} \left\{ A_{xx} \left[ \frac{du_0}{dx} + \frac{1}{2} \left( \frac{dw_0}{dx} \right)^2 \right] \right\} = f \quad (4.3.14)$$

$$-\frac{d}{dx} \left[ S_{xx} \left( \frac{dw_0}{dx} + \phi_x \right) \right] - \frac{d}{dx} \left\{ A_{xx} \frac{dw_0}{dx} \left[ \frac{du_0}{dx} + \frac{1}{2} \left( \frac{dw_0}{dx} \right)^2 \right] \right\} = q \quad (4.3.15)$$

$$-\frac{d}{dx} \left( D_{xx} \frac{d\phi_x}{dx} \right) + S_{xx} \left( \frac{dw_0}{dx} + \phi_x \right) = 0 \quad (4.3.16)$$

### 4.3.3 General Finite Element Model

The finite element model of the Timoshenko beam equations can be constructed using the virtual work statement in Eqs. (4.3.5), where the axial force  $N_{xx}$ , the shear force  $Q_x$ , and bending moment  $M_{xx}$  are known in terms of the generalized displacements  $(u_0, w_0, \phi_x)$  by Eq. (4.3.13b). The virtual work statement (4.3.5) is equivalent to the following three statements

$$0 = \int_{x_a}^{x_b} \left\{ A_{xx} \frac{d\delta u_0}{dx} \left[ \frac{du_0}{dx} + \frac{1}{2} \left( \frac{dw_0}{dx} \right)^2 \right] + f\delta u_0 \right\} dx - Q_1^e \delta u_0(x_a) - Q_4^e \delta u_0(x_b) \quad (4.3.17)$$

$$0 = \int_{x_a}^{x_b} \frac{d\delta w_0}{dx} \left\{ S_{xx}^e \left( \frac{dw_0}{dx} + \phi_x \right) + A_{xx}^e \frac{dw_0}{dx} \left[ \frac{du_0}{dx} + \frac{1}{2} \left( \frac{dw_0}{dx} \right)^2 \right] - \delta w_0 q \right\} dx - Q_2^e \delta w_0(x_a) - Q_5^e \delta w_0(x_b) \quad (4.3.18)$$

$$0 = \int_{x_a}^{x_b} \left[ D_{xx}^e \frac{d\delta\phi_x}{dx} \frac{d\phi_x}{dx} + S_{xx}^e \delta\phi_x \left( \frac{dw_0}{dx} + \phi_x \right) \right] dx - Q_3^e \delta\phi_x(x_a) - Q_6^e \delta\phi_x(x_b) \quad (4.3.19)$$

where  $\delta u_0$ ,  $\delta w_0$ , and  $\delta\phi_x$  are the virtual displacements. The  $Q_i^e$  have the same physical meaning as in the Euler-Bernoulli beam element, and their relationship to the horizontal displacement  $u_0$ , transverse deflection  $w_0$ , and rotation  $\phi_x$ , is

$$\begin{aligned} Q_1^e &= -N_{xx}(x_a), & Q_4^e &= N_{xx}(x_b) \\ Q_2^e &= - \left[ Q_x + N_{xx} \frac{\partial w_0}{\partial x} \right]_{x=x_a}, & Q_5^e &= \left[ Q_x + N_{xx} \frac{\partial w_0}{\partial x} \right]_{x=x_b} \\ Q_3^e &= -M_{xx}(x_a), & Q_6^e &= M_{xx}(x_b) \end{aligned} \quad (4.3.20)$$

An examination of the virtual work statements (4.3.17)–(4.3.19) suggests that  $u_0(x)$ ,  $w_0(x)$ , and  $\phi_x(x)$  are the primary variables and therefore must be carried as nodal degrees of freedom. In general,  $u_0$ ,  $w_0$ , and  $\phi_x$  need not be approximated by polynomials of the same degree. However, the approximations should be such that possible deformation modes (i.e. kinematics) are represented correctly. We will return to this point shortly.

It is also possible to develop the weak forms (4.3.17)–(4.3.19) using the governing equations (4.3.8)–(4.3.10) and introducing the secondary variables (4.3.20). It is left as an exercise to the reader.

Suppose that the displacements are approximated as

$$u_0(x) = \sum_{j=1}^m u_j^e \psi_j^{(1)}, \quad w_0(x) = \sum_{j=1}^n w_j^e \psi_j^{(2)}, \quad \phi_x(x) = \sum_{j=1}^p s_j^e \psi_j^{(3)} \quad (4.3.21)$$

where  $\psi_j^{(\alpha)}(x)$  ( $\alpha = 1, 2, 3$ ) are Lagrange interpolation functions of degree  $(m-1)$ ,  $(n-1)$ , and  $(p-1)$ , respectively. At the moment, the values of  $m$ ,  $n$ , and  $p$  are arbitrary, that is, arbitrary degree of polynomial approximations of  $u_0$ ,  $w_0$ , and  $\phi_x$  may be used. Substitution of (4.3.21) for  $u_0$ ,  $w_0$ , and  $\phi_x$ , and  $\delta u_0 = \psi_i^{(1)}$ ,  $\delta w_0 = \psi_i^{(2)}$ , and  $\delta \phi_x = \psi_i^{(3)}$  into Eqs. (4.3.17)–(4.3.19) yields the finite element model

$$0 = \sum_{j=1}^m K_{ij}^{11} u_j^e + \sum_{j=1}^n K_{ij}^{12} w_j^e + \sum_{j=1}^p K_{ij}^{13} s_j^e - F_i^1 \quad (4.3.22)$$

$$0 = \sum_{j=1}^m K_{ij}^{21} u_j^e + \sum_{j=1}^n K_{ij}^{22} w_j^e + \sum_{j=1}^p K_{ij}^{23} s_j^e - F_i^2 \quad (4.3.23)$$

$$0 = \sum_{j=1}^m K_{ij}^{31} u_j^e + \sum_{j=1}^n K_{ij}^{32} w_j^e + \sum_{j=1}^p K_{ij}^{33} s_j^e - F_i^3 \quad (4.3.24)$$

$$\begin{aligned} K_{ij}^{11} &= \int_{x_a}^{x_b} A_{xx} \frac{d\psi_i^{(1)}}{dx} \frac{d\psi_j^{(1)}}{dx} dx, & K_{ij}^{12} &= \frac{1}{2} \int_{x_a}^{x_b} A_{xx} \frac{dw_0}{dx} \frac{d\psi_i^{(1)}}{dx} \frac{d\psi_j^{(2)}}{dx} dx \\ K_{ij}^{21} &= \int_{x_a}^{x_b} A_{xx} \frac{dw_0}{dx} \frac{d\psi_i^{(2)}}{dx} \frac{d\psi_j^{(1)}}{dx} dx, & K_{ij}^{13} &= 0, & K_{ij}^{31} &= 0 \\ K_{ij}^{22} &= \int_{x_a}^{x_b} S_{xx} \frac{d\psi_i^{(2)}}{dx} \frac{d\psi_j^{(2)}}{dx} dx + \frac{1}{2} \int_{x_a}^{x_b} A_{xx} \left( \frac{dw_0}{dx} \right)^2 \frac{d\psi_i^{(2)}}{dx} \frac{d\psi_j^{(2)}}{dx} dx \\ K_{ij}^{23} &= \int_{x_a}^{x_b} S_{xx} \frac{d\psi_i^{(2)}}{dx} \psi_j^{(3)} dx = K_{ji}^{32} \\ K_{ij}^{33} &= \int_{x_a}^{x_b} \left( D_{xx} \frac{d\psi_i^{(3)}}{dx} \frac{d\psi_j^{(3)}}{dx} + S_{xx} \psi_i^{(3)} \psi_j^{(3)} \right) dx \end{aligned} \quad (4.3.25a)$$

$$\begin{aligned}
F_i^1 &= \int_{x_a}^{x_b} \psi_i^{(1)} f \, dx + Q_1^e \psi_i^{(1)}(x_a) + Q_4^e \psi_i^{(1)}(x_b) \\
F_i^2 &= \int_{x_a}^{x_b} \psi_i^{(2)} q \, dx + Q_2^e \psi_i^{(2)}(x_a) + Q_5^e \psi_i^{(2)}(x_b) \\
F_i^3 &= Q_3^e \psi_i^{(3)}(x_a) + Q_6^e \psi_i^{(3)}(x_b)
\end{aligned} \tag{4.3.25b}$$

The element equations (4.3.22)–(4.3.24) can be expressed in matrix form as

$$\begin{bmatrix} [K^{11}] & [K^{12}] & [K^{13}] \\ [K^{21}] & [K^{22}] & [K^{23}] \\ [K^{31}] & [K^{32}] & [K^{33}] \end{bmatrix} \begin{Bmatrix} \{u\} \\ \{w\} \\ \{s\} \end{Bmatrix} = \begin{Bmatrix} \{F^1\} \\ \{F^2\} \\ \{F^3\} \end{Bmatrix} \tag{4.3.26}$$

The choice of the approximation functions  $\psi_i^{(\alpha)}$  dictates different finite element models. The choice of linear polynomials  $\psi_i^{(1)} = \psi_i^{(2)}$  is known to yield a stiffness matrix that is nearly singular. This will be discussed further in the next section. When  $\psi_i^{(1)}$  are quadratic and  $\psi_i^{(2)}$  are linear, the stiffness matrix is  $5 \times 5$ . It is possible to eliminate the interior degree of freedom for  $w_0$  and obtain  $4 \times 4$  stiffness matrix. This element behaves well. When  $\psi_i^{(1)}$  are cubic and  $\psi_i^{(2)}$  are quadratic, the stiffness matrix is  $7 \times 7$ . If the interior nodal degrees of freedom are eliminated, one obtains  $4 \times 4$  stiffness matrix that is known to yield the exact solution at the nodes in the linear case when the shear stiffness and bending stiffnesses are element-wise constant. More details of various Timoshenko beam elements will be given in the sequel.

#### 4.3.4 Shear and Membrane Locking

A number of Timoshenko beam finite elements for the linear case (i.e. without von Kármán nonlinearity) have appeared in the literature. They differ from each other in the choice of approximation functions used for the transverse deflection  $w_0$  and rotation  $\phi_x$ , or in the variational form used to develop the finite element model. Some are based on equal interpolation and others on unequal interpolation of  $w_0$  and  $\phi_x$ .

The Timoshenko beam finite element with linear interpolation of both  $w_0$  and  $\phi_x$  is the simplest element. Linear interpolation of  $w_0$  means that the slope  $dw_0/dx$  is constant (see Figure 4.3.2). In thin beam limit, that is, as the length-to-thickness ratio becomes large (say, 100), the slope should be equal to  $-\phi_x$ , which is also represented as linear as opposed to being a constant. On the other hand, a constant representation of  $\phi_x$  results in zero bending energy while the transverse shear is non-zero. This inconsistency in the representation of the kinematics through linear approximation of both  $w_0$  and  $\phi_x$  results in zero displacements and rotations, which trivially satisfy the Kirchhoff constraint  $\phi_x = -dw_0/dx$ , and the element is said to be very stiff in the thin beam limit. Such behavior is known as *shear locking*.

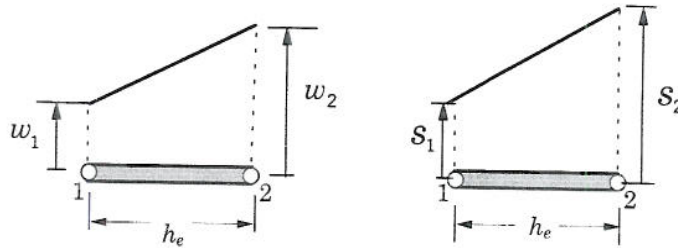


**Figure 4.3.2** Kinematics of deformation of the Timoshenko beam element when both  $w_0$  and  $\phi_x$  are interpolated linearly.

To overcome the locking, one may use equal interpolation for both  $w_0$  and  $\phi_x$  but treat  $\phi_x$  as a constant in the evaluation the shear strain,  $\gamma_{xz} = (dw_0/dx) + \phi_x$ . This is often realized by using selective integration, in which one-point (reduced) Gauss quadrature is used to evaluate the stiffness coefficients associated with the transverse shear strain, and all other coefficients of the stiffness matrix are evaluated using exact (full) integration. A more detailed discussion on the alleviation of shear locking and membrane locking in Timoshenko beam element is presented below.

Since applied distributed loads are represented as point loads in the finite element method, Eq. (4.3.15) with  $q = 0$  and constant  $S_{xx}^e$  implies that

$$\text{(shear strain)} \quad \gamma_{xz}^0 \equiv \phi_x + \frac{dw_0}{dx} = \text{constant} \quad (4.3.27)$$

Similarly, for a problem that involves only bending deformation, the element should experience no stretching [see Eq. (4.3.14) with  $f = 0$ ]:

$$\text{(membrane strain)} \quad \varepsilon_{xx}^0 \equiv \frac{du_0}{dx} + \frac{1}{2} \left( \frac{dw_0}{dx} \right)^2 = 0 \quad (4.3.28)$$

In order to satisfy the above constraints, we must have

$$\phi_x \sim \frac{dw_0}{dx} \quad (4.3.29)$$

$$\frac{du_0}{dx} \sim \left( \frac{dw_0}{dx} \right)^2 \quad (4.3.30)$$

The similarity is in the sense of having the same degree of polynomial variation. For example, when  $\phi_x$  is linear and  $w_0$  is quadratic, the constraint in Eq. (4.3.27) is clearly met. Similarly, when both  $u_0$  and  $w_0$  are linear, the constraint in Eq. (4.3.28) is automatically met; however, when quadratic

interpolation is used for both  $u_0$  and  $w_0$ ,  $du_0/dx$  is linear and  $(dw_0/dx)^2$  is quadratic and the resulting element experiences locking, known as the membrane locking. If  $u_0$  is interpolated using a cubic polynomial,  $w_0$  with a quadratic polynomial, and  $\phi_x$  with a linear polynomial, we have

$$\phi_x \text{ (linear)} \sim \frac{dw_0}{dx} \text{ (linear)} \quad (4.3.31)$$

$$\frac{du_0}{dx} \text{ (quadratic)} \sim \left(\frac{dw_0}{dx}\right)^2 \text{ (quadratic)} \quad (4.3.32)$$

In summary, the constraints would be satisfied for the following two cases:

- $u_0$ ,  $\phi_x$ , and  $w_0$  all linear, with constant representation of  $\gamma_{xz}$ ; the latter can be accomplished by using reduced integration to evaluate the shear stiffness coefficients.
- $u_0$  is cubic,  $w_0$  is quadratic, and  $\phi_x$  is linear. However, this will result in a  $9 \times 9$  stiffness matrix with different degrees of freedom at different nodes, making it difficult (but not impossible) to implement into a computer program.

The membrane locking can also be avoided, in addition to using appropriate interpolation of the variables, by using selective Gauss quadrature, as discussed in Section 4.2.7. In the present study, we shall use equal linear or quadratic interpolation of the variables  $(u_0, w_0, \phi)$  with reduced integration of all nonlinear terms (to avoid membrane locking) and shear terms, that is, stiffness coefficients involving  $S_{xx}$  (to avoid shear locking) of the stiffness matrix.

#### 4.3.5 Tangent Stiffness Matrix

Returning to the nonlinear finite element model (4.3.26) of Section 4.3.3, we compute the tangent stiffness matrix of the Timoshenko beam element. Much of the computer implementation discussion presented in Section 4.2.8 is also valid for the Timoshenko beam element.

The tangent matrix coefficients are defined by

$$T_{ij}^{\alpha\beta} = K_{ij}^{\alpha\beta} + \sum_{\gamma=1}^3 \sum_{k=1}^n \frac{\partial}{\partial \Delta_j^\beta} (K_{ik}^{\alpha\gamma}) \Delta_k^\gamma \quad (4.3.33)$$

In particular, we have

$$T_{ij}^{11} = K_{ij}^{11} + 0$$

$$T_{ij}^{12} = K_{ij}^{12} + \frac{1}{2} \int_{x_a}^{x_b} A_{xx} \frac{dw_0}{dx} \frac{d\psi_i^{(1)}}{dx} \frac{d\psi_j^{(2)}}{dx} dx = 2K_{ij}^{12}$$

$$\begin{aligned}
 T_{ij}^{13} &= K_{ij}^{13} = 0 \\
 T_{ij}^{21} &= K_{ij}^{21} + 0 = K_{ij}^{21} \\
 T_{ij}^{22} &= K_{ij}^{22} + \int_{x_a}^{x_b} A_{xx} \left[ \frac{du_0}{dx} + \left( \frac{dw_0}{dx} \right)^2 \right] \frac{d\psi_i^{(2)}}{dx} \frac{d\psi_j^{(2)}}{dx} dx \\
 T_{ij}^{23} &= K_{ij}^{23} + 0 = K_{ij}^{23} \\
 T_{ij}^{31} &= K_{ij}^{31} + 0 = K_{ij}^{31} \\
 T_{ij}^{32} &= K_{ij}^{32} + 0 = K_{ij}^{32} \\
 T_{ij}^{33} &= K_{ij}^{33} + 0 = K_{ij}^{33}
 \end{aligned} \tag{4.3.34}$$

where the direct stiffness coefficients  $K_{ij}^{\alpha\beta}$  are defined by Eq. (4.3.25a).

As discussed earlier, we must use reduced integration on nonlinear stiffness coefficients and shear stiffness coefficients, while the remaining stiffness coefficients may be evaluated using full integration. For example, consider the following integral expression:

$$\int_{x_a}^{x_b} A_{xx} \left[ \frac{du_0}{dx} \frac{d\psi_i^{(2)}}{dx} \frac{d\psi_j^{(2)}}{dx} + \frac{3}{2} \left( \frac{dw_0}{dx} \right)^2 \frac{d\psi_i^{(2)}}{dx} \frac{d\psi_j^{(2)}}{dx} \right] dx \tag{4.3.35}$$

If quadratic interpolation of both  $u_0$  and  $w_0$  is used (see Figure 4.3.3) and  $A_{xx}$  is constant, then the first term in the integrand is a cubic polynomial while the second term is a fourth-order polynomial. Thus, exact evaluation of the first term requires two-point Gauss quadrature while the second term requires three-point Gauss quadrature. If we use two-point Gauss quadrature to evaluate  $T_{ij}^{22}$  (and  $K_{ij}^{22}$ ), the first term in the coefficient of  $A_{xx}$  is integrated exactly while the second term is integrated approximately. This amounts to approximating  $(dw_0/dx)^2$  as a linear polynomial. Consequently, the constraint  $\epsilon_{xx}^0 = 0$  [see Eq. (4.3.28)] is satisfied.

The rearrangement of the elements of nodal displacement vector, as shown in Eq. (4.2.50), requires rearranging of  $K_{ij}^{\alpha\beta}$  of Eq. (4.3.26). Box 4.3.1 shows the logic for this rearrangement.

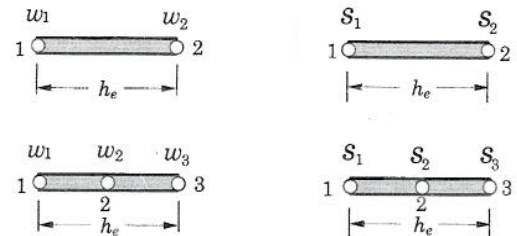


Figure 4.3.3 Linear and quadratic Timoshenko beam finite elements.

**Box 4.3.1** Fortran statements to rearrange stiffness coefficients.

```

C Rearranging of the element stiffness coefficients
C of the TIMOSHENKO beam element (TBT)
C ELK11, ELF1, etc are defined by Eqs. (4.3.25a,b)
C
      II=1
      DO 160 I=1,NPE
        JJ=1
        ELF(II) = ELF1(I)
        ELF(II+1) = ELF2(I)
        DO 150 J=1,NPE
          ELK(II,JJ) = ELK11(I,J)
          ELK(II,JJ+1) = ELK12(I,J)
          ELK(II+1,JJ) = ELK21(I,J)
          ELK(II+1,JJ+1) = ELK22(I,J)
          ELK(II+1,JJ+2) = ELK23(I,J)
          ELK(II+2,JJ+1) = ELK32(I,J)
          ELK(II+2,JJ+2) = ELK33(I,J)
        150      JJ=J*NDF+1
      160      II=I*NDF+1

```

**Example 4.3.1**

Consider the hinged-hinged beam of Example 4.2.1. Using the symmetry about  $x = L/2$ , one-half of the domain is used as the computational domain. The geometric boundary conditions for the computational domain are

$$w_0(0) = u_0\left(\frac{L}{2}\right) = \phi_x\left(\frac{L}{2}\right) = 0 \quad (4.3.36)$$

The load is divided into load increments of equal size  $\Delta q_0 = 1$  lb/in. A tolerance of  $\epsilon = 10^{-3}$  is used in the analysis. The initial solution vector is chosen to be the zero vector, so that the first iteration solution corresponds to the linear problem. The exact linear solution is ( $u_0(x) = 0$ )

$$w_0(x) = \frac{q_0 L^4}{24D_{xx}} \left( \frac{x}{L} - 2\frac{x^3}{L^3} + \frac{x^4}{L^4} \right) + \frac{q_0 L^2}{2S_{xx}} \left( \frac{x}{L} - \frac{x^2}{L^2} \right), \quad \phi_x(x) = \frac{q_0 L^3}{24D_{xx}} \left( 1 - 6\frac{x^2}{L^2} + 4\frac{x^3}{L^3} \right) \quad (4.3.37)$$

The center deflection of the linear problem is ( $q_0 = 1$  lb/in.,  $E = 30 \times 10^6$  psi,  $\nu = 0.25$ , and  $K_s = 5/6$ )

$$w_0\left(\frac{L}{2}\right) = \frac{5q_0 L^4}{384D_{xx}} + \frac{q_0 L^2}{8S_{xx}} = 0.5208 + 0.0125 \times 10^{-4} = 0.5208 \text{ in.} \quad (4.3.38)$$

Thus, the effect of shear deformation is negligible. It should be noted that the reduced-integration (Timoshenko) element (RIE), in general, does not give exact nodal values even for the linear problem (i.e. not a superconvergent element). For a refined mesh and/or higher-order elements, one may expect to get the exact linear solution.



For the mesh of four reduce integration elements, the linear stiffness matrix, force vector, and the global linear solution vector are (with  $\nu = 0.25$  and specified boundary conditions  $\Delta_2 = 0$ ,  $\Delta_{13} = 0$  and  $\Delta_{15} = 0$ )

$$[K^e] = 10^5 \begin{bmatrix} 24 & 0.0 & 0.0 & -24 & 0.0 & 0.0 \\ 0 & 8.0 & -50.0 & 0 & -8.0 & -50.0 \\ 0 & -50.0 & 314.5 & 0 & 50.0 & 310.5 \\ -24 & 0.0 & 0.0 & 24 & 0.0 & 0.0 \\ 0 & -8.0 & 50.0 & 0 & 8.0 & 50.0 \\ 0 & -50.0 & 310.5 & 0 & 50.0 & 314.5 \end{bmatrix}$$

$$\{F^e\} = \begin{Bmatrix} 0.00 \\ 6.25 \\ 0.00 \\ 0.00 \\ 6.25 \\ 0.00 \end{Bmatrix}, \quad \begin{Bmatrix} \Delta_3 \\ \Delta_5 \\ \Delta_6 \\ \Delta_8 \\ \Delta_9 \\ \Delta_{11} \\ \Delta_{12} \\ \Delta_{14} \end{Bmatrix} = \begin{Bmatrix} -0.01641 \\ 0.19659 \\ -0.01504 \\ 0.36142 \\ -0.01133 \\ 0.47009 \\ -0.00605 \\ 0.5079 \end{Bmatrix}$$

Table 4.3.1 contains the results obtained with the Newton-Raphson iteration; FI denotes full integration ( $NGP = LGP = 2$  for linear elements  $NGP = LGP = 3$  for quadratic elements) and RI denotes reduced integration ( $NGP = 2$  and  $LGP = 1$  for linear elements and  $NGP = 3$  and  $LGP = 2$  for quadratic elements). The convergence is reached in 3 iterations. It is clear that the quadratic elements are not as sensitive as the linear elements to locking; also, the effect of locking on the solution becomes less with refined meshes. The convergence of the solution with mesh refinement is also clear.

**Table 4.3.1** Finite element results for the deflections of a *hinged-hinged beam* under uniform load.

Load $q_0$	Integration rule	4L	2Q	8L	4Q	16L	8Q
1.0	RI	0.5079	0.5210	0.5177	0.5210	0.5201	0.5210
	FI	0.0101	0.4943	0.0370	0.5149	0.1223	0.5198
2.0	RI	1.0159	1.0419	1.0354	1.0419	1.0403	1.0419
	FI	0.0201	0.9817	0.0741	1.0294	0.2447	1.0395
3.0	RI	1.5238	1.5629	1.5531	1.5629	1.5604	1.5629
	FI	0.0302	1.4560	0.1111	1.5428	0.3670	1.5592
4.0	RI	2.0318	2.0838	2.0708	2.0838	2.0806	2.0838
	FI	0.0403	1.9130	0.1482	2.0548	0.4893	2.0788
5.0	RI	2.5397	2.6048	2.5885	2.6048	2.6007	2.6048
	FI	0.0504	2.3502	0.1852	2.5654	0.6117	2.5983
10.0	RI	5.0794	5.2096	5.1770	5.2096	5.2014	5.2096
	FI	0.1007	4.2312	0.3704	5.0728	1.2233	5.1927

**Example 4.3.2**

Here we consider the *pinned-pinned* beam of Example 3.2.2. The geometric boundary conditions for the computational domain of the problem are

$$u_0(0) = w_0(0) = u_0\left(\frac{L}{2}\right) = \phi_x\left(\frac{L}{2}\right) = 0 \tag{4.3.39}$$

The load increments of  $\Delta q_0 = 1.0 \text{ lb/in.}$ , a tolerance of  $\epsilon = 10^{-3}$  is used in the analysis. The initial solution vector is chosen to be the zero vector.

Table 4.3.2 contains the results for pinned-pinned beam; the results were obtained with the Newton-Raphson iteration ( $\gamma = 0$ ) method and reduced integration. The convergence of the solution with mesh refinement and higher-order elements is apparent from the results. Also, higher-order elements and refined meshes are less sensitive to shear locking.

**Table 4.3.2** Finite element results for the deflections of a *pinned-pinned* beam under uniformly distributed load.

Load $q_0$	4L	2Q	8L	4Q
1.0	0.3654 (5)*	0.3687 (5)	0.3677 (5)	0.3685 (5)
2.0	0.5439 (4)	0.5458 (4)	0.5451 (4)	0.5454 (4)
3.0	0.6637 (3)	0.6644 (3)	0.6639 (3)	0.6640 (3)
4.0	0.7562 (3)	0.7560 (3)	0.7557 (3)	0.7555 (3)
5.0	0.8327 (3)	0.8318 (3)	0.8316 (3)	0.8312 (3)
6.0	0.8985 (3)	0.8970 (3)	0.8969 (3)	0.8964 (3)
7.0	0.9567 (3)	0.9546 (3)	0.9546 (3)	0.9540 (3)
8.0	1.0090 (3)	1.0065 (3)	1.0066 (3)	1.0058 (3)
9.0	1.0568 (3)	1.0538 (3)	1.0540 (3)	1.0531 (3)
10.0	1.1009 (3)	1.0975 (3)	1.0977 (3)	1.0967 (3)

\* Number of iterations taken to converge.

Table 4.3.3 contains nonlinear deflections,  $\bar{w} = w_{max}10^2(D_{xx}/L^4)$ , of pinned-pinned beams for various length-to-thickness ratios  $L/H$ . The effect of shear deformation is clear from the results; thicker the beams, larger the shear strains and deflections  $\bar{w}$ . Of course, the maximum deflection  $w_{max}$  will be smaller with smaller  $L/H$  ratio (or thicker beams), because thicker beams have larger stiffness. Thus they also exhibit less geometric nonlinearity, as can be seen from Figure 4.3.4, where the deflection at the center,  $w_0(L/2)$ , is plotted as a function of the load  $q_0$  for various values of  $L/H$  ratio. The deflections predicted by the TBT are the same as those predicted by the EBT when  $L/H \geq 100$ .

Lastly, we consider the *clamped-clamped* beam of Example 4.2.3. The geometric boundary conditions for the computational domain of the problem are

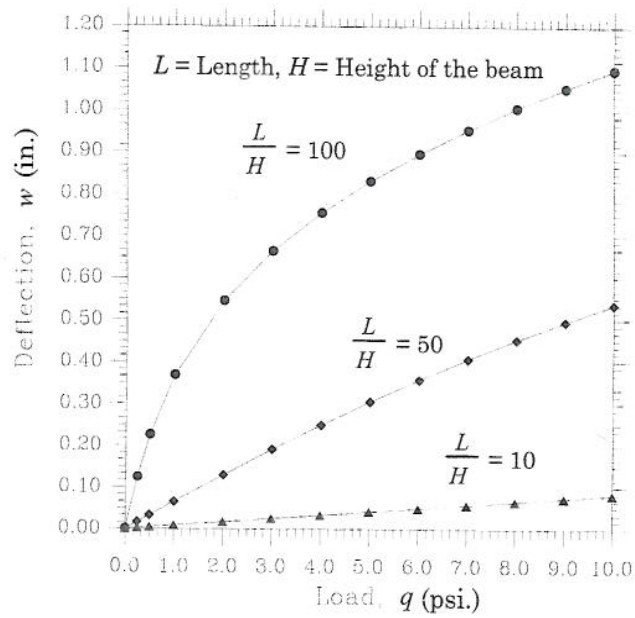
$$u_0(0) = w_0(0) = \phi_x(0) = u_0\left(\frac{L}{2}\right) = \phi_x\left(\frac{L}{2}\right) = 0 \tag{4.3.40}$$

All other parameters are taken to be the same as in the case of the pinned-pinned beam. Table 4.3.4 contains the nonlinear analysis results for clamped-clamped beam; the results were obtained with the direct iteration as well as the Newton-Raphson iteration method using (a) mesh of 8 linear Timoshenko beam elements, and (b) 4 quadratic Timoshenko beam elements. The results obtained with both methods and meshes are virtually the same, although the direct iteration scheme takes more iterations to converge.

**Table 4.3.3** The effect of length-to-thickness ratio on the deflections  $\bar{w} = w_{max}10^2 D_{xx}/L^4$  of a *pinned-pinned beam* under uniformly distributed load (4Q element mesh).

Load $q_0$	Length-to-thickness ratio, $L/H$			
	10	20	25	100
1.0	1.335 (2)*	1.310 (2)	1.307 (2)	0.921 (5)
2.0	2.669 (2)	2.620 (2)	2.614 (2)	1.364 (4)
3.0	4.004 (2)	3.931 (2)	3.921 (2)	1.660 (3)
4.0	5.338 (2)	5.241 (2)	5.228 (2)	1.889 (3)
5.0	6.673 (2)	6.551 (2)	6.534 (2)	2.078 (3)
6.0	8.008 (2)	7.861 (2)	7.840 (2)	2.241 (3)
7.0	9.342 (2)	9.171 (2)	9.145 (2)	2.385 (3)
8.0	10.677 (2)	10.480 (2)	10.450 (2)	2.515 (3)
9.0	12.011 (2)	11.790 (2)	11.753 (2)	2.633 (3)
10.0	13.346 (2)	13.099 (2)	13.056 (2)	2.742 (3)

\* Number of iterations taken to converge.

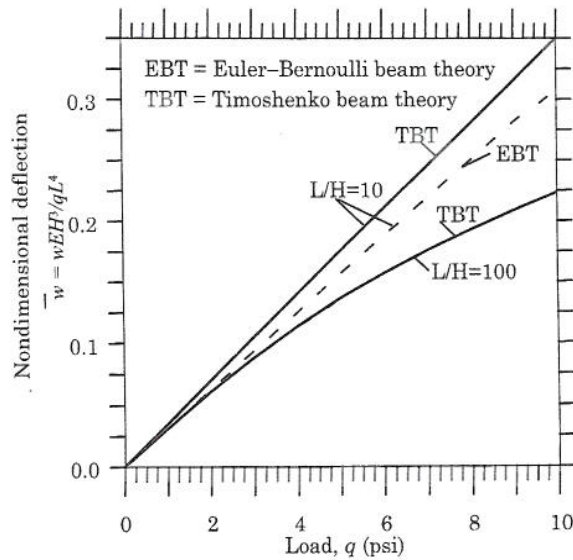


**Figure 4.3.4** Load versus deflection curves for pinned-pinned beam.

**Table 4.3.4** Finite element results for the deflections of a *clamped-clamped* beam under uniformly distributed load ( $\nu = 0.25$ ).

Load $q_0$	Direct iteration		Newton-Raphson Iteration	
	8L	4Q	8L	4Q
1.0	0.1019 (3)*	0.1035 (3)	0.1019 (3)	0.1035 (3)
2.0	0.1997 (4)	0.2025 (4)	0.1997 (3)	0.2025 (3)
3.0	0.2906 (4)	0.2943 (4)	0.2906 (3)	0.2943 (3)
4.0	0.3738 (5)	0.3778 (5)	0.3737 (3)	0.3778 (3)
5.0	0.4493 (5)	0.4535 (5)	0.4492 (3)	0.4534 (3)
6.0	0.5178 (6)	0.5219 (6)	0.5179 (3)	0.5220 (3)
7.0	0.5806 (7)	0.5846 (7)	0.5805 (3)	0.5845 (3)
8.0	0.6379 (8)	0.6416 (8)	0.6380 (3)	0.6418 (3)
9.0	0.6908 (8)	0.6947 (9)	0.6910 (3)	0.6946 (3)
10.0	0.7406 (9)	0.7434 (10)	0.7403 (3)	0.7436 (3)

\* Number of iterations taken to converge.


**Figure 4.3.5** Load-deflection response predicted by the EBT and TBT for clamped-clamped, thin ( $L/H = 100$ ) and thick ( $L/H = 10$ ) beams.

We close this chapter with a note that the geometric nonlinearity considered in the analysis of beams in this chapter is one where the strains are assumed to be small while the rotations are moderately large. In Chapter 9 on continuum formulations, we will revisit this topic in the context of plane elasticity.

## Problems

4.1 Consider the nonlinear differential equations

$$-\frac{dN_{xx}}{dx} = f(x) \quad (\text{a})$$

$$\frac{d^2}{dx^2} \left( D_{xx} \frac{d^2 w_0}{dx^2} \right) - \frac{d}{dx} \left( N_{xx} \frac{dw_0}{dx} \right) = q(x) \quad (\text{b})$$

where  $q(x)$  is the distributed transverse force (positive upward), and

$$N_{xx} = A_{xx} \left[ \frac{du_0}{dx} + \frac{1}{2} \left( \frac{dw_0}{dx} \right)^2 \right] \quad (\text{c})$$

Rewrite the equations (by introducing the bending moment  $M(x)$  as a dependent variable) as a set of second-order equations

$$-\frac{d}{dx} \left\{ A_{xx} \left[ \frac{du_0}{dx} + \frac{1}{2} \left( \frac{dw_0}{dx} \right)^2 \right] \right\} - f(x) = 0 \quad (\text{d})$$

$$-\frac{d^2 w_0}{dx^2} - \frac{M_{xx}}{D_{xx}} = 0 \quad (\text{e})$$

$$-\frac{d^2 M_{xx}}{dx^2} - \frac{d}{dx} \left\{ \frac{dw_0}{dx} A_{xx} \left[ \frac{du_0}{dx} + \frac{1}{2} \left( \frac{dw_0}{dx} \right)^2 \right] \right\} = q(x) \quad (\text{f})$$

Develop: (a) the weak form, and (b) the finite element model using interpolation of the form

$$u_0 = \sum_{j=1}^m u_j^e \psi_j^{(1)}(x), \quad w_0 = \sum_{j=1}^n w_j^e \psi_j^{(2)}(x), \quad M_{xx} = \sum_{j=1}^r M_j^e \psi_j^{(3)}(x) \quad (\text{g})$$

4.2 Consider the problem of (linear) bending of beams according to the Euler–Bernoulli beam theory. The principle of minimum total potential energy states that if the beam is in equilibrium then the total potential energy associated with the equilibrium configuration is the minimum; that is, the equilibrium displacements are those which make the total potential energy a minimum. Thus, solving the equations governing the equilibrium of the Euler–Bernoulli beam is equivalent to minimizing the total potential energy

$$\begin{aligned} \Pi(u_0, w_0) = & \int_{x_a}^{x_b} \left\{ \frac{A_{xx}}{2} \left[ \frac{du_0}{dx} + \frac{1}{2} \left( \frac{dw_0}{dx} \right)^2 \right]^2 + \frac{D_{xx}}{2} \left( \frac{d^2 w_0}{dx^2} \right)^2 \right\} dx \\ & - \int_{x_a}^{x_b} (f u_0 + q w_0) dx \end{aligned} \quad (\text{a})$$

where  $A_{xx} = E_x A$  and  $D_{xx} = E_x I_{yy}$  are the extensional and bending stiffnesses. The necessary condition for the minimum of a functional is that its first variation be zero:  $\delta \Pi = 0$ , which yields the governing equations of equilibrium. As you know, the statement  $\delta \Pi = 0$  is the same as the weak forms of the governing equations of the Euler–Bernoulli beam theory. The weak form requires Hermite cubic interpolation of the transverse deflection  $w_0$ . Now suppose that we wish to relax the continuity required of the interpolation used for  $w_0(x)$  by introducing the relation

$$\frac{dw_0}{dx} = \varphi(x) \quad (\text{b})$$

Then the total potential energy functional takes the form

$$\begin{aligned} \Pi(u_0, w_0, \varphi) = & \int_{x_a}^{x_b} \left\{ \frac{A_{xx}}{2} \left[ \frac{du_0}{dx} + \frac{1}{2} \left( \frac{dw_0}{dx} \right)^2 \right]^2 + \frac{D_{xx}}{2} \left( \frac{d\varphi}{dx} \right)^2 \right\} dx \\ & - \int_{x_a}^{x_b} (fu_0 + qw_0) dx - \sum_{i=1}^6 \Delta_i^e Q_i^e \end{aligned} \quad (c)$$

Since the functional now contains only the first derivative of  $u_0$  and  $\varphi$ , linear Lagrange (minimum) interpolation can be used. Thus the original problem is replaced with the following equivalent problem:

Minimize  $\Pi(u_0, w_0, \varphi)$  in Eq. (c) subjected to the constraint

$$\frac{dw_0}{dx} - \varphi(x) = 0 \quad (d)$$

Develop the penalty function formulation of the constrained problem by deriving (a) the weak form, and (b) the finite element model.

4.3 Develop the weak forms of the governing equations (4.3.8)–(4.3.10); make use of the definitions in Eq. (4.3.20).

4.4 Analyze a clamped (at both ends) beam under uniformly distributed load (of intensity,  $q_0$ ) using the Newton–Raphson iteration method and (a) the Euler–Bernoulli beam element, and (b) the Timoshenko beam element. Plot the non-dimensional maximum deflection,  $\bar{w} = w_{max}/L$  versus the load parameter,  $\bar{P} = q_0 L^3/EI$ , with at least twelve points on the graph. Use 8 elements in the beam, with

$$EA = 30 \times 10^6 \left[ 1 + 0.5 \frac{x}{L} \right], \quad EI = \frac{30 \times 10^6}{12} \left[ 1 + 0.5 \frac{x}{L} \right]^3 \quad (a)$$

and  $L = 100$ . Investigate the effect of numerical integration rule on the accuracy of the results.

4.5 The principle of minimum total potential energy for axisymmetric bending of polar orthotropic plates according to the first-order shear deformation theory requires  $\delta\Pi(w_0, \phi) = 0$ , where

$$\begin{aligned} \delta\Pi_m = & 2 \int_b^a \left[ \left( D_{11} \frac{d\phi}{dr} + D_{12} \frac{\phi}{r} \right) \frac{d\delta\phi}{dr} + \frac{1}{r} \left( D_{12} \frac{d\phi}{dr} + D_{22} \frac{\phi}{r} \right) \delta\phi \right. \\ & \left. + A_{55} \left( \phi + \frac{dw_0}{dr} \right) \left( \delta\phi + \frac{d\delta w_0}{dr} \right) - 2q\delta w_0 \right] r dr \end{aligned} \quad (a)$$

where  $b$  is the inner radius and  $a$  the outer radius. Derive the displacement finite element model of the equations. In particular, show that the finite element model is of the form (i.e. define the matrix coefficients of the following equation)

$$\begin{bmatrix} [K^{11}] & [K^{12}] \\ [K^{12}]^T & [K^{22}] \end{bmatrix} \begin{Bmatrix} \{w\} \\ \{\phi\} \end{Bmatrix} = \begin{Bmatrix} \{F\} \\ \{0\} \end{Bmatrix} \quad (b)$$

4.6 Implement the displacement finite element model into a computer program and verify with analytical solutions of simply supported and clamped circular plates (see Reddy [3]).

- 4.7 Include the geometric nonlinearity (by accounting for the von Kármán nonlinear strains) in the total potential energy functional of Problem 4.5, and develop the finite element model.
- 4.8 Implement the nonlinear finite element model of Problem 4.7 into a computer program and validate it with other published results (see Chapter 6).

## References

1. Reddy, J. N., *An Introduction to the Finite Element Method*, 2nd edn, McGraw-Hill, New York (1993).
2. Reddy, J. N., *Energy Principles and Variational Methods in Applied Mechanics*, 2nd edn, John Wiley, New York (2002).
3. Reddy, J. N., *Theory and Analysis of Elastic Plates*, Taylor and Francis, Philadelphia, PA (1999).

---

## Heat Transfer and Other Field Problems in Two Dimensions

---

### 5.1 Model Equation

The finite element analysis of nonlinear two-dimensional problems involves the same basic steps as those described for one-dimensional problems in Chapter 3. Finite element formulation of a model second-order equation was presented in Section 2.3. Here, we extend that development to problems in which the coefficients of the differential equation are possibly functions of the dependent variable and its derivatives.

Consider the problem of finding the solution  $u$  of the following second-order partial differential equation (a slightly more general equation than the one considered in Section 2.3)

$$-\frac{\partial}{\partial x} \left( a_{xx} \frac{\partial u}{\partial x} \right) - \frac{\partial}{\partial y} \left( a_{yy} \frac{\partial u}{\partial y} \right) + a_{00}u = f(x, y) \quad \text{in } \Omega \quad (5.1.1)$$

where  $a_{xx}$ ,  $a_{yy}$ , and  $a_{00}$  are known functions of position  $(x, y)$  and the dependent unknown  $u$  and its derivatives, and  $f$  is a known function of position in a two-dimensional domain  $\Omega$  with boundary  $\Gamma$  [see Figure 5.1.1(a)]. For example,  $a_{xx}$  may be assumed to be of the form

$$a_{xx} = a_{xx} \left( x, y, u, \frac{\partial u}{\partial x}, \frac{\partial u}{\partial y} \right) \quad (5.1.2)$$

The equation is subject to certain boundary conditions, whose form will be apparent from the weak formulation.

In the finite element method, the domain  $\bar{\Omega}$  is discretized into a collection of elements  $\Omega^e$  [see Figure 5.1.1(b)]

$$\bar{\Omega} \approx \Omega_h = \bigcup_{e=1}^N \bar{\Omega}^e, \quad \bar{\Omega} = \Omega \cup \Gamma, \quad \bar{\Omega}^e = \Omega^e \cup \Gamma^e \quad (5.1.3)$$



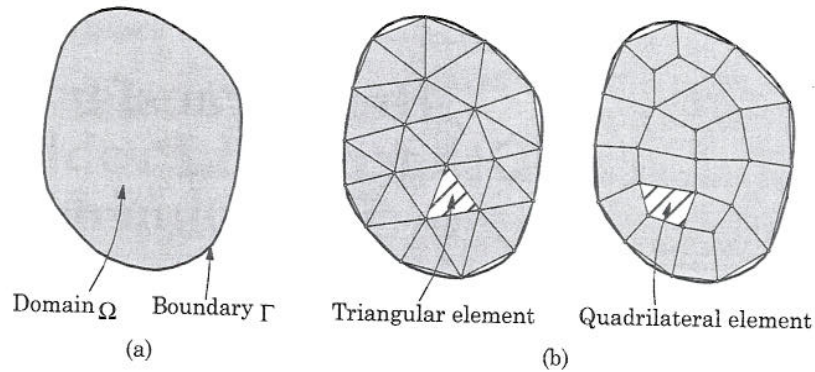


Figure 5.1.1 Finite element discretization of a two-dimensional domain  $\Omega$  and a typical finite element  $\Omega^e$ .

## 5.2 Weak Form

We use a representative element domain  $\Omega^e$  to derive the weak form of the model equation, with the assumption that each element has a unique geometric shape and associated interpolation functions.

Following the steps of Section 2.3, the weak form of Eq. (5.2.1) over a typical finite element  $\Omega^e$ , whether triangular or quadrilateral shape, can be developed. The first step is to multiply Eq. (5.2.1) with a weight function  $w$  which is assumed to be differentiable once with respect to  $x$  and  $y$ , and then integrate the equation over the element domain  $\Omega^e$ :

$$0 = \int_{\Omega^e} w \left[ -\frac{\partial}{\partial x} \left( a_{xx} \frac{\partial u}{\partial x} \right) - \frac{\partial}{\partial y} \left( a_{yy} \frac{\partial u}{\partial y} \right) + a_{00}u - f \right] dx dy \quad (5.2.1)$$

In the second step we distribute the differentiation among  $u$  and  $w$  equally. To achieve this, we integrate the first two terms in Eq. (5.2.1) by parts using the component forms of the Green-Gauss theorem (gradient or divergence theorem).

$$0 = \int_{\Omega^e} \left( a_{xx} \frac{\partial w}{\partial x} \frac{\partial u}{\partial x} + a_{yy} \frac{\partial w}{\partial y} \frac{\partial u}{\partial y} + a_{00}wu - wf \right) dx dy - \oint_{\Gamma^e} w \left( a_{xx} \frac{\partial u}{\partial x} n_x + a_{yy} \frac{\partial u}{\partial y} n_y \right) ds \quad (5.2.2)$$

where  $n_x$  and  $n_y$  are the components (i.e. the direction cosines) of the unit normal vector

$$\hat{\mathbf{n}} = n_x \hat{\mathbf{i}} + n_y \hat{\mathbf{j}} = \cos \alpha \hat{\mathbf{i}} + \sin \alpha \hat{\mathbf{j}} \quad (5.2.3)$$

on the boundary  $\Gamma^e$ , and  $ds$  is the arc length of an infinitesimal line element along the boundary (see Figure 5.2.1). The circle on the boundary integral denotes integration over the closed boundary  $\Gamma^e$ . From an inspection of the boundary term in Eq. (5.2.2), we note that  $u$  is the primary variable. The coefficient of the weight function  $w$  in the boundary expression is

$$a_{xx} \frac{\partial u}{\partial x} n_x + a_{yy} \frac{\partial u}{\partial y} n_y \equiv q_n \quad (5.2.4)$$

and it constitutes the secondary variable. Thus, the weak form of Eq. (5.2.1) is

$$0 = \int_{\Omega^e} \left( a_{xx} \frac{\partial w}{\partial x} \frac{\partial u}{\partial x} + a_{yy} \frac{\partial w}{\partial y} \frac{\partial u}{\partial y} + a_{00} w u - w f \right) dx dy - \oint_{\Gamma^e} w q_n ds \quad (5.2.5)$$

The function  $q_n = q_n(s)$  denotes the outward flux from the boundary as we move counter-clockwise along the boundary  $\Gamma^e$ . The secondary variable  $q_n$  is of physical interest in most problems. For example, in the case of the heat transfer through an anisotropic medium,  $a_{ij}$  denotes the conductivities of the medium, and  $q_n$  denotes the heat flux normal to the boundary of the element. The weak form (or weighted-integral statement) in (5.2.5) forms the basis of the finite element model of Eq. (5.2.1).

### 5.3 Finite Element Model

The weak form in Eq. (5.2.5) requires that the approximation chosen for  $u$  should be at least linear in both  $x$  and  $y$  so that every term in Eq. (5.2.5) has a non-zero contribution to the integral. Since the primary variable is just  $u$ , which must be made continuous between elements, the Lagrange family of interpolation functions is admissible. Hence,  $u$  is approximated over a typical

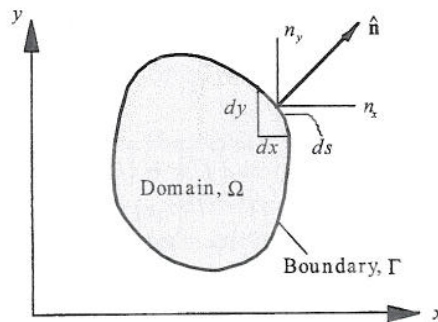


Figure 5.2.1 A typical two-dimensional domain with a curved boundary.

finite element  $\Omega^e$  by the expression

$$u(x, y) \approx u_h^e(x, y) = \sum_{j=1}^n u_j^e \psi_j^e(x, y) \quad (5.3.1)$$

where  $u_j^e$  is the value of  $u_h^e$  at the  $j$ th node of the element, and  $\psi_j^e$  are the Lagrange interpolation functions, which have the property

$$\psi_i^e(x_j, y_j) = \delta_{ij} \quad (5.3.2)$$

where  $(x_j, y_j)$  are the global coordinates of the  $j$ th node of the element  $\Omega^e$ .

Substituting the finite element approximation (5.3.1) for  $u$  into the weak form (5.2.5), we obtain

$$\begin{aligned} 0 &= \int_{\Omega^e} \left[ \frac{\partial w}{\partial x} \left( a_{xx} \sum_{j=1}^n u_j \frac{\partial \psi_j^e}{\partial x} \right) + \frac{\partial w}{\partial y} \left( a_{yy} \sum_{j=1}^n u_j \frac{\partial \psi_j^e}{\partial y} \right) + a_{00} w \sum_{j=1}^n u_j \psi_j^e \right. \\ &\quad \left. - w f \right] dx dy - \oint_{\Gamma^e} w q_n ds \\ &= \sum_{j=1}^n K_{ij}^e u_j^e - f_i^e - Q_i^e \end{aligned} \quad (5.3.3)$$

where

$$\begin{aligned} K_{ij}^e &= \int_{\Omega^e} \left( a_{xx} \frac{\partial \psi_i^e}{\partial x} \frac{\partial \psi_j^e}{\partial x} + a_{yy} \frac{\partial \psi_i^e}{\partial y} \frac{\partial \psi_j^e}{\partial y} + a_{00} \psi_i^e \psi_j^e \right) dx dy \\ f_i^e &= \int_{\Omega^e} \psi_i^e f dx dy \\ Q_i^e &= \oint_{\Gamma^e} \psi_i^e q_n ds \end{aligned} \quad (5.3.4)$$

Note that  $K_{ij}^e = K_{ji}^e$  (i.e.  $[K]$  is symmetric), even though it may be a function of the unknown nodal values  $u_j^e$ . The set of  $n$  nonlinear algebraic equations can be written in matrix form as

$$[K^e]\{u^e\} = \{f^e\} + \{Q^e\} \quad (5.3.5)$$

Equation (5.3.5) represents the finite element model of Eq. (5.1.1). This completes the finite element model development. The usual tasks of assembly of element equations, imposition of boundary conditions, and solution of linear algebraic equations (after an iterative method is applied) are standard and therefore not discussed here (see Reddy [1]).

## 5.4 Solution Procedures

### 5.4.1 Direct Iteration

The assembled form of the nonlinear equation (5.3.5) is

$$[K(\{U\})]\{U\} = \{F\} \quad (5.4.1)$$

where  $[K]$  is the assembled coefficient matrix,  $\{U\}$  the vector of global nodal values, and  $\{F\}$  the assembled source vector. In the direct iteration procedure, the solution at the  $r$ th iteration is determined from the equation

$$[K(\{U\}^{(r-1)})]\{U\}^{(r)} = \{F\} \quad (5.4.2)$$

where the direct matrix  $[K]$  is evaluated using the solution (known) at the  $(r-1)$ st iteration. The direct iteration procedure can be applied to the element equation (5.3.5), as was done in Chapters 3 and 4. We obtain

$$[K^e(\{u^e\}^{(r-1)})]\{u^e\}^{(r)} = \{F^e\} \quad (5.4.3)$$

### 5.4.2 Newton–Raphson Iteration

In the Newton–Raphson procedure, we solve the equation

$$[T(\{U\}^{(r-1)})]\{\delta U\} = -\{R(\{U\}^{(r-1)})\} \quad (5.4.4)$$

where  $\{R\}$  is the residual vector

$$-\{R(\{U\}^{(r-1)})\} = \{F\} - [K(\{U\}^{(r-1)})]\{U\}^{(r-1)} \quad (5.4.5)$$

and  $[T]$  is the tangent matrix

$$[T(\{U\}^{(r-1)})] \equiv \left( \frac{\partial \{R\}}{\partial \{U\}} \right)^{(r-1)} \quad (5.4.6)$$

The solution at the end of the  $r$ th iteration is then given by

$$\{U\}^r = \{U\}^{(r-1)} + \{\delta U\} \quad (5.4.7)$$

At the element level, Eq. (5.4.4) takes the form

$$[T^e(\{u^e\}^{(r-1)})]\{\delta u^e\} = \{F^e(\{u^e\}^{(r-1)})\} - [K^e(\{u^e\}^{(r-1)})]\{u^e\}^{(r-1)} \quad (5.4.8)$$

The coefficients of the tangent matrix can be computed using the definition

$$T_{ij}^e \equiv \frac{\partial R_i^e}{\partial u_j^e} = \sum_{m=1}^n \frac{\partial K_{im}^e}{\partial u_j^e} u_m^e + K_{ij}^e \quad (5.4.9)$$

**Example 5.4.1**

Suppose that  $a_{xx}^e$  and  $a_{yy}^e$  have the form

$$\begin{aligned} a_{xx}^e &= a_{x0}^e(x, y) + a_{xu}^e \cdot u + a_{xux}^e \cdot \frac{\partial u}{\partial x} + a_{xuy}^e \cdot \frac{\partial u}{\partial y} \\ a_{yy}^e &= a_{y0}^e(x, y) + a_{yu}^e \cdot u + a_{yux}^e \cdot \frac{\partial u}{\partial x} + a_{yuy}^e \cdot \frac{\partial u}{\partial y} \end{aligned} \quad (5.4.10)$$

where  $a_{x0}$ ,  $a_{xu}$ , and so on are functions of only  $x$  and  $y$ . In addition, we assume that  $a_{00}$  is only a function of  $x$  and  $y$ . Then we have

$$T_{ij}^e = K_{ij}^e + \sum_{m=1}^n \frac{\partial K_{im}^e}{\partial u_j} u_m^e \quad (5.4.11)$$

where

$$\begin{aligned} \sum_{m=1}^n \frac{\partial K_{im}^e}{\partial u_j} u_m^e &= \sum_{m=1}^n \left[ \int_{\Omega^e} \left( \frac{\partial a_{xx}^e}{\partial u_j} \frac{\partial \psi_i^e}{\partial x} \frac{\partial \psi_m^e}{\partial x} + \frac{\partial a_{yy}^e}{\partial u_j} \frac{\partial \psi_i^e}{\partial y} \frac{\partial \psi_m^e}{\partial y} + \frac{\partial a_{00}^e}{\partial u_j} \psi_i^e \psi_m^e \right) dx dy \right] u_m^e \\ &= \sum_{m=1}^n \left\{ \int_{\Omega^e} \left[ \left( a_{xu}^e \psi_j^e + a_{xux}^e \frac{\partial \psi_j^e}{\partial x} + a_{xuy}^e \frac{\partial \psi_j^e}{\partial y} \right) \frac{\partial \psi_i^e}{\partial x} \frac{\partial \psi_m^e}{\partial x} \right. \right. \\ &\quad \left. \left. + \left( a_{yu}^e \psi_j^e + a_{yux}^e \frac{\partial \psi_j^e}{\partial x} + a_{yuy}^e \frac{\partial \psi_j^e}{\partial y} \right) \frac{\partial \psi_i^e}{\partial y} \frac{\partial \psi_m^e}{\partial y} \right] dx dy \right\} u_m^e \\ &= \int_{\Omega^e} \left[ \frac{\partial u}{\partial x} \frac{\partial \psi_i^e}{\partial x} \left( a_{xu}^e \psi_j^e + a_{xux}^e \frac{\partial \psi_j^e}{\partial x} + a_{xuy}^e \frac{\partial \psi_j^e}{\partial y} \right) \right. \\ &\quad \left. + \frac{\partial u}{\partial y} \frac{\partial \psi_i^e}{\partial y} \left( a_{yu}^e \psi_j^e + a_{yux}^e \frac{\partial \psi_j^e}{\partial x} + a_{yuy}^e \frac{\partial \psi_j^e}{\partial y} \right) \right] dx dy \end{aligned} \quad (5.4.12)$$

Note that, although  $[K^e]$  is symmetric, the symmetry of  $[T^e]$  depends on the nature of the nonlinearity.

## 5.5 Computer Implementation

### 5.5.1 Introduction

An accurate representation of non-rectangular domains and domains with curved boundaries can be accomplished by the use of refined meshes and/or irregularly shaped elements. For example, a non-rectangular region can be represented more accurately by triangular and quadrilateral elements than rectangular elements. However, it is easy to derive interpolation functions for a rectangular element, and it is easier to evaluate integrals over rectangular geometries than over irregular geometries. Therefore, it is practical to use quadrilateral elements with straight or curved sides but have a means to evaluate the integrals involved in the definitions of the coefficient matrices  $K_{ij}^e$  and  $T_{ij}^e$  over the quadrilateral elements. A coordinate transformation

between the coordinates  $(x, y)$  used in the formulation of the problem, called *global coordinates*, and another coordinate system  $(\xi, \eta)$ , called *local coordinate system*, that is convenient in deriving the interpolation functions and evaluating the integrals is needed. The choice of the local coordinate system is dictated by the choice of numerical integration method. Here we shall use, as was done in one-dimensional problems, the Gauss quadrature method to evaluate integrals defined over two-dimensional elements. The main steps in the numerical evaluation of finite element matrices are reviewed here (see Section 2.5 for more details).

### 5.5.2 Numerical Integration

The transformation between  $\Omega^e$  and  $\hat{\Omega}$  is accomplished by a coordinate transformation of the form [cf. Eqs. (2.5.1) and (2.5.2)]

$$x = \sum_{j=1}^m x_j^e \hat{\psi}_j^e(\xi, \eta), \quad y = \sum_{j=1}^m y_j^e \hat{\psi}_j^e(\xi, \eta) \quad (5.5.1)$$

while a typical dependent variable  $u(x, y)$  is approximated by

$$u(x, y) = \sum_{j=1}^n u_j^e \psi_j^e(x, y) = \sum_{j=1}^n u_j^e \psi_j^e(x(\xi, \eta), y(\xi, \eta)) \quad (5.5.2)$$

where  $\hat{\psi}_j^e$  denotes the interpolation functions of the master element  $\hat{\Omega}$  and  $\psi_j^e$  are interpolation functions of a typical element  $\Omega^e$  over which  $u$  is approximated. The transformation (5.5.1) maps a point  $(x, y)$  in a typical element  $\Omega^e$  of the mesh to a point  $(\xi, \eta)$  in the master element  $\hat{\Omega}$  and vice versa, if the Jacobian of the transformation is positive-definite. The positive-definite requirement of the Jacobian dictates admissible geometries of elements in a mesh.

Recall that a finite element model is nothing but a system of algebraic equations among the nodal values of the primary variables and secondary variables. The coefficients of these algebraic equations contain integrals of the physical parameters (e.g. material properties) and approximation functions. The integral expressions are, in general, complicated algebraically due to the spatial variation of the parameters and their dependence on the solution and possibly its derivatives as well as due to the coordinate transformations. Therefore, the integrals are evaluated numerically, which requires evaluation of the integrand at a selective number of points in the domain, multiply their values with suitable weights and summing. Here we discuss the Gauss quadrature to evaluate integrals over quadrilateral elements.



We illustrate the essential elements of the Gauss quadrature by considering the integral expression [see Eq. (5.3.4)]

$$K_{ij}^e = \int_{\Omega^e} \left[ a_{xx}(x, y) \frac{\partial \psi_i^e}{\partial x} \frac{\partial \psi_j^e}{\partial x} + a_{yy}(x, y) \frac{\partial \psi_i^e}{\partial y} \frac{\partial \psi_j^e}{\partial y} + a_{00}(x, y) \psi_i^e \psi_j^e \right] dx dy \quad (5.5.3)$$

We wish to transform the integral from  $\Omega^e$  to the master element  $\hat{\Omega} = \{(\xi, \eta) : -1 \leq \xi \leq 1, -1 \leq \eta \leq 1\}$  so that the Gauss quadrature can be used. From Eq. (2.5.6), we have

$$\begin{Bmatrix} \frac{\partial \psi_i^e}{\partial x} \\ \frac{\partial \psi_i^e}{\partial y} \end{Bmatrix} = [J]^{-1} \begin{Bmatrix} \frac{\partial \psi_i^e}{\partial \xi} \\ \frac{\partial \psi_i^e}{\partial \eta} \end{Bmatrix} \quad (5.5.4)$$

which gives the derivatives of  $\psi_i^e$  with respect to the global coordinates  $(x, y)$  in terms of the derivatives of  $\psi_i^e$  with respect to the local coordinates  $(\xi, \eta)$ . The matrix  $[J^e]$  is the Jacobian matrix of the transformation (5.5.1)

$$[J]^e = \begin{bmatrix} \frac{\partial x}{\partial \xi} & \frac{\partial y}{\partial \xi} \\ \frac{\partial x}{\partial \eta} & \frac{\partial y}{\partial \eta} \end{bmatrix}^e \quad (5.5.5)$$

and its determinant  $|J|$  is the Jacobian, which must be greater than zero in order to invert Eq. (5.5.4). Negative non-zero values of  $|J|$  imply that a right-hand coordinate system is transformed to a left-hand coordinate system, which should be avoided. The Jacobian matrix can be computed using the transformation (5.5.1) in Eq. (5.5.5). We have

$$\begin{aligned} [J]^e &= \begin{bmatrix} \frac{\partial x}{\partial \xi} & \frac{\partial y}{\partial \xi} \\ \frac{\partial x}{\partial \eta} & \frac{\partial y}{\partial \eta} \end{bmatrix}^e = \begin{bmatrix} \sum_{i=1}^m x_i \frac{\partial \hat{\psi}_i}{\partial \xi} & \sum_{i=1}^m y_i \frac{\partial \hat{\psi}_i}{\partial \xi} \\ \sum_{i=1}^m x_i \frac{\partial \hat{\psi}_i}{\partial \eta} & \sum_{i=1}^m y_i \frac{\partial \hat{\psi}_i}{\partial \eta} \end{bmatrix}^e \\ &= \begin{bmatrix} \frac{\partial \hat{\psi}_1}{\partial \xi} & \frac{\partial \hat{\psi}_2}{\partial \xi} & \cdots & \frac{\partial \hat{\psi}_m}{\partial \xi} \\ \frac{\partial \hat{\psi}_1}{\partial \eta} & \frac{\partial \hat{\psi}_2}{\partial \eta} & \cdots & \frac{\partial \hat{\psi}_m}{\partial \eta} \end{bmatrix}^e \begin{bmatrix} x_1 & y_1 \\ x_2 & y_2 \\ \vdots & \vdots \\ x_m & y_m \end{bmatrix}^e \end{aligned} \quad (5.5.6)$$

Thus, given the global coordinates  $(x_j, y_j)$  of element nodes and the interpolation functions  $\hat{\psi}_j^e$  used for geometry, the Jacobian matrix can be evaluated using Eq. (5.5.6). Note that  $\hat{\psi}_j^e$  are different, in general, from  $\psi_j^e$  used in the approximation of the dependent variables. The Jacobian is given by

$$|J| = J_{11}J_{22} - J_{12}J_{21} \quad (5.5.7)$$

We have from Eq. (5.5.4)

$$\begin{Bmatrix} \frac{\partial \psi_i^e}{\partial x} \\ \frac{\partial \psi_i^e}{\partial y} \end{Bmatrix} = [J]^{-1} \begin{Bmatrix} \frac{\partial \psi_i^e}{\partial \xi} \\ \frac{\partial \psi_i^e}{\partial \eta} \end{Bmatrix} \equiv [J^*] \begin{Bmatrix} \frac{\partial \psi_i^e}{\partial \xi} \\ \frac{\partial \psi_i^e}{\partial \eta} \end{Bmatrix} \quad (5.5.8)$$

where

$$J_{11}^* = \frac{J_{22}}{|J|}, \quad J_{12}^* = -\frac{J_{12}}{|J|}, \quad J_{22}^* = \frac{J_{11}}{|J|}, \quad J_{21}^* = -\frac{J_{21}}{|J|} \quad (5.5.9)$$

Returning to the coefficients  $K_{ij}^e$  in Eq. (5.5.3), we can write it now in terms of the natural coordinates  $(\xi, \eta)$  as

$$\begin{aligned} K_{ij}^e &= \int_{\hat{\Omega}} \left\{ a_{xx}(\xi, \eta) \left( J_{11}^* \frac{\partial \psi_i^e}{\partial \xi} + J_{12}^* \frac{\partial \psi_i^e}{\partial \eta} \right) \left( J_{11}^* \frac{\partial \psi_j^e}{\partial \xi} + J_{12}^* \frac{\partial \psi_j^e}{\partial \eta} \right) \right. \\ &\quad + a_{yy}(\xi, \eta) \left( J_{21}^* \frac{\partial \psi_j^e}{\partial \xi} + J_{22}^* \frac{\partial \psi_j^e}{\partial \eta} \right) \left( J_{21}^* \frac{\partial \psi_i^e}{\partial \xi} + J_{22}^* \frac{\partial \psi_i^e}{\partial \eta} \right) \\ &\quad \left. + a_{00}(\xi, \eta) \psi_i^e \psi_j^e \right\} |J| \, d\xi \, d\eta \\ &\equiv \int_{\hat{\Omega}} F_{ij}(\xi, \eta) \, d\xi \, d\eta \end{aligned} \quad (5.5.10)$$

where the element area  $dA = dx dy$  in element  $\Omega^e$  is transformed to  $|J| \, d\xi \, d\eta$  in the master element  $\hat{\Omega}$ .

Using the Gauss quadrature formulas for integrals defined over a rectangular master element  $\hat{\Omega}$ , which are the same as those for the one-dimensional quadrature, we obtain

$$\begin{aligned} \int_{\hat{\Omega}} F_{ij}(\xi, \eta) \, d\xi \, d\eta &= \int_{-1}^1 \left[ \int_{-1}^1 F_{ij}(\xi, \eta) \, d\eta \right] d\xi \approx \int_{-1}^1 \left[ \sum_{J=1}^N F_{ij}(\xi, \eta_J) W_J \right] d\xi \\ &\approx \sum_{I=1}^M \sum_{J=1}^N F_{ij}(\xi_I, \eta_J) W_I W_J \end{aligned} \quad (5.5.11)$$

where  $M$  and  $N$  denote the number of Gauss quadrature points in the  $\xi$  and  $\eta$  directions,  $(\xi_I, \eta_J)$  denote the Gauss points, and  $W_I$  and  $W_J$  denote the corresponding Gauss weights (see Table 2.5.1).

As already discussed, the number of Gauss points required to evaluate an integral accurately is based on the following rule: if the integrand is a polynomial of degree  $p$ , it is integrated exactly by employing  $NGP \equiv N = \text{int}[\frac{1}{2}(p+1)]$ ; that is, the smallest integer greater than  $\frac{1}{2}(p+1)$ . In most cases, the interpolation functions are of the same degree in both  $\xi$  and  $\eta$ , and we take  $NGP = MGP \equiv M$ .

### 5.5.3 Element Calculations

Calculation of element coefficients require evaluation of interpolation functions and their derivatives. The Fortran statements for the calculation of the



Jacobian matrix and determinant are given in the subroutine SHPRCT (see Appendix 2 of Reddy [1]). The notation used is as follows:

$$SF(i) = \psi_i^e, \quad DSF(1, i) = \frac{\partial \psi_i^e}{\partial \xi}, \quad DSF(2, i) = \frac{\partial \psi_i^e}{\partial \eta}$$

$[ELXY]$  = array of the global coordinates of element nodes  
 $ELXY(i, 1) = x_i, \quad ELXY(i, 2) = y_i$   
 $[GJ]$  = the Jacobian matrix,  $[J]; [GJ] = [DSF][ELXY]$   
 $[GJINV]$  = inverse of the Jacobian matrix,  $[GJ]^{-1}$   
 $DET$  = the determinant of the Jacobian matrix,  $|J|$   
 $GDSF(1, i) = \frac{\partial \psi_i^e}{\partial x}, \quad GDSF(2, i) = \frac{\partial \psi_i^e}{\partial y}$   
 $[GDSF] = [GJINV][DSF]$

The above calculations are carried out in the subroutine SHPRECT.

The subroutine ELECOFNT that calculates  $[K^e]$ ,  $[T^e]$ , and  $\{f^e\}$  for the direct iteration and Newton-Raphson iteration is listed in Box 5.5.1. The following notation is used ( $n = NPE$ ):

$$ELF(i) = f_i^e, \quad ELK(i, j) = K_{ij}^e, \quad TANG(i, j) = \sum_{m=1}^n \frac{\partial K_{im}^e}{\partial u_j} u_m^e$$

$GAUSPT(I, J)$  =  $I$ th Gauss point in the  $J$ th Gauss-point rule ( $I \leq J$ )  
 $GAUSWT(I, J)$  =  $I$ th Gauss weight in the  $J$ th Gauss-point rule ( $I \leq J$ )  
 $ELU(I) = u_i^e$  from the previous iteration

Other variables have the same meaning as indicated earlier. It is assumed that the coefficients  $a_{x0}$  and  $a_{y0}$  are linear functions of  $x$  and  $y$

$$a_{x0} = a_{x00} + a_{x0x}x + a_{x0y}y, \quad a_{y0} = a_{y00} + a_{y0x}x + a_{y0y}y \quad (5.5.12)$$

Of course, other variations of the coefficients may be assumed and implemented without difficulty.

### Example 5.5.1

Consider heat transfer in an isotropic medium [ $a_{xx} = a_{yy}$  in Eq. (5.2.1)] of rectangular shape  $a \times b = 0.18 \times 0.1$  m. The conductivity  $a_{xx} = a_{yy} = k$  is assumed to vary according to the relation ( $a_{00} = 0$ )

$$k = k_0 (1 + \beta T) \quad (5.5.13)$$

where  $k_0$  is the constant thermal conductivity,  $\beta$  the temperature coefficient of thermal conductivity, and  $T$  the temperature. Suppose that there is no internal heat generation (i.e.  $f = 0$ ) and the boundary conditions are

$$T(0, y) = 500^\circ\text{K}, \quad T(a, y) = 300^\circ\text{K} \quad (5.5.14a)$$

$$\frac{\partial T}{\partial y} = 0 \quad \text{at } y = 0, b \text{ for any } x \quad (5.5.14b)$$

**Box 5.5.1** Subroutine (in Fortran) ELECOFNT for the calculation of element matrices  $[K^e]$ ,  $[T^e]$ , and  $\{f^e\}$  of the model problem in Eq. (5.2.1).

```

SUBROUTINE ELECOEF(NPE,NGP,ITYPE,NONLN)
C
C
C Element calculations based on linear and quadratic rectangular
C elements and isoparametric formulation are carried out for the
C model equation in (4.2.1).
C
C NPE - Nodes per element (4: linear; 8: serendipity quadratic,
C 9: complete quadratic)
C NGP - Number of Gauss points.
C ITYPE - Type of iterative method used:
C ITYPE=1, Direct iteration, ITYPE>1, Newton-Raphson iteration
C
C
C IMPLICIT REAL*8(A-H,O-Z)
COMMON/STF/ELF(7),ELK(9,9),ELXY(9,2),ELU(9)
COMMON/PST/A10,A1X,A1Y,A20,A2X,A2Y,A00,F0,FX,FY,
* A1U,A1UX,A1UY,A2U,A2UX,A2UY
COMMON/SHP/SF(9),GDSF(2,9)
DIMENSION GAUSPT(5,5),GAUSWT(5,5),TANG(9,9)
C
DATA GAUSPT/5*0.0D0, -0.57735027D0, 0.57735027D0, 3*0.0D0,
2 -0.77459667D0, 0.0D0, 0.77459667D0, 2*0.0D0, -0.86113631D0,
3 -0.33998104D0, 0.33998104D0, 0.86113631D0, 0.0D0, -0.90617984D0,
4 -0.53846931D0,0.0D0,0.53846931D0,0.90617984D0/
C
DATA GAUSWT/2.0D0, 4*0.0D0, 2*1.0D0, 3*0.0D0, 0.55555555D0,
2 0.88888888D0, 0.55555555D0, 2*0.0D0, 0.34785485D0,
3 2*0.65214515D0, 0.34785485D0, 0.0D0, 0.23692688D0,
4 0.47862867D0, 0.56888888D0, 0.47862867D0, 0.23692688D0/
C
C Initialize the arrays
C
DO 100 I = 1,NPE
ELF(I) = 0.0
DO 100 J = 1,NPE
IF(ITYPE.GT.1)THEN
TANG(I,J)=0.0
ENDIF
100 ELK(I,J)= 0.0
C
C Do-loops on numerical (Gauss) integration begin here. Subroutine
C SHPRCT (SHaPe functions for ReCTangular elements) is called here
C
DO 200 NI = 1,NGP
DO 200 NJ = 1,NGP
XI = GAUSPT(NI,NGP)
ETA = GAUSPT(NJ,NGP)
CALL SHPRCT (NPE,XI,ETA,DET,ELXY)
CNST = DET*GAUSWT(NI,NGP)*GAUSWT(NJ,NGP)
X=0.0
Y=0.0
U = 0.0
UX= 0.0
UY= 0.0

```

## Box 5.5.1 (continued)

```

DO 140 I=1,NPE
  U=U+ELU(I)*SF(I)
  UX=UX+ELU(I)*GDSF(1,I)
  UY=UY+ELU(I)*GDSF(2,I)
  X=X+ELXY(I,1)*SF(I)
  Y=Y+ELXY(I,2)*SF(I)
140
CC
CC  Define the coefficients of the differential equation
CC
  FXY=F0+FX*X+FY*Y
  AXX=AX0+AXX*X+AXY*Y
  AYY=AY0+AYX*X+AYY*Y
  IF(NONLN.GT.0)THEN
    AXX=AXX+AXU*U+AXUX*UX+AXUY*UY
    AYY=AYY+AYU*U+AYUX*UX+AYUY*UY
  ENDIF
CC
CC  Define the element source vector and coefficient matrix
CC
  DO 180 I=1,NPE
    ELF(I)=ELF(I)+FX*SF(I)*CNST
    DO 160 J=1,NPE
      S00=SF(I)*SF(J)*CNST
      S11=GDSF(1,I)*GDSF(1,J)*CNST
      S22=GDSF(2,I)*GDSF(2,J)*CNST
      ELK(I,J)=ELK(I,J)+A11*S11+A22*S22+A00*S00
    DO
CC
CC  Define the part needed to add to [K] to define [T]
CC
    IF(ITYPE.GT.1)THEN
      S10=GDSF(1,I)*SF(J)*CNST
      S20=GDSF(2,I)*SF(J)*CNST
      S12=GDSF(1,I)*GDSF(2,J)*CNST
      S21=GDSF(2,I)*GDSF(1,J)*CNST
      TANG(I,J)=TANG(I,J)
      *      +UX*(A1U*S10+AXUX*SXX+AXUY*S12)
      *      +UY*(A2U*S20+AYUX*SYX+AYUY*S22)
    ENDIF
160  CONTINUE
180  CONTINUE
200  CONTINUE
CC
CC  Compute the residual vector and tangent matrix
CC
  IF(ITYPE.GT.1)THEN
    DO 220 I=1,NPE
      DO 220 J=1,NPE
220    ELF(I)=ELF(I)-ELK(I,J)*ELU(J)
      DO 240 I=1,NPE
        DO 240 J=1,NPE
240    ELK(I,J)=ELK(I,J)+TANG(I,J)
      ENDIF
    RETURN
  END
END

```

This is essentially a one-dimensional problem (in the  $x$  coordinate), and can be solved as such (see Table 3.5.1).

Table 5.5.1 shows the linear and nonlinear solutions  $T(x, y_0)$  for any  $y_0$ . Direct iteration is used to solve the problem. It took two iterations to converge ( $\epsilon = 0.01$ ). Also, the solution is independent of the mesh in the  $y$ -direction. The present results were found to be identical to those obtained with the one-dimensional model (for the same tolerance of  $\epsilon = 0.01$ ).

**Table 5.5.1** Finite element solutions of a nonlinear heat conduction equation [ $k_0 = 0.2 \text{ W/(m } ^\circ\text{K)}$  and  $\beta = 2 \times 10^{-3} \text{ (} ^\circ\text{K}^{-1}\text{)}$ ].

$x$	Linear	$4 \times 4\text{L}^*$	$2 \times 2\text{Q9}$	$8 \times 8\text{L4}$	$4 \times 4\text{Q9}$
0.0000	500.00	500.00	500.00	500.00	500.00
0.0225	475.00	—	—	477.31	477.31
0.0450	450.00	454.02	454.03	454.03	454.03
0.0675	425.00	—	—	430.12	430.12
0.0900	400.00	405.56	405.57	405.57	405.57
0.1125	375.00	—	—	380.32	380.32
0.1350	350.00	354.33	354.34	354.34	354.34
0.1575	325.00	—	—	327.58	327.58
0.1800	300.00	300.00	300.00	300.00	300.00

\*  $m \times n\text{L4}$ , for example, denotes a mesh of the four-node linear (L) elements.

## Problems

- 5.1** Consider the nonlinear problem of Example 5.5.1 (heat transfer in two dimensions). Use the uniform  $4 \times 4$  nine-node quadratic element mesh to analyze the problem using the following data and boundary conditions:

$$a = 0.18 \text{ m}, \quad b = 0.1 \text{ m}, \quad f_0 = 0 \text{ W/m}^3 \quad (\text{a})$$

$$k = k_0 (1 + \beta T), \quad k_0 = 25 \text{ W/(m } ^\circ\text{C)} \quad (\text{b})$$

$$T(0, y) = 100 \text{ } ^\circ\text{C}, \quad T(a, y) = 50 \text{ } ^\circ\text{C}$$

$$k \frac{\partial T}{\partial n} + h_c(T - T_\infty) = 0 \text{ at } y = 0, b \quad (\text{c})$$

Use  $\beta = 0.2$ ,  $T_\infty = 10^\circ\text{C}$ , and  $h_c = 50 \text{ W/(m}^2 \text{ } ^\circ\text{C)}$ .

- 5.2** The energy equation for simultaneous conduction and radiation in a participating medium can be expressed by

$$-\nabla \cdot [k_e(T)\nabla T] = g$$

where

$$k_e(T) = k + \frac{16\sigma n^2 T^3}{3\beta}$$

Here  $T$  is the temperature,  $g$  is the internal heat generation,  $n$  denotes the refractive index of the medium,  $\sigma$  is the Stefan-Boltzman constant, and  $\beta$  is the Roseland mean extinction coefficient (see Özisik [4]). Develop the finite element model of the equation and determine the tangent coefficient matrix for a planar (two-dimensional) domain.

- 5.3** Repeat Problem 5.2 for a radially axisymmetric domain.
- 5.4** Suppose that the boundary of a typical finite element is subject to both convective and enclosed radiation heat transfer [cf. Eq. (2.3.36)]:

$$\left( a_{xx} \frac{\partial u}{\partial x} n_x + a_{yy} \frac{\partial u}{\partial y} n_y \right) + h_c(u - u_c) + \sigma \epsilon (u^4 - u_c^4) = q_n$$

where  $\sigma$  is the Stefan-Boltzman constant and  $\epsilon$  is the emissivity of the surface. Reformulate the finite element equations in (2.3.39) to account for the radiation term. *Hint:*  $\sigma \epsilon (u^4 - u_c^4) = \sigma \epsilon (u^2 + u_c^2)(u + u_c)(u - u_c) \equiv h_r(u)(u - u_c)$ .

- 5.5 Compute the tangent coefficient matrix associated with the nonlinear radiation boundary condition of Problem 5.4.

## References

1. Reddy, J. N., *An Introduction to the Finite Element Method*, 2nd edn, McGraw-Hill, New York (1993).
2. Reddy, J. N. and Gartling, D. K., *The Finite Element Method in Heat Transfer and Fluid Dynamics*, 2nd edn, CRC Press, Boca Raton, FL (2001).
3. Reddy, J. N., *Energy Principles and Variational Methods in Applied Mechanics*, 2nd edn, John Wiley, New York (2002).
4. Özisik, M. N., *Finite Difference Methods in Heat Transfer*, CRC Press, Boca Raton, FL (1994).
5. Holman, J. P., *Heat Transfer*, 7th edn, McGraw-Hill, New York (1990).

---

# Nonlinear Bending of Elastic Plates and Shells

---

## 6.1 Introduction

A *plate* is a flat structural element with planform dimensions that are large compared to its thickness and is subjected to loads that cause bending deformation in addition to stretching. In most cases, the thickness is no greater than one-tenth of the smallest in-plane dimension. A *shell* is much like a plate except that it is not flat but curved. Because of the smallness of thickness dimension, it is often not necessary to model them using three-dimensional elasticity equations. Simple two-dimensional plate and shell theories can be developed to study the deformation and stresses in plate structures undergoing small strains, small to moderate rotations, and large displacements (i.e.  $w_0/h \geq 1$ ).

Here we derive governing equations of the classical and first-order theories of plates and shells with the von Kármán strains, and develop their displacement finite element models. The principle of virtual displacements is used to derive the weak forms, and the displacement finite element models are developed using the weak forms.

## 6.2 Classical Plate Theory

### 6.2.1 Assumptions of the Kinematics

The *classical plate theory* (CPT) is one in which the displacement field is selected so as to satisfy the *Kirchhoff hypothesis*. The *Kirchhoff hypothesis* has the following three assumptions (see Figure 6.2.1):

- (1) Straight lines perpendicular to the mid-surface (i.e. transverse normals) before deformation, remain straight after deformation.
- (2) The transverse normals do not experience elongation (i.e. they are inextensible).
- (3) The transverse normals rotate such that they remain perpendicular to the mid-surface after deformation.

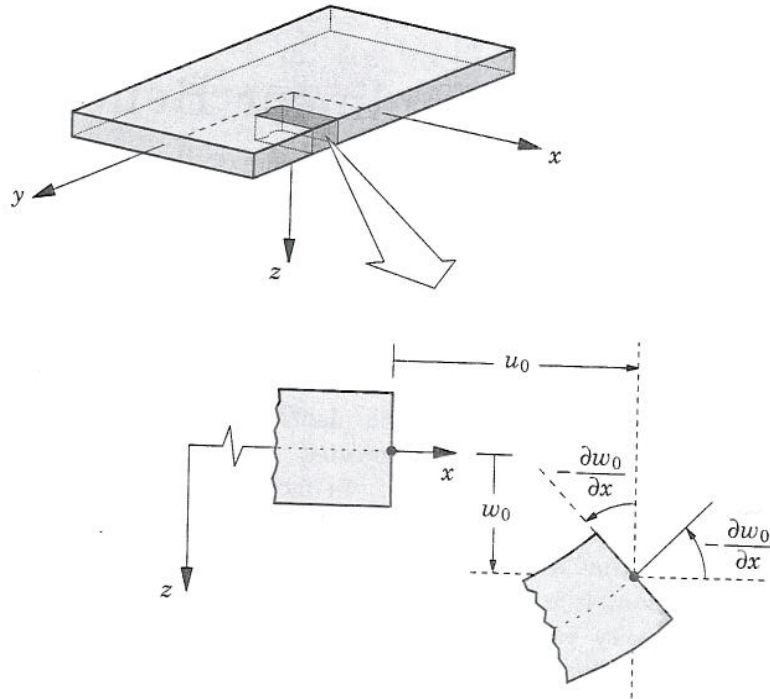


Figure 6.2.1 Undeformed and deformed geometries of an edge of a plate under the Kirchhoff assumptions.

### 6.2.2 Displacement Field and Strains

Let us denote the undeformed mid-plane of the plate with the symbol  $\Omega_0$ . The total domain of the plate is the tensor product  $\Omega_0 \times (-h/2, h/2)$ . The boundary of the total domain consists of surfaces  $S_t(z = h/2)$  and  $S_b(z = -h/2)$ , and the edge  $\bar{\Gamma} \equiv \Gamma \times (-h/2, h/2)$ . In general,  $\Gamma$  is a curved surface, with outward normal  $\hat{\mathbf{n}} = n_x \hat{\mathbf{e}}_x + n_y \hat{\mathbf{e}}_y$ , where  $n_x$  and  $n_y$  are the direction cosines of the unit normal.

The Kirchhoff hypothesis implies the following form of the displacement field (see Reddy [1-3] and Figure 6.2.1)

$$\begin{aligned} u(x, y, z) &= u_0(x, y) - z \frac{\partial w_0}{\partial x} \\ v(x, y, z) &= v_0(x, y) - z \frac{\partial w_0}{\partial y} \\ w(x, y, z) &= w_0(x, y) \end{aligned} \quad (6.2.1)$$

where  $(u_0, v_0, w_0)$  denote the displacements of a material point at  $(x, y, 0)$  in  $(x, y, z)$  coordinate directions. The nonlinear strains are given by

$$\begin{aligned}
 E_{11} &= \frac{\partial u}{\partial x} + \frac{1}{2} \left[ \left( \frac{\partial u}{\partial x} \right)^2 + \left( \frac{\partial v}{\partial x} \right)^2 + \left( \frac{\partial w}{\partial x} \right)^2 \right] \\
 E_{12} &= \frac{1}{2} \left( \frac{\partial u}{\partial y} + \frac{\partial v}{\partial x} + \frac{\partial u}{\partial x} \frac{\partial u}{\partial y} + \frac{\partial v}{\partial x} \frac{\partial v}{\partial y} + \frac{\partial w}{\partial x} \frac{\partial w}{\partial y} \right) \\
 E_{13} &= \frac{1}{2} \left( \frac{\partial u}{\partial z} + \frac{\partial w}{\partial x} + \frac{\partial u}{\partial x} \frac{\partial u}{\partial z} + \frac{\partial v}{\partial x} \frac{\partial v}{\partial z} + \frac{\partial w}{\partial x} \frac{\partial w}{\partial z} \right) \\
 E_{22} &= \frac{\partial v}{\partial y} + \frac{1}{2} \left[ \left( \frac{\partial u}{\partial y} \right)^2 + \left( \frac{\partial v}{\partial y} \right)^2 + \left( \frac{\partial w}{\partial y} \right)^2 \right] \\
 E_{23} &= \frac{1}{2} \left( \frac{\partial v}{\partial z} + \frac{\partial w}{\partial y} + \frac{\partial u}{\partial y} \frac{\partial u}{\partial z} + \frac{\partial v}{\partial y} \frac{\partial v}{\partial z} + \frac{\partial w}{\partial y} \frac{\partial w}{\partial z} \right) \\
 E_{33} &= \frac{\partial w}{\partial z} + \frac{1}{2} \left[ \left( \frac{\partial u}{\partial z} \right)^2 + \left( \frac{\partial v}{\partial z} \right)^2 + \left( \frac{\partial w}{\partial z} \right)^2 \right]
 \end{aligned} \tag{6.2.2}$$

If the components of the displacement gradients are of the order  $\epsilon$ , i.e.

$$\frac{\partial u}{\partial x}, \frac{\partial u}{\partial y}, \frac{\partial v}{\partial x}, \frac{\partial v}{\partial y}, \frac{\partial w}{\partial z} = O(\epsilon) \tag{6.2.3}$$

then the small strain assumption implies that terms of the order  $\epsilon^2$  are omitted in the strains. If the rotations of transverse normals are moderate (say  $10^\circ - 15^\circ$ ), then the following terms are small but *not* negligible compared to  $\epsilon$

$$\left( \frac{\partial w}{\partial x} \right)^2, \left( \frac{\partial w}{\partial y} \right)^2, \frac{\partial w}{\partial x} \frac{\partial w}{\partial y} \tag{6.2.4}$$

Thus for small strains and moderate rotations, the strain-displacement relations (6.2.2) take the form

$$\begin{aligned}
 \epsilon_{xx} &= \frac{\partial u}{\partial x} + \frac{1}{2} \left( \frac{\partial w}{\partial x} \right)^2, & \epsilon_{xy} &= \frac{1}{2} \left( \frac{\partial u}{\partial y} + \frac{\partial v}{\partial x} + \frac{\partial w}{\partial x} \frac{\partial w}{\partial y} \right) \\
 \epsilon_{xz} &= \frac{1}{2} \left( \frac{\partial u}{\partial z} + \frac{\partial w}{\partial x} \right), & \epsilon_{yy} &= \frac{\partial v}{\partial y} + \frac{1}{2} \left( \frac{\partial w}{\partial y} \right)^2 \\
 \epsilon_{yz} &= \frac{1}{2} \left( \frac{\partial v}{\partial z} + \frac{\partial w}{\partial y} \right), & \epsilon_{zz} &= \frac{\partial w}{\partial z}
 \end{aligned} \tag{6.2.5}$$

where, for this special case of geometric nonlinearity (i.e. small strains but moderate rotations), the notation  $\epsilon_{ij}$  is used in place of  $E_{ij}$ . The corresponding Second-Piola Kirchhoff stresses will be denoted  $\sigma_{ij}$ .

For the displacement field in Eq. (6.2.1),  $\partial w / \partial z = 0$ . In view of the assumptions in Eqs. (6.2.3) and (6.2.4), the strains (6.2.5) for the displacement



field (6.2.1) reduce to

$$\begin{aligned}\varepsilon_{xx} &= \frac{\partial u_0}{\partial x} + \frac{1}{2} \left( \frac{\partial w_0}{\partial x} \right)^2 - z \frac{\partial^2 w_0}{\partial x^2} \\ \varepsilon_{xy} &= \frac{1}{2} \left( \frac{\partial u_0}{\partial y} + \frac{\partial v_0}{\partial x} + \frac{\partial w_0}{\partial x} \frac{\partial w_0}{\partial y} - 2z \frac{\partial^2 w_0}{\partial x \partial y} \right)\end{aligned}\quad (6.2.6)$$

$$\begin{aligned}\varepsilon_{yy} &= \frac{\partial v_0}{\partial y} + \frac{1}{2} \left( \frac{\partial w_0}{\partial y} \right)^2 - z \frac{\partial^2 w_0}{\partial y^2} \\ \varepsilon_{xz} &= \frac{1}{2} \left( -\frac{\partial w_0}{\partial x} + \frac{\partial w_0}{\partial x} \right) = 0 \\ \varepsilon_{yz} &= \frac{1}{2} \left( -\frac{\partial w_0}{\partial y} + \frac{\partial w_0}{\partial y} \right) = 0 \\ \varepsilon_{zz} &= 0\end{aligned}\quad (6.2.7)$$

The strains in Eqs. (6.2.6) and (6.2.7) are called the *von Kármán strains*, and the associated plate theory is termed the *classical plate theory with the von Kármán strains*. Note that the transverse strains ( $\varepsilon_{xz}, \varepsilon_{yz}, \varepsilon_{zz}$ ) are identically zero in the classical plate theory.

In matrix notation, Eq. (6.2.6) can be written as

$$\begin{Bmatrix} \varepsilon_{xx} \\ \varepsilon_{yy} \\ \gamma_{xy} \end{Bmatrix} = \begin{Bmatrix} \varepsilon_{xx}^0 \\ \varepsilon_{yy}^0 \\ \gamma_{xy}^0 \end{Bmatrix} + z \begin{Bmatrix} \varepsilon_{xx}^1 \\ \varepsilon_{yy}^1 \\ \gamma_{xy}^1 \end{Bmatrix}\quad (6.2.8a)$$

$$\begin{Bmatrix} \varepsilon_{xx}^0 \\ \varepsilon_{yy}^0 \\ \gamma_{xy}^0 \end{Bmatrix} = \begin{Bmatrix} \frac{\partial u_0}{\partial x} + \frac{1}{2} \left( \frac{\partial w_0}{\partial x} \right)^2 \\ \frac{\partial v_0}{\partial y} + \frac{1}{2} \left( \frac{\partial w_0}{\partial y} \right)^2 \\ \frac{\partial u_0}{\partial y} + \frac{\partial v_0}{\partial x} + \frac{\partial w_0}{\partial x} \frac{\partial w_0}{\partial y} \end{Bmatrix}, \quad \begin{Bmatrix} \varepsilon_{xx}^1 \\ \varepsilon_{yy}^1 \\ \gamma_{xy}^1 \end{Bmatrix} = \begin{Bmatrix} -\frac{\partial^2 w_0}{\partial x^2} \\ -\frac{\partial^2 w_0}{\partial y^2} \\ -2 \frac{\partial^2 w_0}{\partial x \partial y} \end{Bmatrix}\quad (6.2.8b)$$

## 6.3 Variational Formulation of CPT

### 6.3.1 Virtual Work

Here, the weak form based on the principle of virtual displacements applied to the classical plate theory is derived for a typical finite element  $\Omega^e$ . In the derivation, we account for thermal (and hence, moisture) effects only with the understanding that the material properties are independent of the temperature and that the temperature  $T$  is a known function of position (hence,  $\delta T = 0$ ). Thus, the temperature enters the formulation only through constitutive equations.

As noted earlier, the transverse strains ( $\gamma_{xz}, \gamma_{yz}, \varepsilon_{zz}$ ) are identically zero in the classical plate theory. Consequently, the transverse stresses ( $\sigma_{xz}, \sigma_{yz}, \sigma_{zz}$ )

do not enter the formulation because the virtual strain energy of these stresses is zero (due to the fact that kinematically consistent virtual strains must be zero):

$$\delta\varepsilon_{xz} = 0, \quad \delta\varepsilon_{yz} = 0, \quad \delta\varepsilon_{zz} = 0 \quad (6.3.1)$$

Whether the transverse stresses are accounted for or not in a theory, they are present in reality to keep the plate in equilibrium. In addition, these stress components may be specified on the boundary. Thus, the transverse stresses do not enter the virtual strain energy expression but must be accounted for in the boundary conditions and equilibrium of forces.

The principle of virtual displacements is

$$0 = \delta W^e \equiv (\delta U^e + \delta V^e) \quad (6.3.2)$$

where  $U^e$  is the strain energy stored and  $V^e$  is the work done by applied forces in an element. Suppose that  $q$  is the distributed force at  $z = -h/2$ , and  $(\sigma_{nn}, \sigma_{ns}, \sigma_{nz})$  are the stress components on the boundary  $\bar{\Gamma}^e = \Gamma^e \times (-\frac{h}{2}, \frac{h}{2})$  of the plate element (see Figure 6.3.1).

The virtual strain energy in element  $\Omega^e$  is given by

$$\begin{aligned} \delta U^e &= \int_{\Omega^e} \int_{-\frac{h}{2}}^{\frac{h}{2}} (\sigma_{xx} \delta\varepsilon_{xx} + \sigma_{yy} \delta\varepsilon_{yy} + 2\sigma_{xy} \delta\varepsilon_{xy}) \, dz \, dx \, dy \\ &= \int_{\Omega^e} \left( N_{xx} \delta\varepsilon_{xx}^0 + M_{xx} \delta\varepsilon_{xx}^1 + N_{yy} \delta\varepsilon_{yy}^0 + M_{yy} \delta\varepsilon_{yy}^1 \right. \\ &\quad \left. + N_{xy} \delta\gamma_{xy}^0 + M_{xy} \delta\gamma_{xy}^1 \right) dx \, dy \end{aligned} \quad (6.3.3)$$

where  $(N_{xx}, N_{yy}, N_{xy})$  are the forces per unit length and  $(M_{xx}, M_{yy}, M_{xy})$  are the moments per unit length (see Figure 6.3.2):

$$\begin{Bmatrix} N_{xx} \\ N_{yy} \\ N_{xy} \end{Bmatrix} = \int_{-\frac{h}{2}}^{\frac{h}{2}} \begin{Bmatrix} \sigma_{xx} \\ \sigma_{yy} \\ \sigma_{xy} \end{Bmatrix} dz, \quad \begin{Bmatrix} M_{xx} \\ M_{yy} \\ M_{xy} \end{Bmatrix} = \int_{-\frac{h}{2}}^{\frac{h}{2}} \begin{Bmatrix} \sigma_{xx} \\ \sigma_{yy} \\ \sigma_{xy} \end{Bmatrix} z \, dz \quad (6.3.4)$$

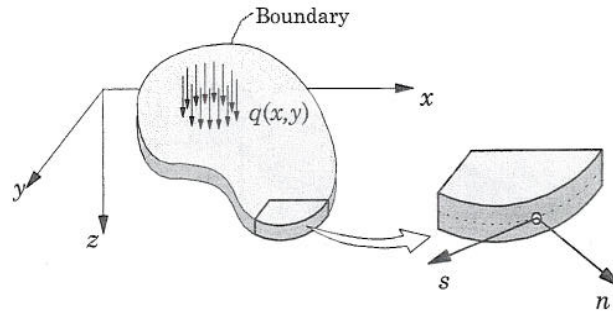


Figure 6.3.1 Geometry of a plate element with curved boundary.

The virtual work done by the distributed transverse load  $q(x, y)$  applied at  $z = -h/2$ , the transverse reaction force of an elastic foundation at  $z = h/2$ , in-plane normal stress  $\sigma_{nn}$ , in-plane tangential stress  $\sigma_{ns}$ , and transverse shear stress  $\sigma_{nz}$  is

$$\delta V^e = - \left\{ \int_{\Omega^e} q(x, y) \delta w(x, y, \frac{-h}{2}) dx dy + \int_{\Omega^e} F_s(x, y) \delta w(x, y, \frac{h}{2}) dx dy + \oint_{\Gamma^e} \int_{-\frac{h}{2}}^{\frac{h}{2}} [\sigma_{nn} \delta u_n + \sigma_{ns} \delta u_s + \sigma_{nz} \delta w] dz ds \right\} \quad (6.3.5)$$

$$= - \left\{ \int_{\Omega^e} (q - k w_0) \delta w_0 dx dy + \oint_{\Gamma^e} \left( N_{nn} \delta u_{0n} - M_{nn} \frac{\partial \delta w_0}{\partial n} + N_{ns} \delta u_{0s} - M_{ns} \frac{\partial \delta w_0}{\partial s} + Q_n \delta w_0 \right) ds \right\} \quad (6.3.6)$$

where  $F_s = -k w_0$ ,  $k$  is the foundation modulus,  $u_{0n}, u_{0s}$ , and  $w_0$  are the displacements along the normal, tangential, and transverse directions, respectively, and (see Figure 6.3.2)

$$\begin{Bmatrix} N_{nn} \\ N_{ns} \end{Bmatrix} = \int_{-\frac{h}{2}}^{\frac{h}{2}} \begin{Bmatrix} \sigma_{nn} \\ \sigma_{ns} \end{Bmatrix} dz, \quad \begin{Bmatrix} M_{nn} \\ M_{ns} \end{Bmatrix} = \int_{-\frac{h}{2}}^{\frac{h}{2}} \begin{Bmatrix} \sigma_{nn} \\ \sigma_{ns} \end{Bmatrix} z dz \quad (6.3.7a)$$

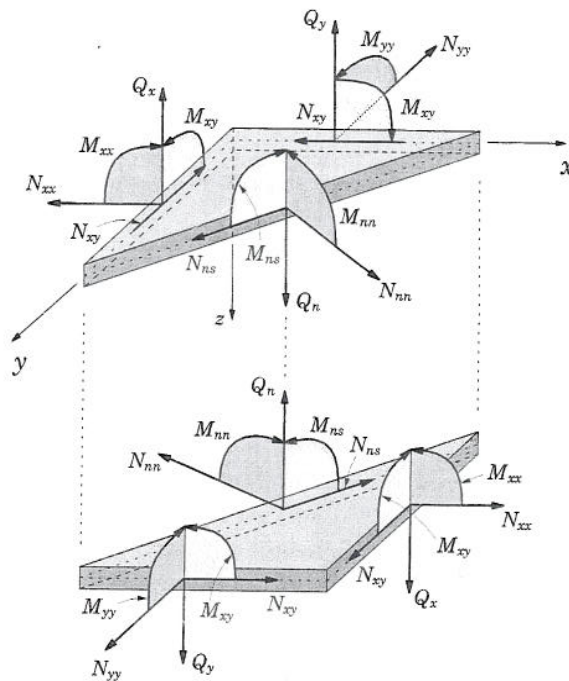


Figure 6.3.2 Forces and moments per unit length on a plate element.

$$Q_n = \int_{-\frac{h}{2}}^{\frac{h}{2}} \sigma_{nz} dz \quad (6.3.7b)$$

The stresses  $(\sigma_{nn}, \sigma_{ns})$  on the boundary  $\Gamma^e$  are related to  $(\sigma_{xx}, \sigma_{yy}, \sigma_{xy})$  in the interior of  $\Omega^e$  by the transformation

$$\begin{Bmatrix} \sigma_{nn} \\ \sigma_{ns} \end{Bmatrix} = \begin{bmatrix} n_x^2 & n_y^2 & 2n_x n_y \\ -n_x n_y & n_x n_y & n_x^2 - n_y^2 \end{bmatrix} \begin{Bmatrix} \sigma_{xx} \\ \sigma_{yy} \\ \sigma_{xy} \end{Bmatrix} \quad (6.3.8)$$

### 6.3.2 Weak Forms

Substituting for  $\delta U^e$  and  $\delta V^e$  from Eqs. (6.3.3) and (6.3.6) into the virtual work statement in Eq. (6.3.2), we obtain the weak form

$$\begin{aligned} 0 &= \int_{\Omega^e} \left( N_{xx} \delta \varepsilon_{xx}^0 + M_{xx} \delta \varepsilon_{xx}^1 + N_{yy} \delta \varepsilon_{yy}^0 + M_{yy} \delta \varepsilon_{yy}^1 + N_{xy} \delta \gamma_{xy}^0 \right. \\ &\quad \left. + M_{xy} \delta \gamma_{xy}^1 + k w_0 \delta w_0 - q \delta w_0 \right) dx dy \\ &\quad - \oint_{\Gamma^e} \left( N_{nn} \delta u_{0n} + N_{ns} \delta u_{0s} - M_{nn} \frac{\partial \delta w_0}{\partial n} - M_{ns} \frac{\partial \delta w_0}{\partial s} + Q_n \delta w_0 \right) ds \\ &= \int_{\Omega^e} \left[ \left( \frac{\partial \delta u_0}{\partial x} + \frac{\partial w_0}{\partial x} \frac{\partial \delta w_0}{\partial x} \right) N_{xx} + \left( \frac{\partial \delta v_0}{\partial y} + \frac{\partial w_0}{\partial y} \frac{\partial \delta w_0}{\partial y} \right) N_{yy} \right. \\ &\quad \left. + \left( \frac{\partial \delta u_0}{\partial y} + \frac{\partial \delta v_0}{\partial x} + \frac{\partial w_0}{\partial x} \frac{\partial \delta w_0}{\partial y} + \frac{\partial w_0}{\partial y} \frac{\partial \delta w_0}{\partial x} \right) N_{xy} \right. \\ &\quad \left. - \frac{\partial^2 \delta w_0}{\partial x^2} M_{xx} - \frac{\partial^2 \delta w_0}{\partial y^2} M_{yy} - 2 \frac{\partial^2 \delta w_0}{\partial x \partial y} M_{xy} + k \delta w_0 w_0 - \delta w_0 q \right] dx dy \\ &\quad - \oint_{\Gamma^e} \left( N_{nn} \delta u_{0n} + N_{ns} \delta u_{0s} - M_{nn} \frac{\partial \delta w_0}{\partial n} - M_{ns} \frac{\partial \delta w_0}{\partial s} + Q_n \delta w_0 \right) ds \end{aligned} \quad (6.3.9)$$

The statement (6.3.9) is equivalent to the following three weak forms:

$$0 = \int_{\Omega^e} \left( \frac{\partial \delta u_0}{\partial x} N_{xx} + \frac{\partial \delta u_0}{\partial y} N_{xy} \right) dx dy - \oint_{\Gamma^e} N_{nn} \delta u_{0n} ds \quad (6.3.10)$$

$$0 = \int_{\Omega^e} \left( \frac{\partial \delta v_0}{\partial x} N_{xy} + \frac{\partial \delta v_0}{\partial y} N_{yy} \right) dx dy - \oint_{\Gamma^e} N_{ns} \delta u_{0s} ds \quad (6.3.11)$$

$$\begin{aligned} 0 &= \int_{\Omega^e} \left[ \frac{\partial \delta w_0}{\partial x} \left( \frac{\partial w_0}{\partial x} N_{xx} + \frac{\partial w_0}{\partial y} N_{xy} \right) + \frac{\partial \delta w_0}{\partial y} \left( \frac{\partial w_0}{\partial x} N_{xy} + \frac{\partial w_0}{\partial y} N_{yy} \right) \right. \\ &\quad \left. - \frac{\partial^2 \delta w_0}{\partial x^2} M_{xx} - \frac{\partial^2 \delta w_0}{\partial y^2} M_{yy} - 2 \frac{\partial^2 \delta w_0}{\partial x \partial y} M_{xy} + k \delta w_0 w_0 - \delta w_0 q \right] dx dy \\ &\quad - \oint_{\Gamma^e} \left( -M_{nn} \frac{\partial \delta w_0}{\partial n} - M_{ns} \frac{\partial \delta w_0}{\partial s} + Q_n \delta w_0 \right) ds \end{aligned} \quad (6.3.12)$$

### 6.3.3 Equilibrium Equations

To obtain the governing equations of the CPT, integrate expressions in Eqs. (6.3.10)–(6.3.12) by parts to relieve the virtual displacements ( $\delta u_0, \delta v_0, \delta w_0$ ) in  $\Omega^e$  of any differentiation (so that we can use the fundamental lemma of variational calculus); we obtain

$$\begin{aligned}
 0 = & \int_{\Omega^e} \left[ - (N_{xx,x} + N_{xy,y}) \delta u_0 - (N_{xy,x} + N_{yy,y}) \delta v_0 \right. \\
 & \left. - \left( M_{xx,xx} + 2M_{xy,xy} + M_{yy,yy} + \mathcal{N} - kw_0 + q \right) \delta w_0 \right] dx dy \\
 & + \oint_{\Gamma^e} \left[ (N_{xx}n_x + N_{xy}n_y) \delta u_0 + (N_{xy}n_x + N_{yy}n_y) \delta v_0 \right. \\
 & \left. + \left( M_{xx,x}n_x + M_{xy,y}n_x + M_{yy,y}n_y + M_{xy,x}n_y + \mathcal{P} \right) \delta w_0 \right. \\
 & \left. - (M_{xx}n_x + M_{xy}n_y) \frac{\partial \delta w_0}{\partial x} - (M_{xy}n_x + M_{yy}n_y) \frac{\partial \delta w_0}{\partial y} \right] ds \\
 & - \oint_{\Gamma^e} \left( N_{nn} \delta u_{0n} + N_{ns} \delta u_{0s} - M_{nn} \frac{\partial \delta w_0}{\partial n} - M_{ns} \frac{\partial \delta w_0}{\partial s} + Q_n \delta w_0 \right) ds
 \end{aligned} \tag{6.3.13}$$

where a comma followed by subscripts denotes differentiation with respect to the subscripts:  $N_{xx,x} = \partial N_{xx} / \partial x$ , and so on, and

$$\mathcal{N}(u_0, v_0, w_0) = \frac{\partial}{\partial x} \left( N_{xx} \frac{\partial w_0}{\partial x} + N_{xy} \frac{\partial w_0}{\partial y} \right) + \frac{\partial}{\partial y} \left( N_{xy} \frac{\partial w_0}{\partial x} + N_{yy} \frac{\partial w_0}{\partial y} \right)$$

$$\mathcal{P}(u_0, v_0, w_0) = \left( N_{xx} \frac{\partial w_0}{\partial x} + N_{xy} \frac{\partial w_0}{\partial y} \right) n_x + \left( N_{xy} \frac{\partial w_0}{\partial x} + N_{yy} \frac{\partial w_0}{\partial y} \right) n_y \tag{6.3.14}$$

The equations of equilibrium are obtained by setting the coefficients of  $\delta u_0$ ,  $\delta v_0$ , and  $\delta w_0$  in  $\Omega^e$  to zero:

$$\delta u_0 : \quad \frac{\partial N_{xx}}{\partial x} + \frac{\partial N_{xy}}{\partial y} = 0 \tag{6.3.15}$$

$$\delta v_0 : \quad \frac{\partial N_{xy}}{\partial x} + \frac{\partial N_{yy}}{\partial y} = 0 \tag{6.3.16}$$

$$\begin{aligned}
 \delta w_0 : \quad & \frac{\partial^2 M_{xx}}{\partial x^2} + 2 \frac{\partial^2 M_{xy}}{\partial y \partial x} + \frac{\partial^2 M_{yy}}{\partial y^2} \\
 & + \mathcal{N}(u_0, v_0, w_0) - kw_0 + q = 0
 \end{aligned} \tag{6.3.17}$$

### 6.3.4 Boundary Conditions

To cast the boundary conditions on an arbitrary edge whose normal is  $\hat{n}$ , we express all generalized displacements ( $u_0, v_0, w_0, \frac{\partial w_0}{\partial x}, \frac{\partial w_0}{\partial y}$ ) from the  $(x, y, z)$  system in terms of the corresponding generalized displacements in the normal, tangential, and transverse directions. We have

$$u_0 = u_{0n}n_x - u_{0s}n_y, \quad v_0 = u_{0n}n_y + u_{0s}n_x \quad (6.3.18a)$$

$$\frac{\partial w_0}{\partial x} = \frac{\partial w_0}{\partial n}n_x - \frac{\partial w_0}{\partial s}n_y, \quad \frac{\partial w_0}{\partial y} = \frac{\partial w_0}{\partial n}n_y + \frac{\partial w_0}{\partial s}n_x \quad (6.3.18b)$$

The boundary expression of Eq. (6.3.13) takes the form

$$\begin{aligned} & \oint_{\Gamma^e} \left[ (N_{xx}n_x + N_{xy}n_y) (\delta u_{0n}n_x - \delta u_{0s}n_y) \right. \\ & \quad + (N_{xy}n_x + N_{yy}n_y) (\delta u_{0n}n_y + \delta u_{0s}n_x) \\ & \quad + \left( M_{xx,x}n_x + M_{xy,y}n_x + M_{yy,y}n_y + M_{xy,x}n_y + \mathcal{P} \right) \delta w_0 \\ & \quad - (M_{xx}n_x + M_{xy}n_y) \left( \frac{\partial \delta w_0}{\partial n}n_x - \frac{\partial \delta w_0}{\partial s}n_y \right) \\ & \quad \left. - (M_{xy}n_x + M_{yy}n_y) \left( \frac{\partial \delta w_0}{\partial n}n_y + \frac{\partial \delta w_0}{\partial s}n_x \right) \right] ds \\ & - \oint_{\Gamma^e} \left( N_{nn}\delta u_{0n} + N_{ns}\delta u_{0s} - M_{nn}\frac{\partial \delta w_0}{\partial n} - M_{ns}\frac{\partial \delta w_0}{\partial s} + Q_n\delta w_0 \right) ds \\ & = \oint_{\Gamma^e} \left\{ (N_{xx}n_x^2 + 2N_{xy}n_xn_y + N_{yy}n_y^2 - N_{nn}) \delta u_{0n} \right. \\ & \quad + [(N_{yy} - N_{xx})n_xn_y + N_{xy}(n_x^2 - n_y^2) - N_{ns}] \delta u_{0s} \\ & \quad + (M_{xx,x}n_x + M_{xy,y}n_x + M_{yy,y}n_y + M_{xy,x}n_y + \mathcal{P} - Q_n) \delta w_0 \\ & \quad - (M_{xx}n_x^2 + 2M_{xy}n_xn_y + M_{yy}n_y^2 - M_{nn}) \frac{\partial \delta w_0}{\partial n} \\ & \quad \left. - [(M_{yy} - M_{xx})n_xn_y + M_{xy}(n_x^2 - n_y^2) - M_{ns}] \frac{\partial \delta w_0}{\partial s} \right\} ds \quad (6.3.19) \end{aligned}$$

The natural boundary conditions are obtained by setting the coefficients of  $\delta u_0, \delta v_0, \delta w_0, \frac{\partial \delta w_0}{\partial n}$  and  $\frac{\partial \delta w_0}{\partial s}$  on  $\Gamma^e$  to zero:

$$\begin{aligned} \delta u_{0n} : N_{nn} &= N_{xx}n_x^2 + 2N_{xy}n_xn_y + N_{yy}n_y^2 \\ \delta u_{0s} : N_{ns} &= (N_{yy} - N_{xx})n_xn_y + N_{xy}(n_x^2 - n_y^2) \\ \delta w_0 : Q_n &= M_{xx,x}n_x + M_{xy,y}n_x + M_{yy,y}n_y + M_{xy,x}n_y + \mathcal{P} \end{aligned} \quad (6.3.20a)$$

$$\begin{aligned} \frac{\partial \delta w_0}{\partial n} : M_{nn} &= M_{xx}n_x^2 + 2M_{xy}n_xn_y + M_{yy}n_y^2 \\ \frac{\partial \delta w_0}{\partial s} : M_{ns} &= (M_{yy} - M_{xx})n_xn_y + M_{xy}(n_x^2 - n_y^2) \end{aligned} \quad (6.3.20b)$$

From Eq. (6.3.20), it is clear that the primary variables (i.e. generalized displacements) and secondary variables (i.e. generalized forces) of the theory are:

$$\begin{aligned} \text{Primary variables: } & u_{0n}, u_{0s}, w_0, \frac{\partial w_0}{\partial n}, \frac{\partial w_0}{\partial s} \\ \text{Secondary variables: } & N_{nn}, N_{ns}, Q_n, M_{nn}, M_{ns} \end{aligned} \quad (6.3.21)$$

We note that the equations of equilibrium in Eqs. (6.3.15)–(6.3.17) have the total spatial differential order of eight. In other words, if the governing equations are expressed in terms of the displacements  $(u_0, v_0, w_0)$ , they would contain second-order spatial derivatives of  $u_0$  and  $v_0$  and fourth-order spatial derivatives of  $w_0$ . This implies that there should be only eight (four essential and four natural) boundary conditions, whereas Eq. (6.3.21) shows five essential and five natural boundary conditions, giving a total of ten boundary conditions. To eliminate this discrepancy, one may integrate the tangential derivative term by parts to obtain the boundary term

$$-\oint_{\Gamma} M_{ns} \frac{\partial \delta w_0}{\partial s} ds = \oint_{\Gamma} \frac{\partial M_{ns}}{\partial s} \delta w_0 ds - [M_{ns} \delta w_0]_{\Gamma} \quad (6.3.22)$$

The term  $[M_{ns} \delta w_0]_{\Gamma}$  is zero when the end points of a closed curve coincide or when  $M_{ns} = 0$ . If  $M_{ns} = 0$  is not specified at corners of the boundary  $\Gamma$  of a polygonal plate, concentrated forces of magnitude  $F_c = -2M_{ns}$  will be produced at the corners. The factor of 2 appears because  $M_{ns}$  from two sides of the corner are added there.

The remaining boundary term in Eq. (6.3.22) is added to the shear force  $Q_n$  (because it is a coefficient of  $\delta w_0$  on  $\Gamma^e$ ) to obtain the effective shear force

$$V_n \equiv Q_n + \frac{\partial M_{ns}}{\partial s} \quad (6.3.23)$$

The specification of this effective shear force  $V_n$  is known as the *Kirchhoff free-edge condition*. Finally, the correct boundary conditions of the CPT involve specifying the following quantities:

$$\begin{aligned} \text{Generalized displacements: } & u_{0n}, u_{0s}, w_0, \frac{\partial w_0}{\partial n} \\ \text{Generalized forces: } & N_{nn}, N_{ns}, V_n, M_{nn} \end{aligned} \quad (6.3.24)$$

Thus, at every boundary point one must know  $u_{0n}$  or  $N_{nn}$ ,  $u_{0s}$  or  $N_{ns}$ ,  $w_0$  or  $V_n$ , and  $\partial w_0 / \partial n$  or  $M_{nn}$ . On an edge parallel to the  $x$ -axis (i.e.  $s = x$  and

$n = y$ ), for example, the above boundary conditions become

$$u_{0n} = v_0, \quad u_{0s} = u_0, \quad w_0, \quad \frac{\partial w_0}{\partial n} = \frac{\partial w_0}{\partial y} \quad (6.3.25a)$$

$$N_{nn} = N_{yy}, \quad N_{ns} = N_{yx}, \quad V_n = V_y, \quad M_{nn} = M_{yy} \quad (6.3.25b)$$

Next we discuss some common types of boundary conditions for the linear bending of a rectangular plate with edges parallel to the  $x$  and  $y$  coordinates. Here we use the edge at  $y = 0$  ( $n_x = 0$  and  $n_y = -1$ ) to discuss the boundary conditions (see Figure 6.3.2). It should be noted that only one element of each of the four pairs may (and should) be specified on an edge of a plate. The force boundary conditions may be expressed in terms of the generalized displacements using the plate constitutive equations discussed in the next section.

**Free edge,  $y = 0$ :** A free edge is one that is geometrically not restrained in any way. Hence, we have

$$u_0 \neq 0, \quad v_0 \neq 0, \quad w_0 \neq 0, \quad \frac{\partial w_0}{\partial y} \neq 0 \quad (6.3.26a)$$

However, the edge may have applied forces and/or moments

$$N_{xy} = \hat{N}_{xy}, \quad N_{yy} = \hat{N}_{yy}, \quad V_n \equiv -Q_y - \frac{\partial M_{xy}}{\partial x} = \hat{V}_n, \quad M_{yy} = \hat{M}_{yy} \quad (6.3.26b)$$

where quantities with a hat are specified forces/moments. For free rectangular plates,  $M_{xy} = 0$ , hence no corner forces are developed.

**Fixed (or clamped) edge,  $y = 0$ :** A fixed edge is one that is geometrically fully restrained

$$u_0 = 0, \quad v_0 = 0, \quad w_0 = 0, \quad \frac{\partial w_0}{\partial y} = 0 \quad (6.3.27)$$

Therefore, the forces and moments on a fixed edge are not known a priori (i.e. they are reactions to be determined as a part of the analysis). For clamped rectangular plates,  $M_{xy} = 0$ , hence no corner forces are developed.

**Simply supported edge  $y = 0$ :** The phrase "simply supported" does not uniquely define the boundary conditions, and one must indicate what it means, especially when both in-plane and bending deflections are involved. Here we *define* two types of simply supported boundary conditions:

$$\text{SS-1:} \quad u_0 = 0, \quad w_0 = 0; \quad N_{yy} = \hat{N}_{yy}, \quad M_{yy} = \hat{M}_{yy} \quad (6.3.28)$$

$$\text{SS-2:} \quad v_0 = 0, \quad w_0 = 0; \quad N_{xy} = \hat{N}_{xy}, \quad M_{yy} = \hat{M}_{yy} \quad (6.3.29)$$



### 6.3.5 Stress Resultant-Deflections Relations

To express the forces and moments ( $\{N\}, \{M\}$ ) per unit length in terms of the generalized displacements ( $u_0, v_0, w_0$ ), we must invoke appropriate stress-strain relations. In the CPT, all three transverse strain components ( $\varepsilon_{zz}, \varepsilon_{xz}, \varepsilon_{yz}$ ) are zero by definition. Since  $\varepsilon_{zz} = 0$ , the transverse normal stress  $\sigma_{zz}$ , though not zero identically, does not appear in the virtual work statement and hence in the equations of motion. Consequently, it amounts to neglecting the transverse normal stress. Thus we have, in theory, a case of both plane strain and plane stress. However, from practical considerations, a thin to moderately thick plate is in a state of plane stress because the thickness is small compared to the in-plane dimensions. Hence, the plane stress-reduced constitutive relations may be used.

For an orthotropic material with principal materials axes ( $x_1, x_2, x_3$ ) coinciding with the plate coordinates ( $x, y, z$ ), the plane stress-reduced thermoelastic constitutive equations can be expressed as (see Reddy [3,40])

$$\begin{Bmatrix} \sigma_{xx} \\ \sigma_{yy} \\ \sigma_{xy} \end{Bmatrix} = \begin{bmatrix} Q_{11} & Q_{12} & 0 \\ Q_{12} & Q_{22} & 0 \\ 0 & 0 & Q_{66} \end{bmatrix} \begin{Bmatrix} \varepsilon_{xx} - \alpha_1 \Delta T \\ \varepsilon_{yy} - \alpha_2 \Delta T \\ \gamma_{xy} \end{Bmatrix} \quad (6.3.30)$$

where  $Q_{ij}$  are the plane stress-reduced stiffnesses

$$Q_{11} = \frac{E_1}{1 - \nu_{12}\nu_{21}}, \quad Q_{12} = \frac{\nu_{12}E_2}{1 - \nu_{12}\nu_{21}} = \frac{\nu_{21}E_1}{1 - \nu_{12}\nu_{21}} \quad (6.3.31a)$$

$$Q_{22} = \frac{E_2}{1 - \nu_{12}\nu_{21}}, \quad Q_{66} = G_{12} \quad (6.3.31b)$$

and ( $\sigma_i, \varepsilon_i$ ) are the stress and strain components, respectively,  $\alpha_1$  and  $\alpha_2$  are the coefficients of thermal expansion, and  $\Delta T$  is the temperature increment from a reference state,  $\Delta T = T - T_0$ . The moisture strains are similar to thermal strains (i.e. for moisture strains replace  $\Delta T$  and  $\alpha_i$  with the moisture concentration increment and coefficients of hygroscopic expansion, respectively).

The plate constitutive equations relate the forces and moments per unit length in Eq. (6.3.4) to the strains (6.2.8b) of the plate theory. For a plate made of a single or multiple orthotropic layers, the plate constitutive relations are obtained using the definitions in Eq. (6.3.4). For plates laminated of multiple orthotropic layers whose material axes are arbitrarily oriented with respect to the plate axes, the plate constitutive relations couple the in-plane displacements to the out-of-plane displacements even for linear problems (see Reddy [40] for details). For a single orthotropic layer, the plate constitutive relations are greatly simplified. They are

$$\begin{Bmatrix} N_{xx} \\ N_{yy} \\ N_{xy} \end{Bmatrix} = \int_{-\frac{h}{2}}^{\frac{h}{2}} \begin{bmatrix} Q_{11} & Q_{12} & 0 \\ Q_{12} & Q_{22} & 0 \\ 0 & 0 & Q_{66} \end{bmatrix} \begin{Bmatrix} \varepsilon_{xx}^0 + z\varepsilon_{xx}^1 - \alpha_1 \Delta T \\ \varepsilon_{yy}^0 + z\varepsilon_{yy}^1 - \alpha_2 \Delta T \\ \gamma_{xy}^0 + z\gamma_{xy}^1 \end{Bmatrix} dz$$

$$= \begin{bmatrix} A_{11} & A_{12} & 0 \\ A_{12} & A_{22} & 0 \\ 0 & 0 & A_{66} \end{bmatrix} \begin{Bmatrix} \varepsilon_{xx}^0 \\ \varepsilon_{yy}^0 \\ \gamma_{xy}^0 \end{Bmatrix} - \begin{Bmatrix} N_{xx}^T \\ N_{yy}^T \\ 0 \end{Bmatrix} \quad (6.3.32)$$

$$\begin{aligned} \begin{Bmatrix} M_{xx} \\ M_{yy} \\ M_{xy} \end{Bmatrix} &= \int_{-\frac{h}{2}}^{\frac{h}{2}} \begin{bmatrix} Q_{11} & Q_{12} & 0 \\ Q_{12} & Q_{22} & 0 \\ 0 & 0 & Q_{66} \end{bmatrix} \begin{Bmatrix} \varepsilon_{xx}^0 + z\varepsilon_{xx}^1 - \alpha_1 \Delta T \\ \varepsilon_{yy}^0 + z\varepsilon_{yy}^1 - \alpha_2 \Delta T \\ \gamma_{xy}^0 + z\gamma_{xy}^1 \end{Bmatrix} z \, dz \\ &= \begin{bmatrix} D_{11} & D_{12} & 0 \\ D_{12} & D_{22} & 0 \\ 0 & 0 & D_{66} \end{bmatrix} \begin{Bmatrix} \varepsilon_{xx}^1 \\ \varepsilon_{yy}^1 \\ \gamma_{xy}^1 \end{Bmatrix} - \begin{Bmatrix} M_{xx}^T \\ M_{yy}^T \\ 0 \end{Bmatrix} \end{aligned} \quad (6.3.33)$$

where  $A_{ij}$  are *extensional stiffnesses* and  $D_{ij}$  are *bending stiffnesses*, which are defined in terms of the elastic stiffnesses  $Q_{ij}$  as

$$(A_{ij}, D_{ij}) = \int_{-\frac{h}{2}}^{\frac{h}{2}} Q_{ij}(1, z^2) dz \quad \text{or} \quad A_{ij} = hQ_{ij}, \quad D_{ij} = \frac{h^3}{12} Q_{ij} \quad (6.3.34)$$

and  $\{N^T\}$  and  $\{M^T\}$  are thermal stress resultants

$$\begin{Bmatrix} N_{xx}^T \\ N_{yy}^T \end{Bmatrix} = \begin{Bmatrix} Q_{11}\alpha_1 + Q_{12}\alpha_2 \\ Q_{12}\alpha_1 + Q_{22}\alpha_2 \end{Bmatrix} \int_{-\frac{h}{2}}^{\frac{h}{2}} \Delta T(x, y, z) \, dz \quad (6.3.35a)$$

$$\begin{Bmatrix} M_{xx}^T \\ M_{yy}^T \end{Bmatrix} = \begin{Bmatrix} Q_{11}\alpha_1 + Q_{12}\alpha_2 \\ Q_{12}\alpha_1 + Q_{22}\alpha_2 \end{Bmatrix} \int_{-\frac{h}{2}}^{\frac{h}{2}} \Delta T(x, y, z) \, z \, dz \quad (6.3.35b)$$

where  $\alpha_1$  and  $\alpha_2$  are the thermal coefficients of expansion, and  $\Delta T$  is the temperature change (above a stress-free temperature), which is a known function of position. For isotropic plates, Eqs. (6.3.35a,b) simplify to

$$N_{xx}^T = N_{yy}^T = \frac{N_T}{(1-\nu)}, \quad N_T = E\alpha \int_{-\frac{h}{2}}^{\frac{h}{2}} \Delta T \, dz \quad (6.3.36a)$$

$$M_{xx}^T = M_{yy}^T = \frac{M_T}{(1-\nu)}, \quad M_T = E\alpha \int_{-\frac{h}{2}}^{\frac{h}{2}} \Delta T \, z \, dz \quad (6.3.36b)$$

## 6.4 Finite Element Models of CPT

### 6.4.1 General Formulation

In this section, the displacement finite element model of Eqs. (6.3.15)–(6.3.17) governing plates according to the CPT is developed. The virtual work statements of the CPT over a typical orthotropic plate finite element  $\Omega^e$

are given by [from Eqs. (6.3.10)–(6.3.12)]

$$0 = \int_{\Omega^e} \left( \frac{\partial \delta u_0}{\partial x} \left\{ A_{11} \left[ \frac{\partial u_0}{\partial x} + \frac{1}{2} \left( \frac{\partial w_0}{\partial x} \right)^2 \right] + A_{12} \left[ \frac{\partial v_0}{\partial y} + \frac{1}{2} \left( \frac{\partial w_0}{\partial y} \right)^2 \right] \right\} \right. \\ \left. + A_{66} \frac{\partial \delta u_0}{\partial y} \left[ \frac{\partial u_0}{\partial y} + \frac{\partial v_0}{\partial x} + \frac{\partial w_0}{\partial x} \frac{\partial w_0}{\partial y} \right] \right) dx dy \\ - \int_{\Omega^e} \frac{\partial \delta u_0}{\partial x} N_{xx}^T dx dy - \oint_{\Gamma^e} N_n \delta u_{0n} ds \quad (6.4.1a)$$

$$0 = \int_{\Omega^e} \left( \frac{\partial \delta v_0}{\partial y} \left\{ A_{12} \left[ \frac{\partial u_0}{\partial x} + \frac{1}{2} \left( \frac{\partial w_0}{\partial x} \right)^2 \right] + A_{22} \left[ \frac{\partial v_0}{\partial y} + \frac{1}{2} \left( \frac{\partial w_0}{\partial y} \right)^2 \right] \right\} \right. \\ \left. + A_{66} \frac{\partial \delta v_0}{\partial x} \left[ \frac{\partial u_0}{\partial y} + \frac{\partial v_0}{\partial x} + \frac{\partial w_0}{\partial x} \frac{\partial w_0}{\partial y} \right] \right) dx dy \\ - \int_{\Omega^e} \frac{\partial \delta v_0}{\partial y} N_{yy}^T dx dy - \oint_{\Gamma^e} N_s \delta u_{0s} ds \quad (6.4.1b)$$

$$0 = \int_{\Omega^e} \left\{ \frac{\partial \delta w_0}{\partial x} \left[ \frac{\partial w_0}{\partial x} \left\{ A_{11} \left[ \frac{\partial u_0}{\partial x} + \frac{1}{2} \left( \frac{\partial w_0}{\partial x} \right)^2 \right] + A_{12} \left[ \frac{\partial v_0}{\partial y} + \frac{1}{2} \left( \frac{\partial w_0}{\partial y} \right)^2 \right] \right\} \right. \right. \\ \left. + A_{66} \frac{\partial w_0}{\partial y} \left( \frac{\partial u_0}{\partial y} + \frac{\partial v_0}{\partial x} + \frac{\partial w_0}{\partial x} \frac{\partial w_0}{\partial y} \right) \right] \\ + \frac{\partial \delta w_0}{\partial y} \left[ \frac{\partial w_0}{\partial y} \left\{ A_{12} \left[ \frac{\partial u_0}{\partial x} + \frac{1}{2} \left( \frac{\partial w_0}{\partial x} \right)^2 \right] + A_{22} \left[ \frac{\partial v_0}{\partial y} + \frac{1}{2} \left( \frac{\partial w_0}{\partial y} \right)^2 \right] \right\} \right. \\ \left. + A_{66} \frac{\partial w_0}{\partial x} \left( \frac{\partial u_0}{\partial y} + \frac{\partial v_0}{\partial x} + \frac{\partial w_0}{\partial x} \frac{\partial w_0}{\partial y} \right) \right] \\ + \frac{\partial^2 \delta w_0}{\partial x^2} \left( D_{11} \frac{\partial^2 w_0}{\partial x^2} + D_{12} \frac{\partial^2 w_0}{\partial x^2} \right) + \frac{\partial^2 \delta w_0}{\partial y^2} \left( D_{12} \frac{\partial^2 w_0}{\partial x^2} + D_{22} \frac{\partial^2 w_0}{\partial x^2} \right) \\ \left. + 4D_{66} \frac{\partial^2 \delta w_0}{\partial x \partial y} \frac{\partial^2 w_0}{\partial x \partial y} + k \delta w_0 w_0 - \delta w_0 q \right\} dx dy \\ + \int_{\Omega^e} \left( \frac{\partial^2 \delta w_0}{\partial x^2} M_{xx}^T + \frac{\partial^2 \delta w_0}{\partial y^2} M_{yy}^T \right) dx dy - \oint_{\Gamma^e} \left( V_n \delta w_0 - M_n \frac{\partial \delta w_0}{\partial n} \right) ds \quad (6.4.1c)$$

where

$$N_n = N_{xx} n_x + N_{xy} n_y, \quad N_s = N_{xy} n_x + N_{yy} n_y \\ V_n = Q_n + \frac{\partial M_{ns}}{\partial s} \\ M_n = M_{xx} n_x + M_{xy} n_y, \quad M_s = M_{xy} n_x + M_{yy} n_y \quad (6.4.2)$$

and  $(n_x, n_y)$  denote the direction cosines of the unit normal on the element boundary  $\Gamma^e$ . We note from the boundary terms in Eqs. (6.4.1a-c) that  $u_0$ ,  $v_0$ ,  $w_0$ , and  $\partial w_0/\partial n$  are used as the primary variables (or generalized displacements), and  $\hat{N}_n$ ,  $\hat{N}_s$ ,  $\hat{V}_n$ , and  $\hat{M}_n$  as the secondary degrees of freedom (or generalized forces). Thus, finite elements based on the CPT require continuity of the transverse deflection  $w_0$  and its derivatives across element boundaries (i.e.  $C^1$ -continuity of  $w_0$ ). Also, to satisfy the constant displacement (rigid body mode) and constant strain requirements, the polynomial expansion for  $w_0$  should be a complete quadratic. The in-plane displacements  $u_0$  and  $v_0$  need only be  $C^0$  continuous.

Assume finite element approximation of the form

$$\begin{aligned} u_0(x, y) &= \sum_{j=1}^m u_j^e \psi_j^e(x, y) \\ v_0(x, y) &= \sum_{j=1}^m v_j^e \psi_j^e(x, y) \\ w_0(x, y) &= \sum_{j=1}^n \bar{\Delta}_j^e \varphi_j^e(x, y) \end{aligned} \quad (6.4.3)$$

where  $\psi_j^e$  are the Lagrange interpolation functions,  $\bar{\Delta}_j^e$  are the values of  $w_0$  and its derivatives at the nodes, and  $\varphi_j^e$  are the interpolation functions, the specific form of which will depend on the geometry of the element and the nodal degrees of freedom interpolated. Substituting approximations (6.4.3) for  $(u_0, v_0, w_0)$  and  $(\psi_i^e, \psi_j^e, \varphi_i^e)$  for the virtual displacements  $(\delta u_0, \delta v_0, \delta w_0)$  into Eqs. [6.4.1(a)-(c)], we obtain

$$\begin{bmatrix} [K^{11}] & [K^{12}] & [K^{13}] \\ [K^{21}] & [K^{22}] & [K^{23}] \\ [K^{31}] & [K^{32}] & [K^{33}] \end{bmatrix} \begin{Bmatrix} \{u\} \\ \{v\} \\ \{\bar{\Delta}\} \end{Bmatrix} = \begin{Bmatrix} \{F^1\} \\ \{F^2\} \\ \{F^3\} \end{Bmatrix} + \begin{Bmatrix} \{F^{1T}\} \\ \{F^{2T}\} \\ \{F^{3T}\} \end{Bmatrix} \quad (6.4.4)$$

The stiffness coefficients  $K_{ij}^{\alpha\beta}$  (not symmetric) and force vectors  $F_i^\alpha$  and  $F_i^{\alpha T}$  ( $\alpha, \beta = 1, 2, 3$ ) are defined as follows:

$$\begin{aligned} K_{ij}^{11} &= \int_{\Omega^e} \left( A_{11} \frac{\partial \psi_i^e}{\partial x} \frac{\partial \psi_j^e}{\partial x} + A_{66} \frac{\partial \psi_i^e}{\partial y} \frac{\partial \psi_j^e}{\partial y} \right) dx dy \\ K_{ij}^{12} &= \int_{\Omega^e} \left( A_{12} \frac{\partial \psi_i^e}{\partial x} \frac{\partial \psi_j^e}{\partial y} + A_{66} \frac{\partial \psi_i^e}{\partial y} \frac{\partial \psi_j^e}{\partial x} \right) dx dy = K_{ji}^{21} \\ K_{ij}^{13} &= \frac{1}{2} \int_{\Omega^e} \left[ \frac{\partial \psi_i^e}{\partial x} \left( A_{11} \frac{\partial w_0}{\partial x} \frac{\partial \varphi_j^e}{\partial x} + A_{12} \frac{\partial w_0}{\partial y} \frac{\partial \varphi_j^e}{\partial y} \right) \right. \\ &\quad \left. + A_{66} \frac{\partial \psi_i^e}{\partial y} \left( \frac{\partial w_0}{\partial x} \frac{\partial \varphi_j^e}{\partial y} + \frac{\partial w_0}{\partial y} \frac{\partial \varphi_j^e}{\partial x} \right) \right] dx dy \end{aligned}$$

$$\begin{aligned}
K_{ij}^{22} &= \int_{\Omega^e} \left( A_{66} \frac{\partial \psi_i^e}{\partial x} \frac{\partial \psi_j^e}{\partial x} + A_{22} \frac{\partial \psi_i^e}{\partial y} \frac{\partial \psi_j^e}{\partial y} \right) dx dy \\
K_{ij}^{23} &= \frac{1}{2} \int_{\Omega^e} \left[ \frac{\partial \psi_i^e}{\partial y} \left( A_{12} \frac{\partial w_0}{\partial x} \frac{\partial \varphi_j^e}{\partial x} + A_{22} \frac{\partial w_0}{\partial y} \frac{\partial \varphi_j^e}{\partial y} \right) \right. \\
&\quad \left. + A_{66} \frac{\partial \psi_i^e}{\partial x} \left( \frac{\partial w_0}{\partial x} \frac{\partial \varphi_j^e}{\partial y} + \frac{\partial w_0}{\partial y} \frac{\partial \varphi_j^e}{\partial x} \right) \right] dx dy \\
K_{ij}^{31} &= \int_{\Omega^e} \left[ \frac{\partial \varphi_i^e}{\partial x} \left( A_{11} \frac{\partial w_0}{\partial x} \frac{\partial \psi_j^e}{\partial x} + A_{66} \frac{\partial w_0}{\partial y} \frac{\partial \psi_j^e}{\partial y} \right) \right. \\
&\quad \left. + \frac{\partial \varphi_i^e}{\partial y} \left( A_{66} \frac{\partial w_0}{\partial x} \frac{\partial \psi_j^e}{\partial y} + A_{12} \frac{\partial w_0}{\partial y} \frac{\partial \psi_j^e}{\partial x} \right) \right] dx dy \\
K_{ij}^{32} &= \int_{\Omega^e} \left[ \frac{\partial \varphi_i^e}{\partial x} \left( A_{12} \frac{\partial w_0}{\partial x} \frac{\partial \psi_j^e}{\partial y} + A_{66} \frac{\partial w_0}{\partial y} \frac{\partial \psi_j^e}{\partial x} \right) \right. \\
&\quad \left. + \frac{\partial \varphi_i^e}{\partial y} \left( A_{66} \frac{\partial w_0}{\partial x} \frac{\partial \psi_j^e}{\partial x} + A_{22} \frac{\partial w_0}{\partial y} \frac{\partial \psi_j^e}{\partial y} \right) \right] dx dy \\
K_{ij}^{33} &= \int_{\Omega^e} \left[ D_{11} \frac{\partial^2 \varphi_i^e}{\partial x^2} \frac{\partial^2 \varphi_j^e}{\partial x^2} + D_{22} \frac{\partial^2 \varphi_i^e}{\partial y^2} \frac{\partial^2 \varphi_j^e}{\partial y^2} \right. \\
&\quad \left. + D_{12} \left( \frac{\partial^2 \varphi_i^e}{\partial x^2} \frac{\partial^2 \varphi_j^e}{\partial y^2} + \frac{\partial^2 \varphi_i^e}{\partial y^2} \frac{\partial^2 \varphi_j^e}{\partial x^2} \right) \right. \\
&\quad \left. + 4D_{66} \frac{\partial^2 \varphi_i^e}{\partial x \partial y} \frac{\partial^2 \varphi_j^e}{\partial x \partial y} + k \varphi_i^e \varphi_j^e \right] dx dy \\
&\quad + \frac{1}{2} \int_{\Omega^e} \left\{ \left[ A_{11} \left( \frac{\partial w_0}{\partial x} \right)^2 + A_{66} \left( \frac{\partial w_0}{\partial y} \right)^2 \right] \frac{\partial \varphi_i^e}{\partial x} \frac{\partial \varphi_j^e}{\partial x} \right. \\
&\quad \left. + \left[ A_{66} \left( \frac{\partial w_0}{\partial x} \right)^2 + A_{22} \left( \frac{\partial w_0}{\partial y} \right)^2 \right] \frac{\partial \varphi_i^e}{\partial y} \frac{\partial \varphi_j^e}{\partial y} \right. \\
&\quad \left. + (A_{12} + A_{66}) \frac{\partial w_0}{\partial x} \frac{\partial w_0}{\partial y} \left( \frac{\partial \varphi_i^e}{\partial x} \frac{\partial \varphi_j^e}{\partial y} + \frac{\partial \varphi_i^e}{\partial y} \frac{\partial \varphi_j^e}{\partial x} \right) \right\} dx dy \quad (6.4.5)
\end{aligned}$$

$$\begin{aligned}
F_i^1 &= \oint_{\Gamma^e} N_n \psi_i^e ds, \quad F_i^2 = \oint_{\Gamma^e} N_s \psi_i^e ds \\
F_i^3 &= \int_{\Omega^e} q \varphi_i^e dx dy + \oint_{\Gamma^e} \left( V_n \varphi_i^e - M_n \frac{\partial \varphi_i^e}{\partial n} \right) ds \\
F_i^{1T} &= \int_{\Omega^e} N_{xx}^T \frac{\partial \psi_i^e}{\partial x} dx dy, \quad F_i^{2T} = \int_{\Omega^e} N_{yy}^T \frac{\partial \psi_i^e}{\partial y} dx dy \\
F_i^{3T} &= - \int_{\Omega^e} \left( \frac{\partial^2 \varphi_i^e}{\partial x^2} M_{xx}^T + \frac{\partial^2 \varphi_i^e}{\partial y^2} M_{yy}^T \right) dx dy \quad (6.4.6)
\end{aligned}$$

where  $N_{xx}^T, M_{xx}^T$ , etc. are the thermal forces and moments defined in Eqs. (6.3.35a,b).

This completes the general finite element model development of the classical plate theory. The finite element model in Eq. (6.4.4) is called a *displacement finite element model* because it is based on equations of motion expressed in terms of the displacements, and the generalized displacements are the primary nodal degrees of freedom.

### 6.4.2 Tangent Stiffness Coefficients

The solution of nonlinear algebraic equations arising in the analysis of structural problems, one often uses the Newton-Raphson method or its improvements. To this end it useful to derive the tangent stiffness coefficients associated with the CPT.

The Newton-Raphson iterative method involves solving equations of the form

$$\begin{bmatrix} [T^{11}] & [T^{12}] & [T^{13}] \\ [T^{21}] & [T^{22}] & [T^{23}] \\ [T^{31}] & [T^{32}] & [T^{33}] \end{bmatrix} \begin{Bmatrix} \{\delta\Delta^1\} \\ \{\delta\Delta^2\} \\ \{\delta\Delta^3\} \end{Bmatrix} = - \begin{Bmatrix} \{R^1\} \\ \{R^2\} \\ \{R^3\} \end{Bmatrix} \quad (6.4.7)$$

where

$$\Delta_i^1 = u_i, \quad \Delta_i^2 = v_i, \quad \Delta_i^3 = \bar{\Delta}_i^3 \quad (6.4.8)$$

the coefficients of the submatrices  $[T^{\alpha\beta}]$  are defined by

$$T_{ij}^{\alpha\beta} = \frac{\partial R_i^\alpha}{\partial \Delta_j^\beta} \quad (6.4.9)$$

the components of the residual vector  $\{R^\alpha\}$  are

$$R_i^\alpha = \sum_{\gamma=1}^3 \sum_{k=1}^{n^*} K_{ik}^{\alpha\gamma} \Delta_k^\gamma - F_i^\alpha \quad (6.4.10)$$

and  $n^*$  denotes  $n$  or  $m$ , depending on the nodal degree of freedom. Thus, we have

$$T_{ij}^{\alpha\beta} = \frac{\partial}{\partial \Delta_j^\beta} \left( \sum_{\gamma=1}^3 \sum_{k=1}^{n^*} K_{ik}^{\alpha\gamma} \Delta_k^\gamma - F_i^\alpha \right) = \sum_{\gamma=1}^3 \sum_{k=1}^{n^*} \frac{\partial K_{ik}^{\alpha\gamma}}{\partial \Delta_j^\beta} \Delta_k^\gamma + K_{ij}^{\alpha\beta} \quad (6.4.11)$$

The only coefficients that depend on the displacements are  $K_{ij}^{13}, K_{ij}^{23}, K_{ij}^{31}, K_{ij}^{32}$ , and  $K_{ij}^{33}$ , and they are functions of only the transverse displacement  $\Delta_i^3 = \bar{\Delta}_i^3$ . Hence, derivatives of all submatrices with respect to  $\Delta_j^1 = u_j$  and

$\Delta_j^2 = v_j$  are zero. We have

$$\begin{aligned}
 T_{ij}^{11} &= \sum_{\gamma=1}^3 \sum_{k=1}^{n^*} \frac{\partial K_{ik}^{1\gamma}}{\partial u_j} \Delta_k^\gamma + K_{ij}^{11} = K_{ij}^{11}, & T_{ij}^{12} &= \sum_{\gamma=1}^3 \sum_{k=1}^{n^*} \frac{\partial K_{ik}^{1\gamma}}{\partial v_j} \Delta_k^\gamma + K_{ij}^{12} = K_{ij}^{12} \\
 T_{ij}^{21} &= \sum_{\gamma=1}^3 \sum_{k=1}^{n^*} \frac{\partial K_{ik}^{2\gamma}}{\partial u_j} \Delta_k^\gamma + K_{ij}^{21} = K_{ij}^{21}, & T_{ij}^{22} &= \sum_{\gamma=1}^3 \sum_{k=1}^{n^*} \frac{\partial K_{ik}^{2\gamma}}{\partial v_j} \Delta_k^\gamma + K_{ij}^{22} = K_{ij}^{22} \\
 T_{ij}^{31} &= \sum_{\gamma=1}^3 \sum_{k=1}^{n^*} \frac{\partial K_{ik}^{3\gamma}}{\partial u_j} \Delta_k^\gamma + K_{ij}^{31} = K_{ij}^{31}, & T_{ij}^{32} &= \sum_{\gamma=1}^3 \sum_{k=1}^{n^*} \frac{\partial K_{ik}^{3\gamma}}{\partial v_j} \Delta_k^\gamma + K_{ij}^{32} = K_{ij}^{32} \\
 T_{ij}^{13} &= \sum_{\gamma=1}^3 \sum_{k=1}^{n^*} \frac{\partial K_{ik}^{1\gamma}}{\partial \Delta_j^3} \Delta_k^\gamma + K_{ij}^{13} = \sum_{k=1}^n \frac{\partial K_{ik}^{13}}{\partial \Delta_j^3} \bar{\Delta}_k^3 + K_{ij}^{13} \\
 &= \frac{1}{2} \sum_{k=1}^n \bar{\Delta}_k^3 \frac{\partial}{\partial \Delta_j^3} \left\{ \int_{\Omega^e} \left[ \frac{\partial \psi_i^e}{\partial x} \left( A_{11} \frac{\partial w_0}{\partial x} \frac{\partial \varphi_k^e}{\partial x} + A_{12} \frac{\partial w_0}{\partial y} \frac{\partial \varphi_k^e}{\partial y} \right) \right. \right. \\
 &\quad \left. \left. + A_{66} \frac{\partial \psi_i^e}{\partial y} \left( \frac{\partial w_0}{\partial x} \frac{\partial \varphi_k^e}{\partial y} + \frac{\partial w_0}{\partial y} \frac{\partial \varphi_k^e}{\partial x} \right) \right] dx dy \right\} + K_{ij}^{13} \\
 &= \frac{1}{2} \sum_{k=1}^n \bar{\Delta}_k^3 \left\{ \int_{\Omega^e} \left[ \frac{\partial \psi_i^e}{\partial x} \left( A_{11} \frac{\partial \varphi_j^e}{\partial x} \frac{\partial \varphi_k^e}{\partial x} + A_{12} \frac{\partial \varphi_j^e}{\partial y} \frac{\partial \varphi_k^e}{\partial y} \right) \right. \right. \\
 &\quad \left. \left. + A_{66} \frac{\partial \psi_i^e}{\partial y} \left( \frac{\partial \varphi_j^e}{\partial x} \frac{\partial \varphi_k^e}{\partial y} + \frac{\partial \varphi_j^e}{\partial y} \frac{\partial \varphi_k^e}{\partial x} \right) \right] dx dy \right\} + K_{ij}^{13} \\
 &= \frac{1}{2} \int_{\Omega^e} \left[ \frac{\partial \psi_i^e}{\partial x} \left( A_{11} \frac{\partial w_0}{\partial x} \frac{\partial \varphi_j^e}{\partial x} + A_{12} \frac{\partial w_0}{\partial y} \frac{\partial \varphi_j^e}{\partial y} \right) \right. \\
 &\quad \left. + A_{66} \frac{\partial \psi_i^e}{\partial y} \left( \frac{\partial w_0}{\partial x} \frac{\partial \varphi_j^e}{\partial y} + \frac{\partial w_0}{\partial y} \frac{\partial \varphi_j^e}{\partial x} \right) \right] dx dy + K_{ij}^{13} \\
 &= K_{ij}^{13} + K_{ij}^{13} = 2K_{ij}^{13} (= T_{ji}^{31}) \\
 T_{ij}^{23} &= \sum_{\gamma=1}^3 \sum_{k=1}^{n^*} \frac{\partial K_{ik}^{2\gamma}}{\partial \Delta_j^3} \Delta_k^\gamma + K_{ij}^{23} = \sum_{k=1}^n \frac{\partial K_{ik}^{23}}{\partial \Delta_j^3} \bar{\Delta}_k^3 + K_{ij}^{23} \\
 &= \frac{1}{2} \sum_{k=1}^n \bar{\Delta}_k^3 \frac{\partial}{\partial \Delta_j^3} \left\{ \int_{\Omega^e} \left[ \frac{\partial \psi_i^e}{\partial y} \left( A_{12} \frac{\partial w_0}{\partial x} \frac{\partial \varphi_k^e}{\partial x} + A_{22} \frac{\partial w_0}{\partial y} \frac{\partial \varphi_k^e}{\partial y} \right) \right. \right. \\
 &\quad \left. \left. + A_{66} \frac{\partial \psi_i^e}{\partial x} \left( \frac{\partial w_0}{\partial x} \frac{\partial \varphi_k^e}{\partial y} + \frac{\partial w_0}{\partial y} \frac{\partial \varphi_k^e}{\partial x} \right) \right] dx dy \right\} + K_{ij}^{23} \\
 &= \frac{1}{2} \sum_{k=1}^n \bar{\Delta}_k^3 \left\{ \int_{\Omega^e} \left[ \frac{\partial \psi_i^e}{\partial y} \left( A_{12} \frac{\partial \varphi_j^e}{\partial x} \frac{\partial \varphi_k^e}{\partial x} + A_{22} \frac{\partial \varphi_j^e}{\partial y} \frac{\partial \varphi_k^e}{\partial y} \right) \right. \right. \\
 &\quad \left. \left. + A_{66} \frac{\partial \psi_i^e}{\partial x} \left( \frac{\partial \varphi_j^e}{\partial x} \frac{\partial \varphi_k^e}{\partial y} + \frac{\partial \varphi_j^e}{\partial y} \frac{\partial \varphi_k^e}{\partial x} \right) \right] dx dy \right\} + K_{ij}^{23}
 \end{aligned}$$

$$\begin{aligned}
 &= \frac{1}{2} \int_{\Omega^e} \left[ \frac{\partial \psi_i^e}{\partial y} \left( A_{12} \frac{\partial w_0}{\partial x} \frac{\partial \varphi_j^e}{\partial x} + A_{22} \frac{\partial w_0}{\partial y} \frac{\partial \varphi_j^e}{\partial y} \right) \right. \\
 &\quad \left. + A_{66} \frac{\partial \psi_i^e}{\partial x} \left( \frac{\partial w_0}{\partial y} \frac{\partial \varphi_j^e}{\partial x} + \frac{\partial w_0}{\partial x} \frac{\partial \varphi_j^e}{\partial y} \right) \right] dx dy + K_{ij}^{23} \\
 &= K_{ij}^{23} + K_{ij}^{23} = 2K_{ij}^{23} (= T_{ji}^{32})
 \end{aligned} \tag{6.4.12}$$

The computation of  $T_{ij}^{33}$  requires the calculation of three parts:

$$\begin{aligned}
 T_{ij}^{33} &= \sum_{\gamma=1}^3 \sum_{k=1}^{n^*} \frac{\partial K_{ik}^{3\gamma}}{\partial \Delta_j^3} \Delta_k^\gamma + K_{ij}^{33} \\
 &= \sum_{k=1}^{n^*} \left( \frac{\partial K_{ik}^{31}}{\partial \Delta_j^3} u_k + \frac{\partial K_{ik}^{32}}{\partial \Delta_j^3} v_k + \frac{\partial K_{ik}^{33}}{\partial \Delta_j^3} \Delta_k^3 \right) + K_{ij}^{33}
 \end{aligned} \tag{6.4.13}$$

We shall compute these terms first. We have

$$\begin{aligned}
 &\sum_{k=1}^{n^*} u_k \frac{\partial K_{ik}^{31}}{\partial \Delta_j^3} \\
 &= \sum_{k=1}^m u_k \frac{\partial}{\partial \Delta_j^3} \left\{ \int_{\Omega^e} \left[ \frac{\partial \varphi_i^e}{\partial x} \left( A_{11} \frac{\partial w_0}{\partial x} \frac{\partial \psi_k^e}{\partial x} + A_{66} \frac{\partial w_0}{\partial y} \frac{\partial \psi_k^e}{\partial y} \right) \right. \right. \\
 &\quad \left. \left. + \frac{\partial \varphi_i^e}{\partial y} \left( A_{66} \frac{\partial w_0}{\partial x} \frac{\partial \psi_k^e}{\partial y} + A_{12} \frac{\partial w_0}{\partial y} \frac{\partial \psi_k^e}{\partial x} \right) \right] dx dy \right\} \\
 &= \sum_{k=1}^m u_k \left\{ \int_{\Omega^e} \left[ \frac{\partial \varphi_i^e}{\partial x} \left( A_{11} \frac{\partial \varphi_j^e}{\partial x} \frac{\partial \psi_k^e}{\partial x} + A_{66} \frac{\partial \varphi_j^e}{\partial y} \frac{\partial \psi_k^e}{\partial y} \right) \right. \right. \\
 &\quad \left. \left. + \frac{\partial \varphi_i^e}{\partial y} \left( A_{66} \frac{\partial \varphi_j^e}{\partial x} \frac{\partial \psi_k^e}{\partial y} + A_{12} \frac{\partial \varphi_j^e}{\partial y} \frac{\partial \psi_k^e}{\partial x} \right) \right] dx dy \right\} \\
 &= \int_{\Omega^e} \left[ \frac{\partial \varphi_i^e}{\partial x} \left( A_{11} \frac{\partial u_0}{\partial x} \frac{\partial \varphi_j^e}{\partial x} + A_{66} \frac{\partial u_0}{\partial y} \frac{\partial \varphi_j^e}{\partial y} \right) \right. \\
 &\quad \left. + \frac{\partial \varphi_i^e}{\partial y} \left( A_{66} \frac{\partial u_0}{\partial y} \frac{\partial \varphi_j^e}{\partial x} + A_{12} \frac{\partial u_0}{\partial x} \frac{\partial \varphi_j^e}{\partial y} \right) \right] dx dy
 \end{aligned} \tag{6.4.14}$$

$$\begin{aligned}
 &\sum_{k=1}^{n^*} v_k \frac{\partial K_{ik}^{32}}{\partial \Delta_j^3} \\
 &= \sum_{k=1}^m v_k \frac{\partial}{\partial \Delta_j^3} \left\{ \int_{\Omega^e} \left[ \frac{\partial \varphi_i^e}{\partial x} \left( A_{12} \frac{\partial w_0}{\partial x} \frac{\partial \psi_k^e}{\partial y} + A_{66} \frac{\partial w_0}{\partial y} \frac{\partial \psi_k^e}{\partial x} \right) \right. \right. \\
 &\quad \left. \left. + \frac{\partial \varphi_i^e}{\partial y} \left( A_{66} \frac{\partial w_0}{\partial x} \frac{\partial \psi_k^e}{\partial x} + A_{22} \frac{\partial w_0}{\partial y} \frac{\partial \psi_k^e}{\partial y} \right) \right] dx dy \right\}
 \end{aligned}$$



$$\begin{aligned}
 &= \sum_{k=1}^m v_k \left\{ \int_{\Omega^e} \left[ \frac{\partial \varphi_i^e}{\partial x} \left( A_{12} \frac{\partial \varphi_j^e}{\partial x} \frac{\partial \psi_k^e}{\partial y} + A_{66} \frac{\partial \varphi_j^e}{\partial y} \frac{\partial \psi_k^e}{\partial x} \right) \right. \right. \\
 &\quad \left. \left. + \frac{\partial \varphi_i^e}{\partial y} \left( A_{66} \frac{\partial \varphi_j^e}{\partial x} \frac{\partial \psi_k^e}{\partial x} + A_{22} \frac{\partial \varphi_j^e}{\partial y} \frac{\partial \psi_k^e}{\partial y} \right) \right] dx dy \right\} \\
 &= \int_{\Omega^e} \left[ \frac{\partial \varphi_i^e}{\partial x} \left( A_{12} \frac{\partial v_0}{\partial y} \frac{\partial \varphi_j^e}{\partial x} + A_{66} \frac{\partial v_0}{\partial x} \frac{\partial \varphi_j^e}{\partial y} \right) \right. \\
 &\quad \left. + \frac{\partial \varphi_i^e}{\partial y} \left( A_{66} \frac{\partial v_0}{\partial x} \frac{\partial \varphi_j^e}{\partial x} + A_{22} \frac{\partial v_0}{\partial y} \frac{\partial \varphi_j^e}{\partial y} \right) \right] dx dy \tag{6.4.15}
 \end{aligned}$$

$$\begin{aligned}
 &\sum_{k=1}^{n^*} \bar{\Delta}_k^3 \frac{\partial K_{ik}^{33}}{\partial \bar{\Delta}_j^3} \\
 &= \frac{1}{2} \sum_{k=1}^n \bar{\Delta}_k^3 \frac{\partial}{\partial \bar{\Delta}_j^3} \left\{ \int_{\Omega^e} \left\{ \left[ A_{11} \left( \frac{\partial w_0}{\partial x} \right)^2 + A_{66} \left( \frac{\partial w_0}{\partial y} \right)^2 \right] \frac{\partial \varphi_i^e}{\partial x} \frac{\partial \varphi_k^e}{\partial x} \right. \right. \\
 &\quad \left. \left. + \left[ A_{66} \left( \frac{\partial w_0}{\partial x} \right)^2 + A_{22} \left( \frac{\partial w_0}{\partial y} \right)^2 \right] \frac{\partial \varphi_i^e}{\partial y} \frac{\partial \varphi_k^e}{\partial y} \right. \right. \\
 &\quad \left. \left. + (A_{12} + A_{66}) \frac{\partial w_0}{\partial x} \frac{\partial w_0}{\partial y} \left( \frac{\partial \varphi_i^e}{\partial x} \frac{\partial \varphi_k^e}{\partial y} + \frac{\partial \varphi_i^e}{\partial y} \frac{\partial \varphi_k^e}{\partial x} \right) \right\} dx dy \right\} \\
 &= \frac{1}{2} \sum_{k=1}^n \bar{\Delta}_k^3 \left\{ \int_{\Omega^e} \left[ \left( 2A_{11} \frac{\partial w_0}{\partial x} \frac{\partial \varphi_j^e}{\partial x} + 2A_{66} \frac{\partial w_0}{\partial y} \frac{\partial \varphi_j^e}{\partial y} \right) \frac{\partial \varphi_i^e}{\partial x} \frac{\partial \varphi_k^e}{\partial x} \right. \right. \\
 &\quad \left. \left. + \left( 2A_{66} \frac{\partial w_0}{\partial x} \frac{\partial \varphi_j^e}{\partial x} + 2A_{22} \frac{\partial w_0}{\partial y} \frac{\partial \varphi_j^e}{\partial y} \right) \frac{\partial \varphi_i^e}{\partial y} \frac{\partial \varphi_k^e}{\partial y} + (A_{12} + A_{66}) \right. \right. \\
 &\quad \left. \left. \times \left( \frac{\partial w_0}{\partial x} \frac{\partial \varphi_j^e}{\partial y} + \frac{\partial w_0}{\partial y} \frac{\partial \varphi_j^e}{\partial x} \right) \left( \frac{\partial \varphi_i^e}{\partial x} \frac{\partial \varphi_k^e}{\partial y} + \frac{\partial \varphi_i^e}{\partial y} \frac{\partial \varphi_k^e}{\partial x} \right) \right] dx dy \right\} \\
 &= \int_{\Omega^e} \left[ A_{11} \left( \frac{\partial w_0}{\partial x} \right)^2 \frac{\partial \varphi_i^e}{\partial x} \frac{\partial \varphi_j^e}{\partial x} + A_{66} \frac{\partial w_0}{\partial x} \frac{\partial w_0}{\partial y} \frac{\partial \varphi_i^e}{\partial x} \frac{\partial \varphi_j^e}{\partial y} \right. \\
 &\quad \left. + A_{66} \frac{\partial w_0}{\partial x} \frac{\partial w_0}{\partial y} \frac{\partial \varphi_i^e}{\partial y} \frac{\partial \varphi_j^e}{\partial x} + A_{22} \left( \frac{\partial w_0}{\partial y} \right)^2 \frac{\partial \varphi_i^e}{\partial y} \frac{\partial \varphi_j^e}{\partial y} \right. \\
 &\quad \left. + \left( \frac{A_{12} + A_{66}}{2} \right) \left( \frac{\partial w_0}{\partial x} \frac{\partial \varphi_j^e}{\partial y} + \frac{\partial w_0}{\partial y} \frac{\partial \varphi_j^e}{\partial x} \right) \left( \frac{\partial \varphi_i^e}{\partial x} \frac{\partial w_0}{\partial y} + \frac{\partial \varphi_i^e}{\partial y} \frac{\partial w_0}{\partial x} \right) \right] dx dy \\
 &= \int_{\Omega^e} \left[ A_{11} \left( \frac{\partial w_0}{\partial x} \right)^2 \frac{\partial \varphi_i^e}{\partial x} \frac{\partial \varphi_j^e}{\partial x} + A_{22} \left( \frac{\partial w_0}{\partial y} \right)^2 \frac{\partial \varphi_i^e}{\partial y} \frac{\partial \varphi_j^e}{\partial y} \right. \\
 &\quad \left. + A_{66} \frac{\partial w_0}{\partial x} \frac{\partial w_0}{\partial y} \left( \frac{\partial \varphi_i^e}{\partial x} \frac{\partial \varphi_j^e}{\partial y} + \frac{\partial \varphi_i^e}{\partial y} \frac{\partial \varphi_j^e}{\partial x} \right) + \left( \frac{A_{12} + A_{66}}{2} \right) \right]
 \end{aligned}$$

$$\times \left( \frac{\partial \varphi_i^e}{\partial x} \frac{\partial w_0}{\partial y} + \frac{\partial \varphi_i^e}{\partial y} \frac{\partial w_0}{\partial x} \right) \left( \frac{\partial w_0}{\partial x} \frac{\partial \varphi_j^e}{\partial y} + \frac{\partial w_0}{\partial y} \frac{\partial \varphi_j^e}{\partial x} \right) dx dy \quad (6.4.16)$$

Therefore,  $T_{ij}^{33}$  is given by combining the expressions in Eqs. (6.4.14)–(6.4.16) and  $K_{ij}^{33}$ . We obtain

$$\begin{aligned} T_{ij}^{33} = & \int_{\Omega^e} \left[ D_{11} \frac{\partial^2 \varphi_i^e}{\partial x^2} \frac{\partial^2 \varphi_j^e}{\partial x^2} + D_{22} \frac{\partial^2 \varphi_i^e}{\partial y^2} \frac{\partial^2 \varphi_j^e}{\partial y^2} \right. \\ & + D_{12} \left( \frac{\partial^2 \varphi_i^e}{\partial x^2} \frac{\partial^2 \varphi_j^e}{\partial y^2} + \frac{\partial^2 \varphi_i^e}{\partial y^2} \frac{\partial^2 \varphi_j^e}{\partial x^2} \right) \\ & \left. + 4D_{66} \frac{\partial^2 \varphi_i^e}{\partial x \partial y} \frac{\partial^2 \varphi_j^e}{\partial x \partial y} + k \varphi_i^e \varphi_j^e \right] dx dy \\ & + \int_{\Omega^e} \left\{ (N_{xx} + N_{xx}^T) \frac{\partial \varphi_i^e}{\partial x} \frac{\partial \varphi_j^e}{\partial x} + (N_{yy} + N_{yy}^T) \frac{\partial \varphi_i^e}{\partial y} \frac{\partial \varphi_j^e}{\partial y} \right. \\ & + N_{xy} \left( \frac{\partial \varphi_i^e}{\partial x} \frac{\partial \varphi_j^e}{\partial y} + \frac{\partial \varphi_i^e}{\partial y} \frac{\partial \varphi_j^e}{\partial x} \right) \\ & + (A_{12} + A_{66}) \frac{\partial w_0}{\partial x} \frac{\partial w_0}{\partial y} \left( \frac{\partial \varphi_i^e}{\partial x} \frac{\partial \varphi_j^e}{\partial y} + \frac{\partial \varphi_i^e}{\partial y} \frac{\partial \varphi_j^e}{\partial x} \right) \\ & + \left[ A_{11} \left( \frac{\partial w_0}{\partial x} \right)^2 + A_{66} \left( \frac{\partial w_0}{\partial y} \right)^2 \right] \frac{\partial \varphi_i^e}{\partial x} \frac{\partial \varphi_j^e}{\partial x} \\ & \left. + \left[ A_{66} \left( \frac{\partial w_0}{\partial x} \right)^2 + A_{22} \left( \frac{\partial w_0}{\partial y} \right)^2 \right] \frac{\partial \varphi_i^e}{\partial y} \frac{\partial \varphi_j^e}{\partial y} \right\} dx dy \quad (6.4.17) \end{aligned}$$

Clearly, the tangent stiffness matrix of an element is symmetric (while the original element stiffness is *not* symmetric).

### 6.4.3 Some Plate Finite Elements

There exists a large body of literature on triangular and rectangular plate bending finite elements of isotropic or orthotropic plates based on the CPT (e.g. see [13–20]). There are two kinds of plate bending elements of the CPT. A *conforming element* is one in which the inter-element continuity of  $w_0$ ,  $\theta_x \equiv \partial w_0 / \partial x$ , and  $\theta_y \equiv \partial w_0 / \partial y$  (or  $\partial w_0 / \partial n$ ) are satisfied, and a *non-conforming element* is one in which the continuity of the normal slope,  $\partial w_0 / \partial n$ , is not satisfied.

An effective non-conforming triangular element (the BCIZ triangle) was developed by Bazeley et al. [14], and it consists of three degrees of freedom ( $w_0, \theta_x, \theta_y$ ) at the three vertex nodes (see Figure 6.4.1). The element performs very well in bending as well as vibration problems (with a consistent mass matrix).

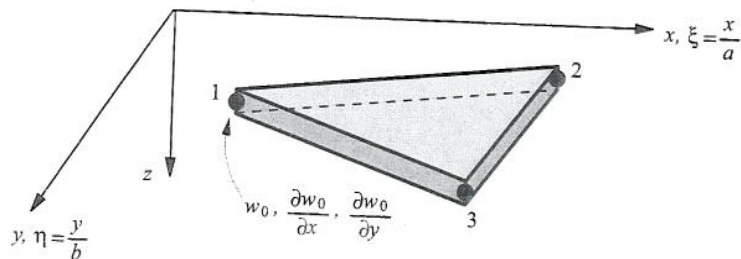


Figure 6.4.1 A non-conforming triangular element with three degrees freedom ( $w_0, \partial w_0/\partial x, \partial w_0/\partial y$ ) per node.

A conforming triangular element due to Clough and Tocher [15] is an assemblage of three triangles as shown in Figure 6.4.2. The normal slope continuity is enforced at the mid-side nodes between the sub-triangles. In each sub-triangle, the transverse deflection is represented by the polynomial

$$w_0^i(x, y) = a_i + b_i \xi + c_i \eta + d_i \xi \eta + e_i \xi^2 + f_i \eta^2 + g_i \xi^3 + h_i \xi^2 \eta + k_i \xi \eta^2 + l_i \eta \tag{6.4.18}$$

where  $(\xi, \eta)$  are the local coordinates, as shown in Figure 6.4.2. The thirty coefficients are reduced to nine, three ( $w_0, \partial w_0/\partial x, \partial w_0/\partial y$ ) at each vertex of the triangle, by equating the variables from the vertices of each sub-triangle at the common points and normal slope between the mid-side points of sub-triangles.

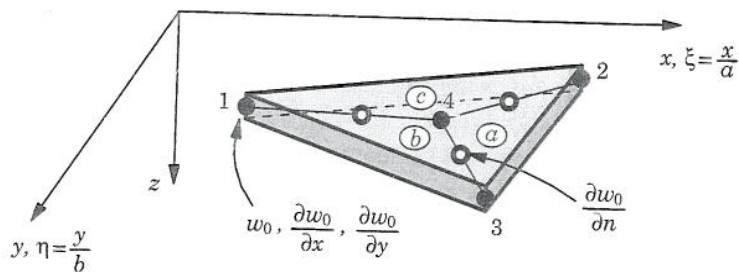


Figure 6.4.2 A conforming triangular element.

A non-conforming rectangular element has  $w_0$ ,  $\theta_x$ , and  $\theta_y$  as the nodal variables (see Figure 6.4.3). The element was developed by Melosh [16] and Zienkiewicz and Cheung [17]. The normal slope variation is cubic along an edge, whereas there are only two values of  $\partial w_0/\partial n$  available on the edge. Therefore, the cubic polynomial for the normal derivative of  $w_0$  is not the same on the edge common to two elements. The interpolation functions for this element can be expressed compactly as

$$\begin{aligned} \varphi_i^e &= g_{i1} \quad (i = 1, 4, 7, 10); & \varphi_i^e &= g_{i2} \quad (i = 2, 5, 8, 11) \\ \varphi_i^e &= g_{i3} \quad (i = 3, 6, 9, 12) \\ g_{i1} &= \frac{1}{8}(1 + \xi_0)(1 + \eta_0)(2 + \xi_0 + \eta_0 - \xi^2 - \eta^2) & (6.4.19) \\ g_{i2} &= \frac{1}{8}\xi_i(\xi_0 - 1)(1 + \eta_0)(1 + \xi_0)^2, & g_{i3} &= \frac{1}{8}\eta_i(\eta_0 - 1)(1 + \xi_0)(1 + \eta_0)^2 \\ \xi &= (x - x_c)/a, \quad \eta = (y - y_c)/b, \quad \xi_0 = \xi\xi_i, \quad \eta_0 = \eta\eta_i \end{aligned}$$

where  $2a$  and  $2b$  are the sides of the rectangle,  $(x_c, y_c)$  are the global coordinates of the center of the rectangle, and  $(\xi_i, \eta_i)$  are the coordinates of the nodes in  $(\xi, \eta)$  coordinate system [e.g.  $(\xi_1, \eta_1) = (-1, -1)$ ,  $(\xi_2, \eta_2) = (1, -1)$ , etc.].

A conforming rectangular element with  $w_0$ ,  $\partial w_0/\partial x$ ,  $\partial w_0/\partial y$ , and  $\partial^2 w_0/\partial x \partial y$  as the nodal variables (see Figure 6.4.4) was developed by Bogner et al. [18]. The interpolation functions for this element are

$$\begin{aligned} \varphi_i^e &= g_{i1} \quad (i = 1, 5, 9, 13); & \varphi_i^e &= g_{i2} \quad (i = 2, 6, 10, 14) \\ \varphi_i^e &= g_{i3} \quad (i = 3, 7, 11, 15); & \varphi_i^e &= g_{i4} \quad (i = 4, 8, 12, 16) \\ g_{i1} &= \frac{1}{16}(\xi + \xi_i)^2(\xi_0 - 2)(\eta + \eta_i)^2(\eta_0 - 2) \end{aligned}$$

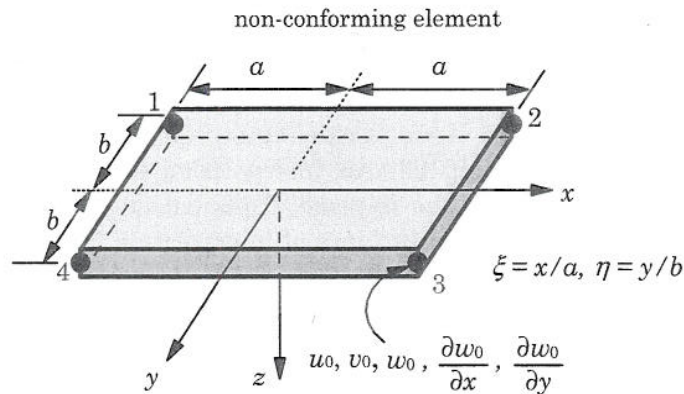


Figure 6.4.3 A non-conforming rectangular element.

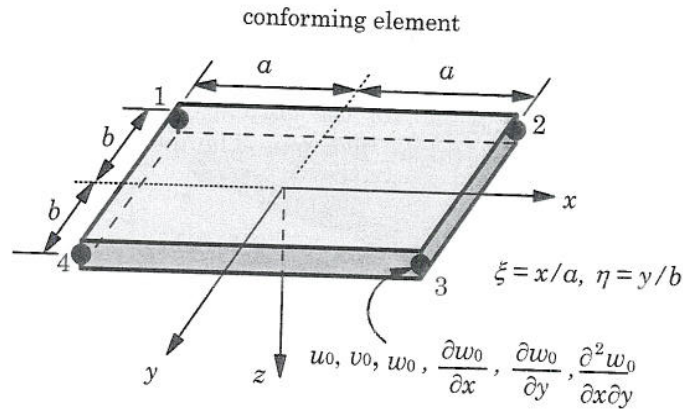


Figure 6.4.4 A conforming rectangular element.

$$\begin{aligned}
 g_{i2} &= \frac{1}{16} \xi_i (\xi + \xi_i)^2 (1 - \xi_0) (\eta + \eta_i)^2 (\eta_0 - 2) \\
 g_{i3} &= \frac{1}{16} \eta_i (\xi + \xi_i)^2 (\xi_0 - 2) (\eta + \eta_i)^2 (1 - \eta_0) \\
 g_{i4} &= \frac{1}{16} \xi_i \eta_i (\xi + \xi_i)^2 (1 - \xi_0) (\eta + \eta_i)^2 (1 - \eta_0)
 \end{aligned} \quad (6.4.20)$$

The conforming element has four degrees of freedom per node, whereas the non-conforming element has three degrees of freedom per node. For the conforming rectangular element the total number of in-plane and bending nodal degrees of freedom per element is  $8 + 16 = 24$ , and for the non-conforming element, the total number is  $8 + 12 = 20$ .

## 6.5 Computer Implementation Aspects and Numerical Results of CPT Elements

### 6.5.1 Computer Implementation

The conforming and non-conforming rectangular finite elements developed in this chapter are implemented into a computer program using bilinear interpolation of  $(u_0, v_0)$  and Hermite cubic interpolation of  $w_0$ . The element geometry is represented using bilinear interpolation functions. In view of the different interpolation of the in-plane displacements and the transverse deflection, one must compute both types of interpolation functions and their first and second derivatives (see Problem 6.24) in each call of the shape functions subroutine. In addition, one must rearrange the stiffness coefficients such that the finite element nodal displacement vector is of the form (to minimize the bandwidth of the stiffness matrix)

$$\{\Delta\} = \{u_{01}, v_{01}, w_{01}, \theta_{x1}, \theta_{y1}, \theta_{xy1}, u_{02}, v_{02}, w_{02}, \theta_{x2}, \theta_{y2}, \theta_{xy2}, \dots\}$$

where  $(u_{0i}, v_{0i}, w_{0i}, \theta_{xi}, \theta_{yi}, \theta_{xyi})$  are the displacements at node  $i$ . The same logic as in the case of Euler-Bernoulli beams may be used to rearrange the stiffness coefficients of the CPT elements (see Box 4.2.1) as discussed next.

First, one must compute all element forces  $F_i^\alpha$ , element stiffnesses  $K_{ij}^{\alpha\beta}$ , and extra stiffness terms to form the total tangent matrix. Two separate do-loops on Gauss quadrature are required to compute all the force and stiffness coefficients. The full integration loop is used to evaluate all force components and all linear stiffnesses. The reduced integration loop is used to compute the nonlinear stiffness terms. One may use separate arrays (say,  $EXT13(I, J)$ ,  $EXT33(I, J)$ , and so on) to store the extra terms (to those of  $K_{ij}^{\alpha\beta}$ ) of the tangent stiffness coefficients. Next, the stiffness coefficients  $K_{ij}^{31}$  and  $K_{ij}^{32}$ , for example, are rearranged as follows:

```

II = 1
DO 300 I = 1, NPE
  DO 200 K = 1, NWD
    K0 = (I - 1) * NWD + K
    KK = II + K + 1
    JJ = 1
    DO 100 J = 1, NPE
      ELK(KK, JJ) = ELK31(I, J)
      ELK(KK, JJ + 1) = ELK32(I, J)
100    JJ = J * NDF + 1
200    CONTINUE
300    II = I * NDF + 1

```

where  $NWD$  is equal to 3 for non-conforming element and 4 for the conforming element; it denotes the number of degrees of freedom per node associated with the transverse deflection. Similar logic may be used to rearrange the coefficients  $K_{ij}^{13}$ ,  $K_{ij}^{23}$ , and  $K_{ij}^{33}$ . The logic to rearrange  $K_{ij}^{11}$ ,  $K_{ij}^{12}$ ,  $K_{ij}^{21}$ , and  $K_{ij}^{22}$  is the same as shown in Box 4.3.1.

Note that the addition of the extra terms to the direct stiffness matrix  $[K]$  in order to obtain the tangent stiffness matrix,  $[K]^{tan}$ , must be carried out only after the imbalance (or residual) vector is computed:

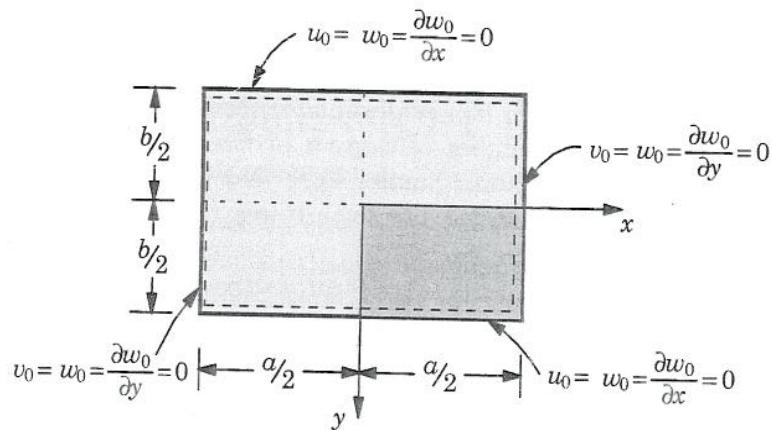
$$\begin{aligned}
 -\{R\} &= [K]\{\Delta\} - \{F\} \rightarrow ELF(I) = ELF(I) - ELK(I, J) * ELU(J) \\
 [K]^{tan} &= [K] + [EXT] \rightarrow ELK(I, J) = ELK(I, J) + EXT(I, J)
 \end{aligned}$$

where  $[EXT]$  in the present discussion is used only for the extra terms that are added to  $[K]$  to obtain the tangent stiffness matrix. The above two operations must be carried out sequentially in separate do-loops.

Solution symmetries available in a problem should be taken advantage of to identify the computational domain because they reduce computational effort. For example, a  $2 \times 2$  mesh in a quadrant of the plate is the same as a  $4 \times 4$  mesh in the total plate, and the results obtained with the two meshes would be identical, within the round-off errors of the computation, if the solution exhibits biaxial symmetry. A solution is symmetric about a line only if (a) the geometry, including boundary conditions, (b) the material properties, and (c) the loading are symmetric about the line. The boundary conditions along a line of symmetry should be correctly identified and imposed in the finite element model. The boundary conditions along the edges and the symmetry lines of a simply supported rectangular plate are shown in Figure 6.5.1. In the case of the conforming element, we may also set  $\theta_{xy} \equiv \partial^2 w_0 / \partial x \partial y = 0$  at the center of the plate. When one is not sure of the solution symmetry, it is advised that the whole plate be modeled.

### 6.5.2 Results of Linear Analysis

We consider the bending of rectangular plates with various edge conditions to evaluate the elements developed herein. The foundation modulus  $k$  is set to zero in all examples. The linear stiffness coefficients are evaluated using a  $4 \times 4$  Gauss rule, while the stresses were computed at the center of the elements (i.e. one-point quadrature is used). The effect of the integration rule on the accuracy of solutions will be examined in the sequel.



$$\text{Symm. B.C.: } u_0 = \frac{\partial w_0}{\partial x} = 0 \text{ at } x=0; \quad v_0 = \frac{\partial w_0}{\partial y} = 0 \text{ at } y=0$$

Figure 6.5.1 Boundary conditions for rectangular plates with biaxial symmetry.

**Example 6.5.1**

Consider a simply supported (SS-1) rectangular plate under uniformly distributed load. The geometric boundary conditions of the computational domain (see the shaded quadrant in Figure 6.5.1) are

$$u_0 = \frac{\partial w_0}{\partial x} = 0 \text{ at } x = 0; \quad v_0 = \frac{\partial w_0}{\partial y} = 0 \text{ at } y = 0 \tag{6.5.1}$$

$$v_0 = w_0 = \frac{\partial w_0}{\partial y} = 0 \text{ at } x = \frac{a}{2}; \quad u_0 = w_0 = \frac{\partial w_0}{\partial x} = 0 \text{ at } y = \frac{b}{2}$$

$$\frac{\partial^2 w_0}{\partial x \partial y} = 0 \text{ at } x = y = 0 \text{ (for conforming element only)} \tag{6.5.2}$$

Table 6.5.1 shows a comparison of non-dimensionalized finite element solutions with the analytical solutions (see Reddy [3]) of isotropic and orthotropic square plates under uniformly distributed transverse load  $q_0$ . The stresses were evaluated at the center of the element. Hence, the locations of the maximum normal stresses are  $(a/8, b/8)$ ,  $(a/16, b/16)$ , and  $(a/32, b/32)$  for uniform meshes  $2 \times 2$ ,  $4 \times 4$ , and  $8 \times 8$ , respectively, while those of  $\sigma_{xy}$  are  $(3a/8, 3b/8)$ ,  $(7a/16, 7b/16)$ , and  $(15a/32, 15b/32)$  for the three meshes. The analytical solutions were evaluated using  $m, n = 1, 3, \dots, 19$ . The exact maximum deflection occurs at  $x = y = 0$ , maximum stresses  $\sigma_{xx}$  and  $\sigma_{yy}$  occur at  $(0, 0, h/2)$ , and the maximum shear stress  $\sigma_{xy}$  occurs at  $(a/2, b/2, -h/2)$ .

**Table 6.5.1** Maximum transverse deflections and stresses\* of simply supported square plates under a uniformly distributed load  $q_0$  (linear analysis).

Variable	Non-conforming			Conforming			Analytical solution
	$2 \times 2$	$4 \times 4$	$8 \times 8$	$2 \times 2$	$4 \times 4$	$8 \times 8$	
<i>Isotropic plate</i> ( $\nu = 0.25$ )							
$\bar{w} \times 10^2$	4.8571	4.6425	4.5883	4.7619	4.5952	4.5739	4.5698
$\bar{\sigma}_{xx}$	0.2405	0.2673	0.2740	0.2239	0.2637	0.2731	0.2762
$\bar{\sigma}_{xy}$	0.1713	0.1964	0.2050	0.1688	0.1935	0.2040	0.2085
<i>Orthotropic plate</i> ( $E_1/E_2 = 25, G_{12} = G_{13} = 0.5E_2, \nu_{12} = 0.25$ )							
$\bar{w} \times 10^2$	0.7082	0.6635	0.6531	0.7710	0.6651	0.6522	0.6497
$\bar{\sigma}_{xx}$	0.7148	0.7709	0.7828	0.5560	0.7388	0.7743	0.7866
$\bar{\sigma}_{yy}$	0.0296	0.0253	0.0246	0.0278	0.0249	0.0245	0.0244
$\bar{\sigma}_{xy}$	0.0337	0.0421	0.0444	0.0375	0.0416	0.0448	0.0463

\* $\bar{w} = w_0 E_2 h^3 / (q_0 a^4)$ ,  $\bar{\sigma} = \sigma h^2 / (q_0 a^2)$ .

**Example 6.5.2**

Here we consider a clamped square plate under uniformly distributed load. The boundary conditions are taken to be

$$u_0 = \frac{\partial w_0}{\partial x} = 0 \text{ at } x = 0; \quad v_0 = \frac{\partial w_0}{\partial y} = 0 \text{ at } y = 0 \tag{6.5.3a}$$



$$u_0 = v_0 = w_0 = \frac{\partial w_0}{\partial x} = \frac{\partial w_0}{\partial y} = 0 \text{ at } x = \frac{a}{2}; \quad u_0 = v_0 = w_0 = \frac{\partial w_0}{\partial x} = \frac{\partial w_0}{\partial y} = 0 \text{ at } y = \frac{b}{2};$$

$$\frac{\partial^2 w_0}{\partial x \partial y} = 0 \text{ on clamped edges (for conforming element only)} \tag{6.5.3}$$

Table 6.5.2 contains the non-dimensionalized deflections and stresses. The locations of the normal stresses reported for the three meshes are:

$$2 \times 2: \left(\frac{a}{8}, \frac{b}{8}\right); \quad 4 \times 4: \left(\frac{a}{16}, \frac{b}{16}\right); \quad 8 \times 8: \left(\frac{a}{32}, \frac{b}{32}\right)$$

and shear stresses reported for the three meshes are

$$2 \times 2: \left(\frac{3a}{8}, \frac{3b}{8}\right); \quad 4 \times 4: \left(\frac{7a}{16}, \frac{7b}{16}\right); \quad 8 \times 8: \left(\frac{15a}{32}, \frac{15b}{32}\right)$$

These stresses are not necessarily the maximum ones in the plate. For example for an  $8 \times 8$  mesh, the maximum normal stress in the isotropic plate is found to be 0.2300 at  $(0.46875a, 0.03125b, -h/2)$  and the maximum shear stress is 0.0226 at  $(0.28125a, 0.09375b, -h/2)$  for the non-conforming element. The conforming element yields slightly better solutions than the non-conforming element for deflections but not for the stresses, and both elements show good convergence.

**Table 6.5.2** Maximum transverse deflections and stresses\* of clamped (CCCC), isotropic and orthotropic, square plates ( $a = b$ ) under a uniformly distributed load  $q_0$  (linear analysis).

Variable	Non-conforming			Conforming		
	2 × 2	4 × 4	8 × 8	2 × 2	4 × 4	8 × 8
<i>Isotropic plate</i> ( $\nu = 0.25$ )						
$\bar{w} \times 10^2$	1.5731	1.4653	1.4342	1.4778	1.4370	1.4249
$\bar{\sigma}_{xx}$	0.0987	0.1238	0.1301	0.0861	0.1197	0.1288
$\bar{\sigma}_{xy}$	0.0497	0.0222	0.0067	0.0489	0.0224	0.0068
<i>Orthotropic plate</i> ( $E_1/E_2 = 25, G_{12} = G_{13} = 0.5E_2, \nu_{12} = 0.25$ )						
$\bar{w} \times 10^2$	0.1434	0.1332	0.1314	0.1402	0.1330	0.1311
$\bar{\sigma}_{xx}$	0.1962	0.2491	0.2598	0.1559	0.2358	0.2576
$\bar{\sigma}_{yy}$	0.0085	0.0046	0.0042	0.0066	0.0047	0.0043
$\bar{\sigma}_{xy}$	0.0076	0.0046	0.0019	0.0083	0.0048	0.0020

\* $\bar{w} = w_0 E_2 h^3 / (q_0 a^4), \quad \bar{\sigma} = \sigma h^2 / (q_0 a^2).$

### 6.5.3 Results of Nonlinear Analysis

Here we investigate geometrically nonlinear response of plates using the conforming and non-conforming plate finite elements. The nonlinear terms are evaluated using reduced integration. Full integration (F) means  $4 \times 4$  Gauss rule and reduced integration (R) means  $1 \times 1$  Gauss rule.

**Example 6.5.3**

First, we consider the nonlinear bending of an isotropic ( $\nu = 0.3$ ) square plate under uniformly distributed transverse load,  $q_0$  (see Lévy [32], Wang [33], and Kawai and Yoshimura [34]). The following simply supported (SS-3) geometric boundary conditions are used:

$$u_0 = v_0 = w_0 = 0 \quad \text{on all four edges} \quad (6.5.5)$$

Since  $\theta_x = (\partial w_0 / \partial x)$  and  $\theta_y = (\partial w_0 / \partial y)$  are not specified in SS 3, it follows that the following boundary conditions are

$$\text{on } y = 0, b: M_{xy} = M_{yy} = 0; \quad \text{on } x = 0, a: M_{xx} = M_{xy} = 0 \quad (6.5.6)$$

satisfied in the integral sense [see Eq. (6.4.7)].

Using the biaxial symmetry, only a quadrant is modeled with a uniform  $4 \times 4$  or  $8 \times 8$  mesh of rectangular elements. The boundary conditions along the lines of symmetry are shown in Figure 6.5.1. The following geometric and material parameters are used, although the non-dimensional transverse deflection and stresses presented here are independent of them (but may depend on  $\nu$ ):

$$a = b = 10 \text{ in.}, \quad h = 0.1 \text{ in.}, \quad E = 30 \times 10^6 \text{ psi}, \quad \nu = 0.3 \quad (6.5.7)$$

The notation F-F means full integration ( $4 \times 4$  Gauss rule) is used for the numerical evaluation of all coefficients, while F-R means full integration is used for all but nonlinear terms and reduced integration ( $1 \times 1$  Gauss rule) is used for the nonlinear terms. The number in front of F-F or F-R stands for the mesh (4 refers to  $4 \times 4$  mesh and so on). Stresses are evaluated at the center of the element (i.e.  $1 \times 1$  Gauss point). A load increment of  $\Delta q_0 = 7.5$ , which is equal to the increment of load parameter,  $\Delta \bar{P} \equiv \Delta q_0 a^4 / Eh^4 = 25$ , is used along with the convergence tolerance of  $\epsilon = 10^{-2}$ . Except for the first load step, which took 5 iterations, the convergence was achieved for 2 or 3 iterations.

The center deflection,  $\bar{w} = w_0/h$ , and total stresses (i.e. membrane and flexural contributions included),  $\bar{\sigma}_{xx} = \sigma_{xx}(A, A, h/2)(a^2/Eh^2)$  and  $\bar{\sigma}_{xy} = \sigma_{xy}(B, B, -h/2)(a^2/Eh^2)$  as functions of the load parameter,  $\bar{P} = q_0 a^4 / Eh^4$  are presented in Table 6.5.3. The location  $(A, A, h/2)$  refers to the Gauss point nearest to the center ( $x = y = 0$ ) but at the top of the plate, while  $(B, B, -h/2)$  refers to the Gauss point nearest to the corner  $x = y = a/2$ , at the bottom of the plate (see Figure 6.5.1). There is very little difference between the results obtained with reduced and full integration of the nonlinear stiffness coefficients.

Plots of the load parameter  $\bar{P}$  versus the deflection  $\bar{w}$  and  $\bar{P}$  versus various stresses are presented in Figure 6.5.2. Although the linear and nonlinear values of  $\bar{\sigma}_{xx}$  for the load parameter  $\bar{P} = 25$  are maximum at the center of the plate, the location of the maximum normal stress  $\bar{\sigma}_{xx}$  in the nonlinear analysis changes as the load value is increased. For example, the maximum value of  $\bar{\sigma}_{xx}$  at  $\bar{P} = 250$  in the finite element analysis occurs at  $(x, y) = (2.8125, 0.3125)$ , and its value is found to be 21.177. It is clear that the membrane stresses are a significant part of the total stresses.

**Example 6.5.4**

This example is concerned with the bending of a simply supported (SS-1) orthotropic square plate under a uniformly distributed transverse load  $q_0$ . The geometry and material properties used are given below.

$$\begin{aligned} a = b = 12 \text{ in.}, \quad h = 0.138 \text{ in.}, \quad E_1 = 3 \times 10^6 \text{ psi}, \quad E_2 = 1.28 \times 10^6 \text{ psi} \\ G_{12} = G_{23} = G_{13} = 0.37 \times 10^6 \text{ psi.}, \quad \nu_{12} = \nu_{23} = \nu_{13} = 0.32 \end{aligned} \quad (6.5.8)$$

A load increment of  $\Delta q_0 = 0.2$  psi and a uniform mesh of  $4 \times 4$  in a quarter plate was used. Figure 6.5.3 shows plots of the center deflection versus the intensity of the distributed load. The finite element results are in close agreement with the experimental results of Zaghlool and Kennedy [35].

**Table 6.5.3** Maximum transverse deflections and stresses\* of simply supported (SS-3), isotropic ( $\nu = 0.3$ ) square plates ( $a = b$ ) under a uniformly distributed load  $q_0$  (nonlinear analysis).

Load parameter	Linear $\bar{w} \rightarrow$	Non-conforming			Conforming		
		4F-F	4F-R	8F-R	4F-F	4F-R	8F-R
		1.127	1.127	1.113	1.116	1.116	1.110
25	$\bar{w}$	0.670	0.673	0.670	0.669	0.670	0.669
	$\bar{\sigma}_{xx}$	5.279	5.321	5.423	5.252	5.324	5.426
	$\bar{\sigma}_{xy}$	3.014	3.028	3.179	2.994	3.019	3.172
50	$\bar{w}$	0.944	0.951	0.946	0.943	0.949	0.945
	$\bar{\sigma}_{xx}$	8.035	8.142	8.227	8.018	8.219	8.247
	$\bar{\sigma}_{xy}$	4.510	4.552	4.818	4.484	4.566	4.810
75	$\bar{w}$	1.124	1.136	1.128	1.123	1.135	1.127
	$\bar{\sigma}_{xx}$	10.057	10.231	10.271	10.048	10.390	10.309
	$\bar{\sigma}_{xy}$	5.600	5.674	6.036	5.569	5.719	6.029
100	$\bar{w}$	1.262	1.280	1.268	1.262	1.279	1.267
	$\bar{\sigma}_{xx}$	11.731	11.974	11.961	11.729	12.217	12.017
	$\bar{\sigma}_{xy}$	6.493	6.599	7.049	6.457	6.679	7.042
125	$\bar{w}$	1.377	1.400	1.383	1.377	1.400	1.383
	$\bar{\sigma}_{xx}$	13.197	13.509	13.440	13.201	13.838	13.513
	$\bar{\sigma}_{xy}$	7.265	7.403	7.933	7.224	7.521	7.927
150	$\bar{w}$	1.475	1.504	1.483	1.476	1.505	1.483
	$\bar{\sigma}_{xx}$	14.519	14.902	14.777	14.529	15.317	14.867
	$\bar{\sigma}_{xy}$	7.951	8.122	8.726	7.905	8.280	8.722
175	$\bar{w}$	1.563	1.597	1.571	1.563	1.598	1.571
	$\bar{\sigma}_{xx}$	15.737	16.191	16.009	15.752	16.693	16.117
	$\bar{\sigma}_{xy}$	8.573	8.778	9.451	8.524	8.979	9.449
200	$\bar{w}$	1.641	1.681	1.651	1.642	1.683	1.651
	$\bar{\sigma}_{xx}$	16.874	17.401	17.162	16.894	17.989	17.287
	$\bar{\sigma}_{xy}$	9.147	9.385	10.123	9.094	9.631	10.123
225	$\bar{w}$	1.713	1.758	1.724	1.713	1.761	1.724
	$\bar{\sigma}_{xx}$	17.946	18.546	18.251	17.970	19.222	18.393
	$\bar{\sigma}_{xy}$	9.681	9.952	10.751	9.625	10.244	10.754
250	$\bar{w}$	1.779	1.830	1.791	1.779	1.834	1.791
	$\bar{\sigma}_{xx}$	18.965	19.638	19.287	18.993	20.401	19.446
	$\bar{\sigma}_{xy}$	10.182	10.486	11.344	10.122	10.827	11.349

\* $\bar{w} = w_0/h, \bar{\sigma} = \sigma(a^2/Eh^2)$ .

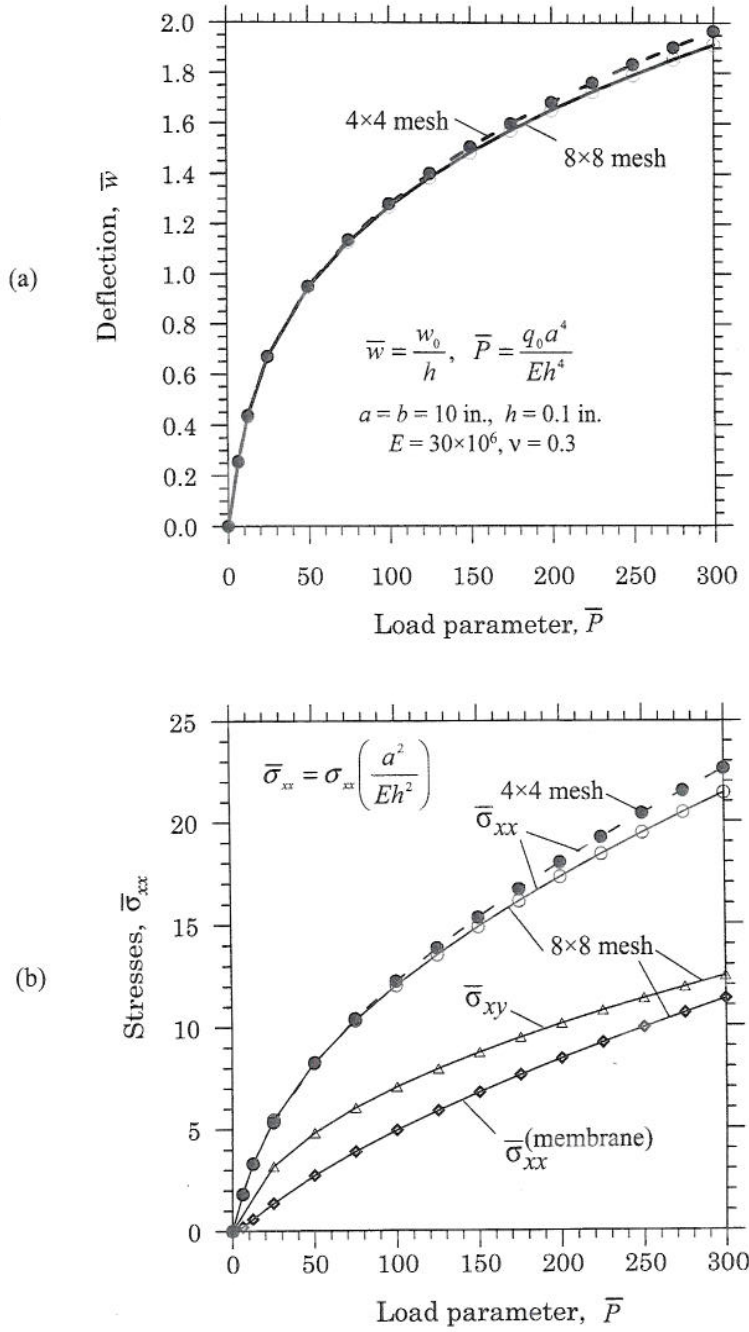


Figure 6.5.2 (a) Load versus deflection and (b) load versus stress plots for simply supported (SS-3) isotropic ( $\nu = 0.3$ ) square plates under uniformly distributed transverse load  $q_0$ .

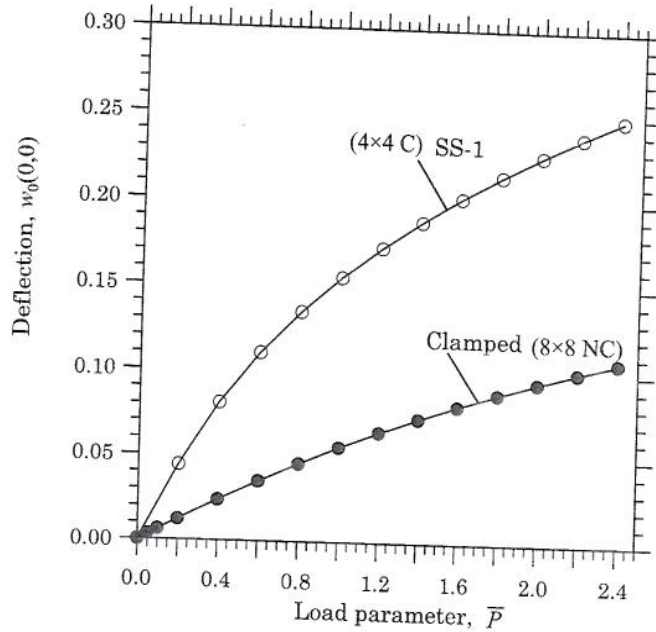


Figure 6.5.3 Load-deflection curves for simply supported and clamped orthotropic square plates under uniform load.

#### Example 6.5.5

The last example of this section is concerned with the bending of a clamped square plate under uniformly distributed load  $q_0$ . The geometric and material parameters used are the same as those in Eq. (6.5.8). The boundary conditions of a clamped edge are taken to be

$$u_0 = v_0 = w_0 = \frac{\partial w_0}{\partial x} = \frac{\partial w_0}{\partial y} = 0 \quad (6.5.9)$$

Of course, for conforming element, one may also impose  $(\partial^2 w_0 / \partial x \partial y) = 0$ .

A uniform mesh of  $8 \times 8$  non-conforming elements in a quarter plate is used, and a load increments of  $\{\Delta q_0\} = \{0.05, 0.05, 0.1, 0.2, 0.2, \dots, 0.2\}$  psi was used. The linear solution at  $q_0 = 0.05$  is found to be  $w_0(0,0) = 0.00302$  in. A plot of the center deflection versus the intensity of the distributed load for the clamped orthotropic plate is included in Figure 6.5.3 (see [36-38]).

We close this section with a note that the plate bending elements of the CPT discussed here are adequate for most engineering applications, which involve thin, isotropic plate structures and shear deformation is negligible. In the coming sections, we discuss plate elements based on the first-order shear deformation plate theory (FSDT), which can be used to analyze both thin and thick plates.

## 6.6 First-Order Shear Deformation Plate Theory

### 6.6.1 Introduction

The preceding sections of the book were devoted to the study of bending of plates using the CPT, in which transverse normal and shear stresses are neglected. The FSDT extends the kinematics of the CPT by relaxing the normality restriction (see Section 6.2) and allowing for arbitrary but constant rotation of transverse normals.

In this chapter, we develop displacement finite element models of the FSDT. As we shall see in the sequel, the formulation requires only  $C^0$  interpolation of all generalized displacements. Consequently, the element is much simpler to implement on a computer. Of course, the element can be used to analyze thick as well as thin plates. We begin with the theoretical formulation of the theory (see Reddy [3] for additional details).

### 6.6.2 Displacement Field

Under the same assumptions and restrictions as in the classical laminate theory but relaxing the normality condition, the displacement field of the FSDT can be expressed in the form

$$\begin{aligned} u(x, y, z) &= u_0(x, y) + z\phi_x(x, y) \\ v(x, y, z) &= v_0(x, y) + z\phi_y(x, y) \\ w(x, y, z) &= w_0(x, y) \end{aligned} \quad (6.6.1)$$

where  $(u_0, v_0, w_0, \phi_x, \phi_y)$  are unknown functions to be determined. As before,  $(u_0, v_0, w_0)$  denote the displacements of a point on the plane  $z = 0$  and  $\phi_x$  and  $\phi_y$  are the rotations of a transverse normal about the  $y$ - and  $x$ -axes, respectively (see Figure 6.6.1). The quantities  $(u_0, v_0, w_0, \phi_x, \phi_y)$  are called the *generalized displacements*.

The notation that  $\phi_x$  denotes the rotation of a transverse normal about the  $y$ -axis and  $\phi_y$  denotes the rotation about the  $x$ -axis may be confusing to some because they do not follow the right-hand rule. However, the notation has been used extensively in the literature, and we will not depart from it. If  $(\beta_x, \beta_y)$  denote the rotations about the  $x$ - and  $y$ -axes, respectively, that follow the right-hand rule, then

$$\beta_x = -\phi_y, \quad \beta_y = \phi_x \quad (6.6.2)$$

For thin plates, that is, when the plate in-plane characteristic dimension to thickness ratio is on the order of 50 or greater, the rotation functions  $\phi_x$  and  $\phi_y$  should approach the respective slopes of the transverse deflection [21]:

$$\phi_x = -\frac{\partial w_0}{\partial x}, \quad \phi_y = -\frac{\partial w_0}{\partial y} \quad (6.6.3)$$

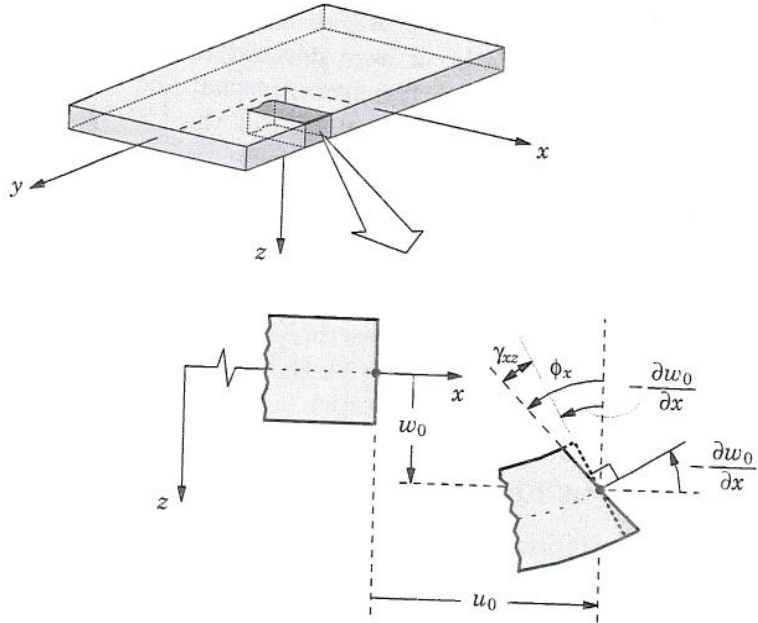


Figure 6.6.1 Undeformed and deformed geometries of an edge of a plate under the assumptions of the FSDT.

The von Kármán nonlinear strains associated with the displacement field (6.6.1) are ( $\epsilon_{zz} = 0$ )

$$\begin{Bmatrix} \epsilon_{xx} \\ \epsilon_{yy} \\ \gamma_{yz} \\ 0 \\ \gamma_{xz} \\ \gamma_{xy} \end{Bmatrix} = \begin{Bmatrix} \epsilon_{xx}^0 \\ \epsilon_{yy}^0 \\ \gamma_{yz}^0 \\ 0 \\ \gamma_{xz}^0 \\ \gamma_{xy}^0 \end{Bmatrix} + z \begin{Bmatrix} \epsilon_{xx}^1 \\ \epsilon_{yy}^1 \\ 0 \\ 0 \\ \gamma_{xz}^1 \\ \gamma_{xy}^1 \end{Bmatrix} = \begin{Bmatrix} \frac{\partial u_0}{\partial x} + \frac{1}{2} \left( \frac{\partial w_0}{\partial x} \right)^2 \\ \frac{\partial v_0}{\partial y} + \frac{1}{2} \left( \frac{\partial w_0}{\partial y} \right)^2 \\ \frac{\partial w_0}{\partial y} + \phi_y \\ \frac{\partial w_0}{\partial x} + \phi_x \\ \frac{\partial u_0}{\partial y} + \frac{\partial v_0}{\partial x} + \frac{\partial w_0}{\partial x} \frac{\partial w_0}{\partial y} \end{Bmatrix} + z \begin{Bmatrix} \frac{\partial \phi_x}{\partial x} \\ \frac{\partial \phi_y}{\partial y} \\ 0 \\ 0 \\ \frac{\partial \phi_x}{\partial y} + \frac{\partial \phi_y}{\partial x} \end{Bmatrix} \quad (6.6.4)$$

Note that the strains ( $\epsilon_{xx}, \epsilon_{yy}, \gamma_{xy}$ ) are linear through the plate thickness, while the transverse shear strains ( $\gamma_{xz}, \gamma_{yz}$ ) are constant.

### 6.6.3 Weak Formulation

The weak form of the FSDT can be derived using the principle of virtual displacements

$$0 = \delta W^e \equiv \delta U^e + \delta V^e \quad (6.6.5)$$

where the virtual strain energy  $\delta U^e$  and the virtual work done by applied

forces  $\delta V^e$  in an element  $\Omega^e$  are given by

$$\delta U^e = \int_{\Omega^e} \left\{ \int_{-\frac{h}{2}}^{\frac{h}{2}} \left[ \sigma_{xx} (\delta \varepsilon_{xx}^0 + z \delta \varepsilon_{xx}^1) + \sigma_{yy} (\delta \varepsilon_{yy}^0 + z \delta \varepsilon_{yy}^1) \right. \right. \\ \left. \left. + \sigma_{xy} (\delta \gamma_{xy}^0 + z \delta \gamma_{xy}^1) + \sigma_{xz} \delta \gamma_{xz}^0 + \sigma_{yz} \delta \gamma_{yz}^0 \right] dz \right\} dx dy \quad (6.6.6)$$

$$\delta V^e = - \left\{ \int_{\Gamma^e} \int_{-\frac{h}{2}}^{\frac{h}{2}} \left[ \sigma_{nn} (\delta u_{0n} + z \delta \phi_n) + \sigma_{ns} (\delta u_{0s} + z \delta \phi_s) + \sigma_{nz} \delta w_0 \right] dz ds \right. \\ \left. + \int_{\Omega^e} (q - k w_0) \delta w_0 dx dy \right\} \quad (6.6.7)$$

where  $\Omega^e$  denotes the undeformed mid-plane of a typical plate element,  $h$  the total thickness,  $\rho_0$  the density of the plate,  $k$  the modulus of the elastic foundation (if any), and  $(\sigma_{nn}, \sigma_{ns}, \sigma_{nz})$  are the edge stresses along the  $(n, s, z)$  coordinates.

Substituting for  $\delta U^e$  and  $\delta V^e$  from Eqs. (6.6.6) and (6.6.7) into the virtual work statement in Eq. (6.6.5) and integrating through the thickness, we obtain

$$0 = \int_{\Omega^e} \left[ N_{xx} \delta \varepsilon_{xx}^0 + M_{xx} \delta \varepsilon_{xx}^1 + N_{yy} \delta \varepsilon_{yy}^0 + M_{yy} \delta \varepsilon_{yy}^1 + N_{xy} \delta \gamma_{xy}^0 \right. \\ \left. + M_{xy} \delta \gamma_{xy}^1 + Q_x \delta \gamma_{xz}^0 + Q_y \delta \gamma_{yz}^0 + k w_0 \delta w_0 - q \delta w_0 \right] dx dy \\ - \int_{\Gamma^e} (N_{nn} \delta u_{0n} + N_{ns} \delta u_{0s} + M_{nn} \delta \phi_n + M_{ns} \delta \phi_s + Q_n \delta w_0) ds \quad (6.6.8)$$

where the stress resultants  $(N_{xx}, N_{yy}, N_{xy}, M_{xx}, M_{yy}, M_{xy})$  were defined in Eq. (6.3.4),  $(N_{nn}, N_{ns}, M_{nn}, M_{ns}, Q_n)$  in Eqs. (6.3.6a,b)-(6.3.7), and the transverse forces per unit length  $(Q_x, Q_y)$  are defined by

$$\begin{Bmatrix} Q_x \\ Q_y \end{Bmatrix} = \int_{-\frac{h}{2}}^{\frac{h}{2}} \begin{Bmatrix} \sigma_{xz} \\ \sigma_{yz} \end{Bmatrix} dz \quad (6.6.9)$$

and  $\phi_n$  and  $\phi_s$  are the rotations of a transverse normal about  $s$  and  $-n$  coordinates, respectively.

Since the transverse shear strains are represented as constant through the laminate thickness, it follows that the transverse shear stresses will also be constant. It is well known from elementary theory of homogeneous beams that the transverse shear stress variation is parabolic through the beam thickness. This discrepancy between the actual stress state and the constant stress state predicted by the FSDT is often corrected in computing the transverse shear forces  $(Q_x, Q_y)$  by multiplying the integrals in Eq. (6.6.9) with a parameter  $K_s$ , called *shear correction coefficient*:

$$\begin{Bmatrix} Q_x \\ Q_y \end{Bmatrix} = K_s \int_{-\frac{h}{2}}^{\frac{h}{2}} \begin{Bmatrix} \sigma_{xz} \\ \sigma_{yz} \end{Bmatrix} dz \quad (6.6.10)$$



This amounts to modifying the plate transverse shear stiffnesses. The factor  $K_s$  is computed such that the strain energy due to transverse shear stress in Eq. (6.6.10) equals the strain energy due to the true transverse stress predicted by the three-dimensional elasticity theory.

To obtain the governing equations of equilibrium, first we substitute the virtual strains in terms of the virtual displacements into Eq. (6.6.8), and then integrate-by-parts the expressions to relieve the virtual displacements ( $\delta u_0, \delta v_0, \delta w_0, \delta \phi_x, \delta \phi_y$ ) in  $\Omega^e$  of any differentiation. We obtain

$$\begin{aligned}
 0 = & \int_{\Omega^e} \left[ - (N_{xx,x} + N_{xy,y}) \delta u_0 - (N_{xy,x} + N_{yy,y}) \delta v_0 \right. \\
 & - (M_{xx,x} + M_{xy,y} - Q_x) \delta \phi_x - (M_{xy,x} + M_{yy,y} - Q_y) \delta \phi_y \\
 & \left. - (Q_{x,x} + Q_{y,y} - kw_0 + \mathcal{N} + q) \delta w_0 \right] dx dy \\
 & + \oint_{\Gamma^e} \left[ (N_{xx}n_x + N_{xy}n_y) \delta u_0 + (N_{xy}n_x + N_{yy}n_y) \delta v_0 \right. \\
 & + (M_{xx}n_x + M_{xy}n_y) \delta \phi_x - (M_{xy}n_x + M_{yy}n_y) \delta \phi_y \\
 & \left. + (Q_xn_x + Q_y n_y + \mathcal{P}) \delta w_0 \right] ds \\
 & - \oint_{\Gamma^e} (N_{nn} \delta u_{0n} + N_{ns} \delta u_{0s} + M_{nn} \delta \phi_n + M_{ns} \delta \phi_s + Q_n \delta w_0) ds \quad (6.6.11)
 \end{aligned}$$

where  $\mathcal{N}$  and  $\mathcal{P}$  are defined by Eqs. (6.3.14a,b). The boundary terms can be expressed in terms of the normal and tangential components  $u_{0n}$ ,  $u_{0s}$ ,  $\phi_n$ , and  $\phi_s$  using Eqs. (6.3.18a,b) and

$$\phi_x = n_x \phi_n - n_y \phi_s, \quad \phi_y = n_y \delta \phi_n + n_x \delta \phi_s \quad (6.6.12)$$

This will yield the natural boundary conditions given in Eq. (6.3.20), which relate the forces and moments on an arbitrary edge to those on edges parallel to the coordinates  $(x, y, z)$ .

The Euler-Lagrange equations are

$$\delta u_0 : \quad \frac{\partial N_{xx}}{\partial x} + \frac{\partial N_{xy}}{\partial y} = 0 \quad (6.6.13)$$

$$\delta v_0 : \quad \frac{\partial N_{xy}}{\partial x} + \frac{\partial N_{yy}}{\partial y} = 0 \quad (6.6.14)$$

$$\delta w_0 : \quad \frac{\partial Q_x}{\partial x} + \frac{\partial Q_y}{\partial y} - kw_0 + \mathcal{N} + q = 0 \quad (6.6.15)$$

$$\delta \phi_x : \quad \frac{\partial M_{xx}}{\partial x} + \frac{\partial M_{xy}}{\partial y} - Q_x = 0 \quad (6.6.16)$$

$$\delta \phi_y : \quad \frac{\partial M_{xy}}{\partial x} + \frac{\partial M_{yy}}{\partial y} - Q_y = 0 \quad (6.6.17)$$

The primary and secondary variables of the theory are

$$\begin{aligned} \text{primary variables: } & u_{0n}, u_{0s}, w_0, \phi_n, \phi_s \\ \text{secondary variables: } & N_{nn}, N_{ns}, Q_n, M_{nn}, M_{ns} \end{aligned} \quad (6.6.18)$$

The plate constitutive equations in Eqs. (6.3.32) and (6.3.33) are valid also for the first-order plate theory. In addition, we have the following constitutive equations for transverse shear forces of an orthotropic plate::

$$\begin{Bmatrix} Q_y \\ Q_x \end{Bmatrix} = K_s \int_{-\frac{h}{2}}^{\frac{h}{2}} \begin{Bmatrix} \sigma_{yz} \\ \sigma_{xz} \end{Bmatrix} dz = K_s \begin{bmatrix} A_{44} & 0 \\ 0 & A_{55} \end{bmatrix} \begin{Bmatrix} \gamma_{yz} \\ \gamma_{xz} \end{Bmatrix} \quad (6.6.19)$$

where the extensional stiffnesses  $A_{44}$  and  $A_{55}$  are defined by

$$(A_{44}, A_{55}) = \int_{-\frac{h}{2}}^{\frac{h}{2}} (Q_{44}, Q_{55}) dz, \quad Q_{44} = G_{23}, \quad Q_{55} = G_{13} \quad (6.6.20)$$

The stress resultants in an orthotropic plate are related to the generalized displacements  $(u_0, v_0, w_0, \phi_x, \phi_y)$  by [see Eqs. (6.3.32) and (6.3.33)]

$$\begin{Bmatrix} N_{xx} \\ N_{yy} \\ N_{xy} \end{Bmatrix} = \begin{bmatrix} A_{11} & A_{12} & 0 \\ A_{12} & A_{22} & 0 \\ 0 & 0 & A_{66} \end{bmatrix} \begin{Bmatrix} \varepsilon_{xx}^0 \\ \varepsilon_{yy}^0 \\ \gamma_{xy}^0 \end{Bmatrix} - \begin{Bmatrix} N_{xx}^T \\ N_{yy}^T \\ 0 \end{Bmatrix} \quad (6.6.21)$$

$$\begin{Bmatrix} M_{xx} \\ M_{yy} \\ M_{xy} \end{Bmatrix} = \begin{bmatrix} D_{11} & D_{12} & 0 \\ D_{12} & D_{22} & 0 \\ 0 & 0 & D_{66} \end{bmatrix} \begin{Bmatrix} \varepsilon_{xx}^1 \\ \varepsilon_{yy}^1 \\ \gamma_{xy}^1 \end{Bmatrix} - \begin{Bmatrix} M_{xx}^T \\ M_{yy}^T \\ 0 \end{Bmatrix} \quad (6.6.22)$$

$$\begin{Bmatrix} Q_y \\ Q_x \end{Bmatrix} = K_s \begin{bmatrix} A_{44} & 0 \\ 0 & A_{55} \end{bmatrix} \begin{Bmatrix} \gamma_{yz}^0 \\ \gamma_{xz}^0 \end{Bmatrix} \quad (6.6.23)$$

## 6.7 Finite Element Models of FSDT

### 6.7.1 Virtual Work Statements

Using the weak form (6.6.9) developed in Section 6.6, we can construct the finite element models of the equations governing the FSDT. The stress resultants in Eq. (6.6.9) are understood to be known in terms of the generalized displacements  $(u_0, v_0, w_0, \phi_x, \phi_y)$  via Eqs. (6.6.22)–(6.6.24). The virtual work statement (6.6.9) is equivalent to (collecting the terms involving  $\delta u_0$ ,  $\delta v_0$ ,  $\delta w_0$ ,  $\delta \phi_x$ , and  $\delta \phi_y$  separately) the following five weak forms

$$0 = \int_{\Omega^e} \left( \frac{\partial \delta u_0}{\partial x} N_{xx} + \frac{\partial \delta u_0}{\partial y} N_{xy} \right) dx dy - \oint_{\Gamma^e} (N_{xx} n_x + N_{xy} n_y) \delta u_0 ds \quad (6.7.1)$$

$$0 = \int_{\Omega^e} \left( \frac{\partial \delta v_0}{\partial x} N_{xy} + \frac{\partial \delta v_0}{\partial y} N_{yy} \right) dx dy - \oint_{\Gamma^e} (N_{xy} n_x + N_{yy} n_y) \delta v_0 ds \quad (6.7)$$

$$0 = \int_{\Omega^e} \left[ \frac{\partial \delta w_0}{\partial x} Q_x + \frac{\partial \delta w_0}{\partial y} Q_y + \frac{\partial \delta w_0}{\partial x} \left( N_{xx} \frac{\partial w_0}{\partial x} + N_{xy} \frac{\partial w_0}{\partial y} \right) + \frac{\partial \delta w_0}{\partial y} \left( N_{xy} \frac{\partial w_0}{\partial x} + N_{yy} \frac{\partial w_0}{\partial y} \right) - \delta w_0 q + k w_0 \delta w_0 \right] dx dy - \oint_{\Gamma^e} \left[ \left( Q_x + N_{xx} \frac{\partial w_0}{\partial x} + N_{xy} \frac{\partial w_0}{\partial y} \right) n_x + \left( Q_y + N_{xy} \frac{\partial w_0}{\partial x} + N_{yy} \frac{\partial w_0}{\partial y} \right) n_y \right] \delta w_0 ds \quad (6.7.1)$$

$$0 = \int_{\Omega^e} \left( \frac{\partial \delta \phi_x}{\partial x} M_{xx} + \frac{\partial \delta \phi_x}{\partial y} M_{xy} + \delta \phi_x Q_x \right) dx dy - \oint_{\Gamma^e} (M_{xx} n_x + M_{xy} n_y) \delta \phi_x ds \quad (6.7.2)$$

$$0 = \int_{\Omega^e} \left( \frac{\partial \delta \phi_y}{\partial x} M_{xy} + \frac{\partial \delta \phi_y}{\partial y} M_{yy} + \delta \phi_y Q_y \right) dx dy - \oint_{\Gamma^e} (M_{xy} n_x + M_{yy} n_y) \delta \phi_y ds \quad (6.7.3)$$

We note from the boundary terms in Eqs. (6.7.1)–(6.7.3) that  $u_0$ ,  $v_0$ ,  $w_0$ ,  $\phi_x$ ,  $\phi_y$  are used as the primary variables (or generalized displacements) as opposed to  $u_{0n}$ ,  $u_{0s}$ ,  $w_0$ ,  $\phi_n$ ,  $\phi_s$ . Unlike in the CPT, the rotations ( $\phi_x$ ,  $\phi_y$ ) are independent of  $w_0$ . Since no derivatives of ( $u_0$ ,  $v_0$ ,  $w_0$ ,  $\phi_x$ ,  $\phi_y$ ) appear in the list of the primary variables, all generalized displacements may be interpolated using the Lagrange interpolation functions. Hence, the element is called  $C^0$  element with respect to all dependent unknowns.

We identify the secondary variables of the formulation as

$$\hat{N}_n \equiv N_{xx} n_x + N_{xy} n_y, \quad \hat{N}_s \equiv N_{xy} n_x + N_{yy} n_y \quad (6.7.4a)$$

$$\hat{M}_n \equiv M_{xx} n_x + M_{xy} n_y, \quad \hat{M}_s \equiv M_{xy} n_x + M_{yy} n_y \quad (6.7.4b)$$

$$\hat{Q}_n \equiv \left( Q_x + N_{xx} \frac{\partial w_0}{\partial x} + N_{xy} \frac{\partial w_0}{\partial y} \right) n_x + \left( Q_y + N_{xy} \frac{\partial w_0}{\partial x} + N_{yy} \frac{\partial w_0}{\partial y} \right) n_y \quad (6.7.4c)$$

### 6.7.2 Finite Element Model

The virtual work statements in Eqs. (6.7.1)–(6.7.3) contain at the most only the first derivatives of the dependent variables ( $u_0$ ,  $v_0$ ,  $w_0$ ,  $\phi_x$ ,  $\phi_y$ ). Therefore,

they can all be approximated using the Lagrange interpolation functions. In principle,  $(u_0, v_0)$ ,  $w_0$ , and  $(\phi_x, \phi_y)$  can be approximated with differing degrees of Lagrange interpolation functions. Let

$$u_0(x, y) = \sum_{j=1}^m u_j \psi_j^{(1)}(x, y), \quad v_0(x, y) = \sum_{j=1}^m v_j \psi_j^{(1)}(x, y) \quad (6.7.8)$$

$$w_0(x, y) = \sum_{j=1}^n w_j \psi_j^{(2)}(x, y) \quad (6.7.9)$$

$$\phi_x(x, y) = \sum_{j=1}^p S_j^1 \psi_j^{(3)}(x, y), \quad \phi_y(x, y) = \sum_{j=1}^p S_j^2 \psi_j^{(3)}(x, y) \quad (6.7.10)$$

where  $\psi_j^{(\alpha)}$  ( $\alpha = 1, 2, 3$ ) are Lagrange interpolation functions. One can use linear, quadratic, or higher-order interpolations of these variables. Although the development is general, in the implementation of this element, we shall use equal interpolation of all variables.

Substituting Eqs. (6.7.8)–(6.7.10) for  $(u_0, v_0, w_0, \phi_x, \phi_y)$  into Eqs. (6.7.1)–(6.7.5), we obtain the following finite element model:

$$\begin{bmatrix} [K^{11}] & [K^{12}] & [K^{13}] & [K^{14}] & [K^{15}] \\ [K^{21}] & [K^{22}] & [K^{23}] & [K^{24}] & [K^{25}] \\ [K^{31}] & [K^{32}] & [K^{33}] & [K^{34}] & [K^{35}] \\ [K^{41}] & [K^{42}] & [K^{43}] & [K^{44}] & [K^{45}] \\ [K^{51}] & [K^{52}] & [K^{53}] & [K^{54}] & [K^{55}] \end{bmatrix} \begin{Bmatrix} \{u^e\} \\ \{v^e\} \\ \{w^e\} \\ \{S^1\} \\ \{S^2\} \end{Bmatrix} = \begin{Bmatrix} \{F^1\} \\ \{F^2\} \\ \{F^3\} \\ \{F^4\} \\ \{F^5\} \end{Bmatrix} + \begin{Bmatrix} \{F^{1T}\} \\ \{F^{2T}\} \\ \{0\} \\ \{F^{4T}\} \\ \{F^{5T}\} \end{Bmatrix} \quad (6.7.11)$$

or, in generic matrix form

$$[K^e] \{\Delta^e\} = \{F^e\} \quad (6.7.12)$$

where the coefficients of the submatrices  $[K^{\alpha\beta}]$  and vectors  $\{F^\alpha\}$  and  $\{F^{\alpha T}\}$  are defined for  $(\alpha, \beta = 1, 2, 3, 4, 5)$  by the expressions

$$\begin{aligned} K_{ij}^{11} &= \int_{\Omega^e} \left( A_{11} \frac{\partial \psi_i^{(1)}}{\partial x} \frac{\partial \psi_j^{(1)}}{\partial x} + A_{66} \frac{\partial \psi_i^{(1)}}{\partial y} \frac{\partial \psi_j^{(1)}}{\partial y} \right) dx dy \\ K_{ij}^{12} &= \int_{\Omega^e} \left( A_{12} \frac{\partial \psi_i^{(1)}}{\partial x} \frac{\partial \psi_j^{(1)}}{\partial y} + A_{66} \frac{\partial \psi_i^{(1)}}{\partial y} \frac{\partial \psi_j^{(1)}}{\partial x} \right) dx dy \\ K_{ij}^{13} &= \frac{1}{2} \int_{\Omega^e} \left[ \frac{\partial \psi_i^{(1)}}{\partial x} \left( A_{11} \frac{\partial w_0}{\partial x} \frac{\partial \psi_j^{(2)}}{\partial x} + A_{12} \frac{\partial w_0}{\partial y} \frac{\partial \psi_j^{(2)}}{\partial y} \right) \right. \\ &\quad \left. + A_{66} \frac{\partial \psi_i^{(1)}}{\partial y} \left( \frac{\partial w_0}{\partial x} \frac{\partial \psi_j^{(2)}}{\partial y} + \frac{\partial w_0}{\partial y} \frac{\partial \psi_j^{(2)}}{\partial x} \right) \right] dx dy \end{aligned}$$

$$\begin{aligned}
K_{ij}^{22} &= \int_{\Omega^e} \left( A_{66} \frac{\partial \psi_i^{(1)}}{\partial x} \frac{\partial \psi_j^{(1)}}{\partial x} + A_{22} \frac{\partial \psi_i^{(1)}}{\partial y} \frac{\partial \psi_j^{(1)}}{\partial y} \right) dx dy \\
K_{ij}^{23} &= \frac{1}{2} \int_{\Omega^e} \left[ \frac{\partial \psi_i^{(1)}}{\partial y} \left( A_{12} \frac{\partial w_0}{\partial x} \frac{\partial \psi_j^{(2)}}{\partial x} + A_{22} \frac{\partial w_0}{\partial y} \frac{\partial \psi_j^{(2)}}{\partial y} \right) \right. \\
&\quad \left. + A_{66} \frac{\partial \psi_i^{(1)}}{\partial x} \left( \frac{\partial w_0}{\partial x} \frac{\partial \psi_j^{(2)}}{\partial y} + \frac{\partial w_0}{\partial y} \frac{\partial \psi_j^{(2)}}{\partial x} \right) \right] dx dy \\
K_{ij}^{31} &= \int_{\Omega^e} \left[ \frac{\partial \psi_i^{(2)}}{\partial x} \left( A_{11} \frac{\partial w_0}{\partial x} \frac{\partial \psi_j^{(1)}}{\partial x} + A_{66} \frac{\partial w_0}{\partial y} \frac{\partial \psi_j^{(1)}}{\partial y} \right) \right. \\
&\quad \left. + \frac{\partial \psi_i^{(2)}}{\partial y} \left( A_{66} \frac{\partial w_0}{\partial x} \frac{\partial \psi_j^{(1)}}{\partial y} + A_{12} \frac{\partial w_0}{\partial y} \frac{\partial \psi_j^{(1)}}{\partial x} \right) \right] dx dy \\
K_{ij}^{32} &= \int_{\Omega^e} \left[ \frac{\partial \psi_i^{(2)}}{\partial x} \left( A_{12} \frac{\partial w_0}{\partial x} \frac{\partial \psi_j^{(1)}}{\partial y} + A_{66} \frac{\partial w_0}{\partial y} \frac{\partial \psi_j^{(1)}}{\partial x} \right) \right. \\
&\quad \left. + \frac{\partial \psi_i^{(2)}}{\partial y} \left( A_{66} \frac{\partial w_0}{\partial x} \frac{\partial \psi_j^{(1)}}{\partial x} + A_{22} \frac{\partial w_0}{\partial y} \frac{\partial \psi_j^{(1)}}{\partial y} \right) \right] dx dy \\
K_{ij}^{33} &= \int_{\Omega^e} \left( K_s A_{55} \frac{\partial \psi_i^{(e)}}{\partial x} \frac{\partial \psi_j^{(2)}}{\partial x} + K_s A_{44} \frac{\partial \psi_i^{(2)}}{\partial y} \frac{\partial \psi_j^{(2)}}{\partial y} + k \psi_i^{(e)} \psi_j^{(2)} \right) dx dy \\
&\quad + \frac{1}{2} \int_{\Omega^e} \left\{ \left[ A_{11} \left( \frac{\partial w_0}{\partial x} \right)^2 + A_{66} \left( \frac{\partial w_0}{\partial y} \right)^2 \right] \frac{\partial \psi_i^{(e)}}{\partial x} \frac{\partial \psi_j^{(2)}}{\partial x} \right. \\
&\quad + \left[ A_{66} \left( \frac{\partial w_0}{\partial x} \right)^2 + A_{22} \left( \frac{\partial w_0}{\partial y} \right)^2 \right] \frac{\partial \psi_i^{(2)}}{\partial y} \frac{\partial \psi_j^{(2)}}{\partial y} \\
&\quad \left. + (A_{12} + A_{66}) \frac{\partial w_0}{\partial x} \frac{\partial w_0}{\partial y} \left( \frac{\partial \psi_i^{(2)}}{\partial x} \frac{\partial \psi_j^{(2)}}{\partial y} + \frac{\partial \psi_i^{(2)}}{\partial y} \frac{\partial \psi_j^{(2)}}{\partial x} \right) \right\} dx dy \\
K_{ij}^{34} &= \int_{\Omega^e} K_s A_{55} \frac{\partial \psi_i^{(2)}}{\partial x} \psi_j^{(3)} dx dy, \quad K_{ij}^{35} = \int_{\Omega^e} K_s A_{44} \frac{\partial \psi_i^{(2)}}{\partial y} \psi_j^{(3)} dx dy \\
K_{ij}^{44} &= \int_{\Omega^e} \left( D_{11} \frac{\partial \psi_i^{(3)}}{\partial x} \frac{\partial \psi_j^{(3)}}{\partial x} + D_{66} \frac{\partial \psi_i^{(3)}}{\partial y} \frac{\partial \psi_j^{(3)}}{\partial y} + K_s A_{55} \psi_i^{(3)} \psi_j^{(3)} \right) dx dy \\
K_{ij}^{45} &= \int_{\Omega^e} \left( D_{12} \frac{\partial \psi_i^{(3)}}{\partial x} \frac{\partial \psi_j^{(3)}}{\partial y} + D_{66} \frac{\partial \psi_i^{(3)}}{\partial y} \frac{\partial \psi_j^{(3)}}{\partial x} \right) dx dy
\end{aligned}$$

$$\begin{aligned}
 K_{ij}^{55} &= \int_{\Omega^e} \left( D_{66} \frac{\partial \psi_i^{(3)}}{\partial x} \frac{\partial \psi_j^{(3)}}{\partial x} + D_{22} \frac{\partial \psi_i^{(3)}}{\partial y} \frac{\partial \psi_j^{(3)}}{\partial y} + K_s A_{44} \psi_i^{(3)} \psi_j^{(3)} \right) dx dy \\
 F_i^1 &= \oint_{\Gamma^e} \hat{N}_n \psi_i^{(1)} ds, \quad F_i^2 = \oint_{\Gamma^e} \hat{N}_s \psi_i^{(1)} ds \\
 F_i^3 &= \int_{\Omega^e} q \psi_i^{(2)} dx dy + \oint_{\Gamma^e} \hat{Q}_n \psi_i^{(2)} ds \\
 F_i^4 &= \oint_{\Gamma^e} \hat{M}_n \psi_i^{(3)} ds, \quad F_i^5 = \oint_{\Gamma^e} \hat{M}_s \psi_i^{(3)} ds \\
 F_i^{1T} &= \oint_{\Omega^e} \frac{\partial \psi_i^{(1)}}{\partial x} N_{xx}^T ds, \quad F_i^{2T} = \oint_{\Omega^e} \frac{\partial \psi_i^{(1)}}{\partial y} N_{yy}^T ds \\
 F_i^{4T} &= \oint_{\Omega^e} \frac{\partial \psi_i^{(3)}}{\partial x} M_{xx}^T ds, \quad F_i^{5T} = \oint_{\Omega^e} \frac{\partial \psi_i^{(3)}}{\partial y} M_{yy}^T ds \\
 K_{ij}^{21} &= K_{ji}^{12}; \quad K_{ij}^{43} = K_{ji}^{34}; \quad K_{ij}^{54} = K_{ji}^{45}
 \end{aligned} \tag{6.7.13}$$

and all other stiffness coefficients are zero. Here  $N_{xx}^T$  and  $N_{yy}^T$  denote thermal forces and  $M_{xx}^T$  and  $M_{yy}^T$  the thermal moments. It is noted that the element stiffness matrix is *not* symmetric.

The displacement-based  $C^0$  plate bending element of Eq. (6.7.12) is often referred to in the finite element literature as the *Mindlin plate element*, which is labeled in this book as the first-order shear deformation theory (FSDT) element. When the bilinear rectangular element is used for all generalized displacements  $(u_0, v_0, w_0, \phi_x, \phi_y)$ , the element stiffness matrices are of the order  $20 \times 20$ ; and for the nine-node quadratic element they are  $45 \times 45$  (see Figure 6.7.1).

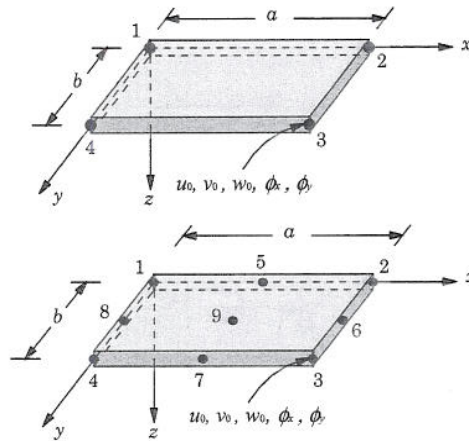


**Figure 6.7.1** Linear and nine-node quadratic rectangular elements for the FSDT.

### 6.7.3 Tangent Stiffness Coefficients

The tangent stiffness matrix coefficients needed for the Newton-Raphson method of solving the nonlinear equations in Eq. (6.7.12) can be computed using the definition. Since the source of nonlinearity in the CPT and FSDT is the same, the nonlinear parts of the tangent stiffness coefficients derived for the CPT are also applicable to the FSDT.

Suppose that the tangent stiffness matrix is of the same form as the direct stiffness matrix in Eq. (6.7.1). Then the coefficients of the submatrices  $[T^{\alpha\beta}]$  are defined by

$$T_{ij}^{\alpha\beta} = \frac{\partial R_i^\alpha}{\partial \Delta_j^\beta} \quad (6.7.14)$$

where the components of the residual vector  $\{R^\alpha\}$  are given by

$$R_i^\alpha = \sum_{\gamma=1}^5 \sum_{k=1}^{n^*} K_{ik}^{\alpha\gamma} \Delta_k^\gamma - F_i^\alpha \quad (6.7.15)$$

$$\Delta_i^1 = u_i, \quad \Delta_i^2 = v_i, \quad \Delta_i^3 = w_i, \quad \Delta_i^4 = S_i^1, \quad \Delta_i^5 = S_i^2 \quad (6.7.16)$$

and  $n^*$  denotes  $n$ ,  $m$ , or  $p$ , depending on the nodal degree of freedom. Thus, we have

$$T_{ij}^{\alpha\beta} = \frac{\partial}{\partial \Delta_j^\beta} \left( \sum_{\gamma=1}^5 \sum_{k=1}^{n^*} K_{ik}^{\alpha\gamma} \Delta_k^\gamma - F_i^\alpha \right) = \sum_{\gamma=1}^5 \sum_{k=1}^{n^*} \frac{\partial K_{ik}^{\alpha\gamma}}{\partial \Delta_j^\beta} \Delta_k^\gamma + K_{ij}^{\alpha\beta} \quad (6.7.17)$$

It should be noted that only coefficients that depend on the solution are  $K_{ij}^{13}$ ,  $K_{ij}^{23}$ ,  $K_{ij}^{31}$ ,  $K_{ij}^{32}$ , and  $K_{ij}^{33}$ . Further, they are functions of only  $w_0$  (or functions of  $w_j$ ). Hence, derivatives of all submatrices with respect to  $u_j$ ,  $v_j$ ,  $S_j^1$ , and  $S_j^2$  are zero. Thus, we have

$$\begin{aligned} T_{ij}^{11} &= \sum_{\gamma=1}^5 \sum_{k=1}^{n^*} \frac{\partial K_{ik}^{1\gamma}}{\partial u_j} \Delta_k^\gamma + K_{ij}^{11} = K_{ij}^{11}, & T_{ij}^{12} &= \sum_{\gamma=1}^5 \sum_{k=1}^{n^*} \frac{\partial K_{ik}^{1\gamma}}{\partial v_j} \Delta_k^\gamma + K_{ij}^{12} = K_{ij}^{12} \\ T_{ij}^{13} &= \sum_{\gamma=1}^5 \sum_{k=1}^{n^*} \frac{\partial K_{ik}^{1\gamma}}{\partial w_j} \Delta_k^\gamma + K_{ij}^{13} = \sum_{k=1}^n \frac{\partial K_{ik}^{13}}{\partial w_j} w_k + K_{ij}^{13} \\ &= \frac{1}{2} \int_{\Omega^e} \left[ \frac{\partial \psi_i^{(1)}}{\partial x} \left( A_{11} \frac{\partial w_0}{\partial x} \frac{\partial \psi_j^{(2)}}{\partial x} + A_{12} \frac{\partial w_0}{\partial y} \frac{\partial \psi_j^{(2)}}{\partial y} \right) \right. \\ &\quad \left. + A_{66} \frac{\partial \psi_i^{(1)}}{\partial y} \left( \frac{\partial w_0}{\partial x} \frac{\partial \psi_j^{(2)}}{\partial y} + \frac{\partial w_0}{\partial y} \frac{\partial \psi_j^{(2)}}{\partial x} \right) \right] dx dy + K_{ij}^{13} \end{aligned}$$

$$\begin{aligned}
 &= K_{ij}^{13} + K_{ij}^{13} = 2K_{ij}^{13} \quad (= T_{ji}^{31} = K_{ji}^{31}) \\
 T_{ij}^{14} &= \sum_{\gamma=1}^5 \sum_{k=1}^{n^*} \frac{\partial K_{ik}^{1\gamma}}{\partial S_j^1} \Delta_k^\gamma + K_{ij}^{14} = K_{ij}^{14}, \quad T_{ij}^{15} = \sum_{\gamma=1}^5 \sum_{k=1}^{n^*} \frac{\partial K_{ik}^{1\gamma}}{\partial S_j^2} \Delta_k^\gamma + K_{ij}^{15} = K_{ij}^{15} \\
 T_{ij}^{21} &= \sum_{\gamma=1}^5 \sum_{k=1}^{n^*} \frac{\partial K_{ik}^{2\gamma}}{\partial u_j} \Delta_k^\gamma + K_{ij}^{21} = K_{ij}^{21}, \quad T_{ij}^{22} = \sum_{\gamma=1}^5 \sum_{k=1}^{n^*} \frac{\partial K_{ik}^{2\gamma}}{\partial v_j} \Delta_k^\gamma + K_{ij}^{22} = K_{ij}^{22} \\
 T_{ij}^{23} &= \sum_{\gamma=1}^5 \sum_{k=1}^{n^*} \frac{\partial K_{ik}^{2\gamma}}{\partial w_j} \Delta_k^\gamma + K_{ij}^{23} = \sum_{k=1}^n \frac{\partial K_{ik}^{23}}{\partial w_j} w_k + K_{ij}^{23} \\
 &= \frac{1}{2} \int_{\Omega^e} \left[ \frac{\partial \psi_i^{(1)}}{\partial y} \left( A_{12} \frac{\partial w_0}{\partial x} \frac{\partial \psi_j^{(2)}}{\partial x} + A_{22} \frac{\partial w_0}{\partial y} \frac{\partial \psi_j^{(2)}}{\partial y} \right) \right. \\
 &\quad \left. + A_{66} \frac{\partial \psi_i^{(1)}}{\partial x} \left( \frac{\partial w_0}{\partial y} \frac{\partial \psi_j^{(2)}}{\partial x} + \frac{\partial w_0}{\partial x} \frac{\partial \psi_j^{(2)}}{\partial y} \right) \right] dx dy + K_{ij}^{23} \\
 &= K_{ij}^{23} + K_{ij}^{23} = 2K_{ij}^{23} \quad (= T_{ji}^{32} = K_{ji}^{32}) \\
 T_{ij}^{24} &= \sum_{\gamma=1}^5 \sum_{k=1}^{n^*} \frac{\partial K_{ik}^{2\gamma}}{\partial S_j^1} \Delta_k^\gamma + K_{ij}^{24} = K_{ij}^{24}, \quad T_{ij}^{25} = \sum_{\gamma=1}^5 \sum_{k=1}^{n^*} \frac{\partial K_{ik}^{2\gamma}}{\partial S_j^2} \Delta_k^\gamma + K_{ij}^{25} = K_{ij}^{25} \\
 T_{ij}^{31} &= \sum_{\gamma=1}^5 \sum_{k=1}^{n^*} \frac{\partial K_{ik}^{3\gamma}}{\partial u_j} \Delta_k^\gamma + K_{ij}^{31} = K_{ij}^{31}, \quad T_{ij}^{32} = \sum_{\gamma=1}^5 \sum_{k=1}^{n^*} \frac{\partial K_{ik}^{3\gamma}}{\partial v_j} \Delta_k^\gamma + K_{ij}^{32} = K_{ij}^{32} \\
 T_{ij}^{33} &= \sum_{\gamma=1}^5 \sum_{k=1}^{n^*} \frac{\partial K_{ik}^{3\gamma}}{\partial w_j} \Delta_k^\gamma + K_{ij}^{33} = \sum_{k=1}^{n^*} \left( \frac{\partial K_{ik}^{31}}{\partial w_j} u_k + \frac{\partial K_{ik}^{32}}{\partial w_j} v_k + \frac{\partial K_{ik}^{33}}{\partial w_j} w_k \right) + K_{ij}^{33} \\
 &= \int_{\Omega^e} \left( K_s A_{55} \frac{\partial \psi_i^{(2)}}{\partial x} \frac{\partial \psi_j^{(2)}}{\partial x} + K_s A_{44} \frac{\partial \psi_i^{(2)}}{\partial y} \frac{\partial \psi_j^{(2)}}{\partial y} + k \psi_i^{(2)} \psi_j^{(2)} \right) dx dy \\
 &+ \int_{\Omega^e} \left\{ (N_{xx} + N_{xx}^T) \frac{\partial \psi_i^{(2)}}{\partial x} \frac{\partial \psi_j^{(2)}}{\partial x} + (N_{yy} + N_{yy}^T) \frac{\partial \psi_i^{(2)}}{\partial y} \frac{\partial \psi_j^{(2)}}{\partial y} \right. \\
 &\quad \left. + N_{xy} \left( \frac{\partial \psi_i^{(2)}}{\partial x} \frac{\partial \psi_j^{(2)}}{\partial y} + \frac{\partial \psi_i^{(2)}}{\partial y} \frac{\partial \psi_j^{(2)}}{\partial x} \right) \right. \\
 &\quad \left. + (A_{12} + A_{66}) \frac{\partial w_0}{\partial x} \frac{\partial w_0}{\partial y} \left( \frac{\partial \psi_i^{(2)}}{\partial x} \frac{\partial \psi_j^{(2)}}{\partial y} + \frac{\partial \psi_i^{(2)}}{\partial y} \frac{\partial \psi_j^{(2)}}{\partial x} \right) \right. \\
 &\quad \left. + \left[ A_{11} \left( \frac{\partial w_0}{\partial x} \right)^2 + A_{66} \left( \frac{\partial w_0}{\partial y} \right)^2 \right] \frac{\partial \psi_i^{(2)}}{\partial x} \frac{\partial \psi_j^{(2)}}{\partial x} \right. \\
 &\quad \left. + \left[ A_{66} \left( \frac{\partial w_0}{\partial x} \right)^2 + A_{22} \left( \frac{\partial w_0}{\partial y} \right)^2 \right] \frac{\partial \psi_i^{(2)}}{\partial y} \frac{\partial \psi_j^{(2)}}{\partial y} \right\} dx dy
 \end{aligned}$$



$$\begin{aligned}
T_{ij}^{34} &= \sum_{\gamma=1}^5 \sum_{k=1}^{n^*} \frac{\partial K_{ik}^{3\gamma}}{\partial S_j^1} \Delta_k^\gamma + K_{ij}^{34} = K_{ij}^{34}, & T_{ij}^{35} &= \sum_{\gamma=1}^5 \sum_{k=1}^{n^*} \frac{\partial K_{ik}^{3\gamma}}{\partial S_j^2} \Delta_k^\gamma + K_{ij}^{35} = K_{ij}^{35}, \\
T_{ij}^{44} &= \sum_{\gamma=1}^5 \sum_{k=1}^{n^*} \frac{\partial K_{ik}^{4\gamma}}{\partial S_j^1} \Delta_k^\gamma + K_{ij}^{44} = K_{ij}^{44}, & T_{ij}^{45} &= \sum_{\gamma=1}^5 \sum_{k=1}^{n^*} \frac{\partial K_{ik}^{4\gamma}}{\partial S_j^2} \Delta_k^\gamma + K_{ij}^{45} = K_{ij}^{45}, \\
T_{ij}^{55} &= \sum_{\gamma=1}^5 \sum_{k=1}^{n^*} \frac{\partial K_{ik}^{5\gamma}}{\partial S_j^2} \Delta_k^\gamma + K_{ij}^{55} = K_{ij}^{55}
\end{aligned} \tag{6.7.18}$$

Note that all nonlinear coefficients are the same as those derived for the CPT. Once again, we note that the tangent stiffness matrix of the FSDT element is symmetric.

#### 6.7.4 Shear and Membrane Locking

The  $C^0$ -plate bending elements based on the FSDT are among the simplest available in the literature. Unfortunately, when lower order (quadratic or less) equal interpolation of the generalized displacements is used, the elements become excessively stiff in the thin plate limit, yielding displacements that are too small compared to the true solution. As discussed earlier for beams, this type of behavior is known as shear locking. There are a number of papers on the subject of shear locking and elements developed to alleviate the problem (see [23–28]). A commonly used technique is to use selective integration [29,30]: use full integration to evaluate all linear stiffness coefficients and use reduced integration to evaluate the transverse shear stiffnesses (i.e. all coefficients in  $K_{ij}^{\alpha\beta}$  that contain  $A_{44}$  and  $A_{55}$ ) and nonlinear stiffnesses. Higher-order elements or refined meshes of lower-order elements experience relatively less locking, but sometimes at the expense of the rate of convergence. With the suggested Gauss rule, highly distorted elements tend to have slower rates of convergence but they give sufficiently accurate results.

### 6.8 Computer Implementation and Numerical Results of FSDT Elements

#### 6.8.1 Computer Implementation

The FSDT element is quite simple to implement, and the implementation follows the same ideas as discussed in Chapter 5 for single-variables problems in two dimensions. The main difference is that the number of degrees of freedom (NDF) is 5, and one must rearrange the coefficients using the Fortran statements included in Box 4.3.1. Thus, the element displacement vector is of the form

$$\{\Delta\} = \{u_{01}, v_{01}, w_{01}, \phi_{x1}, \phi_{y1}, u_{02}, v_{02}, w_{02}, \phi_{x2}, \phi_{y2}, \dots\}$$

Two separate do-loops on Gauss quadrature are required to compute all the force and stiffness coefficients. The full integration loop is used to evaluate all force components and all linear, except for the transverse shear stiffnesses. The reduced integration loop has two parts: one for the transverse shear terms and the other for nonlinear terms. One may use separate arrays (say,  $EXT13(I, J)$ ,  $EXT33(I, J)$ , and so on to store the extra terms (to those of  $K_{ij}^{\alpha\beta}$ ) of the tangent stiffness coefficients. The stiffness coefficients are rearranged as in Box 4.3.1.

### 6.8.2 Results of Linear Analysis

The effect of the integration rule and the convergence characteristics of the FSDT plate element based on equal interpolation (bilinear as well as biquadratic elements) is illustrated through several examples.

#### Example 6.8.1

Consider a simply supported (SS-1) isotropic ( $\nu = 0.25$  and  $K_s = 5/6$ ) square plate under uniformly distributed transverse load  $q_0$ . The geometric boundary conditions of the computational domain (see the shaded quadrant in Figure 6.8.1) are

$$u_0 = \phi_x = 0 \text{ at } x = 0; \quad v_0 = \phi_y = 0 \text{ at } y = 0 \text{ (symm. lines)} \quad (6.8.1)$$

$$v_0 = w_0 = \phi_y = 0 \text{ at } x = \frac{a}{2}; \quad u_0 = w_0 = \phi_x = 0 \text{ at } y = \frac{b}{2} \quad (6.8.2)$$

The following non-dimensionalizations of the quantities are used:

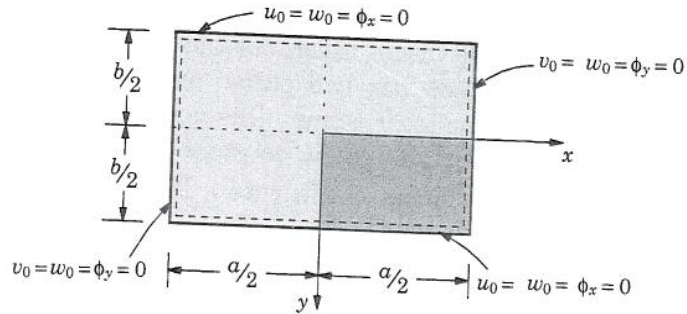
$$\begin{aligned} \bar{w} = w_0(0,0) \frac{E_2 h^3}{a^4 q_0}, \quad \bar{\sigma}_{xx} = \sigma_{xx}(0,0, \frac{h}{2}) \frac{h^2}{b^2 q_0}, \quad \bar{\sigma}_{yy} = \sigma_{yy}(0,0, \frac{h}{4}) \frac{h^2}{b^2 q_0} \\ \bar{\sigma}_{xy} = \sigma_{xy}(\frac{a}{2}, \frac{b}{2}, -\frac{h}{2}) \frac{h^2}{b^2 q_0}, \quad \bar{\sigma}_{xz} = \sigma_{xz}(\frac{a}{2}, 0, -\frac{h}{2}) \frac{h}{b q_0}, \quad \bar{\sigma}_{yz} = \sigma_{yz}(0, \frac{b}{2}, \frac{h}{2}) \frac{h}{b q_0} \end{aligned} \quad (6.8.3)$$

where the origin of the coordinate system is taken at the center of the plate,  $0 \leq x \leq a/2, 0 \leq y \leq b/2$ , and  $-h/2 \leq z \leq h/2$ . The stresses in the finite element analysis are computed at the reduced Gauss points, irrespective of the Gauss rule used for the evaluation of the element stiffness coefficients. The Gauss point coordinates  $A$  and  $B$  are shown in Table 6.8.1. The finite element solutions are compared with the analytical solutions from [2,3] in Table 6.8.2 for two side-to-thickness ratios  $a/h = 10$  and  $100$ . The notation  $nL$  stands for  $n \times n$  uniform mesh of linear rectangular elements and  $nQ9$  for  $n \times n$  uniform mesh of nine-node quadratic elements in a quarter plate.

The stresses are evaluated at the Gauss points as indicated below:

$$\sigma_{xx}(A, A, \frac{h}{2}), \quad \sigma_{xy}(B, B, -\frac{h}{2}), \quad \sigma_{xz}(B, A, -\frac{h}{2}) \quad (6.8.4)$$

Thus, as mesh is refined or higher-order elements are used, the Gauss point locations get closer to the points at which the analytical solutions for stresses are evaluated.



Symm. B.C.:  $u_0 = \phi_x = 0$  at  $x=0$ ;  $v_0 = \phi_y = 0$  at  $y=0$

Figure 6.8.1 Geometric boundary conditions for SS-1 type simply supported rectangular plates.

Table 6.8.1 The Gauss point locations at which the stresses are computed in the finite element analysis of simply supported plates.

Point	2L	4L	8L	1Q9	2Q9	4Q9
A	0.125a	0.0625a	0.03125a	0.10566a	0.05283a	0.02642a
B	0.375a	0.4375a	0.46875a	0.39434a	0.44717a	0.47358a

The following notation is used in Table 6.8.2: F = full integration; R = reduced integration; S = selective integration: full integration of all except the transverse shear coefficients, which are evaluated using reduced integration rule. The CPT solution is independent of side-to-thickness ratio,  $a/h$ .

The results of Table 6.8.2 indicate that the FSDT finite element with equal interpolation of all generalized displacements does not experience shear locking for thick plates even when full integration rule is used for the evaluation of all stiffness coefficients. Shear locking is evident when the element is used to model thin plates ( $a/h \geq 100$ ) with full integration rule (F). Also, higher-order elements are less sensitive to locking but exhibit slower convergence. The element behaves uniformly well for thin and thick plates when the reduced (R) or selectively reduced integration (S) rule is used. The selective integration rule gives the most accurate solutions.

**Example 6.8.2**

Next consider a clamped isotropic ( $\nu = 0.25$  and  $K_s = 5/6$ ) square plate under uniformly distributed load. The non-dimensionalizations used are the same as in Eq. (6.8.3), except for the location of the stresses. The analytical stresses were non-dimensionalized as follows:

$$\bar{\sigma}_{xx} = \sigma_{xx} \left( \frac{a}{2}, 0, -\frac{h}{2} \right) \frac{h^2}{b^2 q_0}, \quad \bar{\sigma}_{zz} = \sigma_{zz} \left( \frac{a}{2}, 0, -\frac{h}{2} \right) \frac{h}{b q_0} \tag{6.8.5}$$

**Table 6.8.2** Effect of integration rule on the linear deflections  $\bar{w}$  and stresses  $\bar{\sigma}$  of simply supported, isotropic ( $\nu = 0.25$  and  $K_s = 5/6$ ), square plates under a uniformly distributed load  $q_0$ .

$a/h$	Mesh	$\bar{w} \times 10^2$	$\bar{\sigma}_{xx}$	$\bar{\sigma}_{xy}$	$\bar{\sigma}_{xz}$
<i>Finite element solutions (FSDT)</i>					
10	2L-F	2.4742	0.1185	0.0727	0.2627
	2L-S	4.7120	0.2350	0.1446	0.2750
	2L-R	4.8887	0.2441	0.1504	0.2750
	1Q-F	4.5304	0.2294	0.1610	0.2813
	1Q-S	4.9426	0.2630	0.1639	0.2847
	1Q-R	4.9711	0.2645	0.1652	0.2886
	4L-F	3.8835	0.2160	0.1483	0.3366
	4L-S	4.7728	0.2661	0.1850	0.3356
	4L-R	4.8137	0.2684	0.1869	0.3356
	2Q-F	4.7707	0.2699	0.1930	0.3437
	2Q-S	4.7989	0.2715	0.1939	0.3424
	2Q-R	4.8005	0.2716	0.1943	0.3425
	8L-F	4.5268	0.2590	0.1891	0.3700
	8L-S	4.7966	0.2743	0.2743	0.2014
	8L-R	4.7866	0.2737	0.2737	0.2008
	4Q-F	4.7897	0.2749	0.2044	0.3737
	4Q-S	4.7916	0.2750	0.2043	0.3735
	4Q-R	4.7917	0.2750	0.2044	0.3735
<i>Anal. solns</i>	[3]	4.7914	0.2762	0.2085	0.3927
<i>Finite element solutions</i>					
100	2L-F	0.0469	0.0024	0.0014	0.2635
	2L-S	4.4645	0.2350	0.1446	0.2750
	2L-R	4.6412	0.2441	0.1504	0.2750
	1Q-F	4.0028	0.2040	0.1591	0.2733
	1Q-S	4.7196	0.2629	0.1643	0.2837
	1Q-R	4.7483	0.2645	0.1652	0.2886
	4L-F	0.1819	0.0108	0.0071	0.3462
	4L-S	4.5481	0.2661	0.1850	0.3356
	4L-R	4.5890	0.2684	0.1869	0.3356
	2Q-F	4.4822	0.2644	0.1893	0.3485
	2Q-S	4.5799	0.2715	0.1941	0.3414
	2Q-R	4.5815	0.2716	0.1943	0.3425
	8L-F	0.6497	0.0401	0.0275	0.3847
	8L-S	4.5664	0.2737	0.2008	0.3691
	8L-R	4.5764	0.2743	0.2014	0.3691
	4Q-F	4.5530	0.2741	0.2020	0.3749
	4Q-S	4.5728	0.2750	0.2044	0.3734
	4Q-R	4.5729	0.2750	0.2044	0.3735
<i>Finite element solutions (CPT)</i>					
	4 × 4C	4.5952	0.2637	0.1935	—
	8 × 8C	4.5734	0.2732	0.2040	—
<i>Anal. solns</i>	[3]	4.5698	0.2762	0.2085	0.3927

while the finite element solutions were non-dimensionalized as

$$\bar{\sigma}_{xx} = \sigma_{xx}(A, B, -\frac{h}{2}) \frac{h^2}{b^2 q_0}, \quad \bar{\sigma}_{xz} = \sigma_{xz}(A, B, -\frac{h}{2}) \frac{h}{b q_0} \tag{6.8}$$

where the values of  $A$  and  $B$  for different meshes are given in Table 6.8.3. Table 6.8.4 contains the non-dimensionalized displacements and stresses. The FSDT element with selective integration or reduced integration is accurate in predicting the bending response

**Table 6.8.3** The Gauss point locations at which the stresses are computed in the finite element analysis of clamped plates (Example 6.8.2)

Point	4L	8L	2Q9	4Q9
A	0.4375a	0.46875a	0.44717a	0.47358a
B	0.0625a	0.03125a	0.05283a	0.02642a

**Table 6.8.4** Effect of integration rule on the linear deflections  $\bar{w}$  and stresses  $\bar{\sigma}$  of clamped, isotropic ( $\nu = 0.25$  and  $K_s = 5/6$ ), square plate under a uniform load  $q_0$ .

a/h	Integ.	Variable	4 × 4L	2 × 2Q9	8 × 8L	4 × 4Q9
10	F	$\bar{w} \times 10^2$	1.2593	1.5983	1.5447	1.6685
		$\bar{\sigma}_{xx}$	0.1190	0.1568	0.2054	0.2301
		$\bar{\sigma}_{xz}$	0.3890	0.4193	0.4463	0.4578
10	S	$\bar{w} \times 10^2$	1.6632	1.6880	1.6721	1.6758
		$\bar{\sigma}_{xx}$	0.1689	0.1813	0.2275	0.2357
		$\bar{\sigma}_{xz}$	0.4056	0.4118	0.4511	0.4566
10	R	$\bar{w} \times 10^2$	1.6854	1.6903	1.6776	1.6760
		$\bar{\sigma}_{xx}$	0.1718	0.1817	0.2204	0.2358
		$\bar{\sigma}_{xz}$	0.4045	0.4120	0.4509	0.4566
100	F	$\bar{w} \times 10^2$	0.0386	1.1222	1.3982	1.3546
		$\bar{\sigma}_{xx}$	0.0041	0.0947	0.0204	0.1825
		$\bar{\sigma}_{xz}$	0.3734	0.4732	0.4229	0.4862
100	S	$\bar{w} \times 10^2$	1.4093	1.4382	1.4219	1.4268
		$\bar{\sigma}_{xx}$	0.1731	0.1846	0.2337	0.2417
		$\bar{\sigma}_{xz}$	0.4236	0.4255	0.4729	0.4776
100	R	$\bar{w} \times 10^2$	1.4334	1.4417	1.4279	1.4271
		$\bar{\sigma}_{xx}$	0.1762	0.1853	0.2346	0.2418
		$\bar{\sigma}_{xz}$	0.4234	0.4284	0.4727	0.4779
100	CPT(C)	4 × 4	$\bar{w} \times 10^2 = 1.4370$ ; $\bar{\sigma}_{xx} = 0.1649$			

6.8.3 Results of Nonlinear Analysis

Here we consider several examples of the nonlinear bending of rectangular plates using the nonlinear FSDT element. The effect of the integration rule to evaluate the nonlinear and transverse shear stiffness coefficients is investigated in the first example. Unless stated otherwise, a uniform mesh of  $4 \times 4$  nine-node quadratic elements is used in a quarter plate for the FSDT. For this choice of mesh, full integration (F) is to use  $3 \times 3$  Gauss rule and reduced integration (R) is to use  $2 \times 2$  Gauss rule. Stresses are calculated at the center of the element. The shear correction coefficient is taken to be  $K_s = 5/6$ .

Example 6.8.3

Consider an isotropic, square plate with

$$a = b = 10 \text{ in.}, \quad h = 1 \text{ in.}, \quad E = 7.8 \times 10^6 \text{ psi}, \quad \nu = 0.3 \quad (6.8.7)$$

Two types of simply supported boundary conditions are studied. The displacement boundary conditions used for SS-1 and SS-3 are (see Figures 6.8.1 and 6.8.2, respectively)

$$\text{SS-1:} \quad \text{At } x = a/2: \quad v_0 = w_0 = \phi_y = 0; \quad \text{At } y = b/2: \quad u_0 = w_0 = \phi_x = 0 \quad (6.8.8)$$

$$\text{SS-3:} \quad u_0 = v_0 = w_0 = 0 \quad \text{on simply supported edges} \quad (6.8.9)$$

Uniformly distributed load of intensity  $q_0$  is used. The boundary conditions along the symmetry lines for both cases are given by Eq. (6.8.1). It is clear that SS-3 provides more edge restraint than SS-1 and therefore should produce lower transverse deflections.

Using the load parameter introduced earlier,  $\bar{P} \equiv q_0 a^4 / E_2 h^4$ , the incremental load vector is chosen to be

$$\{\Delta P\} = \{6.25, 6.25, 12.5, 25.0, 25.0, \dots, 25.0\}$$

A tolerance of  $\epsilon = 10^{-2}$  is used for convergence in the Newton-Raphson iteration scheme to check for convergence of the nodal displacements.

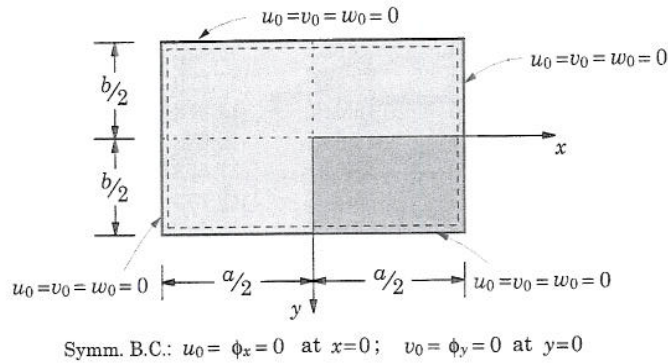


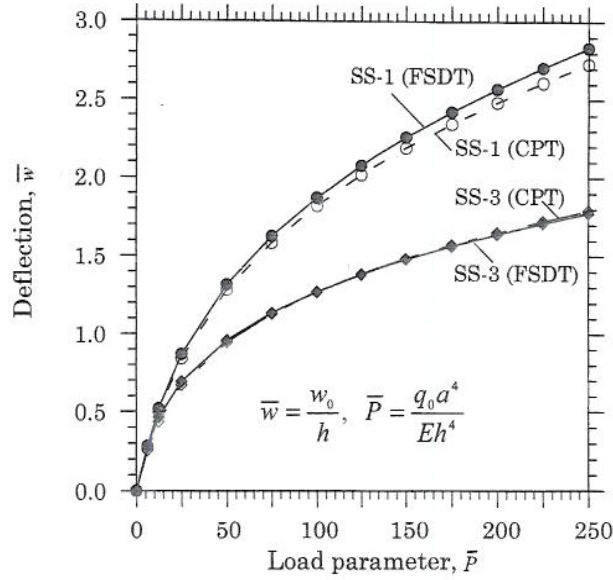
Figure 6.8.2 Geometric boundary conditions used for SS-3 type simply supported rectangular plates.

Table 6.8.5 contains the deflections  $w_0(0,0)$  and normal stresses  $\bar{\sigma}_{xx} = \sigma_{xx}(a^2/Eh)$  obtained with a uniform mesh of  $4 \times 4$  Q9 FSDT elements for various integration rules (also see Figure 6.8.3). The number of iterations taken for convergence are listed in parentheses. The linear FSDT plate solution for load  $q_0 = 4875$ psi (or  $\bar{P} = 6.25$ ) is  $w_0 = 0.2917$ ; for SS-1 and  $w_0 = 0.315$ in. for SS-3 (when reduced integration is used to evaluate transverse shear stiffnesses). As discussed earlier, the  $4 \times 4$  Q9 meshes are not sensitive to shear or membrane locking, and therefore the results obtained with various integration rules are essentially the same.

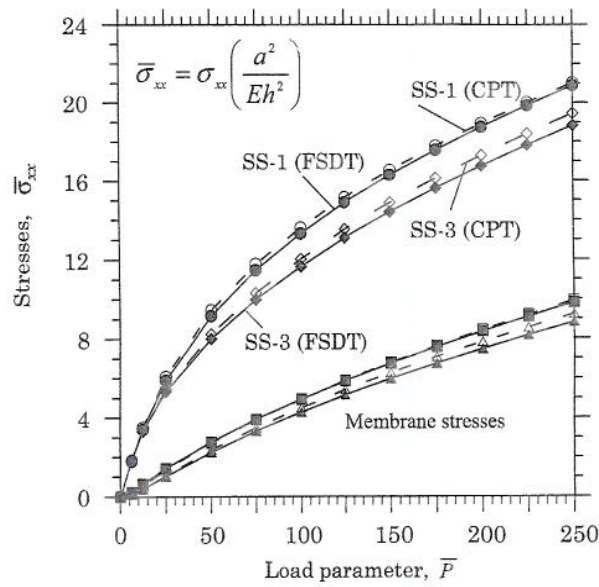
**Table 6.8.5** Center deflection  $\bar{w}$  and stresses  $\bar{\sigma}_{xx}$  of a simply supported (SS-1 and SS-3) plates under uniformly distributed load (Example 6.8.3).

$\bar{P}$	SS-3			SS-1		
	R-R*	F-R	F-F	R-R	F-R	F-F
Deflections, $w_0(0,0)$						
6.25	0.2790 (3)	0.2790 (4)	0.2780 (3)	0.2813 (3)	0.2813 (3)	0.2812 (3)
12.5	0.4630 (3)	0.4630 (3)	0.4619 (3)	0.5186 (3)	0.5186 (3)	0.5185 (3)
25.0	0.6911 (3)	0.6911 (3)	0.6902 (3)	0.8673 (4)	0.8673 (4)	0.8672 (4)
50.0	0.9575 (3)	0.9575 (3)	0.9570 (3)	1.3149 (4)	1.3149 (4)	1.3147 (4)
75.0	1.1333 (3)	1.1333 (3)	1.1330 (3)	1.6241 (3)	1.6239 (3)	1.6237 (3)
100.0	1.2688 (3)	1.2688 (3)	1.2686 (3)	1.8687 (3)	1.8683 (3)	1.8679 (3)
125.0	1.3809 (2)	1.3809 (2)	1.3808 (2)	2.0758 (2)	2.0751 (2)	2.0746 (2)
150.0	1.4774 (2)	1.4774 (2)	1.4774 (2)	2.2567 (2)	2.2556 (2)	2.2549 (2)
175.0	1.5628 (2)	1.5629 (2)	1.5629 (2)	2.4194 (2)	2.4177 (2)	2.4168 (2)
200.0	1.6398 (2)	1.6399 (2)	1.6399 (2)	2.5681 (2)	2.5657 (2)	2.5645 (2)
225.0	1.7102 (2)	1.7103 (2)	1.7103 (2)	2.7056 (2)	2.7023 (2)	2.7009 (2)
250.0	1.7752 (2)	1.7753 (2)	1.7754 (2)	2.8338 (2)	2.8296 (2)	2.8279 (2)
Normal stresses, $\bar{\sigma}_{xx}(0.625, 0.625, h/2)$						
6.25	1.861	1.861	1.856	1.779	1.779	1.780
12.5	3.305	3.305	3.300	3.396	3.396	3.398
25.0	5.319	5.320	5.317	5.882	5.882	5.885
50.0	8.001	8.002	8.001	9.159	9.162	9.165
75.0	9.983	9.984	9.983	11.458	11.462	11.465
100.0	11.633	11.634	11.634	13.299	13.307	13.308
125.0	13.084	13.085	13.085	14.878	14.890	14.889
150.0	14.396	14.398	14.398	16.278	16.293	16.290
175.0	15.608	15.610	15.610	17.553	17.572	17.567
200.0	16.741	16.743	16.743	18.733	18.755	18.748
225.0	17.811	17.813	17.812	19.837	19.863	19.854
250.0	18.828	18.831	18.829	20.880	20.909	20.898

\* The first letter refers to the integration rule used for the nonlinear terms while the second letter refers to the integration rule used for the shear terms.



(a)



(b)

**Figure 6.8.3** Plots of (a) center deflection  $w_0$  versus load  $\bar{P}$  and (b) center normal stress  $\bar{\sigma}_{xx}$  versus load  $\bar{P}$  for isotropic ( $\nu = 0.3$ ), simply supported square plates under uniformly distributed load ( $4 \times 4Q9$  for FSDT and  $8 \times 8C$  for CPT).



**Example 6.8.4**

Orthotropic plates subjected to uniformly distributed transverse load (i.e.  $q = q_0 = \text{constant}$ ) are analyzed. The geometric and material parameters used are

$$a = b = 12 \text{ in.}, \quad h = 0.138 \text{ in.}, \quad E_1 = 3 \times 10^6 \text{ psi}, \quad E_2 = 1.28 \times 10^6 \text{ psi}$$

$$G_{12} = G_{13} = G_{23} = 0.37 \times 10^6 \text{ psi}, \quad \nu_{12} = 0.32 \tag{6.8.1}$$

A uniform mesh of  $4 \times 4Q9$  elements with reduced integration is used in a quadrant. The incremental load vector is chosen to be

$$\{\Delta P\} = \{0.05, 0.05, 0.1, 0.2, 0.2, \dots, 0.2\}$$

Twelve load steps are used, and a tolerance of  $\epsilon = 0.01$  is used for convergence.

Plots of load  $q_0$  (psi) versus center deflection  $w_0$  (in.) and  $q_0$  versus normal stress (total as well as membrane)  $\bar{\sigma}_{xx} = \sigma_{xx}(a^2/E_2h^2)$  are shown in Figure 6.8.4 for SS1 and SS3 plate. The figures also show the results obtained using  $8 \times 8$  mesh of conforming CPT element. Table 6.8.6 contains the center deflection and total normal stress as a function of the load for the two boundary conditions. The linear FSDT solution for load  $q_0 = 0.05$  is  $w_0 = 0.0113$  for SS-1 and  $w_0 = 0.01140$  for SS-3.

**Table 6.8.6** Center deflection  $w_0$  and normal stress  $\bar{\sigma}_{xx}$  for simply supported orthotropic square plates under uniform distributed load ( $4 \times 4Q9$ ; Example 6.8.4).

$q_0$	SS-1			SS-3		
	CPT $w_0$	FSDT $w_0$	FSDT $\bar{\sigma}_{xx}$	CPT $w_0$	FSDT $w_0$	FSDT $\bar{\sigma}_{xx}$
0.05	0.0113 (2)	0.0113	1.034	0.0112	0.0113	1.056
0.10	0.0224 (2)	0.0224	2.070	0.0217	0.0218	2.116
0.20	0.0438 (3)	0.0439	4.092	0.0395	0.0397	4.058
0.40	0.0812 (3)	0.0815	7.716	0.0648	0.0650	7.103
0.60	0.1116 (3)	0.1122	10.702	0.0823	0.0824	9.406
0.80	0.1367 (3)	0.1377	13.169	0.0957	0.0959	11.284
1.00	0.1581 (2)	0.1594	15.255	0.1068	0.1069	12.894
1.20	0.1767 (2)	0.1783	17.050	0.1162	0.1162	14.316
1.40	0.1932 (2)	0.1951	18.631	0.1245	0.1244	15.602
1.60	0.2081 (2)	0.2103	20.044	0.1318	0.1318	16.783
1.80	0.2217 (2)	0.2241	21.324	0.1385	0.1384	17.880
2.00	0.2343 (2)	0.2370	22.495	0.1447	0.1445	18.909

**Example 6.8.5**

Here, we analyze an orthotropic plate with clamped edges, that is, all generalized displacements are zero on the boundary (see Figure 6.8.5). The boundary conditions of a clamped edge are taken to be

$$u_0 = v_0 = w_0 = \phi_x = \phi_y = 0 \tag{6.8.11}$$

The geometric and material parameters used are the same as those listed in Eq. (6.8.10). A uniformly distributed load of intensity  $q_0$  is used.

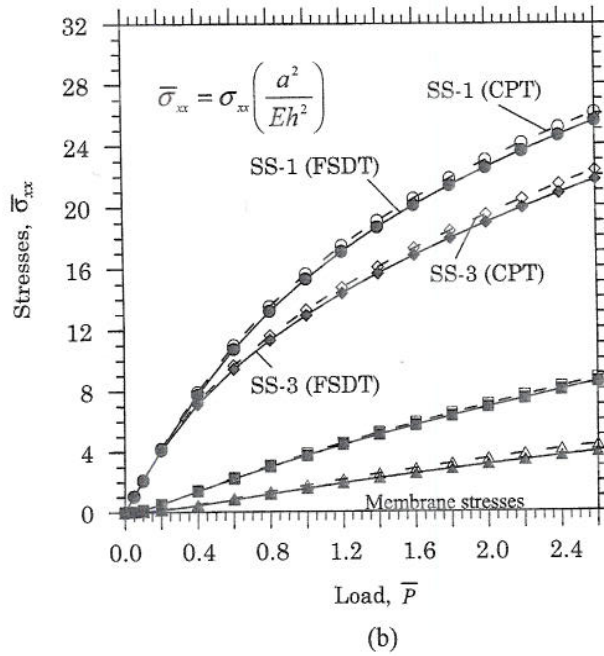
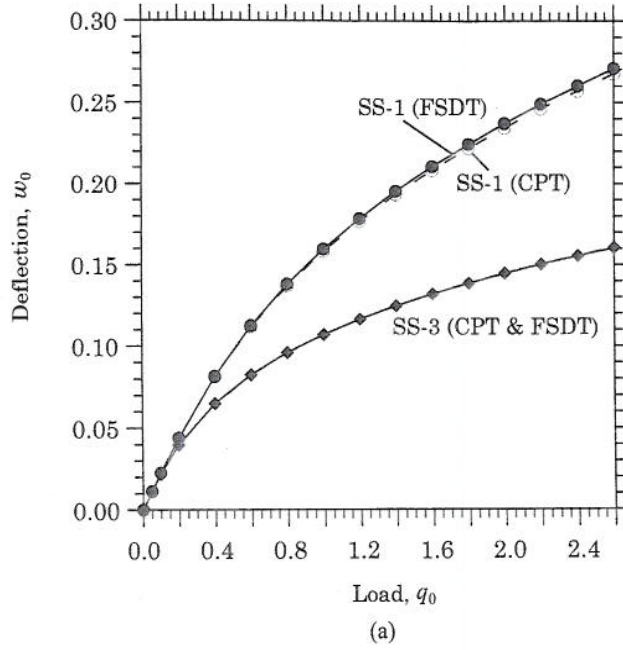
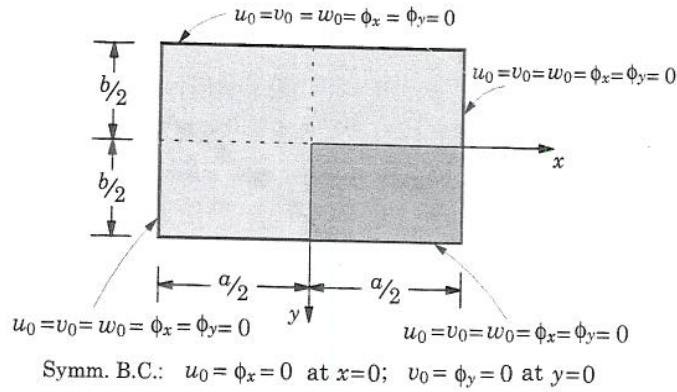
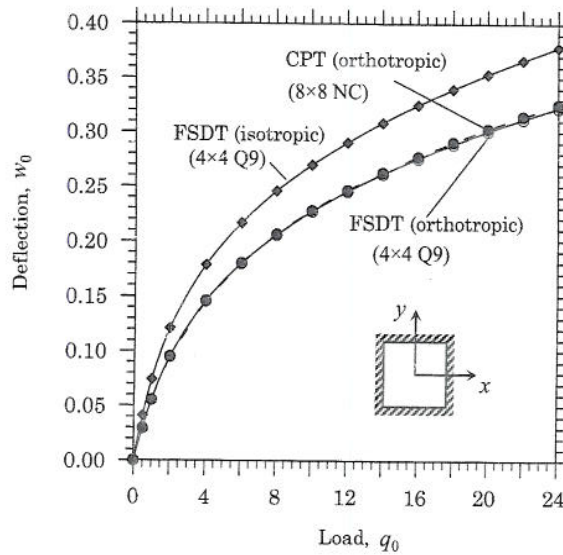


Figure 6.8.4 Center deflection  $w_0(0, 0)$  and stresses  $\bar{\sigma}_{xx}$  as functions of the load  $q_0$  for simply supported, orthotropic, square plates under uniformly distributed load (Example 6.8.4).



**Figure 6.8.5** Boundary conditions for a rectangular plate with clamped edges.

The linear solution for load  $q_0 = 0.5$  is  $w_0 = 0.0301$ . Figure 6.8.6 contains a plot of load versus center deflection, and Table 6.8.7 contains center deflections and stresses for the problem (see [36–38]). Figure 6.8.6 also contains plots of the CPT deflections obtained using  $8 \times 8$  mesh of the non-conforming elements and FSDT deflections of an isotropic plate ( $h = 0.138$  in.,  $E = 1.28 \times 10^6$  psi, and  $\nu = 0.3$ ) obtained with  $4 \times 4$  Q9 mesh.



**Figure 6.8.6** Nonlinear center deflection  $w_0$  versus load parameter  $q_0$  for clamped, orthotropic, square plates under uniform load.

**Table 6.8.7** Center deflection  $w_0$  and normal stress  $\bar{\sigma}_{xx}$  for clamped orthotropic square plates under uniformly distributed load ( $4 \times 4Q9$ ).

$q_0$	$w_0$	$\bar{\sigma}_{xx}$	$q_0$	$w_0$	$\bar{\sigma}_{xx}$
0.5	0.0294 (3)	4.317	12.0	0.2450 (2)	46.001
1.0	0.0552 (3)	8.467	14.0	0.2610 (2)	49.851
2.0	0.0948 (3)	15.309	16.0	0.2754 (2)	53.431
4.0	0.1456 (3)	24.811	18.0	0.2886 (2)	56.800
6.0	0.1795 (3)	31.599	20.0	0.3006 (2)	59.998
8.0	0.2054 (3)	37.078	22.0	0.3119 (2)	63.053
10.0	0.2268 (2)	41.793	24.0	0.3224 (2)	65.986

**Example 6.8.6**

The last example is concerned with the nonlinear bending of a clamped, isotropic, circular plate under uniformly distributed load. Recall that axisymmetric bending of circular plates may be studied using one-dimensional bending elements (see Problems 4.5–4.8).

Figure 6.8.7 shows the finite element mesh and boundary conditions of a quadrant of a circular plate. The exact center deflection for the linear case is given by (see Reddy [2,3])

$$w_0(0) = \frac{q_0 a^4}{64D} \left( 1 + \frac{8}{3(1-\nu)K_s} \frac{h^2}{a^2} \right) \tag{6.8.12}$$

where  $a$  denotes the radius of the plate. For  $\nu = 0.3$ ,  $K_s = 5/6$ , and  $a/h = 10$ , the center deflection is given by  $w_0(0) = 1.0457(q_0 a^4 / 64D)$ . The linear FSDT solution obtained with the mesh of five nine-node quadratic elements is  $w_0(0) = 1.0659(q_0 a^4 / 64D)$  (1.2% error). Figure 6.8.8 shows the load–deflection curve for the problem ( $a = 100$  in.,  $h = 10$  in.,  $E = 10^6$  psi, and  $\nu = 0.3$ ).

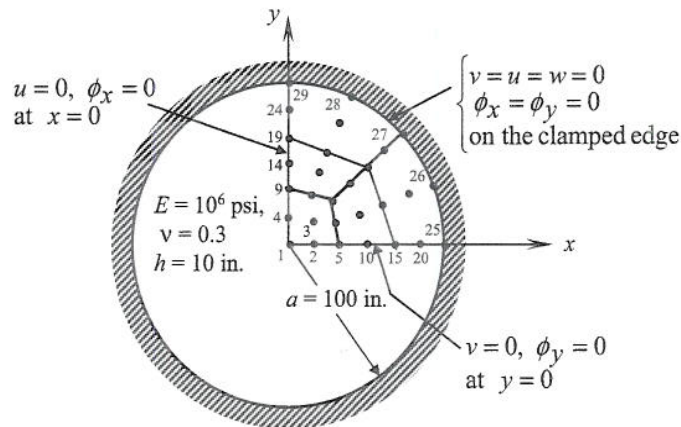


**Figure 6.8.7** Mesh and boundary conditions used for a clamped circular plate.

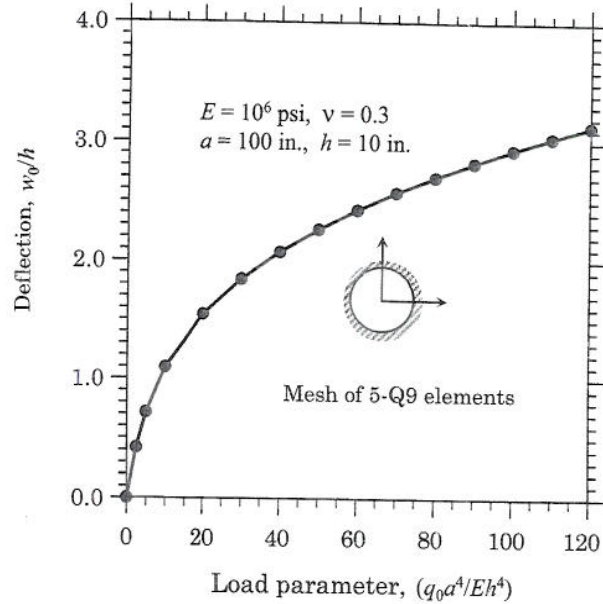


Figure 6.8.8 Load-deflection curve for clamped isotropic circular plate under uniform load.

## 6.9 Theory of Doubly-Curved Shells

### 6.9.1 Introduction

In this section, we review the governing equations of shells. A number of shell theories exist in the literature, and many of these theories were developed originally for thin shells and are based on the Kirchhoff-Love kinematic hypothesis that straight lines normal to the undeformed midsurface remain straight and normal to the middle surface after deformation. A detailed study of thin isotropic shells can be found in the monographs by Ambartsumyan [41-43], Flügge [44], Kraus [45], Timoshenko and Woinowsky-Krieger [46] and Dym [47]. The first-order shear deformation theory of shells, also known as the Sanders' shell theory [48,49], can be found in Kraus [45].

Following this introduction, the equilibrium equations and strain-displacement relations are presented. For additional details, one may consult [40, 44-52]. The finite element models of doubly-curved shells is presented in Section 6.10.

### 6.9.2 Geometric Description

Figure 6.9.1(a) shows a uniform thickness shell, where  $(\xi_1, \xi_2, \zeta)$  denote the orthogonal curvilinear coordinates such that  $\xi_1$  and  $\xi_2$  curves are the lines of curvature on the middle surface ( $\zeta = 0$ ). The position vector of a typical point  $(\xi_1, \xi_2, 0)$  on the middle surface is denoted by  $\mathbf{r}$ , and the position of an arbitrary point  $(\xi_1, \xi_2, \zeta)$  in the shell is denoted by  $\mathbf{R}$ , as shown in Figure 6.9.2(b). The square of the distance  $ds$  between points  $(\xi_1, \xi_2, 0)$  and  $(\xi_1 + d\xi_1, \xi_2 + d\xi_2, 0)$  is determined by (see Reddy [40, 50])

$$(ds)^2 = d\mathbf{r} \cdot d\mathbf{r} = a_1^2(d\xi_1)^2 + a_2^2(d\xi_2)^2 \quad (6.9.1a)$$

$$d\mathbf{r} = \mathbf{g}_1 d\xi_1 + \mathbf{g}_2 d\xi_2, \quad \mathbf{g}_\alpha = \frac{\partial \mathbf{r}}{\partial \xi_\alpha}, \quad g_{\alpha\beta} = \mathbf{g}_\alpha \cdot \mathbf{g}_\beta \quad (6.9.1b)$$

where the vectors  $\mathbf{g}_1$  and  $\mathbf{g}_2$  are tangent to the  $\xi_1$  and  $\xi_2$  coordinate lines,  $g_{\alpha\beta}$  ( $\alpha, \beta = 1, 2$ ) is called the *surface metric tensor* and  $a_\alpha$  ( $\alpha = 1, 2$ ) are

$$a_\alpha = \sqrt{g_{\alpha\alpha}}, \quad (\text{no sum on } \alpha) \quad (6.9.2)$$

Note that  $\mathbf{g}_1 \cdot \mathbf{g}_2 = 0$  when the lines of principal curvature coincide with the coordinate lines.

The unit vector normal to the middle surface can be determined from

$$\hat{\mathbf{n}} = \frac{\mathbf{g}_1 \times \mathbf{g}_2}{a_1 a_2} \quad (6.9.3)$$

Further, we have the Weingarten–Gauss relations

$$\frac{\partial \hat{\mathbf{n}}}{\partial \xi_\alpha} = \frac{\mathbf{g}_\alpha}{R_\alpha}, \quad (\text{no sum on } \alpha) \quad (\text{theorem of Rodrigues}) \quad (6.9.4)$$

$$\frac{\partial}{\partial \xi_2} \left( \frac{a_1}{R_1} \right) = \frac{1}{R_2} \frac{\partial a_1}{\partial \xi_2}, \quad \frac{\partial}{\partial \xi_1} \left( \frac{a_2}{R_2} \right) = \frac{1}{R_1} \frac{\partial a_2}{\partial \xi_1} \quad (\text{Codazzi conditions}) \quad (6.9.5)$$

The values of the principal radii of curvature of the middle surface are denoted by  $R_1$  and  $R_2$  [see Figure 6.9.1(c)]. In general,  $\hat{\mathbf{n}}$ ,  $R_1$  and  $R_2$  are functions of  $\xi_1$  and  $\xi_2$ .

The position vector  $\mathbf{R}$  of a point at a distance  $\zeta$  from the middle surface can be expressed in terms of  $\mathbf{r}$  and  $\hat{\mathbf{n}}$  by [see Figure 6.9.1(b)]

$$\mathbf{R} = \mathbf{r} + \zeta \hat{\mathbf{n}} \quad (6.9.6)$$

By differentiation we have

$$\frac{\partial \mathbf{R}}{\partial \xi_\alpha} = \mathbf{g}_\alpha + \zeta \frac{\partial \hat{\mathbf{n}}}{\partial \xi_\alpha} \equiv \mathbf{G}_\alpha \quad (6.9.7)$$

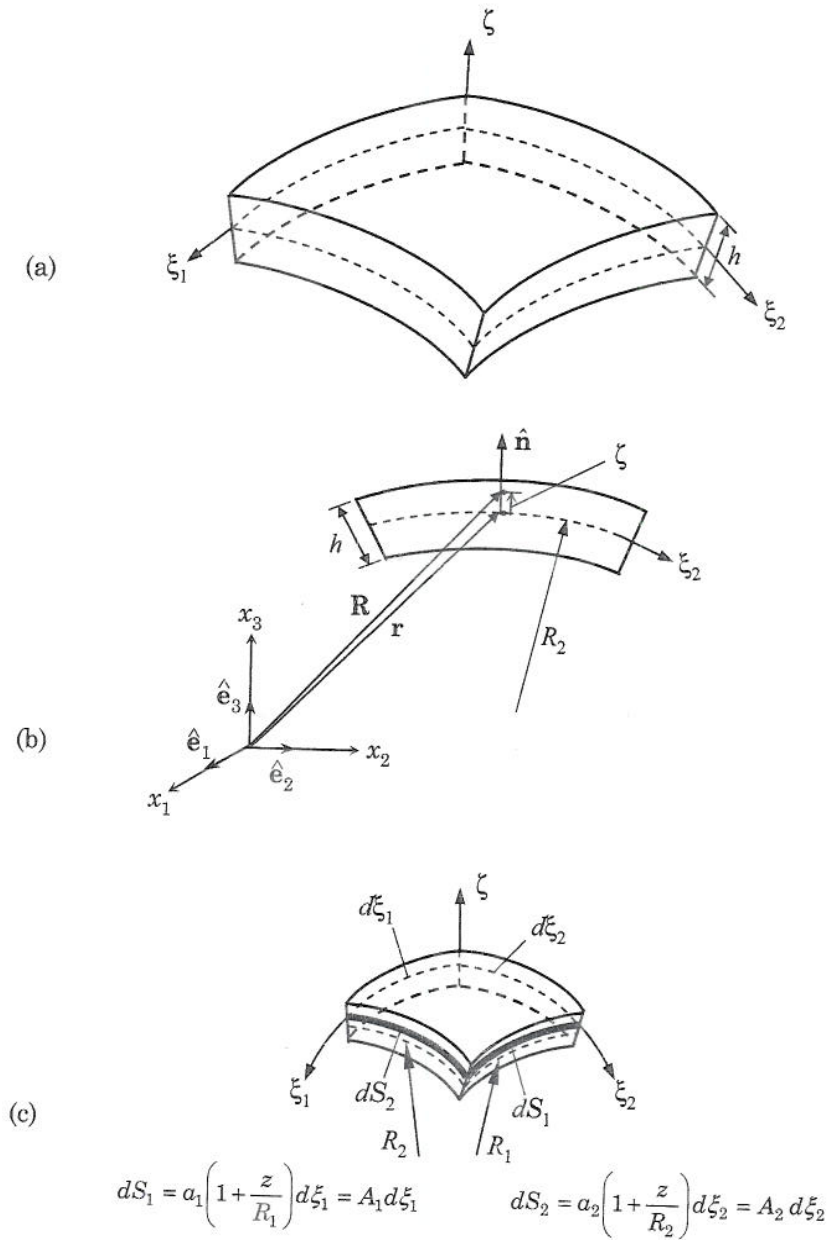


**Figure 6.9.1** Geometry of a doubly-curved shell [50]. (a) Shell geometry. (b) Position vectors of points on the midsurface and above the midsurface. (c) A differential element of the shell ( $dS_1$  and  $dS_2$  denote the arc lengths).

and using Eq. (6.9.4) we obtain

$$\mathbf{G}_\alpha = \frac{\partial \mathbf{R}}{\partial \xi_\alpha} = \left(1 + \frac{\zeta}{R_\alpha}\right) \mathbf{g}_\alpha, \quad (\text{no sum on } \alpha) \quad (6.9.8a)$$

and

$$G_{\alpha\beta} \equiv \mathbf{G}_\alpha \cdot \mathbf{G}_\beta \quad (6.9.8b)$$

Hence, the square of the distance  $dS$  between points  $(\xi_1, \xi_2, \zeta)$  and  $(\xi_1 + d\xi_1, \xi_2 + d\xi_2, \zeta + d\zeta)$  is given by

$$(dS)^2 = d\mathbf{R} \cdot d\mathbf{R} = A_1^2(d\xi_1)^2 + A_2^2(d\xi_2)^2 + A_3^2(d\zeta)^2 \quad (6.9.9a)$$

in which

$$d\mathbf{R} = \mathbf{G}_1 d\xi_1 + \mathbf{G}_2 d\xi_2 + \hat{\mathbf{n}} d\zeta, \quad (6.9.9b)$$

and  $A_1, A_2$ , and  $A_3$  are the Lamé coefficients [see Fig. 6.9.1(c)]

$$A_1 = a_1 \left(1 + \frac{\zeta}{R_1}\right) = \sqrt{G_{11}}, \quad A_2 = a_2 \left(1 + \frac{\zeta}{R_2}\right) = \sqrt{G_{22}}, \quad A_3 = 1 \quad (6.9.10)$$

Note that vector  $\mathbf{G}_\alpha$  is parallel to the vector  $\mathbf{g}_\alpha$ . In view of the Codazzi conditions (6.9.5) and Eq. (6.9.10), it can be shown that the following relations between the derivatives of  $a_\alpha$  and  $A_\alpha$  hold:

$$\frac{1}{A_2} \frac{\partial A_1}{\partial \xi_2} = \frac{1}{a_2} \frac{\partial a_1}{\partial \xi_2}, \quad \frac{1}{A_1} \frac{\partial A_2}{\partial \xi_1} = \frac{1}{a_1} \frac{\partial a_2}{\partial \xi_1} \quad (6.9.11)$$

From Figure 6.9.1(c) the elements of area of the cross sections are

$$\begin{aligned} dS_1 d\zeta &= A_1 d\xi_1 d\zeta = a_1 \left(1 + \frac{\zeta}{R_1}\right) d\xi_1 d\zeta, \\ dS_2 d\zeta &= A_2 d\xi_2 d\zeta = a_2 \left(1 + \frac{\zeta}{R_2}\right) d\xi_2 d\zeta \end{aligned} \quad (6.9.12)$$

An elemental area of the middle surface ( $\zeta = 0$ ) is determined by [see Figure 6.9.2(a)]

$$dA_0 = d\mathbf{r}_1 \times d\mathbf{r}_2 \cdot \hat{\mathbf{n}} = \left(\frac{\partial \mathbf{r}}{\partial \xi_1} \times \frac{\partial \mathbf{r}}{\partial \xi_2} \cdot \hat{\mathbf{n}}\right) d\xi_1 d\xi_2 = a_1 a_2 d\xi_1 d\xi_2 \quad (6.9.13)$$

and an elemental area of the surface at  $\zeta$  is given by [see Figure 6.9.2(b)]

$$dA_\zeta = d\mathbf{R}_1 \times d\mathbf{R}_2 \cdot \hat{\mathbf{n}} = \left(\frac{\partial \mathbf{R}}{\partial \xi_1} \times \frac{\partial \mathbf{R}}{\partial \xi_2} \cdot \hat{\mathbf{n}}\right) d\xi_1 d\xi_2 = A_1 A_2 d\xi_1 d\xi_2 \quad (6.9.14)$$



The volume of a differential element above the midsurface is given by

$$dV = d\mathbf{R}_1 \times d\mathbf{R}_2 \cdot \hat{\mathbf{n}} d\zeta = dA_\zeta d\zeta = A_1 A_2 d\xi_1 d\xi_2 d\zeta \quad (6.9.15)$$

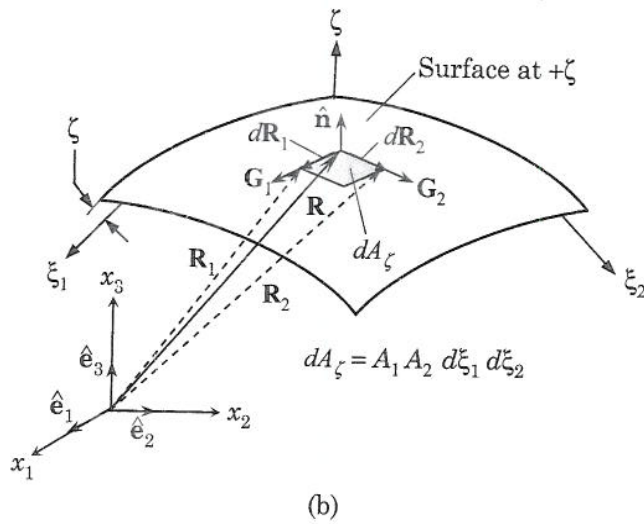
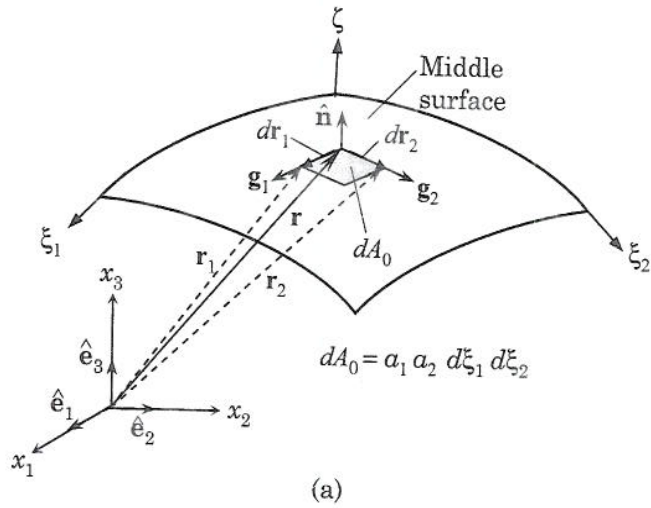


Figure 6.9.2 Surface area elements of a doubly-curved shell [50]. (a) Area element on the midsurface. (b) Area element on a surface at  $+\zeta$ .

### 6.9.3 Strain-Displacement Relations

The engineering components of the Green-Lagrange strain tensor in an orthogonal curvilinear coordinate system are given by (no sum on repeated indices; see [51])

$$\begin{aligned} \varepsilon_i = & \frac{\partial}{\partial \xi_i} \left( \frac{u_i}{A_i} \right) + \frac{1}{A_i} \sum_{k=1}^3 \frac{u_k}{A_k} \frac{\partial A_i}{\partial \xi_k} + \frac{1}{2} \left[ \frac{\partial}{\partial \xi_i} \left( \frac{u_i}{A_i} \right) + \frac{1}{A_i} \sum_{k=1}^3 \frac{u_k}{A_k} \frac{\partial A_i}{\partial \xi_k} \right]^2 \\ & + \frac{1}{2A_i^2} \sum_{k=1, k \neq i}^3 \left( \frac{\partial u_k}{\partial \xi_i} - \frac{u_i}{A_k} \frac{\partial A_i}{\partial \xi_k} \right)^2 \end{aligned} \quad (6.9.16a)$$

$$\begin{aligned} \gamma_{ij} = & \frac{A_i}{A_j} \frac{\partial}{\partial \xi_j} \left( \frac{u_i}{A_i} \right) + \frac{A_j}{A_i} \frac{\partial}{\partial \xi_i} \left( \frac{u_j}{A_j} \right) \\ & + \sum_{k=1, k \neq i}^3 \frac{1}{A_i A_j} \left( \frac{\partial u_k}{\partial \xi_i} - \frac{u_i}{A_k} \frac{\partial A_i}{\partial \xi_k} \right) \left( \frac{\partial u_k}{\partial \xi_j} - \frac{u_j}{A_k} \frac{\partial A_j}{\partial \xi_k} \right) \\ & + \frac{1}{A_j} \left( \frac{\partial u_i}{\partial \xi_j} - \frac{u_j}{A_i} \frac{\partial A_j}{\partial \xi_i} \right) \left[ \frac{\partial}{\partial \xi_i} \left( \frac{u_i}{A_i} \right) + \frac{1}{A_i} \sum_{k=1}^3 \frac{u_k}{A_k} \frac{\partial A_i}{\partial \xi_k} \right] \\ & + \frac{1}{A_i} \left( \frac{\partial u_j}{\partial \xi_i} - \frac{u_i}{A_j} \frac{\partial A_i}{\partial \xi_j} \right) \left[ \frac{\partial}{\partial \xi_j} \left( \frac{u_j}{A_j} \right) + \frac{1}{A_j} \sum_{k=1}^3 \frac{u_k}{A_k} \frac{\partial A_j}{\partial \xi_k} \right] \end{aligned} \quad (6.9.16b)$$

where  $i \neq j$  in Eq. (6.9.16b), and

$$\xi_3 = \zeta, \quad A_1 = a_1 \left( 1 + \frac{\zeta}{R_1} \right), \quad A_2 = a_2 \left( 1 + \frac{\zeta}{R_2} \right), \quad A_3 = a_3 = 1 \quad (6.9.17)$$

Substituting equation (6.9.17) into (6.9.16a,b) and making use of conditions (6.9.10) and (6.9.11), one obtains

$$\begin{aligned} \varepsilon_1 = & \frac{1}{A_1} \left( \frac{\partial u_1}{\partial \xi_1} + \frac{1}{a_2} \frac{\partial a_1}{\partial \xi_2} u_2 + \frac{a_1}{R_1} u_3 \right) + \frac{1}{2A_1^2} \left[ \left( \frac{\partial u_1}{\partial \xi_1} + \frac{u_2}{a_2} \frac{\partial a_1}{\partial \xi_2} + \frac{a_1}{R_1} u_3 \right)^2 \right. \\ & \left. + \left( \frac{\partial u_2}{\partial \xi_1} - \frac{u_1}{a_2} \frac{\partial a_1}{\partial \xi_2} \right)^2 + \left( \frac{\partial u_3}{\partial \xi_1} - \frac{a_1}{R_1} u_1 \right)^2 \right] \\ \varepsilon_2 = & \frac{1}{A_2} \left( \frac{\partial u_2}{\partial \xi_2} + \frac{1}{a_1} \frac{\partial a_2}{\partial \xi_1} u_1 + \frac{a_2}{R_2} u_3 \right) + \frac{1}{2A_2^2} \left[ \left( \frac{\partial u_2}{\partial \xi_2} + \frac{u_1}{a_1} \frac{\partial a_2}{\partial \xi_1} + \frac{a_2}{R_2} u_3 \right)^2 \right. \\ & \left. + \left( \frac{\partial u_1}{\partial \xi_2} - \frac{u_2}{a_1} \frac{\partial a_2}{\partial \xi_1} \right)^2 + \left( \frac{\partial u_3}{\partial \xi_2} - \frac{a_2}{R_2} u_2 \right)^2 \right] \\ \varepsilon_3 = & \frac{\partial u_3}{\partial \zeta} + \frac{1}{2} \left[ \left( \frac{\partial u_1}{\partial \zeta} \right)^2 + \left( \frac{\partial u_2}{\partial \zeta} \right)^2 + \left( \frac{\partial u_3}{\partial \zeta} \right)^2 \right] \end{aligned}$$

$$\begin{aligned}
 \gamma_{23} &= \frac{1}{A_2} \frac{\partial u_3}{\partial \xi_2} + A_2 \frac{\partial}{\partial \zeta} \left( \frac{u_2}{A_2} \right) + \frac{1}{A_2} \left[ \frac{\partial u_2}{\partial \zeta} \left( \frac{\partial u_2}{\partial \xi_2} + \frac{u_1}{a_1} \frac{\partial a_2}{\partial \xi_1} + \frac{a_2}{R_2} u_3 \right) \right. \\
 &\quad \left. + \frac{\partial u_1}{\partial \zeta} \left( \frac{\partial u_1}{\partial \xi_2} - \frac{u_2}{a_1} \frac{\partial a_2}{\partial \xi_1} \right) + \frac{\partial u_3}{\partial \zeta} \left( \frac{\partial u_3}{\partial \xi_2} - \frac{a_2}{R_2} u_2 \right) \right] \\
 \gamma_{13} &= \frac{1}{A_1} \frac{\partial u_3}{\partial \xi_1} + A_1 \frac{\partial}{\partial \zeta} \left( \frac{u_1}{A_1} \right) + \frac{1}{A_1} \left[ \frac{\partial u_1}{\partial \zeta} \left( \frac{\partial u_1}{\partial \xi_1} + \frac{u_2}{a_2} \frac{\partial a_1}{\partial \xi_2} + \frac{a_1}{R_1} u_3 \right) \right. \\
 &\quad \left. + \frac{\partial u_2}{\partial \zeta} \left( \frac{\partial u_2}{\partial \xi_1} - \frac{u_1}{a_2} \frac{\partial a_1}{\partial \xi_2} \right) + \frac{\partial u_3}{\partial \zeta} \left( \frac{\partial u_3}{\partial \xi_1} - \frac{a_1}{R_1} u_1 \right) \right] \\
 \gamma_{12} &= \frac{A_2}{A_1} \frac{\partial}{\partial \xi_1} \left( \frac{u_2}{A_2} \right) + \frac{A_1}{A_2} \frac{\partial}{\partial \xi_2} \left( \frac{u_1}{A_1} \right) \\
 &\quad + \frac{1}{A_1 A_2} \left[ \left( \frac{\partial u_1}{\partial \xi_2} - \frac{u_2}{a_1} \frac{\partial a_2}{\partial \xi_1} \right) \left( \frac{\partial u_1}{\partial \xi_1} + \frac{1}{a_2} \frac{\partial a_1}{\partial \xi_2} u_2 + \frac{a_1}{R_1} u_3 \right) \right. \\
 &\quad + \left( \frac{\partial u_2}{\partial \xi_1} - \frac{u_1}{a_2} \frac{\partial a_1}{\partial \xi_2} \right) \left( \frac{\partial u_2}{\partial \xi_2} + \frac{1}{a_1} \frac{\partial a_2}{\partial \xi_1} u_1 + \frac{a_2}{R_2} u_3 \right) \\
 &\quad \left. + \left( \frac{\partial u_3}{\partial \xi_1} - \frac{a_1}{R_1} u_1 \right) \left( \frac{\partial u_3}{\partial \xi_2} - \frac{a_2}{R_2} u_2 \right) \right] \tag{6.9.18}
 \end{aligned}$$

#### 6.9.4 Stress Resultants

Next, we introduce the stress resultants acting on a shell element. The tensile force measured per unit length along a  $\xi_2$  coordinate line on a cross section perpendicular to a  $\xi_1$  coordinate line [see Figure 6.9.1(c)] is  $\sigma_{11} dS_2$ . The total tensile force on the differential element in the  $\xi_1$  direction can be computed by integrating over the entire thickness of the shell:

$$\int_{-h/2}^{h/2} \sigma_{11} dS_2 d\zeta = a_2 \left[ \int_{-h/2}^{h/2} \sigma_{11} \left( 1 + \frac{\zeta}{R_2} \right) d\zeta \right] d\xi_2 \equiv N_{11} a_2 d\xi_2 \tag{6.9.19}$$

where  $h$  the total thickness of the shell,  $\zeta = -h/2$  and  $\zeta = h/2$  denote the bottom and top surfaces of the shell, and  $N_{11}$  is the membrane force per unit length in  $\xi_1$  direction, acting on a surface perpendicular to the  $\xi_1$ -coordinate (see Figure 6.9.3):

$$N_{11} = \int_{-h/2}^{h/2} \sigma_{11} \left( 1 + \frac{\zeta}{R_2} \right) d\zeta \tag{6.9.20a}$$

Analogously, the moment of the force  $\sigma_{11} dS_2$  about the  $\xi_2$ -axis is

$$M_{11} = \int_{-h/2}^{h/2} \zeta \sigma_{11} \left( 1 + \frac{\zeta}{R_2} \right) d\zeta \tag{6.9.20b}$$

Thus, the stress resultants per unit length can be defined as follows ( $N_1 = N_{11}$ ,  $N_6 = N_{12} = N_{21}$ ,  $N_2 = N_{22}$ ,  $M_1 = M_{11}$ ,  $M_6 = M_{12} = M_{21}$ ,  $M_2 = M_{22}$ ,  $\sigma_1 = \sigma_{11}$ ,  $\sigma_{12} = \sigma_6$ , etc.; see Figure 6.9.3):

$$\begin{Bmatrix} N_{11} \\ N_{22} \\ N_{12} \\ N_{21} \\ M_{11} \\ M_{22} \\ M_{12} \\ M_{21} \end{Bmatrix} = \int_{-h/2}^{h/2} \begin{Bmatrix} \sigma_1 \left(1 + \frac{\zeta}{R_2}\right) \\ \sigma_2 \left(1 + \frac{\zeta}{R_1}\right) \\ \sigma_6 \left(1 + \frac{\zeta}{R_2}\right) \\ \sigma_6 \left(1 + \frac{\zeta}{R_1}\right) \\ \zeta \sigma_1 \left(1 + \frac{\zeta}{R_2}\right) \\ \zeta \sigma_2 \left(1 + \frac{\zeta}{R_1}\right) \\ \zeta \sigma_6 \left(1 + \frac{\zeta}{R_2}\right) \\ \zeta \sigma_6 \left(1 + \frac{\zeta}{R_1}\right) \end{Bmatrix} d\zeta \quad (6.9.21)$$

The shear forces  $Q_i$  are defined as

$$\begin{Bmatrix} Q_1 \\ Q_2 \end{Bmatrix} = K_s \int_{-h/2}^{h/2} \begin{Bmatrix} \sigma_5 \left(1 + \frac{\zeta}{R_2}\right) \\ \sigma_4 \left(1 + \frac{\zeta}{R_1}\right) \end{Bmatrix} d\zeta \quad (6.9.22)$$

where  $K_s$  is the shear correction factor  $K_s$ .

In developing a moderately thick shell theory we make certain assumptions (as we did in the case of plates). They are outlined next.

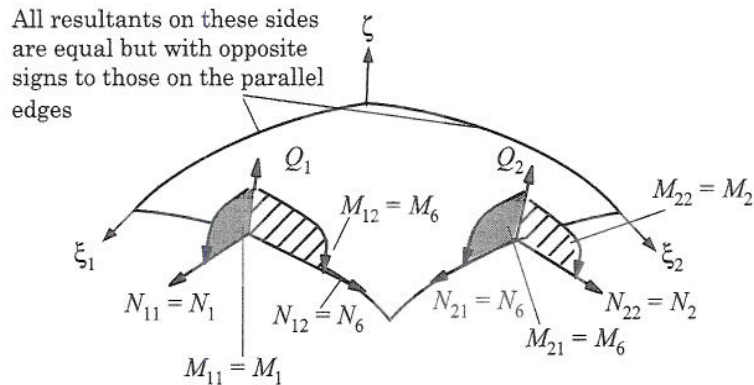


Figure 6.9.3 Stress resultants on a shell element.

1. the transverse normal is inextensible (i.e.  $\epsilon_{33} \approx 0$ ),
2. normals to the reference surface of the shell before deformation remain straight but not necessarily normal after deformation (a relaxed Kirchhoff-Love hypothesis),
3. the shell deflections are small and strains are infinitesimal, and
4. as in the case of plates, we assume that  $\sigma_3$  is negligible and use the plane stress-reduced constitutive relations.

Consistent with the assumptions of a moderately thick shell theory, we assume the following form of the displacement field:

$$\begin{aligned} u_1(\xi_1, \xi_2, \zeta, t) &= u_0(\xi_1, \xi_2, t) + \zeta\phi_1(\xi_1, \xi_2, t) \\ u_2(\xi_1, \xi_2, \zeta, t) &= v_0(\xi_1, \xi_2, t) + \zeta\phi_2(\xi_1, \xi_2, t) \\ u_3(\xi_1, \xi_2, \zeta, t) &= w_0(\xi_1, \xi_2, t) \end{aligned} \tag{6.9.23}$$

in which  $(u_0, v_0, w_0)$  are the displacements of a point  $(\xi_1, \xi_2, 0)$  on the midsurface of the shell, and  $(\phi_1, \phi_2)$  are the rotations of a normal to the reference surface.

The Sanders' [48] nonlinear strain-displacement relations associated with the displacement field in Eq. (6.9.19) are

$$\{\epsilon\} = \{\epsilon^0\} + \zeta\{\epsilon^1\} \tag{6.9.24a}$$

where

$$\begin{Bmatrix} \epsilon_{xx}^0 \\ \epsilon_{yy}^0 \\ \gamma_{xy}^0 \\ \gamma_{xz}^0 \\ \gamma_{yz}^0 \end{Bmatrix} = \begin{Bmatrix} \frac{\partial u_0}{\partial x} + \frac{w_0}{R_1} + \frac{1}{2} \left( \frac{\partial w_0}{\partial x} - \frac{u_0}{R_1} \right)^2 \\ \frac{\partial v_0}{\partial y} + \frac{w_0}{R_2} + \frac{1}{2} \left( \frac{\partial w_0}{\partial y} - \frac{v_0}{R_2} \right)^2 \\ \frac{\partial u_0}{\partial y} + \frac{\partial v_0}{\partial x} + \left( \frac{\partial w_0}{\partial x} - \frac{u_0}{R_1} \right) \left( \frac{\partial w_0}{\partial y} - \frac{v_0}{R_2} \right) \\ \frac{\partial w_0}{\partial x} - \frac{u_0}{R_1} + \phi_x \\ \frac{\partial w_0}{\partial y} - \frac{v_0}{R_2} + \phi_y \end{Bmatrix}, \quad \begin{Bmatrix} \epsilon_{xx}^1 \\ \epsilon_{yy}^1 \\ \gamma_{xy}^1 \\ \gamma_{xz}^1 \\ \gamma_{yz}^1 \end{Bmatrix} = \begin{Bmatrix} \frac{\partial \phi_x}{\partial x} \\ \frac{\partial \phi_y}{\partial y} \\ \frac{\partial \phi_x}{\partial y} + \frac{\partial \phi_y}{\partial x} \\ 0 \\ 0 \end{Bmatrix} \tag{6.9.24b}$$

and  $dx = a_1 d\xi_1$ ,  $dy = a_2 d\xi_2$ , and  $dz = d\zeta$ .

In the remainder of this development, we omit the term  $z/R$  in the definition of the stress resultants and assume that  $a_{\alpha,\beta} = 0$  ( $\alpha, \beta = 1, 2$ ) (i.e. constant radii of curvatures). Thus, for thin shallow shells, we have

$$\left(1 + \frac{\zeta}{R_1}\right) \approx 1, \quad \left(1 + \frac{\zeta}{R_2}\right) \approx 1 \tag{6.9.25}$$

and we have  $N_{12} = N_{21}$  and  $M_{12} = M_{21}$ .

The stress resultants are related to the strains, for an orthotropic shell in the absence of thermal and other influences, as follows:

$$\begin{Bmatrix} N_1 \\ N_2 \\ N_6 \end{Bmatrix} = \begin{bmatrix} A_{11} & A_{12} & 0 \\ A_{12} & A_{22} & 0 \\ 0 & 0 & A_{66} \end{bmatrix} \begin{Bmatrix} \frac{\partial u_0}{\partial x} + \frac{w_0}{R_1} + \frac{1}{2} \left( \frac{\partial w_0}{\partial x} - \frac{u_0}{R_1} \right)^2 \\ \frac{\partial v_0}{\partial y} + \frac{w_0}{R_2} + \frac{1}{2} \left( \frac{\partial w_0}{\partial y} - \frac{v_0}{R_2} \right)^2 \\ \frac{\partial u_0}{\partial y} + \frac{\partial v_0}{\partial x} + \left( \frac{\partial w_0}{\partial x} - \frac{u_0}{R_1} \right) \left( \frac{\partial w_0}{\partial y} - \frac{v_0}{R_2} \right) \end{Bmatrix} \quad (6.9.26a)$$

$$\begin{Bmatrix} M_1 \\ M_2 \\ M_6 \end{Bmatrix} = \begin{bmatrix} D_{11} & D_{12} & 0 \\ D_{12} & D_{22} & 0 \\ 0 & 0 & D_{66} \end{bmatrix} \begin{Bmatrix} \frac{\partial \phi_x}{\partial x} \\ \frac{\partial \phi_y}{\partial y} \\ \frac{\partial \phi_x}{\partial y} + \frac{\partial \phi_y}{\partial x} \end{Bmatrix} \quad (6.9.26b)$$

$$\begin{Bmatrix} Q_2 \\ Q_1 \end{Bmatrix} = K_s \begin{bmatrix} A_{44} & 0 \\ 0 & A_{55} \end{bmatrix} \begin{Bmatrix} \frac{\partial w_0}{\partial y} - \frac{v_0}{R_2} + \phi_y \\ \frac{\partial w_0}{\partial x} - \frac{u_0}{R_1} + \phi_x \end{Bmatrix} \quad (6.9.26c)$$

### 6.9.5 Equations of Motion

The equations of motion of the Sanders' shell theory are

$$-\left( \frac{\partial N_1}{\partial x} + \frac{\partial N_6}{\partial y} \right) - \frac{Q_1 + N_1}{R_1} + I_0 \frac{\partial^2 u_0}{\partial t^2} + I_1 \frac{\partial^2 \phi_x}{\partial t^2} = 0 \quad (6.9.27)$$

$$-\left( \frac{\partial N_6}{\partial x} + \frac{\partial N_2}{\partial y} \right) - \frac{Q_2 + N_2}{R_2} + I_0 \frac{\partial^2 v_0}{\partial t^2} + I_1 \frac{\partial^2 \phi_y}{\partial t^2} = 0 \quad (6.9.28)$$

$$-\left( \frac{\partial Q_1}{\partial x} + \frac{\partial Q_2}{\partial y} \right) + \frac{N_1}{R_1} + \frac{N_2}{R_2} - \mathcal{N}_3(u_0, v_0, w_0) - q + I_0 \frac{\partial^2 w_0}{\partial t^2} = 0 \quad (6.9.29)$$

$$-\left( \frac{\partial M_1}{\partial x} + \frac{\partial M_6}{\partial y} \right) + Q_1 + I_2 \frac{\partial^2 \phi_x}{\partial t^2} + I_1 \frac{\partial^2 u_0}{\partial t^2} = 0 \quad (6.9.30)$$

$$-\left( \frac{\partial M_6}{\partial x} + \frac{\partial M_2}{\partial y} \right) + Q_2 + I_2 \frac{\partial^2 \phi_y}{\partial t^2} + I_1 \frac{\partial^2 v_0}{\partial t^2} = 0 \quad (6.9.31)$$

where

$$I_i = \sum_{k=1}^N \int_{z_k}^{z_{k+1}} \rho^{(k)} \zeta^i d\zeta \quad (6.9.32)$$

$$\begin{aligned} \mathcal{N}_1(u_0, v_0, w_0) &= N_1 \left( \frac{\partial w_0}{\partial x} - \frac{u_0}{R_1} \right) + N_6 \left( \frac{\partial w_0}{\partial y} - \frac{v_0}{R_2} \right) \\ \mathcal{N}_2(u_0, v_0, w_0) &= N_6 \left( \frac{\partial w_0}{\partial x} - \frac{u_0}{R_1} \right) + N_2 \left( \frac{\partial w_0}{\partial y} - \frac{v_0}{R_2} \right) \end{aligned} \quad (6.9.33)$$

$$\mathcal{N}_3(u_0, v_0, w_0) = \frac{\partial N_1}{\partial x} + \frac{\partial N_2}{\partial y}$$

$\rho$  being the mass density.

## 6.10 Finite Element Analysis of Shells

### 6.10.1 Weak Forms

The displacement finite element model of the equations governing doubly curved shells, Eqs. (6.9.27)–(6.9.31), can be derived in a manner similar to that of plates. In fact, the finite element model of doubly-curved shells is identical to that of FSDT with additional terms in the stiffness coefficients. For the sake of completeness, the main equations are presented here.

We begin with the weak forms of Eqs. (6.9.27)–(6.9.31):

$$0 = \int_{\Omega^e} \left[ \frac{\partial \delta u_0}{\partial x} N_1 + \frac{\partial \delta u_0}{\partial y} N_6 - \delta u_0 \frac{Q_1 + N_1}{R_1} + I_0 \delta u_0 \frac{\partial^2 u_0}{\partial t^2} + I_1 \delta u_0 \frac{\partial^2 \phi_1}{\partial t^2} \right] dx dy - \oint_{\Gamma^e} P_1 \delta u_0 ds \quad (6.10.1a)$$

$$0 = \int_{\Omega^e} \left[ \frac{\partial \delta v_0}{\partial x} N_6 + \frac{\partial \delta v_0}{\partial y} N_2 - \delta v_0 \frac{Q_2 + N_2}{R_2} + I_0 \delta v_0 \frac{\partial^2 v_0}{\partial t^2} + I_1 \delta v_0 \frac{\partial^2 \phi_2}{\partial t^2} \right] dx dy - \oint_{\Gamma^e} P_2 \delta v_0 ds \quad (6.10.1b)$$

$$0 = \int_{\Omega^e} \left[ \frac{\partial \delta w_0}{\partial x} Q_1 + \frac{\partial \delta w_0}{\partial y} Q_2 + \delta w_0 \left( \frac{N_1}{R_1} + \frac{N_2}{R_2} \right) - \delta w_0 q + I_0 \delta w_0 \frac{\partial^2 w_0}{\partial t^2} + \frac{\partial \delta w_0}{\partial x} N_1 + \frac{\partial \delta w_0}{\partial y} N_2 \right] dx dy - \oint_{\Gamma^e} V_n \delta w_0 ds \quad (6.10.1c)$$

$$0 = \int_{\Omega^e} \left( \frac{\partial \delta \phi_1}{\partial x} M_1 + \frac{\partial \delta \phi_1}{\partial y} M_6 + \delta \phi_1 Q_1 + I_2 \delta \phi_1 \frac{\partial^2 \phi_1}{\partial t^2} + I_1 \delta \phi_1 \frac{\partial^2 u_0}{\partial t^2} \right) dx dy - \oint_{\Gamma^e} T_1 \delta \phi_1 ds \quad (6.10.1d)$$

$$0 = \int_{\Omega^e} \left( \frac{\partial \delta \phi_2}{\partial x} M_6 + \frac{\partial \delta \phi_2}{\partial y} M_2 + \delta \phi_2 Q_2 + I_2 \delta \phi_2 \frac{\partial^2 \phi_2}{\partial t^2} + I_1 \delta \phi_2 \frac{\partial^2 v_0}{\partial t^2} \right) dx dy - \oint_{\Gamma^e} T_2 \delta \phi_2 ds \quad (6.10.1e)$$

where the stress resultants  $N_i$ ,  $M_i$  and  $Q_i$  are defined by Eqs. (6.9.21) and (6.9.22). We note from the boundary terms in Eq. (6.10.1a–e) that  $u_0$ ,  $v_0$ ,  $w_0$ ,  $\phi_1$ , and  $\phi_2$  are the primary variables. Therefore, we can use the  $C^0$  interpolation of the displacements. The secondary variables are

$$\begin{aligned} P_1 &\equiv N_1 n_1 + N_6 n_2, & P_2 &\equiv N_6 n_1 + N_2 n_2 \\ T_2 &\equiv M_1 n_1 + M_6 n_2, & T_2 &\equiv M_6 n_1 + M_2 n_2 \\ V_n &\equiv (Q_1 + N_1) n_1 + (Q_2 + N_2) n_2 \end{aligned} \quad (6.10.2)$$

where  $(n_1, n_2)$  are the direction cosines of the unit normal to the surface. Note that in the case of shells, surface displacements are coupled to the transverse displacement even for linear analysis of isotropic shells.

### 6.10.2 Finite Element Model

Using interpolation of the form

$$u_0(x, y, t) = \sum_{j=1}^m u_j(t) \psi_j^e(x, y), \quad v_0(x, y, t) = \sum_{j=1}^m v_j(t) \psi_j^e(x, y) \quad (6.10.3)$$

$$w_0(x, y, t) = \sum_{j=1}^n w_j(t) \psi_j^e(x, y) \quad (6.10.4)$$

$$\phi_1(x, y, t) = \sum_{j=1}^p S_j^1(t) \psi_j^e(x, y), \quad \phi_2(x, y, t) = \sum_{j=1}^p S_j^2(t) \psi_j^e(x, y) \quad (6.10.5)$$

where  $\psi_j^e$  are Lagrange interpolation functions. In the present study, equal interpolation ( $m = n = p$ ) of five displacements, with  $p = 1, 2, \dots$  is used. Note that the finite element model developed here for doubly-curved shells contains the FSDT plate element as a special case (set  $1/R_1 = 0$  and  $1/R_2 = 0$ ).

Substituting Eqs. (6.10.3)–(6.10.5) for  $(u_0, v_0, w_0, \phi_1, \phi_2)$  into the weak forms in Eqs. (6.10.1a–c), we obtain the semidiscrete finite element model of the first-order shear deformation shell theory:

$$\begin{aligned} & \left( \begin{bmatrix} [K^{11}] & [K^{12}] & [K^{13}] & [K^{14}] & [K^{15}] \\ [K^{12}]^T & [K^{22}] & [K^{23}] & [K^{24}] & [K^{25}] \\ [K^{13}]^T & [K^{23}]^T & [K^{33}] & [K^{34}] & [K^{35}] \\ [K^{14}]^T & [K^{24}]^T & [K^{34}]^T & [K^{44}] & [K^{45}] \\ [K^{15}]^T & [K^{25}]^T & [K^{35}]^T & [K^{45}]^T & [K^{55}] \end{bmatrix} + \begin{bmatrix} [0] & [0] & [0] & [0] & [0] \\ [0] & [0] & [0] & [0] & [0] \\ [0] & [0] & [G] & [0] & [0] \\ [0] & [0] & [0] & [0] & [0] \\ [0] & [0] & [0] & [0] & [0] \end{bmatrix} \right) \begin{Bmatrix} \{u^e\} \\ \{v^e\} \\ \{w^e\} \\ \{S^1\} \\ \{S^2\} \end{Bmatrix} \\ & + \begin{bmatrix} I_0[M] & [0] & [0] & I_1[M] & [0] \\ [0] & I_0[M] & [0] & [0] & I_1[M] \\ [0] & [0] & I_0[M] & [0] & [0] \\ I_1[M] & [0] & [0] & I_2[M] & [0] \\ [0] & I_1[M] & [0] & [0] & I_2[M] \end{bmatrix} \begin{Bmatrix} \{\ddot{u}^e\} \\ \{\ddot{v}^e\} \\ \{\ddot{w}^e\} \\ \{\dot{S}^1\} \\ \{\dot{S}^2\} \end{Bmatrix} = \begin{Bmatrix} \{F^1\} \\ \{F^2\} \\ \{F^3\} \\ \{F^4\} \\ \{F^5\} \end{Bmatrix} \quad (6.10.6) \end{aligned}$$

where the coefficients of the submatrices  $[K^{\alpha\beta}]$  are defined as follows:

$$\begin{aligned} K_{ij}^{1\alpha} &= \int_{\Omega^e} \left( \frac{\partial \psi_i^e}{\partial x} N_{1j}^\alpha + \frac{\partial \psi_i^e}{\partial y} N_{6j}^\alpha - \psi_i^e \frac{Q_{1j}^\alpha + N_{1j}^\alpha}{R_1} \right) dx dy \\ K_{ij}^{2\alpha} &= \int_{\Omega^e} \left( \frac{\partial \psi_i^e}{\partial x} N_{6j}^\alpha + \frac{\partial \psi_i^e}{\partial y} N_{2j}^\alpha - \psi_i^e \frac{Q_{2j}^\alpha + N_{2j}^\alpha}{R_2} \right) dx dy \\ K_{ij}^{3\alpha} &= \int_{\Omega^e} \left[ \frac{\partial \psi_i^e}{\partial x} Q_{1j}^\alpha + \frac{\partial \psi_i^e}{\partial y} Q_{2j}^\alpha + \psi_i^e \left( \frac{N_{1j}^\alpha}{R_1} + \frac{N_{2j}^\alpha}{R_2} \right) \right] dx dy \end{aligned}$$



$$\begin{aligned}
 K_{ij}^{4\alpha} &= \int_{\Omega^e} \left( \frac{\partial \psi_i^e}{\partial x} M_{1j}^\alpha + \frac{\partial \psi_i^e}{\partial y} M_{6j}^\alpha + \psi_i^e Q_{1j}^\alpha \right) dx dy \\
 K_{ij}^{5\alpha} &= \int_{\Omega^e} \left( \frac{\partial \psi_i^e}{\partial x} M_{6j}^\alpha + \frac{\partial \psi_i^e}{\partial y} M_{2j}^\alpha + \psi_i^e Q_{2j}^\alpha \right) dx dy
 \end{aligned} \quad (6.10)$$

for  $\alpha = 1, 2, \dots, 5$ . The coefficients  $N_{Ij}^\alpha$ ,  $M_{Ij}^\alpha$ , and  $Q_{Ij}^\alpha$  for  $\alpha = 1, 2, \dots, 5$  and  $I = 1, 2, 6$  are given by

$$\begin{aligned}
 N_{1j}^1 &= A_{11} \left[ \frac{\partial \psi_j^e}{\partial x} + \left( \frac{u_0}{2R_1^2} - \frac{1}{R_1} \frac{\partial w_0}{\partial x} \right) \psi_j^e \right] \\
 N_{1j}^2 &= A_{12} \left[ \frac{\partial \psi_j^e}{\partial y} + \left( \frac{v_0}{2R_2^2} - \frac{1}{R_2} \frac{\partial w_0}{\partial x} \right) \psi_j^e \right] \\
 N_{1j}^3 &= \left( \frac{A_{11}}{R_1} + \frac{A_{12}}{R_2} \right) \psi_j^e + \frac{1}{2} \left( A_{11} \frac{\partial w_0}{\partial x} \frac{\partial \psi_j^e}{\partial x} + A_{12} \frac{\partial w_0}{\partial y} \frac{\partial \psi_j^e}{\partial y} \right) \\
 N_{6j}^1 &= A_{66} \left[ \frac{\partial \psi_j^e}{\partial y} - \frac{1}{R_1} \left( \frac{\partial w_0}{\partial y} - \frac{1}{2} \frac{v_0}{R_2} \right) \psi_j^e \right] \\
 N_{6j}^2 &= A_{66} \left[ \frac{\partial \psi_j^e}{\partial x} - \frac{1}{R_2} \left( \frac{\partial w_0}{\partial x} - \frac{1}{2} \frac{u_0}{R_1} \right) \psi_j^e \right] \\
 N_{6j}^3 &= \frac{A_{66}}{2} \left( \frac{\partial w_0}{\partial x} \frac{\partial \psi_j^e}{\partial y} + \frac{\partial w_0}{\partial y} \frac{\partial \psi_j^e}{\partial x} \right) \\
 N_{2j}^1 &= A_{12} \left[ \frac{\partial \psi_j^e}{\partial x} + \left( \frac{u_0}{2R_1^2} - \frac{1}{R_1} \frac{\partial w_0}{\partial x} \right) \psi_j^e \right] \\
 N_{2j}^2 &= A_{22} \left[ \frac{\partial \psi_j^e}{\partial y} + \left( \frac{v_0}{2R_2^2} - \frac{1}{R_2} \frac{\partial w_0}{\partial y} \right) \psi_j^e \right] \\
 N_{2j}^3 &= \left( \frac{A_{12}}{R_1} + \frac{A_{22}}{R_2} \right) \psi_j^e + \frac{1}{2} \left( A_{12} \frac{\partial w_0}{\partial x} \frac{\partial \psi_j^e}{\partial x} + A_{22} \frac{\partial w_0}{\partial y} \frac{\partial \psi_j^e}{\partial y} \right) \\
 N_{6j}^4 &= 0, \quad N_{6j}^5 = 0, \quad N_{1j}^4 = 0, \quad N_{1j}^5 = 0, \quad N_{2j}^4 = 0, \quad N_{2j}^5 = 0 \\
 Q_{1j}^1 &= -\frac{K_s A_{55}}{R_1} \psi_j^e, \quad Q_{1j}^3 = K_s A_{55} \frac{\partial \psi_j^e}{\partial x}, \quad Q_{1j}^4 = K_s A_{55} \psi_j^e \\
 Q_{2j}^2 &= -\frac{K_s A_{44}}{R_2} \psi_j^e, \quad Q_{2j}^3 = K_s A_{44} \frac{\partial \psi_j^e}{\partial y}, \quad Q_{2j}^4 = K_s A_{55} \psi_j^e \\
 Q_{1j}^2 &= 0, \quad Q_{1j}^5 = 0, \quad Q_{2j}^1 = 0, \quad Q_{2j}^5 = 0 \\
 \mathcal{N}_{1j}^1 &= -\frac{N_1}{R_1} \psi_j^e, \quad \mathcal{N}_{1j}^2 = -\frac{N_6}{R_2} \psi_j^e, \quad \mathcal{N}_{1j}^3 = N_1 \frac{\partial \psi_j^e}{\partial x} + N_6 \frac{\partial \psi_j^e}{\partial y} \\
 \mathcal{N}_{2j}^1 &= -\frac{N_6}{R_1} \psi_j^e, \quad \mathcal{N}_{2j}^2 = -\frac{N_2}{R_2} \psi_j^e, \quad \mathcal{N}_{2j}^3 = N_6 \frac{\partial \psi_j^e}{\partial x} + N_2 \frac{\partial \psi_j^e}{\partial y} \\
 \mathcal{N}_{1j}^4 &= 0, \quad \mathcal{N}_{1j}^5 = 0, \quad \mathcal{N}_{2j}^4 = 0, \quad \mathcal{N}_{2j}^5 = 0
 \end{aligned}$$

$$\begin{aligned}
 M_{1j}^1 &= M_{1j}^2 = M_{1j}^3 = 0, & M_{1j}^4 &= D_{11} \frac{\partial \psi_j^e}{\partial x}, & M_{1j}^5 &= D_{12} \frac{\partial \psi_j^e}{\partial y} \\
 M_{2j}^1 &= M_{2j}^2 = M_{2j}^3 = 0, & M_{2j}^4 &= D_{12} \frac{\partial \psi_j^e}{\partial x}, & M_{2j}^5 &= D_{22} \frac{\partial \psi_j^e}{\partial y} \\
 M_{6j}^1 &= M_{6j}^2 = M_{6j}^3 = 0, & M_{6j}^4 &= D_{66} \frac{\partial \psi_j^e}{\partial y}, & M_{6j}^5 &= D_{66} \frac{\partial \psi_j^e}{\partial x}
 \end{aligned} \quad (6.10.8b)$$

$$M_{ij} = \int_{\Omega^e} \psi_i^e \psi_j^e \, dx \, dy \quad (6.10.8c)$$

$$\begin{aligned}
 F_i^1 &= \oint_{\Gamma^e} P_1 \psi_i^e \, dx \, dy, & F_i^2 &= \oint_{\Gamma^e} P_2 \psi_i^e \, dx \, dy \\
 F_i^3 &= \int_{\Omega^e} q \psi_i^e \, dx \, dy + \oint_{\Gamma^e} Q_n \psi_i^e \, ds \\
 F_i^4 &= \oint_{\Gamma^e} T_1 \psi_i^e \, dx \, dy, & F_i^5 &= \oint_{\Gamma^e} T_2 \psi_i^e \, dx \, dy
 \end{aligned} \quad (6.10.8d)$$

The tangent stiffness coefficients can be computed as in the case of plates.

### 6.10.3 Linear Results

Here, numerical results are presented for linear analysis of some benchmark problems from the literature [50]. Quadrilateral elements are used with selective integration rule to evaluate the stiffness coefficients (full integration for bending terms and reduced integration for bending-membrane coupling terms and transverse shear terms). Results are compared with those available in the literature.

#### Example 6.10.1 (*Clamped cylindrical shell*)

Consider the deformation of a cylindrical shell with internal pressure [40]. The shell is clamped at its ends (see Figure 6.10.1). The geometric and material parameters used are:

$$R_1 = 10^{30} \left( \frac{1}{R_1} \approx 0 \right), \quad R_2 = R = 20 \text{ in.}, \quad a = 20 \text{ in.}, \quad h = 1 \text{ in.} \quad (6.10.9a)$$

$$\begin{aligned}
 E_1 &= 7.5 \times 10^6 \text{ psi}, & E_2 &= 2 \times 10^6 \text{ psi}, & G_{12} &= 1.25 \times 10^6 \text{ psi} \\
 G_{13} &= G_{23} = 0.625 \times 10^6 \text{ psi}, & \nu_{12} &= 0.25
 \end{aligned} \quad (6.10.9b)$$

The pressure is taken to be  $p_0 = (6.41/\pi)$  ksi. The numerical results obtained using  $4 \times 4$  mesh of four-node (linear) quadrilateral elements ( $4 \times 4Q4$ ) and  $2 \times 2$  mesh of nine-node (quadratic) quadrilateral elements ( $2 \times 2Q9$ ) in an octant ( $u_0 = \phi_1 = 0$  at  $x_1 = 0$ ;  $v_0 = \phi_2 = 0$  at  $x_2 = 0, \pi R/2$ ; and  $u_0 = v_0 = w_0 = \phi_1 = \phi_2 = 0$  at  $x_1 = a/2$ ) of the shell are presented in Table 6.10.1. The reference solutions by Rao [53] and Timoshenko and Woinowsky-Krieger [46] did not account for the transverse shear strains.



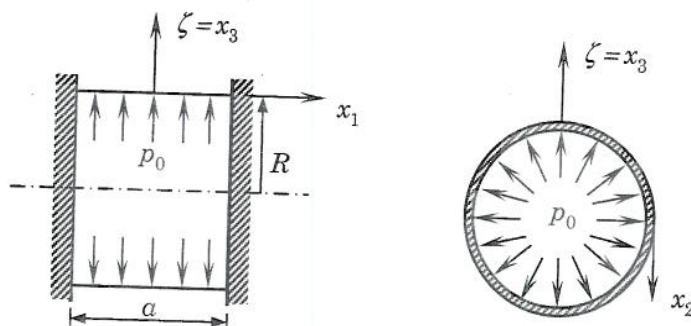


Figure 6.10.1 Clamped cylindrical shell with internal pressure.

Table 6.10.1 Maximum radial deflection ( $w_0$  in.) of a clamped cylindrical shell with internal pressure.

Laminate	Present Solutions			
	4 × 4Q4	2 × 2Q9	Ref. [53]	Ref. [46]
0	0.3754	0.3727	0.3666	0.367

### Example 6.10.2 (Doubly-curved shell panel)

Next, we consider a spherical shell panel ( $R_1 = R_2 = R$ ) under central point load [40]. The shell panel is simply supported at edges (see Figure 6.10.2). The geometric and material parameters used are:

$$R_1 = R_2 = R = 96 \text{ in.}, \quad a = b = 32 \text{ in.}, \quad h = 0.1 \text{ in.} \quad (6.10.10a)$$

$$E_1 = 25E_2, \quad E_2 = 10^6 \text{ psi}, \quad G_{12} = G_{13} = 0.5E_2, \quad G_{23} = 0.2E_2, \quad \nu_{12} = 0.25 \quad (6.10.10b)$$

The point load is taken to be  $F_0 = 100$  lbs. The numerical results obtained using various meshes of linear and quadratic elements in a quadrant of the shell are presented in Table 6.10.2. The finite element solution converges with refinement of the mesh to the series solution of Vlasov [52], who did not consider transverse shear strains in his analysis.

The remaining example problems of this chapter are analyzed using various  $p$  levels [see Eq. (6.10.3)–(6.10.5)]. With five degrees of freedom at each node, the number of degrees of freedom per element for different  $p$  values is given on the next page.

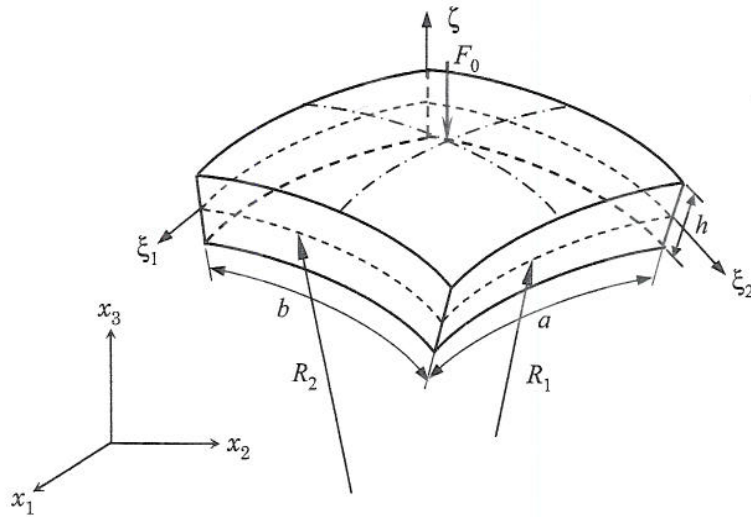


Figure 6.10.2 Simply supported spherical shell panel under central point load.

Table 6.10.2 Maximum radial deflection ( $-w_0 \times 10$  in.) of a simply supported spherical shell panel under central point load.

Material	Present Solutions				Ref. [53]	Ref. [52]
	4 × 4Q4 Uniform	2 × 2Q9 Uniform	4 × 4Q9 Uniform	4 × 4Q9 Nonuniform		
Isotropic	0.3506	0.3726	0.3904	0.3935	0.3866	0.3956
Orthotropic	0.9373	1.0349	—	1.2644	—	—

Table: Number of degrees of freedom per element for different  $p$  values.

Element type	$p$ level	DoF per element
Q4	1	20
Q9	2	45
Q25	4	125
Q49	6	245
Q81	8	405

The numerical integration rule (Gauss quadrature) used is  $I \times J \times K$ , where  $K$  denotes the number of Gauss points (i.e.  $K \times K$  Gauss rule) used to evaluate the transverse shear terms (i.e. those containing  $A_{44}$  and  $A_{55}$ ),  $J$  denotes the number of Gauss points to evaluate the bending-membrane coupling terms (which are zero for the linear analysis of plates), and  $I$  denotes the number of Gauss points used to evaluate all remaining terms in the stiffness matrix. One may use full integration for all terms, reduced integration for all terms or selective integration where reduced integration for transverse shear and coupling terms and full integration for all other terms in the stiffness matrix. The values of  $I$ ,  $J$  and  $K$  used in the present study for different  $p$  levels and integration rules are listed below.

**Table:** The Gauss quadrature rule used for various terms.

$p$ level	Full integration	Selective integration	Reduced integration
1	$2 \times 2 \times 2$	$2 \times 1 \times 1$	$1 \times 1 \times 1$
2	$3 \times 3 \times 3$	$3 \times 2 \times 2$	$2 \times 2 \times 2$
4	$5 \times 5 \times 5$	$5 \times 4 \times 4$	$4 \times 4 \times 4$
6	$7 \times 7 \times 7$	$7 \times 6 \times 6$	$6 \times 6 \times 6$
8	$9 \times 9 \times 9$	$9 \times 8 \times 8$	$8 \times 8 \times 8$

**Example 6.10.3** (*Clamped cylindrical shell panel*)

Here we consider an isotropic cylindrical shell panel with the following geometric and material parameters and subjected to uniformly distributed transverse (normal to the surface) load  $q$  (see Figure 6.10.3):

$$\alpha = 0.1 \text{ rad.}, \quad R = 100 \text{ in.}, \quad a = 20 \text{ in.}, \quad h = 0.125 \text{ in.} \quad (6.10.11a)$$

$$E = 0.45 \times 10^6 \text{ psi}, \quad \nu = 0.3, \quad q = 0.04 \text{ psi} \quad (6.10.11b)$$

Two sets of uniform meshes, one with 81 nodes (405 DoF) and the other with 289 nodes (1,445 DoF), are used in a quadrant of the shell with different  $p$  levels. For example, for  $p = 1$  the mesh is  $8 \times 8Q4$ , for  $p = 2$  the mesh is  $4 \times 4Q9$ , and for  $p = 8$  the mesh is  $1 \times 1Q81$  - all meshes have a total of 81 nodes. Doubling the above meshes will have 289 nodes. The vertical displacement at the center of the shell obtained with various meshes and integration rules are presented in Table 6.10.3. The results obtained with selective and reduced integrations are in close agreement with those of Palazotto and Dennis [51] and Brebbia and Connor [54].

The next example deals with the well-known benchmark problem of Scordelis-Lo roof [55]. A solution to this problem was first discussed by Cantin and Clough [56] (who used  $\nu = 0.3$ ).

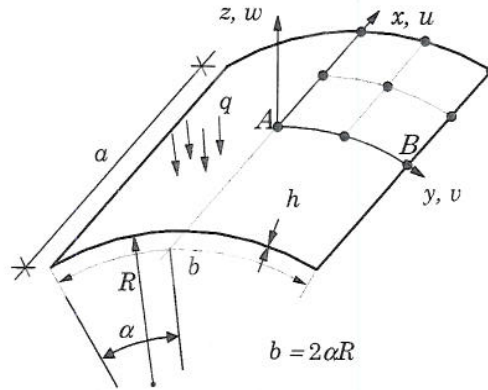


Figure 6.10.3 Clamped cylindrical shell panel under uniform transverse load.

Table 6.10.3 Vertical deflection ( $-w_A \times 10^2$  in.)<sup>†</sup> at the center of the clamped cylindrical panel under uniform transverse load.

p level	Mesh of 81 nodes			Mesh of 289 nodes		
	Full integ.	Selective integ.	Reduced integ.	Full integ.	Selective integ.	Reduced integ.
1	0.3378	1.1562	1.1577	0.7456	1.1401	1.1404
2	1.1721	1.1351	1.1352	1.1427	1.1349	1.1349
4	1.1347	1.1349	1.1349	1.1349	1.1349	1.1349
8	1.1349	1.1348	1.1348	1.1348	1.1349	1.1349

<sup>†</sup> Palazotto and Dennis [51] reported  $-1.144 \times 10^{-2}$  in. while Brebbia and Connor [54] reported a value of  $-1.1 \times 10^{-2}$  in.

**Example 6.10.4 (Barrel vault)**

The problem consists of a cylindrical roof with rigid supports at edges  $x = \pm a/2$  while edges at  $y = \pm b/2$  are free. The shell is assumed to deform under its own weight (i.e.  $q$  acts vertically down, not perpendicular to the surface of the shell). The geometric and material data of the problem is (see Figure 6.10.4)

$$\alpha = 40^\circ (0.698 \text{ rad.}), \quad R = 300 \text{ in.}, \quad a = 600 \text{ in.}, \quad h = 3 \text{ in.} \quad (6.10.12)$$

$$E = 3 \times 10^6 \text{ psi}, \quad \nu = 0.0, \quad q_y = q \sin \frac{y}{R}, \quad q_z = -q \cos \frac{y}{R}, \quad q = 0.625 \text{ psi}$$

The boundary conditions on the computational domain are

$$\begin{aligned} \text{At } x = 0: \quad u_0 = \phi_1 = 0, \quad \text{At } x = a/2: \quad v_0 = w_0 = \phi_2 = 0 \\ \text{At } y = 0: \quad v_0 = \phi_2 = 0, \quad \text{At } y = b/2: \quad \text{Free} \end{aligned} \quad (6.10.13)$$

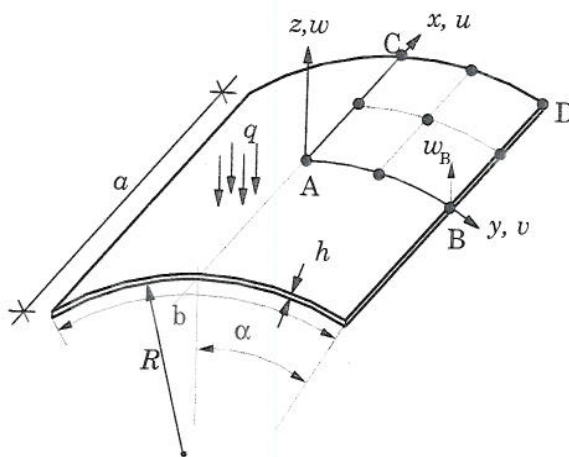


Figure 6.10.4 A cylindrical shell roof under its own weight.

Two sets of uniform meshes, one with 289 nodes (1,445 DoF) and the other with 1,089 nodes (5,445 DoF), are used in a quadrant of the shell with different  $p$  levels. The vertical displacement at  $y = \pm b/2$  (middle of the free edge) of the shell, obtained with various meshes and integration rules, are presented in Table 6.10.4. To avoid shear and membrane locking one must use at least a mesh of  $4 \times 4Q25$  ( $p = 4$ ). The results obtained with selective and reduced integrations are in close agreement with those reported by Simo, Fox and Rifai [57]

Table 6.10.4 Vertical deflection ( $-w_B$  in.)<sup>†</sup> at the center of the free edge of a cylindrical roof panel under its own weight.

$p$ level	Mesh of 289 nodes			Mesh of 1,089 nodes		
	Full integ.	Selective integ.	Reduced integ.	Full integ.	Selective integ.	Reduced integ.
1	0.9002	3.2681	3.6434	1.8387	3.5415	3.6431
2	3.6170	3.6393	3.6430	3.6367	3.6425	3.6428
4	3.6374	3.6430	3.6430	3.6399	3.6428	3.6428
8	3.6392	3.6429	3.6429	3.6419	3.6429	3.6429

<sup>†</sup> Simo, Fox and Rifai [57] reported  $w_{ref} = -3.6288$  in. for deep shells.

Figure 6.10.5 shows the variation of the vertical deflections  $w_0(0, y)$  and  $u_0(300, y)$  as a function of  $y$ , while Figure 6.10.6 shows the convergence of the vertical displacement  $w_B$  for  $p = 1, 2, 4, 8$ . Figure 6.10.5 also contains the results of Zienkiewicz [58].

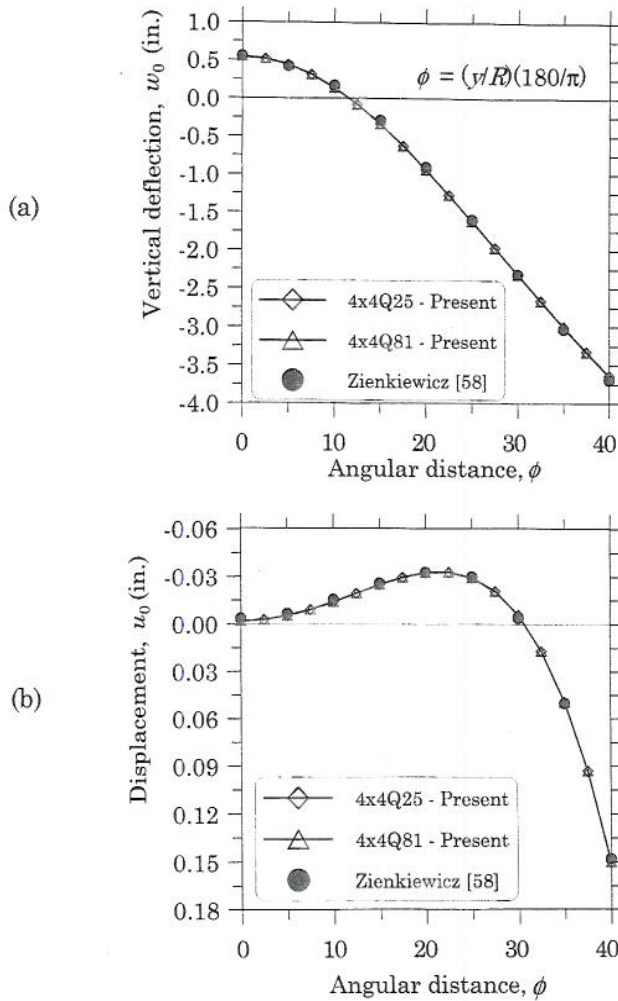


Figure 6.10.5 (a) Deflection  $w_0(0, y)$ . (b) Displacement  $u_0(300, y)$ .

**Example 6.10.5 (Pinched cylinder)**

This is another well-known benchmark problem [44, 59, 60]. The circular cylinder with rigid end diaphragms is subjected to a point load at the center on opposite sides of the cylinder, as shown in Figure 6.10.7. The geometric and material data of the problem is

$$\alpha = \frac{\pi}{2} \text{ rad.}, \quad R = 300 \text{ in.}, \quad a = 600 \text{ in.}, \quad h = 3 \text{ in.}$$

$$E = 3 \times 10^6 \text{ psi}, \quad \nu_{12} = 0.3 \tag{6.10.15}$$



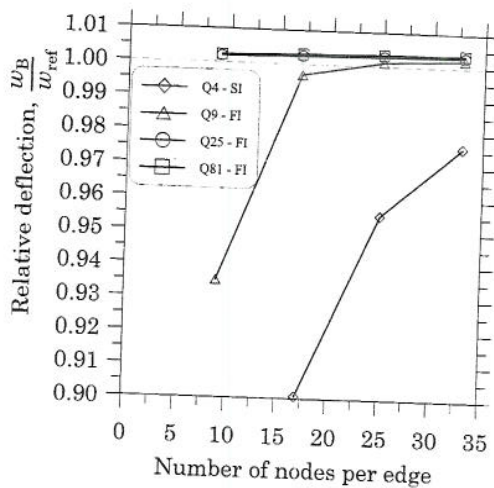


Figure 6.10.6 Convergence of the relative vertical deflection,  $w_B/w_{ref}$ .

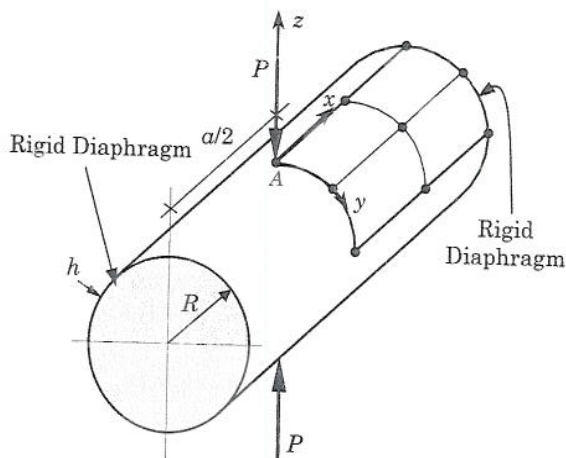


Figure 6.10.7 Geometry of the pinched circular cylinder problem.

The boundary conditions used are:

$$\begin{aligned}
 \text{At } x = 0: \quad u_0 = \phi_1 = 0, \quad \text{At } x = a/2: \quad v_0 = w_0 = \phi_2 = 0 \\
 \text{At } y = 0, b/2: \quad v_0 = \phi_2 = 0
 \end{aligned}
 \tag{6.10.16}$$

Three different meshes with 81 nodes, 289 nodes and 1,089 nodes (with different  $p$  values) are used in the octant of the cylinder. Table 6.10.6 contains radial displacement at the point of load application. The solution of Flügge [44] is based on classical shell theory. It is clear that the problem requires a high  $p$  level to overcome shear and membrane locking. Figure 6.10.8 shows the convergence characteristics of the problem.

**Table 6.10.6** Radial displacement ( $-w_A \times 10^5$ )<sup>†</sup> at node 1 of the pinched circular cylinder problem.

p level	Mesh of 81 nodes			Mesh of 289 nodes			Mesh of 1,089 nodes		
	Full	Selec.	Reduc.	Full	Selec.	Reduc.	Full	Selec.	Reduc.
1	0.1282	1.5784	1.8453	0.2785	1.7724	1.8600	0.6017	1.8432	1.8690
2	0.4184	1.7247	1.8451	1.2238	1.8395	1.8596	1.6844	1.8636	1.8677
4	1.1814	1.8108	1.8438	1.7574	1.8510	1.8586	1.8335	1.8648	1.8667
8	1.7562	1.8309	1.8415	1.8325	1.8548	1.8579	1.8471	1.8653	1.8661

<sup>†</sup> The analytical solution of Flügge [44] is  $-1.8248 \times 10^{-5}$  in.; The value given by Cho and Roh [59] is  $w_{ref} = -1.8541 \times 10^{-5}$  in.

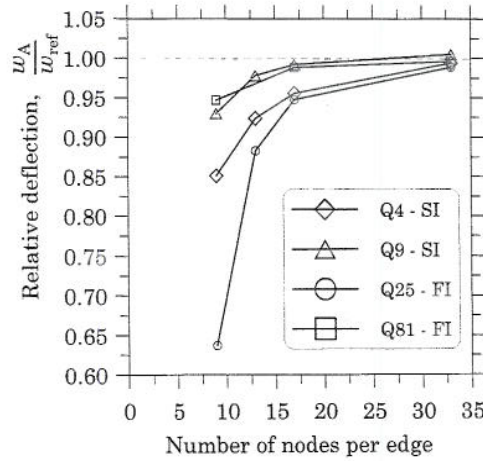


**Figure 6.10.8** Convergence of the relative radial deflection,  $w_A/w_{ref}$ .

### 6.10.4 Nonlinear Results

Here present some few examples of nonlinear bending of shells. The thin shell approximation is used and the results presented are based on the nonlinear strains in Eqs. (6.9.26a-c).

#### Example 6.10.6 (Clamped shallow cylindrical panel)

Here, we consider nonlinear bending of a shallow shell panel clamped on all its four sides, as shown in Figure 6.10.9. The geometric and material parameters used are:

$$E = 0.45 \times 10^6 \text{ psi}, \quad \nu = 0.3, \quad a = 20 \text{ in.}, \quad R = 100 \text{ in.}, \quad h = 0.125 \text{ in.}, \quad \alpha = 0.1 \text{ rad.}$$

Uniformly distributed load, with a load step of  $\Delta q_0 = -0.02$  psi (for a total of 20 load steps) is used. The boundary conditions of the computational domain are

$$\text{At } \xi_1 = 0: \quad u_1 = \phi_1 = 0; \quad \text{At } \xi_2 = 0: \quad u_2 = \phi_2 = 0 \text{ (symmetry)}$$

$$\text{At } \xi_1 = \frac{a}{2} \text{ and } \xi_2 = \alpha: u_1 = u_2 = u_3 = \phi_1 = \phi_2 = 0 \quad (6.10.1)$$

Figure 6.10.10 shows the center deflection versus applied load for various meshes. Full integration is used on all terms. The results are in close agreement with those of Palazotti and Dennis [51].

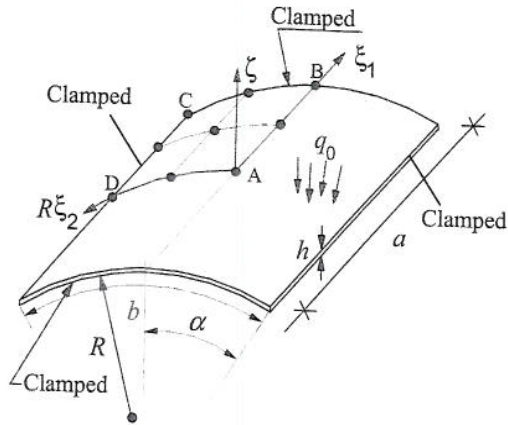


Figure 6.10.9 Geometry and computational domain of the cylindrical shell panel.

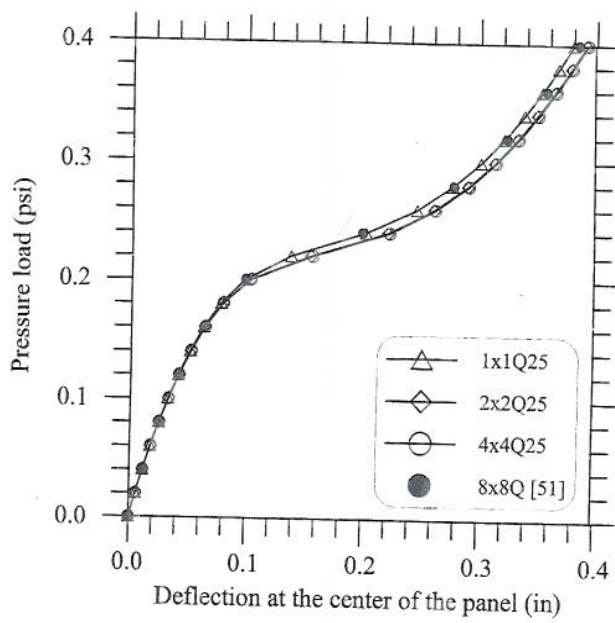


Figure 6.10.10 Center deflection versus load for the clamped cylindrical shell panel.

**Example 6.10.7** (*Hinged shallow cylindrical panel*)

Consider a shallow shell panel hinged on straight edges and free on curved edges, as shown in Figure 6.10.11. The geometric and material parameters used are the same as those in Eq. (6.10.17) except  $h = 1.0$  in. Point load at the center of the panel is used with a load step of  $\Delta P = -100$  lbs (for a total of 12 load steps). Full integration is used on all terms. The boundary conditions of the computational domain are

$$\begin{aligned} \text{At } \xi_1 = 0: \quad u_1 = \phi_1 = 0; \quad \text{At } \xi_2 = 0: \quad u_2 = \phi_2 = 0 \quad (\text{symmetry}) \\ \text{At } \xi_2 = \alpha: \quad u_1 = u_2 = u_3 = \phi_1 = 0; \quad \text{At } \xi_1 = a/2: \quad \text{Free} \end{aligned} \tag{6.10.18}$$

Figure 6.10.12 shows the center deflection versus applied load for various meshes. The results are in close agreement with those of Sabir and Lock [61].

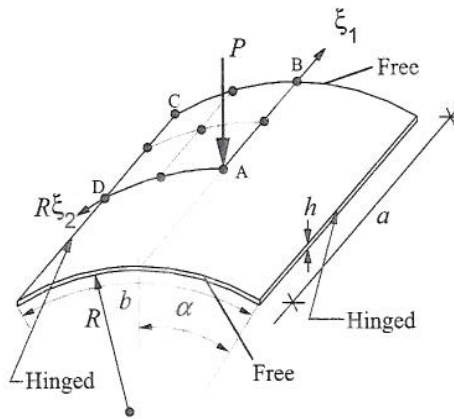


Figure 6.10.11 Geometry and computational domain of the shell panel.

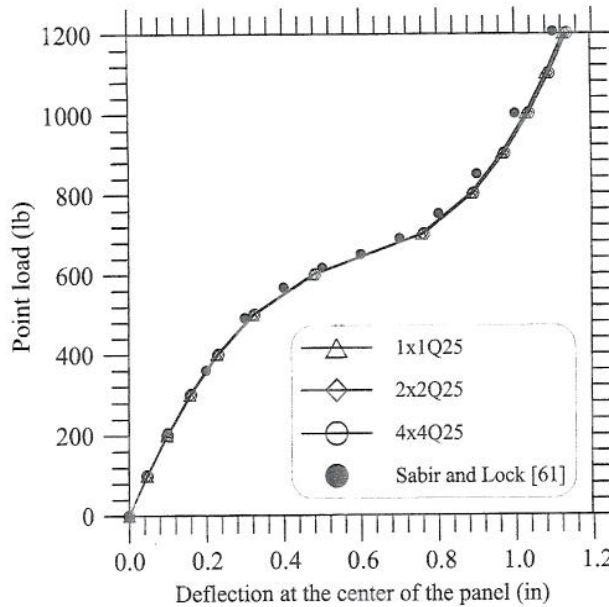


Figure 6.10.12 Deflection versus load for the clamped shell panel.

**Example 6.10.8** (*The Barrel Vault problem*)

Here, we consider the Barrel Vault problem of Example 6.10.4 for nonlinear analysis (see Figure 6.10.4). The geometric and material parameters and the boundary conditions used are the same as those in Eqs. (6.10.12) and (6.10.13). Sixteen load steps of  $\Delta q_0 = -0.625$  psi are used. Figure 6.10.13 shows the center deflection versus applied load for various meshes. For the total load (10 psi) considered, the shell experiences no snap through behavior.

**Example 6.10.9** (*Clamped orthotropic cylinder*)

The last example of this chapter is concerned with the nonlinear bending of an orthotropic cylinder clamped at its ends (see Figure 6.10.14). The following geometric and material parameters (those of glass-epoxy fiber-reinforced composite material) are used:

$$E_1 = 7.5 \times 10^6 \text{ psi}, \quad E_2 = 2.0 \times 10^6 \text{ psi}, \quad G_{12} = 1.25 \times 10^6 \text{ psi}, \quad G_{13} = G_{23} = 0.625 \times 10^6 \text{ psi}$$

$$\nu_{12} = 0.25, \quad a = 10 \text{ in.}, \quad R = 20 \text{ in.}, \quad h = 1.0 \text{ in.}, \quad \alpha = \frac{\pi}{8} \text{ rad.} \quad (6.10.19)$$

The boundary conditions of the computational domain are

$$\text{At } \xi_1 = 0: \quad u_1 = \phi_1 = 0; \quad \text{At } \xi_2 = 0, \alpha: \quad u_2 = \phi_2 = 0 \text{ (symmetry)}$$

$$\text{At } \xi_1 = \frac{a}{2}: \quad u_1 = u_2 = u_3 = \phi_1 = \phi_2 = 0 \quad (6.10.20)$$

Twenty load steps of  $\Delta q_0 = 500$  psi are used. Figure 6.10.15 shows the center deflection versus applied load for various meshes. The results are in close agreement with those of Kreja, Schmidt, and Reddy [60].

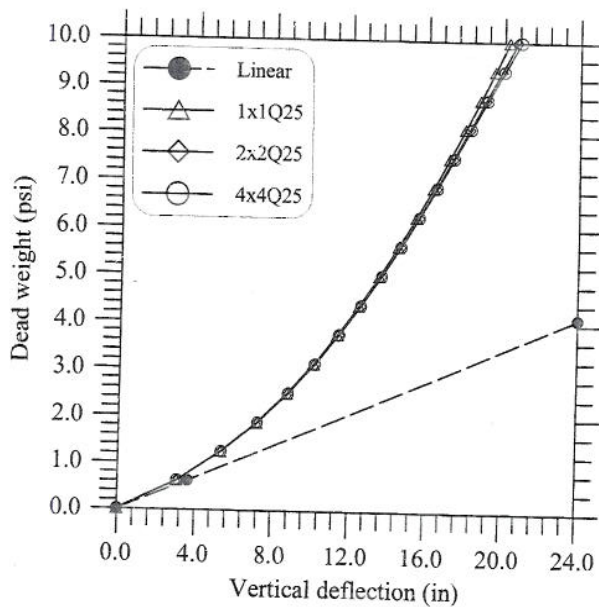


**Figure 6.10.13** Center deflection versus load for a cylindrical shell panel under its own weight.

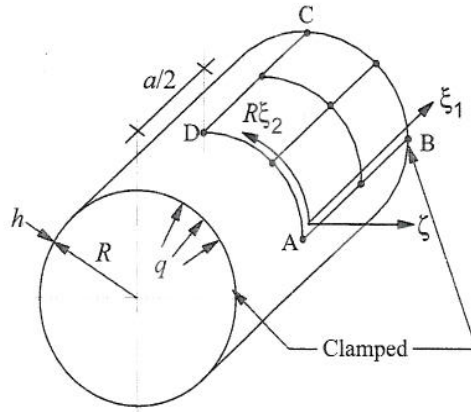


Figure 6.10.14 Geometry and computational domain of a clamped circular cylinder.

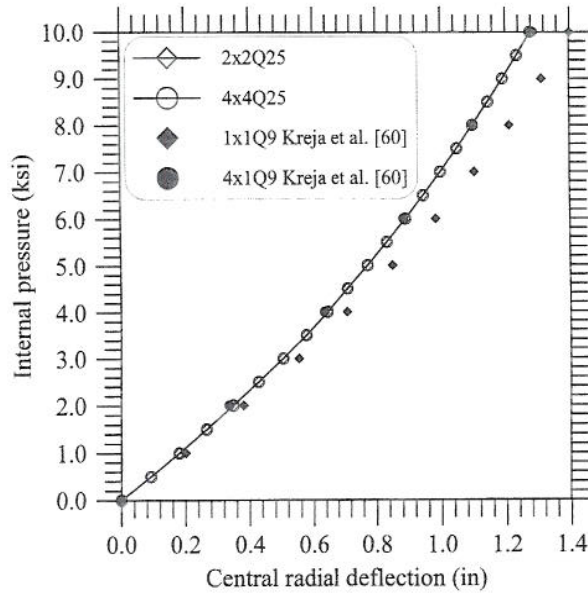


Figure 6.10.15 Center deflection versus load for the clamped orthotropic cylinder.

## Problems

6.1 Develop the weak forms of the following linear equations governing the classical plate theory:

$$-\left(\frac{\partial^2 M_{xx}}{\partial x^2} + 2\frac{\partial^2 M_{xy}}{\partial x \partial y} + \frac{\partial^2 M_{yy}}{\partial y^2}\right) = q \quad (\text{a})$$

$$-\frac{\partial^2 w_0}{\partial x^2} - (\bar{D}_{22} M_{xx} - \bar{D}_{12} M_{yy}) = 0 \quad (\text{b})$$

$$-\frac{\partial^2 w_0}{\partial y^2} - (\bar{D}_{12} M_{xx} - \bar{D}_{11} M_{yy}) = 0 \quad (\text{c})$$

$$-2\frac{\partial^2 w_0}{\partial x \partial y} - (D_{66})^{-1} M_{xy} = 0 \quad (\text{d})$$

where

$$\bar{D}_{ij} = \frac{D_{ij}}{D_0}, \quad D_0 = D_{11}D_{22} - D_{12}^2 \quad (\text{e})$$

$D_{ij}$  being the bending stiffnesses of an orthotropic plate

$$D_{ij} = Q_{ij} \frac{h^3}{12}, \quad (i = 1, 2, 6), \quad (\text{f})$$

and  $Q_{ij}$  are the elastic stiffnesses defined in terms of the principal moduli ( $E_1, E_2$ ), shear modulus  $G_{12}$ , and Poisson's ratio  $\nu_{12}$  as

$$\begin{aligned} Q_{11} &= \frac{E_1}{1 - \nu_{12}\nu_{21}}, & Q_{12} &= \frac{\nu_{12}E_2}{1 - \nu_{12}\nu_{21}}, & Q_{22} &= \frac{E_2}{1 - \nu_{12}\nu_{21}}, \\ Q_{66} &= \frac{1}{S_{66}} = G_{12}, & \nu_{21} &= \nu_{12} \frac{E_2}{E_1} \end{aligned} \quad (\text{g})$$

6.2 Develop the (mixed) finite element model associated with the equations in Problem 6.1. Assume approximation of the form

$$\begin{aligned} w_0 &= \sum_{i=1}^r w_i \psi_i^{(1)}, & M_{xx} &= \sum_{i=1}^s M_{xi} \psi_i^{(2)} \\ M_{yy} &= \sum_{i=1}^p M_{yi} \psi_i^{(3)}, & M_{xy} &= \sum_{i=1}^q M_{xyi} \psi_i^{(4)} \end{aligned}$$

where  $\psi_i^{(\alpha)}$ , ( $\alpha = 1, 2, 3, 4$ ) are appropriate interpolation functions. Discuss the minimum requirements of the interpolation functions.

6.3 Assume

$$\psi_i^1 = \psi_i^2 = \psi_i^3 = \psi_i^4 = \text{bilinear functions of a rectangular element} \quad (\text{a})$$

and develop the finite element program of the mixed model of Problems 1 and 2. The resulting stiffness matrix is of the order 16 by 16. Analytical computation of the coefficient matrices for a rectangular element is simple and straightforward.

6.4 Develop the weak forms of the following nonlinear equations governing the classical plate theory:

$$-\left(\frac{\partial N_{xx}}{\partial x} + \frac{\partial N_{xy}}{\partial y}\right) = 0 \quad (\text{a})$$

$$-\left(\frac{\partial N_{xy}}{\partial x} + \frac{\partial N_{yy}}{\partial y}\right) = 0 \quad (\text{b})$$

$$-\left(\frac{\partial^2 M_{xx}}{\partial x^2} + 2\frac{\partial^2 M_{xy}}{\partial x\partial y} + \frac{\partial^2 M_{yy}}{\partial y^2}\right) - \mathcal{N}(u_0, v_0, w_0) = q \quad (\text{c})$$

$$-\frac{\partial^2 w_0}{\partial x^2} - (\bar{D}_{22}M_{xx} - \bar{D}_{12}M_{yy}) = 0 \quad (\text{d})$$

$$-\frac{\partial^2 w_0}{\partial y^2} - (\bar{D}_{12}M_{xx} - \bar{D}_{11}M_{yy}) = 0 \quad (\text{e})$$

$$-2\frac{\partial^2 w_0}{\partial x\partial y} - (D_{66})^{-1}M_{xy} = 0 \quad (\text{f})$$

where  $(N_{xx}, N_{yy}, N_{xy}, \mathcal{N})$  are known in terms of  $(u_0, v_0, w_0)$  and their derivatives by Eqs. (6.3.32) and (6.3.14a). Note that the dependent unknowns are  $u_0, v_0, w_0, M_{xx}, M_{yy},$  and  $M_{xy}$ .

6.5 Develop the (mixed) nonlinear finite element model of the equations in Problem 6.4. Assume interpolation of the form

$$u_0 = \sum_{i=1}^r u_i \psi_i^{(1)}, \quad v_0 = \sum_{i=1}^r v_i \psi_i^{(1)}, \quad w_0 = \sum_{i=1}^r w_i \psi_i^{(2)}$$

$$M_{xx} = \sum_{i=1}^s M_{xi} \psi_i^{(3)}, \quad M_{yy} = \sum_{i=1}^p M_{yi} \psi_i^{(4)}, \quad M_{xy} = \sum_{i=1}^q M_{xyi} \psi_i^{(5)}$$

6.6 Implement the mixed finite element model of Problem 6.5 and validate your program with the example problems presented in Section 6.5.

6.7 Develop the weak forms of the following nonlinear equations governing the classical plate theory:

$$-\left(\frac{\partial N_{xx}}{\partial x} + \frac{\partial N_{xy}}{\partial y}\right) = 0, \quad -\left(\frac{\partial N_{xy}}{\partial x} + \frac{\partial N_{yy}}{\partial y}\right) = 0$$

$$-\frac{\partial^2 M_{xx}}{\partial x^2} + 4D_{66}\frac{\partial^4 w_0}{\partial x^2\partial y^2} - \frac{\partial^2 M_{yy}}{\partial y^2} - \frac{\partial}{\partial x}\left(N_{xx}\frac{\partial w_0}{\partial x} + N_{xy}\frac{\partial w_0}{\partial y}\right)$$

$$-\frac{\partial}{\partial y}\left(N_{xy}\frac{\partial w_0}{\partial x} + N_{yy}\frac{\partial w_0}{\partial y}\right) = q$$

$$-\frac{\partial^2 w_0}{\partial x^2} - (\bar{D}_{22}M_{xx} + \bar{D}_{12}M_{yy}) = 0, \quad -\frac{\partial^2 w_0}{\partial y^2} - (\bar{D}_{12}M_{xx} + \bar{D}_{11}M_{yy}) = 0$$

where  $(N_{xx}, N_{yy}, N_{xy})$  are known in terms of  $(u_0, v_0, w_0)$  and their derivatives by Eqs. (6.3.32). Note that the dependent unknowns are  $u_0, v_0, w_0, M_{xx},$  and  $M_{yy}$ .

6.8 Develop the (mixed) nonlinear finite element model of the equations in Problem 6.7 by assuming approximations of the form

$$u_0 = \sum_{i=1}^r u_i \psi_i^{(1)}, \quad v_0 = \sum_{i=1}^r v_i \psi_i^{(1)}, \quad w_0 = \sum_{i=1}^r w_i \psi_i^{(2)}$$



$$M_{xx} = \sum_{i=1}^s M_{xi} \psi_i^{(3)}, \quad M_{yy} = \sum_{i=1}^p M_{yi} \psi_i^{(4)}$$

- 6.9 Implement the nonlinear finite element model of Problem 6.8 into a computer program and validate it with the known results of this chapter.
- 6.10 Develop the weak forms of the following nonlinear equations governing the first-order shear deformation plate theory:

$$\begin{aligned} -\left(\frac{\partial N_{xx}}{\partial x} + \frac{\partial N_{xy}}{\partial y}\right) &= 0, & -\left(\frac{\partial N_{xy}}{\partial x} + \frac{\partial N_{yy}}{\partial y}\right) &= 0 \\ -A_{55} \frac{\partial}{\partial x} \left(\frac{\partial w_0}{\partial x} + \phi_x\right) - A_{44} \frac{\partial}{\partial y} \left(\frac{\partial w_0}{\partial y} + \phi_y\right) \\ -\frac{\partial}{\partial x} \left(N_{xx} \frac{\partial w_0}{\partial x} + N_{xy} \frac{\partial w_0}{\partial y}\right) - \frac{\partial}{\partial y} \left(N_{xy} \frac{\partial w_0}{\partial x} + N_{yy} \frac{\partial w_0}{\partial y}\right) &= q \\ -\frac{\partial M_{xx}}{\partial x} - D_{66} \frac{\partial}{\partial y} \left(\frac{\partial \phi_x}{\partial y} + \frac{\partial \phi_y}{\partial x}\right) + K_s A_{55} \left(\frac{\partial w_0}{\partial x} + \phi_x\right) &= 0 \\ -D_{66} \frac{\partial}{\partial x} \left(\frac{\partial \phi_x}{\partial y} + \frac{\partial \phi_y}{\partial x}\right) - \frac{\partial M_{yy}}{\partial y} + K_s A_{44} \left(\frac{\partial w_0}{\partial y} + \phi_y\right) &= 0 \end{aligned}$$

where  $(N_{xx}, N_{yy}, N_{xy})$  are known in terms of  $(u_0, v_0, w_0)$  and their derivatives by Eqs. (6.3.32). Note that the dependent unknowns are  $(u_0, v_0, w_0, \phi_x, \phi_y, M_{xx}, M_{yy})$ .

- 6.11 Develop the (mixed) nonlinear finite element model of the equations in Problem 6.10 by assuming approximations of the form

$$\begin{aligned} u_0 &= \sum_{i=1}^r u_i \psi_i^{(1)}, & v_0 &= \sum_{i=1}^r v_i \psi_i^{(1)}, & w_0 &= \sum_{i=1}^r w_i \psi_i^{(2)} \\ \phi_x &= \sum_{i=1}^r S_i^1 \psi_i^{(3)}, & \phi_y &= \sum_{i=1}^r S_i^2 \psi_i^{(3)} \\ M_{xx} &= \sum_{i=1}^s M_{xi} \psi_i^{(4)}, & M_{yy} &= \sum_{i=1}^p M_{yi} \psi_i^{(5)} \end{aligned}$$

- 6.12 Determine the load-deflection behavior of a rectangular plate with two opposite edges simply supported (SS-1) and the other two edges free, and subjected to uniformly distributed transverse load. Use  $a = 10$  in.,  $h = 1$  in.,  $E_1 = 7.8 \times 10^6$  psi,  $E_2 = 2.6 \times 10^6$  psi,  $\nu_{12} = 0.25$ ,  $G_{12} = G_{13} = G_{23} = 1.3 \times 10^6$  psi, and  $8 \times 8$  uniform mesh of nonconforming CPT elements in a quadrant of the plate. Use load steps such that the load parameter  $P \equiv q_0 a^4 / E_2 h^4$  is equal to 5, and use 12 load steps. Plot (a) load versus center deflection ( $w_0/h$  versus  $P$ ), and (b) load versus maximum stress ( $\sigma_{xx}$  and  $\sigma_{xy}$ ). Use a convergence tolerance of  $\epsilon = 10^{-2}$  and a reasonable value of  $ITMAX$ .
- 6.13 Repeat Problem 6.12 for a rectangular plate with two opposite edges simply supported (SS-1) and the other two edges clamped.
- 6.14 Repeat Problem 6.12 for a rectangular plate with two opposite edges clamped and the other two edges free.
- 6.15 Repeat Problem 6.12 using  $4 \times 4$  Q9 mesh of the FSDT elements.
- 6.16 Repeat Problem 6.13 using  $4 \times 4$  Q9 mesh of the FSDT elements.
- 6.17 Repeat Problem 6.14 using  $4 \times 4$  Q9 mesh of the FSDT elements.
- 6.18 Analyze the circular plate problem of Example 6.8.6 when the edge is simply supported (SS-3). Use all other parameters as in Example 6.8.6.

- 6.19 Verify the strain-displacement relations in Eq. (6.9.18).
- 6.20 Verify the strain-displacement relations associated with the displacement field in Eq. (6.9.19) are given by (6.9.20a,b).
- 6.21 Derive the equations of motion in Eqs. (6.9.27)–(6.9.31).
- 6.22 Derive the tangent stiffness coefficients associated with the finite element model in Eqs. (6.10.6)–(6.10.8).
- 6.23 Analyze the circular cylinder problem of Example 6.10.12 by assuming the fiber direction is  $\xi_2$  (as opposed to  $\xi_1$ ) and compare the results with those in Figure 6.10.15.
- 6.24 Show that the second derivatives of a function  $f(\xi, \eta)$  with respect to the global coordinates  $(x, y)$  are related to its derivatives with respect to the local coordinates  $(\xi, \eta)$  by [see Eqs. (5.5.4)–(5.5.8)]

$$\begin{Bmatrix} \frac{\partial^2 f}{\partial x^2} \\ \frac{\partial^2 f}{\partial y^2} \\ \frac{\partial^2 f}{\partial x \partial y} \end{Bmatrix} = \begin{bmatrix} \left(\frac{\partial x}{\partial \xi}\right)^2 & \left(\frac{\partial y}{\partial \xi}\right)^2 & 2\frac{\partial x}{\partial \xi} \frac{\partial y}{\partial \xi} \\ \left(\frac{\partial x}{\partial \eta}\right)^2 & \left(\frac{\partial y}{\partial \eta}\right)^2 & 2\frac{\partial x}{\partial \eta} \frac{\partial y}{\partial \eta} \\ \frac{\partial x}{\partial \xi} \frac{\partial x}{\partial \eta} & \frac{\partial y}{\partial \xi} \frac{\partial y}{\partial \eta} & \frac{\partial x}{\partial \eta} \frac{\partial y}{\partial \xi} + \frac{\partial y}{\partial \eta} \frac{\partial x}{\partial \xi} \end{bmatrix}^{-1} \left( \begin{Bmatrix} \frac{\partial^2 f}{\partial \xi^2} \\ \frac{\partial^2 f}{\partial \eta^2} \\ \frac{\partial^2 f}{\partial \xi \partial \eta} \end{Bmatrix} - \begin{bmatrix} \frac{\partial^2 x}{\partial \xi^2} & \frac{\partial^2 y}{\partial \xi^2} \\ \frac{\partial^2 x}{\partial \eta^2} & \frac{\partial^2 y}{\partial \eta^2} \\ \frac{\partial^2 x}{\partial \xi \partial \eta} & \frac{\partial^2 y}{\partial \xi \partial \eta} \end{bmatrix} \begin{Bmatrix} \frac{\partial f}{\partial x} \\ \frac{\partial f}{\partial y} \end{Bmatrix} \right)$$

## References

- Reddy, J. N., *An Introduction to the Finite Element Method*, 2nd edn, McGraw-Hill, New York (1993).
- Reddy, J. N., *Energy Principles and Variational Methods in Applied Mechanics*, 2nd edn, John Wiley, New York (2002).
- Reddy, J. N., *Theory and Analysis of Elastic Plates*, Taylor and Francis, Philadelphia, PA (1999).
- Burnett, D. S., *Finite Element Analysis*, Addison-Wesley, Reading, MA (1987).
- Zienkiewicz, O. C. and Taylor, R. L., *The Finite Element Method, Vol. 1: Linear Problems*, McGraw-Hill, New York (1989).
- Hughes, T. J. R., *The Finite Element Method, Linear Static and Dynamic Finite Element Analysis*, Prentice-Hall, Englewood Cliffs, NJ (1987).
- Bathe, K. J., *Finite Element Procedures*, Prentice-Hall, Englewood Cliffs, NJ (1996).
- Gere, J. M. and Weaver, Jr., W., *Analysis of Framed Structures*, D. von Nostrand, New York (1965).
- Przemieniecki, J. S., *Theory of Matrix Structural Analysis*, McGraw-Hill, New York (1968).
- Severn, R. T., "Inclusion of Shear Deflection in the Stiffness Matrix for a Beam Element," *Journal of Strain Analysis*, **5**, 239–241 (1970).
- Nickell, R. E. and Secor, G. A., "Convergence of Consistently Derived Timoshenko Beam Finite Elements," *International Journal for Numerical Methods in Engineering*, **5**, 243–253 (1972).
- Reddy, J. N., "On Locking-Free Shear Deformable Beam Finite Elements," *Computer Methods in Applied Mechanics and Engineering*, **149**, 113–132 (1997).
- Hrabok, M. M. and Hrudey, T. M., "A Review and Catalog of Plate Bending Finite Elements," *Computers and Structures* **19**(3), 479–495 (1984).
- Bazeley, G. P., Cheung, Y. K., Irons, B. M., and Zienkiewicz, O. C., "Triangular Elements in Bending – Conforming and Non-Conforming Solutions," *Proceedings of the Conference on Matrix Methods in Structural Mechanics*, Air Force Institute of Technology, Wright-Patterson Air Force Base, OH, 547–576 (1965).

15. Clough, R. W. and Tocher, J. L., "Finite Element Stiffness Matrices for Analysis of Plates in Bending," *Proceedings of the Conference on Matrix Methods in Structural Mechanics*, Air Force Institute of Technology, Wright-Patterson Air Force Base, OH, 515-545 (1965).
16. Melosh, R. J., "Basis of Derivation of Matrices for the Direct Stiffness Method," *AIAA Journal*, 1, 1631-1637 (1963).
17. Zienkiewicz, O. C. and Cheung, Y. K., "The Finite Element Method for Analysis of Elastic Isotropic and Orthotropic Slabs," *Proceedings of the Institute of Civil Engineers*, London, 28, 471-488 (1964).
18. Bogner, F. K., Fox, R. L., and Schmidt, L. A., Jr., "The Generation of Inter-element Compatible Stiffness and Mass Matrices by the Use of Interpolation Formulas," *Proceedings of the Conference on Matrix Methods in Structural Mechanics*, Air Force Institute of Technology, Wright-Patterson Air Force Base, OH, 397-443 (1965).
19. Fraeijs de Veubeke, B., "A Conforming Finite Element for Plate Bending," *International Journal of Solids and Structures*, 4(1), 95-108 (1968).
20. Irons, B. M., "A Conforming Quartic Triangular Element for Plate Bending," *International Journal for Numerical Methods in Engineering* 1, 29-45 (1969).
21. Reddy, J. N., "Simple Finite Elements with Relaxed Continuity for Non-Linear Analysis of Plates," *Proceedings of the Third International Conference in Australia on Finite Element Methods*, University of New South Wales, Sydney, (1979).
22. Reddy, J. N., "A Penalty Plate-Bending Element for the Analysis of Laminated Anisotropic Composite Plates," *International Journal for Numerical Methods in Engineering*, 15(8), 1187-1206 (1980).
23. Huang, H. C. and Hinton, E., "A Nine-Node Lagrangian Plate Element with Enhanced Shear Interpolation," *Engineering Computations*, 1, 369-379 (1984).
24. Averill, R. C. and Reddy, J. N., "Behavior of Plate Elements Based on the First-Order Shear Deformation Theory," *Engineering Computations*, 7, 57-74 (1990).
25. Zienkiewicz, O. C., Too, J. J. M., and Taylor, R. L., "Reduced Integration Technique in General Analysis of Plates and Shells," *International Journal for Numerical Methods in Engineering*, 3, 275-290 (1971).
26. Hughes, T. J. R., Cohen, M., and Haroun, M., "Reduced and Selective Integration Techniques in the Finite Element Analysis of Plates," *Nuclear Engineering and Design*, 46, 203-222 (1981).
27. Belytschko, T., Tsay, C. S., and Liu, W. K., "Stabilization Matrix for the Bilinear Mindlin Plate Element," *Computer Methods in Applied Mechanics and Engineering*, 29, 313-327 (1981).
28. Bathe, K. J. and Dvorkin, E. N., "A Four-Node Plate Bending Element Based on Mindlin/Reissner Plate Theory and Mixed Interpolation," *International Journal for Numerical Methods in Engineering*, 21, 367-383 (1985).
29. Barlow, J., "Optimal Stress Location in Finite Element Models," *International Journal for Numerical Methods in Engineering*, 10, 243-251 (1976).
30. Barlow, J., "More on Optimal Stress Points - Reduced Integration Element Distortions and Error Estimation," *International Journal for Numerical Methods in Engineering*, 28, 1486-1504 (1989).
31. Reddy, J. N. and Chao, W. C., "A Comparison of Closed-Form and Finite Element Solutions of Thick Laminated Anisotropic Rectangular Plates," *Nuclear Engineering and Design*, 64, 153-167 (1981).
32. Lévy, S., "Bending of Rectangular Plates with Large Deflections," Report No. 737, NACA (1942).

33. Wang, C. T., "Bending of Rectangular Plates with Large Deflections," Report No. 1462, NACA (1948).
34. Kawai, T. and Yoshimura, N., "Analysis of Large Deflection of Plates by the Finite Element Method," *International Journal for Numerical Methods in Engineering*, **1**, 123-133 (1969).
35. Zaghoul, S. A. and Kennedy, J. B., "Nonlinear Behavior of Symmetrically Laminated Plates," *Journal of Applied Mechanics*, **42**, 234-236 (1975).
36. Lévy, S., "Square Plate with Clamped Edges Under Pressure Producing Large Deflections," Tech. Note 847, NACA (1942).
37. Pica, A., Wood, R. D., and Hinton, E., "Finite Element Analysis of Geometrically Nonlinear Plate Behaviour Using a Mindlin Formulation," *Computers and Structures*, **11**, 203-215 (1980).
38. Reddy, J. N., "Analysis of Layered Composite Plates Accounting for Large Deflections and Transverse Shear Strains," in *Recent Advances in Non-Linear Computational Mechanics*, edited by E. Hinton, D. R. J. Owen, and C. Taylor, Chapter 6, 155-202, Pineridge Press, Swansea, UK (1982).
39. Reddy, J. N., "On Mixed Finite-Element Formulations of a Higher-Order Theory of Composite Laminates," *Finite Element Methods for Plate and Shell Structures*, T. J. R. Hughes and E. Hinton (eds.), pp. 31-57, Pineridge Press, UK, (1986).
40. Reddy, J. N., *Mechanics of Laminated Composite Plates and Shells. Theory and Analysis*, 2nd edn, CRC Press, Boca Raton, FL (2004).
41. Ambartsumyan, S. A., "Calculation of Laminated Anisotropic Shells," *Izvestiia Akademiia Nauk Armenskoi SSR, Ser. Fiz. Mat. Est. Tekh. Nauk.*, **6**(3), p.15 (1953).
42. Ambartsumyan, S. A., *Theory of Anisotropic Shells*, NASA Report TT F-118 (1964).
43. Ambartsumyan, S. A., *Theory of Anisotropic Shells*, Moscow, 1961; English translation, NASA-TT-F-118, (1964).
44. Flügge, W., *Stresses in Shells*, Springer, Berlin (1960).
45. Kraus, H., *Thin Elastic Shells*, John Wiley, New York (1967).
46. Timoshenko, S. and Woinowsky-Krieger, S., *Theory of Plates and Shells*, McGraw-Hill, New York (1959).
47. Dym, C. L., *Introduction to the Theory of Shells*, Pergamon, New York (1974).
48. Sanders Jr., J. L., "Nonlinear Theories for Thin Shells," *Quarterly of Applied Mathematics*, **21**(1), 21-36 (1963).
49. Budiansky, B., and Sanders, J. L., "On the 'Best' First Order Linear Shell Theory," *Progress in Applied Mechanics, The Prager Anniversary Volume*, Macmillan, New York, 129-140 (1963).
50. Reddy, J. N., *Energy and Variational Methods in Applied Mechanics*, 1st edn, John Wiley, New York (1984).
51. Palazotto, A. N. and Dennis, S.T., *Nonlinear Analysis of Shell Structures*, AIAA Education Series, Washington, DC (1992).
52. Vlasov, V. Z., *General Theory of Shells and Its Applications in Engineering*, (Translation of *Obshchaya teoriya obolochek i yeye prilozheniya v tekhnike*), NASA TT F-99, National Aeronautics and Space Administration, Washington, DC (1964).
53. Rao, K. P., "A Rectangular Laminated Anisotropic Shallow Thin Shell Finite Element," *Computer Methods in Applied Mechanics and Engineering*, **15**, 13-33 (1978).
54. Brebbia, C. and Connor, J., "Geometrically Nonlinear Finite Element Analysis," *Journal of Engineering Mechanics*, 463-483 (1969).
55. Scordelis, A. C. and Lo, K.S., "Computer Analysis of Cylindrical Shells," *Journal of American Concrete Institute*, 538-560 (1964).

56. Cantin, G. and Clough, R. W., "A Curved Cylindrical Shell Finite Element," *AIAA Journal*, **6**, 1057 (1968).
57. Simo, J. C., Fox, D. D., and Rifai, M. S., "On a Stress Resultant Geometrically Exact Shell Model. Part II: The Linear Theory," *Computer Methods in Applied Mechanics and Engineering*, **73**, 53-92 (1989).
58. Zienkiewicz, O. C., *The Finite Element Method*, McGraw-Hill, New York (1977).
59. Cho, M. and Roh, H. Y., "Development of Geometrically Exact New Elements Based on General Curvilinear Coordinates," *International Journal for Numerical Methods in Engineering*, **56**, 81-115 (2003).
60. Kreja, I., Schmidt, R., and Reddy, J. N., "Finite Elements Based on a First-order Shear Deformation Moderate Rotation Theory with Applications to the Analysis of Composite Structures," *International Journal of Non-Linear Mechanics*, **32**(6), 1123-1142 (1997).
61. Sabir, A. B. and Lock, A. C., "The Application of Finite Elements to the Large Deflection Geometrically Nonlinear Behavior of Cylindrical Shells," *Variational Methods in Engineering, Vol. II* pp. 7/66-7/75, Southampton, UK (1972).

---

## Flows of Viscous Incompressible Fluids

---

### 7.1 Introduction

Fluid mechanics is one of the oldest branches of physics, and is concerned with the motion of gases and liquids and their interaction with the surroundings. For example, the flight of birds in the air and the motion of fish in the water can be understood by the principles of fluid mechanics. Such understanding helps us design airplanes and ships. The formation of tornadoes, hurricanes, and thunderstorms can also be explained with the help of the equations of fluid mechanics.

A fluid state of matter is characterized by the relative mobility of its molecules. Very strong intermolecular attractive forces exist in solids which are responsible for the property of relative rigidity (or stiffness) in solids. The intermolecular forces are weaker in liquids and extremely small in gases. The stress in a solid body is proportional to the strain (i.e. deformation per unit length), while the stress in a fluid is proportional to the time rate of strain (i.e. rate of deformation per unit length). The proportionality parameter in the case of fluids is known as the *viscosity*. It is a measure of the intermolecular forces exerted as layers of fluid attempt to slide past one another. The viscosity of a fluid, in general, is a function of the thermodynamic state of the fluid and in some cases the strain rate.

Fluid mechanics is a very broad area and is traditionally divided into smaller topical areas based on characteristics of the fluid properties or the basic nature of the flow. An *inviscid fluid* is one where the viscosity is assumed to be zero. An *incompressible fluid* is one with constant density or an *incompressible flow* is one in which density variations (compared to a reference density) are negligible. An inviscid and incompressible fluid is termed an *ideal* or a *perfect* fluid. A *real fluid* is one with finite viscosity, and it may or may not be incompressible. When the viscosity of a fluid depends only on thermodynamic properties, and the stress is linearly related to the strain rate, the fluid is said to be *Newtonian*. A *non-Newtonian fluid* is one which does not obey the Newtonian (i.e. linear) stress-strain rate relation. A non-Newtonian constitutive relation can be algebraic, differential, or integral type.

The flow of viscous fluids can also be classified into two major types: smooth, orderly motion is called *laminar flow*, and a random, fluctuating motion is called *turbulent flow*. Viscous flows can be characterized by a non-dimensional parameter known as the *Reynolds number*,  $Re = \rho UL/\mu$ , which is defined as the ratio of inertial forces  $\rho U^2$  to viscous forces  $\mu U/L$ . Here  $\rho$  denotes the density of the fluid,  $\mu$  the fluid viscosity,  $U$  the characteristic flow velocity, and  $L$  is a characteristic dimension of the flow region. High viscosity fluids and/or small velocities produce relatively small Reynolds numbers and a laminar flow. The case of  $Re \ll 1$  corresponds to the flow (called *Stokes flow*) in which the inertial effects are small compared to the viscous effects and therefore neglected. The flow of less viscous fluids and/or higher velocities leads to higher Reynolds numbers and a turbulent flow. High Reynolds number flows contain regions of both laminar and turbulent flows.

The motion of a fluid is governed by the global laws of conservation of mass, momentum, and energy. These equations consist of a set of nonlinear partial differential equations in terms of the velocity components, temperature, and pressure. The equations of motion resulting from the application of the conservation of linear momentum principle are known as the *Navier-Stokes equations*. When temperature effects are not important, the energy equation is uncoupled from the Navier-Stokes equations. Thus for isothermal flows, only the Navier-Stokes equations and continuity equation are solved. One may non-dimensionalize the variables in the Navier-Stokes equations to express them in terms of the Reynolds number. We shall work with physical quantities in this study.

In the present chapter we review the governing equations of flows of incompressible fluids, develop finite element models based on alternative formulations, and discuss computer implementation of the finite element models developed herein. Simple examples of applications of the finite element models are also included.

## 7.2 Governing Equations

### 7.2.1 Introduction

There are two alternative descriptions used to express the conservation laws in analytical form. In the first, one considers the motion of all matter passing through a *fixed spatial location*. Here one is interested in various properties (e.g. velocity, pressure, temperature, density, and so on) of the matter that instantly occupies the fixed spatial location. This description is called the *Eulerian description* or *spatial description*. In the second, one focuses attention on a *set of fixed material particles*, irrespective of their spatial locations. The relative displacements of these particles and the stress caused by external forces and temperature are of interest in this case. This description is known as the *Lagrangian description* or *material description*. The Eulerian

description is most commonly used to study fluid flows and coupled fluid flow and heat transfer, while the Lagrangian description is generally used to study stress and deformation of solid bodies. Here we present the governing equations of a continuous medium based on the Eulerian description. For a derivation of the equations, the reader may consult the books on continuum mechanics (e.g. Bird, Stewart, Lightfoot [1], Malvern [2], and Reddy and Rasmussen [3]), heat transfer (e.g. see Bejan [4], Holman [5], and Özisik [6,7]), and fluid mechanics (e.g. Batchelor [8] and Schlichting [9]).

### 7.2.2 Conservation of Mass

The principle of conservation of mass can be stated as *the time rate of change of mass in a fixed volume is equal to the rate of inflow of mass through the surface*. Application of the principle to an element of the region (called control volume) results in the following equation, known as the *continuity equation*:

$$\frac{\partial \rho}{\partial t} + \nabla \cdot (\rho \mathbf{v}) = 0 \tag{7.2.1}$$

where  $\rho$  is the density (kg/m<sup>3</sup>) of the medium,  $\mathbf{v}$  the velocity vector (m/s), and  $\nabla$  is the vector differential operator. Introducing the *material derivative* or *Eulerian derivative* operator  $D/Dt$

$$\frac{D}{Dt} = \frac{\partial}{\partial t} + \mathbf{v} \cdot \nabla \tag{7.2.2}$$

Eq. (7.2.1) can be expressed in the alternative form

$$\frac{D\rho}{Dt} + \rho \nabla \cdot \mathbf{v} = 0 \tag{7.2.3}$$

For steady-state conditions, the continuity equation becomes

$$\nabla \cdot (\rho \mathbf{v}) = 0 \tag{7.2.4}$$

When the density changes following a fluid particle are negligible, the continuum is termed *incompressible* and we have  $D\rho/Dt = 0$ . The continuity equation (7.2.3) then becomes

$$\nabla \cdot \mathbf{v} = 0 \tag{7.2.5}$$

which is often referred to as the *incompressibility condition*.

The incompressibility condition (7.2.5) expresses the fact that the volume change is zero for an incompressible fluid during its deformation. Since the velocity field  $\mathbf{u}$  is required to satisfy the equations of motion derived in the next section, Eq. (7.2.5) is known as a constraint among the velocity components.



### 7.2.3 Conservation of Momenta

The principle of conservation of linear momentum (or Newton's Second Law of motion) states that *the time rate of change of linear momentum of a given set of particles is equal to the vector sum of all external forces acting on the particles of the set, provided Newton's Third Law of action and reaction governs the internal forces.* Newton's Second Law can be written as

$$\rho \frac{D\mathbf{v}}{Dt} = \nabla \cdot \boldsymbol{\sigma} + \rho \mathbf{f} \quad (7.2.6)$$

where  $\boldsymbol{\sigma}$  is the Cauchy stress tensor ( $\text{N/m}^2$ ) and  $\mathbf{f}$  is the body force vector measured per unit mass. Equation (7.2.6) is known as the Navier-Stokes equations.

The principle of conservation of angular momentum can be stated as *the time rate of change of the total moment of momentum of a given set of particles is equal to the vector sum of the moments of the external forces acting on the system.* In the absence of distributed couples, the principle leads to the symmetry of the stress tensor:

$$\boldsymbol{\sigma} = (\boldsymbol{\sigma})^T \quad (7.2.7)$$

where the superscript  $T$  denotes the transpose of the enclosed quantity.

### 7.2.4 Conservation of Energy

The principle of conservation of energy (or the First Law of Thermodynamics) states that *the time rate of change of the total energy is equal to the sum of the rate of work done by applied forces and the change of heat content per unit time.* For an incompressible fluid, the First Law of Thermodynamics can be expressed as

$$\rho c_v \frac{DT}{Dt} = -\nabla \cdot \mathbf{q} + Q + \Phi \quad (7.2.8)$$

where  $T$  denotes the temperature ( $^{\circ}\text{C}$ ),  $\mathbf{q}$  the heat flux vector ( $\text{W/m}^2$ ),  $Q$  is the internal heat generation ( $\text{W/m}^3$ ),  $\Phi$  is the viscous dissipation function

$$\Phi = \boldsymbol{\tau} : \mathbf{D} \quad (7.2.9)$$

and  $c_v$  is the specific heat [ $\text{J}/(\text{kg} \cdot ^{\circ}\text{C})$ ] at constant volume. In Eq. (7.2.9),  $\boldsymbol{\tau}$  denotes the viscous part of the stress tensor  $\boldsymbol{\sigma}$  and  $\mathbf{D}$  the strain rate tensor, as discussed below. Other types of internal heat generation may arise from other physical processes such as chemical reactions and Joule heating.

### 7.2.5 Constitutive Equations

For most of this study we assume the fluid to be Newtonian (i.e. the constitutive relations are linear). Non-Newtonian fluids will be considered in Chapter 10. Further, the fluids are assumed to be incompressible, and the flow is laminar. For flows involving buoyancy forces, an extended form of the Boussinesq approximation (see Bejan [4]) may be invoked, which allows the density  $\rho$  to vary with temperature  $T$  according to the relation

$$\rho = \rho_0[1 - \beta(T - T_0)] \tag{7.2.10}$$

where  $\beta$  is the coefficient of thermal expansion ( $m/m/^\circ C$ ) and the subscript zero indicates a reference condition. The variation of density as given in Eq. (7.2.10) is permitted only in the description of the body force; the density in all other situations is assumed to be that of the reference state,  $\rho_0$ .

For viscous incompressible fluids the total stress  $\sigma$  can be decomposed into hydrostatic and viscous parts:

$$\sigma = \tau + (-P)\mathbf{I} \tag{7.2.11}$$

where  $P$  is the hydrostatic pressure,  $\mathbf{I}$  the unit tensor, and  $\tau$  is the viscous stress tensor. For Newtonian fluids, the viscous stress tensor is related to the strain rate tensor  $\mathbf{D}$  by

$$\tau = \mathbf{C} : \mathbf{D} \tag{7.2.12}$$

where  $\mathbf{C}$  is the fourth-order tensor of fluid properties. The strain rate tensor  $\mathbf{D}$  is defined by

$$\mathbf{D} = \frac{1}{2}[(\nabla\mathbf{v}) + (\nabla\mathbf{v})^T] \tag{7.2.13}$$

For an isotropic fluid (i.e. whose material properties are independent of direction), the fourth-order tensor  $\mathbf{C}$  can be expressed in terms of two constants,  $\lambda$  and  $\mu$ , called the Lamé constants, and Eq. (7.2.12) takes the form

$$\tau = \lambda(\text{tr}[\mathbf{D}])\mathbf{I} + 2\mu\mathbf{D} \tag{7.2.14}$$

where  $(\text{tr}[\mathbf{D}])$  denotes the *trace* (or sum of the diagonal elements) of the matrix  $[\mathbf{D}]$ , which consists of the elements of the second-order tensor  $\mathbf{D}$ . For an incompressible fluid, we have  $\text{tr}[\mathbf{D}] = 0$  and Eq. (7.2.14) becomes

$$\tau = 2\mu\mathbf{D} \tag{7.2.15}$$

The Fourier heat conduction law states that the heat flux is proportional to the gradient of temperature

$$\mathbf{q} = -\mathbf{k} \cdot \nabla T \tag{7.2.16}$$

where  $\mathbf{k}$  denotes the conductivity tensor of order two. The negative sign Eq. (7.2.16) indicates that heat flows from high-temperature regions to low temperature regions. For an isotropic medium,  $\mathbf{k}$  is of the form

$$\mathbf{k} = k\mathbf{I} \quad (7.2.1)$$

where  $k$  denotes the thermal conductivity [W/(m·°C)] of the medium.

The material coefficients,  $\mu$ ,  $c_v$ ,  $\beta$ , and  $\mathbf{k}$  are generally functions of position and temperature. Conductivity tensor is a symmetric, second-order tensor (i.e.  $\mathbf{k}^T = \mathbf{k}$ ). The volumetric heat source for the fluid and/or solid may be a function of temperature, time, and spatial location. In developing the finite element models, the dependence of the material properties on the spatial location is assumed. The dependence of the viscosity and conductivity on temperature and strain rates is discussed in [10].

### 7.2.6 Boundary Conditions

The boundary conditions for the flow problem (i.e. momentum equations) are given by [10]

$$\mathbf{v} = \hat{\mathbf{v}} \quad \text{on } \Gamma_v \quad (7.2.18a)$$

$$\mathbf{t} \equiv \hat{\mathbf{n}} \cdot \boldsymbol{\sigma} = \hat{\mathbf{t}} \quad \text{on } \Gamma_\sigma \quad (7.2.18b)$$

where  $\hat{\mathbf{n}}$  is the unit normal to the boundary and  $\Gamma_v$  and  $\Gamma_\sigma$  are the boundary portions on which the velocity and tractions are specified, respectively (see Figure 7.2.1).

The boundary conditions for the heat transfer problem (i.e. energy equation) are

$$T = \hat{T} \quad \text{on } \Gamma_T \quad (7.2.19a)$$

$$q_n \equiv \hat{\mathbf{n}} \cdot \mathbf{q} = \hat{q}_n \quad \text{on } \Gamma_q \quad (7.2.19b)$$

where  $\Gamma_T$  and  $\Gamma_q$  are the boundary portions on which the temperature and heat flux are specified, respectively. A more general boundary condition for the heat transfer problem is given by

$$q_{\text{cond}} + q_{\text{conv}} + q_{\text{rad}} = \hat{q}_n \quad \text{on } \Gamma_q \quad (7.2.20)$$

where  $q_{\text{cond}}$ ,  $q_{\text{conv}}$ , and  $q_{\text{rad}}$  are the conductive, convective, and radiative parts of heat flux, respectively,

$$q_{\text{cond}} = -\mathbf{k} \cdot \nabla T, \quad q_{\text{conv}} = h_c(T - T_c), \quad q_{\text{rad}} = h_r(T - T_r) \quad (7.2.21)$$

Here  $h_c$  and  $h_r$  denote the heat transfer coefficients associated with convective and radiative heat transfer, respectively. In general, they are functions of position, time, and temperature.

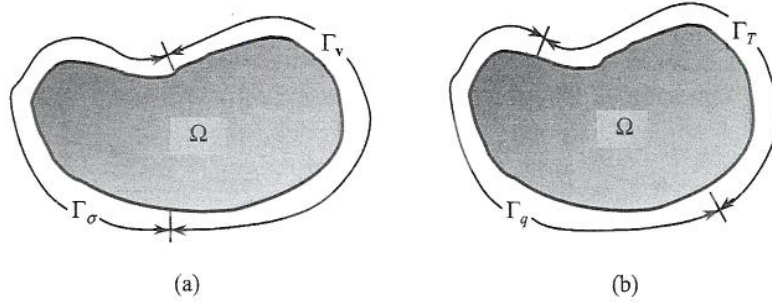


**Figure 7.2.1** A schematic of various boundary portions. (a) For fluid flow. (b) For heat transfer.

The various portions of the boundary  $\Gamma$  must satisfy the requirements

$$\Gamma_v \cup \Gamma_\sigma = \Gamma, \quad \Gamma_v \cap \Gamma_\sigma = \{0\} \tag{7.2.22a}$$

$$\Gamma_T \cup \Gamma_q = \Gamma, \quad \Gamma_T \cap \Gamma_q = \{0\} \tag{7.2.22b}$$

where  $\{0\}$  denotes the empty set. Equations (7.2.22a,b) imply that the total boundary is composed of two disjoint portions,  $\Gamma_v$  and  $\Gamma_\sigma$ , or  $\Gamma_T$  and  $\Gamma_q$ , whose union is the total boundary. Of course, in the analysis of practical problems one may encounter situations where, for example, both velocity and traction are known at a point. This is a mathematical singularity, and one must pick one of the two conditions but not both. Often the primary variables, i.e.  $\mathbf{v}$  and  $T$  are picked over the secondary variables  $\mathbf{t}$  and  $q_n$ .

### 7.3 Governing Equations in Terms of Primitive Variables

#### 7.3.1 Vector Form

Equations (7.2.3), (7.2.6), and (7.2.8) can be expressed in terms of the primitive variables  $(\mathbf{v}, P, T)$  by means of equations (7.2.12)–(7.2.16). The results are summarized below for isotropic, Newtonian, viscous, incompressible fluids in the presence of buoyancy forces:

$$\nabla \cdot \mathbf{v} = 0 \tag{7.3.1}$$

$$\rho_0 \left( \frac{\partial \mathbf{v}}{\partial t} + \mathbf{v} \cdot \nabla \mathbf{v} \right) = -\nabla P + \mu \nabla \cdot [(\nabla \mathbf{v}) + (\nabla \mathbf{v})^T] + \rho_0 \mathbf{f} + \rho_0 \mathbf{g} \beta (T - T_0) \tag{7.3.2}$$

$$\rho_0 c_v \left( \frac{\partial T}{\partial t} + \mathbf{v} \cdot \nabla T \right) = \nabla \cdot (k \nabla T) + Q + \Phi \tag{7.3.3}$$

where  $\mathbf{v}$  represents the velocity vector,  $\rho_0$  the density,  $\mathbf{g}$  the gravity force vector per unit mass,  $T$  the temperature,  $c_v$  the specific heat of the fluid at constant volume, and  $Q$  the rate of heat generation.

The above equations are valid for the fluid region  $\Omega_f$ . In the solid region  $\Omega_s$ , the fluid velocity is zero,  $\mathbf{v} = \mathbf{0}$ , and the only relevant equation is (7.3.3). The energy equation (7.3.3) for the solid region is given by

$$\rho_s C_s \frac{\partial T}{\partial t} = \nabla \cdot (k_s \nabla T) + Q_s \quad (7.3.4)$$

In writing Eq. (7.3.4) it is assumed that the solid is stationary with respect to the coordinate frame such that the convective transport of energy [i.e. the nonlinear part of Eq. (7.3.3)] need not be considered. The finite element model of Eq. (7.3.4) was discussed in Chapter 4 when the conductivity  $k_s$  is a function, in general, of  $x$ ,  $y$ , and  $T$ .

### 7.3.2 Cartesian Component Form

The vector form of the equations in (7.3.1)–(7.3.3) allows us to express them in any coordinate system by expressing the vector operator  $\nabla$  and any other vectors in that coordinate system. In the Cartesian coordinate system  $(x_1, x_2, x_3)$ , the kinematic and constitutive relations take the form

$$D_{ij} = \frac{1}{2} \left( \frac{\partial v_i}{\partial x_j} + \frac{\partial v_j}{\partial x_i} \right) \quad (7.3.5)$$

$$\sigma_{ij} = -P\delta_{ij} + \tau_{ij}; \quad \tau_{ij} = 2\mu D_{ij} \quad (7.3.6)$$

The conservation equations can be expressed as

$$\frac{\partial v_i}{\partial x_i} = 0 \quad (7.3.7)$$

$$\rho_0 \left( \frac{\partial v_i}{\partial t} + v_j \frac{\partial v_i}{\partial x_j} \right) = \frac{\partial}{\partial x_j} \left[ -P\delta_{ij} + \mu \left( \frac{\partial v_i}{\partial x_j} + \frac{\partial v_j}{\partial x_i} \right) \right] + \rho_0 f_i - \rho_0 g_i \beta (T - T_0) \quad (7.3.8)$$

$$\rho_0 C \left( \frac{\partial T}{\partial t} + v_j \frac{\partial T}{\partial x_j} \right) = \frac{\partial}{\partial x_i} \left( k \frac{\partial T}{\partial x_i} \right) + Q + 2\mu D_{ij} D_{ij} \quad (7.3.9)$$

for the fluid region  $\Omega_f$  and

$$\rho_s C_s \frac{\partial T}{\partial t} = \frac{\partial}{\partial x_i} \left( k_s \frac{\partial T}{\partial x_i} \right) + Q_s \quad (7.3.10)$$

for the solid region  $\Omega_s$ . Equations (7.3.5)–(7.3.10) are written for a Cartesian geometry in an Eulerian reference frame, with the indices  $i, j = 1, 2, 3$  (or

$i, j = 1, 2$  for two-dimensional problems); the Einstein summation convention on repeated indices is used (see Reddy and Rasmussen [3], pp. 18–20).

It is possible to express the equations in terms of the stream function and vorticity functions. For example, in the two-dimensional case, we could write equations (7.3.7) and (7.3.8) in terms of the *stream function*  $\psi$  and *vorticity*  $\omega$  which are defined in a two-dimensional case by the relations:

$$v_2 \equiv -\frac{\partial\psi}{\partial x_1}, \quad v_1 \equiv \frac{\partial\psi}{\partial x_2}, \quad \omega \equiv \frac{\partial v_1}{\partial x_2} - \frac{\partial v_2}{\partial x_1} = \nabla^2\psi \quad (7.3.11)$$

Here we chose to use the standard notation for the stream function and vorticity. The symbol  $\psi$  should not be confused with  $\psi_i$  used for interpolation functions. Of course, it would be clear in the context of the discussion.

In the present study, we shall consider two different finite element models of equations (7.3.7) and (7.3.8). The first one is a natural formulation in which the weak forms of equations (7.3.7) and (7.3.8) are used to construct the finite element model. The resulting finite element model is termed the *velocity–pressure model* or *mixed model*. The phrase “mixed” is used because velocity variables are mixed with the force-like variable, pressure, and both types of variables are retained in a single formulation. The second model is based on the interpretation that the continuity equation (7.3.7) is an additional relation among the velocity components (i.e. a constraint among the  $v_i$ ), and the constraint is satisfied in a least-squares (i.e. approximate) sense. This particular method of including the constraint in the formulation is known as the *penalty function method*, and the model is termed the *penalty–finite element model*. In this case, the pressure variable is effectively eliminated from the formulation. It is informative to note that the velocity–pressure (or mixed) formulation is the same as the Lagrange multiplier formulation, wherein the constraint is included by means of the Lagrange multiplier method. The Lagrange multiplier turns out to be the negative of the pressure.

There exist in computational fluid dynamics literature hundreds of papers on finite element models of incompressible flows and their applications. Interested readers may consult the books by Reddy and Gartling [10] and Gresho and Sani [11] for many of these references. Some of these works will be cited at appropriate places of this book.

## 7.4 Velocity–Pressure Finite Element Model

### 7.4.1 Weak Form

The starting point for the development of the finite element models of Eqs. (7.3.7) and (7.3.8) is their weak forms. Here we consider the two-dimensional case, and the three-dimensional case follows in a straightforward manner. First, we write Eqs. (7.3.7) and (7.3.8) for the two-dimensional case using

the notation  $v_1 = v_x, v_2 = v_y, x_1 = x$ , and  $x_2 = y$ . We have

$$\begin{aligned} \frac{\partial v_x}{\partial x} + \frac{\partial v_y}{\partial y} &= 0 \quad (7.4) \\ \rho_0 \left( v_x \frac{\partial v_x}{\partial x} + v_y \frac{\partial v_x}{\partial y} \right) - \frac{\partial}{\partial x} \left( 2\mu \frac{\partial v_x}{\partial x} \right) - \frac{\partial}{\partial y} \left[ \mu \left( \frac{\partial v_x}{\partial y} + \frac{\partial v_y}{\partial x} \right) \right] + \frac{\partial P}{\partial x} &= \rho_0 f_x \quad (7.4) \\ \rho_0 \left( v_x \frac{\partial v_y}{\partial x} + v_y \frac{\partial v_y}{\partial y} \right) - \frac{\partial}{\partial y} \left( 2\mu \frac{\partial v_y}{\partial y} \right) - \frac{\partial}{\partial x} \left[ \mu \left( \frac{\partial v_x}{\partial y} + \frac{\partial v_y}{\partial x} \right) \right] + \frac{\partial P}{\partial y} &= \rho_0 f_y \quad (7.4) \end{aligned}$$

where  $(f_x, f_y)$  are the components of the body force vector.

The weighted-integral statements of these equations over a typical element  $\Omega^e$  are given by

$$\int_{\Omega^e} Q \left( \frac{\partial v_x}{\partial x} + \frac{\partial v_y}{\partial y} \right) dx dy = 0 \quad (7.4.4)$$

$$\int_{\Omega^e} w_x \left\{ \rho_0 \left( v_x \frac{\partial v_x}{\partial x} + v_y \frac{\partial v_x}{\partial y} \right) - \frac{\partial}{\partial x} \left( 2\mu \frac{\partial v_x}{\partial x} \right) - \frac{\partial}{\partial y} \left[ \mu \left( \frac{\partial v_x}{\partial y} + \frac{\partial v_y}{\partial x} \right) \right] + \frac{\partial P}{\partial x} - \rho_0 f_x \right\} dx dy = 0 \quad (7.4.5)$$

$$\int_{\Omega^e} w_y \left\{ \rho_0 \left( v_x \frac{\partial v_y}{\partial x} + v_y \frac{\partial v_y}{\partial y} \right) - \frac{\partial}{\partial y} \left( 2\mu \frac{\partial v_y}{\partial y} \right) - \frac{\partial}{\partial x} \left[ \mu \left( \frac{\partial v_x}{\partial y} + \frac{\partial v_y}{\partial x} \right) \right] + \frac{\partial P}{\partial y} - \rho_0 f_y \right\} dx dy = 0 \quad (7.4.6)$$

where  $(Q, w_x, w_y)$  are weight functions, which will be equated, in the Ritz-Galerkin finite element models, to the interpolation functions used for  $(P, v_x, v_y)$ , respectively (see Reddy and Gartling [10] for details).

Equation (7.4.4) will remain unaffected, as integration-by-parts does not help reduce differentiability on  $(v_x, v_y)$ . In addition, the boundary terms obtained will be in conflict with the physical boundary conditions. The same comment applies to the first expression in Eqs. (7.4.5) and (7.4.6). Note that trading of differentiability between the weight functions and problem variables is subjected to the restriction that the resulting boundary expressions are physically meaningful. Otherwise, the secondary variables of the formulation may not be the quantities the physical problem admits as the boundary conditions. An examination of the boundary stress components  $t_\alpha$  in equation (7.2.18b) shows that the pressure term occurs as a part of the expression [also see Eq. (7.3.6)]. Therefore, the pressure term must also be integrated-by-parts to keep the boundary stresses in tact. The integration-by-parts also allows the pressure variable to have lower-order approximation.

The final expressions for the weak forms are given by

$$\int_{\Omega^e} Q \left( \frac{\partial v_x}{\partial x} + \frac{\partial v_y}{\partial y} \right) dx dy = 0 \tag{7.4.7}$$

$$\int_{\Omega^e} \left[ w_x \rho_0 \left( v_x \frac{\partial v_x}{\partial x} + v_y \frac{\partial v_x}{\partial y} \right) + 2\mu \frac{\partial w_x}{\partial x} \frac{\partial v_x}{\partial x} + \frac{\partial w_x}{\partial x} P + \mu \frac{\partial w_x}{\partial y} \left( \frac{\partial v_x}{\partial y} + \frac{\partial v_y}{\partial x} \right) - \rho_0 w_x f_x \right] dx dy - \int_{\Gamma^e} w_x t_x ds = 0 \tag{7.4.8}$$

$$\int_{\Omega^e} \left[ w_y \rho_0 \left( v_x \frac{\partial v_y}{\partial x} + v_y \frac{\partial v_y}{\partial y} \right) + 2\mu \frac{\partial w_y}{\partial y} \frac{\partial v_y}{\partial y} + \frac{\partial w_y}{\partial y} P + \mu \frac{\partial w_y}{\partial x} \left( \frac{\partial v_x}{\partial y} + \frac{\partial v_y}{\partial x} \right) - \rho_0 w_y f_y \right] dx dy - \int_{\Gamma^e} w_y t_y ds = 0 \tag{7.4.9}$$

where  $(t_x, t_y)$  are the boundary stress (or traction) components

$$t_x = (2\mu \frac{\partial v_x}{\partial x} - P)n_x + \mu \left( \frac{\partial v_x}{\partial y} + \frac{\partial v_y}{\partial x} \right) n_y \tag{7.4.10}$$

$$t_y = \mu \left( \frac{\partial v_x}{\partial y} + \frac{\partial v_y}{\partial x} \right) n_x + (2\mu \frac{\partial v_y}{\partial y} - P)n_y$$

and  $(n_x, n_y)$  are the direction cosines of the unit normal vector  $\hat{n}$  on the boundary  $\Gamma^e$ .

### 7.4.2 Finite Element Model

Since we are developing the Ritz-Galerkin finite element models, the choice of the weight functions is restricted to the spaces of approximation functions used for the pressure and velocity fields. Suppose that the dependent variables  $(v_x, v_y, P)$  are approximated by expansions of the form

$$v_x(x, y, t) = \sum_{m=1}^M \psi_m(x, y) v_x^m(t), \quad v_y(x, y, t) = \sum_{m=1}^M \psi_m(x, y) v_y^m(t) \tag{7.4.11a}$$

$$P(x, y, t) = \sum_{n=1}^N \phi_n(x, y) P_n(t) \tag{7.4.11b}$$

where  $\psi$  and  $\phi$  are interpolation (or shape) functions, and  $(v_x^m, v_y^m, P_n)$  are nodal values of  $(v_x, v_y, P)$ . The weight functions  $(w_x, w_y, Q)$  have the following correspondence (see Reddy [12,13] for further details):

$$Q \approx P, \quad w_x \approx v_x, \quad w_y \approx v_y \tag{7.4.12}$$

Substitution of Eqs. (7.4.11a,b) into Eqs. (7.4.7)–(7.4.9) results in the following finite element equations [10]:

$$\begin{bmatrix} [M] & [0] & [0] \\ [0] & [M] & [0] \\ [0] & [0] & [0] \end{bmatrix} \begin{Bmatrix} \{ \dot{v}_x \} \\ \{ \dot{v}_y \} \\ \{ \dot{P} \} \end{Bmatrix} + \begin{bmatrix} [C(\mathbf{v})] & [0] & [0] \\ [0] & [C(\mathbf{v})] & [0] \\ [0] & [0] & [0] \end{bmatrix} \begin{Bmatrix} \{ v_x \} \\ \{ v_y \} \\ \{ P \} \end{Bmatrix}$$



$$+ \begin{bmatrix} 2[S^{xx}] + [S^{yy}] & [S^{yx}] & -[S^{x0}] \\ [S^{xy}] & [S^{xx}] + 2[S^{yy}] & -[S^{y0}] \\ -[S^{x0}]^T & -[S^{y0}]^T & [0] \end{bmatrix} \begin{Bmatrix} \{v_x\} \\ \{v_y\} \\ \{P\} \end{Bmatrix} = \begin{Bmatrix} \{F^1\} \\ \{F^2\} \\ \{0\} \end{Bmatrix} \quad (7.4.1)$$

The coefficient matrices shown in Eqs. (7.4.13) are defined by

$$\begin{aligned} M_{ij} &= \int_{\Omega^e} \rho_0 \psi_i^e \psi_j^e dx dy \\ C_{ij}^e(\mathbf{v}) &= \int_{\Omega^e} \rho_0 \psi_i^e \left( v_x \frac{\partial \psi_j^e}{\partial x} + v_y \frac{\partial \psi_j^e}{\partial y} \right) dx dy \\ S_{ij}^{\xi\eta} &= \int_{\Omega^e} \mu \frac{\partial \psi_i^e}{\partial \xi} \frac{\partial \psi_j^e}{\partial \eta} dx dy ; \quad \xi, \eta = x, y \\ S_{ij}^{\xi 0} &= \int_{\Omega^e} \frac{\partial \psi_i^e}{\partial \xi} \phi_j^e dx dy ; \quad \xi = x, y \\ F^1 &= \int_{\Omega^e} \rho_0 \psi_i^e f_x dx dy + \oint_{\Gamma^e} \psi_i^e t_x ds \\ F^2 &= \int_{\Omega^e} \rho_0 \psi_i^e f_y dx dy + \oint_{\Gamma^e} \psi_i^e t_y ds \end{aligned} \quad (7.4.1)$$

The two sets of interpolation functions used in Eqs. (7.4.11a,b) should be of the Lagrange type, that is, derived by interpolating only the values of the functions - and not their derivatives. There are two different finite elements associated with the two sets of field variables  $(v_x, v_y)$  and  $P$ , and hence there are two different finite element meshes corresponding to the two variables over the same domain,  $\Omega$ . If one of the meshes contains the other mesh as a subset then we choose to display the first mesh and indicate the nodal degrees of freedom associated with the nodes of a typical element of the mesh.

The interpolation used for the pressure variable should be different from that used for the velocities, because the weak forms in Eqs. (7.4.7)-(7.4.9) contain only the first derivatives of the velocities  $v_x$  and  $v_y$  and no derivative of the pressure  $P$ . In addition, the essential boundary conditions of the formulation do not include specification of the pressure; it enters the boundary conditions as a part of the natural boundary conditions. This implies that the pressure variable need not be carried as a variable that is continuous across interelement boundaries. These observations lead to the conclusion that the pressure variable should be interpolated with functions that are one order less than those used for the velocity field and that the approximation may be discontinuous (i.e. not continuous from one element to other). Thus, quadratic interpolation of  $v_i$  and discontinuous linear interpolation of  $P$  are admissible. Models that use equal interpolation of the velocities and pressure with this formulation are known to give inaccurate results (see [14-26]).

## 7.5 Penalty Finite Element Models

### 7.5.1 Introduction

The penalty function method, like the Lagrange multiplier method (see [3, 10, 13]), allows us to reformulate a problem with constraints as one without constraints. In order to use the penalty function method for the flow of a viscous incompressible fluid, first it is reformulated as a variational problem subjected to a constraint. For the purpose of describing the penalty function method, we consider the steady Stokes flow problem (i.e. without time-dependent and nonlinear terms) in two dimensions. Then the penalty method is applied to the variational problem with a constraint. The development will then be extended to unsteady Navier–Stokes equations.

Consider the weak forms in Eqs. (7.4.7)–(7.4.9), and omit the time derivative and nonlinear terms. These can be expressed in the form

$$B((w_x, w_y, Q), (v_x, v_y, P)) = \ell(w_x, w_y, Q) \tag{7.5.1}$$

where  $(w_x, w_y, Q)$  are the weight functions used for the momentum and continuity equations, respectively,  $B(\cdot, \cdot)$  is a *bilinear form* [i.e. an expression that is linear in  $(w_x, w_y, Q)$  as well as  $(v_x, v_y, P)$ ] and  $\ell(\cdot)$  is a *linear form*, defined by

$$\begin{aligned} & B((w_x, w_y, Q), (v_x, v_y, P)) \\ &= \int_{\Omega^e} \mu \left[ 2 \left( \frac{\partial w_x}{\partial x} \frac{\partial v_x}{\partial x} + \frac{\partial w_y}{\partial y} \frac{\partial v_y}{\partial y} \right) + \left( \frac{\partial w_x}{\partial y} + \frac{\partial w_y}{\partial x} \right) \left( \frac{\partial v_x}{\partial y} + \frac{\partial v_y}{\partial x} \right) \right] dx dy \\ & \quad - \int_{\Omega^e} \left[ \left( \frac{\partial w_x}{\partial x} + \frac{\partial w_y}{\partial y} \right) P + \left( \frac{\partial v_x}{\partial x} + \frac{\partial v_y}{\partial y} \right) Q \right] dx dy \end{aligned} \tag{7.5.2a}$$

$$\ell(w_x, w_y, Q) = \int_{\Omega^e} \rho_0 (w_x f_x + w_y f_y) dx dy + \oint_{\Gamma^e} (w_x t_x + w_y t_y) ds \tag{7.5.2b}$$

and  $(t_x, t_y)$  are the boundary stress components defined in Eq. (7.4.10). The statement in Eq. (7.5.1) is known as the *variational problem* associated with steady-state Stokes problem.

The finite element model based on the variational problem (7.5.1) is a special case of the mixed finite element model in Eq. (7.4.13). Equation (7.4.13) is more general than the problem at hand in that Eq. (7.4.13) is valid for time-dependent Navier–Stokes equations. To make it simple to understand the penalty function method, only the steady-state Stokes problem is considered. The inertial (i.e. time-dependent) and convective (i.e. nonlinear) terms may be added to the equations of the penalty formulation as they are not connected to the divergence-free (i.e. incompressibility) condition, which is central to the penalty formulation.

### 7.5.2 Penalty Function Method

Suppose that the velocity field  $(v_x, v_y)$  is such that the continuity equation (7.4.1) is satisfied identically. Then the weight functions  $(w_x, w_y)$ , being virtual variations of the velocity components, also satisfy the continuity equation

$$\frac{\partial w_x}{\partial x} + \frac{\partial w_y}{\partial y} = 0 \tag{7.5}$$

As a result, the second integral expression in the bilinear form (7.5.2a) drops out, and the pressure, and hence the weight function  $Q$ , does not appear explicitly in the variational problem (7.5.1). The resulting variational problem now can be stated as follows: among all vectors  $\mathbf{v} = v_x \hat{\mathbf{e}}_x + v_y \hat{\mathbf{e}}_y$  that satisfy the continuity equation (7.4.1), find the one that satisfies the variational problem

$$B_0((w_x, w_y), (v_x, v_y)) = \ell_0(w_x, w_y) \tag{7.5}$$

for all admissible weight functions  $\mathbf{w} = w_x \hat{\mathbf{e}}_x + w_y \hat{\mathbf{e}}_y$  [i.e. that which satisfy the condition  $\nabla \cdot \mathbf{w}$  [see Eq. (7.5.3)]. The bilinear and linear forms in Eq. (7.5.4) are defined by

$$B_0(\mathbf{w}, \mathbf{v}) = \int_{\Omega^e} \mu \left[ 2 \left( \frac{\partial w_x}{\partial x} \frac{\partial v_x}{\partial x} + \frac{\partial w_y}{\partial y} \frac{\partial v_y}{\partial y} \right) + \left( \frac{\partial w_x}{\partial y} + \frac{\partial w_y}{\partial x} \right) \left( \frac{\partial v_x}{\partial y} + \frac{\partial v_y}{\partial x} \right) \right] dx dy \tag{7.5.5e}$$

$$\ell_0(\mathbf{w}) = \int_{\Omega^e} \rho_0 (w_x f_x + w_y f_y) dx dy + \oint_{\Gamma^e} (w_x t_x + w_y t_y) ds \tag{7.5.5f}$$

The variational problem in Eq. (7.5.4) is a constrained variational problem because the solution vector  $\mathbf{v}$  is constrained to satisfy the continuity equation. We note that  $B_0(\cdot, \cdot)$  is symmetric

$$B_0(\mathbf{w}, \mathbf{v}) = B_0(\mathbf{v}, \mathbf{w}) \tag{7.5.6}$$

and linear in  $\mathbf{w}$  as well as  $\mathbf{v}$ , that is, the following relations hold for any vectors  $\mathbf{w}_1, \mathbf{w}_2, \mathbf{v}_1$ , and  $\mathbf{v}_2$  that satisfy the incompressibility condition [see Eq. (7.5.3)] and arbitrary constants  $\alpha$  and  $\beta$ :

$$B_0(\alpha \mathbf{w}_1 + \beta \mathbf{w}_2, \mathbf{v}) = \alpha B_0(\mathbf{w}_1, \mathbf{v}) + \beta B_0(\mathbf{w}_2, \mathbf{v}) \tag{7.5.7a}$$

$$B_0(\mathbf{w}, \alpha \mathbf{v}_1 + \beta \mathbf{v}_2) = \alpha B_0(\mathbf{w}, \mathbf{v}_1) + \beta B_0(\mathbf{w}, \mathbf{v}_2) \tag{7.5.7b}$$

Thus,  $B_0(\cdot, \cdot)$  is called *bilinear* if and only if it satisfies conditions in Eq. (7.5.7a,b). Similarly  $\ell_0(\cdot)$  is called *linear* in  $\mathbf{w}$  if and only if it satisfies the condition

$$\ell_0(\alpha \mathbf{w}_1 + \beta \mathbf{w}_2) = \alpha \ell_0(\mathbf{w}_1) + \beta \ell_0(\mathbf{w}_2) \tag{7.5.8}$$

Whenever the bilinear form of a variational problem is symmetric in its arguments, it is possible to construct a quadratic functional such that the minimum of the quadratic functional is equivalent to the variational problem (see Reddy [12,13]). The quadratic functional is given by the expression

$$I_0(\mathbf{v}) = \frac{1}{2}B_0(\mathbf{v}, \mathbf{v}) - \ell_0(\mathbf{v}) \tag{7.5.9}$$

Now we can state that Eqs. (7.4.1)–(7.4.3) governing the steady flow of viscous incompressible fluids are equivalent to minimizing the quadratic functional  $I_0(\mathbf{v})$  [ $\mathbf{v} = (v_x, v_y)$ ] subjected to the constraint

$$G(\mathbf{v}) \equiv \frac{\partial v_x}{\partial x} + \frac{\partial v_y}{\partial y} = 0 \tag{7.5.10}$$

At this point it should be remembered that the discussion presented in this section thus far is to reformulate the problem as one of a constrained problem so that the penalty function method can be used. The advantage of the constrained problem is that the pressure variable  $P$  does not appear in the formulation.

In the penalty function method, the constrained problem is reformulated as an unconstrained problem as follows: minimize the modified functional

$$I_P(\mathbf{v}) \equiv I_0(\mathbf{v}) + \frac{\gamma_e}{2} \int_{\Omega^e} [G(\mathbf{v})]^2 dx \tag{7.5.11}$$

where  $\gamma_e$  is called the *penalty parameter*. Note that the constraint is included in a least-squares sense into the functional. Seeking the minimum of the modified functional  $I_P(\mathbf{v})$  is equivalent to seeking the minimum of both  $I_0(\mathbf{v})$  and  $G(\mathbf{v})$ , the latter with respect to the weight  $\gamma_e$ . The larger the value of  $\gamma_e$ , the more exactly the constraint is satisfied. The necessary condition for the minimum of  $I_P$  is

$$\delta I_P = 0 \tag{7.5.12}$$

We have

$$\begin{aligned} 0 = & \int_{\Omega^e} \left[ 2\mu \frac{\partial \delta v_x}{\partial x} \frac{\partial v_x}{\partial x} + \mu \frac{\partial \delta v_x}{\partial y} \left( \frac{\partial v_x}{\partial y} + \frac{\partial v_y}{\partial x} \right) \right] dx dy - \int_{\Omega^e} \rho_0 \delta v_x f_x dx dy \\ & - \oint_{\Gamma^e} \delta v_x t_x ds + \int_{\Omega^e} \gamma_e \frac{\partial \delta v_x}{\partial x} \left( \frac{\partial v_x}{\partial x} + \frac{\partial v_y}{\partial y} \right) dx dy \end{aligned} \tag{7.5.13a}$$

$$\begin{aligned} 0 = & \int_{\Omega^e} \left[ 2\mu \frac{\partial \delta v_y}{\partial y} \frac{\partial v_y}{\partial y} + \mu \frac{\partial \delta v_y}{\partial x} \left( \frac{\partial v_x}{\partial y} + \frac{\partial v_y}{\partial x} \right) \right] dx dy - \int_{\Omega^e} \rho_0 f_y \delta v_y dx dy \\ & - \oint_{\Gamma^e} \delta v_y t_y ds + \int_{\Omega^e} \gamma_e \frac{\partial \delta v_y}{\partial y} \left( \frac{\partial v_x}{\partial x} + \frac{\partial v_y}{\partial y} \right) dx dy \end{aligned} \tag{7.5.13b}$$

These two statements provide the weak forms for the penalty finite element model with  $\delta v_x = w_x$  and  $\delta v_y = w_y$ . We note that the pressure does not

appear explicitly in the weak forms (7.5.13a,b), although it is a part of the boundary stresses. An approximation for the pressure can be post-computed from the relation

$$P = -\gamma_e \left( \frac{\partial v_x}{\partial x} + \frac{\partial v_y}{\partial y} \right) \quad (7.5.14)$$

where  $\mathbf{v} = \mathbf{v}(\gamma_e)$  is the solution of Eqs. (7.5.13a,b). The time derivative term and nonlinear terms can be added to equations (7.5.13a,b) without affecting the above discussion. We obtain

$$\begin{aligned} 0 = & \int_{\Omega^e} \left[ \delta v_x \rho_0 \left( \frac{\partial v_x}{\partial t} + v_x \frac{\partial v_x}{\partial x} + v_y \frac{\partial v_x}{\partial y} \right) + 2\mu \frac{\partial \delta v_x}{\partial x} \frac{\partial v_x}{\partial x} \right. \\ & \left. + \mu \frac{\partial \delta v_x}{\partial y} \left( \frac{\partial v_x}{\partial y} + \frac{\partial v_y}{\partial x} \right) + \gamma_e \frac{\partial \delta v_x}{\partial x} \left( \frac{\partial v_x}{\partial x} + \frac{\partial v_y}{\partial y} \right) \right] dx dy \\ & - \int_{\Omega^e} \rho_0 \delta v_x f_x dx dy - \int_{\Gamma^e} \delta v_x t_x ds \end{aligned} \quad (7.5.15a)$$

$$\begin{aligned} 0 = & \int_{\Omega^e} \left[ \delta v_y \rho_0 \left( \frac{\partial v_y}{\partial t} + v_x \frac{\partial v_y}{\partial x} + v_y \frac{\partial v_y}{\partial y} \right) + 2\mu \frac{\partial \delta v_y}{\partial y} \frac{\partial v_y}{\partial y} \right. \\ & \left. + \mu \frac{\partial \delta v_y}{\partial x} \left( \frac{\partial v_x}{\partial y} + \frac{\partial v_y}{\partial x} \right) + \gamma_e \frac{\partial \delta v_y}{\partial y} \left( \frac{\partial v_x}{\partial x} + \frac{\partial v_y}{\partial y} \right) \right] dx dy \\ & - \int_{\Omega^e} \rho_0 f_y \delta v_y dx dy - \int_{\Gamma^e} \delta v_y t_y ds \end{aligned} \quad (7.5.15b)$$

### 7.5.3 Reduced Integration Penalty Model

The penalty finite element model is obtained from Eqs. (7.5.15a,b) by substituting finite element interpolation (7.4.11a) for the velocity field, and  $\delta v_x = \psi_i^e$  and  $\delta v_y = \psi_j^e$ :

$$\begin{aligned} & \begin{bmatrix} [C(\mathbf{v})] & [0] \\ [0] & [C(\mathbf{v})] \end{bmatrix} \begin{Bmatrix} \{v_x\} \\ \{v_y\} \end{Bmatrix} + \begin{bmatrix} 2[S^{xx}] + [S^{yy}] & [S^{xy}] \\ [S^{xy}] & [S^{xx}] + 2[S^{yy}] \end{bmatrix} \begin{Bmatrix} \{v_x\} \\ \{v_y\} \end{Bmatrix} \\ & + \begin{bmatrix} [\bar{S}^{xx}] & [\bar{S}^{xy}] \\ [\bar{S}^{xy}] & [\bar{S}^{yy}] \end{bmatrix} \begin{Bmatrix} \{v_x\} \\ \{v_y\} \end{Bmatrix} + \begin{bmatrix} [M] & [0] \\ [0] & [M] \end{bmatrix} \begin{Bmatrix} \{\dot{v}_x\} \\ \{\dot{v}_y\} \end{Bmatrix} = \begin{Bmatrix} \{F^1\} \\ \{F^2\} \end{Bmatrix} \end{aligned} \quad (7.5.16)$$

where  $[M]$ ,  $[C(\mathbf{v})]$ ,  $[S^{\xi\eta}]$ ,  $\{F^1\}$ , and  $\{F^2\}$  are the same as those defined in Eq. (7.4.14), and

$$\bar{S}^{\xi\eta} = \int_{\Omega^e} \gamma_e \frac{\partial \psi_i^e}{\partial \xi} \frac{\partial \psi_j^e}{\partial \eta} dx dy \quad (7.5.17)$$

Equation (7.5.16) can be expressed symbolically as  $(\mathbf{v} = \{\mathbf{v}_x, \mathbf{v}_y\}^T)$

$$[C(\rho, \mathbf{v}) + \mathbf{K}(\mu) + \bar{\mathbf{K}}(\gamma)] \mathbf{v} + \mathbf{M}\dot{\mathbf{v}} = \mathbf{F} \quad (7.5.18)$$

The numerical construction of the penalty terms presented in Eq. (7.5.18) requires special consideration, the details of which are given in Section 7.5.5.

### 7.5.4 Consistent Penalty Model

An alternative formulation (see [10, 15, 17]) of the penalty finite element model is based directly on the use of Eq. (7.5.14). In this formulation, the pressure in the momentum equations (7.4.2) and (7.4.3) is replaced using Eq. (7.5.14) and Eq. (7.4.1) is replaced with Eq. (7.5.14). The weak forms of Eq. (7.5.14) is

$$0 = \int_{\Omega^e} \delta P \left[ P + \gamma_e \left( \frac{\partial v_x}{\partial x} + \frac{\partial v_y}{\partial y} \right) \right] dx dy \tag{7.5.19}$$

The finite element model of Eq. (7.5.19), with  $P$  interpolated as in Eq. (7.4.11b), is given by

$$[M^p]\{P\} + \gamma_e [[S^{0x}] \ [S^{0y}]] \begin{Bmatrix} \{v_x\} \\ \{v_y\} \end{Bmatrix} = \{0\} \tag{7.5.20a}$$

where

$$M_{ij}^p = \int_{\Omega^e} \phi_i \phi_j dx dy, \quad S_{ij}^{0x} = \int_{\Omega^e} \phi_i \frac{\partial \psi_j}{\partial x} dx dy, \quad S_{ij}^{0y} = \int_{\Omega^e} \phi_i \frac{\partial \psi_j}{\partial y} dx dy \tag{7.5.20b}$$

Since  $[M^p]$  is invertible, we can write

$$\{P\} = -\gamma_e [M^p]^{-1} [[S^{0x}] \ [S^{0y}]] \begin{Bmatrix} \{v_x\} \\ \{v_y\} \end{Bmatrix} \tag{7.5.21}$$

Next, we write Eq. (7.4.13) in the alternative form

$$\begin{aligned} & \begin{bmatrix} [M] & [0] \\ [0] & [M] \end{bmatrix} \begin{Bmatrix} \{\dot{v}_x\} \\ \{\dot{v}_y\} \end{Bmatrix} + \begin{bmatrix} [C(\mathbf{v})] & [0] \\ [0] & [C(\mathbf{v})] \end{bmatrix} \begin{Bmatrix} \{v_x\} \\ \{v_y\} \end{Bmatrix} - \begin{Bmatrix} [S^{0x}]^T \\ [S^{0y}]^T \end{Bmatrix} \{P\} \\ & + \begin{bmatrix} 2[S^{xx}] + [S^{yy}] & [S^{yx}] \\ [S^{xy}] & [S^{xx}] + 2[S^{yy}] \end{bmatrix} \begin{Bmatrix} \{v_x\} \\ \{v_y\} \end{Bmatrix} = \begin{Bmatrix} \{F^1\} \\ \{F^2\} \end{Bmatrix} \end{aligned} \tag{7.5.22}$$

$$-\begin{Bmatrix} [S^{0x}]^T \\ [S^{0y}]^T \end{Bmatrix} \begin{Bmatrix} \{v_x\} \\ \{v_y\} \end{Bmatrix} = \{0\} \tag{7.5.23}$$

When Eq. (7.4.21) is substituted for the pressure into Eq. (7.5.22), we obtain

$$\begin{aligned} & \begin{bmatrix} [M] & [0] \\ [0] & [M] \end{bmatrix} \begin{Bmatrix} \{\dot{v}_x\} \\ \{\dot{v}_y\} \end{Bmatrix} + \begin{bmatrix} [C(\mathbf{v})] & [0] \\ [0] & [C(\mathbf{v})] \end{bmatrix} \begin{Bmatrix} \{v_x\} \\ \{v_y\} \end{Bmatrix} \\ & + \gamma_e \begin{bmatrix} [S^{0x}]^T [M^p]^{-1} [S^{0x}] & [S^{0x}]^T [M^p]^{-1} [S^{0y}] \\ [S^{0y}]^T [M^p]^{-1} [S^{0x}] & [S^{0y}]^T [M^p]^{-1} [S^{0y}] \end{bmatrix} \begin{Bmatrix} \{v_x\} \\ \{v_y\} \end{Bmatrix} \\ & + \begin{bmatrix} 2[S^{xx}] + [S^{yy}] & [S^{yx}] \\ [S^{xy}] & [S^{xx}] + 2[S^{yy}] \end{bmatrix} \begin{Bmatrix} \{v_x\} \\ \{v_y\} \end{Bmatrix} = \begin{Bmatrix} \{F^1\} \\ \{F^2\} \end{Bmatrix} \end{aligned} \tag{7.5.24}$$

which can be written in compact form as

$$\mathbf{M}\dot{\mathbf{v}} + [\mathbf{C}(\mathbf{v}) + \mathbf{K}_\mu + \mathbf{K}_\gamma]\mathbf{v} = \mathbf{F} \quad (7.5.2)$$

where [see Eqs. (7.4.14) for the definition of  $M_{ij}$  and  $S_{ij}^{\xi\eta}$ ]

$$\begin{aligned} [\mathbf{M}] &= \begin{bmatrix} [M] & [0] \\ [0] & [M] \end{bmatrix}, \quad [\mathbf{C}] = \begin{bmatrix} [\mathbf{C}(\mathbf{v})] & [0] \\ [0] & [\mathbf{C}(\mathbf{v})] \end{bmatrix} \\ [\mathbf{K}_\gamma] &= \gamma^e \begin{bmatrix} [S^{0x}]^T [M^p]^{-1} [S^{0x}] & [S^{0x}]^T [M^p]^{-1} [S^{0y}] \\ [S^{0y}]^T [M^p]^{-1} [S^{0x}] & [S^{0y}]^T [M^p]^{-1} [S^{0y}] \end{bmatrix} \\ [\mathbf{K}]_\mu &= \begin{bmatrix} 2[S^{xx}] + [S^{yy}] & [S^{yx}] \\ [S^{xy}] & [S^{xx}] + 2[S^{yy}] \end{bmatrix} \end{aligned} \quad (7.5.26)$$

Equation (7.5.25) has the same general form as Eq. (7.5.18). The overall size of the penalty finite element model in Eq. (7.5.18) or (7.5.25) is reduced in comparison to the mixed finite element model in Eq. (7.4.13). To recover the pressure, the inverted form of (7.5.21) is used with the velocity field that is obtained from Eq. (7.5.25). The penalty finite element model described here is commonly termed a *consistent penalty model* because it is derived from the discretized form of equation (7.5.19). This is in contrast to the reduced penalty model described earlier, which falls into the category known as the *reduced integration penalty (RIP)* methods (see Oden [19]). Although the two finite element models are mathematically identical, there are subtle differences that affect the numerical implementation. The successful numerical implementation of the consistent penalty method relies on the ability to efficiently construct the  $\mathbf{K}_p$  matrix, that is, invert  $\mathbf{M}^p$  at the element level. This restricts the choice of the basis functions used to represent the pressure.

## 7.6 Computational Aspects

### 7.6.1 Properties of the Matrix Equations

Some of the properties of the matrix equations in (7.4.13), (7.5.18), and (7.5.25) are listed below because they greatly influence the choice of a solution procedure for the various types of problems [10].

1. The matrix equations (7.4.13), (7.5.18), and (7.5.25) represent discrete analogs of the basic conservation equations with each term representing a particular physical process. For example,  $\mathbf{M}$  represents the mass matrix,  $\mathbf{C}$  represents the velocity dependent convective transport term,  $\mathbf{K}_\mu$  represents the viscous terms, and  $\mathbf{K}_\gamma$  represents the divergence-free condition. The right-hand side  $\mathbf{F}$  contains body forces and surface forces.
2. An inspection of the structure of the individual matrices in (7.4.14) shows that  $\mathbf{M}$  and  $\mathbf{K}_\mu$  are symmetric, while  $\mathbf{C}$  is unsymmetric. This makes the

coefficient matrices of the vector  $\mathbf{v}$  in Eqs. (7.4.13), (7.5.18), and (7.5.25) unsymmetric, and the solution procedure must deal with an unsymmetric system. When material properties are constant and flow velocities are sufficiently small, the convective terms are negligible and the equations are linear and symmetric.

3. An additional difficulty of the mixed finite element model is the presence of zeroes on the matrix diagonals corresponding to the pressure variables [see Eq. (7.4.13)]. Direct equation solving methods must use some type of pivoting strategy, while the use of iterative solvers is severely handicapped by poor convergence behavior attributable mainly to the form of the constraint equation.
4. Equations (7.4.13), (7.5.18), and (7.5.25) represent a set of ordinary differential equations in time. The fact that the pressure does not appear explicitly in the continuity equation [see Eq. (7.4.13)] makes the system time-singular in the pressure and precludes the use of purely explicit time-integration methods.
5. The choice of the penalty parameter is largely dictated by the ratio of the magnitude of penalty terms to the viscous and convective terms (or compared to the Reynolds number,  $Re$ ), the mesh, and the precision of the computer. The following range of  $\gamma$  is used in computations

$$\gamma = 10^4 Re \text{ to } \gamma = 10^{12} Re \quad (7.6.1)$$

### 7.6.2 Choice of Elements

As is clear from the weak statements, the finite element models of conductive heat transfer as well as viscous incompressible flows require only the  $C^0$ -continuous functions to approximate the field variables (i.e. temperature, velocities, and pressure). Thus, any of the Lagrange and serendipity family of interpolation functions are admissible for the interpolation of the velocity field in mixed and penalty finite element models.

The choice of interpolation functions used for the pressure variable in the mixed finite element model is further constrained by the special role the pressure plays in incompressible flows. Recall that the pressure can be interpreted as a Lagrange multiplier that serves to enforce the incompressibility constraint on the velocity field. From Eq. (7.4.11b) it is seen that the approximation functions  $\phi_n$  used for pressure is the weighting function for the continuity equation. In order to prevent an overconstrained system of discrete equations, the interpolation used for pressure must be at least one order lower than that used for the velocity field (i.e. unequal order interpolation). Further, pressure need not be made continuous across elements because the pressure variable does not constitute a primary variable of the



weak form presented in Eqs. (7.4.7)–(7.4.9). Note that the unequal order interpolation criteria can be relaxed for certain “stabilized” formulations such as the methods proposed by Hughes *et al.* [26], which will not be discussed here.

Convergent finite element approximations of problems with constraints are governed by the ellipticity requirement and the *Ladyzhenskaya–Babuska–Brezzi (LBB) condition* (see Reddy [13, pp. 454–461], Oden [19], Oden and Carey [20], and others [21–23]). It is by no means a simple task to rigorously prove whether every new element developed for the viscous incompressible flows satisfies the LBB condition. The discussion of the LBB condition is beyond the scope of the present study and will not be discussed here.

Commonly used elements for two-dimensional flows of viscous incompressible fluids are shown in Figure 7.6.1. In the case of linear elements, pressure is treated as discontinuous between elements; otherwise, the whole domain will have the same pressure. Two different pressure approximations have been used when the velocities are approximated by quadratic Lagrange functions. The first is a continuous bilinear approximation, in which the pressure is defined at the corner nodes of the element and is made continuous across element boundaries. The second pressure approximation involves a discontinuous (between elements) linear variation defined on the element by

$$\Phi = \{\phi\} = \begin{Bmatrix} 1 \\ x \\ y \end{Bmatrix} \quad (7.6.2)$$

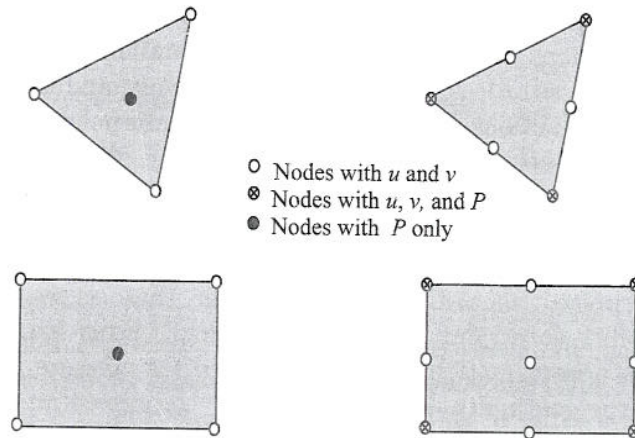


**Figure 7.6.1** The triangular and quadrilateral elements used for the mixed and penalty finite element models.

Here the unknowns are not nodal point values of the pressure but correspond to the coefficients in  $P = a \cdot 1 + b \cdot x + c \cdot y$ . In Eq. (7.6.2) the interpolation functions are written in terms of the global coordinates  $(x, y)$  for the problem.

When the eight-node quadratic element is used to represent the velocity field, a continuous-bilinear pressure approximation may be selected. When a discontinuous pressure variation is utilized with this element, the constant pressure representation over each element must be used. The quadratic quadrilateral elements shown in Figure 7.6.1 are known to satisfy the LBB condition and thus give reliable solutions for velocity and pressure fields. Other elements may yield acceptable solutions for the velocity field but the pressure field is often in error.

### 7.6.3 Evaluation of Element Matrices in Penalty Models

The numerical evaluation of the coefficient matrices appearing in equation (7.5.18) requires special consideration [10]. This aspect is discussed here for the steady-state case. For the steady-state flows with constant material properties, Eq. (7.5.18) is of the form

$$(\rho \hat{\mathbf{C}}(\mathbf{v}) + \mu \hat{\mathbf{K}} + \gamma \bar{\mathbf{K}})\{\mathbf{v}\} = \{\mathbf{F}\} \quad (7.6.3)$$

where  $\hat{\mathbf{C}}$  is the contribution due to the convective terms,  $\hat{\mathbf{K}}$  is the contribution from the viscous terms, and  $\bar{\mathbf{K}}$  is from the penalty terms, which come from the incompressibility constraint. In theory, as we increase the value of  $\gamma$ , the conservation of mass is satisfied more exactly. However, in practice, for some large value of  $\gamma$ , the contribution from the viscous terms would be negligibly small compared to the penalty terms in a computer. Thus, if  $\bar{\mathbf{K}}$  is a non-singular (i.e. invertible) matrix, the solution of Eq. (7.6.3) for a large value of  $\gamma$  is trivial,  $\{\mathbf{v}\} = \{\mathbf{0}\}$ . While the solution satisfies the continuity equation, it does not satisfy the momentum equations. In this case the discrete problem (7.6.3) is said to be overconstrained or "locked". If  $\bar{\mathbf{K}}$  is singular, then the sum  $(\rho \hat{\mathbf{C}} + \mu \hat{\mathbf{K}} + \gamma \bar{\mathbf{K}})$  is non-singular (because  $\rho \hat{\mathbf{C}} + \mu \hat{\mathbf{K}}$  is non-singular), and a non-trivial solution to the problem is obtained.

The numerical problem described above is eliminated by proper evaluation of the integrals in  $\hat{\mathbf{C}}$ ,  $\hat{\mathbf{K}}$ , and  $\bar{\mathbf{K}}$ . It is found that if the coefficients of  $\bar{\mathbf{K}}$  (i.e. penalty matrix coefficients) are evaluated using a numerical integration rule of an order less than that required to integrate them exactly, the finite element equations (7.6.3) give acceptable solutions for the velocity field. This technique of under-integrating the penalty terms is known in the literature as *reduced integration*. For example, if a linear quadrilateral element is used to approximate the velocity field, the matrix coefficients  $\hat{\mathbf{C}}$  and  $\hat{\mathbf{K}}$  (as well as  $\mathbf{M}$  for unsteady problems) are evaluated using the  $2 \times 2$  Gauss quadrature, and  $\bar{\mathbf{K}}$  is evaluated using the one-point ( $1 \times 1$ ) Gauss quadrature. The one-point quadrature yields a singular  $\bar{\mathbf{K}}$ . Therefore, Eq. (7.6.3) can be solved because

$(\rho\hat{\mathbf{C}} + \mu\hat{\mathbf{K}} + \gamma\bar{\mathbf{K}})$  is non-singular and can be inverted (after assembly and imposition of boundary conditions) to obtain a good finite element solution of the original problem. When a quadratic quadrilateral element is used, the  $3 \times 3$  Gauss quadrature is used to evaluate  $\hat{\mathbf{C}}$ ,  $\hat{\mathbf{K}}$ , and  $\mathbf{M}$ , and the  $2 \times 2$  Gauss quadrature is used to evaluate  $\bar{\mathbf{K}}$ . Of course, as the degree of interpolation goes up, or very refined meshes are used, the resulting equations become less sensitive to locking.

Concerning the post-computation of pressure in the penalty model, the pressure should be computed by evaluating Eq. (7.5.14) at integration points corresponding to the reduced Gauss rule. This is equivalent to using an interpolation for pressure that is one order less than the one used for the velocity field. The pressure computed using equation (7.5.14) at the reduced integration points is not always reliable and accurate. The pressures predicted using the linear elements, especially for coarse meshes, are seldom acceptable. Quadratic elements are known to yield more reliable results. In general, triangular elements do not yield stable solutions for pressures. Various techniques have been proposed in the literature to obtain accurate pressure fields (see [27-29]). A procedure for the post-computation of pressure is discussed in [10,29].

#### 7.6.4 Post-Computation of Stresses

The analysis of a flow problem generally includes calculation of not only the velocity field and pressure but also the computation of the stress field. A brief discussion of the stress calculation is presented next [10].

For a plane two-dimensional flow, the stress components  $(\sigma_{xx}, \sigma_{yy}, \sigma_{xy})$  are given by

$$\sigma_{xx} = 2\mu \frac{\partial v_x}{\partial x} - P, \quad \sigma_{yy} = 2\mu \frac{\partial v_y}{\partial y} - P, \quad \sigma_{xy} = \mu \left( \frac{\partial v_x}{\partial y} + \frac{\partial v_y}{\partial x} \right) \quad (7.6.4)$$

where  $\mu$  is the viscosity of the fluid. Substitution of the finite element approximations (7.4.11a,b) for the velocity field and pressure into Eqs. (7.6.4) yields

$$\begin{aligned} \sigma_{xx} &= 2\mu \sum_{j=1}^M \frac{\partial \psi_j}{\partial x} v_x^j - P, & \sigma_{yy} &= 2\mu \sum_{j=1}^M \frac{\partial \psi_j}{\partial y} v_y^j - P \\ \sigma_{xy} &= \mu \sum_{j=1}^M \left( \frac{\partial \psi_j}{\partial y} v_x^j + \frac{\partial \psi_j}{\partial x} v_y^j \right) \end{aligned} \quad (7.6.5)$$

where  $P$  is calculated from [see Eq. (7.5.14)]

$$P(x, y) = \sum_{j=1}^N \phi_j(x, y) P_j \quad (7.6.6a)$$

for the mixed model, and from

$$P_\gamma(x, y) = -\gamma \sum_{j=1}^M \left( \frac{\partial \psi_j}{\partial x} v_x^j + \frac{\partial \psi_j}{\partial y} v_y^j \right) \quad (7.6.6b)$$

for the penalty model.

The spatial derivatives of the interpolation functions in Eqs. (7.6.5a-c) and (7.6.6b) must be evaluated using the reduced Gauss point rule. Thus, the stresses (as well as the pressure) are computed using the one-point Gauss rule for linear elements and with the  $2 \times 2$  Gauss rule for the quadratic elements. The stresses computed at interior integration points can be extrapolated to the nodes by a simple linear extrapolation procedure, and they may be appropriately averaged between adjacent elements to produce a continuous stress field.

## 7.7 Computer Implementation

### 7.7.1 Mixed Model

The computer implementation of the mixed model is somewhat complicated by the fact that the element contains variable degrees of freedom and the coefficient matrix is not positive-definite due to the appearance of zeros on the diagonal. Here, we discuss computer implementation of mixed model with quadratic approximation of the velocity field and bilinear continuous approximation of the pressure. A eight- or nine-node element depicting all nodal values of the formulation will have three degrees of freedom ( $v_x, v_y, P$ ) at the corner nodes and two degrees of freedom ( $v_x, v_y$ ) at the mid-side and interior nodes. This complicates the calculation of element matrices as well as the assembly of element equations to form the global system of equations.

Fortran statements of the element calculations for the mixed finite element model are given in Box 7.7.1. Here  $\{ELV\}$  denotes the element velocity vector,  $AMU$  the viscosity  $\mu$ , and  $RHO$  the density  $\rho$ . The meaning of other variables remain the same as defined in earlier discussions (e.g.  $NGP$  = number of Gauss points;  $GAUSSPT(I, J)$  = array of Gauss points;  $GAUSSWT(I, J)$  = array of Gauss weights;  $DET$  = determinant of the Jacobian matrix;  $NPE$  = number of nodes per element, 8 or 9;  $SF(I) = \psi_i$ , Lagrange interpolation functions of the quadratic element;  $SFL(I) =$  Lagrange interpolation functions of the bilinear element; and  $GDSF(\alpha, i) = \partial \psi_i / \partial x_\alpha$ , etc.).

To facilitate the assembly, we create a companion array  $NFD(I, J)$  to the connectivity array  $NOD(I, J)$ . This array is similar to the array  $NOD$  but it connects the degrees of freedom rather than the global nodes associated with the element nodes:

$NFD(I, J) =$  The last global degree of freedom number associated with the  $J$ th node of the  $I$ th element.

The word 'last' refers to the third degree of freedom at the corner nodes and the second degree of freedom at the mid-side and interior nodes. To see the meaning of array [NFD], consider the mesh of six nine-node elements shown in Figure 7.7.1. First note that the connectivity array for the mesh is given by

$$[NOD] = \begin{matrix} & \begin{matrix} 1 & 2 & 3 & 4 & 5 & 6 & 7 & 8 & 9 \end{matrix} \\ \begin{matrix} 1 \\ 2 \\ 3 \\ 4 \\ 5 \\ 6 \end{matrix} & \begin{bmatrix} 1 & 3 & 17 & 15 & 2 & 10 & 16 & 8 & 9 \\ 3 & 5 & 19 & 17 & 4 & 12 & 18 & 10 & 11 \\ 5 & 7 & 21 & 19 & 6 & 14 & 20 & 12 & 13 \\ 15 & 17 & 31 & 29 & 16 & 24 & 30 & 22 & 23 \\ 17 & 19 & 33 & 31 & 18 & 26 & 32 & 24 & 35 \\ 19 & 21 & 35 & 33 & 20 & 28 & 34 & 26 & 27 \end{bmatrix} \end{matrix}$$

The NFD array is

$$[NFD] = \begin{matrix} & \begin{matrix} 1 & 2 & 3 & 4 & 5 & 6 & 7 & 8 & 9 \end{matrix} \\ \begin{matrix} 1 \\ 2 \\ 3 \\ 4 \\ 5 \\ 6 \end{matrix} & \begin{bmatrix} 3 & 8 & 40 & 35 & 5 & 24 & 37 & 20 & 22 \\ 8 & 13 & 45 & 40 & 10 & 28 & 42 & 24 & 26 \\ 13 & 18 & 50 & 45 & 15 & 32 & 47 & 28 & 30 \\ 35 & 40 & 72 & 67 & 37 & 56 & 69 & 52 & 54 \\ 40 & 45 & 77 & 72 & 42 & 60 & 74 & 56 & 58 \\ 45 & 50 & 82 & 77 & 47 & 64 & 79 & 60 & 62 \end{bmatrix} \end{matrix}$$

In addition, we define an array of the total degrees of freedom of nodes 1 through 9 of the element

$$\{NFR\} = \{ 3 \ 3 \ 3 \ 3 \ 2 \ 2 \ 2 \ 2 \ 2 \}$$

Now with the help of these arrays, we can assemble the element matrices. Fortran statements of the assembly are given in Box 7.7.2.

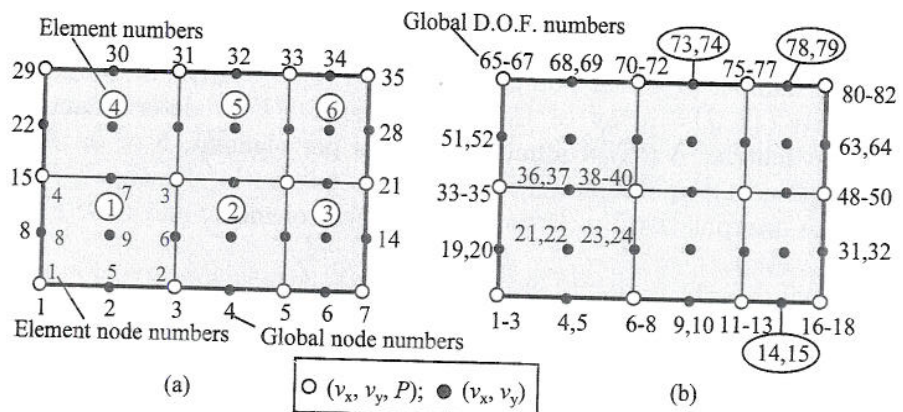


Figure 7.7.1 Element and global degrees of freedom of a mesh of nine-node elements used for the mixed formulation.

Box 7.7.1 Fortran statements of the mixed element calculations.

```

DO 100 NI=1,NGP
  DO 100 NJ=1,NGP
    XI=GAUSS(NI,NGP)
    ETA=GAUSS(NJ,NGP)
    CALL SHP2DPV(NPE,XI,ETA,ELXY,DET)
    CONST=DET*WT(NI,NGP)*WT(NJ,NGP)
  C
    VX=0.0
    VY=0.0
    DO I=1,NPE
      L=2*I-1
      VX=VX+SF(I)*ELV(L)
      VY=VY+SF(I)*ELV(L+1)
    ENDDO
  C
    II=1
    KI = 3
    DO 80 I = 1,NPE
      JJ=1
      KJ = 3
      DO 70 J = 1,NPE
        CONV = SF(I)*(VX*GDSF(1,J)+VY*GDSF(2,J))*CONST
        SX = GDSF(1,I)*GDSF(1,J)*CONST
        SY = GDSF(2,I)*GDSF(2,J)*CONST
        SXY= GDSF(1,I)*GDSF(2,J)*CONST
        SYX= GDSF(2,I)*GDSF(1,J)*CONST
        IF (J.LE.4)THEN
          GX = GDSF(1,I)*SFL(J)*CONST
          GY = GDSF(2,I)*SFL(J)*CONST
        ENDIF
        IF (I.LE.4)THEN
          GXT= GDSF(1,J)*SFL(I)*CONST
          GYT= GDSF(2,J)*SFL(I)*CONST
        ENDIF
      C
        ELK(II,JJ) = ELK(II,JJ) +AMU*(2.0*SX+SY)+RHO*CONV
        ELK(II,JJ+1) = ELK(II,JJ+1) +AMU*SYX
        ELK(II+1,JJ+1) = ELK(II+1,JJ+1)+AMU*(SX+2.0*SY)+RHO*CONV
        ELK(II+1,JJ) = ELK(II+1,JJ) +AMU*SXY
        IF(J .LE. 4)THEN
          ELK(II,JJ+2) = ELK(II,JJ+2) - GX
          ELK(II+1,JJ+2) = ELK(II+1,JJ+2) - GY
        ENDIF
        IF(I .LE. 4)THEN
          ELK(II+2,JJ) = ELK(II+2,JJ) - GXT
          ELK(II+2,JJ+1) = ELK(II+2,JJ+1) - GYT
        ENDIF
      IF(J .GT. 4)KJ=2
    70    JJ = JJ + KJ
      IF(I .GT. 4)KI=2
    80    II = II + KI
  100 CONTINUE

```

**Box 7.7.2** Fortran statements of the assembly procedure used for mixed model.

```

C Assembly of element coefficient matrix and right-hand column vector
C for a typical (Nth) element.
C
DO 90 I=1,NPE
  NDFI=NFR(I)
  NR=NFD(N,I)-NDFI
  DO 90 II=1,NDFI
    NR=NR+1
    IF(I.LE.5)THEN
      L=(I-1)*3+II
    ELSE
      L=12+(I-5)*2+II
    ENDIF
    GLF(NR) = GLF(NR)+ELF(L)
  DO 90 J=1,NPE
    NDFJ=NFR(J)
    NCL=NFD(N,J)-NDFJ
    DO 90 JJ=1,NDFJ
      NCL=NCL+1
      IF(J.LE.5)THEN
        M=(J-1)*3+JJ
      ELSE
        M=12+(J-5)*2+JJ
      ENDIF
      GLK(NR,NCL)=GLK(NR,NCL)+ELK(L,M)
    90 CONTINUE

```

### 7.7.2 Penalty Model

Computer implementation of the penalty finite element model is quite straightforward and is the same as any multi-degree of freedom systems (see Chapters 2 and 5, and Box 7.7.1), and hence not discussed further. One note should be made of the fact that the element calculations involve two Gauss loops: a full integration loop for the evaluations of all terms except for the penalty terms; and the other one is a reduced integration loop for the evaluation of the penalty terms of the coefficient matrix  $[\bar{\mathbf{K}}]$  [see Eq. (7.6.3)].

## 7.8 Numerical Examples

### 7.8.1 Preliminary Comments

In this section, a small number of flow problems solved using the finite element models developed herein are presented. Additional examples may be found in the book by Reddy and Gartling [10]. The examples presented herein were solved using the RIP finite element model and mixed finite element model. The

he

objective of the first several examples is to evaluate the accuracy of the penalty and mixed finite element models by comparing with the available analytical or numerical results and to illustrate the effect of the penalty parameter on the accuracy of the solutions. The remaining examples are for Reynolds numbers greater than unity (i.e. convective terms are included), and the results were obtained using the RIP finite element model.

### 7.8.2 Fluid Squeezed Between Parallel Plates

Consider the slow flow of a viscous incompressible material squeezed between two long parallel plates [see Figure 7.8.1(a)]. When the length of the plates is very large compared to both the width of and the distance between the plates, we have a case of plane flow. Although this is a moving boundary problem, we wish to determine the velocity and pressure fields for a fixed distance between the plates, assuming that a state of plane flow exists.

Let  $V_0$  be the velocity with which the two plates are moving toward each other (i.e. squeezing out the fluid), and let  $2b$  and  $2a$  denote, respectively, the distance between and the length of the plates [see Figure 7.8.1(a)]. Due to the biaxial symmetry present in the problem, it suffices to model only a quadrant of the domain. As a first mesh, we use a  $5 \times 3$  nonuniform mesh of nine-node quadratic elements in the mixed model, and a  $10 \times 6$  mesh of the four-node linear elements and  $5 \times 3$  mesh of nine-node quadratic elements in the penalty model [see Figure 7.8.1(b)]. The non-uniform mesh, with smaller elements near the free surface (i.e. at  $x = a$ ), is used to approximate accurately the singularity in the shear stress at the point  $(a, b) = (6, 2)$ . The mesh used for the penalty model has exactly the same number of nodes as the mesh used for the nine-node mesh of the mixed model. The velocity boundary conditions are shown in Figure 7.8.1(b). The velocity field at  $x = 6$  (outflow boundary)

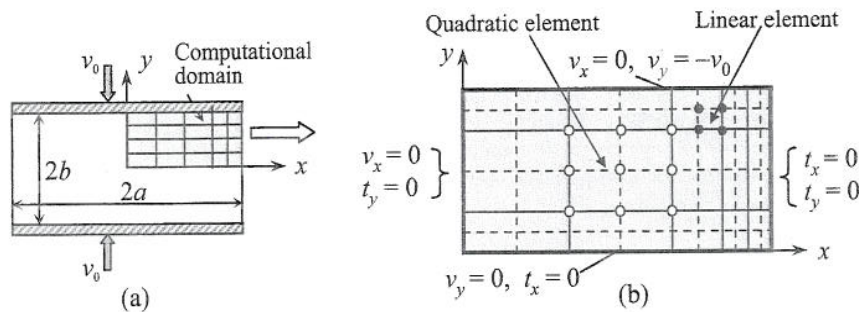


Figure 7.8.1 (a) Geometry, computational domain, and (b) the finite element mesh used for the analysis of slow flow of viscous incompressible fluid between parallel plates.



is not known; if we do not impose any boundary conditions there, it amounts to requiring  $t_x = t_y = 0$  in the integral sense. In the mixed finite element model, it is necessary to specify the pressure at least at one node. In the present case, the node at  $(x, y) = (a, 0)$  is specified to have zero pressure. An approximate analytical solution to this two-dimensional problem is provided by Nadai [30] (also see [12,13]), and it is given by

$$v_x(x, y) = \frac{3V_0x}{2b} \left(1 - \frac{y^2}{b^2}\right), \quad v_y(x, y) = -\frac{3V_0y}{2b} \left(3 - \frac{y^2}{b^2}\right) \quad (7.8.1)$$

$$P(x, y) = \frac{3\mu V_0}{2b^3}(a^2 + y^2 - x^2)$$

The velocities  $v_x(x, 0)$  obtained with the two finite element models compare well with the analytical solution (see Reddy [11]), as shown in Table 7.8.1. The nine-node element gives very good results for both the penalty and mixed models. The influence of the penalty parameter on the accuracy of the solution is clear from the results. Whether the element is linear or quadratic, it is necessary to use a large value of the penalty parameter.

Table 7.8.1 Comparison of finite element solution  $v_x(x, 0)$  with the analytical solution for fluid squeezed between plates.

x	$\gamma = 1.0$		$\gamma = 100$		$\gamma = 10^8$		Mixed model Nine -node	Series solution
	Four -node	Nine* -node	Four -node	Nine -node	Four -node	Nine -node		
1.00	0.0303	0.0310	0.6563	0.6513	0.7576	0.7505	0.7497	0.7500
2.00	0.0677	0.0691	1.3165	1.3062	1.5135	1.4992	1.5031	1.5000
3.00	0.1213	0.1233	1.9911	1.9769	2.2756	2.2557	2.2561	2.2500
4.00	0.2040	0.2061	2.6960	2.6730	3.0541	3.0238	3.0203	3.0000
4.50	0.2611	0.2631	3.0718	3.0463	3.4648	3.4307	3.4292	3.3750
5.00	0.3297	0.3310	3.4347	3.3956	3.8517	3.8029	3.8165	3.7500
5.25	0.3674	0.3684	3.6120	3.5732	4.0441	3.9944	3.9893	3.9375
5.50	0.4060	0.4064	3.7388	3.6874	4.1712	4.1085	4.1204	4.1250
5.75	0.4438	0.4443	3.8316	3.7924	4.2654	4.2160	4.2058	4.3125
6.00	0.4793	0.4797	3.8362	3.7862	4.2549	4.1937	4.2364	4.5000

\*The  $3 \times 3$  Gauss rule for non-penalty terms and the  $2 \times 2$  Gauss rule for penalty terms are used for quadratic elements.

Figure 7.8.2 contains plots of the velocity  $v_x(x, y)$  for  $x = 4$  and  $x = 6$ , and Figure 7.8.3 contains plots of pressure  $P(x, y)$ , for  $y = y_0$ , where  $y_0$  is the  $y$ -coordinate of the Gauss point nearest to the centerline or top plate. These results were obtained with two different meshes:  $5 \times 3$  and  $10 \times 8$ . The pressure in the penalty model was computed using Eq. (7.5.19) with the  $2 \times 2$  Gauss rule for the quadratic rectangular element and the one-point formula

for the linear element, whereas in the mixed model (as well as the analytical solution) it is computed at the nodes. If the pressure in the penalty model were computed using the full quadrature rule for rectangular elements, we would have obtained erroneous values. In general, the same integration rule as that used for the evaluation of the penalty terms in the coefficient matrix must be used to compute the pressure. The oscillations in pressure computed nearest to the top plate are due to the singularity in the boundary conditions at  $(x, y) = (6, 2)$ .

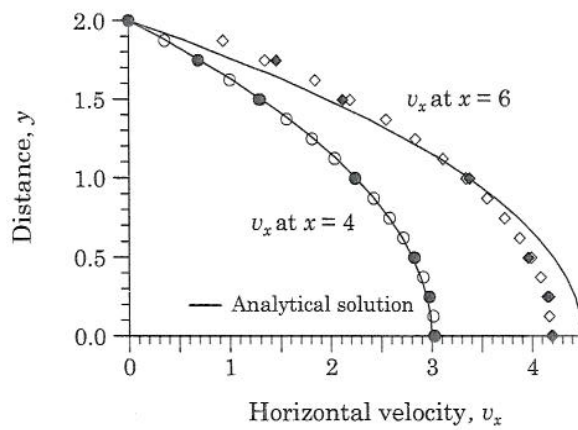


Figure 7.8.2 Velocity fields for fluid squeezed between parallel plates.

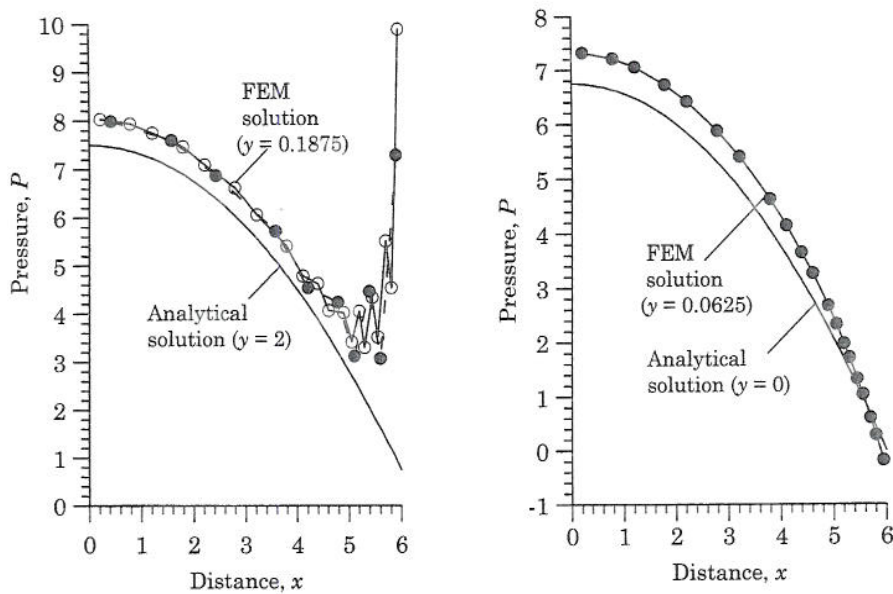


Figure 7.8.3 Pressures for fluid squeezed between parallel plates.

### 7.8.3 Flow of a Viscous Lubricant in a Slider Bearing

The slider (or slipper) bearing consists of a short sliding pad moving a velocity  $u = V_0$  relative to a stationary pad inclined at a small angle with respect to the stationary pad, and the small gap between the two pads is filled with a lubricant [see Figure 7.8.4(a)]. Since the ends of the bearing are generally open, the pressure there is atmospheric,  $P_0$ . If the upper pad is parallel to the base plate, the pressure everywhere in the gap must be atmospheric (because  $dP/dx$  is a constant for flow between parallel plates) and the bearing cannot support any transverse load. If the upper pad is inclined to the base pad, a pressure distribution, in general, a function of  $x$  and  $y$ , is set up in the gap. For large values of  $V_0$ , the pressure generated can be of sufficient magnitude to support heavy loads normal to the base pad.

When the width of the gap and the angle of inclination are small, one may assume that  $v_y = 0$  and the pressure is not a function of  $y$ . Assuming a two-dimensional state of flow and a small angle of inclination, and neglecting the normal stress gradient (in comparison with the shear stress gradient), the equations governing the flow of the lubricant between the pads can be reduced to (see Schlichting [9])

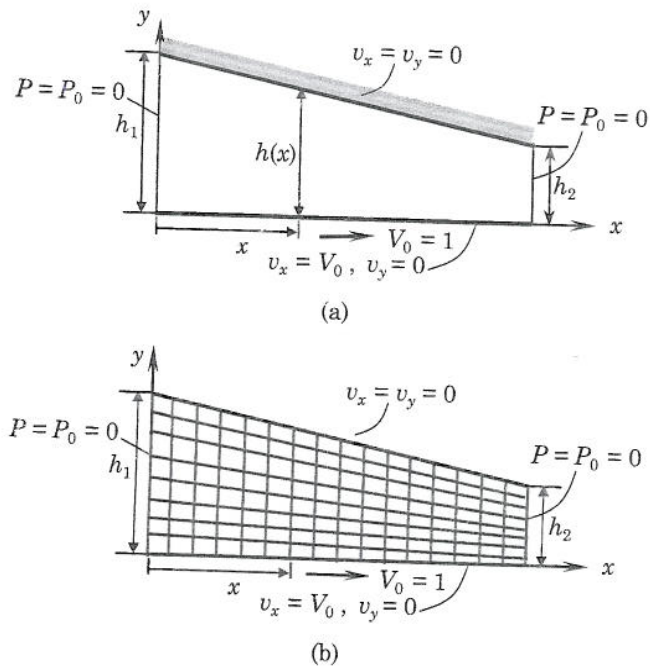


Figure 7.8.4 Schematic and the finite element mesh for slider bearing.

$$\mu \frac{\partial^2 v_x}{\partial y^2} = \frac{dP}{dx}, \quad 0 < x < L \tag{7.8.2a}$$

where the pressure gradient is given by

$$\frac{dP}{dx} = \frac{6\mu V_0}{h^2} \left(1 - \frac{H}{h}\right), \quad H = \frac{2h_1 h_2}{h_1 + h_2} \tag{7.8.2b}$$

The solution of Eqs. (7.8.2a,b), subject to the boundary conditions

$$v_x(0,0) = V_0, \quad v_x(x,h) = 0 \tag{7.8.2c}$$

is

$$v_x(x,y) = \left( V_0 - \frac{h^2}{2\mu} \frac{dP}{dx} \frac{y}{h} \right) \left( 1 - \frac{y}{h} \right) \tag{7.8.3a}$$

$$P(x) = \frac{6\mu V_0 L (h_1 - h)(h - h_2)}{h^2 (h_1^2 - h_2^2)} \tag{7.8.3b}$$

$$\sigma_{xy}(x,y) = \mu \frac{\partial v_x}{\partial y} = \frac{dP}{dx} \left( y - \frac{h}{2} \right) - \mu \frac{V_0}{h} \tag{7.8.3c}$$

where

$$h(x) = h_1 + \frac{h_2 - h_1}{L} x \tag{7.8.4}$$

In the finite element analysis we do not make any assumptions concerning  $v_y$  and the pressure gradient, and solve the Stokes equations [i.e. neglect the convective terms in Eqs. (7.4.2) and (7.4.3)], with the following choice of parameters:

$$h_1 = 2h_2 = 8 \times 10^{-4} \text{ ft}, \quad L = 0.36 \text{ ft}, \quad \mu = 8 \times 10^{-4} \text{ lb/ft}^2, \quad V_0 = 30 \text{ ft} \tag{7.8.5}$$

We use a mesh (Mesh 1) of  $18 \times 8$  linear quadrilateral elements to analyze the problem. The mesh and boundary conditions are shown in Figure 7.8.4(b). The penalty parameter is chosen to be  $\gamma = \mu \times 10^8$ . Table 7.8.2 contains a comparison of the finite element solutions and analytical solutions for the velocity, pressure, and shear stress. Figure 7.8.5 contains plots of the horizontal velocity  $v_x$  at  $x = 0$  ft,  $x = 0.18$  ft, and  $x = 0.36$  ft. Figure 7.8.6 contains plots of pressure and shear stress as a function of  $x$  at  $y = 0$ . The finite element solutions for the pressure and shear stress were computed at the center of the first row of elements along the moving block. The results are in good agreement with the analytical solutions (7.8.3a-c), validating the assumptions made in the development of the analytical solution.

Table 7.8.2 Comparison of finite element solutions velocities with analytical solutions for viscous fluid in a slider bearing.

$\bar{y}$	$v_x(0, y)$		$\bar{y}$	$v_x(0.18, y)$		$\bar{y}$	$v_x(0.36, y)$	
	FEM	Analy.		FEM	Analy.		FEM	Analy.
0.0	30.000	30.000	0.00	30.000	30.000	0.00	30.000	30.000
1.0	22.923	22.969	0.75	25.139	25.156	0.50	29.564	29.531
2.0	16.799	16.875	1.50	20.596	20.625	1.00	28.182	28.125
3.0	11.626	11.719	2.25	16.372	16.406	1.50	25.853	25.781
4.0	7.403	7.500	3.00	12.465	12.500	2.00	22.577	22.500
5.0	4.130	4.219	3.75	8.874	8.906	2.50	18.354	18.281
6.0	1.805	1.875	4.50	5.600	5.625	3.00	13.184	13.125
7.0	0.429	0.469	5.25	2.642	2.656	3.50	7.066	7.031
8.0	0.000	0.000	6.00	0.000	0.000	4.00	0.000	0.000

Analytical solution			FEM Solution			
$x$	$\bar{P}(x, 0)$	$-\sigma_{xy}(x, 0)$	$\bar{x}$	$\bar{y}$	$\bar{P}$	$-\sigma_{xy}$
0.01	7.50	59.99	0.1125	0.4922	8.46	56.61
0.03	22.46	59.89	0.3375	0.4766	25.46	56.60
0.05	37.29	59.67	0.5625	0.4609	42.31	56.47
0.07	51.89	59.30	0.7875	0.4453	58.76	56.17
0.09	66.12	58.77	1.0125	0.4297	74.69	55.69
0.27	129.60	38.40	2.5875	0.3203	134.40	41.77
0.29	118.57	32.71	2.8125	0.3047	125.60	36.93
0.31	99.58	25.70	3.0375	0.2891	107.60	30.76
0.33	70.30	17.04	3.2625	0.2734	77.39	22.89
0.35	27.61	6.31	3.4875	0.2578	30.80	12.82

$\bar{x} = 10x, \bar{y} = y \times 10^4, \bar{P} = P \times 10^{-2}.$

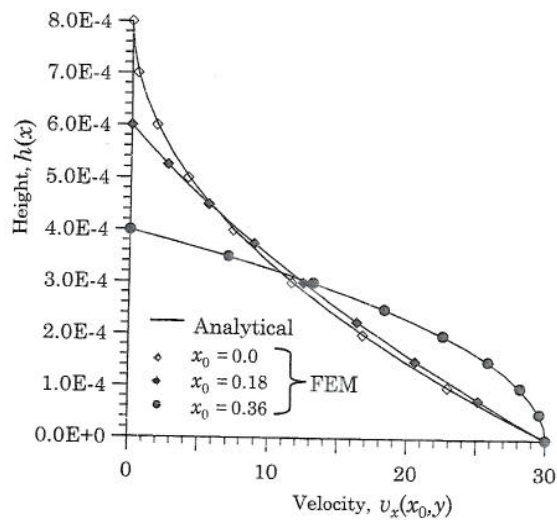


Figure 7.8.5 Velocity distributions for the slider bearing problem.

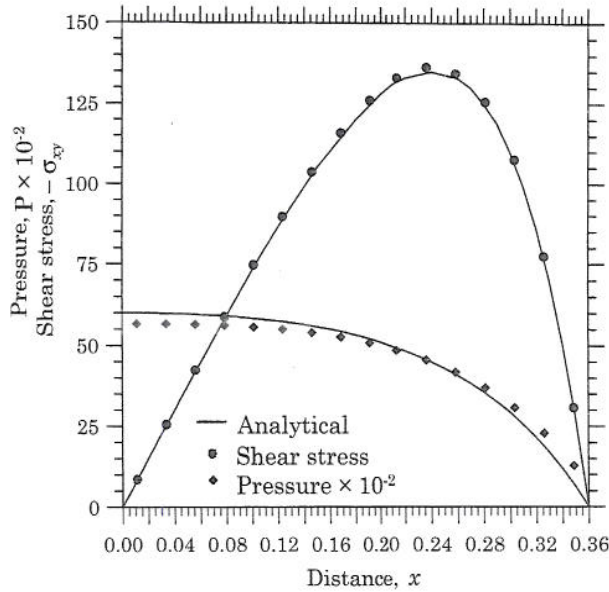


Figure 7.8.6 Pressure and shear stress distributions for the slider bearing problem.

### 7.8.4 Wall-Driven Cavity Flow

Consider the laminar flow of a viscous, incompressible fluid in a square cavity bounded by three motionless walls and a lid moving at a constant velocity in its own plane (see Figure 7.8.7). Singularities exist at each corner where the moving lid meets a fixed wall. This example is one that has been extensively studied by analytical, numerical, and experimental methods (see [31-33], among others), and it is often used as a benchmark problem to test a new numerical method or formulation. In solving this problem, the mesh used should be such that the boundary layer thickness is resolved. The boundary layer thickness is of the order of  $Re^{-\frac{1}{2}}$ , where  $Re = \rho v_0 a / \mu$  is the Reynolds number and  $v_0$  is the lid velocity and  $a$  is the dimension of the cavity.

Assuming a unit square and that the velocity of the top wall is unity, we can discretize the flow region using a uniform,  $8 \times 8$  mesh of linear elements or  $4 \times 4$  of nine-node quadratic elements. At the singular points, namely at the top corners of the lid, we assume that  $v_x(x, 1) = v_0 = 1.0$ . The linear solution for the horizontal velocity along the vertical centerline obtained with the two meshes is shown in Figure 7.8.8, and the variation of pressure along the top wall (computed at the reduced Gauss points) is shown in Figure 7.8.9. The numerical values of the velocity field are tabulated in Table 7.8.3. It is clear that the value of the penalty parameter between  $\gamma = 10^2$  and  $\gamma = 10^8$  has small effect on the solution.

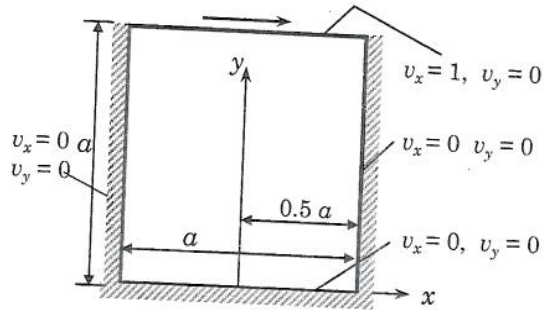


Figure 7.8.7 Wall-driven cavity problem.

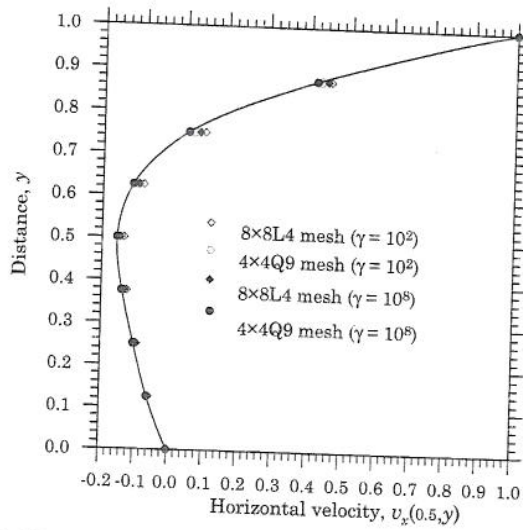


Figure 7.8.8 Plots of horizontal velocity  $v_x(0.5, y)$  along the vertical centerline of the cavity.

Table 7.8.3 Velocity  $v_x(0.5, y)$  obtained with various values of the penalty parameter  $\gamma$  (linear solution).

$y$	Mesh: $8 \times 8L4$		Mesh: $4 \times 4Q9$	
	$\gamma = 10^2$	$\gamma = 10^8$	$\gamma = 10^2$	$\gamma = 10^8$
0.125	-0.0557	-0.0579	-0.0589	-0.0615
0.250	-0.0938	-0.0988	-0.0984	-0.1039
0.375	-0.1250	-0.1317	-0.1320	-0.1394
0.500	-0.1354	-0.1471	-0.1442	-0.1563
0.625	-0.0818	-0.0950	-0.0983	-0.1118
0.750	0.0958	0.0805	0.0641	0.0481
0.875	0.4601	0.4501	0.4295	0.4186

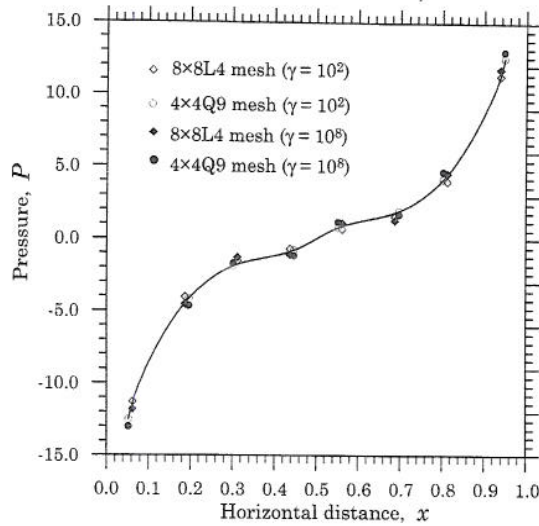


Figure 7.8.9. Plots of pressure  $P(x, y_0)$  along the top wall of the cavity.

Next, we consider the wall-driven cavity problem for nonlinear analysis (i.e. solve Navier-Stokes equations). The role of the load parameter is played by the Reynolds number ( $Re = \rho v_0 a / \mu$ ). For the problem at hand, the Reynolds number can be varied by varying the density while keeping the viscosity constant. Thus, we take (in addition to the the choice of the characteristic velocity  $v_0 = 1$  and characteristic length  $a = 1$ )  $\mu = 1$  so that  $Re = \rho$ . The problem is solved using uniform  $8 \times 8$  mesh of linear elements as well as  $4 \times 4$  mesh of nine-node quadratic elements, and the results are presented in Table 7.8.4 for  $Re = 100, 500$ , and  $700$  ( $\gamma = 10^8$  and  $\epsilon = 10^{-2}$ ). The converged nonlinear solution of the preceding Reynolds number is used as the initial guess in the first iteration of the next Reynolds number. In general, for very high Reynolds numbers underrelaxtion must be used to accelerate the convergence by using the weighted average of velocities from two consecutive iterations

$$\{\bar{\mathbf{v}}\}^r = \beta \{\mathbf{v}\}^{(r)} + (1 - \beta) \{\mathbf{v}\}^{(r-1)} \tag{7.8.6}$$

to compute the coefficient matrix. Here  $\beta$  is the acceleration parameter.

Figure 7.8.10 shows plots of the horizontal velocity along the cavity centerline obtained with  $8 \times 8$  and  $16 \times 20$  mesh of bilinear elements for  $Re = 0$  and  $500$  ( $\beta = 0$ ). The pressure obtained with the two meshes is shown in Figure 7.8.11. Clearly, the pressure exhibits oscillations. Figure 7.8.12 contains plots of the horizontal velocity obtained with  $16 \times 20$  mesh for  $Re = 500, 10^3, 5 \times 10^3, 10^4$  (the increment of  $Re$  is taken to be 500 and  $\beta = 0.5$ ).



Table 7.8.4 Velocity  $v_x(0.5, y)$  obtained with linear and quadratic elements and for various values of the Reynolds number.

$y$	$8 \times 8L$			$4 \times 4Q9$		
	$Re \rightarrow$ 100(5)	500(8)	700(9)	100(5)	500(8)	700(10)
0.125	-0.0498	-0.0242	-0.0140	-0.0554	-0.0141	-0.0106
0.250	-0.0870	-0.0503	-0.0345	-0.0968	-0.0540	-0.0089
0.375	-0.1164	-0.0733	-0.0564	-0.1313	-0.1143	-0.0672
0.500	-0.1231	-0.0700	-0.0586	-0.1414	-0.1252	-0.1181
0.625	-0.0635	0.0027	0.0039	-0.0814	-0.0455	-0.0831
0.750	0.0649	0.0389	0.0354	0.0486	0.1045	0.0808
0.875	0.3750	0.1761	0.1241	0.3629	0.2113	0.1628

\* Number in parentheses denotes the number of iterations taken for convergence.

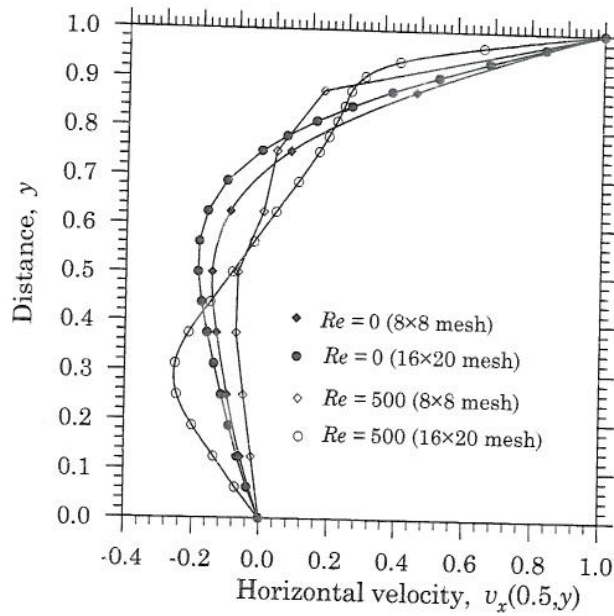


Figure 7.8.10 Velocity  $v_x(0.5, y)$  versus  $y$  for various Reynolds number ( $8 \times 8$  and  $16 \times 20$  meshes of bilinear elements).

Next, a comparison of the present results with the finite difference solution of Ghia *et al.* [34] are presented. The mesh of bilinear elements used in the present study is shown in Figure 7.8.13; a penalty parameter of  $\gamma = 10^8 Re$  and convergence tolerance of  $\epsilon \leq 10^{-2}$  were used. Convergence was achieved with 3 iterations at each Reynolds number step ( $Re = 100, 400, 10^3$ ). Figures 7.8.14 and 7.8.15 show the results for  $Re = 400$  and  $Re = 10^3$ .

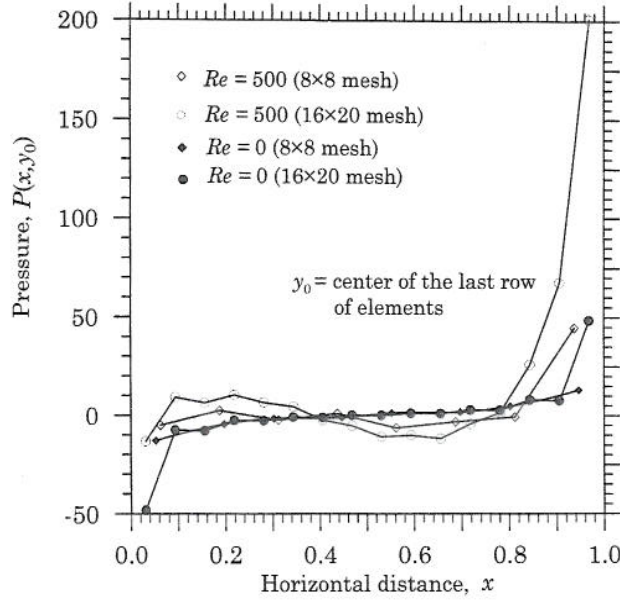


Figure 7.8.11 Plots of pressure  $P(x, y_0)$  along the top wall of the cavity ( $8 \times 8$  and  $16 \times 20$  meshes).

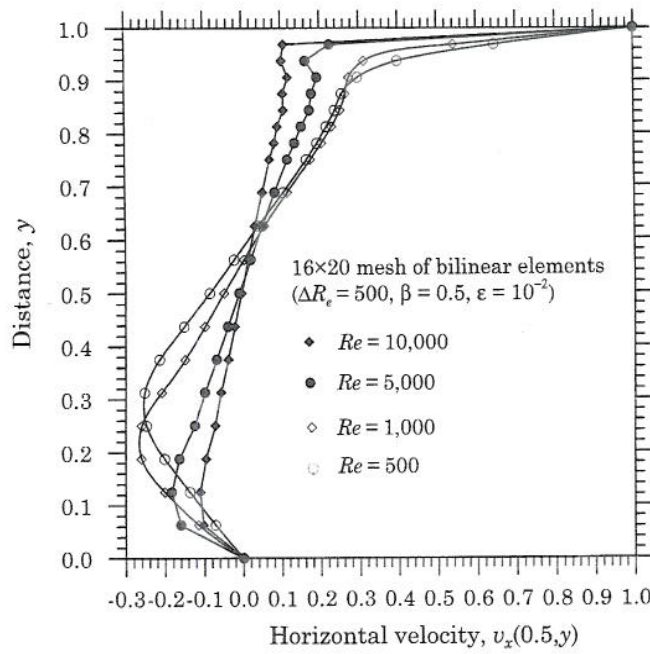


Figure 7.8.12 Velocity  $v_x(0.5, y)$  versus  $y$  for various Reynolds numbers ( $16 \times 20$  mesh of bilinear elements).

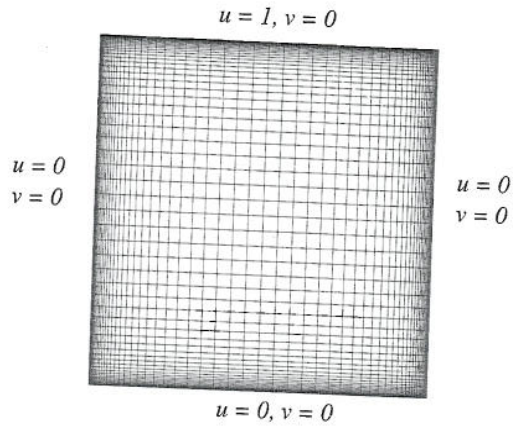


Figure 7.8.13 Mesh used for the wall-driven cavity problems.

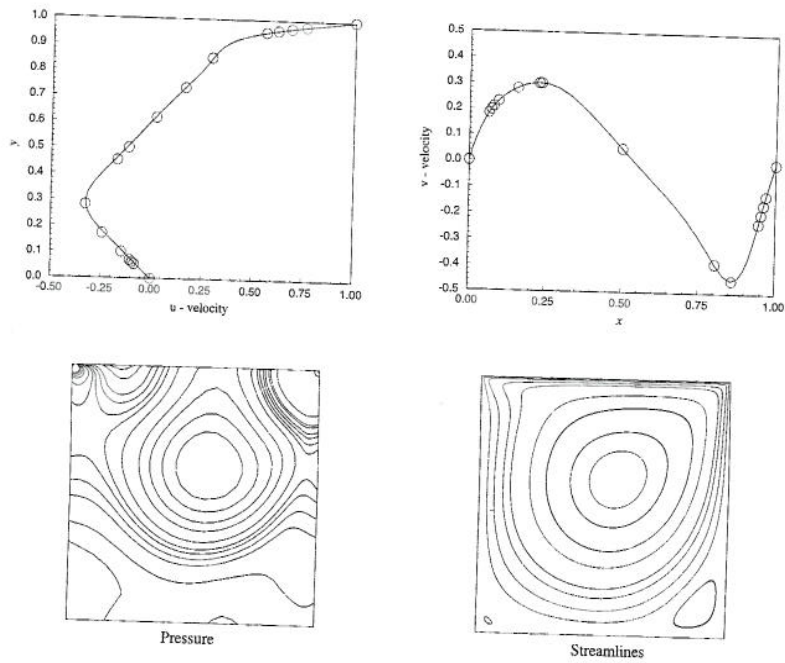
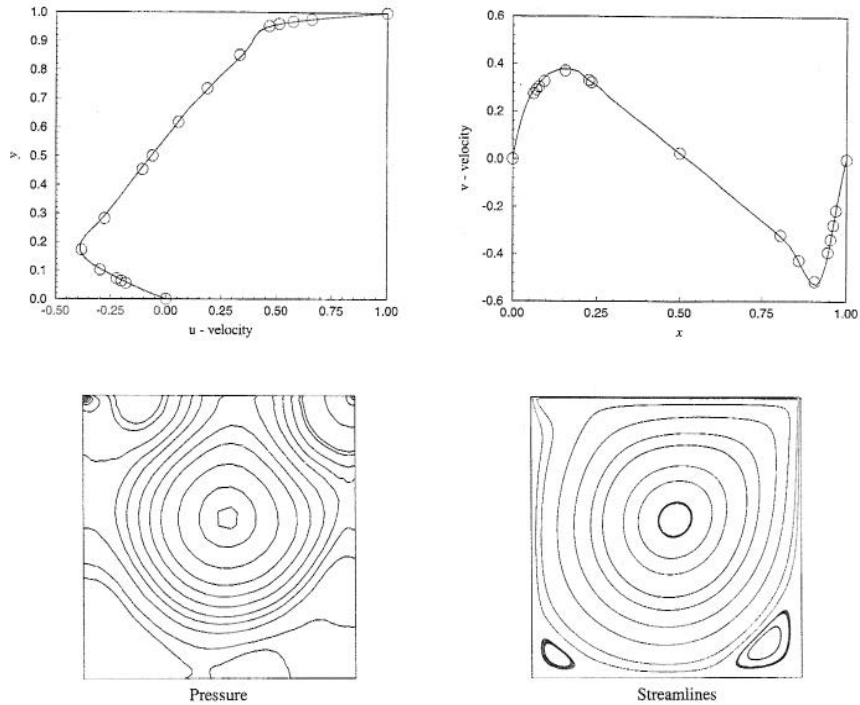


Figure 7.8.14 Normalized horizontal and vertical velocity profiles along the vertical and horizontal mid-sections of the cavity (— computed,  $\circ$  Ghia *et al.* [34]) and pressure contours and streamlines ( $Re = 400$ ).



**Figure 7.8.15** Horizontal and vertical velocity profiles along the vertical and horizontal mid-sections of the cavity for  $Re = 10^3$  (— computed,  $\circ$  Ghia *et al.* [34]). Pressure contours and streamlines.

### 7.8.5 Backward-Facing Step

Here we analyze the well-known backward-facing problem (see Gartling [35] and Reddy and Gartling [10]) using the penalty finite element model. The geometry and boundary conditions of the computational domain are shown in Figure 7.8.16. A penalty parameter of  $\gamma = 10^8 Re$  and convergence tolerance of  $\varepsilon \leq 10^{-2}$  are used. Convergence is achieved with 5 iterations.

Figure 7.8.17 shows contour plots of the streamlines and pressure, while Figure 7.8.18 contains pressure profiles along the upper and lower walls for Reynolds number  $Re = 800$ . The results compare well with those of Gartling [35]. This problem will be revisited in the next section in the context of the least-squares finite element model.

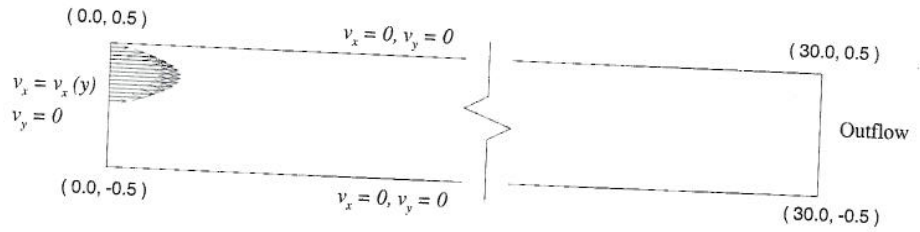
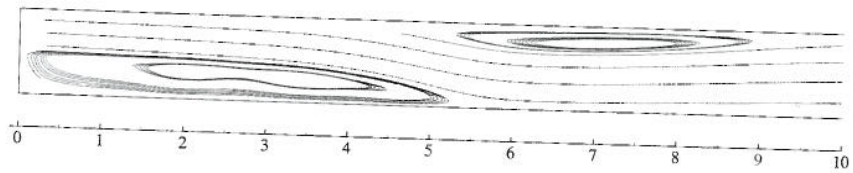


Figure 7.8.16 Geometry and boundary conditions for flow over backward-facing step.

Streamlines



Pressure

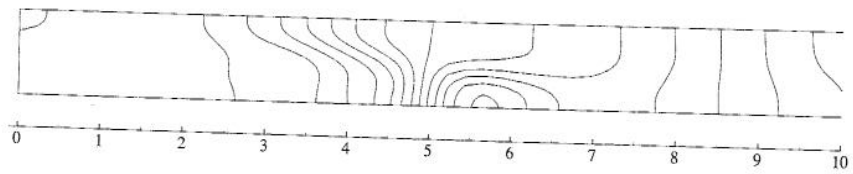


Figure 7.8.17 Streamlines and pressure contours for flow over a backward-facing step ( $Re = 800$ ).

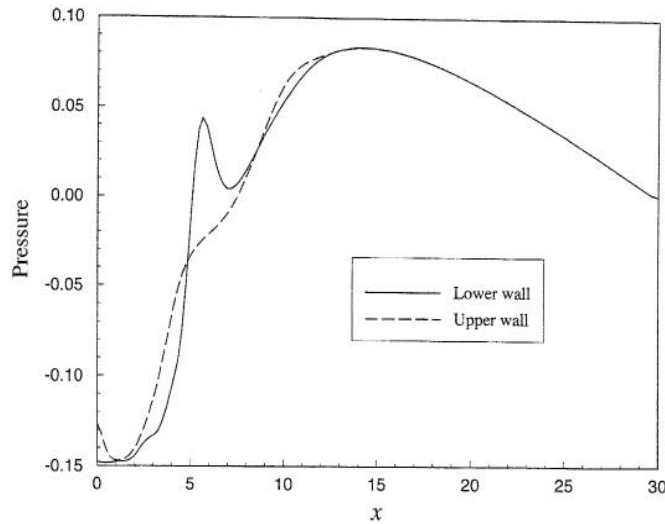


Figure 7.8.18 Pressure profiles along the upper and lower walls of the channel for flow over a backward-facing step ( $Re = 800$ ).

## 7.9 Least-Squares Finite Element Models

### 7.9.1 Introduction

In this section, we present least-squares finite element model of the Navier–Stokes equations [36–39]. The least-squares method has the property of minimizing the residuals in the differential equations. For the Navier–Stokes equations, which have no underlying minimum principles, the least-squares method provides a variational framework [37,38]. The main ideas of the least-squares method are described using the steady Stokes flow problem.

Consider the following vector form of equations governing the steady, slow flow of a viscous incompressible fluid:

$$-\mu \nabla \cdot [(\nabla \mathbf{v}) + (\nabla \mathbf{v})^T] + \nabla P - \rho \mathbf{f} = \mathbf{0} \quad (7.9.1)$$

$$\nabla \cdot \mathbf{v} = 0 \quad (7.9.2)$$

where  $\mathbf{v}$  is the velocity vector,  $P$  is the pressure and  $\mathbf{f}$  is the body force vector. Choosing a suitable finite element approximation of  $(\mathbf{v}, P)$  and their substitution into the governing equations results in residuals

$$\mathcal{R}_1 = -\mu \nabla \cdot [(\nabla \mathbf{v}) + (\nabla \mathbf{v})^T] + \nabla P - \rho \mathbf{f} \quad (7.9.3a)$$

$$\mathcal{R}_2 = \nabla \cdot \mathbf{v} \quad (7.9.3b)$$

In the least-squares method, the sum of the squares of the residuals in the governing equations is minimized: minimize  $I$ , where

$$\begin{aligned} I(\mathbf{v}, P) &\equiv \frac{1}{2} \int_{\Omega^e} (\mathcal{R}_1^2 + \mathcal{R}_2^2) \\ &= \frac{1}{2} \left( \left\| -\mu \nabla \cdot [(\nabla \mathbf{v}) + (\nabla \mathbf{v})^T] + \nabla P - \rho \mathbf{f} \right\|_0^2 + \left\| \nabla \cdot \mathbf{v} \right\|_0^2 \right) \end{aligned} \quad (7.9.4)$$

and  $\|\cdot\|_0$  denotes the  $L_2(\Omega^e)$ -norm of the enclosed quantity

$$\|u\|_0^2 = \int_{\Omega^e} |u|^2 d\Omega \quad (7.9.5)$$

The minimization problem  $\delta I = 0$  is equivalent to the variational problem: find  $(\mathbf{v}, P)$  in a suitable vector space such that for all  $(\mathbf{w}, Q)$  in the same vector space the following equation holds:

$$B((\mathbf{v}, P), (\mathbf{w}, Q)) = \ell((\mathbf{w}, Q)) \quad (7.9.6)$$

where  $B(\cdot, \cdot)$  is a symmetric bilinear form and  $\ell((\mathbf{w}, Q))$  is the linear form

$$\begin{aligned} B((\mathbf{v}, P), (\mathbf{w}, Q)) &= \int_{\Omega^e} \left\{ -\mu \nabla \cdot [(\nabla \mathbf{v}) + (\nabla \mathbf{v})^T] + \nabla P \right\} \cdot \left\{ -\mu \nabla \cdot [(\nabla \mathbf{w}) + (\nabla \mathbf{w})^T] + \nabla Q \right\} d\Omega \\ &\quad + \int_{\Omega^e} (\nabla \cdot \mathbf{v})(\nabla \cdot \mathbf{w}) d\Omega \end{aligned} \quad (7.9.7a)$$

$$\ell((\mathbf{w}, Q)) = \int_{\Omega^e} \rho \mathbf{f} \cdot \left\{ -\mu \nabla \cdot [(\nabla \mathbf{w}) + (\nabla \mathbf{w})^T] + \nabla Q \right\} d\Omega \quad (7.9.7b)$$

The variational problem in (7.9.6) has some nice mathematical as well as computational properties. For example, the finite element model associated with (7.9.6) has a positive-definite coefficient matrix.

Since the variational problem (7.9.6) is based on the differential equation rather than the weak form, it involves the same order derivatives as those appearing in the governing equations, and the variational form does not include the natural boundary terms. Hence, the approximation functions selected must be such that both natural and essential boundary conditions can be imposed. This requires the use of at least  $C^1$ -continuous functions for the velocity field  $\mathbf{v}$ .

In contrast to the weak form finite element models developed earlier, the least-squares finite element model based on the variational problem (7.9.6) has higher differentiability requirements which could be perceived as a practical disadvantage. A way to avoid the use of  $C^1$ -continuous functions is to re-write the governing equations as an equivalent set of first-order equations. The most

common transformation to an equivalent first-order system is to introduce the vorticity vector. In two-dimensional problems, the total number of variables is increased by one, but one has the benefit of directly solving for the vorticity. Yet another approach is to introduce the stresses as independent variables. In two-dimensional problems the total number of variables is increased by three. A third option is to introduce all partial derivatives of the velocity vector field as independent variables. In two-dimensional problems the total number of variables is increased by four and one has the added benefit of easily computing physical quantities of interest (in the post-processing stage) that are linear combinations of the partial derivatives of the velocity vector field; that is, vorticity and stresses. For additional details, see Pontaza and Reddy [37,38].

Here we present a formulation based on the first-order system of equations involving velocities, pressure, and vorticity. To write the second-order equations in (7.9.1) in an equivalent set of first-order equations, we introduce the vorticity vector

$$\omega = \nabla \times \mathbf{v} \tag{7.9.8}$$

Making use of the vector identities

$$\nabla \times \nabla \times \mathbf{v} = -\nabla^2 \mathbf{v} + \nabla (\nabla \cdot \mathbf{v}), \quad \nabla \cdot [(\nabla \mathbf{v}) + (\nabla \mathbf{v})^T] = \nabla^2 \mathbf{v} + \nabla (\nabla \cdot \mathbf{v}) \tag{7.9.9}$$

and the incompressibility condition  $\nabla \cdot \mathbf{v}$ , Eqs. (7.9.1) and (7.9.2) can be replaced by the following first-order system:

$$\mu \nabla \times \omega + \nabla P - \rho \mathbf{f} = \mathbf{0} \tag{7.9.10a}$$

$$\nabla \cdot \mathbf{v} = 0 \tag{7.9.10b}$$

$$\omega - \nabla \times \mathbf{v} = 0 \tag{7.9.10c}$$

The least-squares functional associated with the first-order system (7.9.10a-c) is given by

$$I(\mathbf{v}, P, \omega) = \frac{1}{2} \left( \|\mu \nabla \times \omega + \nabla P - \rho \mathbf{f}\|_0^2 + \|\nabla \cdot \mathbf{v}\|_0^2 + \|\omega - \nabla \times \mathbf{v}\|_0^2 \right) \tag{7.9.11}$$

Like before, we can define the discrete problem by minimizing the functional in (7.9.11) with respect to the chosen approximating spaces. The minimum requirement on approximation functions is that they all be Lagrange family of functions ( $C^0$ -continuity). Because the formulation is based on a variational framework there are no compatibility restrictions between the velocity and pressure approximation spaces, so the same Lagrange basis can be used for all primary variables  $(\mathbf{v}, P, \omega)$ .



### 7.9.2 Finite Element Model

We will now develop the least-squares finite element model of the steady, two dimensional flows of viscous incompressible fluids. The model is developed for the vorticity based equivalent first-order system, which in dimensionless form is written as

$$\frac{\partial v_x}{\partial x} + \frac{\partial v_y}{\partial y} = 0 \quad (7.9.12)$$

$$v_x \frac{\partial v_x}{\partial x} + v_y \frac{\partial v_x}{\partial y} + \frac{\partial P}{\partial x} + \frac{1}{Re} \frac{\partial \omega_z}{\partial y} = f_x \quad (7.9.13)$$

$$v_x \frac{\partial v_y}{\partial x} + v_y \frac{\partial v_y}{\partial y} + \frac{\partial P}{\partial y} - \frac{1}{Re} \frac{\partial \omega_z}{\partial x} = f_y \quad (7.9.14)$$

$$\omega_z + \frac{\partial v_x}{\partial y} - \frac{\partial v_y}{\partial x} = 0 \quad (7.9.15)$$

where  $Re = \rho UL/\mu$  is the Reynolds number. Note that for the two-dimensional case the other two component of the vorticity vector are identically zero,  $\omega = (0, 0, \omega_z)$ .

To develop the least-squares finite element model we define the least-squares functional of the residuals over a typical element  $\Omega^e$ :

$$I^e = \frac{1}{2} \int_{\Omega^e} (\mathcal{R}_1^2 + \mathcal{R}_2^2 + \mathcal{R}_3^2 + \mathcal{R}_4^2) dx dy \quad (7.9.16)$$

where

$$\begin{aligned} \mathcal{R}_1 &= \frac{\partial v_x}{\partial x} + \frac{\partial v_y}{\partial y} \\ \mathcal{R}_2 &= v_x \frac{\partial v_x}{\partial x} + v_y \frac{\partial v_x}{\partial y} + \frac{\partial P}{\partial x} + \frac{1}{Re} \frac{\partial \omega_z}{\partial y} - f_x \\ \mathcal{R}_3 &= v_x \frac{\partial v_y}{\partial x} + v_y \frac{\partial v_y}{\partial y} + \frac{\partial P}{\partial y} - \frac{1}{Re} \frac{\partial \omega_z}{\partial x} - f_y \\ \mathcal{R}_4 &= \omega_z + \frac{\partial v_x}{\partial y} - \frac{\partial v_y}{\partial x} \end{aligned} \quad (7.9.17)$$

and the primary variables  $(v_x, v_y, P, \omega_z)$  are approximated by expansions of the form

$$\begin{aligned} v_x(x, y) &= \sum_{i=1}^N \psi_i(x, y) v_x^i, & v_y(x, y) &= \sum_{i=1}^N \psi_i(x, y) v_y^i \\ P(x, y) &= \sum_{i=1}^N \psi_i(x, y) P_i, & \omega_z(x, y) &= \sum_{i=1}^N \psi_i(x, y) \omega_z^i \end{aligned} \quad (7.9.18)$$

where  $\psi_i$  are the Lagrange family of interpolation functions, and  $(v_x^i, v_y^i, P_i, \omega_z^i)$  are nodal values of  $(v_x, v_y, P, \omega_z)$ .

In developing the finite element model, we assume that the convective term in the residuals associated with the two momentum equations has been linearized; that is,  $v_x$  and  $v_y$  in the convective terms are evaluated from known values of  $v_x^i$  and  $v_y^i$  (from the preceding iteration). In essence this amounts to linearizing the least-squares functional prior to minimization.

Minimizing the least-squares functional in Eq. (7.9.16) with respect to the nodal values of velocities, pressure, and vorticity, we obtain

$$\delta I^e = \frac{\partial I^e}{\partial v_x} \delta v_x + \frac{\partial I^e}{\partial v_y} \delta v_y + \frac{\partial I^e}{\partial P} \delta P + \frac{\partial I^e}{\partial \omega_z} \delta \omega_z = 0 \quad (7.9.19)$$

which yields four sets of  $N$  equations each over a typical element:

$$\frac{\partial I^e}{\partial v_x^i} = 0, \quad \frac{\partial I^e}{\partial v_y^i} = 0, \quad \frac{\partial I^e}{\partial P_i} = 0, \quad \frac{\partial I^e}{\partial \omega_z^i} = 0 \quad (7.9.20)$$

for  $i = 1, 2, \dots, N$ . The resulting finite element equations are given by

$$\begin{aligned} & \begin{bmatrix} [S^{11} + S^{22}] & [S^{12} - S^{21}] & [0] & [S^{20}] \\ [S^{21} - S^{12}] & [S^{11} + S^{22}] & [0] & -[S^{10}] \\ [0] & [0] & [S^{11} + S^{22}] & \frac{1}{Re} [S^{12} - S^{21}] \\ [S^{02}] & -[S^{01}] & \frac{1}{Re} [S^{21} - S^{12}] & \frac{1}{Re^2} [S^{11} + S^{22}] + [S^{00}] \end{bmatrix} \begin{Bmatrix} \{v_x\} \\ \{v_y\} \\ \{P\} \\ \{\omega_z\} \end{Bmatrix} \\ & + \begin{bmatrix} [C^{00}(\mathbf{v})] & [0] & [C^{01}(\mathbf{v})] & \frac{1}{Re} [C^{02}(\mathbf{v})] \\ [0] & [C^{00}(\mathbf{v})] & [C^{02}(\mathbf{v})] & -\frac{1}{Re} [C^{01}(\mathbf{v})] \\ [C^{10}(\mathbf{v})] & [C^{20}(\mathbf{v})] & [0] & [0] \\ \frac{1}{Re} [C^{20}(\mathbf{v})] & -\frac{1}{Re} [C^{10}(\mathbf{v})] & [0] & [0] \end{bmatrix} \begin{Bmatrix} \{v_x\} \\ \{v_y\} \\ \{P\} \\ \{\omega_z\} \end{Bmatrix} = \begin{Bmatrix} \{F^1\} \\ \{F^2\} \\ \{F^3\} \\ \{F^4\} \end{Bmatrix} \end{aligned} \quad (7.9.21)$$

where the coefficient matrices are defined by

$$\begin{aligned} C_{ij}^{00}(\mathbf{v}) &= \int_{\Omega^e} C_i C_j \, dx \, dy, & C_i &= v_x \frac{\partial \psi_i}{\partial x} + v_y \frac{\partial \psi_i}{\partial y} \\ C_{ij}^{01}(\mathbf{v}) &= \int_{\Omega^e} C_i \frac{\partial \psi_j}{\partial x} \, dx \, dy, & C_{ij}^{02}(\mathbf{v}) &= \int_{\Omega^e} C_i \frac{\partial \psi_j}{\partial y} \, dx \, dy \\ C_{ij}^{10}(\mathbf{v}) &= \int_{\Omega^e} \frac{\partial \psi_i}{\partial x} C_j \, dx \, dy, & C_{ij}^{20}(\mathbf{v}) &= \int_{\Omega^e} \frac{\partial \psi_i}{\partial y} C_j \, dx \, dy \\ S_{ij}^{00} &= \int_{\Omega^e} \psi_i \psi_j \, dx \, dy \\ S_{ij}^{01} &= \int_{\Omega^e} \psi_i \frac{\partial \psi_j}{\partial x} \, dx \, dy, & S_{ij}^{02} &= \int_{\Omega^e} \psi_i \frac{\partial \psi_j}{\partial y} \, dx \, dy \\ S_{ij}^{10} &= \int_{\Omega^e} \frac{\partial \psi_i}{\partial x} \psi_j \, dx \, dy, & S_{ij}^{20} &= \int_{\Omega^e} \frac{\partial \psi_i}{\partial y} \psi_j \, dx \, dy \\ S_{ij}^{11} &= \int_{\Omega^e} \frac{\partial \psi_i}{\partial x} \frac{\partial \psi_j}{\partial x} \, dx \, dy, & S_{ij}^{22} &= \int_{\Omega^e} \frac{\partial \psi_i}{\partial y} \frac{\partial \psi_j}{\partial y} \, dx \, dy \end{aligned}$$

$$\begin{aligned}
S_{ij}^{11} &= \int_{\Omega^e} \frac{\partial \psi_i}{\partial x} \frac{\partial \psi_j}{\partial x} dx dy, & S_{ij}^{22} &= \int_{\Omega^e} \frac{\partial \psi_i}{\partial y} \frac{\partial \psi_j}{\partial y} dx dy \\
S_{ij}^{12} &= \int_{\Omega^e} \frac{\partial \psi_i}{\partial x} \frac{\partial \psi_j}{\partial y} dx dy, & S_{ij}^{21} &= \int_{\Omega^e} \frac{\partial \psi_i}{\partial y} \frac{\partial \psi_j}{\partial x} dx dy \\
F_i^1 &= \int_{\Omega^e} C_i f_x dx dy, & F_i^2 &= \int_{\Omega^e} C_i f_y dx dy \\
F_i^3 &= \int_{\Omega^e} \left( \frac{\partial \psi_i}{\partial x} f_x + \frac{\partial \psi_i}{\partial y} f_y \right) dx dy \\
F_i^4 &= \int_{\Omega^e} \frac{1}{Re} \left( \frac{\partial \psi_i}{\partial y} f_x - \frac{\partial \psi_i}{\partial x} f_y \right) dx dy
\end{aligned} \tag{7.9.2}$$

Note that Eq. (7.9.21) cannot be solved until they are assembled and boundary conditions are imposed.

### 7.9.3 Computational Aspects

1. Inspection of the structure of the finite element equations in (7.9.21) reveals that the system is symmetric and positive-definite, even in the convective dominated limit  $1/Re \rightarrow 0$ . In contrast with the mixed finite element model, where the resulting system of discrete equations is unsymmetric and indefinite (zeroes along the diagonal), the least-squares finite element model offers great advantages from a computational point of view.
2. The symmetric positive-definiteness property allows the use of robust iterative methods for the solution of the discrete system of equations. Iterative solution techniques such as preconditioned conjugate gradient methods can be implemented without the need of global assembly. Large scale problems can be solved using element-by-element solution procedure in a fully parallel environment.

In the context of least-squares finite element models for the incompressible Navier-Stokes equations, predominantly low-order expansions, i.e. linear or quadratic Lagrange functions, have been used. Although not commonly emphasized, low-order approximations tend to lock, and reduced integration techniques must be used to obtain acceptable numerical results. When enough redundant degrees of freedom are constrained, the least-squares finite element model using reduced integration yields a collocation finite element model. However, the collocation finite element model may not always be reliable and the least-squares functional cannot be used to measure the quality of the solution. Moreover, the collocation solution may not be smooth at the nodes and post-processing is needed to recover nodal values from the reduced integration points.

Appropriate minimization of the least-squares functional is done using full integration and  $p$ -refinement (see Pontaza and Reddy [37,38] and Winterscheidt and Surana [39]). The quality of the numerical solution may be judged by the value of the least-squares functional, which decays exponentially fast as the expansion order of the basis is increased (see Pontaza and Reddy [38]). Commonly used elements suited for  $p$ -refinement are either of the nodal or modal type. A nodal expansion is of the Lagrange type; when the node spacing is chosen such that the nodes coincide with the location of the roots of a Jacobi polynomial the basis is known as a spectral basis. Modal basis are nodeless expansions whose coefficients are associated with modes of a hierarchical basis. Multi-dimensional nodal and modal basis can be easily constructed by taking tensor product of the one-dimensional basis. Details on the construction of both the nodal and modal expansions can be found in the work of Warburton *et al.* [40].

### 7.9.4 Numerical Examples

#### Kovaszny flow

We consider two-dimensional, steady flow in  $\bar{\Omega} = [-0.5, 1.5] \times [-0.5, 1.5]$ . We use Kovaszny's exact solution to the stationary incompressible Navier-Stokes equations to verify exponentially fast decay of the  $L_2$  least-squares functional and  $L_2$  error norms. The solution is given by

$$v_x = 1 - e^{\lambda x} \cos(2\pi y), \quad v_y = \frac{\lambda}{2\pi} e^{\lambda x} \sin(2\pi y), \quad P = \frac{1}{2} (1 - e^{2\lambda x}) \quad (7.9.23)$$

where  $\lambda = Re/2 - (Re^2/4 + 4\pi^2)^{1/2}$ . Figure 7.9.1(a) shows  $v_x$ -velocity contours of the exact solution for  $Re = 40$  and Figure 7.9.1(b) shows the discretization of the domain using a non-uniform mesh of 8 quadrilateral finite elements.

The exact solution is used to compute the velocity boundary conditions on  $\Gamma$  and pressure is specified at a point. No boundary conditions on vorticity are necessary. The resulting discrete system is solved using Newton's method with Cholesky factorization at each Newton step. Convergence is declared when the normalized norm of the residual in velocities,  $\|\Delta \mathbf{v}\|/\|\mathbf{v}\|$ , was less than  $10^{-4}$ , which typically required 5 Newton iterations. A plot of the  $L_2$  least-squares functional and  $L_2$  error of the velocity and vorticity fields as a function of the expansion order in a logarithmic-linear scale is shown in Figure 7.9.2. Exponentially fast decay of the  $L_2$  least-squares functional and  $L_2$  error is observed.

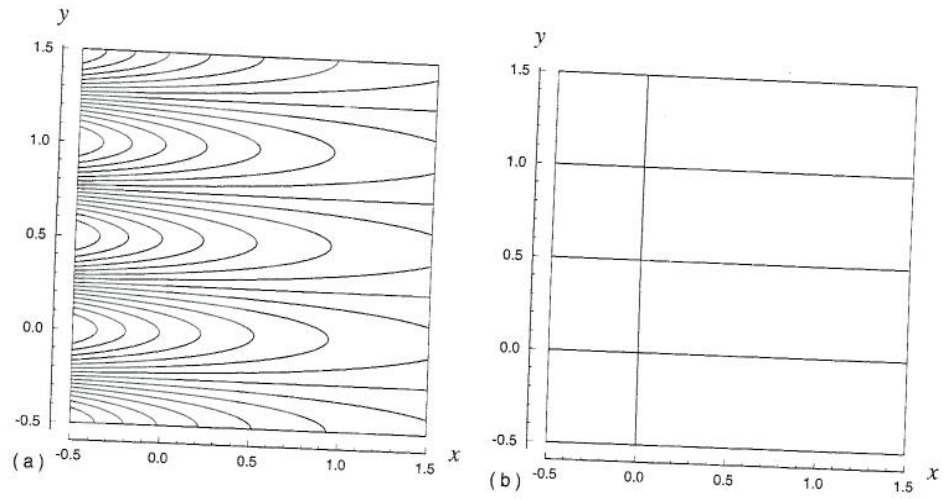


Figure 7.9.1 Kovaszny flow: (a)  $v_x$ -velocity component contours of the exact solution for  $Re = 40$ ; (b) computational domain using 8 quadrilateral elements.

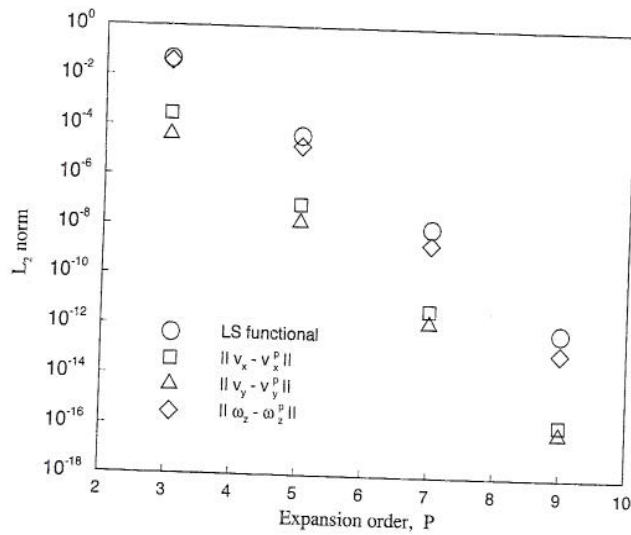


Figure 7.9.2 Decay of the least-squares functional and convergence of the velocity and vorticity fields to the exact Kovaszny solution.

**Flow over a backward-facing step**

We consider two-dimensional, steady flow over a backward-facing step at  $Re = 800$ . The geometry and boundary conditions are taken from the benchmark solution of Gartling [35] and are shown in Figure 7.8.16. As shown in Figure 7.8.16 the standard step geometry was simplified by excluding the channel portion upstream of the step. The boundary conditions for the step geometry include the no-slip condition at all solid surfaces and a parabolic inlet velocity profile given by  $v_x(y) = 24y(0.5 - y)$  for  $0 \leq y \leq 0.5$ . The Reynolds number is based on the mean inlet velocity.

Instead of imposing an outflow boundary condition in a strong sense we impose it in a weak sense through the least-squares functional. For example, if we use the vorticity based first-order system the  $L_2$  least-squares functional is given by

$$I(\mathbf{v}, P, \omega) = \frac{1}{2} \left( \|(\mathbf{v} \cdot \nabla) \mathbf{v} + \nabla P + \frac{1}{Re} \nabla \times \omega - \mathbf{f}\|_0^2 + \|\omega - \nabla \times \mathbf{v}\|_0^2 + \|\nabla \cdot \mathbf{v}\|_0^2 + \|\mathbf{n} \cdot \tilde{\sigma} - \tilde{\mathbf{f}}^s\|_{0, \Gamma_{outflow}}^2 \right) \tag{7.9.24}$$

where  $\tilde{\sigma}$  is a pseudo-stress (see Gresho [35]),  $\tilde{\sigma} = -P\mathbf{I} + (1/Re) \nabla \mathbf{v}$ , and  $\tilde{\mathbf{f}}^s$  are the prescribed pseudo-tractions, typically taken to be zero at an outflow boundary.

The domain,  $\bar{\Omega} = [0, 30] \times [-0.5, 0.5]$ , is discretized using 20 finite elements: two elements along the height of the channel and 10 uniform elements along the length of the channel. The numerical simulation is performed using the two-dimensional incompressible Navier-Stokes equations in the velocity gradient based first-order form (see Pontaza and Reddy [38]). A 11th order modal expansion is used in each element and the resulting discrete system is solved using Newton's method. At each Newton step, the linear system of algebraic equations is solved using the conjugate gradient method with a symmetric Gauss-Seidel preconditioner. Convergence of the conjugate gradient method was declared when the norm of the residual was less than  $10^{-6}$ . Nonlinear convergence was declared when the normalized norm of the residual in velocities,  $\|\Delta \mathbf{v}\|/\|\mathbf{v}\|$ , was less than  $10^{-4}$ , which typically required four Newton iterations. The analysis starts with  $Re = 100$  and steps to  $Re = 800$  using a solution continuation technique with increments of  $Re = 100$ . Away from the corner of the step at  $(x, y) = (0, 0)$ , the  $L_2$  least-squares functional remained below  $10^{-5}$  through the Reynolds number stepping.

Figure 7.9.3 shows the streamlines, the vector velocity field, and pressure contours for  $0 \leq x \leq 10$ , where most of the interesting flow structures occur. The flow separates at the step corner and forms a large recirculation region with a reattachment point on the lower wall of the channel at approximately  $x = 6$ . A second recirculation region forms on the upper wall of the channel beginning near  $x = 5$  with a reattachment point at approximately  $x = 10.5$ .

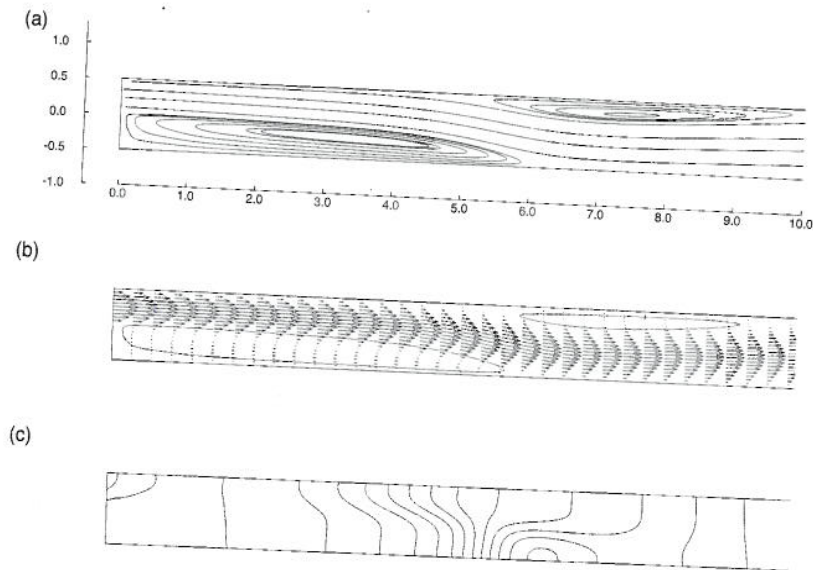


**Figure 7.9.3** Flow over a backward-facing step at  $Re = 800$ : (a) streamlines, (b) vector velocity field, and (c) pressure field.

Figure 7.9.4 shows  $v_x$ -velocity profiles along the channel height at  $x = 7$  and  $x = 15$ . We compare with tabulated values from the benchmark solution of Gartling [35] and find excellent agreement. Gartling's benchmark solution is based on a mixed Galerkin formulation using grid systems ranging from  $6 \times 120$  to  $40 \times 800$  biquadratic elements. Figure 7.9.5 shows pressure profiles along the length of the channel walls. The slopes of the pressure profiles become constant near the exit plane, meaning that the flow has recovered to fully developed conditions at the exit.

### Flow past a circular cylinder at low Reynolds number

The last example deals with the two-dimensional flow of an incompressible fluid past a circular cylinder [37]. The cylinder is of unit diameter and is placed in the finite region  $\bar{\Omega} = [-15.5, 30.5] \times [-20.5, 20.5]$ . The center of the cylinder lies at  $(x, y) = (0, 0)$ , so that the inflow boundary is located at 10.5 cylinder diameters left (or in front) of the center of the cylinder and the outflow boundary is at 30.5 cylinder diameters downstream of the center of the cylinder. The top and bottom boundaries are located each at 20.5 cylinder diameters above and below the center of the cylinder. Having considered a large computational domain allows us to impose free-stream boundary conditions at the top and bottom of the domain without noticeably affecting the solution.

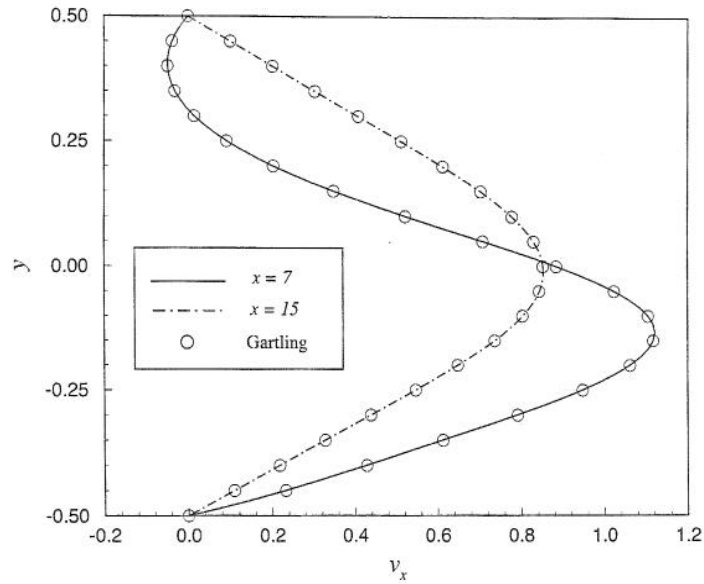


Figure 7.9.4 Flow over a backward-facing step at  $Re = 800$ : Horizontal velocity profiles along the height of the channel at  $x = 7$  and  $x = 15$ . Comparison with the benchmark solution of Gartling [35].

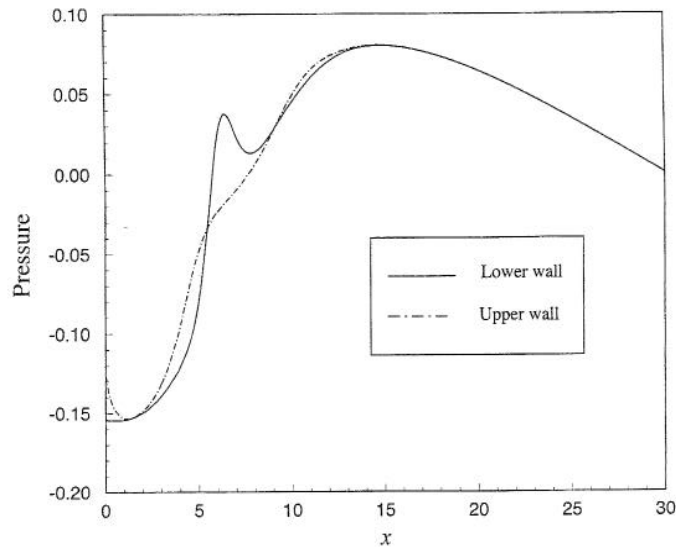
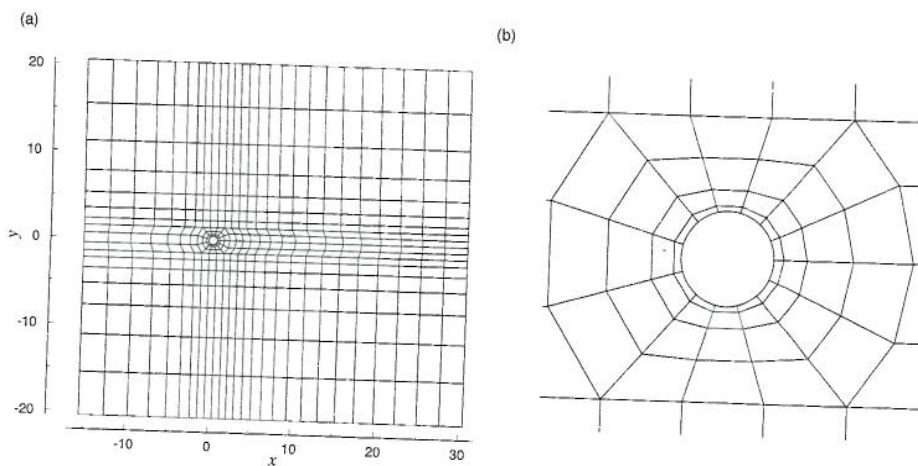


Figure 7.9.5 Flow over a backward-facing step at  $Re = 800$ : Pressure profiles along lower and upper walls of the channel.



The boundary conditions include a specified value of 1.0 for the component of velocity at the inflow, top, and bottom boundaries; that the free-stream velocity  $u_\infty$  is specified to be unity. At these boundaries the  $y$ -component of velocity is set to zero. The outflow boundary conditions are imposed in a weak sense through the least-squares functional. The Reynolds numbers considered here are 20 and 40, for which a steady-state solution exists. The Reynolds number is based on the free-stream velocity and cylinder diameter.

The vorticity based finite element model in Eq. (7.9.21) is used with sixth order nodal expansions in each element. The finite element mesh consists of 501 finite elements (see Figure 7.9.6), where a close-up view of the geometric discretization around the circular cylinder is also shown. To accurately represent the circular arc, the same approximation for the geometry and the solution (i.e. isoparametric formulation) is used. The total number of degrees of freedom for the problem is 73,344. The storage of the assembled system of equations in banded or in compressed sparse row/column format for such large size problems is prohibitively expensive in terms of computer memory. Therefore matrix-free techniques, also known as element-by-element solution algorithms, are implemented in a matrix-free version of the conjugate gradient method with a Jacobi preconditioner.



**Figure 7.9.6** Computational domain and mesh for flow past a circular cylinder. (a) Computational mesh. (b) Close-up view of the geometric discretization around the circular cylinder.

At each Newton step the linear system of equations is solved using the matrix-free conjugate gradient algorithm with a Jacobi preconditioner and convergence tolerance for the norm of the residual to be  $10^{-6}$ . Nonlinear convergence is declared when the relative norm of the residual in velocities between two consecutive iterations was less than  $10^{-4}$ , which required less than six Newton iterations.

Figure 7.9.7 shows the computed surface pressure coefficient distributions along the cylinder surface for  $Re = 20$  and  $40$ , together with experimental measurements of Grove *et al.* [41] for  $Re = 40$ . The finite element results are in good agreement with the experimental measurements. The computed drag coefficients for  $Re = 20$  and  $Re = 40$  are  $C_D = 2.0862$  and  $C_D = 1.5537$ , respectively. Good agreement is found between the computed drag coefficients and the experimental mean curve of Tritton [42], where the corresponding values are  $C_D = 2.05$  and  $C_D = 1.56$ .

Figure 7.9.8 shows computed pressure contours and streamlines in the wake region for  $Re = 20$  and  $Re = 40$ . The predicted wake extends 1.86 and 4.55 cylinder radii measured from the back of the cylinder. The values for the wake lengths are in good agreement with the numerical solution of Dennis and Chang [43], whose computed wake lengths for  $Re = 20$  and  $40$  were reported as 1.88 and 4.69 cylinder radii, respectively. Better agreement for the case  $Re = 40$  is found with the numerical solution of Kawaguti and Jain [44], who reported a computed wake length of 4.50 cylinder radii.

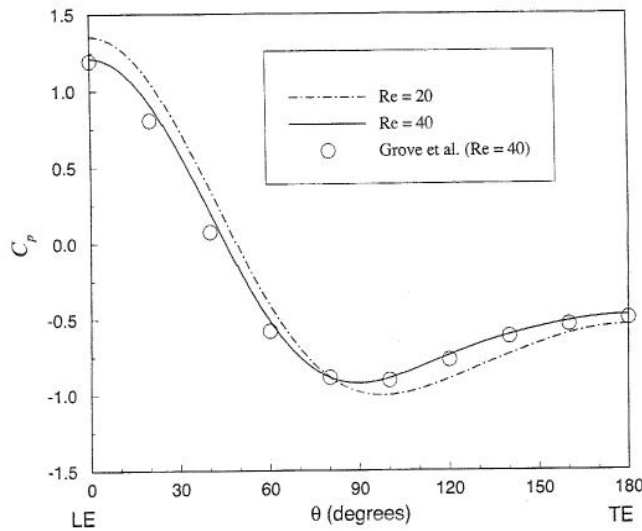


**Figure 7.9.7** Flow past a circular cylinder: comparison of the computed pressure coefficient distributions along the cylinder surface with experimental results of Grove *et al.* [41] for  $Re = 40$ .

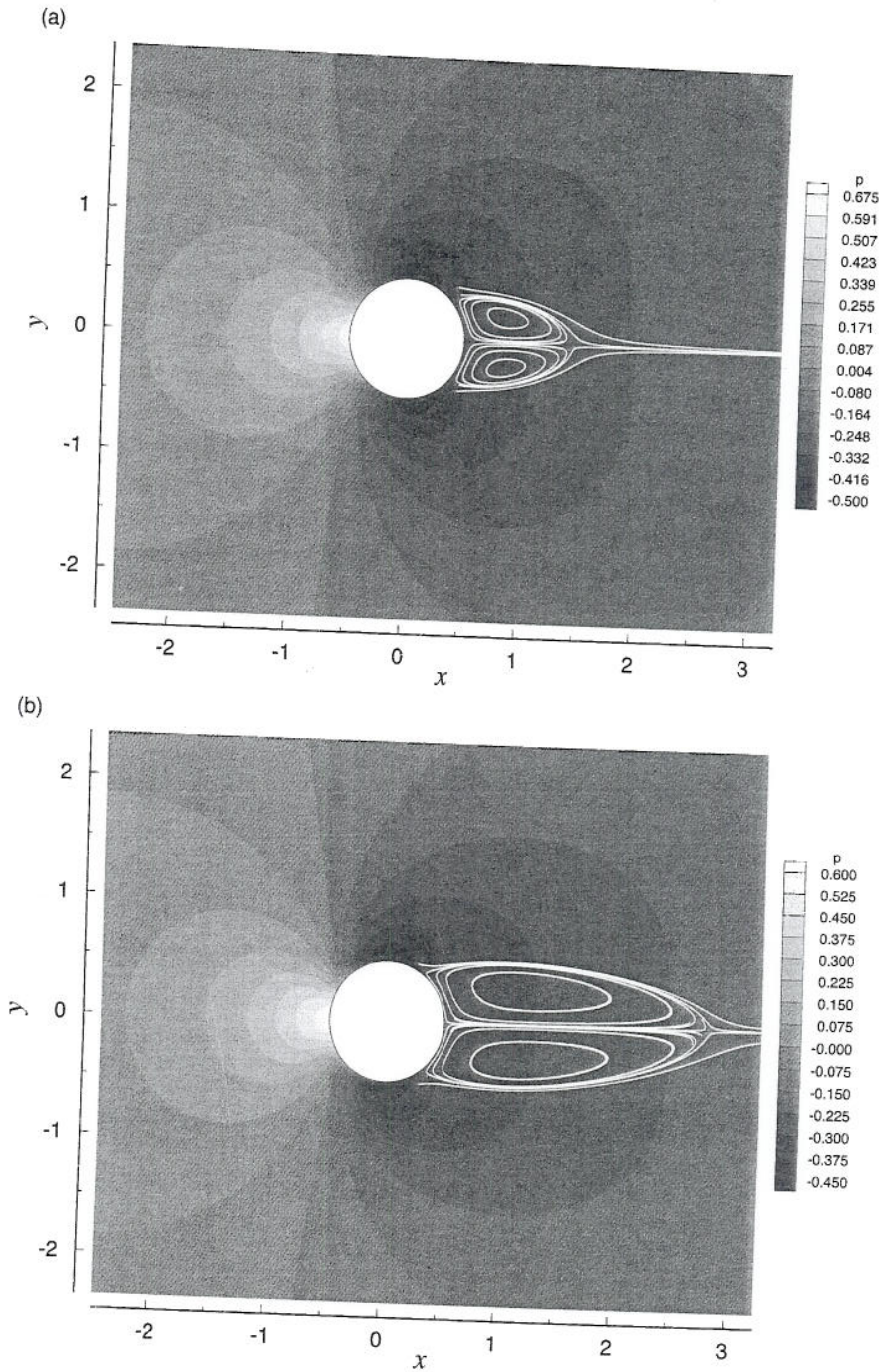


Figure 7.9.8 Flow past a circular cylinder at (a)  $Re = 20$  and (b)  $Re = 40$ : pressure contours and streamlines in the wake region.

## Problems

- 7.1 Consider the vector equations (7.3.1) and (7.3.2). Develop the weak statements of the equations in vector form.
- 7.2 Consider equations (7.4.1)–(7.4.3) in cylindrical coordinates  $(r, \theta, z)$ . For axisymmetric viscous incompressible flows (i.e. the flow field is independent of the  $\theta$  coordinate), and when the convective (nonlinear) terms are neglected, we have

$$\rho \frac{\partial v_x}{\partial t} = \frac{1}{r} \frac{\partial}{\partial r}(r\sigma_r) - \frac{\sigma_\theta}{r} + \frac{\partial \sigma_{rz}}{\partial z} + f_r \quad (\text{i})$$

$$\rho \frac{\partial v_z}{\partial t} = \frac{1}{r} \frac{\partial}{\partial r}(r\sigma_{rz}) + \frac{\partial \sigma_{zz}}{\partial z} + f_z \quad (\text{ii})$$

$$\frac{1}{r} \frac{\partial}{\partial r}(rv_x) + \frac{\partial v_z}{\partial z} = 0 \quad (\text{iii})$$

where

$$\sigma_r = -P + 2\mu \frac{\partial v_x}{\partial r}, \quad \sigma_\theta = -P + 2\mu \frac{v_x}{r}$$

$$\sigma_z = -P + 2\mu \frac{\partial v_z}{\partial z}, \quad \sigma_{rz} = \mu \left( \frac{\partial v_x}{\partial z} + \frac{\partial v_z}{\partial r} \right)$$

Develop the semidiscrete mixed finite element model of the equations.

- 7.3 Develop the semidiscrete penalty finite element model of the equations in Problem 7.2.
- 7.4 The equations governing unsteady slow flow (i.e. Stokes flow) of viscous incompressible fluids in the  $x$ - $y$  plane can be expressed in terms of vorticity  $\omega$  and stream function  $\psi$ :

$$\rho \frac{\partial \omega}{\partial t} - \mu \nabla^2 \omega = 0$$

$$-\omega - \nabla^2 \psi = 0$$

Develop the semidiscrete finite element model of the equations. Discuss the meaning of the secondary variables. Use the  $\alpha$ -family of approximation to reduce the ordinary differential equations to algebraic equations.

- 7.5 Compute the tangent coefficient matrix for the penalty finite element model in equation (7.5.16).
- 7.6 Verify Eqs. (7.9.10)–(7.9.12).
- 7.7 Develop the least-squares finite element model with velocity field and pressure as variables of the Navier-Stokes equations governing axisymmetric flows (see Problem 7.2).
- 7.8 Develop the least-squares finite element model with velocity field, pressure, and vorticity as variables of the Stokes equations governing axisymmetric flows.

## References

1. Bird, R. B., Stewart, W. E., and Lightfoot, E. N., *Transport Phenomena*, John Wiley, New York (1960).
2. Malvern, L. E., *Introduction to the Mechanics of a Continuous Medium*, Prentice-Hall, Englewood Cliffs, NJ(1969).
3. Reddy, J. N. and Rasmussen, M. L., *Advanced Engineering Analysis*, John Wiley & Sons, New York (1982); reprinted by Krieger Publishing, Melbourne, FL (1991).
4. Bejan, A., *Convection Heat Transfer*, 2nd edn, John Wiley, New York (1995).
5. Holman, J. P., *Heat Transfer*, Seventh Edition, McGraw-Hill, New York (1990).
6. Özisik, M. N., *Heat Transfer: A Basic Approach*, McGraw-Hill, New York (1985).

7. Özisik, M. N., *Heat Conduction*, 2nd edn, John Wiley, New York (1993).
8. Batchelor, G. K., *An Introduction to Fluid Dynamics*, Cambridge University Press, Cambridge, UK (1967).
9. Schlichting, H., *Boundary-Layer Theory*, (translated by J. Kestin), 7th edn, McGraw-Hill, New York (1979).
10. Reddy, J. N. and Gartling, D. K., *The Finite Element Method in Heat Transfer and Fluid Dynamics*, CRC Press, Boca Raton, FL (1994); 2nd edn (2000).
11. Gresho, P. M. and Sani, R. L., *Incompressible Flow and the Finite Element Method. Advection-Diffusion and Isothermal Laminar Flow*, John Wiley, Chichester, UK (1999).
12. Reddy, J. N., *An Introduction to the Finite Element Method*, 2nd edn, McGraw-Hill, New York (1993).
13. Reddy, J. N., *Applied Functional Analysis and Variational Methods in Engineering*, McGraw-Hill, New York (1986); reprinted by Krieger Publishing, Melbourne, Florida (1991).
14. Reddy, J. N., "On the Accuracy and Existence of Solutions to Primitive Variable Models of Viscous Incompressible Fluids," *International Journal of Engineering Science*, **16**, 921-929 (1978).
15. Marshall, R. S., Heinrich, J. C., and Zienkiewicz, O. C., "Natural Convection in a Square Enclosure by a Finite Element, Penalty Function Method, Using Primitive Fluid Variables," *Numerical Heat Transfer*, **1**, 315-330 (1978).
16. Reddy, J. N., "On the Finite Element Method with Penalty for Incompressible Fluid Flow Problems," in *The Mathematics of Finite Elements and Applications III*, J. R. Whiteman (ed.), Academic Press, New York (1979).
17. Hughes, T. J. R., Liu, W. K., and Brooks, A., "Review of Finite Element Analysis of Incompressible Viscous Flows by Penalty Function Formulation," *Journal of Computational Physics*, **30**, 1-60 (1979).
18. Reddy, J. N., "On Penalty Function Methods in the Finite Element Analysis of Flow Problems," *International Journal of Numerical Methods in Fluids*, **2**, 151-171 (1982).
19. Oden, J. T., "RIP Methods for Stokesian Flows," in R. H. Gallagher, O. C. Zienkiewicz, J. T. Oden, and D. Norrie (eds.), *Finite Element Method in Flow Problems*, Vol. IV, John Wiley, London, UK (1982).
20. Oden, J. T. and Carey, G. F., *Finite Elements, Mathematical Aspects*, Vol. IV, Prentice-Hall, Englewood Cliffs, NJ (1983).
21. Brezzi, F., and Fortin, M., *Mixed and Hybrid Finite Element Methods*, Springer-Verlag, Berlin, Germany (1991).
22. Le Tallac, P. and Ruas, V., "On the Convergence of the Bilinear-Velocity Constant-Pressure Finite Element Method in Viscous Flow," *Computer Methods in Applied Mechanics and Engineering*, **54**, 235-243 (1986).
23. Temam, R., *Theory and Numerical Analysis of the Navier-Stokes Equations*, North-Holland, Amsterdam, The Netherlands (1977).
24. Bercovier, M. and Engelman, M., "A Finite Element for the Numerical Solution of Viscous Incompressible Flows," *Journal of Computational Physics*, **30**, 181-201 (1979).
25. Engelman, M., Sani, R., Gresho, P. M., and Bercovier, M., "Consistent vs. Reduced Integration Penalty Methods for Incompressible Media Using Several Old and New Elements," *International Journal of Numerical Methods in Fluids*, **2**, 25-42 (1982).
26. Hughes, T. J. R., Franca, L. P., and Balestra, M., "A New Finite Element Formulation for Computational Fluid Dynamics," V. Circumventing the Babuska-Brezzi Condition: A Stable Petrov-Galerkin Formulation for the Stokes Problem Accommodating Equal-Order Interpolations," *Computer Methods in Applied Mechanics and Engineering*, **59**, 85-99 (1986).

27. Salonen, E. M. and Aalto, J., "A Pressure Determination Scheme," *Proceedings of the Fifth International Conference on Numerical Methods in Laminar and Turbulent Flow*, C. Taylor, M. D. Olson, P. M. Gresho, and W. G. Habashi (eds.), Pineridge Press, Swansea, UK (1985).
28. Shiojima, T. and Shimazaki, Y., "A Pressure-Smoothing Scheme for Incompressible Flow Problems," *International Journal of Numerical Methods in Fluids*, **9**, 557-567 (1989).
29. Reddy, M. P. and Reddy, J. N., "Finite-Element Analysis of Flows of Non-Newtonian Fluids in Three-Dimensional Enclosures," *International Journal of Non-Linear Mechanics*, **27**, 9-26 (1992).
30. Nadai, A., *Theory of Flow and Fracture of Solids*, McGraw-Hill, New York (1963).
31. Burggraf, O. R., "Analytical and Numerical Studies of the Structure of Steady Separated Flows," *Journal of Fluid Mechanics*, **24**(1), 113-151 (1966).
32. Pan, F. and Acrivos, A., "Steady Flow in Rectangular Cavities," *Journal of Fluid Mechanics*, **28**, 643 (1967).
33. Reddy, J. N., "Penalty-Finite-Element Analysis of 3-D Navier-Stokes Equations," *Computer Methods in Applied Mechanics and Engineering*, **35**, 87-106 (1982).
34. Ghia, U., Ghia, K. N., and Shin, C. T., "High-Re Solution for Incompressible Flow Using the Navier-Stokes Equations and the Multigrid Method," *Journal of Computational Physics*, **48**, 387-411 (1982).
35. Gartling, D. K., "A Test Problem for Outflow Boundary Conditions - Flow Over a Backward Facing Step," *International Journal for Numerical Methods in Fluids*, **11**, 953-967 (1990).
36. Bochev, P. B., and Gunzburger, M. D., "Finite Element Methods of Least-Squares Type," *SIAM Review*, **40**, 789-837 (1998).
37. Pontaza, J. P. and Reddy, J. N., "Spectral/hp Least-Squares Finite Element Formulation for the Navier-Stokes Equations," *Journal of Computational Physics*, **190**(2), 523-549 (2003).
38. Pontaza, J. P. and Reddy, J. N., "Space-Time Coupled Spectral/hp Least-Squares Finite Element Formulation for the Incompressible Navier-Stokes Equations," *Journal of Computational Physics*, **197**(2), 418-459 (2004).
39. Winterscheidt, D. and Surana, K. S., "p-version Least-Squares Finite Element Formulation for Two-Dimensional Incompressible Fluid Flow," *International Journal for Numerical Methods in Fluids*, **18**, 43-69 (1994).
40. Warburton, T. C., Sherwin, S. J., and Karniadakis, G. E., "Basis Functions for Triangular and Quadrilateral High-Order Elements," *SIAM Journal of Scientific Computing*, **20**, 1671-1695 (1999).
41. Grove, A. S., Shair, F. H., Petersen, E. E., and Acrivos, A., "An Experimental Investigation of the Steady Separated Flow Past a Circular Cylinder," *Journal of Fluid Mechanics*, **19**, 60-80 (1964).
42. Tritton, D. J., "Experiments on the Flow Past a Circular Cylinder at Low Reynolds Numbers," *Journal of Fluid Mechanics*, **6**, 547-567 (1959).
43. Dennis, S. C. R. and Chang, G. Z., "Numerical Solutions for Steady Flow Past a Circular Cylinder at Reynolds Numbers up to 100," *Journal of Fluid Mechanics*, **42**, 471-489 (1970).
44. Kawaguti, M. and Jain, P., "Numerical Study of a Viscous Fluid Past a Circular Cylinder," *Journal of the Physical Society of Japan*, **21**, 2055-2063 (1966).

---

# Nonlinear Analysis of Time-Dependent Problems

---

## 8.1 Introduction

In this chapter, we develop the finite element models of time-dependent problems with nonlinearities and describe some standard time approximation schemes. All classes of problems discussed in the previous chapters will be revisited in the context of transient analysis. We begin with the general discussion of the finite element modeling of time-dependent problems.

The finite element formulation of time-dependent problems involves following two stages:

1. *Spatial approximation*, where the solution  $u(x, t)$  of the equation under consideration is approximated by expressions of the form

$$u(x, t) \approx U^e(x, t) = \sum_{j=1}^n u_j^e(t) \psi_j^e(x) \quad (8.1.1)$$

and the spatial finite element model of the equation is developed using the procedures of static or steady-state problems, while carrying all time-dependent terms in the formulation. This step results in a set of ordinary differential equations (i.e. a semidiscrete system of differential equations) in time for the nodal variables  $u_j^e(t)$  of the element. Equation (8.1.1) represents the spatial approximation of  $u$  for any time  $t$ . When the solution is separable into functions of time only and space only,  $u(x, t) = T(t)X(x)$ , the approximation (8.1.1) is justified for the overall transient response of a structure, in contrast to wave propagation type solutions.

2. *Temporal approximation*, where the system of ordinary differential equations in time are further approximated in time, often using finite difference formulae for the time derivatives. This step allows conversion of the system of ordinary differential equations into a set of algebraic equations among  $u_j^e$  at time  $t_{s+1} = (s + 1)\Delta t$ , where  $\Delta t$  is the time increment and  $s$  is an integer.

At the end of the first step (i.e. after spatial approximation using the finite element method), we obtain, in general, a matrix differential equation of the form

$$[C^e]\{\dot{u}^e\} + [M^e]\{\ddot{u}^e\} + [K^e]\{u^e\} = \{F^e\} \quad (8.1.2)$$

at the element level, which represents a system of ordinary differential equations in time. Here  $\{u\}$  represents a  $m \times 1$  vector of nodal values, and  $[C^e]$ ,  $[M^e]$ , and  $[K^e]$  are  $m \times m$  matrices and  $\{F^e\}$  is  $m \times 1$  vector,  $m$  being the number of nodal degrees of freedom per finite element. The matrices appearing in Eq. (8.1.2) may be functions of the unknown  $u(x, t)$ , making (8.1.2) a set of nonlinear differential equations. Next, using a time approximation scheme, Eq. (8.1.2) is reduced to a set of nonlinear algebraic equations, as will be shown in the sequel, of the form

$$[\hat{K}^e]_{s+1}\{u^e\}_{s+1} = \{\hat{F}^e\}_{s,s+1} \quad (8.1.3)$$

where  $[\hat{K}^e]$  and  $\{\hat{F}^e\}$  are known in terms of  $[C^e]$ ,  $[M^e]$ ,  $[K^e]$ ,  $\{F^e\}$ ,  $\{u^e\}_s$ , and  $\{\dot{u}^e\}_s$ . The subscript  $s + 1$  refers to the time,  $t_{s+1}$ , at which the solution is sought. Equation (8.1.3) is then assembled and solved using known boundary conditions and initial conditions. Thus, at the end of the two-stage approximation, one has a continuous spatial solution at discrete intervals of time:

$$u^e(x, t_s) = \sum_{j=1}^n u_j^e(t_s) \psi_j^e(x) \quad (s = 0, 1, \dots) \quad (8.1.4)$$

In the next section, we study time approximation schemes using Eq. (8.1.2). We discuss stability and accuracy of time approximation schemes in Section 8.3. The two-step procedure is illustrated for all major problems of the previous sections, namely, nonlinear heat conduction (or field problems of that type), bending of plates, and viscous incompressible flows. Of course, the procedure described here can be applied to other problems.

## 8.2 Time Approximations

### 8.2.1 Introduction

All time approximation schemes are broadly classified as *implicit* and *explicit*. In explicit schemes, we find  $u_j$  at time  $t_{s+1}$  using the known value of  $u_j$  at time  $t_s$ . The implicit schemes are based on finding  $u_j$  at time  $t_{s+1}$  using not only the known value of  $u_j$  at time  $t_s$  but also values at  $t_{s+1}$ . Explicit schemes are conditionally stable, that is, the time step size is limited approximately to the time taken for an elastic wave to cross the smallest element dimension in the mesh. Implicit schemes have no such restriction and the time steps used in these schemes can be one or two orders of magnitude larger than the time steps used in simple explicit schemes. However, the accuracy of the implicit



schemes deteriorates as the time step size increases relative to the period of response of the system. The economy of the two schemes depends on (1) the stability limit of the explicit scheme, (2) the cost of the implicit scheme, (3) the relative size of time increments that can yield acceptable accuracy with the implicit scheme compared to the stability limit of the explicit scheme, and (4) the size of the computational model.

In this section, we consider time approximation schemes to reduce Eq. (8.1.2) to Eq. (8.1.3). The case of  $[M] = [0]$  arises in heat transfer and fluid dynamics, and the equation is known as the parabolic equation. Equation (8.1.2), in its general form is known as an hyperbolic equation, and it arises in structural dynamics with damping ( $[C] \neq [0]$ ) and without damping ( $[C] = [0]$ );  $[C]$  denotes the damping matrix and  $[M]$  the mass matrix. The time approximation of (8.1.2) for parabolic and hyperbolic equations will be derived separately. Equation of the form (8.1.2) is also obtained by other spatial approximations methods like the finite difference method and boundary element method, among others. Therefore, the discussion of converting matrix equations of the type (8.1.2) is equally valid for methods used to approximate the spatial variation of the solution.

### 8.2.2 Parabolic Equations

Consider the parabolic equation [i.e. set  $[M]$  equal to zero in Eq. (8.1.2)]

$$[C^e]\{\dot{u}^e\} + [K^e]\{u^e\} = \{F^e\} \quad (8.2.1a)$$

which arises in heat transfer and fluid dynamics problems. The global solution vector is subject to the initial condition

$$\{u(0)\} = \{u\}_0 \quad (8.2.1b)$$

where  $\{u\}_0$  denotes the value of the enclosed quantity  $u$  at time  $t = 0$ .

The eigenvalue problem associated with Eq. (8.2.1a) is obtained by assuming the solution  $u(t)$  to decay with time

$$\{u\} = \{u^0\}e^{-\lambda t}, \quad \{F\} = \{F^0\}e^{-\lambda t} \quad (8.2.2a)$$

where  $\{u^0\}$  is the vector of amplitudes (independent of time) and  $\lambda$  is the eigenvalue. Substitution of Eq. (8.2.2a) into Eq. (8.2.1a) gives

$$[-\lambda[C] + [K]]\{u^0\} = \{F^0\} \quad (8.2.2b)$$

The most commonly used method for solving (8.2.1a,b) is the  $\alpha$ -family of approximation, in which a weighted average of the time derivative of a dependent variable is approximated at two consecutive time steps by linear interpolation of the values of the variable at the two steps:

$$(1 - \alpha)\{\dot{u}\}_s + \alpha\{\dot{u}\}_{s+1} \approx \frac{\{u\}_{s+1} - \{u\}_s}{t_{s+1} - t_s} \quad \text{for } 0 \leq \alpha \leq 1 \quad (8.2.3)$$

where  $\{ \}_s$ , for example, refers to the value of the enclosed quantity at time  $t = t_s$ . In the interest of brevity, the element label  $e$  on various quantities is omitted (i.e. time approximation scheme is used at the element level). Equation (8.2.3) can be expressed alternatively as

$$\begin{aligned} \{u\}_{s+1} &= \{u\}_s + \Delta t \{\dot{u}\}_{s+\alpha} \\ \{\dot{u}\}_{s+\alpha} &= (1 - \alpha)\{\dot{u}\}_s + \alpha\{\dot{u}\}_{s+1} \quad \text{for } 0 \leq \alpha \leq 1 \end{aligned} \quad (8.2.4)$$

where  $\Delta t = t_{s+1} - t_s$ .

Note that when  $\alpha = 0$ , Eq. (8.2.3) reduces, for any nodal value  $u_i(t)$ , to

$$\left( \frac{du_i}{dt} \right)_{t=t_s} \approx \frac{u_i(t_{s+1}) - u_i(t_s)}{t_{s+1} - t_s} \quad (8.2.5)$$

Clearly, it amounts to replacing the time derivative of  $u_i(t)$  at  $t = t_s$  with the *finite difference* of its values at  $t = t_{s+1}$  (i.e. value from a time step ahead) and  $t = t_s$ . Equation (8.2.5) is nothing but an approximation of the derivative of a function, since  $\Delta t = t_{s+1} - t_s$  is finite, i.e. not make it approach zero. The approximation in Eq. (8.2.5) is known as the *forward difference* because it uses the function value ahead of the current position in computing the slope (see Figure 8.2.1). One may also use the value of the function from a time step behind

$$\left( \frac{du_i}{dt} \right)_{t=t_s} \approx \frac{u_i(t_s) - u_i(t_{s-1})}{t_s - t_{s-1}} \quad (8.2.6a)$$

or

$$\left( \frac{du_i}{dt} \right)_{t=t_{s+1}} \approx \frac{u_i(t_{s+1}) - u_i(t_s)}{t_{s+1} - t_s} \quad (8.2.6b)$$

which is the same as that in Eq. (8.2.3) when  $\alpha = 1$ . Equation (8.2.6b) is known as the *backward difference*. If we use the values ahead and behind in computing the slope

$$\left( \frac{du_i}{dt} \right)_{t=t_s} \approx \frac{u_i(t_{s+1}) - u_i(t_{s-1})}{t_{s+1} - t_{s-1}} \quad (8.2.7)$$

it is called the *centered difference*, which is not a special case of Eq. (8.2.3).

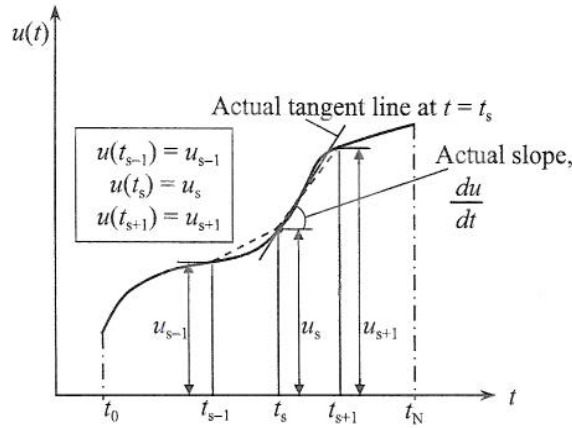


Figure 8.2.1 Approximation of the first derivative of a function.

For different values of  $\alpha$ , we obtain the following well-known numerical integration schemes from Eq. (8.2.3):

$$\alpha = \begin{cases} 0, & \text{the forward difference scheme (conditionally stable);} \\ & \text{Order of accuracy} = O(\Delta t) \\ \frac{1}{2}, & \text{the Crank-Nicolson scheme (stable); } O((\Delta t)^2) \\ \frac{2}{3}, & \text{the Galerkin method (stable); } O((\Delta t)^2) \\ 1, & \text{the backward difference scheme (stable); } O(\Delta t) \end{cases} \quad (8.2.8)$$

The phrases 'stability' and 'conditional stability' will be discussed in Section 8.3.

Equation (8.2.4) can be used to reduce ordinary differential equations (8.2.1a,b) to algebraic equations among the  $u_j$  at time  $t_{s+1}$ . Assuming that  $[C]$  is independent of time  $t$ , we obtain (see Problem 8.1)

$$[\hat{K}]_{s+1}\{u\}_{s+1} = \{\hat{F}\}_{s,s+1} \quad (8.2.9)$$

where

$$[\hat{K}]_{s+1} = [C] + a_1[K]_{s+1}, \quad [\bar{K}]_s = [C] - a_2[K]_s \quad (8.2.10a)$$

$$\{\hat{F}\}_{s,s+1} = [\bar{K}]_s\{u\}_s + a_1\{F\}_{s+1} + a_2\{F\}_s \quad (8.2.10b)$$

$$a_1 = \alpha\Delta t, \quad a_2 = (1 - \alpha)\Delta t \quad (8.2.10c)$$

Equation (8.2.9) provides a means to compute for  $\{u\}_{s+1}$  whenever  $\{u\}_s$  is known. Of course,  $[C]$ ,  $[K]$ , and  $\{F\}$  are known for all times (parts of  $\{F\}$

may not be known at the element level, but after assembly they are known whenever the corresponding  $\{u\}$  are unknown).

Equations (8.2.9) is valid for a typical element. The assembly, imposition of boundary conditions, and solution of the assembled equations are the same as that used for static (or steady-state) problems. Calculation of  $[\hat{K}]$  and  $\{\hat{F}\}$  at time  $t = 0$  requires knowledge of the initial conditions  $\{u\}_0$  and the time dependency of  $[C]$ ,  $[K]$ , and  $\{F\}$ .

Note that for  $\alpha = 0$  (the forward difference scheme), Eq. (8.2.10a) gives  $[\hat{K}^e] = [C^e]$ . When the matrix  $[C^e]$  is diagonal, Eq. (8.2.9) becomes *explicit* in the sense that one can solve for  $\{u\}_{s+1}$  directly without inverting  $[\hat{K}]$ . However, in spatial approximation by the finite element method,  $[C^e]$  is derived using a weak form, and it is never a diagonal matrix. The matrix  $[C^e]$  derived using a weak form is called the *consistent matrix*. Thus, the finite element equations with consistent (mass) matrix  $[C^e]$  never are explicit (in the sense that no inversion of the coefficient matrix is required). In a finite difference method, the matrix  $[C^e]$  is diagonal, and therefore an explicit time integration scheme (such as the forward difference method) results in explicit set of equations, which are quite inexpensive to solve at each time step. To have the advantage of less computational time in dynamic/transient analyses by the finite element method, it is desirable to have  $[C^e]$  diagonalized (see Problem 8.8). Thus, explicit (in the sense that  $[\hat{K}]$  is diagonal) finite element equations can be obtained only when (a) the time approximation scheme is explicit, and (b) the 'mass' matrix  $[C]$  is diagonal.

### 8.2.3 Hyperbolic Equations

Consider the second-order equation

$$[M^e]\{\ddot{u}^e\} + [C^e]\{\dot{u}^e\} + [K^e]\{u^e\} = \{F^e\} \quad (8.2.11)$$

which arises in structural dynamics;  $[C^e]$  denotes the damping matrix,  $[M^e]$  the mass matrix, and  $[K^e]$  the stiffness matrix. The global displacement vector  $\{u\}$  is subject to the initial conditions that the displacement and velocity are known at time  $t = 0$

$$\{u(0)\} = \{u\}_0, \quad \{\dot{u}(0)\} = \{v\}_0 \quad (8.2.12)$$

There are several numerical integration methods available to integrate second-order (i.e. hyperbolic) equations [2,4,5]. Among these, the Newmark family of time integration schemes [4] is widely used in structural dynamics. Other methods, such as the Wilson method and the Houbolt method [5], can be used to develop the algebraic equations from the second-order differential equations (8.2.11).

In the Newmark method, the function and its time derivatives are approximated according to

$$\{u\}_{s+1} = \{u\}_s + \Delta t\{\dot{u}\}_s + \frac{1}{2}(\Delta t)^2\{\ddot{u}\}_{s+\gamma} \quad (8.2.13a)$$

$$\{\dot{u}\}_{s+1} = \{\dot{u}\}_s + \{\ddot{u}\}_{s+\alpha}\Delta t \quad (8.2.13b)$$

$$\{\ddot{u}\}_{s+\alpha} = (1-\alpha)\{\ddot{u}\}_s + \alpha\{\ddot{u}\}_{s+1} \quad (8.2.13c)$$

and  $\alpha$  and  $\gamma$  are parameters that determine the stability and accuracy of the scheme. For  $\alpha = 0.5$ , the following values of  $\gamma$  define various well-known schemes:

$$\gamma = \begin{cases} \frac{1}{2}, & \text{the constant-average acceleration method (stable)} \\ \frac{1}{3}, & \text{the linear acceleration method (conditionally stable)} \\ 0, & \text{the central difference method (conditionally stable)} \\ \frac{8}{5}, & \text{the Galerkin method (stable)} \\ 2, & \text{the backward difference method (stable)} \end{cases} \quad (8.2.14)$$

The set of ordinary differential equations in (8.2.11) can be reduced, with the help of Eqs. (8.2.13a-c), to a set of algebraic equations relating  $\{u\}_{s+1}$  to  $\{u\}_s$  (see Problem 8.2). We have

$$[\hat{K}]_{s+1}\{u\}_{s+1} = \{\hat{F}\}_{s,s+1} \quad (8.2.15)$$

where

$$\begin{aligned} [\hat{K}]_{s+1} &= [K]_{s+1} + a_3[M]_{s+1} + a_6[C]_{s+1} \\ \{\hat{F}\}_{s,s+1} &= \{F\}_{s+1} + [M]_{s+1}\{A\}_s + [C]_{s+1}\{B\}_s \\ \{A\}_s &= a_3\{u\}_s + a_4\{\dot{u}\}_s + a_5\{\ddot{u}\}_s, \quad \{B\}_s = a_6\{u\}_s + a_7\{\dot{u}\}_s + a_8\{\ddot{u}\}_s \end{aligned} \quad (8.2.16)$$

and  $a_i$ ,  $i = 1, 2, \dots, 8$ , are defined as

$$a_1 = \alpha\Delta t, \quad a_2 = (1-\alpha)\Delta t \quad (8.2.17a)$$

$$a_3 = \frac{1}{\beta(\Delta t)^2}, \quad a_4 = a_3\Delta t, \quad a_5 = \frac{1}{\gamma} - 1, \quad \gamma = 2\beta \quad (8.2.17b)$$

$$a_6 = \frac{\alpha}{\beta\Delta t}, \quad a_7 = \frac{\alpha}{\beta} - 1, \quad a_8 = \Delta t \left( \frac{\alpha}{\gamma} - 1 \right) \quad (8.2.17c)$$

The following remarks concerning the Newmark scheme are in order:

1. The calculation of  $[\hat{K}]$  and  $\{\hat{F}\}$  in Newmark's scheme requires knowledge of the initial conditions  $\{u\}_0$ ,  $\{\dot{u}\}_0$ , and  $\{\ddot{u}\}_0$ . In practice, one does not know  $\{\ddot{u}\}_0$ . As an approximation, it can be calculated from the assembled

system of equations associated with (8.2.15) using initial conditions on  $\{u\}$ ,  $\{\dot{u}\}$ , and  $\{F\}$  (often  $\{F\}$  is assumed to be zero at  $t = 0$ ):

$$\{\ddot{u}\}_0 = [M]^{-1} (\{F\}_0 - [K]\{u\}_0 - [C]\{\dot{u}\}_0) \quad (8.2.18)$$

2. At the end of each time step, the new velocity vector  $\{\dot{u}\}_{s+1}$  and acceleration vector  $\{\ddot{u}\}_{s+1}$  are computed using the equations

$$\begin{aligned} \{\ddot{u}\}_{s+1} &= a_3(\{u\}_{s+1} - \{u\}_s) - a_4\{\dot{u}\}_s - a_5\{\ddot{u}\}_s \\ \{\dot{u}\}_{s+1} &= \{\dot{u}\}_s + a_2\{\ddot{u}\}_s + a_1\{\dot{u}\}_{s+1} \end{aligned} \quad (8.2.19)$$

where  $a_1$  and  $a_2$  are defined in Eq. (8.2.17a).

3. Equation (8.2.15) is not valid for the centered difference scheme ( $\gamma = 2\beta = 0$ ), as some of the parameters  $a_i$  are not defined for this scheme. An alternative algebraic manipulation of the equations is required. It can be shown that (see Problem 8.7)

$$[H]_{s+1}\{\ddot{u}\}_{s+1} = \{F\}_{s+1} - [K]_{s+1}\{A\}_s - [C]_{s+1}\{B\}_s \quad (8.2.20)$$

$$\begin{aligned} [H]_{s+1} &= \beta(\Delta t)^2[K]_{s+1} + \alpha\Delta t[C]_{s+1} + [M]_{s+1} \\ \{A\}_s &= \{u\}_s + \Delta t\{\dot{u}\}_s + \frac{1-\gamma}{2}(\Delta t)^2\{\ddot{u}\}_s \\ \{B\}_s &= \{\dot{u}\}_s + (1-\alpha)\Delta t\{\ddot{u}\}_s \end{aligned} \quad (8.2.21)$$

and the displacements and velocities are updated using the relations

$$\{u\}_{s+1} = \{u\}_s + \Delta t\{\dot{u}\}_s + \frac{(\Delta t)^2}{2} [(1-\gamma)\{\ddot{u}\}_s + \gamma\{\ddot{u}\}_{s+1}] \quad (8.2.22)$$

$$\{\dot{u}\}_{s+1} = \{\dot{u}\}_s + \Delta t [(1-\alpha)\{\ddot{u}\}_s + \alpha\{\ddot{u}\}_{s+1}] \quad (8.2.23)$$

4. The centered difference scheme ( $\gamma = 2\beta = 0$ ) with  $\alpha = 0$  yields [see Eqs. (8.2.20) and (8.2.21)]

$$\begin{aligned} [M]_{s+1}\{\ddot{u}\}_{s+1} &= \{F\}_{s+1} - [K]_{s+1} \left( \{u\}_s + \Delta t\{\dot{u}\}_s + \frac{1}{2}(\Delta t)^2\{\ddot{u}\}_s \right) \\ &\quad - [C]_{s+1} \left( \{\dot{u}\}_s + \Delta t\{\ddot{u}\}_s \right) \end{aligned} \quad (8.2.24)$$

Thus, if the mass matrix is diagonalized, the system in Eq. (8.2.24) becomes explicit (no inversion of the coefficient matrix is required).

5. For natural vibration, the forces and the solution is assumed to be periodic

$$\{u\} = \{u^0\}e^{i\omega t}, \quad \{F\} = \{F^0\}e^{i\omega t}, \quad i = \sqrt{-1} \quad (8.2.25)$$

where  $\{u^0\}$  is the vector of amplitudes (independent of time) and  $\omega$  is the frequency of natural vibration of the system. Substitution of Eq. (8.2.25) into Eq. (8.2.11) yields

$$\left[-\omega^2[M] + i\omega[C] + [K]\right] \{u^0\} = \{F^0\} \quad (8.2.26)$$

Equation (8.2.26) is called an eigenvalue problem, which may have complex eigenvalues when damping  $[C]$  is included.

### 8.3 Stability and Accuracy

#### 8.3.1 Preliminary Comments

In general, the application of a time approximation scheme to an initial-value problem results in equation of the type

$$[\hat{K}]\{u\}_{s+1} = [\bar{K}]\{u\}_s \quad \text{or} \quad \{u\}_{s+1} = [A]\{u\}_s \quad (8.3.1)$$

where  $[A] = [\hat{K}]^{-1}[\bar{K}]$  is called the *amplification* matrix, and  $[\hat{K}]$  and  $[\bar{K}]$  are matrix operators that depend on the problem parameters, for example, geometric and material properties and finite element mesh parameter, and  $\{u\}_{s+1}$  is the solution vector at time  $t_{s+1}$ .

Since Eq. (8.2.3), for example, represents an approximation that is used to derive equation of the type (8.3.1), error is introduced into the solution  $\{u\}_{s+1}$  at each time step. Since the solution  $\{u\}_{s+1}$  at time  $t_{s+1}$  depends on the solution  $\{u\}_s$  at time  $t_s$ , the error can grow with time. The time approximation scheme is said to be stable if the error introduced in  $\{u\}_s$  does not grow unbounded as Eq. (8.3.1) is solved repeatedly for  $s = 0, 1, \dots$ . In order that the error to remain bounded, it is necessary and sufficient that the largest eigenvalue of the amplification matrix  $[A]$  is less than or equal to unity:

$$|\lambda_{\max}| \leq 1 \quad (8.3.2)$$

where  $\lambda_{\max}$  is the largest value that satisfies the equation

$$\left([A] - \lambda^A[I]\right) \{u\} = \{0\} \quad (8.3.3)$$

Equation (8.3.3) represents an eigenvalue problem. If condition (8.3.2) is satisfied for any value of  $\Delta t$ , the scheme is said to be *unconditionally stable* or simply stable. If Eq. (8.3.2) places a restriction on the size of the time step  $\Delta t$ , the scheme is said to be *conditionally stable*.

*Accuracy* of a numerical scheme is a measure of the closeness between the approximate solution and the exact solution, whereas *stability* of a solution is a measure of the boundedness of the approximate solution with time. As

one might expect, the size of the time step can influence both accuracy and stability. When we construct an approximate solution, we like it to converge to the true solution when the number of elements or the degree of approximation is increased and the time step  $\Delta t$  is decreased. A time approximation scheme is said to be *convergent* if, for fixed  $t_s$  and  $\Delta t$ , the numerical value  $\{u\}_s$  converges to its true value  $\{u(t_s)\}$  as  $\Delta t \rightarrow 0$ . Accuracy is measured in terms of the rate at which the approximate solution converges. If a numerical scheme is stable and consistent, it is also convergent.

### 8.3.2 Stability Criteria

The  $\alpha$ -family of approximations is stable for all numerical schemes in which  $\alpha < \frac{1}{2}$ , only if the time step satisfies the following (stability) condition:

$$\Delta t < \Delta t_{cr} \equiv \frac{2}{(1 - 2\alpha)\lambda_{\max}} \quad (8.3.4)$$

where  $\lambda_{\max}$  is the largest eigenvalue of the finite element equations (8.2.2b):

$$([K^e] - \lambda[C^e])\{u^0\}^e = \{F^0\}^e \quad (8.3.5a)$$

Note that the same mesh as that used for the transient analysis must be used to calculate the eigenvalues of the assembled system (8.3.5a); after assembly and imposition of boundary conditions, the eigenvalue problem in Eq. (8.3.5a) becomes homogeneous

$$([K] - \lambda[C])\{U^0\} = \{0\} \quad (8.3.5b)$$

The stability criterion in Eq. (8.3.4) is arrived using Eq. (8.3.2). The amplification matrix for the  $\alpha$ -family of approximations is given by

$$[A] = [\hat{K}]^{-1}[\bar{K}] = ([C] + a_1[K])^{-1}([C] - a_2[K]) \quad (8.3.6)$$

Let  $\lambda_{\max}$  be the maximum eigenvalue of Eq. (8.3.5b). Then it can be shown that (using spectral decomposition of  $[A]$ ) the maximum eigenvalue of  $[A]$  is equal to

$$\lambda_{\max}^A = \left| \frac{1 - (1 - \alpha)\Delta t \lambda_{\max}}{1 + \alpha \Delta t \lambda_{\max}} \right| \leq 1 \quad (8.3.7)$$

from which it follows that the  $\alpha$ -family of approximations is unconditionally stable if  $\alpha \geq \frac{1}{2}$ . In the case  $\alpha < \frac{1}{2}$ , the method is stable only if condition (8.3.4) is satisfied.

Similarly, all Newmark schemes in which  $\gamma < \alpha$  and  $\alpha \geq \frac{1}{2}$ , the stability requirement is

$$\Delta t \leq \Delta t_{cr} = \left[ \frac{1}{2} \omega_{\max}^2 (\alpha - \gamma) \right]^{-1/2} \quad (8.3.6)$$



where  $\omega_{\max}$  is the maximum natural frequency of the undamped system (8.2.26)

$$([K] - \omega^2[M])\{\Delta\} = \{0\} \quad (8.3.7)$$

## 8.4 Transient Analysis of Nonlinear Problems

### 8.4.1 Introduction

Here we discuss time approximations of the problems considered in heat transfer, fluid mechanics, and solid mechanics with nonlinearities. The discussion mainly focused on developing the fully discretized finite element equations for transient response. It should be noted that the stability criteria discussed in the previous sections for conditionally stable schemes are valid only for linear problems, and no such estimates are available for nonlinear problems.

### 8.4.2 Heat Transfer

Consider the model equation (4.2.1). For time-dependent problems, it takes the form

$$c_0 \frac{\partial u}{\partial t} - \frac{\partial}{\partial x} \left( a_{11} \frac{\partial u}{\partial x} \right) - \frac{\partial}{\partial y} \left( a_{22} \frac{\partial u}{\partial y} \right) + a_{00}u = f(x, y, t) \quad (8.4.1)$$

where  $a_{ij}$  are, in general, functions of position and time. In addition,  $a_{ij}$  ( $i, j = 1, 2$ ) are functions of  $u$ ,  $\partial u/\partial x$ , and  $\partial u/\partial y$ . However, we assume that  $c_0$  is only a function of position but not time. The semidiscretization follows the same steps as in the steady-state case (see Chapter 4). The weak form of Eq. (8.4.1) is given by

$$0 = \int_{\Omega^e} \left( c_0 w \frac{\partial u}{\partial t} + a_{11} \frac{\partial w}{\partial x} \frac{\partial u}{\partial x} + a_{22} \frac{\partial w}{\partial y} \frac{\partial u}{\partial y} + a_{00} w u - w f \right) dx dy - \oint_{\Gamma^e} w q_n ds \quad (8.4.2)$$

The finite element approximation is assumed to be of the form

$$u(x, y, t) \approx u_h^e(x, y, t) = \sum_{j=1}^n u_j^e(t) \psi_j^e(x, y) \quad (8.4.3)$$

where the nodal values  $u_j^e$  are now assumed to be functions of time. Substitution of Eq. (8.4.3) into Eq. (8.4.2) gives rise to the finite element equations

$$[C^e]\{\dot{u}^e\} + [K^e]\{u^e\} = \{f^e\} + \{Q^e\} \quad (8.4.4)$$

where

$$\begin{aligned}
 C_{ij}^e &= \int_{\Omega^e} c_0 \psi_i^e \psi_j^e \, dx \, dy \\
 K_{ij}^e &= \int_{\Omega^e} \left( a_{11} \frac{\partial \psi_i^e}{\partial x} \frac{\partial \psi_j^e}{\partial x} + a_{22} \frac{\partial \psi_i^e}{\partial y} \frac{\partial \psi_j^e}{\partial y} + a_{00} \psi_i^e \psi_j^e \right) \, dx \, dy \\
 f_i^e &= \int_{\Omega^e} \psi_i^e f \, dx \, dy, \quad Q^e = \oint_{\Gamma^e} \psi_i^e q_n \, ds
 \end{aligned} \tag{8.4.5}$$

The fully discretized set of equations associated with (8.4.4) is given by

$$[\hat{K}(\{u_{s+1}\})]\{u\}_{s+1} = [\bar{K}(\{u_s\})]\{u\}_s + \{\hat{F}\}_{s,s+1} \equiv \{\bar{F}\} \tag{8.4.6}$$

where

$$\begin{aligned}
 [\hat{K}(\{u_{s+1}\})] &= [C] + a_1 [K(\{u_{s+1}\})], \quad [\bar{K}(\{u_s\})] = [C] - a_2 [K(\{u_s\})] \\
 \{\hat{F}\}_{s,s+1} &= a_1 \{F\}_{s+1} + a_2 \{F\}_s, \quad a_1 = \alpha \Delta t, \quad a_2 = (1 - \alpha) \Delta t
 \end{aligned} \tag{8.4.7}$$

Note that only  $[K]$  is a function of the nodal unknowns  $\{u\}$ .

When the direct iteration is used to solve the nonlinear equations, at the  $(r + 1)$ st iteration we solve the equation

$$[\hat{K}(\{u_{s+1}^r\})]\{u\}_{s+1}^{r+1} = \{\bar{F}\} \tag{8.4.8a}$$

with

$$\{\bar{F}\} = ([C] - a_2 [K(\{u_s\})]) \{u\}_s + a_1 \{F\}_{s+1} + a_2 \{F\}_s \tag{8.4.8b}$$

Note that  $\{\bar{F}\}$  remains unchanged during the nonlinear iteration for a given time step, whereas  $[\hat{K}]$  changes during the iteration due to the latest known solution  $\{u\}_{s+1}^{r+1}$ .

### 8.4.3 Flows of Viscous Incompressible Fluids

#### Weak form finite element model

The weak form (Ritz–Galerkin) finite element models developed in Chapter 7 already include time-dependent terms [see Eqs. (7.4.13), and (7.5.16) or (7.5.18)]. The fully discretized equations of (7.5.18) are discussed here. We have

$$[\hat{\mathbf{K}}(\{\mathbf{v}_{s+1}\})]\{\mathbf{v}\}_{s+1} = [\tilde{\mathbf{K}}(\{\mathbf{v}_s\})]\{\mathbf{v}\}_s + \{\hat{\mathbf{F}}\}_{s,s+1} \tag{8.4.9a}$$

where

$$\begin{aligned}
 [\hat{\mathbf{K}}(\{\mathbf{v}_{s+1}\})] &= [\mathbf{M}] + a_1 ([\mathbf{C}(\{\mathbf{v}_{s+1}\})] + [\mathbf{K}(\{\mathbf{v}_{s+1}\})] + [\bar{\mathbf{K}}]) \\
 [\tilde{\mathbf{K}}(\{\mathbf{v}_s\})]_s &= [\mathbf{M}] - a_2 ([\mathbf{C}(\{\mathbf{v}_s\})] + [\mathbf{K}(\{\mathbf{v}_s\})] + [\bar{\mathbf{K}}]) \\
 \{\hat{\mathbf{F}}\}_{s,s+1} &= a_1 \{\mathbf{F}\}_{s+1} + a_2 \{\mathbf{F}\}_s
 \end{aligned} \tag{8.4.9b}$$

where  $[M]$ ,  $[C]$ ,  $[K]$ , and  $[\bar{K}]$  are defined in Eqs. (7.4.14) and (7.5.17).

Dependence of  $[C]$  on the nodal values  $\{v\}$  is due to the convective terms, and dependence of  $[K]$  on  $\{v\}$  is due to viscosity being a function of the strain rates (e.g. power-law fluids). If viscosity is constant, that is, Newtonian fluids, then  $[K]$  is independent of the nodal values  $\{v\}$  of the velocity field. For direct iteration solution, Eq. (8.4.9a) takes the form

$$[\hat{K}(\{v_{s+1}^r\})]\{v\}_{s+1}^{r+1} = [\bar{K}(\{v_s\})]\{v\}_s + \{\hat{F}\}_{s,s+1} \tag{8.4.10}$$

**Least-squares finite element models**

The least-squares finite element models of time-dependent Navier-Stokes equations (see Section 7.9) are discussed next. We consider two alternative least-squares formulations [6,7]: (1) velocity-pressure-vorticity model, and (2) velocity-pressure-velocity gradient model.

The velocity-pressure-vorticity formulation is based on the minimization of the least-squares functional

$$I_1(v, P, \omega) = \frac{1}{2} \left[ \left\| \frac{\partial v}{\partial t} + (v \cdot \nabla) v + \nabla P - \frac{1}{Re} \nabla \times \omega - f \right\|_0^2 + \|\omega - \nabla \times v\|_0^2 + \|\nabla \cdot v\|_0^2 + \|\nabla \cdot \omega\|_0^2 \right] \tag{8.4.11}$$

where  $\|\cdot\|_0$  denotes the  $L_2(\Omega)$ -norm

$$\|u\|_0 = \int_{\Omega^e} |u(x, t)|^2 d\Omega, \quad t \in (0, \tau) \tag{8.4.12}$$

The finite element model based on minimization of  $I_1$  requires that we choose at least piecewise bilinear (in two dimensions) or trilinear (in three dimensions) polynomials for  $v$ ,  $P$ , and  $\omega$ . The temporal terms are approximated using the backward (Euler) difference scheme.

The velocity-pressure-velocity gradient formulation is based on minimization of the functional

$$I_2(v, P, U) = \frac{1}{2} \left[ \left\| \frac{\partial v}{\partial t} + (v \cdot U)^T + \nabla P - \frac{1}{Re} (\nabla \cdot U)^T - f \right\|_0^2 + \|U - (\nabla v)^T\|_0^2 + \|\nabla \cdot v\|_0^2 + \|\nabla(\text{tr } U)\|_0^2 \right] \tag{8.4.13}$$

where  $U$  is the velocity gradient tensor. The finite element model based on minimization of  $I_2$  also requires, at the minimum, piecewise bilinear (in two dimensions) or trilinear (in three dimensions) polynomials for  $v$ ,  $P$ , and  $U$ .

## 8.4.4 Plate Bending (FSDT)

Here we consider the FSDT with von Kármán nonlinearity (see Chapter 6). We begin with the following equations of motion of the theory (see Reddy [5-7]):

$$\begin{aligned}
 I_0 \frac{\partial^2 u_0}{\partial t^2} - \frac{\partial N_{xx}}{\partial x} - \frac{\partial N_{xy}}{\partial y} &= 0, & I_0 \frac{\partial^2 v_0}{\partial t^2} - \frac{\partial N_{xy}}{\partial x} - \frac{\partial N_{yy}}{\partial y} &= 0 \\
 I_0 \frac{\partial^2 w_0}{\partial t^2} - \frac{\partial}{\partial x} \left( N_{xx} \frac{\partial w_0}{\partial x} + N_{xy} \frac{\partial w_0}{\partial y} \right) - \frac{\partial}{\partial y} \left( N_{xy} \frac{\partial w_0}{\partial x} + N_{yy} \frac{\partial w_0}{\partial y} \right) \\
 &\quad - \frac{\partial Q_x}{\partial x} - \frac{\partial Q_y}{\partial y} - q = 0 \\
 I_2 \frac{\partial^2 \phi_x}{\partial t^2} - \frac{\partial M_{xx}}{\partial x} - \frac{\partial M_{xy}}{\partial y} + Q_x &= 0, & I_2 \frac{\partial^2 \phi_y}{\partial t^2} - \frac{\partial M_{xy}}{\partial x} - \frac{\partial M_{yy}}{\partial y} + Q_y &= 0
 \end{aligned} \tag{8.4.14a}$$

where  $I_0$  and  $I_2$  are the principal and rotatory inertias

$$I_0 = \rho h, \quad I_2 = \frac{\rho h^3}{12} \tag{8.4.14b}$$

and the inplane forces ( $N_{xx}, N_{xy}, N_{yy}$ ), transverse shear forces ( $Q_x, Q_y$ ), and moments ( $M_{xx}, M_{xy}, M_{yy}$ ) were defined in Eqs. (6.3.4) and (6.6.11).

The weak forms of Eqs. (8.4.14a) are given by

$$0 = \int_{\Omega^e} \left( \frac{\partial \psi_i}{\partial x} N_{xx} + \frac{\partial \psi_i}{\partial y} N_{xy} + I_0 \psi_i \frac{\partial^2 u_0}{\partial t^2} \right) dx dy - \int_{\Gamma^e} N_{nn} \psi_i ds \tag{8.4.15a}$$

$$0 = \int_{\Omega^e} \left( \frac{\partial \psi_i}{\partial x} N_{xy} + \frac{\partial \psi_i}{\partial y} N_{yy} + I_0 \psi_i \frac{\partial^2 v_0}{\partial t^2} \right) dx dy - \int_{\Gamma^e} N_{ns} \psi_i ds \tag{8.4.15b}$$

$$\begin{aligned}
 0 = \int_{\Omega^e} \left[ \frac{\partial \psi_i}{\partial x} \left( Q_x + N_{xx} \frac{\partial w_0}{\partial x} + N_{xy} \frac{\partial w_0}{\partial y} \right) + \frac{\partial \psi_i}{\partial y} \left( Q_y + N_{xy} \frac{\partial w_0}{\partial x} + N_{yy} \frac{\partial w_0}{\partial y} \right) \right. \\
 \left. + I_0 \psi_i \frac{\partial^2 w_0}{\partial t^2} - \psi_i q \right] dx dy - \int_{\Gamma^e} Q_n \psi_i ds
 \end{aligned} \tag{8.4.15c}$$

$$0 = \int_{\Omega^e} \left( \frac{\partial \psi_i}{\partial x} M_{xx} + \frac{\partial \psi_i}{\partial y} M_{xy} + \psi_i Q_x + I_2 \psi_i \frac{\partial^2 \phi_x}{\partial t^2} \right) dx dy - \int_{\Gamma^e} M_{nn} \psi_i ds \tag{8.4.15d}$$

$$0 = \int_{\Omega^e} \left( \frac{\partial \psi_i}{\partial x} M_{xy} + \frac{\partial \psi_i}{\partial y} M_{yy} + \psi_i Q_y + I_2 \psi_i \frac{\partial^2 \phi_y}{\partial t^2} \right) dx dy - \int_{\Gamma^e} M_{ns} \psi_i ds \tag{8.4.15e}$$

where  $(N_{nn}, N_{ns}, M_{nn}, M_{ns}, Q_n)$  are the stress resultants on an edge with unit normal  $\hat{\mathbf{n}}$ , and they are defined in Eqs. (6.3.7a,b), (6.3.9), and (6.4.2). Note that the nonlinearity in Eqs. (8.4.15a-e) is solely due to  $w_0$ , and the nonlinear terms are present only in  $(N_{xx}, N_{xy}, N_{yy})$ .

For convenience of writing the finite element equations, the linear and nonlinear parts of the inplane forces  $(N_{xx}, N_{xy}, N_{yy})$  are denoted as

$$\{N\} = \{N^0\} + \{N^1\} \quad (8.4.16)$$

where  $\{N^0\}$  is the linear part and  $\{N^1\}$  is the nonlinear part. For an orthotropic plate (with the principal material axes coinciding with the plate axes), the forces and moments are related to the generalized displacements  $(u_0, v_0, w_0, \phi_x, \phi_y)$  as follows:

$$\begin{aligned} N_{xx}^0 &= A_{11} \frac{\partial u_0}{\partial x} + A_{12} \frac{\partial v_0}{\partial y}, & N_{yy}^0 &= A_{12} \frac{\partial u_0}{\partial x} + A_{22} \frac{\partial v_0}{\partial y} \\ N_{xy}^0 &= A_{66} \left( \frac{\partial u_0}{\partial y} + \frac{\partial v_0}{\partial x} \right), & M_{xx} &= D_{11} \frac{\partial \phi_x}{\partial x} + D_{12} \frac{\partial \phi_y}{\partial y} \\ M_{yy} &= D_{12} \frac{\partial \phi_x}{\partial x} + D_{22} \frac{\partial \phi_y}{\partial y}, & M_{xy} &= D_{66} \left( \frac{\partial \phi_x}{\partial y} + \frac{\partial \phi_y}{\partial x} \right) \\ Q_x &= A_{55} \left( \phi_x + \frac{\partial w_0}{\partial x} \right), & Q_y &= A_{44} \left( \phi_y + \frac{\partial w_0}{\partial y} \right) \\ N_{xx}^1 &= \frac{1}{2} \left[ A_{11} \left( \frac{\partial w_0}{\partial x} \right)^2 + A_{12} \left( \frac{\partial w_0}{\partial y} \right)^2 \right] \\ N_{yy}^1 &= \frac{1}{2} \left[ A_{12} \left( \frac{\partial w_0}{\partial x} \right)^2 + A_{22} \left( \frac{\partial w_0}{\partial y} \right)^2 \right] \\ N_{xy}^1 &= A_{66} \frac{\partial w_0}{\partial x} \frac{\partial w_0}{\partial y} \end{aligned} \quad (8.4.17a)$$

and  $A_{ij}$  and  $D_{ij}$  are the plate stiffnesses [see Eq. (6.3.34)]

$$A_{ij} = hQ_{ij}, \quad D_{ij} = \frac{h^3}{12} Q_{ij} \quad (8.4.17b)$$

and  $Q_{ij}$  are defined in Eqs. (6.3.31a,b).

The finite element model based on equal interpolation of all generalized displacements

$$\begin{aligned} u_0(x, y, t) &= \sum_{j=1}^n \Delta_j^1(t) \psi_j(x, y), & v_0(x, y, t) &= \sum_{j=1}^n \Delta_j^2(t) \psi_j(x, y) \\ w_0(x, y, t) &= \sum_{j=1}^n \Delta_j^3(t) \psi_j(x, y) \\ \phi_x(x, y, t) &= \sum_{j=1}^n \Delta_j^4(t) \psi_j(x, y), & \phi_y(x, y, t) &= \sum_{j=1}^n \Delta_j^5(t) \psi_j(x, y) \end{aligned} \quad (8.4.18)$$

can be expressed as

$$0 = \sum_{\beta=1}^5 \sum_{j=1}^n M_{ij}^{\alpha\beta} \ddot{\Delta}_j^\beta + \sum_{\beta=1}^5 \sum_{j=1}^n K_{ij}^{\alpha\beta} \Delta_j^\beta - F_i^\alpha \equiv R_i^\alpha \quad (8.4.19)$$

for  $\alpha = 1, 2, \dots, 5$ , where  $\Delta_i^\alpha$  denotes the value of the  $\alpha$ th variable, in the order  $(u_0, v_0, w_0, \phi_x, \phi_y)$ , at the  $i$ th node ( $i = 1, 2, \dots, n$ ) of the element. The non-zero coefficients of Eq. (8.4.19) are defined by

$$\begin{aligned} M_{ij}^{11} &= \int_{\Omega^e} I_0 \psi_i \psi_j \, dx \, dy, \quad M_{ij}^{22} = M_{ij}^{33} = M_{ij}^{11} \\ M_{ij}^{44} &= M_{ij}^{55} = \int_{\Omega^e} I_2 \psi_i \psi_j \, dx \, dy \\ F_i^1 &= \oint_{\Gamma^e} N_{nn} \psi_i \, ds, \quad F_i^2 = \oint_{\Gamma^e} N_{ns} \psi_i \, ds \\ F_i^3 &= \int_{\Omega^e} q \psi_i \, dx \, dy + \oint_{\Gamma^e} Q_n \psi_i \, ds \\ F_i^4 &= \oint_{\Gamma^e} M_{nn} \psi_i \, ds, \quad F_i^5 = \oint_{\Gamma^e} M_{ns} \psi_i \, ds \\ K_{ij}^{1\alpha} &= \int_{\Omega^e} \left( \frac{\partial \psi_i}{\partial x} N_{1j}^\alpha + \frac{\partial \psi_i}{\partial y} N_{6j}^\alpha \right) dx \, dy \\ K_{ij}^{2\alpha} &= \int_{\Omega^e} \left( \frac{\partial \psi_i}{\partial x} N_{6j}^\alpha + \frac{\partial \psi_i}{\partial y} N_{2j}^\alpha \right) dx \, dy \\ K_{ij}^{3\alpha} &= \int_{\Omega^e} \left[ \frac{\partial \psi_i}{\partial x} \left( Q_{1j}^\alpha + \frac{\partial w_0}{\partial x} N_{1j}^\alpha + \frac{\partial w_0}{\partial y} N_{6j}^\alpha \right) \right. \\ &\quad \left. + \frac{\partial \psi_i}{\partial y} \left( Q_{2j}^\alpha + \frac{\partial w_0}{\partial x} N_{6j}^\alpha + \frac{\partial w_0}{\partial y} N_{2j}^\alpha \right) \right] dx \, dy \\ K_{ij}^{4\alpha} &= \int_{\Omega^e} \left( Q_{1j}^\alpha \psi_i + \frac{\partial \psi_i}{\partial x} M_{1j}^\alpha + \frac{\partial \psi_i}{\partial y} M_{6j}^\alpha \right) dx \, dy \\ K_{ij}^{5\alpha} &= \int_{\Omega^e} \left( Q_{2j}^\alpha \psi_i + \frac{\partial \psi_i}{\partial x} M_{6j}^\alpha + \frac{\partial \psi_i}{\partial y} M_{2j}^\alpha \right) dx \, dy \end{aligned} \quad (8.4.20)$$

and  $K_{ij}^{\alpha\beta}$  denotes the coefficient matrix of the  $\alpha$ th variable in the  $\beta$ th equation ( $\alpha, \beta = 1, 2, 3, 4, 5$ ). Thus,  $N_{ij}^I$  denotes the contribution from  $N_I (= N_I^0 + N_I^1)$  to the  $\alpha$ th variable, where  $j$  denotes the node number. The non-zero terms appearing in the definition of  $K_{ij}^{\alpha\beta}$  are given below:

$$\begin{aligned} N_{ij}^1 &= A_{11} \frac{\partial \psi_j}{\partial x}, \quad N_{6j}^1 = A_{66} \frac{\partial \psi_j}{\partial y} \\ N_{1j}^2 &= A_{12} \frac{\partial \psi_j}{\partial y}, \quad N_{6j}^2 = A_{66} \frac{\partial \psi_j}{\partial x} \\ N_{1j}^3 &= \frac{1}{2} \left( A_{11} \frac{\partial w}{\partial x} \frac{\partial \psi_j}{\partial x} + A_{12} \frac{\partial w}{\partial y} \frac{\partial \psi_j}{\partial y} \right) \end{aligned}$$

$$\begin{aligned}
 N_{6j}^3 &= \frac{A_{66}}{2} \left( \frac{\partial w}{\partial x} \frac{\partial \psi_j}{\partial y} + \frac{\partial w}{\partial y} \frac{\partial \psi_j}{\partial x} \right) \\
 N_{2j}^1 &= A_{12} \frac{\partial \psi_j}{\partial x}, \quad N_{2j}^2 = A_{22} \frac{\partial \psi_j}{\partial y} \\
 N_{2j}^3 &= \frac{1}{2} \left( A_{12} \frac{\partial w}{\partial x} \frac{\partial \psi_j}{\partial x} + A_{22} \frac{\partial w}{\partial y} \frac{\partial \psi_j}{\partial y} \right) \\
 Q_{1j}^3 &= A_{55} \frac{\partial \psi_j}{\partial x}, \quad Q_{2j}^3 = A_{44} \frac{\partial \psi_j}{\partial y} \\
 Q_{1j}^4 &= A_{55} \psi_j, \quad Q_{2j}^5 = A_{44} \psi_j \\
 M_{1j}^4 &= D_{11} \frac{\partial \psi_j}{\partial x}, \quad M_{6j}^4 = D_{66} \frac{\partial \psi_j}{\partial y} \\
 M_{2j}^4 &= D_{12} \frac{\partial \psi_j}{\partial x}, \quad M_{1j}^5 = D_{12} \frac{\partial \psi_j}{\partial y} \\
 M_{6j}^5 &= D_{66} \frac{\partial \psi_j}{\partial x}, \quad M_{2j}^5 = D_{22} \frac{\partial \psi_j}{\partial y}
 \end{aligned} \tag{8.4.21}$$

Equation (8.4.19), when generalized to include structural damping, has the form

$$[M]\{\ddot{\Delta}\} + [C]\{\dot{\Delta}\} + [K]\{\Delta\} = \{F\} \tag{8.4.22}$$

The fully discretized equations are

$$[\hat{K}(\{\Delta\}_{s+1})]\{\Delta\}_{s+1} = \{\hat{F}\}_{s,s+1} \tag{8.4.23}$$

where

$$\begin{aligned}
 [\hat{K}(\{\Delta\}_{s+1})] &= [K(\{\Delta\}_{s+1})] + a_3[M]_{s+1} + a_6[C]_{s+1} \\
 \{\hat{F}\}_{s,s+1} &= \{F\}_{s+1} + [M]_{s+1}\{A\}_s + [C]_{s+1}\{B\}_s \\
 \{A\}_s &= a_3\{\Delta\}_s + a_4\{\dot{\Delta}\}_s + a_5\{\ddot{\Delta}\}_s \\
 \{B\}_s &= a_6\{\Delta\}_s + a_7\{\dot{\Delta}\}_s + a_8\{\ddot{\Delta}\}_s
 \end{aligned} \tag{8.4.24a}$$

and  $a_i$  are defined as ( $\gamma = 2\beta$ )

$$\begin{aligned}
 a_1 &= \alpha \Delta t, \quad a_2 = (1 - \alpha) \Delta t, \quad a_3 = \frac{1}{\beta(\Delta t)^2}, \quad a_4 = a_3 \Delta t, \\
 a_5 &= \frac{1}{\gamma} - 1, \quad a_6 = \frac{\alpha}{\beta \Delta t}, \quad a_7 = \frac{\alpha}{\beta} - 1, \quad a_8 = \Delta t \left( \frac{\alpha}{\gamma} - 1 \right)
 \end{aligned} \tag{8.4.24b}$$

At the end of each time step, the new velocity vector  $\{\dot{\Delta}\}_{s+1}$  and acceleration vector  $\{\ddot{\Delta}\}_{s+1}$  are computed using the equations

$$\{\ddot{\Delta}\}_{s+1} = a_3(\{\Delta\}_{s+1} - \{\Delta\}_s) - a_4\{\dot{\Delta}\} - a_5\{\ddot{\Delta}\}_s \tag{8.4.25a}$$

$$\{\dot{\Delta}\}_{s+1} = \{\dot{\Delta}\}_s + a_2\{\ddot{\Delta}\}_s + a_1\{\ddot{\Delta}\}_{s+1} \tag{8.4.25b}$$

Solution of Eq. (8.4.23) by the Newton-Raphson iteration method results in the following linearized equations for the incremental solution at the  $(r+1)$ st iteration

$$\{\delta\Delta\} = -[\hat{K}^T(\{\Delta\}_{s+1}^r)]^{-1}\{R\}_{s+1}^r \quad (8.4.26)$$

$$[\hat{K}^T(\{\Delta\}_{s+1}^r)] \equiv \left[ \frac{\partial\{R\}}{\partial\{\Delta\}} \right]_{s+1}^r, \{R\}_{s+1}^r = [\hat{K}(\{\Delta\}_{s+1}^r)]\{\Delta\}_{s+1}^r - \{\hat{F}\}_{s,s+1} \quad (8.4.27)$$

The total solution is obtained from

$$\{\Delta\}_{s+1}^{r+1} = \{\Delta\}_{s+1}^r + \{\delta\Delta\} \quad (8.4.28)$$

Note that the tangent stiffness matrix is evaluated using the latest known solution, while the residual vector contains contributions from the latest known solution in computing  $[\hat{K}(\{\Delta\}_{s+1}^r)]\{\Delta\}_{s+1}^r$  and previous time step solution in computing  $\{\hat{F}\}_{s,s+1}$ . The velocity and acceleration vectors are updated using Eqs. (8.4.25a,b) only after convergence is reached for a given time step.

## 8.5 Computer Implementation

Computer implementation of nonlinear time-dependent problems is complicated by the fact that one must keep track of the solution vectors at different loads, times, and iterations. Thus, there are three levels of calculations. Often, for a fixed value of load (or Reynolds number in the case of fluid flows), one wishes to obtain the transient solution. Therefore, the outer loop is on the number of load steps, followed by a loop on the number of time steps, and the inner most loop being on nonlinear iterations. Flow chart shown in Figure 8.5.1 illustrates the general idea.

As an example, Fortran statements showing the transfer of global solution vectors from previous time step and current iteration of the current time step to subroutine to calculate element matrices and residual vector are given below. Here variable *IDYN* is a flag: *IDYN* = 0 is for static analysis and *IDYN* > 0 is for transient analysis. Also we have

$W0(I)$  = element displacement vector at time  $t_s$

$W1(I)$  = element velocity vector at time  $t_s$

$W2(I)$  = element acceleration vector at time  $t_s$

$W(I)$  = element displacement vector at  $t_{s+1}$  in the latest iteration.

Fortran statements showing the transfer of global solution vectors to element solution vectors are given in Box 8.5.1. Statements showing the residual vector calculation inside the subroutine are given in Box 8.5.2.



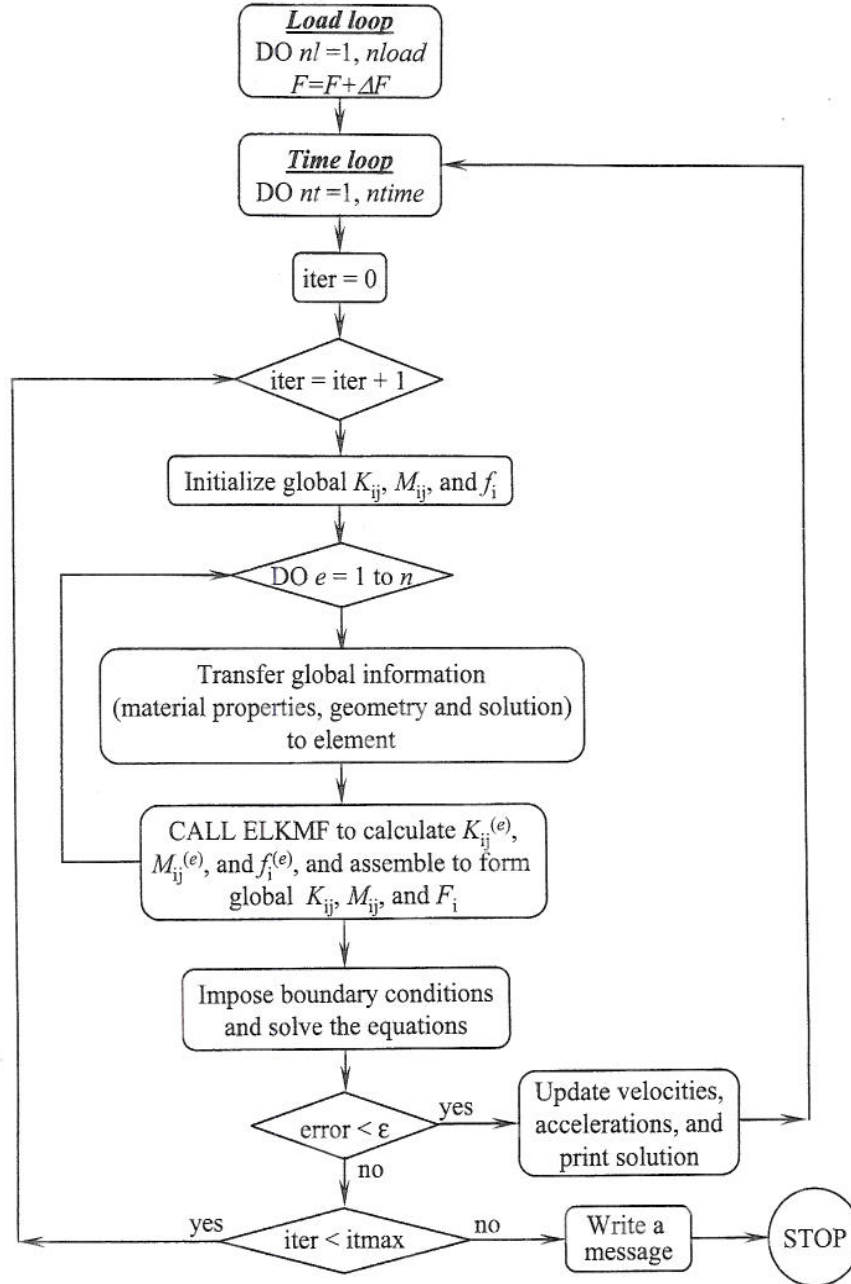


Figure 8.5.1 Flow chart of the nonlinear transient analysis of a problem.

Box 8.5.1 Fortran statements showing the transfer of global solution vectors to element solution vectors.

```

C
C Initialize the global coefficient matrices and vectors
C
DO 180 I=1,NEQ
GLF(I)=0.0
DO 180 J=1,NHBW
180 GLK(I,J)=0.0
C
C Do-loop on the number of ELEMENTS to compute element matrices
C and their assembly begins here (IDYN > 0, flag for dynamic anal.)
C
DO 200 N=1,NEM
L=0
DO 190 I=1,NPE
NI=NOD(N,I)
ELXY(I,1)=X(NI)
ELXY(I,2)=Y(NI)
LI=(NI-1)*NDF
DO 190 J=1,NDF
LI=LI+1
L=L+1
IF(IDYN.GT.0)THEN
ELP(L)=GLP(LI) !GLP - Global solution vector at time  $t_s$ 
ELV(L)=GLV(LI) !GLV - Global velocity vector at time  $t_s$ 
ELA(L)=GLA(LI) !GLA - Global acceleration vector at time  $t_s$ 
ENDIF
ELU(L)=GLU(LI) !GLU - Global solution vector at  $t_{s+1}$  & current iteration.
190 CONTINUE
C
C Call subroutine to compute [ELK], [ELM], [ELC] and {ELF}
C
.....
200 CONTINUE

```

Box 8.5.2 Fortran statements for the calculation of  $[\hat{K}]$  and  $\{\hat{F}\}$ .

```

C
C ELM(I,J) - mass matrix; ELK(I,J) - current coefficient matrix (updated in each
C iteration for nonlinear problems); ELKP(I,J) - coefficient matrix based on
C previous step solution (ELK=ELKP for linear problems); ELP(J) - solution vector
C from previous time step; ELU(J) - solution vector at current time and iteration.
C
IF(IDYN.EQ.1)THEN !Parabolic equations
DO 120 I=1,NN
SUM=0.0
DO 100 J=1,NN
SUM=SUM + (ELM(I,J)-A2*ELKP(I,J))*ELP(J)
100 ELK(I,J)=ELM(I,J)+A1*ELK(I,J)
120 ELF(I)=(A1+A2)*ELF(I) + SUM !Assumed time-independent source
C
ELSE !Hyperbolic equations
C
C ELC(I,J) - Damping matrix; ELP, ELV, ELA are displacement, velocity, and
C acceleration vectors from previous time step (do not change during iteration).
C
DO 150 I=1,NN
SUM=0.0
DO 140 J=1,NN
SUM=SUM+ELM(I,J)*(A3*ELP(J)+A4*ELV(J)+A5*ELA(J))
* +ELC(I,J)*(A6*ELP(J)+A7*ELV(J)+A8*ELA(J))
140 ELK(I,J)=ELK(I,J)+A3*ELM(I,J)+A6*ELC(I,J)
150 ELF(I)=ELF(I)+SUM
ENDIF
RETURN
END

```

## 8.6 Numerical Examples

### 8.6.1 Linear Problems

Here we consider several representative examples of time-dependent linear problems. We begin with a heat conduction problem.

#### Example 8.6.1

Consider the transient heat conduction equation

$$\frac{\partial \theta}{\partial t} - \left( \frac{\partial^2 \theta}{\partial x^2} + \frac{\partial^2 \theta}{\partial y^2} \right) = 1 \quad \text{in } \Omega \quad (8.6.1)$$

where  $\theta$  is the non-dimensional temperature and  $\Omega$  is the square domain of side 2. The boundary condition is that  $\theta = 0$  on the boundary for  $t > 0$  (see Figure 8.6.1). The initial condition is that  $\theta(x, y, 0) = 0$ . We wish to find the temperature field inside the domain for  $t > 0$ .

In view of the biaxial symmetry, it is sufficient to model one quadrant of the domain. The boundary conditions along the lines of symmetry require that the heat flux be zero there. Thus, the boundary conditions of the computational domain are

$$\frac{\partial \theta}{\partial x}(0, y, t) = 0, \quad \frac{\partial \theta}{\partial y}(x, 0, t) = 0, \quad \theta(1, y, t) = 0, \quad \theta(x, 1, t) = 0 \quad (8.6.2)$$

We choose a uniform mesh  $8 \times 8$  of linear rectangular elements to model the domain, and investigate the stability and accuracy of various schemes. Since the Crank–Nicolson ( $\alpha = 0.5$ ) and backward difference ( $\alpha = 1.0$ ) methods are unconditionally stable schemes, one can choose any value of  $\Delta t$ . However, if  $\Delta t$  is too large, the solution may not be accurate even when it is stable. In order to estimate the time step, one must calculate the maximum eigenvalue for the mesh used in the transient analysis. The solution of the eigenvalue problem associated with the  $8 \times 8$  mesh of linear elements yields 64 eigenvalues, of which the maximum eigenvalue is  $\lambda_{\max} = 1492.56$ . Therefore, the critical time step for the forward difference scheme ( $\alpha = 0.0$ ) is given by  $\Delta t_{\text{cr}} = (2/1492.56) = 0.00134$ .

Figure 8.6.2 shows plots of the temperature  $\theta(0, 0, t)$  versus time  $t$  for a  $\Delta t = 0.002$ , which is greater than the critical time step. For very small times,  $\theta(0, 0, t) \approx t$ , and both backward difference and Crank–Nicolson schemes show stable behavior while the forward difference is unstable. For  $\Delta t = 0.001$ , the forward difference too gives the same result as the stable schemes using  $\Delta t = 0.05$ . Table 8.6.1 shows the numerical values of  $\theta(0, 0, t)$  predicted by various schemes and two different meshes. One must note that the critical time step for the  $4 \times 4$  mesh is different as the maximum eigenvalue is different ( $\Delta t_{\text{cr}}$  is likely to be smaller for the mesh of quadratic elements). Figure 8.6.3 contains plots of the evolution of  $\theta(0, 0, t)$  with time, reaching a steady-state at around  $t = 1.2$ . Finally, Figure 8.6.4 shows plots of  $\theta(x, 0, t)$  versus  $x$  for  $t = 0.2, 0.5, \text{ and } 1.0$ . The difference between the solutions obtained by the two meshes and different time approximation schemes cannot be seen in the plots.



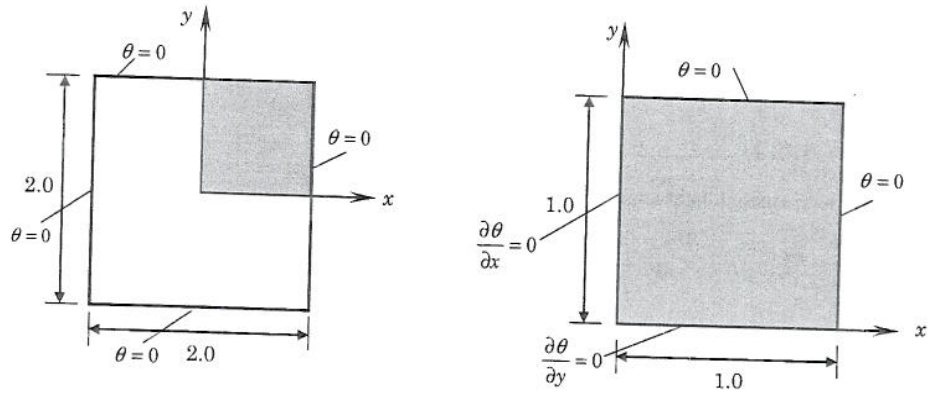


Figure 8.6.1 Actual and computational domains of the transient heat transfer problem.

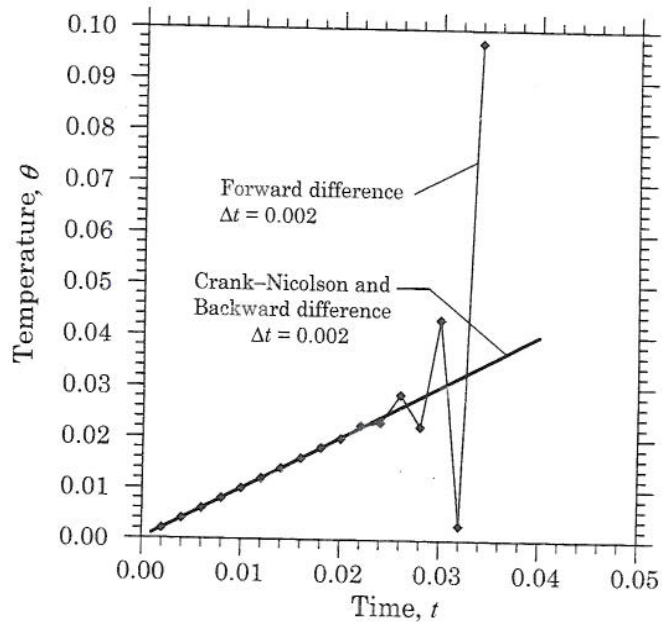


Figure 8.6.2 Transient response predicted by various schemes.

**Table 8.6.1** Evolution of  $\theta(0,0,t)$  obtained with various time approximation schemes ( $\Delta t = 0.05$  for Crank-Nicolson and backward difference schemes, and  $\Delta t = 0.001$  for the forward difference scheme).

Time	8 × 8L			4 × 4Q9		
	Crank-Nicolson	Backward difference	Forward difference	Crank-Nicolson	Backward difference	Forward difference
0.05	0.0497	0.0480	0.0500	0.0496	0.0479	0.0500
0.10	0.0975	0.0916	0.0983	0.0971	0.0913	0.0979
0.15	0.1398	0.1294	0.1400	0.1390	0.1288	0.1393
0.20	0.1740	0.1612	0.1737	0.1730	0.1604	0.1728
0.25	0.2006	0.1873	0.2004	0.1996	0.1864	0.1994
0.30	0.2215	0.2085	0.2213	0.2205	0.2075	0.2202
0.35	0.2379	0.2257	0.2376	0.2368	0.2247	0.2365
0.40	0.2506	0.2395	0.2503	0.2495	0.2385	0.2493
0.45	0.2605	0.2506	0.2603	0.2594	0.2496	0.2592
0.50	0.2682	0.2595	0.2680	0.2672	0.2585	0.2670
0.55	0.2743	0.2667	0.2741	0.2732	0.2656	0.2731
0.60	0.2790	0.2724	0.2788	0.2779	0.2714	0.2778
0.65	0.2826	0.2770	0.2825	0.2816	0.2760	0.2815
0.70	0.2855	0.2807	0.2854	0.2845	0.2797	0.2844
0.75	0.2877	0.2837	0.2876	0.2867	0.2827	0.2866
0.80	0.2895	0.2860	0.2894	0.2885	0.2850	0.2884
0.85	0.2908	0.2879	0.2908	0.2898	0.2870	0.2898
0.90	0.2919	0.2895	0.2918	0.2909	0.2885	0.2909
0.95	0.2927	0.2907	0.2926	0.2917	0.2897	0.2917
1.00	0.2933	0.2916	0.2933	0.2924	0.2907	0.2924

### Example 8.6.2

Here we consider the transient response  $u(x,y,t)$  of a square membrane fixed ( $u = 0$ ) on its boundary. The governing equation is

$$\frac{\partial^2 u}{\partial t^2} - \left( \frac{\partial^2 u}{\partial x^2} + \frac{\partial^2 u}{\partial y^2} \right) = 1 \quad \text{in } \Omega \quad (8.6.3)$$

See Figure 8.6.1 for the domain and boundary conditions with  $\theta$  replaced by  $u$ . We use  $8 \times 8$  mesh of linear elements in the quarter of the domain to determine the response. The critical time step for the linear acceleration method ( $\alpha = 0.5$  and  $\gamma = 1/3$ ) is ( $\lambda_{\max} = 1492.56$ )  $\Delta t_{\text{cr}} = 0.0897$ .

Figure 8.6.5 shows plots of the transverse deflection  $u(0,0,t)$  versus time  $t$  for a  $\Delta t = 0.1$ , which is greater than the critical time step. The linear acceleration method ( $\alpha = 0.5$  and  $\gamma = 1/3$ ) gives almost the same response as the constant-average acceleration method ( $\alpha = 0.5$  and  $\gamma = 0.5$ ) when  $\Delta t = 0.05$  (see Table 8.6.2).

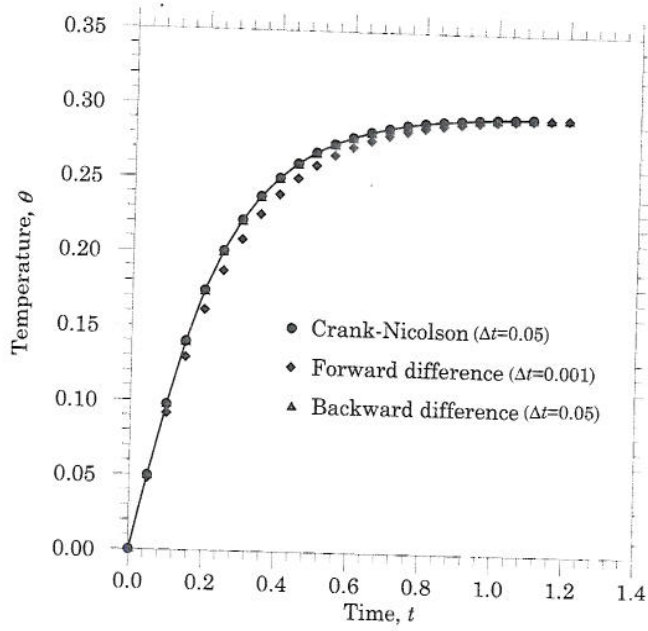


Figure 8.6.3 Evolution of the temperature  $\theta(0, 0, t)$ .

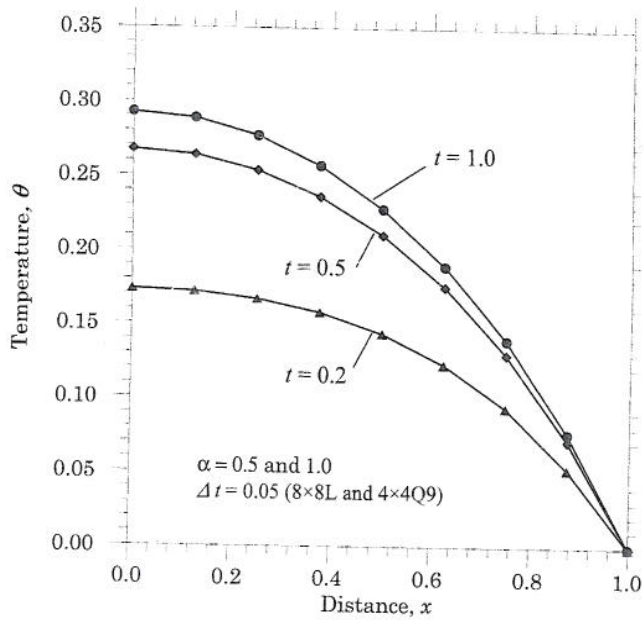


Figure 8.6.4 Transient response of the heat conduction problem of Example 8.6.1.

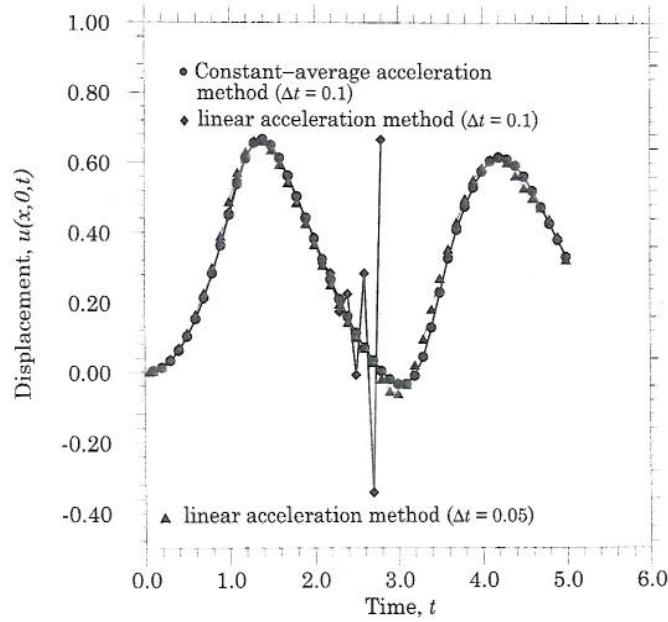


Figure 8.6.5 Evolution of the deflection  $u(x, 0, t)$  of the membrane.

Table 8.6.2 Deflection  $u(x, 0, t)$  versus time  $t$  for a square membrane fixed on its edges and subjected to uniform load ( $8 \times 8L^4$ ).

$t$	$u$ CAM*	$u$ LAM*	$u$ LAM†	$t$	$u$ CAM*	$u$ LAM*	$u$ LAM†
0.1	0.0025	0.0017	0.0029	1.7	0.5624	0.5578	0.5424
0.2	0.0125	0.0117	0.0154	1.8	0.5025	0.5023	0.4858
0.3	0.0325	0.0317	0.0379	1.9	0.4419	0.4397	0.4260
0.4	0.0625	0.0617	0.0704	2.0	0.3833	0.3872	0.3661
0.5	0.1025	0.1017	0.1129	2.1	0.3243	0.3122	0.3069
0.6	0.1525	0.1517	0.1657	2.2	0.2655	0.2841	0.2511
0.7	0.2125	0.2117	0.2269	2.3	0.2105	0.1740	0.1959
0.8	0.2825	0.2812	0.2989	2.4	0.1601	0.2250	0.1427
0.9	0.3624	0.3626	0.3896	2.5	0.1131	-0.0078	0.1014
1.0	0.4500	0.4565	0.4876	2.6	0.0706	0.2833	0.0693
1.1	0.5378	0.5482	0.5701	2.7	0.0343	-0.3422	0.0289
1.2	0.6110	0.6161	0.6301	2.8	0.0038	0.6653	-0.0196
1.3	0.6550	0.6546	0.6619	2.9	-0.0204	-1.1816	-0.0553
1.4	0.6656	0.6658	0.6608	3.0	-0.0348	1.9455	-0.0625
1.5	0.6492	0.6482	0.6359	3.1	-0.0339	-3.5061	-0.0358
1.6	0.6133	0.6079	0.5939	3.2	-0.0102	5.9403	0.0207

\*CAM = constant-average acceleration method ( $\Delta t = 0.1$ ); LAM = linear acceleration method ( $\Delta t = 0.1$ ).

† LAM with  $\Delta t = 0.05$ .

**Example 8.6.3**

Next, we consider the transient response  $w_0(x, y, t)$  of a simply supported (SS-1), isotropic square plate under uniform load of intensity  $q(x, y, t) = q_0 H(t)$ , where  $H(t)$  denotes the Heaviside step function. We use  $4 \times 4Q9$  mesh in the quarter of the domain to determine the response. The constant-average acceleration method ( $\alpha = 0.5$ ,  $\gamma = 0.5$ ) is used with  $\Delta t = 20 \mu\text{s} = 20 \times 10^{-6}$  s. The geometric and material parameters used are

$$\begin{aligned} a = b = 25 \text{ cm}, \quad h = 1 \text{ or } 2.5 \text{ cm}, \quad E_1 = E_2 = 2.1 \times 10^6 \text{ N/cm}^2 \\ \nu_{12} = 0.25, \quad \rho = 8 \times 10^{-6} \text{ N-s}^2/\text{cm}^4 \end{aligned} \quad (8.6.4)$$

Figure 8.6.6 shows plots of the non-dimensionalized transverse deflection  $\bar{w} = 10^3 w_0(0, 0, t) E_2 h^3 / q_0 a^4$  versus time  $t$  (in  $\mu\text{s}$ ) for thin ( $h = 1$  cm) and thick ( $h = 2.5$  cm), simply supported, isotropic ( $\nu = 0.25$ ) plates ( $4 \times 4Q9$  mesh;  $\Delta t = 20 \mu\text{s}$ ). Note that the effect of shear deformation is to increase the amplitude and reduce the period of the transverse deflection (see Table 8.6.3).

**Example 8.6.4**

Lastly, we study the motion (for  $Re = 0$ ) of a viscous fluid inside a wall-driven cavity (see Section 7.8.4). We use  $16 \times 20Q4$  non-uniform mesh (of four-node rectangular elements) in the domain. The mesh size in each coordinate direction are given by

$$\{DX\} = \{0.0625, 0.0625, \dots, 0.0625\}, \quad \{DY\} = \{0.0625, \dots, 0.0625, 0.03125, \dots, 0.03125\}$$

The Crank-Nicolson method ( $\alpha = 0.5$ ) with two different time steps  $\Delta t = 0.01$  and  $\Delta t = 0.001$  are used. Table 8.6.4 contains the velocity field  $v_x(0.5, y, t) \times 10$  for times  $t = 0.01, 0.05$ , and  $0.1$ . The solution reaches the steady state ( $\epsilon = 10^{-2}$ ) at time  $t = 0.1$  when  $\Delta t = 0.01$  is used. Figure 8.6.7 shows the evolution of  $v_x(0.5, y, t)$  ( $\Delta t = 0.01$ ).

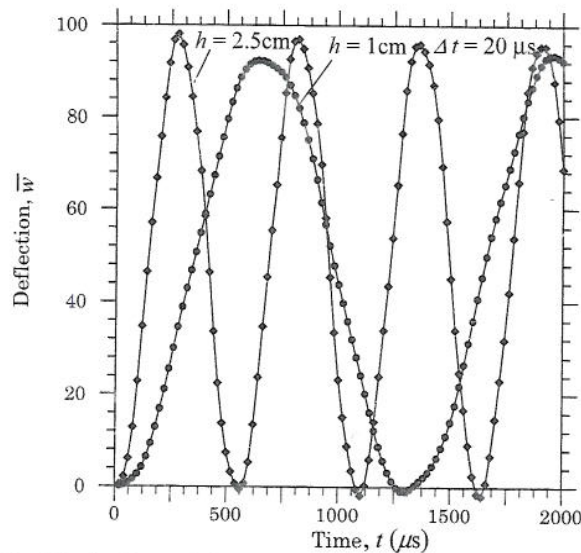


**Figure 8.6.6** Evolution of the transverse deflection  $\bar{w}$  of a simply supported, isotropic plate under uniform load.



**Table 8.6.3** Non-dimensionalized center deflection  $\bar{w}$  versus time  $t$  for simply supported, isotropic, square plates.

$t$ ( $\mu\text{s}$ )	$\bar{w}$		$t$ ( $\mu\text{s}$ )	$\bar{w}$	
	$h = 1$	$h = 2.5$		$h = 1$	$h = 2.5$
20	0.067	0.426	360	50.661	76.739
40	0.334	2.193	380	54.768	68.263
60	0.860	6.074	400	58.922	58.352
80	1.626	12.813	420	63.078	46.337
100	2.674	22.770	440	67.238	33.574
120	4.189	34.696	460	71.368	22.403
140	6.405	46.408	480	75.488	13.751
160	9.348	56.971	500	79.533	7.423
180	12.871	66.677	520	83.218	3.213
200	16.819	75.708	540	86.276	0.605
220	21.044	84.185	560	88.635	-0.511
240	25.459	91.721	580	90.348	0.728
260	30.002	96.806	600	91.472	5.332
280	34.532	98.062	620	92.084	13.441
300	38.861	95.669	640	92.323	23.727
320	42.878	90.826	660	92.251	34.641
340	46.718	84.384	680	91.849	45.351

**Table 8.6.4** The horizontal velocity field  $v_x(0.5, y, t) \times 10$  versus time  $t$  for the wall-driven cavity problem ( $16 \times 20\text{Q4}$  mesh).

$y$	$t = 0.01$	$t = 0.01$	$t = 0.05$	$t = 0.05$	$t = 0.10$	Steady state
	$\Delta t = 0.01$	$\Delta t = 0.001$	$\Delta t = 0.01$	$\Delta t = 0.001$	$\Delta t = 0.01$	
0.0625	-0.1342	-0.1953	-0.3103	-0.3247	-0.3655	-0.3688
0.1250	-0.1936	-0.3140	-0.5624	-0.5841	-0.6558	-0.6631
0.1875	-0.2314	-0.3940	-0.7888	-0.8163	-0.9108	-0.9198
0.2500	-0.2691	-0.4651	-1.0122	-1.0435	-1.1499	-1.1593
0.3125	-0.3157	-0.5475	-1.2346	-1.2746	-1.3802	-1.3886
0.3750	-0.3759	-0.6536	-1.4790	-1.5053	-1.5967	-1.6028
0.4375	-0.4516	-0.7902	-1.6964	-1.7151	-1.7793	-1.7820
0.5000	-0.5435	-0.9605	-1.8536	-1.8643	-1.8906	-1.8895
0.5625	-0.6465	-1.1577	-1.8846	-1.8878	-1.8700	-1.8652
0.6250	-0.7474	-1.3479	-1.7011	-1.6946	-1.6336	-1.6250
0.6875	-0.8097	-1.4428	-1.1889	-1.1653	-1.0700	-1.0572
0.7500	-0.7536	-1.1523	-0.2093	-0.1693	-0.0520	-0.0382
0.7813	-0.6325	-0.7744	0.5100	0.5471	0.6713	0.6820
0.8125	-0.4077	-0.1695	1.4014	1.4197	1.5467	1.5526
0.8438	-0.0054	0.7336	2.4885	2.4716	2.5918	2.5965
0.8750	0.6329	1.9318	3.7259	3.6716	3.7646	3.7824
0.9063	1.7000	3.5232	5.1185	5.0707	5.1198	5.1616
0.9375	3.3334	5.3837	6.5139	6.5756	6.6082	6.6410
0.9688	5.9470	7.5970	7.9975	8.2488	8.3805	8.2838

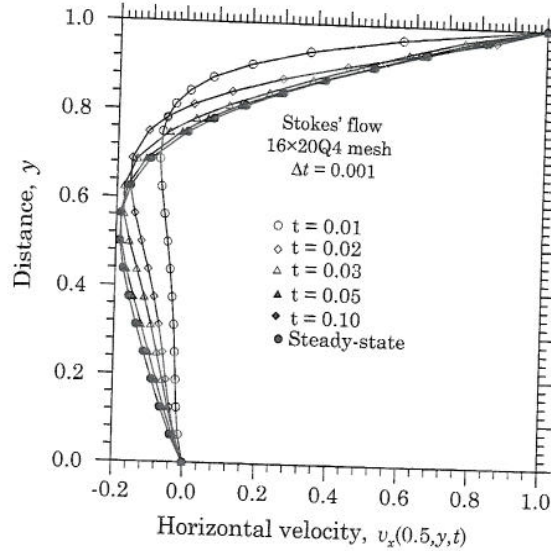


Figure 8.6.7 Evolution of the horizontal velocity  $v_x(0.5, y, t)$  inside a wall-driven cavity.

### 8.6.2 Nonlinear Problems

The nonlinear results of time-dependent problems are presented for heat transfer, plate bending, and fluid flow problems.

#### Example 8.6.5

Consider the equation

$$\frac{\partial T}{\partial t} - \frac{\partial}{\partial x} \left( k \frac{\partial T}{\partial x} \right) - \frac{\partial}{\partial y} \left( k \frac{\partial T}{\partial y} \right) = 0 \text{ in } \Omega \quad (8.6.5)$$

where  $T$  is the temperature and  $k$  is the conductivity. The domain  $\Omega$  is a rectangle of dimensions  $a = 0.18$  m and  $b = 0.1$  m along the  $x$  and  $y$  coordinates, respectively; the conductivity  $k$  is of the form

$$k = k_0 (1 + \beta T) \quad (8.6.6)$$

where  $k_0$  is the constant thermal conductivity, and  $\beta$  is the temperature coefficient of thermal conductivity. We take  $k_0 = 0.2$  W/(m °C) and  $\beta = 2 \times 10^{-3}$  (°C<sup>-1</sup>), and the boundary conditions to be

$$T(0, y, t) = 500^\circ\text{C}, \quad T(a, y, t) = 300^\circ\text{C}, \quad \frac{\partial T}{\partial y} = 0 \text{ at } y = 0, b \quad (8.6.7)$$

The initial condition is assumed to be

$$T(x, y, 0) = 0^\circ\text{C} \quad (8.6.8)$$

This is essentially a one-dimensional problem.

Table 8.6.5 contains numerical results of the finite element analysis using  $4 \times 2Q9$  mesh; Figures 8.6.8(a) and (b) show the evolution of the temperature at different locations of the domain.

**Table 8.6.5** The temperature field  $T(x, y, t)$  (for any fixed  $y$ ) of the heat transfer problem ( $4 \times 2Q9$  mesh,  $\Delta t = 0.005$ ).

$x$	$t = 0.01$	$t = 0.02$	$t = 0.03$	$t = 0.05$	$t = 0.10$	S-State
0.0225	426.96	456.51	471.49	477.91	477.55	477.31
0.0450	289.94	386.79	427.71	448.57	453.08	454.03
0.0675	178.69	343.34	401.45	427.63	430.45	430.12
0.0900	119.17	311.90	375.40	402.23	404.97	405.57
0.1125	118.00	289.10	350.39	377.39	380.54	380.32
0.1350	167.10	278.42	326.87	350.13	353.99	354.34
0.1575	250.20	293.20	316.46	327.12	327.80	327.58

#### Example 8.6.6

Here we consider the nonlinear transient response of the plate considered in Example 8.6.3. The problem data used is the same as given in Eq. (8.6.4), except  $h = 2.5$  cm and  $\Delta t = 10 \mu\text{s}$ . Figure 8.6.9 shows plots of the linear and nonlinear center deflections versus time for  $q_0 = 10^3$ ,  $q_0 = 5 \times 10^3$ , and  $q_0 = 10^4$  (also see Table 8.6.6). The deflection is non-dimensionalized as  $\bar{w} = 10^3 w_0(0, 0, t) E_2 h^3 / q_0 a^4$ .

#### Example 8.6.7

The next example is concerned with the nonlinear transient analysis of the wall-driven cavity problem of Example 8.6.4. A mesh of  $16 \times 20$  four-node quadrilateral elements is used with  $\Delta t = 0.001$ . The transient response is calculated for Reynolds numbers  $Re = 1,000$  and  $Re = 2,500$  separately. Figures 8.6.10(a) and (b) show plots of the nonlinear steady-state and transient center horizontal velocity  $v_x(0.5, y, t)$  versus  $y$  for various times.

#### Example 8.6.8 (Least-squares model)

The last example of this chapter deals with the transient flow past a circular cylinder [6,7]. The interest of this problem is in the periodic flow pattern that develops when the free stream Reynolds number is greater than  $Re_c \approx 46$  and the modeling of the outflow boundary conditions. The outflow boundary condition is a particularly challenging one since the computational domain must be truncated in a region where the vortex street is fully developed.

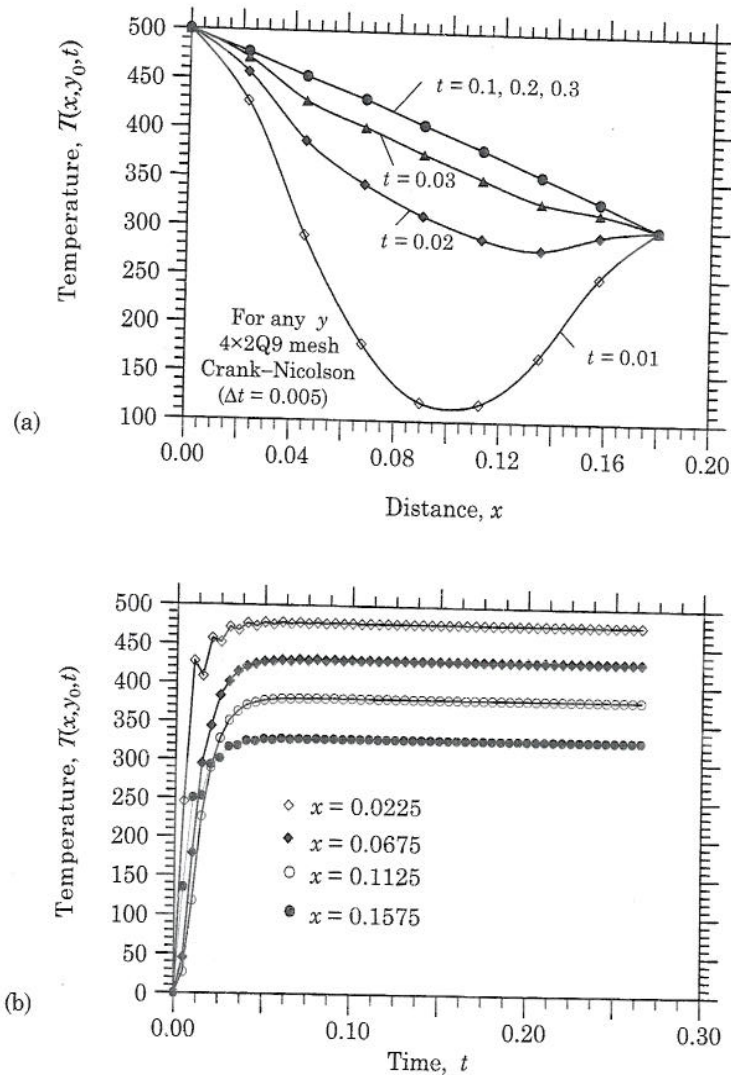


**Figure 8.6.8** Evolution of the temperature  $T(x, y, t)$  for the nonlinear heat transfer problem. (a) Temperature,  $T(x, y_0, t)$  for any value of  $y_0$ . (b) Evolution of temperatures for different values of  $x$ .

We consider a circular cylinder of unit diameter placed in the finite region  $\{\bar{\Omega} : -8 \leq x \leq 25, -8 \leq y \leq 8\}$ . The boundary conditions include a specified value of 1.0 for the  $x$ -component of velocity at the inflow, top, and bottom boundaries. At these boundaries the  $y$ -component of velocity is set to zero, see Figure 8.6.11(a). At these boundaries no boundary conditions for vorticity or velocity gradients are specified. We consider flow at a free stream Reynolds number of 100. The finite element mesh used for the computations is shown in Figure 8.6.11(b) and consists of 6,052 bilinear elements and 6,226 nodes. A collocation

solution will be sought for this problem. One collocation point per element is used, with the collocation point located at the center of each element. For the bilinear elements, the collocation point coincides with the reduced integration point.

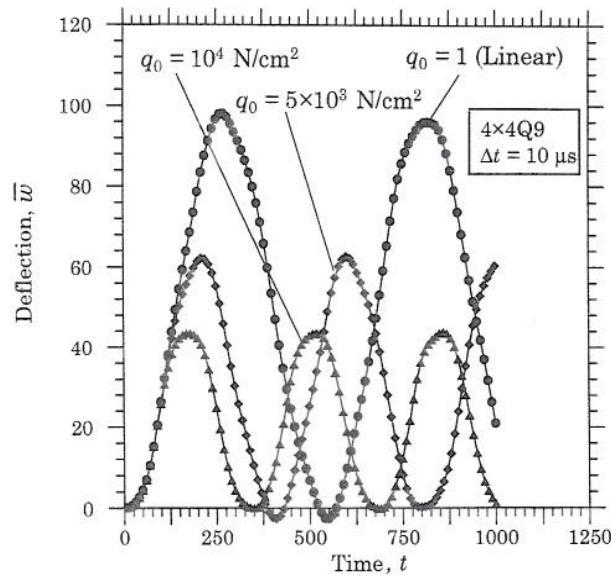


Figure 8.6.9 Plots of the linear and nonlinear center deflections  $\bar{w}$  versus time  $t$  ( $\mu\text{s}$ ) for simply supported square plate under uniform load ( $4 \times 4\text{Q9}$  mesh,  $\Delta t = 10\mu\text{s}$ ).

Table 8.6.6 Center deflections  $\bar{w}$  versus time  $t$  ( $\mu\text{s}$ ) for simply supported square plate under uniform load.

$t$ ( $\mu\text{s}$ )	Linear $q_0 = 1$	Nonlinear		
		$q_0 = 10^3$	$q_0 = 5 \times 10^3$	$q_0 = 10^4$
10	0.105	0.105	0.105	0.105
20	0.525	0.525	0.525	0.525
40	2.637	2.637	2.637	2.637
80	15.119	15.119	15.116	15.108
100	26.282	26.277	26.147	25.746
200	78.605	77.565	61.334	42.258
300	93.457	86.558	30.263	4.352
400	53.509	41.715	-2.343	7.872
500	6.760	2.214	25.179	42.854
600	9.727	17.908	62.625	18.889
700	59.089	69.535	33.608	0.115
800	95.215	90.271	0.151	36.143
900	73.660	51.497	23.921	37.009
1,000	20.968	5.232	60.393	1.060

In the weak form (Galerkin) finite element model, the outflow boundary conditions [see Figure 8.6.11(a)]

$$-P + \frac{1}{Re} \frac{\partial v_x}{\partial x} = 0, \quad \frac{\partial v_y}{\partial x} = 0 \quad (8.6)$$

are imposed in a weak sense rather than in a pointwise manner. They are imposed in least-squares sense in the least-squares finite element model.

*The velocity-pressure-vorticity formulation*

In the velocity-pressure-vorticity formulation we are left to model the outflow boundary condition by specifying both velocity components or a velocity component and either pressure or vorticity. We can set a reference pressure of  $P = 0$  at the outflow boundary; however, we can say nothing about either of the velocity components or about the vorticity. Just setting  $P = 0$  at the outflow boundary is not sufficient and would lead to a mathematically ill-posed problem.

Taking advantage of the flexibility of the least-squares method, we can modify the velocity-pressure-vorticity  $L_2$  least-squares functional  $I_1$  of Eq. (8.4.11) to enforce the outflow boundary conditions (8.6.9) in a weak sense:

$$I_1(\mathbf{v}, P, \omega) = \frac{1}{2} \left[ \left\| \frac{\partial \mathbf{v}}{\partial t} + (\mathbf{v} \cdot \nabla) \mathbf{v} + \nabla P + \frac{1}{Re} \nabla \times \omega - \mathbf{f} \right\|_0^2 + \|\omega - \nabla \times \mathbf{v}\|_0^2 + \|\nabla \cdot \mathbf{v}\|_0^2 \right. \\ \left. + \|\nabla \cdot \omega\|_0^2 + \left\| -P + \frac{1}{Re} \frac{\partial v_x}{\partial x} \right\|_{0, \Gamma_{\text{outflow}}}^2 + \left\| \frac{\partial v_y}{\partial x} \right\|_{0, \Gamma_{\text{outflow}}}^2 \right] \quad (8.6.10)$$

We consider a space-time decoupled formulation, where the temporal terms are discretized using the trapezoidal rule (see [7] for details on space-time coupled and decoupled least-squares formulations). The collocation solution is most accurate at the collocation points, i.e. at the reduced integration points. In a post-processing stage the nodal values for all degrees of freedom are recovered by taking an average of abutting elements to a node.

We choose the point  $(x, y) = (2, 0)$  to trace the change of the velocity component  $v_y$  with time. We use a fixed time increment of  $\Delta t = 0.1$  for the simulation. Even though the least-squares method is stable for large time increments, a small time increment is desirable for accuracy reasons. When a small time increment is used, the solution at the previous time step serves as a very good initial guess for the solution at the current time step, thus the conjugate gradient method takes only a few iterations to converge.

Figure 8.6.12 shows the time history of the velocity component  $v_y$  at the point  $(x, y) = (2, 0)$ . From the figure we see that shedding starts around  $t = 50$ . The shedding period measured from Figure 8.6.12 is found to be  $\mathcal{T} = 6.10$ , which gives a dimensionless shedding frequency of  $St = 0.164$ . Our result is in good agreement with the experimental result  $St = 0.166$  of Hammache and Gharib [16].

Figure 8.6.13 shows contour plots of the  $v_x$ - and  $v_y$ -velocity components. From visual inspection of the contour plots we see that the outflow boundary condition is modelled in a satisfactory manner. By definition, an outflow boundary condition should permit the flow to exit the domain gracefully and passively and not have any effect on the behavior of the solution in the domain near the open boundary and especially far from it (see Sani and Gresho [14]). Clearly, the outflow boundary condition did not have any effect on the behavior of the solution immediately behind the cylinder or near the open boundary. The imposition of the outflow boundary condition through the least-squares functional is not only efficient but very elegant.

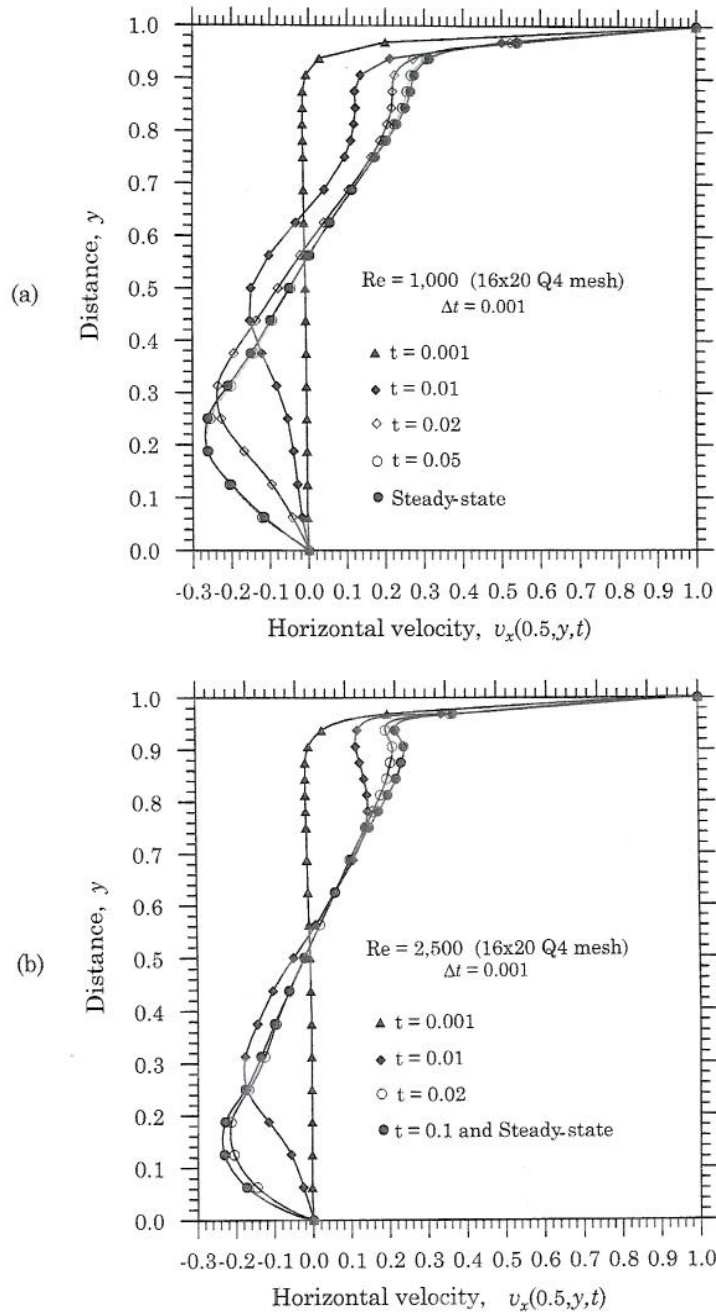


Figure 8.6.10 Evolution of the horizontal velocity field  $v_x(0.5, y, t)$  for the wall-driven cavity problem (nonlinear analysis).

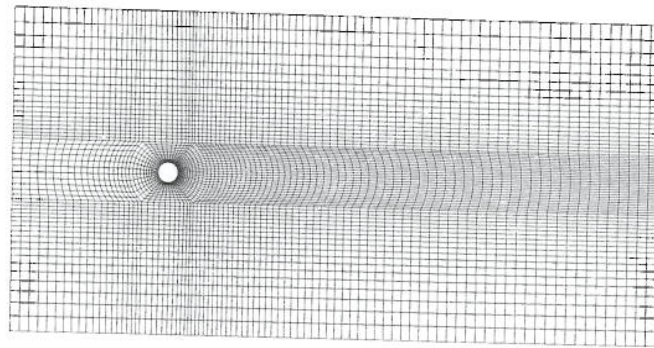
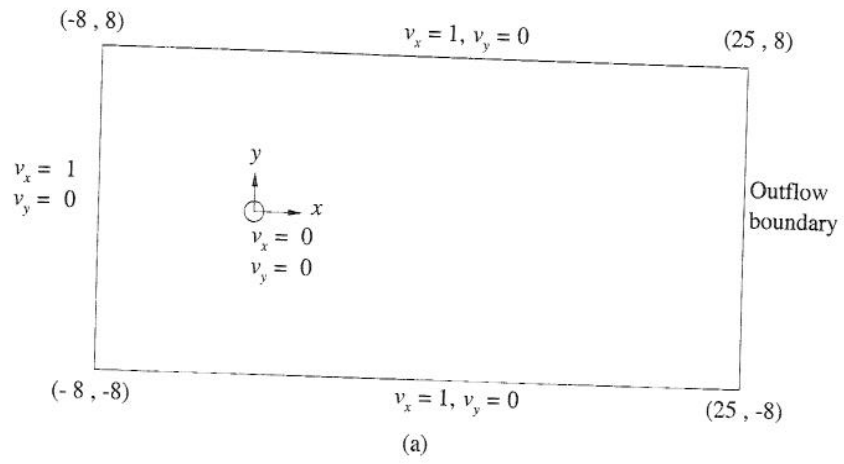


Figure 8.6.11 (a) Geometry and boundary conditions for flow past a circular cylinder. (b) Finite element mesh for flow past a circular cylinder.

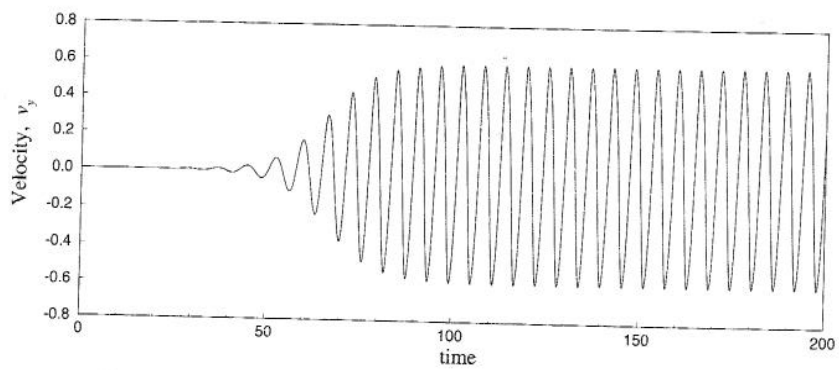
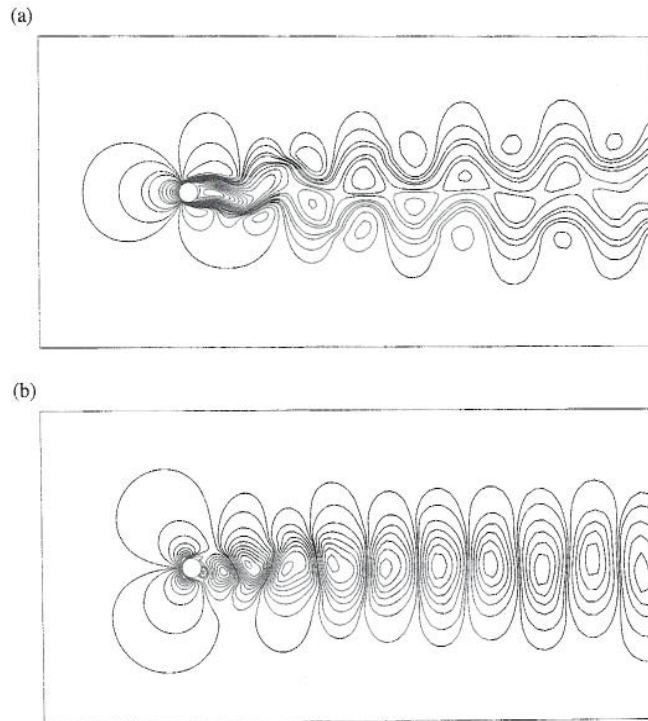


Figure 8.6.12 Time history of  $v_y$ -velocity component at  $(x, y) = (2, 0)$ .





**Figure 8.6.13** Numerical results for cylinder in cross flow using the velocity-pressure-vorticity formulation: (a)  $v_x$ -velocity contours and (b)  $v_y$ -velocity contours.

Yet another approach is to carry out the simulation using a space-time coupled formulation [7]. In such an approach the least-squares functional

$$I_1(\mathbf{v}, P, \omega) = \frac{1}{2} \left( \left\| \frac{\partial \mathbf{v}}{\partial t} + (\mathbf{v} \cdot \nabla) \mathbf{v} + \nabla P + \frac{1}{Re} \nabla \times \omega - \mathbf{f} \right\|_{0, \Omega \times (0, \tau]}^2 \right. \\ \left. + \|\omega - \nabla \times \mathbf{v}\|_{0, \Omega \times (0, \tau]}^2 + \|\nabla \cdot \mathbf{v}\|_{0, \Omega \times (0, \tau]}^2 + \|\nabla \cdot \omega\|_{0, \Omega \times (0, \tau]}^2 \right)$$

is minimized in space-time, where  $\|\cdot\|_{0, \Omega \times (0, \tau]}$  denotes the  $L_2$  norm of the enclosed quantity in space-time, i.e.,

$$\|u\|_{0, \Omega \times (0, \tau]}^2 = \int_0^\tau \int_\Omega |u(\mathbf{x}, t)|^2 d\Omega dt$$

Details and applications of such a formulation to this and other problems can be found in Pontaza and Reddy [7].

*The velocity–pressure–velocity gradient formulation*

In the velocity–pressure–velocity gradient formulation we have the added freedom of specifying any of the velocity gradients at the outflow boundary. Here we set  $P = 0$  and  $U_{12} = \partial v_y / \partial x = 0$  at the outflow boundary to model the outflow boundary condition. Again we choose the point  $(x, y) = (2, 0)$  to trace the change of the  $v_y$ -velocity component with time and use a fixed time increment of  $\Delta t = 0.1$  for the simulation.

Figure 8.6.14 shows the time history of the  $v_y$ -velocity component at the point  $(x, y) = (2, 0)$ . Like in the velocity–pressure–vorticity formulation, the outflow boundary condition is satisfactory (see Figure 8.6.15) and the shedding period is found to be  $\mathcal{T} = 6.10$ , which gives a dimensionless shedding frequency of  $St = 0.164$ .

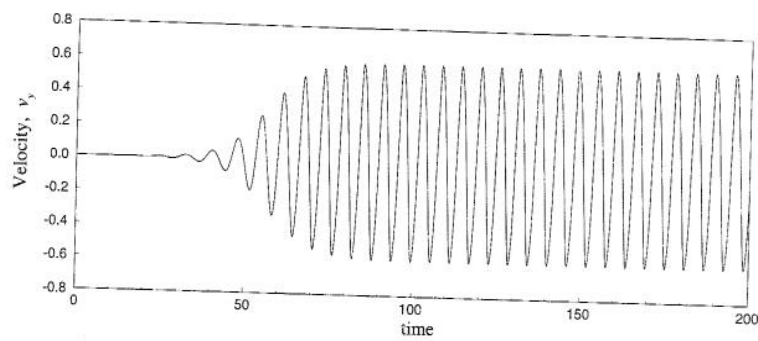


Figure 8.6.14 Time history of  $v_y$ -velocity component at  $(x, y) = (2, 0)$ .

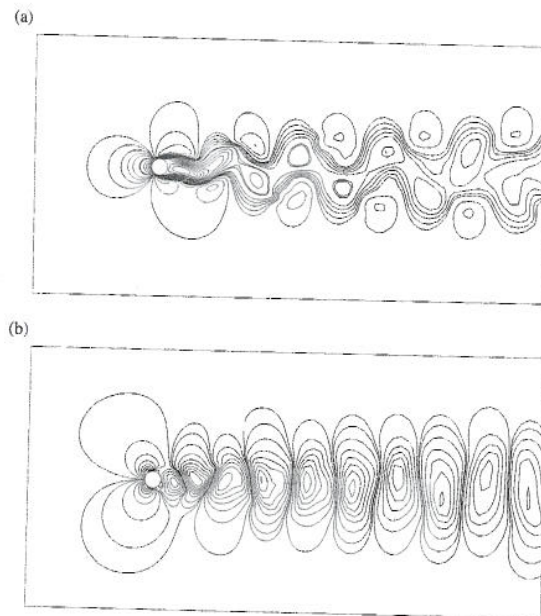


Figure 8.6.15 Numerical results for cylinder in cross flow using the velocity–pressure–velocity gradient formulation: (a)  $v_x$ -velocity contours and (b)  $v_y$ -velocity contours.

### Problems

- 8.1 Derive Eq. (8.2.9) for parabolic equations. What if  $[C]$  is a function of time?
- 8.2 Derive Eq. (8.2.15) for hyperbolic equations.
- 8.3 The  $\alpha$ -family of approximation and a general class of time approximation schemes can be derived using the finite element method in time domain. Consider a first-order differential equation of the form

$$C \frac{du}{dt} + Ku(t) = F(t) \tag{i}$$

The weighted-integral statement of Eq. (i) over a typical time interval  $(t_s, t_{s+1})$  is given by

$$\int_{t_s}^{t_{s+1}} w(t) (C\dot{u} + Ku - F) dt \tag{ii}$$

where  $w$  is a weight function, which is arbitrary at the moment. Suppose that  $u$  is approximated as

$$u(t) \approx \sum_{j=1}^n U_j \psi_j(t) \tag{iii}$$

where  $U_j$  denotes the value of  $u(t)$  at 'time node'  $t = t_j$  and  $\psi_j(t)$  is the associated interpolation function. In general, to obtain  $n$  independent relations  $w(t)$  can be chosen to be  $n$  independent functions  $\phi_i \neq \psi_j$  ( $j = 1, 2, \dots, n$ ). Such a scheme is known as the Petrov-Galerkin method [10]. When  $\phi_j = \psi_j$ , it is known as the Galerkin method. Obtain (a) the Petrov-Galerkin finite element model of the weighted-integral statement (ii), and (b) for the choice of  $n = 2$  in Eq. (iii) [i.e. linear interpolation of  $u(t)$ ] and

$$\phi_1(t) = -1 + 3t + 3\alpha(1 - 2t), \quad \phi_2(t) = 2 - 3t - 3\alpha(1 - 2t) \tag{iv}$$

show that the finite element equations are given by

$$\left( \frac{C}{2} \begin{bmatrix} -1 & 1 \\ -1 & 1 \end{bmatrix} + \frac{K\Delta t}{2} \begin{bmatrix} \alpha & 1-\alpha \\ 1-\alpha & \alpha \end{bmatrix} \right) \begin{Bmatrix} U_1 \\ U_2 \end{Bmatrix} = \frac{\Delta t}{2} \begin{Bmatrix} \alpha F_1 + (1-\alpha)F_2 \\ (1-\alpha)F_1 + \alpha F_2 \end{Bmatrix} \tag{v}$$

where  $F(t)$  is also interpolated as

$$F(t) = F_1\psi_1(t) + F_2\psi_2(t) \tag{vi}$$

Solve the second equation of (v) for  $U_2 = u_{s+1}$  in terms of  $U_1 = u_s$ , and obtain

$$[C + \alpha\Delta tK] u_{s+1} = [C - (1-\alpha)\Delta tK] u_s + \Delta t[(1-\alpha)F_s + \alpha F_{s+1}] \tag{vii}$$

- 8.4 Use quadratic approximation of  $u(t)$  with  $\phi_i = \psi_i$  (i.e. Galerkin's method) in the weak form (ii) of Problem 8.1 and arrive at the finite element equations

$$\left( \frac{C}{6} \begin{bmatrix} -3 & 4 & -1 \\ -4 & 0 & 4 \\ 1 & -4 & 3 \end{bmatrix} + \frac{K\Delta t}{30} \begin{bmatrix} 4 & 2 & -1 \\ 2 & 16 & 2 \\ -1 & 2 & 4 \end{bmatrix} \right) \begin{Bmatrix} U_1 \\ U_2 \\ U_3 \end{Bmatrix} = \frac{\Delta t}{30} \begin{bmatrix} 4 & 2 & -1 \\ 2 & 16 & 2 \\ -1 & 2 & 4 \end{bmatrix} \begin{Bmatrix} F_1 \\ F_2 \\ F_3 \end{Bmatrix} \tag{i}$$

where

$$U_1 = u_s, \quad U_2 = u_{s+\frac{1}{2}}, \quad U_3 = u_{s+1} \tag{ii}$$

and similar definition holds for  $F_i$ . Determine the values of  $U_2$  and  $U_3$  in terms of  $U_1$ .  
**8.5** Consider the second-order equation

$$M \frac{d^2 u}{dt^2} + C \frac{du}{dt} + Ku = F \tag{i}$$

The weighted-integral statement over an element is given by

$$\int_{t_s}^{t_{s+1}} w(t) (M\ddot{u} + C\dot{u} + Ku - F) dt \tag{ii}$$

The 'weak form' is given by

$$\int_{t_s}^{t_{s+1}} (-M\dot{w}\dot{u} + Cw\dot{u} + Kwu - wF) dt = Mw(t_s)v(t_s) - Mw(t_{s+1})v(t_{s+1}) \tag{iii}$$

where  $v(t) = \dot{u}(t)$ . The weighted-integral form in Eq. (ii) requires quadratic or higher-order interpolation while that in Eq. (iii) admits linear or higher-order approximations. Use the weighted-integral statement in Eq. (ii) with  $w(t) = \phi_i = \psi_i$  and  $n = 3$  (i.e. quadratic approximation) and obtain

$$\left( \frac{M}{3\Delta t} \begin{bmatrix} 2 & -4 & 2 \\ 8 & -16 & 8 \\ -2 & 4 & -2 \end{bmatrix} + \frac{C}{6} \begin{bmatrix} -3 & 4 & -1 \\ -4 & 0 & 4 \\ 1 & -4 & 3 \end{bmatrix} + \frac{K\Delta t}{30} \begin{bmatrix} 4 & 2 & -1 \\ 2 & 16 & 2 \\ -1 & 2 & 4 \end{bmatrix} \right) \begin{Bmatrix} U_1 \\ U_2 \\ U_3 \end{Bmatrix} = \frac{\Delta t}{30} \begin{bmatrix} 4 & 2 & -1 \\ 2 & 16 & 2 \\ -1 & 2 & 4 \end{bmatrix} \begin{Bmatrix} F_1 \\ F_2 \\ F_3 \end{Bmatrix} \tag{iv}$$

where

$$U_1 = u_s, \quad U_2 = u_{s+\frac{1}{2}}, \quad U_3 = u_{s+1} \tag{v}$$

Equation (iv) can be solved for  $u_{s+\frac{1}{2}}$  and  $U_3 = u_{s+1}$  in terms of  $u_s$ .

**8.6** Use the weak form (iii) of Problem 8.5 with  $w(t) = \phi_i = \psi_i$  and  $n = 2$  (i.e. linear approximation), and obtain

$$\left( -\frac{M}{\Delta t} \begin{bmatrix} 1 & -1 \\ -1 & 1 \end{bmatrix} + \frac{C}{2} \begin{bmatrix} -1 & 1 \\ -1 & 1 \end{bmatrix} + \frac{K\Delta t}{6} \begin{bmatrix} 2 & 1 \\ 1 & 2 \end{bmatrix} \right) \begin{Bmatrix} U_1 \\ U_2 \end{Bmatrix} = \frac{\Delta t}{6} \begin{bmatrix} 2 & 1 \\ 1 & 2 \end{bmatrix} \begin{Bmatrix} F_1 \\ F_2 \end{Bmatrix} + M \begin{Bmatrix} \dot{U}_1 \\ -\dot{U}_2 \end{Bmatrix} \tag{i}$$

and then solve for  $U_2 = u_{s+1}$  in terms of quantities known at time  $t_s$ . *Hint:* Replace  $F_1 = F_s$  with  $F_s = M\ddot{u}_s + C\dot{u}_s + Ku_s$ , and solve for  $u_{s+1}$

$$\left( \frac{6M}{(\Delta t)^2} + \frac{3C}{\Delta t} + K \right) u_{s+1} = M \left( \frac{6}{(\Delta t)^2} u_s + \frac{6}{\Delta t} \dot{u}_s + 2\ddot{u}_s \right) + C \left( \frac{3}{\Delta t} u_s + 2\dot{u}_s \right) + F_{s+1} \tag{ii}$$

which is the same as the Newmark scheme with  $\alpha = 1/2$  and  $\gamma = 1/3$  (and  $a_7 = 0$ ).

**8.7** Use the Newmark scheme in Eqs. (8.2.22) and (8.2.23) to reduce Eq. (8.2.11) to that in Eq. (8.2.20). *Hint:* Use Eqs. (8.2.22), (8.2.23), and (8.2.11) to eliminate  $\{u\}_{s+1}$  and  $\{\dot{u}\}_{s+1}$  to arrive at the desired equation.

- 8.8 The mass matrices of the finite element formulations are always non-diagonal. They may be replaced with rationally derived diagonal matrices, also called lumped mass matrices, for use in explicit formulations. The *row-sum lumping* and *proportional lumping* techniques are two ways to compute diagonal matrices. In row-sum lumping the sum of the coefficients of each row of the consistent 'mass' matrix is used as the diagonal element and the off-diagonal elements are set to zero:

$$M_{ii}^e = \sum_{j=1}^n \int_{\Omega^e} \rho \psi_i^e \psi_j^e dx = \int_{\Omega^e} \rho \psi_i^e dx, \quad M_{ij} = 0 \quad \text{for } i \neq j \quad (\text{i})$$

where the property  $\sum_{j=1}^n \psi_j^e = 1$  of the interpolation functions is used. In proportional lumping the diagonal elements are computed to be proportional to the diagonal elements of the consistent mass matrix while conserving the total mass of the element:

$$M_{ii}^e = \alpha \int_{\Omega^e} \rho \psi_i^e \psi_i^e dx, \quad \alpha = \frac{\int_{\Omega^e} \rho dx}{\sum_{i=1}^n \int_{\Omega^e} \rho \psi_i^e \psi_i^e dx} \quad (\text{ii})$$

Compute the lumped mass matrices for linear and quadratic one-dimensional elements and show that the critical time step computed using lumped mass matrices is greater than that computed using the consistent mass matrix.

- 8.9 The equation governing bending of beams according to the Euler-Bernoulli assumptions and in the presence of viscous (velocity-dependent) damping is given by

$$\frac{\partial^2}{\partial x^2} \left( EI \frac{\partial^2 w_0}{\partial x^2} + c_s I \frac{\partial^3 w_0}{\partial x^2 \partial t} \right) + I_0 \frac{\partial^2 w_0}{\partial t^2} + c \frac{\partial w_0}{\partial t} = q(x, t) \quad (\text{i})$$

where  $I$  denotes the moment of inertia,  $I_0$  the principal mass inertia,  $c_s$  the viscous resistance to strain velocity, and  $c$  the viscous resistance to transverse displacement. Develop the semidiscrete finite element model and fully discretized finite element model using the Newmark scheme.

- 8.10 Establish the stability condition in Eq. (8.3.4).

## References

1. Argyris, J. H. and Scharpf, O. W., "Finite Elements in Time and Space," *Aeronautical Journal of the Royal Society*, **73**, 1041-1044 (1969).
2. Bathe, K. J., *Finite Element Procedures*, Prentice-Hall, Englewood Cliffs, NJ (1996).
3. Engelman, M. S. and Jamnia, M. A., "Transient Flow Past a Circular Cylinder: a Benchmark Solution," *International Journal for Numerical Methods in Fluids*, **11**, 985-1000 (1990).
4. Newmark, N. M., "A Method for Computation of Structural Dynamics," *Journal of Engineering Mechanics*, **85**, 67-94 (1959).
5. Nickell, R. E., "On the Stability of Approximation Operators in Problems of Structural Dynamics," *International Journal of Solids and Structures*, **7**, 301-319 (1971).
6. Pontaza, J. P. and Reddy, J. N., "Spectral/hp Least-Squares Finite Element Formulation for the Navier-Stokes Equations," *Journal of Computational Physics*, **190**(2), 523-549 (2003).
7. Pontaza, J. P. and Reddy, J. N., "Space-Time Coupled Spectral/hp Least-Squares Finite Element Formulation for the Incompressible Navier-Stokes Equations," *Journal of Computational Physics* (to appear).

8. Reddy, J.N. and Gartling, D. K., *The Finite Element Method in Heat Transfer and Fluid Dynamics*, 2nd edn, CRC Press, Boca Raton, FL (2000).
9. Reddy, J. N., *An Introduction to the Finite Element Method*, 2nd edn, McGraw-Hill, New York (1993).
10. Reddy, J. N., *Applied Functional Analysis and Variational Methods in Engineering*, McGraw-Hill, New York (1986); reprinted by Krieger Publishing, Melbourne, FL (1991).
11. Reddy, J. N., *Energy Principles and Variational Methods in Applied Mechanics*, Second Edition, John Wiley, New York (2002).
12. Reddy, J. N., *Theory and Analysis of Elastic Plates*, Taylor and Francis, Philadelphia, PA (1999).
13. Reddy, J. N., *Mechanics of Laminated Composite Plates and Shells. Theory and Analysis*, 2nd edn, CRC Press, Boca Raton, FL (2004).
14. Sani, R. L. and Gresho, P. M., "Resume and Remarks on the Open Boundary Condition Minisymposium," *International Journal for Numerical Methods in Fluids*, **18**, 983-1008 (1994).
15. Wood, W. L., "Control of Crank-Nicolson Noise in the Numerical Solution of the Heat Conduction Equation," *International Journal for Numerical Methods in Engineering*, **11**, 1059-1065 (1977).
16. Hammache, M. and Gharib, M., "An Experimental Study of the Parallel and Oblique Vortex Shedding from Circular Cylinders," *Journal of Fluid Mechanics*, **232**, 567-590 (1991).

---

# Finite Element Formulations of Solid Continua

---

## 9.1 Introduction

### 9.1.1 Background

In the linear description of the motion of solid bodies one assumes that the displacements and strains are very small and that the material is linearly elastic. In addition, the equilibrium equations were derived using the undeformed configuration of the body. In geometrically nonlinear analysis of beams and plates that was considered in earlier chapters the assumption of small strains allowed us to ignore the changes in the geometry of the body and the distinction between various measures of stress and strain, as we proceeded to determine the deformation for the next load. In this chapter, we shall study geometrically nonlinear behavior in which changes in geometry, however large or small, have a significant effect on the load-displacement characteristics of solid bodies. When the geometric changes are significant, that is, displacements and strains are large, the geometry of the body must be updated to determine the new position  $\mathbf{x}$  of the material point  $\mathbf{X}$ . Consequently, it becomes necessary to distinguish between various measures of stress and strain, and descriptions of motion. Intuition tells us that if strain energy is based on the product of stress and strain, it is not expected to change simply because of our choice of stress or strain measure. Thus, "energetically conjugate" pairs of stress and strain that produce the same strain energy must be used [1-6].

Before we develop geometrically nonlinear finite element formulations of solid continua, it is useful to familiarize ourselves with the associated nonlinear continuum mechanics. The knowledge of nonlinear continuum mechanics enables us to understand better the restrictions placed on the model, better interpret and apply the results of the analysis, and prevent the use of a computer program beyond the range of its applicability.

### 9.1.2 Descriptions of Motion

Consider a deformable body of known geometry, constitution, and loading. For a given geometry and loading, the body will undergo deformation (i.e. macroscopic geometric changes within the body). If the applied loads are time-dependent, the deformation of the body will be a function of time, that is, the geometry of the body will change continuously with time. If the loads are applied slowly so that the deformation is only dependent on the loads, the body will take a definitive shape at the end of each load application. Whether the deformation is time-dependent or not, the forces in the deformed body will be in equilibrium at all times.

Suppose that the body initially occupies a configuration  $C_0$ , in which a particle  $X$  of the body occupies the position  $\mathbf{X}$ , referred to a rectangular Cartesian system  $(X_1, X_2, X_3)$ . Note that  $X$  is the name of the particle that occupies the location  $\mathbf{X}$  in configuration  $C_0$ , and therefore  $(X_1, X_2, X_3)$  are called the *material coordinates*. After the application of the loads, the body deforms and assumes a new configuration  $C$ . The particle  $X$  now occupies the position  $\mathbf{x}$  in the deformed configuration  $C$  (see Figure 9.1.1).

An analytical description of the deformation of a continuous body follows one of the two approaches [1-3,5,6]. In the first approach, called the *material* or *Lagrangian description*, the motion of the body is referred to a reference configuration  $C_R$ , which is often chosen to be the undeformed configuration,  $C_R = C_0$ . Thus, in the Lagrangian description, the current coordinates  $(x_1, x_2, x_3)$  are expressed in terms of the reference coordinates  $(X_1, X_2, X_3)$ :

$$\mathbf{x} = \mathbf{x}(\mathbf{X}, t) \quad (9.1.1)$$

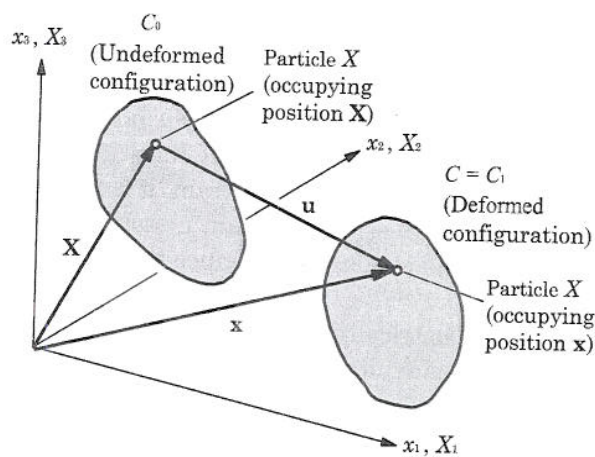


Figure 9.1.1 Reference and deformed configurations of a body.



and the variation of a typical variable  $\phi$  over the body is described with respect to the material coordinates  $(X_1, X_2, X_3)$ :

$$\phi = \phi(\mathbf{X}, t) \quad (9.1.2)$$

In the *spatial* or *Eulerian description*, the motion is referred to the current configuration  $\mathcal{C}$  occupied by the body, and  $\phi$  is described with respect to the position  $(x_1, x_2, x_3)$  in space, currently occupied by material particle  $X$ :

$$\phi = \phi(\mathbf{x}, t), \quad \mathbf{X} = \mathbf{X}(\mathbf{x}, t) \quad (9.1.3)$$

The coordinates  $(x_1, x_2, x_3)$  are termed the *spatial coordinates*.

Equations (9.1.2) and (9.1.3) each convey a different information [1-3]. In Eq. (9.1.2), a change in time  $t$  implies that the *same* material particle  $X$ , occupying position  $\mathbf{X}$  in  $\mathcal{C}_0$ , has a different value  $\phi$ . Thus the attention is focused on the material particle  $X$ . In Eq. (9.1.3), a change in time  $t$  implies that a different value  $\phi$  is observed at the *same* spatial location  $\mathbf{x}$ , now probably occupied by a different material particle  $X$ . Hence, attention is focused on a spatial position  $\mathbf{x}$ .

In the study of solid bodies, the Eulerian description is less useful since the configuration  $\mathcal{C}$  is unknown. On the other hand, it is the preferred description for the study of motion of fluids because the configuration is known and remains unchanged, and we wish to determine the changes in the fluid velocities, pressure, density and so on. Thus, in the Eulerian description, attention is focused on a given region of space instead of a given body of matter. The development of continuum equations in the Eulerian description of fluid flows was presented in Chapter 7. Here we focus our attention on the Lagrangian description of the motion of solid bodies undergoing geometric changes.

## 9.2 Strain and Stress Measures

### 9.2.1 Deformation Gradient Tensor

Consider two material particles  $P$  and  $Q$  in the neighborhood of each other in the reference configuration  $\mathcal{C}_0$  (see Figure 9.2.1). The positions of  $P$  and  $Q$  are denoted by  $\mathbf{X}_P$  and  $\mathbf{X}_Q$ , respectively. The position of  $Q$  relative to  $P$  is given by the elemental vector  $d\mathbf{X}$  in  $\mathcal{C}_0$ :

$$d\mathbf{X} = \mathbf{X}_Q - \mathbf{X}_P$$

After deformation the material particles  $P$  and  $Q$  occupy spatial positions  $\mathbf{x}_P$  and  $\mathbf{x}_Q$ , respectively in  $\mathcal{C}$ ; they are now labeled as  $\bar{P}$  and  $\bar{Q}$ . The position of  $\bar{Q}$  relative to  $\bar{P}$  is denoted by  $d\mathbf{x}$  and it is given by

$$d\mathbf{x} = \mathbf{x}_Q - \mathbf{x}_P$$

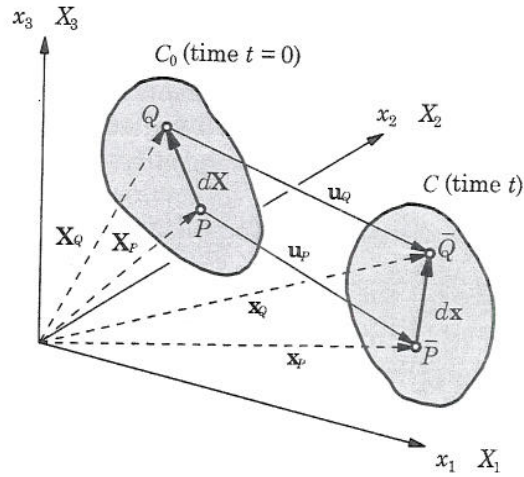


Figure 9.2.1 Deformation of a line segment  $PQ$  in a continuous medium.

The displacements of the material particles  $P$  and  $Q$  are given by

$$\mathbf{u}_P = \mathbf{x}_P - \mathbf{X}_P, \quad \mathbf{u}_Q = \mathbf{x}_Q - \mathbf{X}_Q \quad (9.2.1)$$

One of the key quantities in finite deformation analysis is the *deformation gradient tensor*  $\mathbf{F}$ , which gives the relationship of a material line  $d\mathbf{X}$  before deformation to the line  $d\mathbf{x}$  after deformation. It is defined as [1-3]

$$d\mathbf{x} = \mathbf{F} \cdot d\mathbf{X} = d\mathbf{X} \cdot \mathbf{F}^T \quad \text{where } \mathbf{F} = \left( \frac{\partial \mathbf{x}}{\partial \mathbf{X}} \right)^T \equiv (\nabla_o \mathbf{x})^T \quad (9.2.2)$$

and  $\nabla_o$  is the gradient operator with respect to  $\mathbf{X}$ . We also have

$$d\mathbf{X} = \mathbf{F}^{-1} \cdot d\mathbf{x} = d\mathbf{x} \cdot \mathbf{F}^{-T}, \quad \text{where } \mathbf{F}^{-T} = \frac{\partial \mathbf{X}}{\partial \mathbf{x}} \equiv \nabla \mathbf{X} \quad (9.2.3)$$

and  $\nabla$  is the gradient operator with respect to  $\mathbf{x}$ . In indicial notation, Eqs (9.2.2) and (9.2.3) can be written as

$$\mathbf{F} = F_{iI} \hat{\mathbf{e}}_i \hat{\mathbf{E}}_I, \quad F_{iI} = \frac{\partial x_i}{\partial X_I} \quad (9.2.4a)$$

$$\mathbf{F}^{-1} = F_{Ii}^{-1} \hat{\mathbf{E}}_I \hat{\mathbf{e}}_i, \quad F_{Ii}^{-1} = \frac{\partial X_I}{\partial x_i} \quad (9.2.4b)$$

Here the lower case indices refer to the current (spatial) Cartesian coordinates, whereas upper case indices refer to the reference (material) Cartesian

coordinates. The determinant of  $\mathbf{F}$  is called the *Jacobian of the motion* and it is denoted by  $J$ . The deformation tensor  $\mathbf{F}$  can be expressed in terms of the displacement vector as

$$\mathbf{F} = (\nabla_o \mathbf{x})^T = (\nabla_o \mathbf{u} + \mathbf{I})^T, \quad \mathbf{F}^T = \nabla_o \mathbf{x} = \nabla_o \mathbf{u} + \mathbf{I} \quad (9.2.5)$$

The deformation tensor conveys no information about the translation of the body. Further, if  $\mathbf{F} = \mathbf{I}$  everywhere in the body, then the body is not rotated and is undeformed. If  $\mathbf{F}$  has the same value at every material point in a body, then the mapping  $\mathbf{x} = \mathbf{x}(\mathbf{X}, t)$  is said to be a *homogeneous motion* of the body.

### 9.2.2 Green and Almansi Strain Tensors

Next we discuss a general measure of deformation, independent of both translation and rotation. Consider two material particles  $P$  and  $Q$  in the neighborhood of each other (separated by  $d\mathbf{X}$ ) in the reference configuration (see Figure 9.2.1). In the deformed configuration the material points  $P$  and  $Q$  are denoted by  $\bar{P}$  and  $\bar{Q}$ , and they are separated by  $d\mathbf{x}$ . We wish to determine the change in the distance  $d\mathbf{X}$  between the material points  $P$  and  $Q$  as the body deforms and the material points move to the new locations  $\bar{P}$  and  $\bar{Q}$ .

The distances between points  $P$  and  $Q$  and points  $\bar{P}$  and  $\bar{Q}$  are given, respectively, by

$$(dS)^2 = d\mathbf{X} \cdot d\mathbf{X} \quad (9.2.6a)$$

$$\begin{aligned} (ds)^2 &= d\mathbf{x} \cdot d\mathbf{x} = (\mathbf{F} \cdot d\mathbf{X}) \cdot (\mathbf{F} \cdot d\mathbf{X}) = d\mathbf{X} \cdot (\mathbf{F}^T \cdot \mathbf{F}) \cdot d\mathbf{X} \\ &\equiv d\mathbf{X} \cdot \mathbf{C} \cdot d\mathbf{X} \end{aligned} \quad (9.2.6b)$$

where  $\mathbf{C}$  is the *right Cauchy–Green deformation tensor*

$$\mathbf{C} = \mathbf{F}^T \cdot \mathbf{F} \quad (9.2.7)$$

The change in the squared lengths that occurs as the body deforms from the initial to the current configuration can be expressed relative to the original length as

$$(ds)^2 - (dS)^2 = 2 d\mathbf{X} \cdot \mathbf{E} \cdot d\mathbf{X} \quad (9.2.8)$$

where  $\mathbf{E}$  is called the *Green–Lagrange strain tensor* or simply the *Green strain tensor*, which can be expressed as

$$\mathbf{E} = \frac{1}{2} (\mathbf{F}^T \cdot \mathbf{F} - \mathbf{I}) = \frac{1}{2} (\mathbf{C} - \mathbf{I}) \quad (9.2.9)$$

$$= \frac{1}{2} [(\nabla_o \mathbf{u})^T + \nabla_o \mathbf{u} + (\nabla_o \mathbf{u})^T \cdot (\nabla_o \mathbf{u})] \quad (9.2.10)$$

Clearly, the Green strain tensor is symmetric. Also, the change in the squared lengths is zero if and only if  $\mathbf{E} = \mathbf{0}$ .

Alternatively, the change in the squared lengths that occurs as the body deforms from the initial to the current configuration can be expressed relative to the current length as

$$(ds)^2 - (dS)^2 = 2 \, dx \cdot e \cdot dx \quad (9.2.11)$$

where  $e$  is called the *Almansi-Hamel (Eulerian) strain tensor* or simply the *Euler strain tensor*, which can be expressed as

$$e = \frac{1}{2} (\mathbf{I} - \mathbf{F}^{-T} \cdot \mathbf{F}^{-1}) = \frac{1}{2} (\mathbf{I} - \mathbf{B}^{-1}) \quad (9.2.12)$$

$$= \frac{1}{2} [(\nabla \mathbf{u})^T + \nabla \mathbf{u} - (\nabla \mathbf{u})^T \cdot (\nabla \mathbf{u})] \quad (9.2.13)$$

where  $\mathbf{B} = \mathbf{F} \cdot \mathbf{F}^T$  is the *Cauchy strain tensor*, and its inverse is called the *left Cauchy-Green* or *Finger tensor*.

In the Cartesian component form, we can write

$$\mathbf{E} = E_{IJ} \hat{\mathbf{E}}_I \hat{\mathbf{E}}_J \quad (9.2.14)$$

$$e = e_{ij} \hat{\mathbf{e}}_i \hat{\mathbf{e}}_j \quad (9.2.15)$$

with components

$$E_{IJ} = \frac{1}{2} \left( \frac{\partial x_m}{\partial X_I} \frac{\partial x_m}{\partial X_J} - \delta_{IJ} \right) \quad (9.2.16a)$$

$$= \frac{1}{2} \left( \frac{\partial u_I}{\partial X_J} + \frac{\partial u_J}{\partial X_I} + \frac{\partial u_K}{\partial X_I} \frac{\partial u_K}{\partial X_J} \right) \quad (9.2.16b)$$

$$e_{ij} = \frac{1}{2} \left( \delta_{ij} - \frac{\partial X_K}{\partial x_i} \frac{\partial X_K}{\partial x_j} \right) \quad (9.2.17a)$$

$$= \frac{1}{2} \left( \frac{\partial u_i}{\partial x_j} + \frac{\partial u_j}{\partial x_i} - \frac{\partial u_k}{\partial x_i} \frac{\partial u_k}{\partial x_j} \right) \quad (9.2.17b)$$

In expanded notation, the Green strain components, for example, are given by

$$\begin{aligned} E_{11} &= \frac{\partial u_1}{\partial X_1} + \frac{1}{2} \left[ \left( \frac{\partial u_1}{\partial X_1} \right)^2 + \left( \frac{\partial u_2}{\partial X_1} \right)^2 + \left( \frac{\partial u_3}{\partial X_1} \right)^2 \right] \\ E_{22} &= \frac{\partial u_2}{\partial X_2} + \frac{1}{2} \left[ \left( \frac{\partial u_1}{\partial X_2} \right)^2 + \left( \frac{\partial u_2}{\partial X_2} \right)^2 + \left( \frac{\partial u_3}{\partial X_2} \right)^2 \right] \\ E_{33} &= \frac{\partial u_3}{\partial X_3} + \frac{1}{2} \left[ \left( \frac{\partial u_1}{\partial X_3} \right)^2 + \left( \frac{\partial u_2}{\partial X_3} \right)^2 + \left( \frac{\partial u_3}{\partial X_3} \right)^2 \right] \\ E_{12} &= \frac{1}{2} \left( \frac{\partial u_1}{\partial X_2} + \frac{\partial u_2}{\partial X_1} + \frac{\partial u_1}{\partial X_1} \frac{\partial u_1}{\partial X_2} + \frac{\partial u_2}{\partial X_1} \frac{\partial u_2}{\partial X_2} + \frac{\partial u_3}{\partial X_1} \frac{\partial u_3}{\partial X_2} \right) \\ E_{13} &= \frac{1}{2} \left( \frac{\partial u_1}{\partial X_3} + \frac{\partial u_3}{\partial X_1} + \frac{\partial u_1}{\partial X_1} \frac{\partial u_1}{\partial X_3} + \frac{\partial u_2}{\partial X_1} \frac{\partial u_2}{\partial X_3} + \frac{\partial u_3}{\partial X_1} \frac{\partial u_3}{\partial X_3} \right) \\ E_{23} &= \frac{1}{2} \left( \frac{\partial u_2}{\partial X_3} + \frac{\partial u_3}{\partial X_2} + \frac{\partial u_1}{\partial X_2} \frac{\partial u_1}{\partial X_3} + \frac{\partial u_2}{\partial X_2} \frac{\partial u_2}{\partial X_3} + \frac{\partial u_3}{\partial X_2} \frac{\partial u_3}{\partial X_3} \right) \end{aligned} \quad (9.2.18)$$

**Example 9.2.1**

Consider a rectangular block of dimensions  $a \times b \times h$ , where  $h$  is very small compared to  $a$  and  $b$  [5]. Suppose that the block is deformed into the diamond shape shown in Figure 9.2.2. By inspection, the geometry of the deformed body can be described as follows: let  $(X_1, X_2, X_3)$  denote the coordinates of a material point in the undeformed configuration. Thus the coordinate mapping and its inverse are given by

$$\begin{aligned} x_1 &= X_1 + \frac{e_0}{b} X_2, & X_1 &= \frac{ab}{ab - e_0^2} x_1 - \frac{ae_0}{ab - e_0^2} x_2 \\ x_2 &= X_2 + \frac{e_0}{a} X_1, & X_2 &= -\frac{be_0}{ab - e_0^2} x_1 + \frac{ab}{ab - e_0^2} x_2 \\ x_3 &= X_3, & X_3 &= x_3. \end{aligned}$$

Thus, the displacement components of a material point in the Lagrangian description are

$$u_1 = x_1 - X_1 = \frac{e_0}{b} X_2, \quad u_2 = x_2 - X_2 = \frac{e_0}{a} X_1, \quad u_3 = x_3 - X_3 = 0.$$

The only non-zero Green strain tensor components are given by

$$E_{11} = \frac{1}{2} \left( \frac{e_0}{a} \right)^2, \quad E_{12} = \frac{e_0}{2b} + \frac{e_0}{2a}, \quad E_{22} = \frac{1}{2} \left( \frac{e_0}{b} \right)^2.$$

The Almansi strain tensor components are

$$\begin{aligned} e_{11} &= -\frac{e_0^2}{ab - e_0^2} - \frac{1}{2} \left[ \frac{e_0^2(e_0^2 + b^2)}{(ab - e_0^2)^2} \right], \\ e_{12} &= \frac{e_0(a + b)}{(ab - e_0^2)} + \frac{e_0^3(a + b)}{(ab - e_0^2)^2}, \\ e_{22} &= -\frac{e_0^2}{ab - e_0^2} - \frac{1}{2} \left[ \frac{e_0^2(e_0^2 + a^2)}{(ab - e_0^2)^2} \right]. \end{aligned}$$

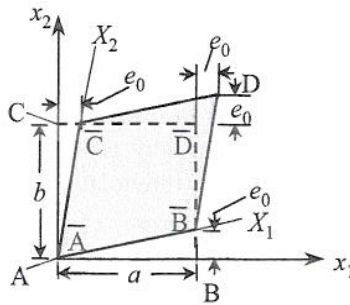


**Figure 9.2.2** Undeformed and deformed rectangular block.

### 9.2.3 Polar Decomposition

Recall that the deformation gradient tensor  $\mathbf{F}$  transforms a material vector  $d\mathbf{X}$  into the corresponding spatial vector  $d\mathbf{x}$ , and it forms an essential part of the definition of any strain measure. Another role of  $\mathbf{F}$  in connection with the strain measures is discussed with the help of the polar decomposition theorem of Cauchy, which enables  $\mathbf{F}$  to be written as [1-3]

$$\mathbf{F} = \mathbf{R} \cdot \mathbf{U} = \mathbf{V} \cdot \mathbf{R} \quad (9.2.19)$$

where  $\mathbf{R}$  is an orthogonal *rotation tensor* and  $\mathbf{U}$  and  $\mathbf{V}$  are symmetric *stretch tensors*. An orthogonal rotation tensor  $\mathbf{R}$  is one that satisfies  $\mathbf{R}^T \cdot \mathbf{R} = \mathbf{I}$ .

To evaluate the tensors  $\mathbf{R}$  and  $\mathbf{U}$ , we recall the definition of  $\mathbf{C}$ :

$$\mathbf{C} = \mathbf{F}^T \cdot \mathbf{F} = \mathbf{U}^T \cdot \mathbf{R}^T \cdot \mathbf{R} \cdot \mathbf{U} = \mathbf{U}^T \cdot \mathbf{U} \quad (9.2.20)$$

To compute  $\mathbf{U}$  using Eq. (9.2.20), it is necessary to write  $\mathbf{C}$  in terms of its eigenvalues and eigenvectors:

$$\mathbf{C} = \sum_{\alpha=1}^3 \lambda_{\alpha}^2 \hat{\mathbf{N}}_{\alpha} \hat{\mathbf{N}}_{\alpha} \quad (9.2.21)$$

where  $\lambda_{\alpha}^2$  are the eigenvalues and  $\hat{\mathbf{N}}_{\alpha}$  are the eigenvectors of  $\mathbf{C}$ . Then

$$\mathbf{U} = \sum_{\alpha=1}^3 \lambda_{\alpha} \hat{\mathbf{N}}_{\alpha} \hat{\mathbf{N}}_{\alpha} \quad (9.2.22)$$

and the rotation tensor  $\mathbf{R}$  can be obtained from Eq. (9.2.19) as  $\mathbf{R} = \mathbf{F} \cdot \mathbf{U}^{-1}$ .

### 9.2.4 Stress Tensors

The equations of motion or equilibrium must be derived for the deformed configuration of the structure at time  $t$ . However, since the geometry of the deformed configuration is not known, the equations must be written in terms of the known reference configuration. In doing so we introduce various measures of stress. They emerge in a natural way as we transform volumes and areas from the deformed configuration to undeformed configuration [1-3].

First we introduce the true stress, that is, stress in the deformed configuration. Consider a deformed body at its current position. If we denote by  $d\mathbf{f}(\hat{\mathbf{n}})$  the force on a small area  $\hat{\mathbf{n}} da$  located at the position  $\mathbf{x}$ , the *stress vector* can be defined as  $\mathbf{t}(\hat{\mathbf{n}}) = \frac{d\mathbf{f}}{da}$ . The *Cauchy stress tensor*  $\sigma$  is defined to be the *current force per unit deformed area*:

$$d\mathbf{f} = \mathbf{t} da = da \cdot \sigma, \quad \text{where } da = da \hat{\mathbf{n}} \quad (9.2.23a)$$

where Cauchy's formula,  $\mathbf{t} = \boldsymbol{\sigma} \cdot \hat{\mathbf{n}}$ , is used (see Problem 9.5).

To express  $d\mathbf{f}$  in terms of a stress times the initial undeformed area  $dA$  requires a new stress tensor  $\mathbf{P}$ ,

$$d\mathbf{f} = d\mathbf{A} \cdot \mathbf{P}, \quad \text{where } d\mathbf{A} = dA \hat{\mathbf{N}} \quad (9.2.23b)$$

where  $\hat{\mathbf{N}}$  is the unit normal to the undeformed area  $dA$ . The stress tensor  $\mathbf{P}$  is called the *first Piola-Kirchhoff stress tensor*, and it gives the *current force* per unit *undeformed area*. The first Piola-Kirchhoff stress tensor is not symmetric.

The *second Piola-Kirchhoff stress tensor*  $\mathbf{S}$ , which is used in the total Lagrangian formulation of geometrically nonlinear analysis, is introduced as follows. Recall from Eq. (9.2.3) that  $d\mathbf{X} = \mathbf{F}^{-1} \cdot d\mathbf{x}$ . Analogously, we can transform the force  $d\mathbf{f}$  on the deformed elemental area  $da$  to the force  $d\mathbf{F}$  on the undeformed elemental area  $d\mathbf{A}$  (not to be confused between the force  $d\mathbf{F}$  and deformation tensor  $\mathbf{F}$ )

$$d\mathbf{F} = \mathbf{F}^{-1} \cdot d\mathbf{f} = \mathbf{F}^{-1} \cdot (d\mathbf{A} \cdot \mathbf{P}) = d\mathbf{A} \cdot \mathbf{P} \cdot \mathbf{F}^{-T} \equiv d\mathbf{A} \cdot \mathbf{S} \quad (9.2.24)$$

Thus, the second Piola-Kirchhoff stress tensor gives the *transformed current force* per unit *undeformed area*. The second Piola-Kirchhoff stress tensor is symmetric whenever the Cauchy stress tensor is symmetric.

In summary, we have the following relationships between various stress measures ( $J$  denotes the determinant of  $\mathbf{F}$ ):

$$\mathbf{P} = J \mathbf{F}^{-1} \cdot \boldsymbol{\sigma} = \mathbf{S} \cdot \mathbf{F}^T \quad (9.2.25a)$$

$$\boldsymbol{\sigma} = \frac{1}{J} \mathbf{F} \cdot \mathbf{P} = \frac{1}{J} \mathbf{F} \cdot \mathbf{S} \cdot \mathbf{F}^T \quad (9.2.25b)$$

$$\mathbf{S} = J \mathbf{F}^{-1} \cdot \boldsymbol{\sigma} \cdot \mathbf{F}^{-T} = \mathbf{P} \cdot \mathbf{F}^{-T} \quad (9.2.25c)$$

### 9.2.5 Energetically-Conjugate Stresses and Strains

The rate of internal work done (power) in a continuous medium in the current configuration can be expressed as (see [3])

$$W = \frac{1}{2} \int_v \boldsymbol{\sigma} : \mathbf{d} \, dv \quad (9.2.26)$$

where  $\boldsymbol{\sigma}$  is the Cauchy stress tensor and  $\mathbf{d}$  is the symmetric part of the *velocity gradient tensor*

$$\mathbf{d} = \frac{1}{2} [(\nabla \mathbf{v})^T + \nabla \mathbf{v}], \quad \mathbf{v} = \frac{d\mathbf{x}}{dt} \quad (9.2.27)$$

The pair  $(\sigma, \mathbf{d})$  is said to be *energetically-conjugate* since it produces the (strain) energy stored in the deformable medium. We can show that the second Piola-Kirchhoff stress tensor  $\mathbf{S}$  is energetically-conjugate to the rate of Green-Lagrange strain tensor  $\dot{\mathbf{E}}$ :

$$W = \frac{1}{2} \int_V \mathbf{S} : \dot{\mathbf{E}} \, dV \quad (9.2.28)$$

The proof of the above statement requires the use of a number of identities [3], which are presented next.

The first one is a relation between the *rate of deformation gradient tensor*  $\dot{\mathbf{F}}$  and  $\nabla_0 \mathbf{v}$ . We have

$$\dot{\mathbf{F}} \equiv \frac{d\mathbf{F}}{dt} = \frac{d}{dt} \left( \frac{\partial \mathbf{x}}{\partial \mathbf{X}} \right)^T = \left[ \frac{\partial}{\partial \mathbf{X}} \left( \frac{d\mathbf{x}}{dt} \right) \right]^T = \left( \frac{\partial \mathbf{v}}{\partial \mathbf{X}} \right)^T = (\nabla_0 \mathbf{v})^T, \quad \frac{d\mathbf{x}}{dt} = \mathbf{v} \quad (9.2.29)$$

Next, we note that

$$\dot{\mathbf{F}} = \left( \frac{\partial \mathbf{v}}{\partial \mathbf{X}} \right)^T = \left( \frac{\partial \mathbf{v}}{\partial \mathbf{x}} \right)^T \cdot \left( \frac{\partial \mathbf{x}}{\partial \mathbf{X}} \right)^T = \mathbf{L} \cdot \mathbf{F}, \quad \mathbf{L} \equiv \left( \frac{\partial \mathbf{v}}{\partial \mathbf{x}} \right)^T = \dot{\mathbf{F}} \cdot \mathbf{F}^{-1} \quad (9.2.30)$$

where  $\mathbf{L}$  is the *velocity gradient tensor*.

The time derivative of the Lagrangian strain tensor,  $\dot{\mathbf{E}}$ , is known as the *material strain rate tensor*. We have

$$\dot{\mathbf{E}} \equiv \frac{d\mathbf{E}}{dt} = \frac{1}{2} \frac{d}{dt} (\mathbf{F}^T \cdot \mathbf{F} - \mathbf{I}) = \frac{1}{2} (\dot{\mathbf{F}}^T \cdot \mathbf{F} + \mathbf{F}^T \cdot \dot{\mathbf{F}}) \quad (9.2.31)$$

The symmetric part of the velocity gradient tensor can be related to the strain rate tensor

$$\begin{aligned} \mathbf{d} &= \frac{1}{2} (\mathbf{L}^T + \mathbf{L}) \\ &= \frac{1}{2} \left[ \left( \dot{\mathbf{F}} \cdot \mathbf{F}^{-1} \right)^T + \dot{\mathbf{F}} \cdot \mathbf{F}^{-1} \right] = \frac{1}{2} (\mathbf{F}^{-T} \cdot \dot{\mathbf{F}}^T + \dot{\mathbf{F}} \cdot \mathbf{F}^{-1}) \\ &= \frac{1}{2} \mathbf{F}^{-T} \cdot (\dot{\mathbf{F}}^T + \mathbf{F}^T \cdot \dot{\mathbf{F}} \cdot \mathbf{F}^{-1}) \\ &= \frac{1}{2} \mathbf{F}^{-T} \cdot (\dot{\mathbf{F}}^T \cdot \mathbf{F} + \mathbf{F}^T \cdot \dot{\mathbf{F}}) \cdot \mathbf{F}^{-1} \\ &= \mathbf{F}^{-T} \cdot \dot{\mathbf{E}} \cdot \mathbf{F}^{-1} \end{aligned} \quad (9.2.32)$$

Now returning to Eq. (9.2.26) for the rate of work done, we have

$$\frac{1}{2} \int_v \sigma : \mathbf{d} \, dv = \frac{1}{2} \int_v \sigma : \mathbf{L} \, dv \quad (\text{by symmetry of } \sigma \text{ and } \mathbf{d})$$



$$\begin{aligned}
&= \frac{1}{2} \int_V J \sigma : (\dot{\mathbf{F}} \cdot \mathbf{F}^{-1}) dV \quad [\text{by Eq. (9.2.30)}] \\
&= \frac{1}{2} \int_V J (\sigma_{ij} \hat{\mathbf{e}}_i \hat{\mathbf{e}}_j) : \left[ (\dot{F}_{pI} \hat{\mathbf{e}}_p \hat{\mathbf{E}}_I) \cdot ((\mathbf{F}^{-1})_{Jq} \hat{\mathbf{E}}_J \hat{\mathbf{e}}_q) \right] dV \\
&= \frac{1}{2} \int_V J \sigma_{ij} \dot{F}_{jI} (\mathbf{F}^{-1})_{Ii} dV = \frac{1}{2} \int_V J \sigma_{ji} \dot{F}_{jI} (\mathbf{F}^{-1})_{Ii} dV \quad (\text{since } \sigma_{ij} = \sigma_{ji}) \\
&= \frac{1}{2} \int_V J \sigma_{ij} \dot{F}_{iI} (\mathbf{F}^{-1})_{Ij} dV \quad (\text{by renaming } i \text{ to be } j \text{ and } j \text{ to be } i) \\
&= \frac{1}{2} \int_V J \left[ ((\mathbf{F}^{-1})_{Iq} \hat{\mathbf{E}}_I \hat{\mathbf{e}}_q) \cdot (\sigma_{ij} \hat{\mathbf{e}}_i \hat{\mathbf{e}}_j) \right] : (\dot{F}_{pJ} \hat{\mathbf{e}}_p \hat{\mathbf{E}}_J) dV \\
&= \frac{1}{2} \int_V (J \mathbf{F}^{-1} \cdot \sigma) : \dot{\mathbf{F}} dV = \frac{1}{2} \int_V \mathbf{P} : \dot{\mathbf{F}} dV \tag{9.2.33}
\end{aligned}$$

Thus, the first Piola–Kirchhoff stress tensor  $\mathbf{P}$  is work conjugate to the rate of the deformation gradient tensor  $\dot{\mathbf{F}}$ . Similarly,

$$\begin{aligned}
&\frac{1}{2} \int_v \sigma : \mathbf{d} dv \\
&= \frac{1}{2} \int_V J \sigma : (\mathbf{F}^{-T} \cdot \dot{\mathbf{E}} \cdot \mathbf{F}^{-1}) dV \quad [\text{using Eq. (9.2.32)}] \\
&= \frac{1}{2} \int_V J (\sigma_{ij} \hat{\mathbf{e}}_i \hat{\mathbf{e}}_j) : \left( (\mathbf{F}^{-1})_{Ip} \hat{\mathbf{e}}_p \dot{E}_{IJ} (\mathbf{F}^{-1})_{Jq} \hat{\mathbf{e}}_q \right) dV \\
&= \frac{1}{2} \int_V J \left( (\mathbf{F}^{-1})_{Ii} \sigma_{ij} (\mathbf{F}^{-1})_{Jj} \right) \dot{E}_{IJ} dV \quad (E_{IJ} = E_{JI}) \\
&= \frac{1}{2} \int_V J \left( (\mathbf{F}^{-1})_{Ii} \sigma_{ij} (\mathbf{F}^{-1})_{Jj} \right) \dot{E}_{JI} dV \\
&= \frac{1}{2} \int_V J \left[ \left( (\mathbf{F}^{-1})_{Ip} \hat{\mathbf{E}}_I \hat{\mathbf{e}}_p \right) \cdot (\sigma_{ij} \hat{\mathbf{e}}_i \hat{\mathbf{e}}_j) \cdot \left( (\mathbf{F}^{-1})_{Jq} \hat{\mathbf{E}}_J \hat{\mathbf{e}}_q \right)^T \right] : (\dot{E}_{PQ} \hat{\mathbf{E}}_P \hat{\mathbf{E}}_Q) dV \\
&= \frac{1}{2} \int_V J (\mathbf{F}^{-1} \cdot \sigma \cdot \mathbf{F}^{-T}) : \dot{\mathbf{E}} dV = \frac{1}{2} \int_V \mathbf{S} : \dot{\mathbf{E}} dV \tag{9.2.34}
\end{aligned}$$

Thus, the second Piola–Kirchhoff stress tensor  $\mathbf{S}$  is work conjugate to the rate of the Green–Lagrangian strain tensor  $\dot{\mathbf{E}}$ .

## 9.3 Strain and Stress Measures Between Configurations

### 9.3.1 Notation

The determination of the final configuration of a solid body undergoing large deformation is not an easy task. A practical way of determining the final configuration  $\mathcal{C}$  from a known initial configuration  $\mathcal{C}_0$  is to assume that the total load is applied in increments so that the body occupies several intermediate configurations,  $\mathcal{C}_i$  ( $i = 1, 2, \dots$ ), prior to occupying the final configuration.

The magnitude of load increments should be such that the computation method used is capable of predicting the deformed configuration at each load step. In the determination of an intermediate configuration  $C_i$ , the Lagrangian description of motion can use any of the previously known configurations  $C_1, \dots, C_{i-1}$  as the reference configuration  $C_R$ . If the initial configuration is used as the reference configuration with respect to which all quantities are measured, it is called the *total Lagrangian description*. If the latest known configuration  $C_{i-1}$  is used as the reference configuration, it is called the *updated Lagrangian description*.

Here we introduce the notation used for positions, displacements, strain stresses, etc. in the rest of this chapter. We consider three equilibrium configurations of the body, namely,  $C_0$ ,  $C_1$ , and  $C_2$ , which correspond to three different loads. As shown in Figure 9.3.1, the three configurations of the body can be thought of as the initial undeformed configuration  $C_0$ , the last known deformed configuration  $C_1$ , and the current deformed configuration  $C_2$  to be determined. It is assumed that all variables, such as the displacements, strains, and stresses are known up to the  $C_1$  configuration. We wish to develop a formulation for determining the displacement field of the body in the current deformed configuration  $C_2$ . It is assumed that the deformation of the body from  $C_1$  to  $C_2$  due to an increment in the load is small, and the accumulated deformation of the body from  $C_0$  to  $C_1$  can be arbitrarily large but continuous (i.e. neighborhoods move into neighborhoods).

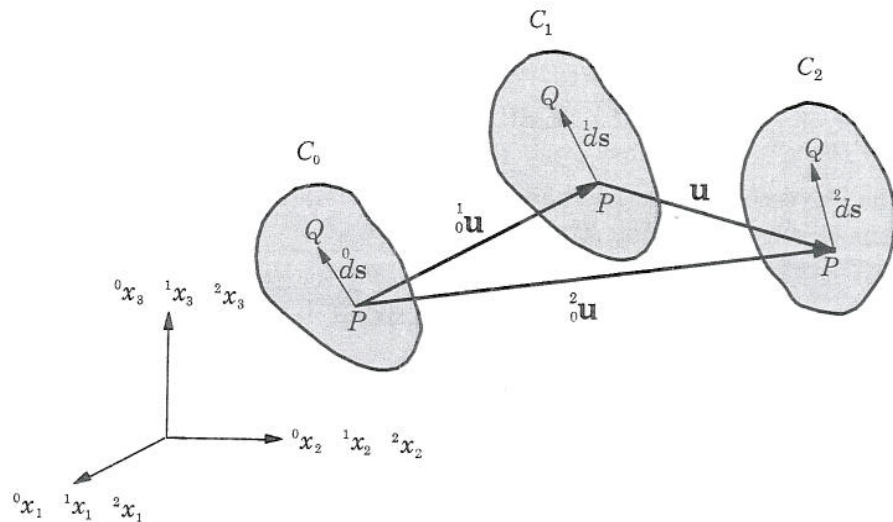


Figure 9.3.1 Initial and two consecutive configurations of a body.

The following notation is adopted in the present study (see Bathe [4]). A left *superscript* on a quantity denotes the configuration in which the quantity occurs, and a left *subscript* denotes the configuration with respect to which the quantity is *measured*. Thus  ${}^i_j Q$  indicates that the quantity  $Q$  occurs in configuration  $\mathcal{C}_i$  but measured in configuration  $\mathcal{C}_j$ . When the quantity under consideration is measured in the same configuration in which it occurs, the left subscript may not be used. The left superscript will be omitted on incremental quantities that occur between configurations  $\mathcal{C}_1$  and  $\mathcal{C}_2$ . Of course, right subscript(s) refer to components in rectangular Cartesian coordinate systems, as will be clear in the context of the discussion. Although somewhat cumbersome, the notation conveys the meaning more directly.

Since we are dealing with three different configurations, it is necessary to introduce the following symbols in the three configurations [4,25]:

configuration:	$\mathcal{C}_0$	$\mathcal{C}_1$	$\mathcal{C}_2$	
coordinates of a point:	${}^0\mathbf{x}$	${}^1\mathbf{x}$	${}^2\mathbf{x}$	
volumes:	${}^0V$	${}^1V$	${}^2V$	
areas:	${}^0A$	${}^1A$ ,	${}^2A$	(9.3.1)
density:	${}^0\rho$	${}^1\rho$	${}^2\rho$	
total displacements of a point:		${}^1_0\mathbf{u}$	${}^2_0\mathbf{u}$	

We use a rectangular Cartesian coordinate system to formulate the equations. We rewrite the equations presented earlier in a form suitable for the current study. When the body deforms under the action of external forces, a particle  $X$  occupying the position  ${}^0\mathbf{x} = ({}^0x_1, {}^0x_2, {}^0x_3) = (X_1, X_2, X_3)$  in configuration  $\mathcal{C}_0$  moves to a new position  ${}^1\mathbf{x} = ({}^1x_1, {}^1x_2, {}^1x_3)$  in configuration  $\mathcal{C}_1$  and position  ${}^2\mathbf{x} = ({}^2x_1, {}^2x_2, {}^2x_3)$  in configuration  $\mathcal{C}_2$ . The total displacements of the particle  $X$  in the two configurations  $\mathcal{C}_1$  and  $\mathcal{C}_2$  can be written as

$${}^1_0\mathbf{u} = {}^1\mathbf{x} - {}^0\mathbf{x} \quad \text{or} \quad {}^1_0u_i = {}^1x_i - {}^0x_i \quad (i = 1, 2, 3) \quad (9.3.2)$$

$${}^2_0\mathbf{u} = {}^2\mathbf{x} - {}^0\mathbf{x} \quad \text{or} \quad {}^2_0u_i = {}^2x_i - {}^0x_i \quad (i = 1, 2, 3) \quad (9.3.3)$$

and the displacement increment of the point from  $\mathcal{C}_1$  to  $\mathcal{C}_2$  is

$$\mathbf{u} = {}^2_0\mathbf{u} - {}^1_0\mathbf{u} \quad \text{or} \quad u_i = {}^2_0u_i - {}^1_0u_i \quad (i = 1, 2, 3) \quad (9.3.4)$$

### 9.3.2 Conservation of Mass

The relations among the mass densities  ${}^0\rho$ ,  ${}^1\rho$ , and  ${}^2\rho$  of materials in configurations  $\mathcal{C}_0$ ,  $\mathcal{C}_1$ , and  $\mathcal{C}_2$ , respectively, can be established using the

principle of conservation of mass. The principle requires that the mass of a material body be conserved in moving through different configurations

$$\int_{2V} {}^2\rho \, d^2V = \int_{1V} {}^1\rho \, d^1V = \int_{0V} {}^0\rho \, d^0V \quad (9.3.5)$$

where  ${}^iV$  is the volume of the body when it occupies the configuration  $C_i$ . By a change of coordinates of integration from  ${}^2x_i$  to  ${}^0x_i$ , we have

$$\int_{2V} {}^2\rho \, d^2V = \int_{0V} {}^2\rho {}^2_0J \, d^0V \quad (9.3.6)$$

where  ${}^2_0J$  is the determinant of the deformation gradient tensor  ${}^2_0\mathbf{F}$  (or the *Jacobian* of the transformation)

$${}^2_0J = \det({}^2_0\mathbf{F}) = \left| \frac{\partial^2 x_i}{\partial^0 x_j} \right| = \begin{vmatrix} \frac{\partial^2 x_1}{\partial^0 x_1} & \frac{\partial^2 x_1}{\partial^0 x_2} & \frac{\partial^2 x_1}{\partial^0 x_3} \\ \frac{\partial^2 x_2}{\partial^0 x_1} & \frac{\partial^2 x_2}{\partial^0 x_2} & \frac{\partial^2 x_2}{\partial^0 x_3} \\ \frac{\partial^2 x_3}{\partial^0 x_1} & \frac{\partial^2 x_3}{\partial^0 x_2} & \frac{\partial^2 x_3}{\partial^0 x_3} \end{vmatrix} \quad (9.3.7)$$

Equation (9.3.5) implies, in view of Eq. (9.3.6), that

$${}^0\rho = {}^2\rho {}^2_0J \quad (9.3.8)$$

Similarly, we have

$${}^1\rho = {}^2\rho {}^2_1J \quad (9.3.9)$$

### 9.3.3 Green Strain Tensors for Various Configurations

The Cartesian components of the *Green-Lagrange strain tensors*,  ${}^1_0E_{ij}$  and  ${}^2_0E_{ij}$ , in the two configurations  $C_1$  and  $C_2$  are defined by

$${}^1_0E_{ij} = \frac{1}{2} \left( \frac{\partial^1 x_k}{\partial^0 x_i} \frac{\partial^1 x_k}{\partial^0 x_j} - \delta_{ij} \right) \quad (9.3.10)$$

$${}^2_0E_{ij} = \frac{1}{2} \left( \frac{\partial^2 x_k}{\partial^0 x_i} \frac{\partial^2 x_k}{\partial^0 x_j} - \delta_{ij} \right) \quad (9.3.11)$$

The strain components in Eqs. (9.3.10) and (9.3.11) can be expressed in terms of the displacement components  ${}^1_0u_i$  and  ${}^2_0u_i$ . First, using Eqs. (9.3.2) and (9.3.3), we can write

$$\frac{\partial^1 x_k}{\partial^0 x_i} = \frac{\partial^1_0 u_k}{\partial^0 x_i} + \delta_{ki}, \quad \frac{\partial^2 x_k}{\partial^0 x_i} = \frac{\partial^2_0 u_k}{\partial^0 x_i} + \delta_{ki} \quad (9.3.12)$$

Note that  ${}^0x_i = X_i$ . Substituting into Eqs. (9.3.10) and (9.3.11), we obtain

$${}^1_0E_{ij} = \frac{1}{2} \left( \frac{\partial {}^1_0u_i}{\partial {}^0x_j} + \frac{\partial {}^1_0u_j}{\partial {}^0x_i} + \frac{\partial {}^1_0u_k}{\partial {}^0x_i} \frac{\partial {}^1_0u_k}{\partial {}^0x_j} \right) \quad (9.3.13)$$

$${}^2_0E_{ij} = \frac{1}{2} \left( \frac{\partial {}^2_0u_i}{\partial {}^0x_j} + \frac{\partial {}^2_0u_j}{\partial {}^0x_i} + \frac{\partial {}^2_0u_k}{\partial {}^0x_i} \frac{\partial {}^2_0u_k}{\partial {}^0x_j} \right) \quad (9.3.14)$$

### Green-Lagrange Incremental Strain Tensor

It is useful in the sequel to define the incremental strain components  ${}^0\varepsilon_{ij}$ , that is, strains induced in moving from configuration  $\mathcal{C}_1$  to configuration  $\mathcal{C}_2$ . The Green-Lagrange strain increment tensor is defined as

$$\begin{aligned} 2 {}^0\varepsilon_{ij} d^0x_i d^0x_j &= ({}^2ds)^2 - ({}^1ds)^2 \\ &= [({}^2ds)^2 - ({}^0ds)^2] - [({}^1ds)^2 - ({}^0ds)^2] \\ &= 2 \left( {}^2_0E_{ij} - {}^1_0E_{ij} \right) d^0x_i d^0x_j \end{aligned} \quad (9.3.15)$$

$$\equiv 2 ({}^0e_{ij} + {}^0\eta_{ij}) d^0x_i d^0x_j \quad (9.3.16)$$

where  ${}^0e_{ij}$  are linear components of strain increment tensor

$${}^0e_{ij} = \frac{1}{2} \left( \frac{\partial u_i}{\partial x_j} + \frac{\partial u_j}{\partial x_i} + \frac{\partial u_k}{\partial x_i} \frac{\partial u_k}{\partial x_j} + \frac{\partial u_k}{\partial x_i} \frac{\partial u_k}{\partial x_j} \right) \quad (9.3.17)$$

and  ${}^0\eta_{ij}$  are the nonlinear components

$${}^0\eta_{ij} = \frac{1}{2} \frac{\partial u_k}{\partial x_i} \frac{\partial u_k}{\partial x_j} \quad (9.3.18)$$

The linearity of  ${}^0e_{ij}$  and nonlinearity of  ${}^0\eta_{ij}$  is understood to be in terms of the incremental displacement components  $u_i$ .

For geometrically linear analysis, that is, when strains are infinitesimal, only two configurations  $\mathcal{C}_1 = \mathcal{C}_0$  and  $\mathcal{C}_2$  are involved,  ${}^1u_i = 0$ ,  ${}^2u_i = u_i$ , and  $u_{i,k}$  are small enough to neglect their products. Consequently, the linear components of strain increment tensor  ${}^0e_{ij}$  become the same as the components of the Green-Lagrange strain tensor  ${}^2_0E_{ij}$ , and both reduce to the *infinitesimal strain components*

$${}^0e_{ij} = \frac{1}{2} \left( \frac{\partial u_i}{\partial x_j} + \frac{\partial u_j}{\partial x_i} \right) \quad (9.3.19)$$

*Updated Green-Lagrange Strain Tensor*

The Green-Lagrange strain tensor  ${}^2_0E_{ij}$  introduced earlier is useful in the total Lagrangian formulation. With the updated Lagrangian formulation in mind we define the components of Green-Lagrange strain tensor with respect to configuration  $\mathcal{C}_1$ . Such a strain tensor, denoted as  ${}^2_1\varepsilon_{ij}$ , is called the *updated Green-Lagrange strain tensor*. It is defined by

$$2({}^2_1\varepsilon_{ij})d^1x_i d^1x_j = ({}^2ds)^2 - ({}^1ds)^2 \quad (9.3.20)$$

Using (note that all are first-order derivatives)

$$d^2x_i = \frac{\partial^2x_i}{\partial^1x_j} d^1x_j, \quad ({}^2ds)^2 = \frac{\partial^2x_k}{\partial^1x_i} \frac{\partial^2x_k}{\partial^1x_j} d^1x_i d^1x_j \quad (9.3.21)$$

$$u_i = {}^2x_i - {}^1x_i, \quad \frac{\partial^2x_k}{\partial^1x_i} = \frac{\partial u_k}{\partial^1x_i} + \delta_{ki} \quad (9.3.22)$$

we can write

$$\begin{aligned} {}^2_1\varepsilon_{ij} &= \frac{1}{2} \left( \frac{\partial^2x_k}{\partial^1x_i} \frac{\partial^2x_k}{\partial^1x_j} - \delta_{ij} \right) \\ &= \frac{1}{2} \left( \frac{\partial u_i}{\partial^1x_j} + \frac{\partial u_j}{\partial^1x_i} + \frac{\partial u_k}{\partial^1x_i} \frac{\partial u_k}{\partial^1x_j} \right) \end{aligned} \quad (9.3.23)$$

$$\equiv {}^1e_{ij} + {}^1\eta_{ij} \quad (9.3.24)$$

where

$${}^1e_{ij} = \frac{1}{2} \left( \frac{\partial u_i}{\partial^1x_j} + \frac{\partial u_j}{\partial^1x_i} \right), \quad {}^1\eta_{ij} = \frac{1}{2} \left( \frac{\partial u_k}{\partial^1x_i} \frac{\partial u_k}{\partial^1x_j} \right) \quad (9.3.25)$$

Note that the definition of  ${}^2_1\varepsilon_{ij}$  involves the components of the displacement increment vector  $\mathbf{u}$ . Therefore,  ${}^2_1\varepsilon_{ij}$  are also called the *updated Green-Lagrange strain increment components*.

**9.3.4 Euler Strain Tensor**

Suppose that a body occupying the undeformed configuration  $\mathcal{C}_0$  takes a number of intermediate configurations before occupying the deformed configuration  $\mathcal{C}_1$ , and we wish to determine the next configuration  $\mathcal{C}_2$  in a single incremental step. Although the accumulated displacements  ${}^1u_i$  of the body from configuration  $\mathcal{C}_0$  to configuration  $\mathcal{C}_1$  can be large, the incremental displacements  $u_i$  within the incremental step from  $\mathcal{C}_1$  to  $\mathcal{C}_2$  are assumed to be small. Hence, we may refer the strains to configuration  $\mathcal{C}_2$ . The

strains occurring in the body at configuration  $\mathcal{C}_2$  and measured in the same configuration are defined by

$${}^1_1\varepsilon_{ij} d^1x_i d^1x_j = ({}^1ds)^2 - ({}^0ds)^2 \quad (9.3.26)$$

$${}^2_2\varepsilon_{ij} d^2x_i d^2x_j = ({}^2ds)^2 - ({}^1ds)^2 \quad (9.3.27a)$$

$$= \left( \delta_{ij} - \frac{\partial^1x_k}{\partial^2x_i} \frac{\partial^1x_k}{\partial^2x_j} \right) d^2x_i d^2x_j \quad (9.3.27b)$$

These strains are called the *Euler strain tensor components*. Using

$${}^1x_k = {}^2x_k - u_k, \quad \frac{\partial^1x_k}{\partial^2x_j} = \delta_{kj} - \frac{\partial u_k}{\partial^2x_j} \quad (9.3.28)$$

we obtain ( ${}^2_2\varepsilon_{ij} \equiv {}^2\varepsilon_{ij}$ )

$${}^2\varepsilon_{ij} = \frac{1}{2} \left( \frac{\partial u_i}{\partial^2x_j} + \frac{\partial u_j}{\partial^2x_i} - \frac{\partial u_k}{\partial^2x_i} \frac{\partial u_k}{\partial^2x_j} \right) \quad (9.3.29)$$

The linear part of the Euler strain tensor  ${}^2\varepsilon_{ij}$  is called the infinitesimal strain tensor and denoted  ${}^2e_{ij}$

$${}^2e_{ij} = \frac{1}{2} \left( \frac{\partial u_i}{\partial^2x_j} + \frac{\partial u_j}{\partial^2x_i} \right) \quad (9.3.30)$$

which is identical in form to the infinitesimal strain tensor  ${}^0e_{ij}$  given in Eq. (9.3.19), except that the reference configuration is changed to  $\mathcal{C}_2$ . These strain components are energetically-conjugate to the Cauchy stress components.

### 9.3.5 Relationships Between Various Stress Tensors

The Cauchy stress components  $\sigma_{ij}$  in configurations  $\mathcal{C}_1$  and  $\mathcal{C}_2$  are denoted by

$${}^1\sigma_{ij} = \frac{1}{1}\sigma_{ij}, \quad {}^2\sigma_{ij} = \frac{2}{2}\sigma_{ij} \quad (9.3.31)$$

The Cauchy stress components  ${}^1\sigma_{ij}$ , for example, can be depicted in the configuration  $\mathcal{C}_1$  by selecting a rectangular parallelepiped with faces parallel to the  ${}^1x_1 - {}^1x_2$ ,  ${}^1x_2 - {}^1x_3$ ,  ${}^1x_3 - {}^1x_1$  planes – much the same way as in small strain formulations.

Recall that the second Piola–Kirchhoff stress tensor characterizes the current force in  $\mathcal{C}_2$  but transformed to  $\mathcal{C}_0$  and measured per unit area in  $\mathcal{C}_0$ :

$$({}^0\hat{\mathbf{n}} \cdot \mathbf{S})d^0A = d^0\mathbf{f} \quad (9.3.32)$$

where  ${}^0\hat{\mathbf{n}}$  denotes the unit normal to the area element  $d^0A$  in  $\mathcal{C}_0$ . The force  $d^0\mathbf{f}$  is related to the force  $d^2\mathbf{f}$  by

$$d^0\mathbf{f} = {}^2_0\mathbf{F}^{-1} \cdot d^2\mathbf{f}, \quad {}^2_0\mathbf{F} = \frac{\partial^2\mathbf{x}}{\partial^0\mathbf{x}} \quad (9.3.33)$$

where  ${}^2_0\mathbf{F}$  is the deformation gradient tensor between configurations  $\mathcal{C}_0$  and  $\mathcal{C}_2$ .

It is useful in the updated Lagrangian formulation to define another kind of stress tensor called the *updated Kirchhoff stress tensor*. Consider the infinitesimal rectangular parallelepiped containing the point P in configuration  $\mathcal{C}_1$  enclosed by the six surfaces

$${}^1x_i = \text{const.}, \quad {}^1x_i + d^1x_i = \text{const.} \quad (i = 1, 2, 3) \quad (9.3.34)$$

The Cauchy stress components on this rectangular parallelepiped are  ${}^1\sigma_{ij}$ . As the body deforms from configuration  $\mathcal{C}_1$  to  $\mathcal{C}_2$ , this rectangular parallelepiped will deform into, in general, a non-rectangular parallelepiped. Using the configuration  $\mathcal{C}_1$  as the reference, we can define the updated Kirchhoff stress components  ${}^2_1S_{ij}$  as the internal forces per unit area acting along the normal and two tangential directions of each of the side surfaces of the parallelepiped in the  $\mathcal{C}_2$  configuration. The updated Kirchhoff stresses  ${}^2_1S_{ij}$  can be decomposed as

$${}^2_1S_{ij} = {}^1\sigma_{ij} + {}^1S_{ij} \quad (9.3.35)$$

where  ${}^1\sigma_{ij} = {}^1_1S_{ij}$  are the Cauchy stress components in  $\mathcal{C}_1$  configuration and  ${}^1S_{ij}$  are the *updated Kirchhoff stress increment tensor* components.

The second Piola-Kirchhoff stress tensor components in the  $\mathcal{C}_1$  and  $\mathcal{C}_2$  configurations are denoted by  ${}^1_0S_{ij}$  and  ${}^2_0S_{ij}$ , respectively. The components in the two configurations are related by

$${}^2_0S_{ij} = {}^1_0S_{ij} + {}^0S_{ij} \quad (9.3.36)$$

where  ${}^0S_{ij}$  are the components of the *Kirchhoff stress increment tensor*.

Recall from Eqs. (9.2.25a,b) that the stress tensors  ${}^2\sigma$  and  ${}^2_0\mathbf{S}$  are related by

$${}^2\sigma = ({}^2_0J)^{-1} \mathbf{F} \cdot {}^2_0\mathbf{S} \cdot \mathbf{F}^T, \quad {}^2\sigma_{ij} = ({}^2_0J)^{-1} \left( \frac{\partial^2x_i}{\partial^0x_m} \right) {}^2_0S_{mn} \left( \frac{\partial^2x_j}{\partial^0x_n} \right) \quad (9.3.37)$$

$${}^2_0\mathbf{S} = {}^2_0J \mathbf{F}^{-1} \cdot {}^2\sigma \cdot \mathbf{F}^{-T}, \quad {}^2_0S_{ij} = {}^2_0J \left( \frac{\partial^0x_i}{\partial^2x_m} \right) {}^2\sigma_{mn} \left( \frac{\partial^0x_j}{\partial^2x_n} \right) \quad (9.3.38)$$

where  ${}^2_0J$  is the determinant of  ${}^2_0\mathbf{F}$ .



The relations between the Cauchy stress tensor components  ${}^2\sigma_{ij}$  and the second Piola–Kirchhoff stress tensor components  ${}^2S_{ij}$  can also be written as [ ${}^0\rho = {}^2\rho {}^2J$ ; see Eq. (9.3.8)]

$${}^2\sigma_{ij} = \frac{{}^2\rho}{{}^0\rho} \frac{\partial^2 x_i}{\partial^0 x_p} \frac{\partial^2 x_j}{\partial^0 x_q} {}^2S_{pq} \quad (9.3.39)$$

$${}^2S_{ij} = \frac{{}^0\rho}{{}^2\rho} \frac{\partial^0 x_i}{\partial^2 x_p} \frac{\partial^0 x_j}{\partial^2 x_q} {}^2\sigma_{pq} \quad (9.3.40)$$

where  ${}^0\rho$  and  ${}^2\rho$  represent the mass densities of the material in configurations  $\mathcal{C}_0$  and  $\mathcal{C}_2$ , respectively.

The Cauchy stress tensor components  ${}^2\sigma_{ij}$  in  $\mathcal{C}_2$  can be related to the updated Kirchhoff stress tensor components  ${}^2_1S_{ij}$  by the following formulae:

$${}^2_1S_{ij} = \frac{{}^1\rho}{{}^2\rho} \frac{\partial^1 x_i}{\partial^2 x_p} \frac{\partial^1 x_j}{\partial^2 x_q} {}^2\sigma_{pq} \quad (9.3.41)$$

$${}^2\sigma_{ij} = \frac{{}^2\rho}{{}^1\rho} \frac{\partial^2 x_i}{\partial^1 x_p} \frac{\partial^2 x_j}{\partial^1 x_q} {}^2_1S_{pq} \quad (9.3.42)$$

The transformation between the second Piola–Kirchhoff stress tensor components in different reference configurations is provided by the following relations:

$${}^2_0S_{ij} = \frac{{}^0\rho}{{}^1\rho} \frac{\partial^0 x_i}{\partial^1 x_p} \frac{\partial^0 x_j}{\partial^1 x_q} {}^2_1S_{pq} \quad (9.3.43)$$

$${}^1_0S_{ij} = \frac{{}^0\rho}{{}^1\rho} \frac{\partial^0 x_i}{\partial^1 x_p} \frac{\partial^0 x_j}{\partial^1 x_q} {}^1\sigma_{pq} \quad (9.3.44)$$

Finally, from Eqs. (9.3.43) and (9.3.44), we obtain the relations between the incremental stresses  ${}^0S_{ij}$  and  ${}^1S_{pq}$ :

$${}^0S_{ij} = \frac{{}^0\rho}{{}^1\rho} \frac{\partial^0 x_i}{\partial^1 x_p} \frac{\partial^0 x_j}{\partial^1 x_q} {}^1S_{pq} \quad (9.3.45)$$

$${}^1S_{ij} = \frac{{}^1\rho}{{}^0\rho} \frac{\partial^1 x_i}{\partial^0 x_p} \frac{\partial^1 x_j}{\partial^0 x_q} {}^0S_{pq} \quad (9.3.46)$$

These relations are useful in the calculation of the material coefficients for large strain problems in the updated Lagrangian formulation, as will be seen shortly.

## 9.4 Constitutive Equations

Materials for which the constitutive behavior is only a function of the current state of deformation are known as *elastic*. In the special case in which the work done by the stresses during a deformation is dependent only on the initial state and the current configuration, the material is called *hyperelastic*. For hyperelastic materials we assume that there exists a stored strain energy function,  $U_0$  per unit undeformed volume, such that the components of the *material elasticity tensor*  $\mathbf{C}$  are given by

$$C_{ijkl} = \frac{\partial S_{ij}}{\partial E_{kl}} \quad (9.4.1)$$

In the derivation of finite element models of incremental nonlinear analysis of solid continua, it is necessary to specify the stress-strain relations in incremental form. In the total Lagrangian formulation, for example, the constitutive relations can be expressed in terms of the Kirchhoff stress increment tensor components  ${}_0S_{ij}$  and Green-Lagrange strain increment tensor components  ${}_0\varepsilon_{ij}$  as

$${}_0S_{ij} = {}_0C_{ijkl} {}_0\varepsilon_{kl} \quad (9.4.2)$$

In the updated Lagrangian formulation, it can be expressed in terms of the updated Kirchhoff stress increment tensor components  ${}_1S_{ij}$  and updated Green-Lagrange strain increment tensor components  ${}_1\varepsilon_{ij}$ :

$${}_1S_{ij} = {}_1C_{ijkl} {}_1\varepsilon_{kl} \quad (9.4.3)$$

where  ${}_0C_{ijkl}$  and  ${}_1C_{ijkl}$  denote the incremental constitutive tensors with respect to the configurations  $\mathcal{C}_0$  and  $\mathcal{C}_1$ , respectively. It can be shown that the following transformation rules hold between the components of the elasticity tensor  $\mathbf{C}$  in different configurations:

$${}_0C_{ijkl} = \frac{{}_0\rho}{{}_1\rho} \frac{\partial {}^0x_i}{\partial {}^1x_p} \frac{\partial {}^0x_j}{\partial {}^1x_q} \frac{\partial {}^0x_k}{\partial {}^1x_r} \frac{\partial {}^0x_l}{\partial {}^1x_s} {}_1C_{pqrs} \quad (9.4.4)$$

$${}_1C_{ijkl} = \frac{{}_1\rho}{{}_0\rho} \frac{\partial {}^1x_i}{\partial {}^0x_p} \frac{\partial {}^1x_j}{\partial {}^0x_q} \frac{\partial {}^1x_k}{\partial {}^0x_r} \frac{\partial {}^1x_l}{\partial {}^0x_s} {}_0C_{pqrs} \quad (9.4.5)$$

With these two equations, only one set of coefficients, namely,  ${}_0C_{ijkl}$  or  ${}_1C_{ijkl}$ , need to be known or given. The other set of coefficients can be obtained simply by transformation. We can therefore ensure that the material properties implied by the total and updated Lagrangian formulations are identical to each other, provided that the same step sizes are used in both formulations.

Often, the incremental material laws (9.4.2) and (9.4.3) with identical coefficients, that is,  ${}_0C_{ijkl} = {}_1C_{ijkl}$ , are employed in the total and updated

Lagrangian finite element formulations. Of course, the error introduced by the assumption can be negligible if the strains are relatively small but the difference can be significant in large deformation problems, for example, in high velocity impact problems.

## 9.5 Total Lagrangian and Updated Lagrangian Formulations of Continua

### 9.5.1 Principle of Virtual Displacements

The equations of the Lagrangian incremental description of motion can be derived from the principles of virtual work (i.e. virtual displacements, virtual forces, or mixed virtual displacements and forces). Since our ultimate objective is to develop the finite element model of the equations governing a body, we will not actually derive the differential equations of motion but utilize the virtual work statements to develop the finite element models.

The *displacement finite element model* is based on the principle of virtual displacements. The principle requires that the sum of the external virtual work done on a body and the internal virtual work stored in the body should be equal to zero:

$$\delta W \equiv \int_{2V} {}^2\sigma : \delta({}_2\mathbf{e}) d^2V - \delta^2 R = 0 \quad (9.5.1a)$$

$$= \int_{2V} {}^2\sigma_{ij} \delta({}_2e_{ij}) d^2V - \delta^2 R = 0 \quad (9.5.1b)$$

where  $\delta^2 R$  denotes the virtual work done by applied forces

$$\delta^2 R = \int_{2V} {}^2\mathbf{f} \cdot \delta\mathbf{u} d^2V + \int_{2S} {}^2\mathbf{t} \cdot \delta\mathbf{u} d^2S \quad (9.5.2a)$$

$$= \int_{2V} {}^2f_i \delta u_i d^2V + \int_{2S} {}^2t_i \delta u_i d^2S \quad (9.5.2b)$$

and  $d^2S$  denotes surface element and  ${}^2\mathbf{f}$  is the body force vector (measured per unit volume) and  ${}^2\mathbf{t}$  is the boundary stress (or traction) vector (measured per unit surface area) in configuration  $\mathcal{C}_2$ . The variational symbol ' $\delta$ ' is understood to operate on unknown displacement variables ( ${}^2u_i$  and  $u_i$ ).

Equation (9.5.1) cannot be solved directly since the configuration  $\mathcal{C}_2$  is unknown. This is an important difference compared with the linear analysis in which we assume that the displacements are infinitesimally small so that the configuration of the body does not change. In a large deformation analysis special attention must be given to the fact that the configuration of the body is changing continuously. This change in configuration can be dealt with by defining appropriate stress and strain measures. The objective of their

introduction into the analysis is to express the internal work in Eq. (9.5.1) in terms of an integral over a configuration that is known. The stress and strain measures that we shall use are the 2nd Piola–Kirchhoff stress tensor and the Green–Lagrange strain tensor, which are “energetically conjugate” to each other [see Eq. (9.2.34)].

### 9.5.2 Total Lagrangian Formulation

In the total Lagrangian formulation, all quantities are measured with respect to the initial configuration  $C_0$ . Hence, the virtual work statement in Eq. (9.5.1) must be expressed in terms of quantities referred to the reference configuration. We use the following identities [4]

$$\int_{2V} {}^2\sigma_{ij} \delta({}^2e_{ij}) d^2V = \int_{0V} {}^2S_{ij} \delta({}^2_0E_{ij}) d^0V \quad (9.5.3)$$

$$\int_{2V} {}^2f_i \delta u_i d^2V = \int_{0V} {}^2_0f_i \delta u_i d^0V \quad (9.5.4)$$

$$\int_{2S} {}^2t_i \delta u_i d^2S = \int_{0S} {}^2_0t_i \delta u_i d^0S \quad (9.5.5)$$

where  ${}^2_0f_i$  and  ${}^2_0t_i$  are the body force and boundary traction components referred to the configuration  $C_0$ . Using Eqs. (9.5.3)–(9.5.5) in Eq. (9.5.1b) we arrive at

$$\int_{0V} {}^2_0S_{ij} \delta({}^2_0E_{ij}) d^0V - \delta({}^2_0R) = 0 \quad (9.5.6)$$

where

$$\delta({}^2_0R) = \int_{0V} {}^2_0f_i \delta u_i d^0V + \int_{0S} {}^2_0t_i \delta u_i d^0S \quad (9.5.7)$$

Next we simplify the virtual work statement (9.5.6). First, we note that [see Eqs. (9.3.15) and (9.3.16)]

$$\begin{aligned} \delta({}^2_0E_{ij}) &= \delta({}^1_0E_{ij}) + \delta({}_0\varepsilon_{ij}) = \delta({}_0\varepsilon_{ij}) \\ &= \delta({}_0e_{ij}) + \delta({}_0\eta_{ij}) \end{aligned} \quad (9.5.8)$$

where  $\delta({}^1_0E_{ij}) = 0$  because it is not a function of the unknown displacements. The virtual strains are given by

$$\delta({}_0e_{ij}) = \frac{1}{2} \left( \frac{\partial \delta u_i}{\partial {}^0x_j} + \frac{\partial \delta u_j}{\partial {}^0x_i} + \frac{\partial \delta u_k}{\partial {}^0x_i} \frac{\partial {}^1_0u_k}{\partial {}^0x_j} + \frac{\partial {}^1_0u_k}{\partial {}^0x_i} \frac{\partial \delta u_k}{\partial {}^0x_j} \right) \quad (9.5.9)$$

$$\delta({}_0\eta_{ij}) = \frac{1}{2} \left( \frac{\partial \delta u_k}{\partial {}^0x_i} \frac{\partial u_k}{\partial {}^0x_j} + \frac{\partial u_k}{\partial {}^0x_i} \frac{\partial \delta u_k}{\partial {}^0x_j} \right) \quad (9.5.10)$$

Substituting Eqs. (9.5.8) for  $\delta({}_0^2E_{ij})$  and Eq. (9.3.36) for  ${}_0^2S_{ij}$  into Eq. (9.5.6), we arrive at the expression

$$\begin{aligned} 0 &= \int_{0V} {}_0^2S_{ij} \delta({}_0^2E_{ij}) d^0V - \delta({}_0^2R) \\ &= \int_{0V} ({}_0^1S_{ij} + {}_0S_{ij}) \delta({}_0\varepsilon_{ij}) d^0V - \delta({}_0^2R) \\ &= \int_{0V} \{ {}_0S_{ij} \delta({}_0\varepsilon_{ij}) + {}_0^1S_{ij} [\delta({}_0e_{ij}) + \delta({}_0\eta_{ij})] \} d^0V - \delta({}_0^2R) \\ &= \int_{0V} {}_0S_{ij} \delta({}_0\varepsilon_{ij}) d^0V + \int_{0V} {}_0^1S_{ij} \delta({}_0\eta_{ij}) d^0V + \delta({}_0^1R) - \delta({}_0^2R) \end{aligned} \quad (9.5.11)$$

where  $\delta({}_0^1R)$  is the virtual internal energy (in moving the actual internal forces through virtual displacements) stored in the body at configuration  $\mathcal{C}_1$

$$\delta({}_0^1R) = \int_{0V} {}_0^1S_{ij} \delta({}_0e_{ij}) d^0V \quad (9.5.12)$$

Since the body is in equilibrium at configuration  $\mathcal{C}_1$ , by the principle of virtual work applied to configuration  $\mathcal{C}_1$  we have

$$0 = \int_{0V} {}_0^1S_{ij} \delta({}_0e_{ij}) d^0V - \int_{0V} {}_0^1f_i \delta u_i d^0V - \int_{0S} {}_0^1t_i \delta u_i d^0S \quad (9.5.13)$$

and therefore

$$\delta({}_0^1R) = \int_{0V} {}_0^1f_i \delta u_i d^0V + \int_{0S} {}_0^1t_i \delta u_i d^0S \quad (9.5.14)$$

Equation (9.5.11) forms the basis for the finite element model. We only need to replace  ${}_0S_{ij}$  in terms of the strains and ultimately the displacement increments using an appropriate constitutive relation. The first term of Eq. (9.5.11) represents the change in the virtual strain energy due to the virtual incremental displacements  $u_i$  between configurations  $\mathcal{C}_1$  and  $\mathcal{C}_2$ . The second term represents the virtual work done by forces due to initial stresses  ${}_0^1S_{ij}$ . The last two terms together denote the change in the virtual work done by applied body forces and surface tractions in moving from  $\mathcal{C}_1$  to  $\mathcal{C}_2$ . This is primarily due to the geometric changes that take place between the two configurations. Equation (9.5.11) represents the statement of virtual work for the incremental deformation between the configurations  $\mathcal{C}_1$  and  $\mathcal{C}_2$ , and no approximations are made in arriving at it.

Towards constructing the displacement finite element model of Eq. (9.5.11), we invoke the constitutive relation (9.4.2) to express  ${}_0S_{ij}$  in terms of the incremental strain components  ${}_0\varepsilon_{ij}$ . Equation (9.5.11) takes the form

$$\int_{0V} {}_0C_{ijkl} {}_0\varepsilon_{kl} \delta({}_0\varepsilon_{ij}) d^0V + \int_{0V} {}_0^1S_{ij} \delta({}_0\eta_{ij}) d^0V = \delta({}_0^2R) - \delta({}_0^1R) \quad (9.5.15)$$

Equation (9.5.15) is nonlinear in the displacement increments  $u_i$ . To make it computationally tractable, we assume that the displacements  $u_i$  are small (which is indeed the case provided the load step is small in moving from  $\mathcal{C}_1$  to  $\mathcal{C}_2$ ) so that the following approximations hold:

$${}^0S_{ij} \approx {}^0C_{ijkl} {}^0e_{kl} \quad \text{and} \quad \delta({}^0\varepsilon_{ij}) \approx \delta({}^0e_{ij}) \quad (9.5.16)$$

Then Eq. (9.5.15) can be simplified to

$$\int_{0V} {}^0C_{ijkl} {}^0e_{kl} \delta({}^0e_{ij}) d^0V + \int_{0V} {}^1S_{ij} \delta({}^0\eta_{ij}) d^0V = \delta({}^2_0R) - \delta({}^1_0R) \quad (9.5.17)$$

Equation (9.5.17) is the weak form for the development of the finite element model based on the total Lagrangian formulation. The total stress components  ${}^1S_{ij}$  are evaluated using the constitutive relation

$${}^1S_{ij} = {}^0C_{ijkl} {}^1E_{kl} \quad (9.5.18)$$

where  ${}^1E_{kl}$  are the Green-Lagrange strain tensor components defined in Eq. (9.3.13).

A summary of all the pertinent equations of the total Lagrangian formulation is presented in Table 9.5.1.

### 9.5.3 Updated Lagrangian Formulation

In the updated Lagrangian formulation, all quantities are referred to the latest known configuration, namely  $\mathcal{C}_1$ . Hence, the virtual work statement in Eq. (9.5.1b) must be recast in terms of quantities referred to  $\mathcal{C}_1$ . We use the identities

$$\int_{2V} {}^2\sigma_{ij} \delta({}^2e_{ij}) d^2V = \int_{1V} {}^2S_{ij} \delta({}^2_1\varepsilon_{ij}) d^1V \quad (9.5.19a)$$

$$\int_{2V} {}^2f_i \delta u_i d^2V = \int_{1V} {}^2f_i \delta u_i d^1V \quad (9.5.19b)$$

$$\int_{2S} {}^2t_i \delta u_i d^2S = \int_{1S} {}^2t_i \delta u_i d^1S \quad (9.5.19c)$$

where  ${}^2f_i$  and  ${}^2t_i$  are the body force and boundary traction components referred to the configuration  $\mathcal{C}_1$ , and  ${}^2_1\varepsilon_{ij}$  are the components of the updated Green-Lagrange strain tensor components defined in Eq. (9.3.23). Using Eqs. (9.5.19a-c), Eq. (9.5.1b) can be expressed as

$$\int_{1V} {}^2S_{ij} \delta({}^2_1\varepsilon_{ij}) d^1V - \delta({}^2_1R) = 0 \quad (9.5.20)$$

where

$$\delta({}_1^2R) = \int_{1V} {}_1^2f_i \delta u_i d^1V + \int_{1S} {}_1^2t_i \delta u_i d^1S \quad (9.5.21)$$

**Table 9.5.1** Summary of equations of the total Lagrangian formulation.

1. Weak form

$$0 = \int_{0V} {}_0^2S_{ij} \delta({}_0^2E_{ij}) d^0V - \delta({}_0^2R) \quad (9.5.6)$$

$${}_0^2S_{ij} = {}_0^2J \left( \frac{\partial {}^0x_i}{\partial {}^2x_m} \right) {}_2\sigma_{mn} \left( \frac{\partial {}^0x_j}{\partial {}^2x_n} \right) \quad (9.3.40)$$

$${}_0^2E_{ij} = \frac{1}{2} \left( \frac{\partial {}^2u_i}{\partial {}^0x_j} + \frac{\partial {}^2u_j}{\partial {}^0x_i} + \frac{\partial {}^2u_k}{\partial {}^0x_i} \frac{\partial {}^2u_k}{\partial {}^0x_j} \right) \quad (9.3.14)$$

$$\delta({}_0^2R) = \int_{0V} {}_0^2f_i \delta u_i d^0V + \int_{0S} {}_0^2t_i \delta u_i d^0S \quad (9.5.7)$$

2. Incremental decompositions

$${}_0^2S_{ij} = {}_0^1S_{ij} + {}_0S_{ij} \quad (9.3.36)$$

$${}_0^2E_{ij} = {}_0^1E_{ij} + {}_0\varepsilon_{ij}, \quad {}_0\varepsilon_{ij} = {}_0e_{ij} + {}_0\eta_{ij} \quad (9.3.15) \& (9.3.16)$$

$${}_0^1S_{ij} = {}_0C_{ijkl} {}_0^1E_{kl}, \quad {}_0S_{ij} = {}_0C_{ijkl} {}_0\varepsilon_{kl} \quad (9.4.2)$$

$${}_0^1E_{ij} = \frac{1}{2} \left( \frac{\partial {}^1u_i}{\partial {}^0x_j} + \frac{\partial {}^1u_j}{\partial {}^0x_i} + \frac{\partial {}^1u_k}{\partial {}^0x_i} \frac{\partial {}^1u_k}{\partial {}^0x_j} \right) \quad (9.3.13)$$

$${}_0e_{ij} = \frac{1}{2} \left( \frac{\partial u_i}{\partial {}^0x_j} + \frac{\partial u_j}{\partial {}^0x_i} + \frac{\partial {}^1u_k}{\partial {}^0x_i} \frac{\partial u_k}{\partial {}^0x_j} + \frac{\partial u_k}{\partial {}^0x_i} \frac{\partial {}^1u_k}{\partial {}^0x_j} \right) \quad (9.3.17)$$

$${}_0\eta_{ij} = \frac{1}{2} \frac{\partial u_k}{\partial {}^0x_i} \frac{\partial u_k}{\partial {}^0x_j} \quad (9.3.18)$$

3. Weak form with incremental decompositions

$$\int_{0V} {}_0S_{ij} \delta({}_0\varepsilon_{ij}) d^0V + \int_{0V} {}_0^1S_{ij} \delta({}_0\eta_{ij}) d^0V = \delta({}_0^2R) - \int_{0V} {}_0^1S_{ij} \delta({}_0e_{ij}) d^0V \quad (9.5.11) \& (9.5.12)$$

4. Linearized weak form with incremental decompositions Use the approximations

$${}_0S_{ij} = {}_0C_{ijkl} {}_0\varepsilon_{kl} \approx {}_0C_{ijkl} {}_0e_{kl}, \quad \delta({}_0\varepsilon_{ij}) \approx \delta({}_0e_{ij}) \quad (9.5.16)$$

to rewrite the weak form as

$$\begin{aligned} & \int_{0V} {}_0C_{ijkl} {}_0e_{kl} \delta({}_0e_{ij}) d^0V + \int_{0V} {}_0^1S_{ij} \delta({}_0\eta_{ij}) d^0V \\ & = \delta({}_0^2R) - \int_{0V} {}_0^1S_{ij} \delta({}_0e_{ij}) d^0V \end{aligned} \quad (9.5.17)$$

The virtual strains are given by  $\delta({}_1^2\varepsilon_{ij}) = \delta({}_1e_{ij}) + \delta({}_1\eta_{ij})$  [see Eq. (9.3.24)] where

$$\delta({}_1e_{ij}) = \frac{1}{2} \left( \frac{\partial \delta u_i}{\partial {}^1x_j} + \frac{\partial \delta u_j}{\partial {}^1x_i} \right) \quad (9.5.22)$$

$$\delta({}_1\eta_{ij}) = \frac{1}{2} \left( \frac{\partial \delta u_k}{\partial {}^1x_i} \frac{\partial u_k}{\partial {}^1x_j} + \frac{\partial u_k}{\partial {}^1x_i} \frac{\partial \delta u_k}{\partial {}^1x_j} \right) \quad (9.5.23)$$

Now using Eqs. (9.3.24) and (9.3.35), we can write Eq. (9.5.20) as

$$\begin{aligned} 0 &= \int_{1V} {}_1^2S_{ij} \delta({}_1^2\varepsilon_{ij}) d^1V - \delta({}_1^2R) \\ &= \int_{1V} ({}^1\sigma_{ij} + {}_1S_{ij}) \delta({}_1^2\varepsilon_{ij}) d^1V - \delta({}_1^2R) \\ &= \int_{1V} \{ {}_1S_{ij} \delta({}_1^2\varepsilon_{ij}) + {}^1\sigma_{ij} [\delta({}_1e_{ij}) + \delta({}_1\eta_{ij})] \} d^1V - \delta({}_1^2R) \\ &= \int_{1V} {}_1S_{ij} \delta({}_1^2\varepsilon_{ij}) d^1V + \int_{1V} {}^1\sigma_{ij} \delta({}_1\eta_{ij}) d^1V + \delta({}_1^1R) - \delta({}_1^2R) \end{aligned} \quad (9.5.24)$$

where  $\delta({}_1^1R)$  is the virtual internal energy stored in the body at configuration  $\mathcal{C}_1$

$$\delta({}_1^1R) = \int_{1V} {}^1\sigma_{ij} \delta({}_1e_{ij}) d^1V \quad (9.5.25)$$

Since the body is in equilibrium at configuration  $\mathcal{C}_1$ , the principle of virtual work applied to configuration  $\mathcal{C}_1$  yields

$$\delta({}_1^1R) = \int_{1V} {}^1f_i \delta u_i d^1V + \int_{1S} {}^1t_i \delta u_i d^1S \quad (9.5.26)$$

Next, we invoke the constitutive relation (9.4.3) to express  ${}_1S_{ij}$  in terms of the incremental strain components  ${}_1^2\varepsilon_{ij}$ . Equation (9.5.24) takes the form

$$\begin{aligned} &\int_{1V} {}_1C_{ijkl} {}_1^2\varepsilon_{kl} \delta({}_1^2\varepsilon_{ij}) d^1V + \int_{1V} {}^1\sigma_{ij} \delta({}_1\eta_{ij}) d^1V \\ &= \delta({}_1^2R) - \int_{1V} {}^1\sigma_{ij} \delta({}_1e_{ij}) d^1V \end{aligned} \quad (9.5.27)$$

As before, we assume that the displacements  $u_i$  are small so that the following approximations hold:

$${}_1S_{ij} \approx {}_1C_{ijkl} {}_1e_{kl} \quad \text{and} \quad \delta({}_1^2\varepsilon_{ij}) \approx \delta({}_1e_{ij}) \quad (9.5.28)$$

Then Eq. (9.5.27) takes the form

$$\begin{aligned} &\int_{1V} {}_1C_{ijkl} {}_1e_{kl} \delta({}_1e_{ij}) d^1V + \int_{1V} {}^1\sigma_{ij} \delta({}_1\eta_{ij}) d^1V \\ &= \delta({}_1^2R) - \int_{1V} {}^1\sigma_{ij} \delta({}_1e_{ij}) d^1V \end{aligned} \quad (9.5.29)$$



Equation (9.5.29) is the weak form for the development of the finite element model based on the updated Lagrangian formulation. The total Cauchy stress components  ${}^1\sigma_{ij}$  are evaluated using the constitutive relation

$${}^1\sigma_{ij} = {}_1C_{ijkl} {}^1\varepsilon_{kl} \quad (9.5.30)$$

where  ${}^1\varepsilon_{kl}$  are the Almansi strain tensor components defined by [see Eq. (9.3.26)]

$$2 {}^1\varepsilon_{ij} d^1x_i d^1x_j = ({}^1ds)^2 - ({}^0ds)^2 \quad (9.5.31)$$

which gives

$${}^1\varepsilon_{ij} = \frac{1}{2} \left( \frac{\partial {}^1u_i}{\partial {}^1x_j} + \frac{\partial {}^1u_j}{\partial {}^1x_i} - \frac{\partial {}^1u_k}{\partial {}^1x_i} \frac{\partial {}^1u_k}{\partial {}^1x_j} \right) \quad (9.5.32)$$

A summary of all the pertinent equations of the updated Lagrangian formulation is presented in Table 9.5.2.

## 9.6 Finite Element Models of Two-Dimensional Continua

### 9.6.1 Introduction

Here we discuss finite element models based on the total and updated Lagrangian formulations presented in the last section. Attention is focused here on two-dimensional problems under the assumption of linear elastic behavior. Further, we assume orthotropic behavior.

### 9.6.2 Total Lagrangian Formulation

We introduce the notation

$${}^0x_1 = x, \quad {}^0x_2 = y, \quad {}^1u_1 = u, \quad {}^1u_2 = v, \quad u_1 = \bar{u}, \quad u_2 = \bar{v} \quad (9.6.1)$$

We can write the first expression of Eq. (9.5.17) in the alternate form

$$\begin{aligned} \int_{{}^0V} {}_0C_{ijkl} {}_0e_{kl} \delta({}_0e_{ij}) d^0V &= \int_{{}^0V} \{\delta_0e\}^T [{}_0C] \{0e\} d^0V \\ &= \int_{{}^0V} \{\delta\bar{u}\}^T ([D] + [D_u])^T [{}_0C] ([D] + [D_u]) \{\bar{u}\} d^0V \end{aligned} \quad (9.6.2)$$

where

$$\{0e\} = \begin{Bmatrix} {}_0e_{xx} \\ {}_0e_{yy} \\ 2 {}_0e_{xy} \end{Bmatrix} = \begin{Bmatrix} \frac{\partial \bar{u}}{\partial x} \\ \frac{\partial \bar{v}}{\partial y} \\ \frac{\partial \bar{u}}{\partial y} + \frac{\partial \bar{v}}{\partial x} \end{Bmatrix} + \begin{Bmatrix} \frac{\partial u}{\partial x} \frac{\partial \bar{u}}{\partial x} + \frac{\partial v}{\partial x} \frac{\partial \bar{v}}{\partial x} \\ \frac{\partial u}{\partial y} \frac{\partial \bar{u}}{\partial y} + \frac{\partial v}{\partial y} \frac{\partial \bar{v}}{\partial y} \\ \frac{\partial u}{\partial x} \frac{\partial \bar{u}}{\partial y} + \frac{\partial v}{\partial x} \frac{\partial \bar{v}}{\partial y} + \frac{\partial \bar{u}}{\partial x} \frac{\partial u}{\partial y} + \frac{\partial \bar{v}}{\partial x} \frac{\partial v}{\partial y} \end{Bmatrix}$$

$$\begin{aligned}
 &= \left( \begin{bmatrix} \frac{\partial}{\partial x} & 0 \\ 0 & \frac{\partial}{\partial y} \\ \frac{\partial}{\partial y} & \frac{\partial}{\partial x} \end{bmatrix} + \begin{bmatrix} \frac{\partial u}{\partial x} \frac{\partial}{\partial x} & \frac{\partial v}{\partial x} \frac{\partial}{\partial x} \\ \frac{\partial u}{\partial y} \frac{\partial}{\partial y} & \frac{\partial v}{\partial y} \frac{\partial}{\partial y} \\ \frac{\partial u}{\partial y} \frac{\partial}{\partial x} + \frac{\partial u}{\partial x} \frac{\partial}{\partial y} & \frac{\partial v}{\partial y} \frac{\partial}{\partial x} + \frac{\partial v}{\partial x} \frac{\partial}{\partial y} \end{bmatrix} \right) \begin{Bmatrix} \bar{u} \\ \bar{v} \end{Bmatrix} \\
 &\equiv ([D] + [D_u]) \{\bar{u}\} \tag{9.6.3}
 \end{aligned}$$

Table 9.5.2 Summary of equations of the updated Lagrangian formulation.

1. Weak form

$$0 = \int_{1V} {}^2S_{ij} \delta({}^2\varepsilon_{ij}) d^1V - \delta({}^2R) \tag{9.5.20}$$

$${}^2S_{ij} = \frac{1}{2\rho} \frac{\partial^1x_i}{\partial^2x_p} \frac{\partial^1x_j}{\partial^2x_q} {}^2\sigma_{pq} \tag{9.3.41}$$

$${}^2\varepsilon_{ij} = \frac{1}{2} \left( \frac{\partial u_i}{\partial^1x_j} + \frac{\partial u_j}{\partial^1x_i} + \frac{\partial u_k}{\partial^1x_i} \frac{\partial u_k}{\partial^1x_j} \right) \tag{9.3.23}$$

$$\delta({}^2R) = \int_{1V} {}^2f_i \delta u_i d^1V + \int_{1S} {}^2t_i \delta u_i d^1S \tag{9.5.21}$$

2. Incremental decompositions

$${}^2S_{ij} = {}^1\sigma_{ij} + {}^1S_{ij}, \quad {}^1S_{ij} = {}^1\sigma_{ij} \tag{9.3.35}$$

$${}^2\varepsilon_{ij} = {}^1e_{ij} + {}^1\eta_{ij} \tag{9.3.24}$$

$${}^1\sigma_{ij} = {}^1C_{ijkl} {}^1\varepsilon_{kl}, \quad {}^1S_{ij} = {}^1C_{ijkl} {}^2\varepsilon_{kl} \tag{9.5.30}$$

$${}^1\varepsilon_{ij} = \frac{1}{2} \left( \frac{\partial {}^1u_i}{\partial^1x_j} + \frac{\partial {}^1u_j}{\partial^1x_i} - \frac{\partial {}^1u_k}{\partial^1x_i} \frac{\partial {}^1u_k}{\partial^1x_j} \right) \tag{9.5.32}$$

$${}^1e_{ij} = \frac{1}{2} \left( \frac{\partial u_i}{\partial^1x_j} + \frac{\partial u_j}{\partial^1x_i} \right), \quad {}^1\eta_{ij} = \frac{1}{2} \left( \frac{\partial u_k}{\partial^1x_i} \frac{\partial u_k}{\partial^1x_j} \right) \tag{9.3.25}$$

3. Weak form with incremental decompositions

$$\int_{1V} {}^1S_{ij} \delta({}^2\varepsilon_{ij}) d^1V + \int_{1V} {}^1\sigma_{ij} \delta({}^1\eta_{ij}) d^1V = \delta({}^2R) - \int_{1V} {}^1\sigma_{ij} \delta({}^1e_{ij}) d^1V \tag{9.5.24} \& \tag{9.5.25}$$

4. Linearized weak form with incremental decompositions Use the approximations

$${}^1S_{ij} = {}^1C_{ijkl} {}^2\varepsilon_{kl} \approx {}^1C_{ijkl} {}^1e_{kl}, \quad \delta({}^1\varepsilon_{ij}) \approx \delta({}^1e_{ij}) \tag{9.5.28}$$

to rewrite the weak form as

$$\begin{aligned}
 &\int_{1V} {}^1C_{ijkl} {}^1e_{kl} \delta({}^1e_{ij}) d^1V + \int_{1V} {}^1\sigma_{ij} \delta({}^1\eta_{ij}) d^1V \\
 &= \delta({}^2R) - \int_{1V} {}^1\sigma_{ij} \delta({}^1e_{ij}) d^1V \tag{9.5.29}
 \end{aligned}$$

$$\{\delta \text{ }_0e\} = \begin{Bmatrix} \delta \text{ }_0e_{xx} \\ \delta \text{ }_0e_{yy} \\ 2\delta \text{ }_0e_{xy} \end{Bmatrix} = ([D] + [D_{\mathbf{u}}]) \{\delta \bar{\mathbf{u}}\} \quad (9.6.4)$$

$$[_0C] = \begin{bmatrix} {}_0C_{11} & {}_0C_{12} & 0 \\ {}_0C_{12} & {}_0C_{22} & 0 \\ 0 & 0 & {}_0C_{66} \end{bmatrix} \quad (9.6.5)$$

The second expression of Eq. (9.5.17) can be written as

$$\int_{^0V} {}_1S_{ij} \delta({}_0\eta_{ij}) d^0V = \int_{^0V} \{\delta \text{ }_0\eta\}^T \{^1S\} d^0V \quad (9.6.6)$$

$$\begin{aligned} \{\delta \text{ }_0\eta\} &= \begin{Bmatrix} {}_0\eta_{xx} \\ {}_0\eta_{yy} \\ 2 \text{ }_0\eta_{xy} \end{Bmatrix} = \frac{1}{2} \begin{Bmatrix} \frac{\partial \bar{u}}{\partial x} \frac{\partial \bar{u}}{\partial x} + \frac{\partial \bar{v}}{\partial x} \frac{\partial \bar{v}}{\partial x} \\ \frac{\partial \bar{u}}{\partial y} \frac{\partial \bar{u}}{\partial y} + \frac{\partial \bar{v}}{\partial y} \frac{\partial \bar{v}}{\partial y} \\ 2 \left( \frac{\partial \bar{u}}{\partial x} \frac{\partial \bar{u}}{\partial y} + \frac{\partial \bar{v}}{\partial x} \frac{\partial \bar{v}}{\partial y} \right) \end{Bmatrix} \\ &= \frac{1}{2} \begin{bmatrix} \frac{\partial \bar{u}}{\partial x} \frac{\partial}{\partial x} & \frac{\partial \bar{v}}{\partial x} \frac{\partial}{\partial x} \\ \frac{\partial \bar{u}}{\partial y} \frac{\partial}{\partial y} & \frac{\partial \bar{v}}{\partial y} \frac{\partial}{\partial y} \\ \frac{\partial \bar{u}}{\partial y} \frac{\partial}{\partial x} + \frac{\partial \bar{u}}{\partial x} \frac{\partial}{\partial y} & \frac{\partial \bar{v}}{\partial y} \frac{\partial}{\partial x} + \frac{\partial \bar{v}}{\partial x} \frac{\partial}{\partial y} \end{bmatrix} \begin{Bmatrix} \bar{u} \\ \bar{v} \end{Bmatrix} \\ &= \frac{1}{2} [D_{\bar{\mathbf{u}}}] \{\bar{\mathbf{u}}\} \end{aligned} \quad (9.6.7)$$

$$\begin{aligned} \{\delta \text{ }_0\eta\} &= \begin{Bmatrix} \delta \text{ }_0\eta_{xx} \\ \delta \text{ }_0\eta_{yy} \\ 2\delta \text{ }_0\eta_{xy} \end{Bmatrix} = \begin{Bmatrix} \frac{\partial \delta \bar{u}}{\partial x} \frac{\partial \bar{u}}{\partial x} + \frac{\partial \delta \bar{v}}{\partial x} \frac{\partial \bar{v}}{\partial x} \\ \frac{\partial \delta \bar{u}}{\partial y} \frac{\partial \bar{u}}{\partial y} + \frac{\partial \delta \bar{v}}{\partial y} \frac{\partial \bar{v}}{\partial y} \\ \frac{\partial \delta \bar{u}}{\partial x} \frac{\partial \bar{u}}{\partial y} + \frac{\partial \delta \bar{u}}{\partial y} \frac{\partial \bar{u}}{\partial x} + \frac{\partial \delta \bar{v}}{\partial x} \frac{\partial \bar{v}}{\partial y} + \frac{\partial \delta \bar{v}}{\partial y} \frac{\partial \bar{v}}{\partial x} \end{Bmatrix} \\ &= [D_{\delta \bar{\mathbf{u}}}] \{\delta \bar{\mathbf{u}}\} = [D_{\delta \bar{\mathbf{u}}}] \{\bar{\mathbf{u}}\} \end{aligned} \quad (9.6.8)$$

$$\{^1_0S\} = \begin{Bmatrix} {}^1_0S_{xx} \\ {}^1_0S_{yy} \\ {}^1_0S_{xy} \end{Bmatrix} = \begin{bmatrix} {}_0C_{11} & {}_0C_{12} & 0 \\ {}_0C_{12} & {}_0C_{22} & 0 \\ 0 & 0 & {}_0C_{66} \end{bmatrix} \begin{Bmatrix} {}^1_0E_{xx} \\ {}^1_0E_{yy} \\ 2 \text{ }^1_0E_{xy} \end{Bmatrix} \quad (9.6.9a)$$

$$\{^1_0E\} = \begin{Bmatrix} {}^1_0E_{xx} \\ {}^1_0E_{yy} \\ 2 \text{ }^1_0E_{xy} \end{Bmatrix} = \begin{Bmatrix} \frac{\partial u}{\partial x} + \frac{1}{2} \left[ \left( \frac{\partial u}{\partial x} \right)^2 + \left( \frac{\partial v}{\partial x} \right)^2 \right] \\ \frac{\partial v}{\partial y} + \frac{1}{2} \left[ \left( \frac{\partial u}{\partial y} \right)^2 + \left( \frac{\partial v}{\partial y} \right)^2 \right] \\ \frac{\partial u}{\partial y} + \frac{\partial v}{\partial x} + \left( \frac{\partial u}{\partial x} \frac{\partial u}{\partial y} + \frac{\partial v}{\partial x} \frac{\partial v}{\partial y} \right) \end{Bmatrix} \quad (9.6.9b)$$

However, the expression (9.6.6) is not convenient for the finite element development since the vector  $\{\delta \text{ }_0\eta\}$  is a nonlinear function of the vector

of displacement increments  $\bar{\mathbf{u}}$ . It must be written in an alternate way to facilitate the construction of finite element matrices. We have

$$\begin{aligned} & \int_{0V} \{\delta \ 0\eta\}^T \{^1_0S\} d^0V \\ &= \int_{0V} \left[ ^1_0S_{xx} \left( \frac{\partial \delta \bar{u}}{\partial x} \frac{\partial \bar{u}}{\partial x} + \frac{\partial \delta \bar{v}}{\partial x} \frac{\partial \bar{v}}{\partial x} \right) + ^1_0S_{yy} \left( \frac{\partial \delta \bar{u}}{\partial y} \frac{\partial \bar{u}}{\partial y} + \frac{\partial \delta \bar{v}}{\partial y} \frac{\partial \bar{v}}{\partial y} \right) \right. \\ & \quad \left. + ^1_0S_{xy} \left( \frac{\partial \delta \bar{u}}{\partial x} \frac{\partial \bar{u}}{\partial y} + \frac{\partial \delta \bar{v}}{\partial x} \frac{\partial \bar{v}}{\partial y} + \frac{\partial \bar{u}}{\partial x} \frac{\partial \delta \bar{u}}{\partial y} + \frac{\partial \bar{v}}{\partial x} \frac{\partial \delta \bar{v}}{\partial y} \right) \right] d^0V \\ &= \int_{0V} \left\{ \begin{matrix} \frac{\partial \delta \bar{u}}{\partial x} \\ \frac{\partial \delta \bar{u}}{\partial y} \\ \frac{\partial \delta \bar{v}}{\partial x} \\ \frac{\partial \delta \bar{v}}{\partial y} \end{matrix} \right\}^T \begin{bmatrix} ^1_0S_{xx} & ^1_0S_{xy} & 0 & 0 \\ ^1_0S_{xy} & ^1_0S_{yy} & 0 & 0 \\ 0 & 0 & ^1_0S_{xx} & ^1_0S_{xy} \\ 0 & 0 & ^1_0S_{xy} & ^1_0S_{yy} \end{bmatrix} \left\{ \begin{matrix} \frac{\partial \bar{u}}{\partial x} \\ \frac{\partial \bar{u}}{\partial y} \\ \frac{\partial \bar{v}}{\partial x} \\ \frac{\partial \bar{v}}{\partial y} \end{matrix} \right\} d^0V \\ &= \int_{0V} \{\delta \bar{\mathbf{u}}\}^T [\bar{D}]^T [^1_0S] [\bar{D}] \{\bar{\mathbf{u}}\} d^0V \end{aligned} \tag{9.6.10}$$

where

$$[^1_0S] = \begin{bmatrix} ^1_0S_{xx} & ^1_0S_{xy} & 0 & 0 \\ ^1_0S_{xy} & ^1_0S_{yy} & 0 & 0 \\ 0 & 0 & ^1_0S_{xx} & ^1_0S_{xy} \\ 0 & 0 & ^1_0S_{xy} & ^1_0S_{yy} \end{bmatrix} \tag{9.6.11a}$$

$$\{^1_0S\} = \left\{ \begin{matrix} ^1_0S_{xx} \\ ^1_0S_{xy} \\ ^1_0S_{yy} \\ ^1_0S_{xy} \end{matrix} \right\}, \quad [\bar{D}] = \begin{bmatrix} \frac{\partial}{\partial x} & 0 \\ \frac{\partial}{\partial y} & 0 \\ 0 & \frac{\partial}{\partial x} \\ 0 & \frac{\partial}{\partial y} \end{bmatrix} \left\{ \begin{matrix} \bar{u} \\ \bar{v} \end{matrix} \right\} \tag{9.6.11b}$$

This completes the development of alternate form of the expressions in the virtual work statement (9.5.17).

Suppose that the total and incremental displacement fields are interpolated as

$$\{\mathbf{u}\} = \begin{Bmatrix} u \\ v \end{Bmatrix} = \begin{Bmatrix} \sum_{j=1}^n u_j \psi_j(\mathbf{x}) \\ \sum_{j=1}^n v_j \psi_j(\mathbf{x}) \end{Bmatrix} = [\Psi] \{\Delta\} \tag{9.6.12}$$

$$\{\bar{\mathbf{u}}\} = \begin{Bmatrix} \bar{u} \\ \bar{v} \end{Bmatrix} = \begin{Bmatrix} \sum_{j=1}^n \bar{u}_j \psi_j(\mathbf{x}) \\ \sum_{j=1}^n \bar{v}_j \psi_j(\mathbf{x}) \end{Bmatrix} = [\Psi] \{\bar{\Delta}\} \tag{9.6.13}$$

where

$$[\Psi] = \begin{bmatrix} \psi_1 & 0 & \psi_2 & 0 & \dots & \psi_n & 0 \\ 0 & \psi_1 & 0 & \psi_2 & \dots & 0 & \psi_n \end{bmatrix} \tag{9.6.14a}$$

$$\{\Delta\}^T = \{u_1, v_1, u_2, v_2, \dots, u_n, v_n\} \tag{9.6.14b}$$

$$\{\bar{\Delta}\}^T = \{\bar{u}_1, \bar{v}_1, \bar{u}_2, \bar{v}_2, \dots, \bar{u}_n, \bar{v}_n\} \tag{9.6.14c}$$

We have

$$\begin{aligned}
 & \int_{0V} {}_0\{\delta_0e\}^T [{}_0C] \{0e\} d^0V \\
 &= \int_{0V} \{\delta\bar{u}\}^T ([D] + [D_u])^T [{}_0C] ([D] + [D_u]) \{\bar{u}\} d^0V \\
 &= \int_{0V} \{\delta\bar{\Delta}\}^T \{([D] + [D_u]) [\Psi]\}^T [{}_0C] ([D] + [D_u]) [\Psi] \{\bar{\Delta}\} d^0V \\
 &= \int_{0V} \{\delta\bar{\Delta}\}^T [B_L]^T [{}_0C] [B_L] \{\bar{\Delta}\} d^0V \quad (9.6.15)
 \end{aligned}$$

$$\begin{aligned}
 & \int_{0V} \{\delta_0\eta\}^T \{{}_0^1S\} d^0V \\
 &= \int_{0V} \{\delta\bar{u}\}^T [\bar{D}]^T [{}_0^1S] [\bar{D}] \{\bar{u}\} d^0V \\
 &= \int_{0V} \{\delta\bar{\Delta}\}^T [B_{NL}]^T [{}_0^1S] [B_{NL}] \{\bar{\Delta}\} d^0V \quad (9.6.16)
 \end{aligned}$$

$$\begin{aligned}
 \delta({}_0^1R) &= \int_{0V} {}_0^1S_{ij} \delta(0e_{ij}) d^0V \\
 &= \int_{0V} \{\delta_0e\}^T \{{}_0^1S\} d^0V \\
 &= \int_{0V} \{\delta\bar{\Delta}\}^T [B_L]^T \{{}_0^1S\} d^0V \quad (9.6.17)
 \end{aligned}$$

$$\begin{aligned}
 \delta({}_0^2R) &= \int_{0V} {}_0^2f_i \delta u_i d^0V + \int_{0S} {}_0^2t_i \delta u_i d^0S \\
 &= \int_{0V} \{\delta\bar{\Delta}\}^T [\Psi]^T \{{}_0^2f\} d^0V + \int_{0S} \{\delta\bar{\Delta}\}^T [\Psi]^T \{{}_0^2t\} d^0S \quad (9.6.18)
 \end{aligned}$$

where  $[B_L]$  is the  $3 \times 2n$  matrix and  $[B_{NL}]$  is the  $4 \times 2n$  matrix defined by

$$[B_L] = ([D] + [D_u]) [\Psi], \quad [B_{NL}] = [\bar{D}] [\Psi] \quad (9.6.19)$$

Substitution of Eqs. (9.6.15)–(9.6.18) into Eq. (9.5.17), and use of the fundamental Lemma of calculus of variations (i.e.  $\{\delta\bar{\Delta}\}$  arbitrary variations), yields the following finite element model associated with the total Lagrangian formulation of two-dimensional nonlinear continua:

$$([K_L] + [K_{NL}]) \{\bar{\Delta}\} = \{{}_0^2F\} - \{{}_0^1F\} \quad (9.6.20)$$

where

$$[K_L] = \int_{0V} [B_L]^T [{}_0C] [B_L] d^0V \quad (9.6.21)$$

$$[K_{NL}] = \int_{0V} [B_{NL}]^T [{}_0^1S] [B_{NL}] d^0V \quad (9.6.22)$$

$$\{^1_0F\} = \int_{^0V} [B_L]^T \{^1_0S\} d^0V \tag{9.6.23}$$

$$\{^2_0F\} = \int_{^0V} [\Psi]^T \{^2_0f\} d^0V + \int_{^0S} [\Psi]^T \{^2_0t\} d^0S \tag{9.6.24}$$

$$\{^2_0f\} = \left\{ \begin{matrix} ^2_0f_x \\ ^2_0f_y \end{matrix} \right\}, \quad \{^2_0t\} = \left\{ \begin{matrix} ^2_0t_x \\ ^2_0t_y \end{matrix} \right\} \tag{9.6.25}$$

Note that the stiffness matrix  $[K] = [K_L] + [K_{NL}]$  is symmetric since  $[^1_0S]$  and  $[^0C]$  are symmetric. Also, the total and updated Lagrangian formulations are incremental formulations, that is, determining  $\{\delta\Delta\} \equiv \{\bar{\Delta}\}$ , the stiffness matrix in Eq. (9.6.20) is the tangent stiffness matrix. The direct stiffness matrix is implicit in the vector  $\{^1_0F\}$ . For a linear analysis, we have  $\{\bar{\Delta}\} = \{\Delta\}$ ,  $\{^1_0F\} = \{0\}$ , and  $[K_{NL}] = [0]$ . The formulation presented above is easily extendable to three-dimensional problems.

For two-dimensional problems, the matrices  $[B_L]$  and  $[B_{NL}]$  are given by

$$[B_L] = [B_L^0] + [B_L^u] + [B_L^v] \tag{9.6.26}$$

$$[B_L^0] = \begin{bmatrix} \frac{\partial\psi_1}{\partial x} & 0 & \frac{\partial\psi_2}{\partial x} & 0 & \dots & \frac{\partial\psi_n}{\partial x} & 0 \\ 0 & \frac{\partial\psi_1}{\partial y} & 0 & \frac{\partial\psi_2}{\partial y} & \dots & 0 & \frac{\partial\psi_n}{\partial y} \\ \frac{\partial\psi_1}{\partial y} & \frac{\partial\psi_1}{\partial x} & \frac{\partial\psi_2}{\partial y} & \frac{\partial\psi_2}{\partial x} & \dots & \frac{\partial\psi_n}{\partial y} & \frac{\partial\psi_n}{\partial x} \end{bmatrix} \tag{9.6.27a}$$

$$[B_L^u] = \begin{bmatrix} \frac{\partial u}{\partial x} \frac{\partial\psi_1}{\partial x} & 0 & \frac{\partial u}{\partial x} \frac{\partial\psi_2}{\partial x} & \dots & \frac{\partial u}{\partial x} \frac{\partial\psi_n}{\partial x} & 0 \\ \frac{\partial u}{\partial y} \frac{\partial\psi_1}{\partial y} & 0 & \frac{\partial u}{\partial y} \frac{\partial\psi_2}{\partial y} & \dots & \frac{\partial u}{\partial y} \frac{\partial\psi_n}{\partial y} & 0 \\ \frac{\partial u}{\partial x} \frac{\partial\psi_1}{\partial y} + \frac{\partial u}{\partial y} \frac{\partial\psi_1}{\partial x} & 0 & \frac{\partial u}{\partial x} \frac{\partial\psi_2}{\partial y} + \frac{\partial u}{\partial y} \frac{\partial\psi_2}{\partial x} & \dots & \frac{\partial u}{\partial x} \frac{\partial\psi_n}{\partial y} + \frac{\partial u}{\partial y} \frac{\partial\psi_n}{\partial x} & 0 \end{bmatrix} \tag{9.6.27b}$$

$$[B_L^v] = \begin{bmatrix} 0 & \frac{\partial v}{\partial x} \frac{\partial\psi_1}{\partial x} & 0 & \frac{\partial v}{\partial x} \frac{\partial\psi_2}{\partial x} & \dots & \frac{\partial v}{\partial x} \frac{\partial\psi_n}{\partial x} \\ 0 & \frac{\partial v}{\partial y} \frac{\partial\psi_1}{\partial y} & 0 & \frac{\partial v}{\partial y} \frac{\partial\psi_2}{\partial y} & \dots & \frac{\partial v}{\partial y} \frac{\partial\psi_n}{\partial y} \\ 0 & \frac{\partial v}{\partial x} \frac{\partial\psi_1}{\partial y} + \frac{\partial v}{\partial y} \frac{\partial\psi_1}{\partial x} & 0 & \frac{\partial v}{\partial x} \frac{\partial\psi_2}{\partial y} + \frac{\partial v}{\partial y} \frac{\partial\psi_2}{\partial x} & \dots & \frac{\partial v}{\partial x} \frac{\partial\psi_n}{\partial y} + \frac{\partial v}{\partial y} \frac{\partial\psi_n}{\partial x} \end{bmatrix} \tag{9.6.27c}$$

$$[B_{NL}] = \begin{bmatrix} \frac{\partial\psi_1}{\partial x} & 0 & \frac{\partial\psi_2}{\partial x} & 0 & \dots & \frac{\partial\psi_n}{\partial x} & 0 \\ \frac{\partial\psi_1}{\partial y} & 0 & \frac{\partial\psi_2}{\partial y} & 0 & \dots & \frac{\partial\psi_n}{\partial y} & 0 \\ 0 & \frac{\partial\psi_1}{\partial x} & 0 & \frac{\partial\psi_2}{\partial x} & \dots & 0 & \frac{\partial\psi_n}{\partial x} \\ 0 & \frac{\partial\psi_1}{\partial y} & 0 & \frac{\partial\psi_2}{\partial y} & \dots & 0 & \frac{\partial\psi_n}{\partial y} \end{bmatrix} \tag{9.6.28}$$

The finite element equations (9.6.20) can be written in explicit form as

$$\begin{bmatrix} [K^{11L}] + [K^{11N}] & [K^{12L}] \\ [K^{21L}] & [K^{22L}] + [K^{22N}] \end{bmatrix} \begin{Bmatrix} \{\bar{u}\} \\ \{\bar{v}\} \end{Bmatrix} = \begin{Bmatrix} \{^2_0F^1\} - \{^1_0F^1\} \\ \{^2_0F^2\} - \{^1_0F^2\} \end{Bmatrix} \tag{9.6.29}$$

where

$$\begin{aligned}
 K_{ij}^{11L} &= h_e \int_{\Omega^e} \left\{ {}_0C_{11} \left( 1 + \frac{\partial u}{\partial x} \right)^2 \frac{\partial \psi_i}{\partial x} \frac{\partial \psi_j}{\partial x} + {}_0C_{22} \left( \frac{\partial u}{\partial y} \right)^2 \frac{\partial \psi_i}{\partial y} \frac{\partial \psi_j}{\partial y} \right. \\
 &\quad + {}_0C_{12} \left( 1 + \frac{\partial u}{\partial x} \right) \frac{\partial u}{\partial y} \left( \frac{\partial \psi_i}{\partial x} \frac{\partial \psi_j}{\partial y} + \frac{\partial \psi_i}{\partial y} \frac{\partial \psi_j}{\partial x} \right) \\
 &\quad + {}_0C_{66} \left[ \left( 1 + \frac{\partial u}{\partial x} \right) \frac{\partial \psi_i}{\partial y} + \frac{\partial u}{\partial y} \frac{\partial \psi_i}{\partial x} \right] \\
 &\quad \left. \times \left[ \left( 1 + \frac{\partial u}{\partial x} \right) \frac{\partial \psi_j}{\partial y} + \frac{\partial u}{\partial y} \frac{\partial \psi_j}{\partial x} \right] \right\} dx dy \\
 K_{ij}^{12L} &= h_e \int_{\Omega^e} \left\{ {}_1C_{11} \left( 1 + \frac{\partial u}{\partial x} \right) \frac{\partial v}{\partial x} \frac{\partial \psi_i}{\partial x} \frac{\partial \psi_j}{\partial x} + {}_0C_{22} \left( 1 + \frac{\partial v}{\partial y} \right) \frac{\partial u}{\partial y} \frac{\partial \psi_i}{\partial y} \frac{\partial \psi_j}{\partial y} \right. \\
 &\quad + {}_0C_{12} \left[ \left( 1 + \frac{\partial u}{\partial x} \right) \left( 1 + \frac{\partial v}{\partial y} \right) \frac{\partial \psi_i}{\partial x} \frac{\partial \psi_j}{\partial y} + \frac{\partial u}{\partial y} \frac{\partial v}{\partial x} \frac{\partial \psi_i}{\partial y} \frac{\partial \psi_j}{\partial x} \right] \\
 &\quad + {}_0C_{66} \left[ \left( 1 + \frac{\partial u}{\partial x} \right) \frac{\partial \psi_i}{\partial y} + \frac{\partial u}{\partial y} \frac{\partial \psi_i}{\partial x} \right] \\
 &\quad \left. \times \left[ \left( 1 + \frac{\partial v}{\partial y} \right) \frac{\partial \psi_j}{\partial x} + \frac{\partial v}{\partial x} \frac{\partial \psi_j}{\partial y} \right] \right\} dx dy = K_{ji}^{21L} \\
 K_{ij}^{22L} &= h_e \int_{\Omega^e} \left\{ {}_0C_{11} \left( \frac{\partial v}{\partial x} \right)^2 \frac{\partial \psi_i}{\partial x} \frac{\partial \psi_j}{\partial x} + {}_0C_{22} \left( 1 + \frac{\partial v}{\partial y} \right)^2 \frac{\partial \psi_i}{\partial y} \frac{\partial \psi_j}{\partial y} \right. \\
 &\quad + {}_0C_{12} \left( 1 + \frac{\partial v}{\partial y} \right) \frac{\partial v}{\partial x} \left( \frac{\partial \psi_i}{\partial x} \frac{\partial \psi_j}{\partial y} + \frac{\partial \psi_i}{\partial y} \frac{\partial \psi_j}{\partial x} \right) \\
 &\quad + {}_0C_{66} \left[ \left( 1 + \frac{\partial v}{\partial y} \right) \frac{\partial \psi_i}{\partial x} + \frac{\partial v}{\partial x} \frac{\partial \psi_i}{\partial y} \right] \\
 &\quad \left. \times \left[ \left( 1 + \frac{\partial v}{\partial y} \right) \frac{\partial \psi_j}{\partial x} + \frac{\partial v}{\partial x} \frac{\partial \psi_j}{\partial y} \right] \right\} dx dy \\
 K_{ij}^{11N} &= h_e \int_{\Omega^e} \left[ {}_1S_{xx} \frac{\partial \psi_i}{\partial x} \frac{\partial \psi_j}{\partial x} + {}_1S_{xy} \left( \frac{\partial \psi_i}{\partial y} \frac{\partial \psi_j}{\partial x} + \frac{\partial \psi_i}{\partial x} \frac{\partial \psi_j}{\partial y} \right) \right. \\
 &\quad \left. + {}_1S_{yy} \frac{\partial \psi_i}{\partial y} \frac{\partial \psi_j}{\partial y} \right] dx dy = K_{ij}^{22N} \tag{9.6.30a}
 \end{aligned}$$

$${}_0^2F_i^1 = h_e \int_{\Omega^e} {}_0^2f_x \psi_i dx dy + h_e \oint_{\Gamma^e} {}_0^2t_x \psi_i ds$$

$${}_0^2F_i^2 = h_e \int_{\Omega^e} {}_0^2f_y \psi_i dx dy + h_e \oint_{\Gamma^e} {}_0^2t_y \psi_i ds$$

$$\begin{aligned}
 {}_1^0F_i^1 &= h_e \int_{\Omega^e} \left\{ \left( 1 + \frac{\partial u}{\partial x} \right) \frac{\partial \psi_i}{\partial x} {}_1^0S_{xx} + \frac{\partial u}{\partial y} \frac{\partial \psi_i}{\partial y} {}_1^0S_{yy} \right. \\
 &\quad \left. + \left[ \left( 1 + \frac{\partial u}{\partial x} \right) \frac{\partial \psi_i}{\partial y} + \frac{\partial u}{\partial y} \frac{\partial \psi_i}{\partial x} \right] {}_1^0S_{xy} \right\} dx dy
 \end{aligned}$$

$$\begin{aligned}
 {}^1_0F_i^2 = h_e \int_{\Omega^e} \left\{ \frac{\partial v}{\partial x} \frac{\partial \psi_i}{\partial x} {}^1_0S_{xx} + \left( 1 + \frac{\partial v}{\partial y} \right) \frac{\partial \psi_i}{\partial y} {}^1_0S_{yy} \right. \\
 \left. + \left[ \left( 1 + \frac{\partial v}{\partial y} \right) \frac{\partial \psi_i}{\partial x} + \frac{\partial v}{\partial x} \frac{\partial \psi_i}{\partial y} \right] {}^1_0S_{xy} \right\} dx dy
 \end{aligned} \quad (9.6.30b)$$

where  $h_e$  is the thickness of the element (for the plane elastic problem).

### 9.6.3 Updated Lagrangian Formulation

In view of the detailed discussion of the finite element model development for the total Lagrangian formulation and the similarity between Eqs. (9.5.17) and (9.5.29), the finite element model based on the updated Lagrangian formulation can be simply written as

$$([K_L] + [K_{NL}]) \{\bar{\Delta}\} = \{^2F\} - \{^1F\} \quad (9.6.31)$$

where

$$[K_L] = \int_{0V} [B_L^0]^T [{}^1C] [B_L^0] d^1V \quad (9.6.32)$$

$$[K_{NL}] = \int_{1V} [B_{NL}]^T [{}^1\sigma] [B_{NL}] d^1V \quad (9.6.33)$$

$$\{^1F\} = \int_{1V} [B_L^0]^T \{^1\sigma\} d^1V \quad (9.6.34)$$

$$\{^2F\} = \int_{1V} [\Psi]^T \{^2f\} d^1V + \int_{1S} [\Psi]^T \{^2t\} d^1S \quad (9.6.35)$$

$$\{^2f\} = \begin{Bmatrix} {}^2f_x \\ {}^2f_y \end{Bmatrix}, \quad \{^2t\} = \begin{Bmatrix} {}^2t_x \\ {}^2t_y \end{Bmatrix} \quad (9.6.36)$$

where  $[B_L^0]$  and  $[B_{NL}]$  are defined by Eqs. (9.6.27a) and (9.6.28), respectively, and

$$[{}^1\sigma] = \begin{bmatrix} {}^1\sigma_{xx} & {}^1\sigma_{xy} & 0 & 0 \\ {}^1\sigma_{xy} & {}^1\sigma_{yy} & 0 & 0 \\ 0 & 0 & {}^1\sigma_{xx} & {}^1\sigma_{xy} \\ 0 & 0 & {}^1\sigma_{xy} & {}^1\sigma_{yy} \end{bmatrix} \quad (9.6.37a)$$

$$\{^1\sigma\} = \begin{Bmatrix} {}^1\sigma_{xx} \\ {}^1\sigma_{yy} \\ {}^1\sigma_{xy} \end{Bmatrix} = \begin{bmatrix} {}^1C_{11} & {}^1C_{12} & 0 \\ {}^1C_{12} & {}^1C_{22} & 0 \\ 0 & 0 & {}^1C_{66} \end{bmatrix} \begin{Bmatrix} {}^1\varepsilon_{xx} \\ {}^1\varepsilon_{yy} \\ 2 {}^1\varepsilon_{xy} \end{Bmatrix} \quad (9.6.37b)$$

$$\{^1\varepsilon\} = \begin{Bmatrix} {}^1\varepsilon_{xx} \\ {}^1\varepsilon_{yy} \\ 2 {}^1\varepsilon_{xy} \end{Bmatrix} = \begin{Bmatrix} \frac{\partial u}{\partial x} - \frac{1}{2} \left[ \left( \frac{\partial u}{\partial x} \right)^2 + \left( \frac{\partial v}{\partial x} \right)^2 \right] \\ \frac{\partial v}{\partial y} - \frac{1}{2} \left[ \left( \frac{\partial u}{\partial y} \right)^2 + \left( \frac{\partial v}{\partial y} \right)^2 \right] \\ \frac{\partial u}{\partial y} + \frac{\partial v}{\partial x} - \left( \frac{\partial u}{\partial x} \frac{\partial u}{\partial y} + \frac{\partial v}{\partial x} \frac{\partial v}{\partial y} \right) \end{Bmatrix} \quad (9.6.37c)$$



The finite element equations (9.6.31) can be written in explicit form as

$$\begin{bmatrix} [K^{11L}] + [K^{11N}] & [K^{12L}] \\ [K^{21L}] & [K^{22L}] + [K^{22N}] \end{bmatrix} \begin{Bmatrix} \{\bar{u}\} \\ \{\bar{v}\} \end{Bmatrix} = \begin{Bmatrix} \{ {}^2F^1 \} - \{ {}^1F^1 \} \\ \{ {}^2F^2 \} - \{ {}^1F^2 \} \end{Bmatrix} \quad (9.6.38)$$

where

$$\begin{aligned} K_{ij}^{11L} &= h_e \int_{\Omega^e} \left( {}^1C_{11} \frac{\partial \psi_i}{\partial x} \frac{\partial \psi_j}{\partial x} + {}^1C_{66} \frac{\partial \psi_i}{\partial y} \frac{\partial \psi_j}{\partial y} \right) dx dy \\ K_{ij}^{12L} &= h_e \int_{\Omega^e} \left( {}^1C_{12} \frac{\partial \psi_i}{\partial x} \frac{\partial \psi_j}{\partial y} + {}^1C_{66} \frac{\partial \psi_i}{\partial y} \frac{\partial \psi_j}{\partial x} \right) dx dy = K_{ji}^{21L} \\ K_{ij}^{22L} &= h_e \int_{\Omega^e} \left( {}^1C_{66} \frac{\partial \psi_i}{\partial x} \frac{\partial \psi_j}{\partial x} + {}^1C_{22} \frac{\partial \psi_i}{\partial y} \frac{\partial \psi_j}{\partial y} \right) dx dy \\ K_{ij}^{11N} &= h_e \int_{\Omega^e} \left[ {}^1\sigma_{xx} \frac{\partial \psi_i}{\partial x} \frac{\partial \psi_j}{\partial x} + {}^1\sigma_{xy} \left( \frac{\partial \psi_i}{\partial y} \frac{\partial \psi_j}{\partial x} + \frac{\partial \psi_i}{\partial x} \frac{\partial \psi_j}{\partial y} \right) \right. \\ &\quad \left. + {}^1\sigma_{yy} \frac{\partial \psi_i}{\partial y} \frac{\partial \psi_j}{\partial y} \right] dx dy = K_{ij}^{22N} \end{aligned} \quad (9.6.39a)$$

$$\begin{aligned} {}^2_1F_i^1 &= h_e \int_{\Omega^e} {}^2_1f_x \psi_i dx dy + h_e \oint_{\Gamma^e} {}^2_1t_x \psi_i ds \\ {}^2_1F_i^2 &= h_e \int_{\Omega^e} {}^2_1f_y \psi_i dx dy + h_e \oint_{\Gamma^e} {}^2_1t_y \psi_i ds \\ {}^1_1F_i^1 &= h_e \int_{\Omega^e} \left( \frac{\partial \psi_i}{\partial x} {}^1\sigma_{xx} + \frac{\partial \psi_i}{\partial y} {}^1\sigma_{xy} \right) dx dy \\ {}^1_1F_i^2 &= h_e \int_{\Omega^e} \left( \frac{\partial \psi_i}{\partial x} {}^1\sigma_{xy} + \frac{\partial \psi_i}{\partial y} {}^1\sigma_{yy} \right) dx dy \end{aligned} \quad (9.6.39b)$$

where  $h_e$  is the thickness of the element  ${}^1x_1 = x$  and  ${}^1x_2 = y$ .

### 9.6.4 Computer Implementation

The computer implementation of the two nonlinear formulations discussed in this chapter follows along the same lines as discussed for the Newton-Raphson procedure used for plate bending. Box 9.6.1 contains the portion of the main program where element information is passed on to the element subroutine and error check, while Box 9.6.2 contains the main parts of the element subroutine.

### 9.6.5 Numerical Results

Here we present numerical results obtained for a cantilever beam under uniformly distributed load using the total and updated Lagrangian formulations. Suppose that the beam is of length  $a = 10$  in., height  $b = 1$  in., and thickness  $h = 1$  in. A mesh of five eight-node quadratic elements are used, and load increment of  $\Delta q_0 = -0.5$  psi (acting downward) is used. The

## Box 9.6.1 Fortran statements showing the transfer of element information and error check.

```

P0=0.0
NFLAG=0
DO 500 LOAD=1,NLS
P0=P0+DP(LOAD)
ITER=0
220 ITER=ITER+1
.
.
C
C Compute and assemble element matrices
C
DO 340 N=1,NEM
DO 260 I=1,NPE
NI=NOD(N,I)
ELXY(I,1)=X(NI)
ELXY(I,2)=Y(NI)
L=NI*NDF-1
K=I*NDF-1
ELU(K) =GLU(L)
ELU(K+1)=GLU(L+1)
260 CONTINUE
C
270 CALL STIFF (IEL,NGP,NN,NPE,P,NAXIS,ITER,NEWTON,LFORM)
.
.
340 CONTINUE
C
C Impose the specified displacement and force dof and solve the equations (GF is the
C incremental displacement vector). Update the total solution vector GT and coordinates.
C
DO 420 I=1,NNM
L=(I-1)*NDF+1
GLU(L) =GLU(L) +GF(L)
GLU(L+1)=GLU(L+1)+GF(L+1)
IF(LFORM.GT.1)THEN
X(I)=X(I)+GF(L)
Y(I)=Y(I)+GF(L+1)
ENDIF
420 CONTINUE
C
SNORM=0.0
ENORM=0.0
DO 430 I=1,NEQ
SNORM=SNORM+GLU(I)*GLU(I)
430 ENORM=ENORM+GF(I)*GF(I)
TOL=DSQRT(ENORM/SNORM)
IF (TOL.GT.EPS) THEN
IF (ITER.GT.ITMAX) THEN
write a message
STOP
ELSE
GOTO 220
ENDIF
ENDIF
.
.
500 CONTINUE

```

**Box 9.6.2** Fortran statements showing the element matrix calculations for the total and updated Lagrangian formulations.

```

SUBROUTINE STIFF(IEL,IDYN,NGP,NN,NPE,P,NAXIS,ITER,NEWTON,LFORM)
C
C
C STIFFNESS MATRIX FOR ISOPARAMETRIC QUADRILATERAL ELEMENTS
C (Total and Updated Lagrangian Formulations)
C
C LFORM.....Indicator for the type of formulation:
C LFORM=1, TOTAL Lagrangian formulation
C LFORM>1, UPDATED Lagrangian formulation
C
C
C
C Initialize element force vector and stiffness matrix
C
DO 10 I=1,NN
F(I)=0.0
DO 10 J=1,NN
ELSTIF(I,J)=0.0
10 CONTINUE
C
C Numerical integration to evaluate the element matrices
C
DO 60 NI=1,NGP
DO 60 NJ=1,NGP
XI =GAUSSPT(NI,NGP)
ETA=GAUSSPT(NJ,NGP)
CALL SHAPE (NPE,XI,ETA,SF,GDSF,DET,ELXY)
CONST=DET*GAUSSWT(NI,NGP)*GAUSSWT(NJ,NGP)
C
C Define the gradients of displacements and strains
C
X=0.0
U=0.0
UX=0.0
UY=0.0
VX=0.0
VY=0.0
DO 20 I=1,NPE
L=(I-1)*NDF+1
X=X+SF(I)*ELXY(I,1)
U=U+SF(I)*ELU(L)
UX=UX+GDSF(1,I)*ELU(L)
UY=UY+GDSF(2,I)*ELU(L)
VX=VX+GDSF(1,I)*ELU(L+1)
20 VY=VY+GDSF(2,I)*ELU(L+1)
UX2=UX*UX
UY2=UY*UY
VX2=VX*VX
VY2=VY*VY

```

(Box 9.6.2 continued)

```

C
  IF(LFORM.EQ.1)THEN
    UXP1=1.0+UX
    UXP2=UXP1*UXP1
    VYP1=1.0+VY
    VYP2=VYP1*VYP1
  C
    EX=UX+0.5*(UX2+VX2)
    EY=VY+0.5*(UY2+VY2)
    EXY=UY+VX+UX*UY+VX*VY
    S11=C(1,1)*EX+C(1,2)*EY
    S22=C(1,2)*EX+C(2,2)*EY
    S12=C(3,3)*EXY
  ELSE
  C
  C Compute the Almansi strains and Cauchy stresses
  C
    EX=UX-0.5*(UX2+VX2)
    EY=VY-0.5*(UY2+VY2)
    EXY=UY+VX-UX*UY-VX*VY
    S11=C(1,1)*EX+C(1,2)*EY
    S22=C(1,2)*EX+C(2,2)*EY
    S12=C(3,3)*EXY
  ENDIF
  C
  C Compute element force vector and stiffness matrix
  C
    II=1
    DO 50 I=1,NPE
  C
  C Imbalance force coefficients for the TOTAL Lagrangian formulation
  C
    IF(LFORM.EQ.1)THEN
      F(II) =F(II) +(P*SF(I)-UXP1*GDSF(1,I)*S11-UY*GDSF(2,I)*S22
      * -(UXP1*GDSF(2,I)+UY*GDSF(1,I))*S12)*CONST
      F(II+1)=F(II+1)+(P*SF(I)-VX*GDSF(1,I)*S11-VYP1*GDSF(2,I)*S22
      * -(VYP1*GDSF(1,I)+VX*GDSF(2,I))*S12)*CONST
    C
    C Imbalance force coefficients for the UPDATED Lagrangian formulation
    C
      ELSE
        F(II)=F(II)+(P*SF(I)-GDSF(1,I)*S11-GDSF(2,I)*S12)*CONST
        F(II+1)=F(II+1)+(P*SF(I)-GDSF(1,I)*S12-GDSF(2,I)*S22)*CONST
      ENDIF
      JJ=1
      DO 40 J=1,NPE
        SIG=S11*GDSF(1,I)*GDSF(1,J)+S22*GDSF(2,I)*GDSF(2,J)
        * +S12*(GDSF(1,I)*GDSF(2,J)+GDSF(2,I)*GDSF(1,J))
      C
      IF(LFORM.EQ.1)THEN

```

(Box 9.6.2 continued)

```

C
C Stiffness coefficients for the TOTAL Lagrangian formulation
C
  ELSTIF(II,JJ)=ELSTIF(II,JJ)+(C(1,1)*UXP2*GDSF(1,I)*GDSF(1,J)
*   +C(2,2)*UY2*GDSF(2,I)*GDSF(2,J)
*   +C(1,2)*UXP1*UY*(GDSF(1,I)*GDSF(2,J)+GDSF(2,I)*GDSF(1,J))
*   +C(3,3)*(UXP1*GDSF(2,I)+UY*GDSF(1,I))*
*   (UXP1*GDSF(2,J)+UY*GDSF(1,J))+SIG)*CONST
  ELSTIF(II+1,JJ+1)=ELSTIF(II+1,JJ+1)+(C(1,1)*VX2*GDSF(1,I)
*   *GDSF(1,J)+C(2,2)*VYP2*GDSF(2,I)*GDSF(2,J)
*   +C(1,2)*VYP1*VX*(GDSF(1,I)*GDSF(2,J)+GDSF(2,I)*GDSF(1,J))
*   +C(3,3)*(VYP1*GDSF(1,I)+VX*GDSF(2,I))*
*   (VYP1*GDSF(1,J)+VX*GDSF(2,J))+SIG)*CONST
  ELSTIF(II,JJ+1)=ELSTIF(II,JJ+1)+(C(1,1)*UXP1*VX*GDSF(1,I)
*   *GDSF(1,J)+C(2,2)*VYP1*UY*GDSF(2,I)*GDSF(2,J)
*   +C(1,2)*(UXP1*VYP1*GDSF(1,I)*GDSF(2,J)
*   +UY*VX*GDSF(2,I)*GDSF(1,J))
*   +C(3,3)*(UXP1*GDSF(2,I)+UY*GDSF(1,I))*
*   (VYP1*GDSF(1,J)+VX*GDSF(2,J))*CONST
  ELSTIF(II+1,JJ)=ELSTIF(II+1,JJ)+(C(1,1)*UXP1*VX*GDSF(1,I)
*   *GDSF(1,I)+C(2,2)*VYP1*UY*GDSF(2,I)*GDSF(2,I)
*   +C(1,2)*(UXP1*VYP1*GDSF(1,I)*GDSF(2,I)
*   +UY*VX*GDSF(2,I)*GDSF(1,I))
*   +C(3,3)*(UXP1*GDSF(2,I)+UY*GDSF(1,I))*
*   (VYP1*GDSF(1,I)+VX*GDSF(2,I))*CONST
C
C Stiffness coefficients for the UPDATED Lagrangian formulation
C
  ELSE
  ELSTIF(II,JJ)=ELSTIF(II,JJ)+(C(1,1)*GDSF(1,I)*GDSF(1,I)
*   +C(3,3)*GDSF(2,I)*GDSF(2,I)+SIG)*CONST
  ELSTIF(II+1,JJ+1)=ELSTIF(II+1,JJ+1)+(C(3,3)*GDSF(1,I)
*   *GDSF(1,I)+C(2,2)*GDSF(2,I)*GDSF(2,I)+SIG)*CONST
  ELSTIF(II,JJ+1)=ELSTIF(II,JJ+1)+(C(1,2)*GDSF(1,I)*GDSF(2,I)
*   +C(3,3)*GDSF(2,I)*GDSF(1,I))*CONST
  ELSTIF(II+1,JJ)=ELSTIF(II+1,JJ)+(C(1,2)*GDSF(2,I)*GDSF(1,I)
*   +C(3,3)*GDSF(1,I)*GDSF(2,I))*CONST
  ENDIF
40 JJ=NDF*J+1
50 II=NDF*I+1
60 CONTINUE
  RETURN
  END

```

material properties used are

$$E = 1.2 \times 10^4 \text{ psi}, \quad \nu = 0.2 \quad (9.6.40)$$

The beam assumed to be in the *plane state of stress* so that (no distinction is made between  ${}_1C_{ij}$  and  ${}_0C_{ij}$  for the two formulations, and they are assumed to remain constant during the deformation).

Table 9.6.1 contains the numerical results obtained with the updated Lagrangian formulation for the center deflection at the free end (also see Figure 9.6.1), while Table 9.6.2 contains (also see Figure 9.6.2) the Cauchy and second Piola-Kirchhoff stresses at the fixed end of the beam (at the Gauss point located nearest to the top left end). The load was distributed equally at the top and bottom of the beam. Surprisingly, the solution without iteration is very good, except for initial oscillations. It took only 2 or 3 iterations to converge for each load step.

**Table 9.6.1** Transverse deflections of a cantilevered beam under uniform load (applied equally at the top and bottom), obtained with the updated Lagrangian formulation ( $5 \times 1Q8$  mesh).

$-q_0$	$x$	$y$	$u(10, 0.5)$	$v(10, 0.5)$
1.0	9.914	-0.730	-0.086	-1.230*
	9.968	-0.287	-0.032	-0.787
2.0	9.674	-1.884	-0.326	-2.384
	9.822	-1.291	-0.178	-1.791
3.0	9.327	-2.893	-0.673	-3.393
	9.530	-2.373	-0.470	-2.873
4.0	8.920	-3.750	-1.080	-4.250
	9.145	-3.327	-0.855	-3.827
5.0	8.493	-4.460	-1.507	-4.960
	8.699	-4.153	-1.301	-4.653
6.0	8.070	-5.045	-1.930	-5.545
	8.244	-4.831	-1.756	-5.331
8.0	7.286	-5.926	-2.714	-6.426
	7.391	-5.831	-2.609	-6.331
10.0	6.609	-6.540	-3.391	-7.040
	6.656	-6.506	-3.344	-7.006
12.0	6.035	-6.981	-3.965	-7.481
	6.052	-6.971	-3.948	-7.471
14.0	5.550	-7.309	-4.450	-7.809
	5.557	-7.305	-4.443	-7.805
16.0	5.137	-7.562	-4.863	-8.062
	5.142	-7.559	-4.858	-8.059

\*The first row corresponds to iteration and the second row to the no iteration.

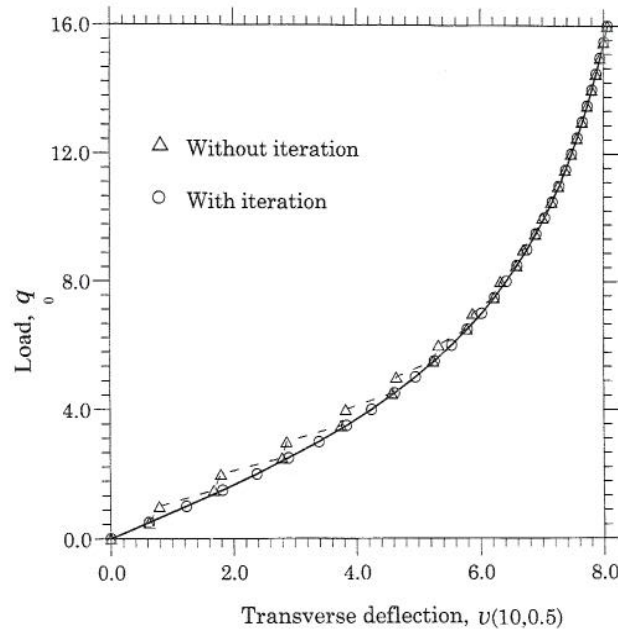


Figure 9.6.1 Transverse deflection  $v(10, 0.5)$  versus load  $q_0$  for a cantilever beam under uniform load of intensity  $q_0$ .

Table 9.6.2 A comparison of the stresses  ${}^1\sigma_{xx}$  and  ${}^1_0S_{xx}$  obtained with the updated Lagrangian formulation.

$-q_0$	${}^1\sigma_{xx}$	${}^1_0S_{xx}$	${}^1\sigma_{yy}$	${}^1_0S_{yy}$
1.0	153.55	161.76	23.15	28.88
2.0	300.14	332.20	43.65	65.41
3.0	434.44	503.43	61.50	107.05
4.0	555.38	671.46	77.11	151.82
5.0	662.83	833.34	90.87	198.02
6.0	758.08	988.19	103.17	244.66
8.0	918.14	1277.32	124.61	337.16
10.0	1046.77	1542.59	143.15	427.19
12.0	1152.26	1788.70	159.78	514.33
14.0	1240.32	2019.60	175.11	598.72
16.0	1314.87	2238.26	189.50	680.62

Table 9.6.3 contains the numerical results for the center deflection at the free end and the second Piola–Kirchhoff stresses at the fixed end of the beam (at the Gauss point located nearest to the top left end). The results were obtained with the total Lagrangian description and with nonlinear iteration. Results are included only for selective loads. Only 2 to 3 iterations were taken to converge at each load step.

Table 9.6.3 Transverse deflections of a cantilevered beam obtained with the total Lagrangian formulation.

$-q_0^*$	$u(10, 0.5)$	$v(10, 0.5)$	${}^1\sigma_{xx}$	${}^1_0S_{xx}$
1.0	-0.087	-1.230	143.84	151.97
2.0	-0.331	-2.382	263.28	294.79
4.0	-1.091	-4.237	426.04	538.12
6.0	-1.942	-5.516	509.29	728.24
8.0	-2.721	-6.380	539.85	877.75
10.0	-3.391	-6.979	536.14	998.51
12.0	-3.957	-7.408	509.23	1098.78
14.0	-4.434	-7.726	465.82	1184.04
16.0	-4.839	-7.971	410.10	1257.97

\*The linear solution at  $q_0 = -0.5$  is  $v(10, 0.5) = -0.6227$ .

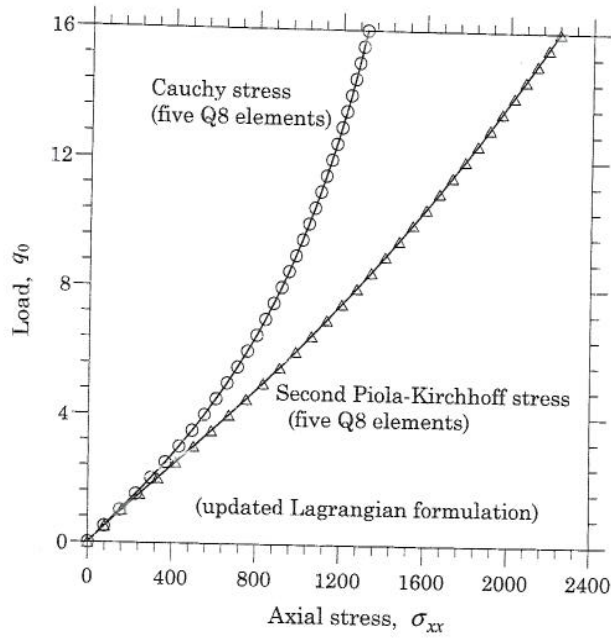


Figure 9.6.2 Normal stresses versus load for a cantilever beam under uniform load of intensity  $q_0$ .

This completes the development of finite element models of nonlinear continua. The procedures developed herein can be readily extended to axisymmetric problems, three-dimensional problems, problems with assumed displacements and/or strains [7-9], and composite plates and shells [10]. The extension of the formulations to transient problems is straightforward.



## 9.7 Shell Finite Elements

### 9.7.1 Introduction

In previous chapters, the beam and plate elements were developed using beam and plate theories that were derived from an assumed displacement field. Such theories are limited to geometrically linear analyses and nonlinear analysis with small strains and moderate rotations. The finite element models to be developed in this section are based on three-dimensional elasticity equations, and the geometry and the displacement fields of the structure are directly discretized by imposing some geometric and static constraints to satisfy the assumptions of a beam or shell theory. Both shell and beam elements can have a variable number of nodes, and the shell element can be modified as transition elements to model shell intersections or solid-to-shell transition regions. Such formulations would appear to be especially applicable to material and geometrical nonlinear analysis of shell-type structures in which large displacements and rotations are experienced (see [2,10-27]).

### 9.7.2 Incremental Equations of Motion

Consider the motion of a body in a fixed Cartesian coordinate system. Assuming that the body may experience large displacements and rotations, we wish to determine deformed configurations of the body for different times/loads. We assume that all configurations from time  $t = 0$  to the current time  $t$ , both inclusive, have been determined, and the configuration  $C_2$  for time  $t = t + \Delta t$  is sought next. The total Lagrangian description with the principle of virtual displacements (9.5.17) is used to express the dynamic equilibrium of the body in the configuration  $C_2$ .

For dynamic analysis, the principle of virtual displacements (9.5.17) must be modified to include inertial terms. In this case we have

$$\int_{2V} {}^2\rho {}^2\ddot{u}_i \delta^2 u_i d^2V = \int_{0V} {}^0\rho {}^2\ddot{u}_i \delta^2 u_i d^0V \quad (9.7.1)$$

and hence the mass matrix can be evaluated using the initial configuration of the body. Using Hamilton's principle we obtain the equations of motion of the moving body at time  $t + \Delta t$  in the variational form as

$$\begin{aligned} \int_{0V} {}^0\rho {}^2\ddot{u}_i \delta^2 u_i d^0V + \int_{0V} {}^0C_{ijrs} {}^0e_{rs} \delta {}^0e_{ij} d^0V + \int_{0V} {}^1S_{ij} \delta {}^0\eta_{ij} d^0V \\ = {}^2R - \int_{0V} {}^1S_{ij} \delta {}^0e_{ij} d^0V \end{aligned} \quad (9.7.2)$$

where  $\delta^2 u_i = \delta u_i$ .

### 9.7.3 Finite Element Model of a Continuum

Equation (9.7.2) can be used to develop the nonlinear displacement finite element model for any continuum. The basic step in deriving the finite element equations for a shell element is the selection of proper interpolation functions for the displacement field and geometry. In the case of beam and shell elements, the approximation for the geometry is chosen such that the beam or shell kinematic hypotheses are realized. First, we derive the finite element model of a continuum and then specialize it to shells [24-26].

It is important that the coordinates and displacements are interpolated using the same interpolation functions (isoparametric formulation) so that the displacement compatibility across element boundaries can be preserved in all configurations. Let

$${}^0x_i = \sum_{k=1}^n \psi_k {}^0x_i^k, \quad {}^1x_i = \sum_{k=1}^n \psi_k {}^1x_i^k, \quad {}^2x_i = \sum_{k=1}^n \psi_k {}^2x_i^k \quad (9.7.3)$$

$${}^1u_i = \sum_{k=1}^n \psi_k {}^1u_i^k, \quad u_i = \sum_{k=1}^n \psi_k u_i^k \quad (i = 1, 2, 3) \quad (9.7.4)$$

where the right superscript  $k$  indicates the quantity at nodal point  $k$ ,  $\psi_k$  is the interpolation function corresponding to nodal point  $k$ , and  $n$  is the number of element nodal points.

Substitution of Eqs. (9.7.3) and (9.7.4) in Eq. (9.7.2) yields the finite element model

$${}^1_0[M]\{\ddot{\Delta}^e\} + ({}^1_0[K_L] + {}^1_0[K_{NL}])\{\Delta^e\} = {}^2\{R\} - {}^1_0\{F\} \quad (9.7.5)$$

where  $\{\Delta^e\}$  is the vector of nodal incremental displacements from time  $t$  to time  $t + \Delta t$  in an element, and  ${}^1_0[M]\{\ddot{\Delta}^e\}$ ,  ${}^1_0[K_L]\{\Delta^e\}$ ,  ${}^1_0[K_{NL}]\{\Delta^e\}$ , and  ${}^1_0\{F\}$  are obtained by evaluating the integrals, respectively:

$$\int_{0V} {}^0\rho {}^2\ddot{u}_i \delta {}^2u_i d^0V, \quad \int_{0V} {}^0C_{ijrs} {}^0e_{rs} \delta {}^0e_{ij} d^0V$$

$$\int_{0V} {}^1S_{ij} \delta {}^0\eta_{ij} d^0V, \quad \int_{0V} {}^1S_{ij} \delta {}^0e_{ij} d^0V$$

Various matrices are defined by

$${}^1_0[K_L] = \int_{0A} {}^1_0[B_L]^T {}^0[C] {}^1_0[B_L] d^0V \quad (9.7.6a)$$

$${}^1_0[K_{NL}] = \int_{0V} {}^1_0[B_{NL}]^T {}^0[S] {}^1_0[B_{NL}] d^0V \quad (9.7.6b)$$

$${}^1_0[M] = \int_{0V} {}^0\rho {}^1[H]^T {}^1[H] d^0V \quad (9.7.6c)$$

$${}^1_0\{F\} = \int_{0V} {}^1_0[B_L]^T {}^1\{\hat{S}\} d^0V \quad (9.7.6d)$$

In the above equations,  ${}^1_0[B_L]$  and  ${}^1_0[B_{NL}]$  are the linear and nonlinear strain-displacement transformation matrices,  ${}^0[C]$  is the incremental stress-strain material property matrix,  ${}^0[S]$  is a matrix of 2nd Piola-Kirchhoff stress components,  ${}^0\{\hat{S}\}$  is a vector of these stresses, and  ${}^1[H]$  is the incremental displacement interpolation matrix. All matrix elements correspond to the configuration at time  $t$  and are defined with respect to the configuration at time  $t = 0$ . It is important to note that Eq. (9.7.5) is only an approximation to the actual solution to be determined in each time step [see Eq. (9.5.15)]. Therefore, it may be necessary to iterate in each time step until Eq. (9.5.15), with inertia terms, is satisfied to a required tolerance.

The finite element equations (9.7.5) are second-order differential equations in time. In order to obtain numerical solutions at each time step, Eq. (9.7.5) needs to be converted to algebraic equations using a time approximation scheme, as explained in Chapter 8. In the present study the Newmark scheme (see Section 8.2.3 for details) is used.

In the Newmark time integration scheme, the displacements and velocities are approximated by [see Eqs. (8.2.22) and (8.2.23)]

$$\begin{aligned} {}^{t+\Delta t}\{\Delta\} &= \Delta t {}^t\{\Delta\} + {}^t\{\dot{\Delta}\} + (\Delta t)^2 \left[ \left( \frac{1}{2} - \beta \right) {}^t\{\ddot{\Delta}\} + \beta {}^{t+\Delta t}\{\ddot{\Delta}\} \right] \\ {}^{t+\Delta t}\{\dot{\Delta}\} &= {}^t\{\dot{\Delta}\} + \Delta t \left[ (1 - \alpha) {}^t\{\ddot{\Delta}\} + \alpha {}^{t+\Delta t}\{\ddot{\Delta}\} \right] \end{aligned} \quad (9.7.7)$$

where  $\alpha = \frac{1}{2}$  and  $\beta = \frac{1}{4}$  for the constant-average acceleration method, and  $\Delta t$  is the time step. Rearranging Eqs. (9.7.5) and (9.7.7), we obtain  ${}^1_0[M] \approx {}^2_0[M]$ ; see Eq. (8.2.15)]

$${}^1_0[\hat{K}]\{\Delta\} = {}^2\{\hat{R}\} \quad (9.7.8)$$

where  $\{\Delta\}$  is the vector of nodal incremental displacements at time  $t$ ,  $\{\Delta\} = {}^{t+\Delta t}\{\Delta\} - {}^t\{\Delta\}$ , and

$${}^1_0[\hat{K}] = a_3 {}^1_0[M] + {}^1_0[K_L] + {}^1_0[K_{NL}] \quad (9.7.9a)$$

$${}^2\{\hat{R}\} = {}^2\{R\} - {}^1_0\{F\} + {}^1_0[M] \left( a_3 {}^t\{\Delta\} + a_4 {}^t\{\dot{\Delta}\} + a_5 {}^t\{\ddot{\Delta}\} \right) \quad (9.7.9b)$$

$$a_3 = \frac{1}{\beta(\Delta t)^2}, \quad a_4 = a_3 \Delta t, \quad a_5 = \frac{1}{2\beta} - 1 \quad (9.7.10)$$

Once Eq. (9.7.8) is solved for  $\{\Delta\}$  at time  $t + \Delta t$ , the acceleration and velocity vectors are obtained using  $[a_1 = \alpha \Delta t$  and  $a_2 = (1 - \alpha) \Delta t$ ; see Eqs. (8.2.19)]

$$\begin{aligned} {}^{t+\Delta t}\{\ddot{\Delta}\} &= a_3 \{\Delta\} - a_4 {}^t\{\dot{\Delta}\} - a_5 {}^t\{\ddot{\Delta}\} \\ {}^{t+\Delta t}\{\dot{\Delta}\} &= {}^t\{\dot{\Delta}\} + a_1 {}^{t+\Delta t}\{\ddot{\Delta}\} + a_2 {}^t\{\ddot{\Delta}\} \end{aligned} \quad (9.7.11)$$

The finite element equations (9.7.8) are solved, after assembly and imposition of boundary conditions, iteratively at each time step until Eq. (9.5.15) is satisfied within a required tolerance. The Newton–Raphson method with Riks–Wempner algorithm (see Appendix A1) is used in the present study.

#### 9.7.4 Shell Finite Element

The shell element is deduced from the three-dimensional continuum element by imposing two kinematic constraints: (1) straight line normal to the mid-surface of the shell before deformation remains straight but not normal after deformation; (2) the transverse normal components of strain and stress are ignored in the development. However, the shell element admits arbitrarily large displacements and rotations but small strains since the shell thickness is assumed not to change and the normal is not allowed to distort [22, 24–26, 28].

Consider the solid three-dimensional element shown in Figure 9.7.1. Let  $(\xi, \eta)$  be the curvilinear coordinates in the middle surface of the shell and  $\zeta$  be the coordinate in the thickness direction. The coordinates  $(\xi, \eta, \zeta)$  are normalized such that they vary between  $-1$  and  $+1$ . The coordinates of a typical point in the element can be written as

$$x_i = \sum_{k=1}^n \psi_k(\xi, \eta) \left[ \frac{1+\zeta}{2} (x_i^k)_{\text{top}} + \frac{1-\zeta}{2} (x_i^k)_{\text{bottom}} \right] \quad (9.7.12)$$

where  $n$  is the number of nodes in the element, and  $\psi_k(\zeta, \eta)$  is the finite element interpolation function associated with node  $k$ . If  $\psi_k(\xi, \eta)$  are derived as interpolation functions of a parent element, square or triangular in-plane, then compatibility is achieved at the interfaces of curved space shell elements. Define

$$V_{3i}^k = (x_i^k)_{\text{top}} - (x_i^k)_{\text{bottom}}, \quad \hat{e}_3^k = \mathbf{V}_3^k / |\mathbf{V}_3^k| \quad (9.7.13)$$

where  $\mathbf{V}_3^k$  is the vector connecting the upper and lower points of the normal at node  $k$ . Equation (9.7.12) can be rewritten as

$$x_i = \sum_{k=1}^n \psi_k(\xi, \eta) \left[ (x_i^k)_{\text{mid}} + \frac{\zeta}{2} V_{3i}^k \right] = \sum_{k=1}^n \psi_k(\xi, \eta) \left[ (x_i^k)_{\text{mid}} + \frac{\zeta}{2} h_k e_{3i}^k \right] \quad (9.7.14)$$

where  $h_k = |\mathbf{V}_3^k|$  is the thickness of the shell element at node  $k$ . Hence, the coordinates of any point in the element at time  $t$  are interpolated by the expression

$${}^1x_i = \sum_{k=1}^n \psi_k(\xi, \eta) \left[ {}^1x_i^k + \frac{\zeta}{2} h_k {}^1e_{3i}^k \right] \quad (9.7.15)$$

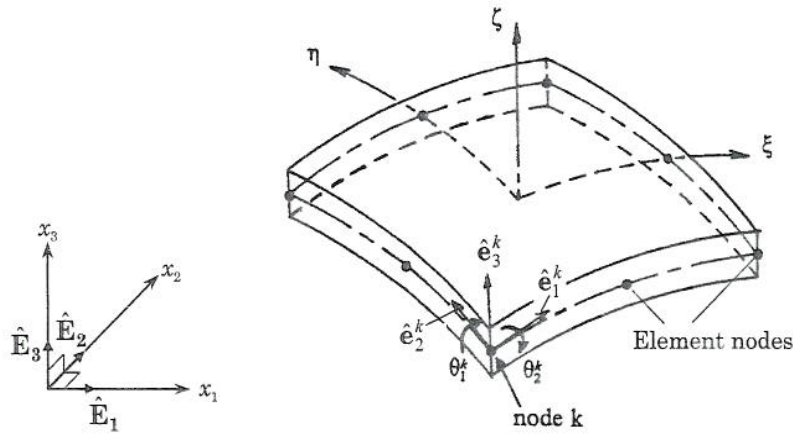


Figure 9.7.1 Geometry and coordinate system of a curved shell element.

and the displacements and incremental displacements by

$${}^1u_i = {}^1x_i - {}^0x_i = \sum_{k=1}^n \psi_k(\xi, \eta) \left[ {}^1u_i^k + \frac{\zeta}{2} h_k ({}^1e_{3i}^k - {}^0e_{3i}^k) \right] \quad (9.7.16)$$

$$u_i = {}^2u_i - {}^1u_i = \sum_{k=1}^n \psi_k(\xi, \eta) \left[ u_i^k + \frac{\zeta}{2} h_k ({}^2e_{3i}^k - {}^1e_{3i}^k) \right] \quad (9.7.17)$$

Here  ${}^1u_i^k$  and  $u_i^k$  denote, respectively, the displacement and incremental displacement components in the  $x_i$ -direction at the  $k$ th node and time  $t$ . For small rotation  $d\Omega$  at each node, we have

$$d\Omega = \theta_2^k {}^1\hat{e}_1^k + \theta_1^k {}^1\hat{e}_2^k + \theta_3^k {}^1\hat{e}_3^k \quad (9.7.18)$$

the increment of vector  ${}^1\hat{e}_3^k$  can be written as

$$\Delta {}^1\hat{e}_3^k = {}^2\hat{e}_3^k - {}^1\hat{e}_3^k = d\Omega \times {}^1\hat{e}_3^k = \theta_1^k {}^1\hat{e}_1^k - \theta_2^k {}^1\hat{e}_2^k \quad (9.7.19)$$

Then Eq. (9.7.17) becomes

$$u_i = \sum_{k=1}^n \psi_k(\xi, \eta) \left[ u_i^k + \frac{\zeta}{2} h_k (\theta_1^k {}^1e_{1i}^k - \theta_2^k {}^1e_{2i}^k) \right] \quad (i = 1, 2, 3) \quad (9.7.20)$$

The unit vectors  ${}^1\hat{e}_1^k$  and  ${}^1\hat{e}_2^k$  at node  $k$  can be obtained from the relations

$${}^1\hat{e}_1^k = \frac{\hat{\mathbf{E}}_2 \times {}^1\hat{e}_3^k}{|\hat{\mathbf{E}}_2 \times {}^1\hat{e}_3^k|}, \quad {}^1\hat{e}_2^k = {}^1\hat{e}_3^k \times {}^1\hat{e}_1^k \quad (9.7.21)$$

where  $\hat{E}_i$  are the unit vectors of the stationary global coordinate system ( ${}^0x_1, {}^0x_2, {}^0x_3$ ). Equation (9.7.35) can be written in matrix form as

$$\{u\} = \{u_1 \ u_2 \ u_3\}^T = {}^1[H]_{3 \times 5n} \{\Delta^e\}^{5n \times 1} \tag{9.7.22}$$

where  $\{\Delta^e\} = \{u_i^k \ \theta_1^k \ \theta_2^k\}^T$ , ( $i = 1, 2, 3, k = 1, 2, \dots, n$ , and  $n$  is the number of nodes) is the vector of nodal incremental displacements (five per node), and  ${}^1[H]$  is the incremental displacement interpolation matrix

$${}^1[H]_{3 \times 5n} = \begin{bmatrix} \dots & \psi_k & 0 & 0 & \frac{1}{2}\psi_k\zeta h_k {}^1e_{11}^k & -\frac{1}{2}\psi_k\zeta h_k {}^1e_{21}^k & \dots \\ \dots & 0 & \psi_k & 0 & \frac{1}{2}\psi_k\zeta h_k {}^1e_{12}^k & -\frac{1}{2}\psi_k\zeta h_k {}^1e_{22}^k & \dots \\ \dots & 0 & 0 & \psi_k & \frac{1}{2}\psi_k\zeta h_k {}^1e_{13}^k & -\frac{1}{2}\psi_k\zeta h_k {}^1e_{23}^k & \dots \end{bmatrix} \tag{9.7.23}$$

For each time step or iteration step one can find three unit vectors at each node from Eqs. (9.7.19) and (9.7.21).

From Eq. (9.3.17) the linear strain increments  $\{0e\} = \{0e_{11} \ 0e_{22} \ 0e_{33} \ 2_0e_{12} \ 2_0e_{13} \ 2_0e_{23}\}^T$  can be expressed as

$$\{0e\} = {}^1[A]\{0u\} \tag{9.7.24a}$$

where  $\{0u\}$  is the vector of derivatives of increment displacements,

$$\begin{aligned} \{0u\} &= \{0u_{1,1} \ 0u_{1,2} \ 0u_{1,3} \ 0u_{2,1} \ 0u_{2,2} \ 0u_{2,3} \ 0u_{3,1} \ 0u_{3,2} \ 0u_{3,3}\}^T \\ {}^1[A]_{6 \times 9} &= \begin{bmatrix} 1 + \frac{1}{0}u_{1,1} & 0 & 0 & \dots & \frac{1}{0}u_{3,1} & 0 & 0 \\ 0 & \frac{1}{0}u_{1,2} & 0 & \dots & 0 & \frac{1}{0}u_{3,2} & 0 \\ 0 & 0 & \frac{1}{0}u_{1,3} & \dots & 0 & 0 & 1 + \frac{1}{0}u_{3,3} \\ \frac{1}{0}u_{1,2} & 1 + \frac{1}{0}u_{1,1} & 0 & \dots & \frac{1}{0}u_{3,2} & \frac{1}{0}u_{3,1} & 0 \\ \frac{1}{0}u_{1,3} & 0 & 1 + \frac{1}{0}u_{1,1} & \dots & 1 + \frac{1}{0}u_{3,3} & 0 & \frac{1}{0}u_{3,1} \\ 0 & \frac{1}{0}u_{1,3} & \frac{1}{0}u_{1,2} & \dots & 0 & 1 + \frac{1}{0}u_{3,3} & \frac{1}{0}u_{3,2} \end{bmatrix} \end{aligned} \tag{9.7.24b}$$

The dots correspond to the entries (not displayed due to the page width)

$$\begin{aligned} &\dots \quad \frac{1}{0}u_{2,1} \quad 0 \quad 0 \\ &\dots \quad 0 \quad 1 + \frac{1}{0}u_{2,2} \quad 0 \\ &\dots \quad 0 \quad 0 \quad \frac{1}{0}u_{2,3} \\ &\dots = 1 + \frac{1}{0}u_{2,2} \quad \frac{1}{0}u_{3,1} \quad 0 \\ &\dots \quad \frac{1}{0}u_{2,3} \quad 0 \quad \frac{1}{0}u_{2,1} \\ &\dots \quad 0 \quad \frac{1}{0}u_{2,3} \quad 1 + \frac{1}{0}u_{2,2} \end{aligned}$$

and  $0u_{i,j} = \partial u_i / \partial {}^0x_j$ . The vectors  $\{0u\}$  and  $\{0e\}$  are related to the displacement increments at nodes by

$$\begin{aligned} \{0u\} &= [N] \{u\} = [N] {}^1[H] \{\Delta^e\} \\ \{0e\} &= {}^1[A]\{0u\} = {}^1[A][N] {}^1[H] \{\Delta^e\} \equiv \frac{1}{0}[B_L] \{\Delta^e\} \tag{9.7.25a} \\ \frac{1}{0}[B_L] &= {}^1[A][N] {}^1[H] \end{aligned}$$

where  $[N]^T$  is the operator of differentials

$$[N]^T = \begin{bmatrix} \frac{\partial}{\partial^0 x_1} & \frac{\partial}{\partial^0 x_2} & \frac{\partial}{\partial^0 x_3} & 0 & 0 & 0 & 0 & 0 & 0 \\ 0 & 0 & 0 & \frac{\partial}{\partial^0 x_1} & \frac{\partial}{\partial^0 x_2} & \frac{\partial}{\partial^0 x_3} & 0 & 0 & 0 \\ 0 & 0 & 0 & 0 & 0 & 0 & \frac{\partial}{\partial^0 x_1} & \frac{\partial}{\partial^0 x_2} & \frac{\partial}{\partial^0 x_3} \end{bmatrix} \quad (9.7.25b)$$

The components of  ${}^1[A]$  include  ${}^1_0 u_{i,j}$ . From Eq. (9.7.16) the global displacements are related to the natural curvilinear coordinates  $(\xi, \eta)$  and the linear coordinate  $\zeta$ . Hence the derivatives of these displacements  ${}^1_0 u_{i,j}$  with respect to the global coordinates  ${}^0 x_1, {}^0 x_2,$  and  ${}^0 x_3$  are obtained through the relation

$$[{}^1_0 u_{i,j}] = \begin{bmatrix} \frac{\partial^1 u_1}{\partial^0 x_1} & \frac{\partial^1 u_2}{\partial^0 x_1} & \frac{\partial^1 u_3}{\partial^0 x_1} \\ \frac{\partial^1 u_1}{\partial^0 x_2} & \frac{\partial^1 u_2}{\partial^0 x_2} & \frac{\partial^1 u_3}{\partial^0 x_2} \\ \frac{\partial^1 u_1}{\partial^0 x_3} & \frac{\partial^1 u_2}{\partial^0 x_3} & \frac{\partial^1 u_3}{\partial^0 x_3} \end{bmatrix} = {}^0[J]^{-1} \begin{bmatrix} \frac{\partial^1 u_1}{\partial \xi} & \frac{\partial^1 u_2}{\partial \xi} & \frac{\partial^1 u_3}{\partial \xi} \\ \frac{\partial^1 u_1}{\partial \eta} & \frac{\partial^1 u_2}{\partial \eta} & \frac{\partial^1 u_3}{\partial \eta} \\ \frac{\partial^1 u_1}{\partial \zeta} & \frac{\partial^1 u_2}{\partial \zeta} & \frac{\partial^1 u_3}{\partial \zeta} \end{bmatrix} \quad (9.7.26)$$

The Jacobian matrix  ${}^0[J]$  is defined as

$${}^0[J] = \begin{bmatrix} \frac{\partial^0 x_1}{\partial \xi} & \frac{\partial^0 x_2}{\partial \xi} & \frac{\partial^0 x_3}{\partial \xi} \\ \frac{\partial^0 x_1}{\partial \eta} & \frac{\partial^0 x_2}{\partial \eta} & \frac{\partial^0 x_3}{\partial \eta} \\ \frac{\partial^0 x_1}{\partial \zeta} & \frac{\partial^0 x_2}{\partial \zeta} & \frac{\partial^0 x_3}{\partial \zeta} \end{bmatrix} \quad (9.7.27)$$

and is computed from the coordinate definition of Eq. (9.7.15). The derivatives of displacements  ${}^1 u_i$  with respect to the coordinates  $\xi, \eta,$  and  $\zeta$  can be computed from Eq. (9.7.16). In the evaluations of element matrices in Eqs (9.7.6a-d), the integrands of  ${}^1_0[B_L], {}^0[C], {}^1_0[B_{NL}], {}^1_0[S], {}^1[H],$  and  ${}^1_0\{\hat{S}\}$  should be expressed in the same coordinate system, namely the global coordinate system  $({}^0 x_1, {}^0 x_2, {}^0 x_3)$  or the local curvilinear system  $(x'_1, x'_2, x'_3)$ .

The number of stress and strain components are reduced to five since we neglect the transverse normal components of stress and strain. Hence, the global derivatives of displacements,  $[{}^1_0 u_{i,j}]$  which are obtained in Eq. (9.7.26), are transformed to the local derivatives of the local displacements along the orthogonal coordinates by the following relation

$$\begin{bmatrix} \frac{\partial^1 u'_1}{\partial x'_1} & \frac{\partial^1 u'_2}{\partial x'_1} & \frac{\partial^1 u'_3}{\partial x'_1} \\ \frac{\partial^1 u'_1}{\partial x'_2} & \frac{\partial^1 u'_2}{\partial x'_2} & \frac{\partial^1 u'_3}{\partial x'_2} \\ \frac{\partial^1 u'_1}{\partial x'_3} & \frac{\partial^1 u'_2}{\partial x'_3} & \frac{\partial^1 u'_3}{\partial x'_3} \end{bmatrix} = [\theta]_{3 \times 3}^T [{}^1_0 u_{i,j}] [\theta]_{3 \times 3} \quad (9.7.28)$$

where  $[\theta]^T$  is the transformation matrix between the local coordinate system  $(x'_1, x'_2, x'_3)$  and the global coordinate system  $({}^0 x_1, {}^0 x_2, {}^0 x_3)$  at the integration

point. The transformation matrix  $[\theta]$  is obtained by interpolating the three orthogonal unit vectors ( ${}^1\hat{e}_1, {}^1\hat{e}_2, {}^1\hat{e}_3$ ) at each node:

$$[\theta] = \begin{bmatrix} \sum_{k=1}^n \psi_k^1 e_{11}^k & \sum_{k=1}^n \psi_k^1 e_{21}^k & \sum_{k=1}^n \psi_k^1 e_{31}^k \\ \sum_{k=1}^n \psi_k^1 e_{12}^k & \sum_{k=1}^n \psi_k^1 e_{22}^k & \sum_{k=1}^n \psi_k^1 e_{32}^k \\ \sum_{k=1}^n \psi_k^1 e_{13}^k & \sum_{k=1}^n \psi_k^1 e_{23}^k & \sum_{k=1}^n \psi_k^1 e_{33}^k \end{bmatrix} \quad (9.7.29)$$

Since the element matrices are evaluated using numerical integration, the transformation must be performed at each integration point during the numerical integration.

In order to obtain  ${}^0[B_L]$ , the vector of derivatives of incremental displacements  $\{u_0\}$  needs to be evaluated. Equations (9.7.26) and (9.7.28) can be used again except that  ${}^1u_i$  are replaced by  $u_i$  and the interpolation equation for  $u_i$ , Eq. (9.7.17), is applied.

The development of the matrix of material stiffness,  ${}^0[C']$ , is discussed next. Here we wish to present it for shell element composed of orthotropic material layers with the principal material coordinates  $(x_1, x_2, x_3)$  oriented arbitrarily with respect to the local coordinate system  $(x'_1, x'_2, x'_3)$  (with  $x_3 = x'_3$ ). For a  $k$ th lamina of a laminated composite shell the matrix of material stiffnesses is given by

$${}^0[C']_{(k)} = \begin{bmatrix} C'_{11} & C'_{12} & C'_{16} & 0 & 0 \\ C'_{12} & C'_{22} & C'_{26} & 0 & 0 \\ C'_{16} & C'_{26} & C'_{66} & 0 & 0 \\ 0 & 0 & 0 & C'_{44} & C'_{45} \\ 0 & 0 & 0 & C'_{45} & C'_{55} \end{bmatrix} \quad (9.7.30)$$

where

$$\begin{aligned} C'_{11} &= m^4 Q_{11} + 2m^2 n^2 (Q_{12} + 2Q_{66}) + n^4 Q_{22} \\ C'_{12} &= m^2 n^2 (Q_{11} + Q_{22} - 4Q_{66}) + (m^4 + n^4) Q_{12} \\ C'_{16} &= mn [m^2 Q_{11} - n^2 Q_{22} - (m^2 - n^2)(Q_{12} + 2Q_{66})] \\ C'_{22} &= n^4 Q_{11} + 2m^2 n^2 (Q_{12} + 2Q_{66}) + m^4 Q_{22} \\ C'_{26} &= mn [n^2 Q_{11} - m^2 Q_{22} + (m^2 - n^2)(Q_{12} + 2Q_{66})] \\ C'_{66} &= m^2 n^2 (Q_{11} + Q_{22} - 2Q_{12}) + (m^2 - n^2)^2 Q_{66} \\ C'_{44} &= m^2 Q_{44} + n^2 Q_{55}, \quad C'_{45} = mn (Q_{55} - Q_{44}) \\ C'_{55} &= m^2 Q_{55} + n^2 Q_{44} \\ m &= \cos \theta_{(k)}, \quad n = \sin \theta_{(k)} \end{aligned} \quad (9.7.31)$$

where  $Q_{ij}$  are the plane stress-reduced stiffnesses of the  $k$ th orthotropic lamina in the material coordinate system. The  $Q_{ij}$  can be expressed in terms of engineering constants of a lamina

$$Q_{11} = \frac{E_1}{1 - \nu_{12}\nu_{21}}, \quad Q_{12} = \frac{\nu_{12}E_2}{1 - \nu_{12}\nu_{21}}, \quad Q_{22} = \frac{E_2}{1 - \nu_{12}\nu_{21}}$$



$$Q_{44} = G_{23}, \quad Q_{55} = G_{13}, \quad Q_{66} = G_{12} \quad (9.7.32)$$

where  $E_i$  is the modulus in the  $x_i$ -direction,  $G_{ij}$  ( $i \neq j$ ) are the shear moduli in the  $x_i$ - $x_j$  plane, and  $\nu_{ij}$  are the associated Poisson's ratios (see Reddy [10]).

To evaluate element matrices in Eqs. (9.7.6a-d), we employ the Gauss quadrature. Since we are dealing with laminated composite structures, integration through the thickness involves individual lamina. One way is to use Gauss quadrature through the thickness direction. Since the constitutive relation  ${}^0[C]$  is different from layer to layer and is not a continuous function in the thickness direction, the integration should be performed separately for each layer. This increases the computational time as the number of layers is increased. An alternative way is to perform explicit integration through the thickness and reduce the problem to a two-dimensional one. The Jacobian matrix, in general, is a function of  $(\xi, \eta, \zeta)$ . The terms in  $\zeta$  may be neglected provided the thickness to curvature ratios are small. Thus the Jacobian matrix  ${}^0[J]$  becomes independent of  $\zeta$  and explicit integration can be employed. If  $\zeta$  terms are retained in  ${}^0[J]$ , Gauss points through the thickness should be added. In the present study we assume that the Jacobian matrix is independent of  $\zeta$  in the evaluation of element matrices and the internal nodal force vector.

Since the explicit integration is performed through the thickness, the expression for

$$\left[ \frac{\partial^1 u'_i}{\partial x'_j} \right], \quad {}^1_0[A'], \quad \{ {}^1_0 u' \}, \quad {}^1[H], \quad {}^1_0[B'], \quad \{ {}^1_0 \varepsilon'_{ij} \}$$

are now expressed in an explicit form in terms of  $\zeta$ . Hence, we can use exact integration through the thickness and use the Gauss quadrature to perform numerical integration on the mid-surface of the shell element.

For thin shell structures, in order to avoid "locking" we use reduced integration scheme to evaluate the stiffness coefficients associated with the transverse shear deformation. Hence we split the constitutive matrix  ${}^0[C']$  into two parts, one without transverse shear moduli  ${}^0[C']_B$ , and the other with only transverse shear moduli  ${}^0[C']_S$ . Full integration is used to evaluate the stiffness coefficients containing  ${}^0[C']_B$ , and reduced integration is used for those containing  ${}^0[C']_S$ .

If a shell element is subjected to a distributed load (such as the weight or pressure), the corresponding load vector  ${}^2\{R\}$  from Eq. (9.7.6) is given by

$${}^2\{R\}_{5n \times 1} = \int_{{}^0A} {}^1[H]^T \begin{Bmatrix} {}^2P_1 \\ {}^2P_2 \\ {}^2P_3 \end{Bmatrix} d{}^0A \quad (9.7.33)$$

where  ${}^2P_i$  is the component of distributed load in the  ${}^0x_i$ -direction at time  $t + \Delta t$ ,  ${}^0A$  is the area of upper or middle or bottom surface of the shell

element depending on the position of the loading and the loading is assumed deformation-independent.

Substituting  ${}^1[H]$  into Eq. (9.7.33) yields

$$\begin{aligned}
 {}^2\{R\}_{5n \times 1} &= \int_{{}^0A} \begin{bmatrix} \dots & \dots & \dots \\ \psi_k & 0 & 0 \\ 0 & \psi_k & 0 \\ 0 & 0 & \psi_k \\ \frac{1}{2}\zeta\psi_k h_k {}^1e_{11}^k & \frac{1}{2}\zeta\psi_k h_k {}^1e_{12}^k & -\frac{1}{2}\zeta\psi_k h_k {}^1e_{13}^k \\ -\frac{1}{2}\zeta\psi_k h_k {}^1e_{21}^k & \frac{1}{2}\zeta\psi_k h_k {}^1e_{22}^k & -\frac{1}{2}\zeta\psi_k h_k {}^1e_{23}^k \\ \dots & \dots & \dots \end{bmatrix} \begin{Bmatrix} {}^2P_1 \\ {}^2P_2 \\ {}^2P_3 \end{Bmatrix} d^0A \\
 &= \sum_{r=1}^{NGP} \sum_{s=1}^{NGP} \begin{Bmatrix} \dots \\ \psi_k {}^2P_1 \\ \psi_k {}^2P_2 \\ \psi_k {}^2P_3 \\ \frac{1}{2}\zeta\psi_k h_k \sum_{i=1}^3 {}^2P_i {}^1e_{1i}^k \\ -\frac{1}{2}\zeta\psi_k h_k \sum_{i=1}^3 {}^2P_i {}^1e_{2i}^k \\ \dots \end{Bmatrix} W_{\xi_r} W_{\eta_s} |{}^0J|_{(\xi_r, \eta_s)} \frac{2}{h} \quad (9.7.34)
 \end{aligned}$$

where  $h = \sum_{k=1}^{NPE} \psi_k(\xi, \eta) h_k$  is the shell thickness at each Gauss point, and  $W$  is the weight at each Gauss point, and  $|{}^0J|$  is the determinant of the Jacobian matrix in Eq. (9.7.27) at each Gauss point. Here the  $\zeta$  terms are retained in Jacobian matrix and let  $\zeta$  equal to 1, -1, or 0, respectively, when the distributed loading is at the top, bottom, or middle surface.

### 9.7.5 Numerical Examples

A number of numerical examples of isotropic and orthotropic plates and shells are presented. Only static bending problems of plates and shells are included. The Riks-Wempner method is employed for tracing the nonlinear load-deflection path (see Appendix 1). For most of the problems the reduced/selective integration scheme is used to evaluate the element stiffness coefficients. For additional examples, the reader may refer to [22,24-26].

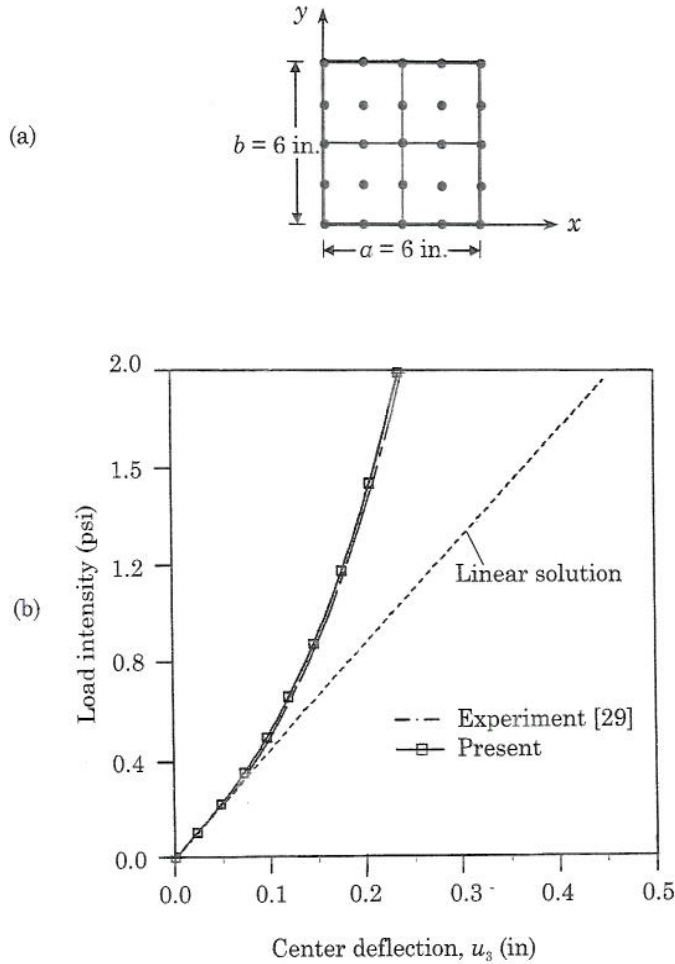
#### *Simply-supported (BC1) orthotropic plate under uniform load*

Figure 9.7.2(a) shows the plate and material properties used. A quarter of the plate with the boundary and symmetry conditions shown in the figure is modeled with four nine-node shell elements. The results are shown in Figure 9.7.2(b) along with the experimental results of Zaghoul and Kennedy [29]. For this simply-supported plate, the finite element results are in good agreement with the experimental results of Zaghoul and Kennedy [29].

$$E_1 = 3 \times 10^6 \text{ psi}, E_2 = 1.28 \times 10^6 \text{ psi},$$

$$G_{12} = G_{13} = G_{23} = 0.37 \times 10^6 \text{ psi}, \nu_{12} = 0.32$$

$$h = 0.138 \text{ in.}$$



**Figure 9.7.2** Geometrically nonlinear response of an orthotropic plate. (a) Geometry and mesh. (b) Load-deflection curves.

*Four-layer (0/90/90/0) clamped plate under uniform load*

Figure 9.7.3(a) shows a clamped, symmetrically laminated, square plate under uniform load. The material properties of a typical layer and finite element mesh are also shown in the figure. A quarter of the plate is modeled using four nine-node elements. The present results along with the experimental

results of Zaghoul and Kennedy [29] are shown in Figure 9.7.3(b). The two results are not in good agreement in this case. The difference between the theoretical and experimental results is attributed to possible difference in the support conditions used in the finite element analysis and those used in the experiment (i.e. the exact nature of clamped boundary conditions used in the test may not be the ones used in the finite element analysis), because the present results are verified against independent finite element study by Putch and Reddy [30].

$$E_1 = 1.8282 \times 10^6 \text{ psi}, E_2 = 1.8315 \times 10^6 \text{ psi},$$

$$G_{12} = G_{13} = G_{23} = 0.3125 \times 10^6 \text{ psi}, \nu_{12} = 0.2395$$

$$h = 0.096 \text{ in.}$$

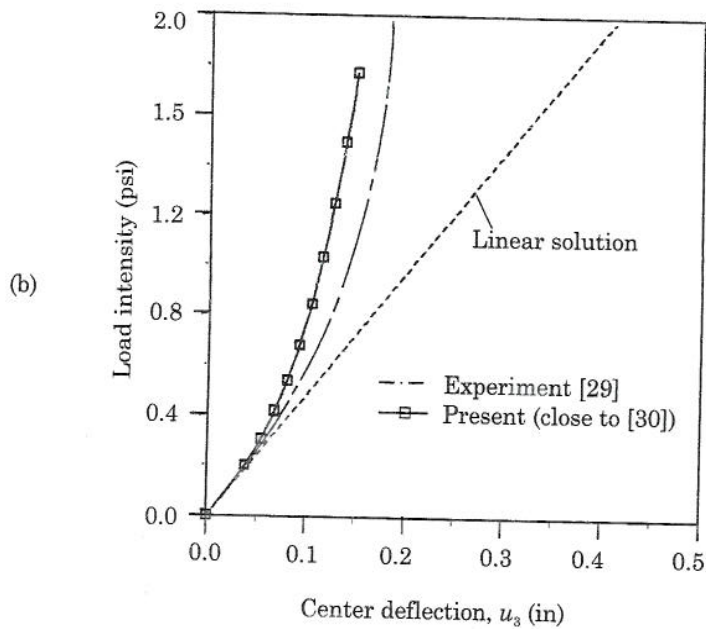
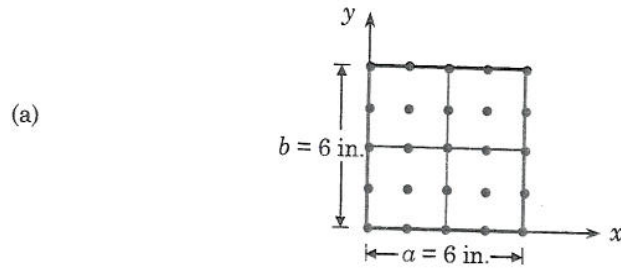


Figure 9.7.3 Nonlinear response of a clamped cross-ply laminated plate. (a) Geometry and mesh. (b) Load-deflection curves.

*Cylindrical shell roof under self-weight*

Here we consider the linear analysis of a cylindrical panel under its own weight [see Figure 9.7.4(a)]. This is often used as a benchmark problem [27] in the literature to validate numerical methods (i.e. assessment of the performance of shell finite elements). It was shown in [28] that with the uniform (i.e. for all stiffness coefficients) reduction of integration order the quadratic and cubic shell elements show a more rapid convergence and better accuracy than with the reduced integration order applied to transverse shear terms only. The linear results obtained in the present study with the nine-node quadratic element and uniform reduced integration order are shown in Figures 9.7.4(b) and 9.7.4(c). Even with one element the results show good agreement with the exact solution [27], and for further mesh refinement the results are close to the exact one.

*Simply-supported spherical shell under point load*

A simply supported isotropic spherical shell panel under central point load [see Figure 9.7.5(a)] is analyzed for its large displacement response using a meshes of sixteen four-node elements and four nine-node elements in a quarter of the shell. Figure 9.7.5(b) shows the responses calculated, including the postbuckling range, with the modified Riks–Wempner method. The figure also includes the results of Bathe and Ho [17].

*Shallow cylindrical shell under point load*

An isotropic shallow cylindrical shell hinged along the longitudinal edges and free at the curved boundaries and subjected to a point load is analyzed [see Figure 9.7.6(a)]. One-quarter of the shell is modeled with four nine-node shell elements. The structure exhibits snap-through as well as snap-back phenomena, as shown in 9.7.6(b). The solution obtained by Crisfield [18] is also shown in Figure 9.7.6(b) to be compared with the present results.

**Problems**

- 9.1 Consider the uniform deformation of a square of side 2 units initially centered at  $\mathbf{X} = (0, 0)$ . The deformation is given by the mapping [3]

$$x_1 = \frac{1}{4}(18 + 4X_1 + 6X_2), \quad x_2 = \frac{1}{4}(14 + 6X_2)$$

- (a) Sketch the deformed configuration of the body.
- (b) Compute the components of the deformation gradient tensor  $\mathbf{F}$  and its inverse (display them in matrix form).
- (c) Compute the components of the right and left Cauchy–Green deformation tensors (display them in matrix form).
- (d) Compute the Green’s and Almansi’s strain tensor components (display them in matrix form).

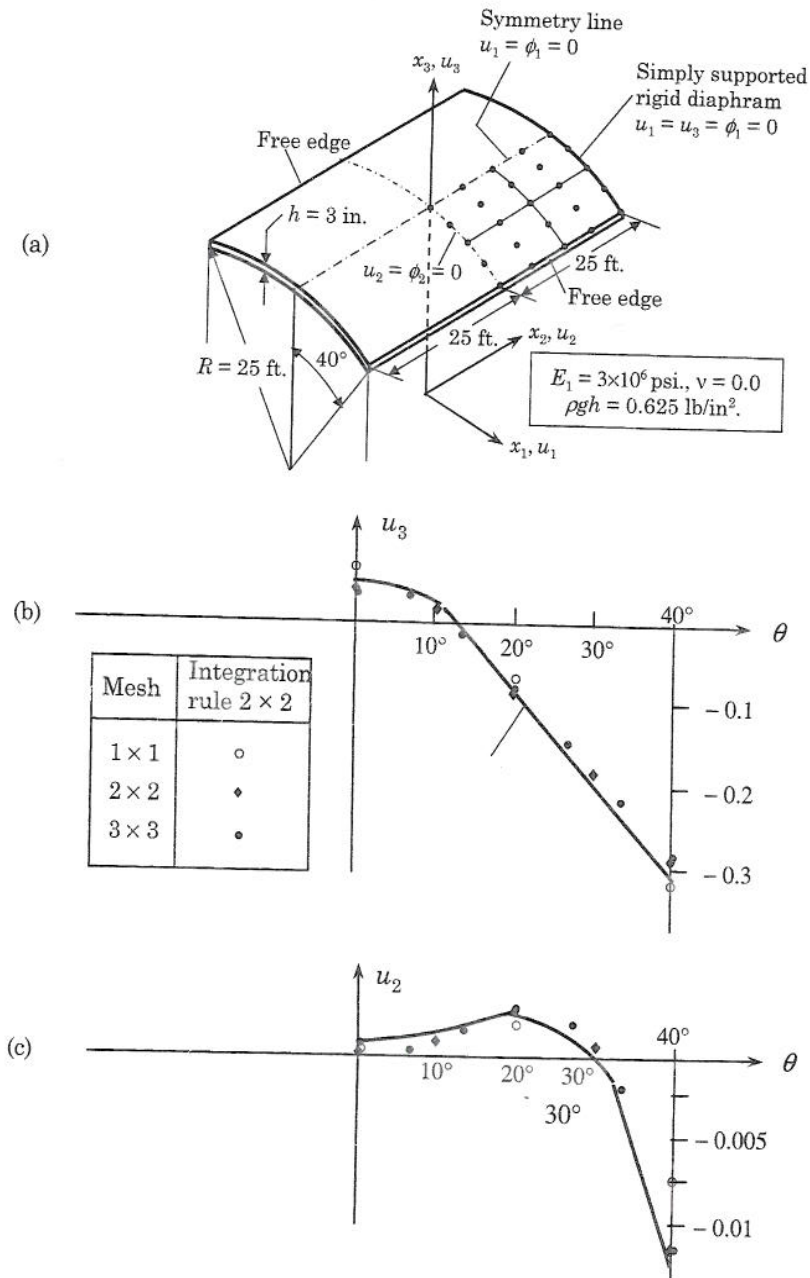
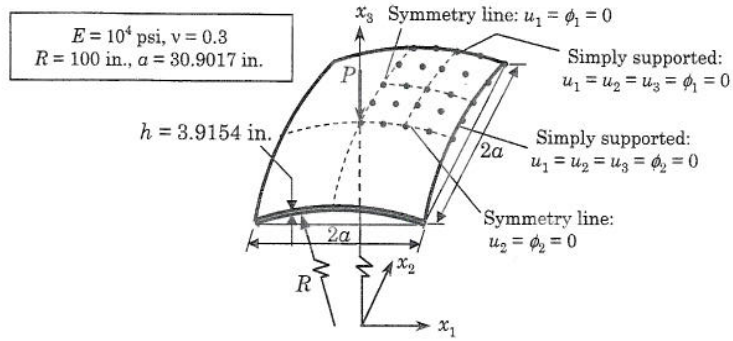
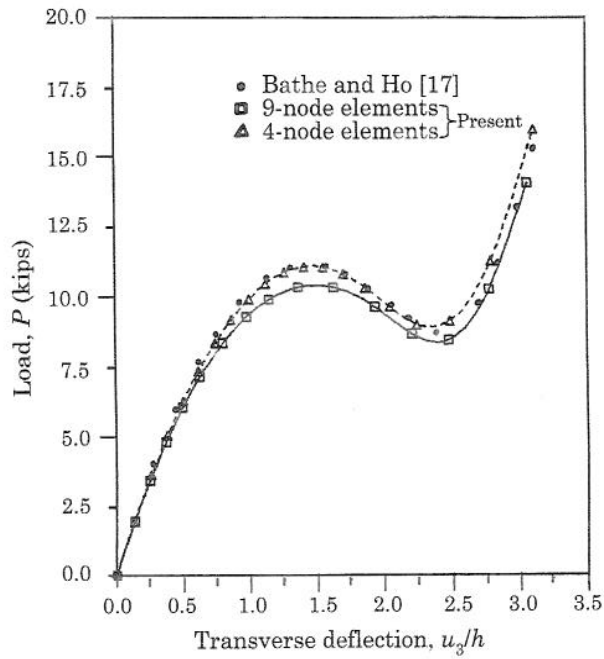


Figure 9.7.4 A cylindrical shell roof under self-weight. (a) Geometry and the finite element mesh. (b) Vertical displacement on mid-section. (c) Axial displacement at support.



(a)



(b)

Figure 9.7.5 A simply supported spherical shell panel. (a) Geometry and finite element mesh. (b) Load-deflection curves.

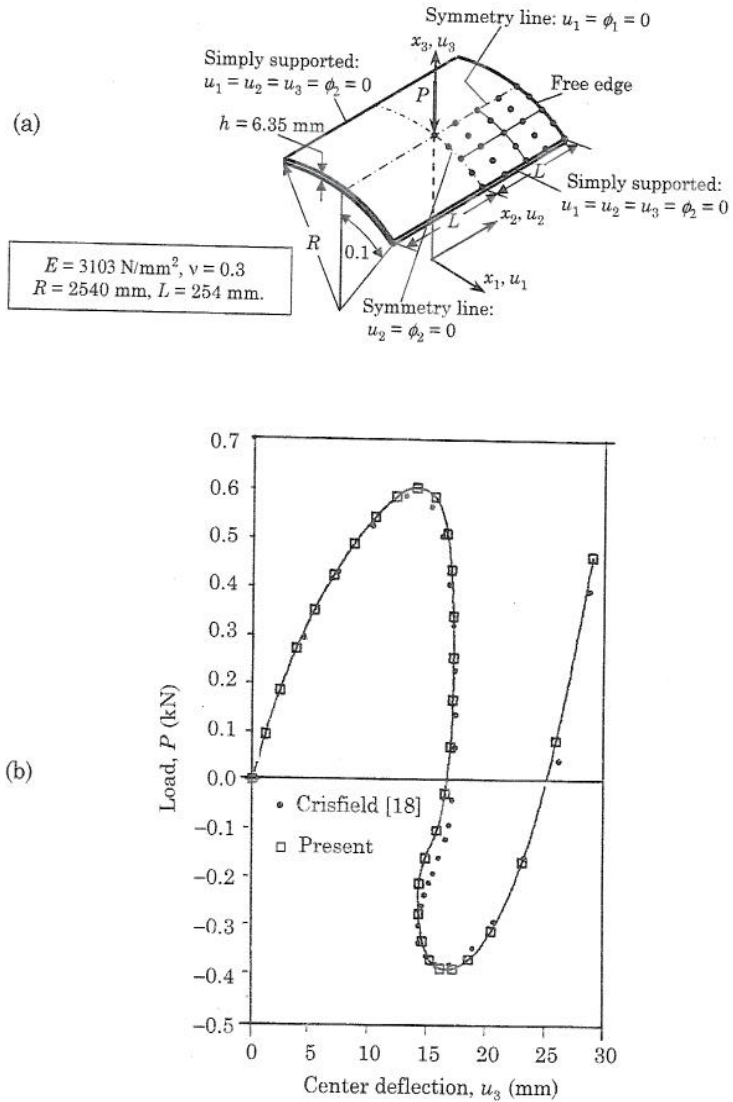


Figure 9.7.6 Geometrically nonlinear response of a shallow cylindrical shell. (a) Geometry and finite element mesh. (b) Load-deflection curves.

9.2 Consider the deformation given by the mapping [3]

$$x_1 = \frac{1}{4} [4X_1 + (9 - 3X_1 - 5X_2 - X_1X_2)t], \quad x_2 = \frac{1}{4} [4X_2 + (16 + 8X_1)t]$$

(a) For  $\mathbf{X} = (0, 0)$  and  $t = 1$  determine the deformation gradient tensor  $\mathbf{F}$  and right Cauchy-Green tensor  $\mathbf{C}$ .



- (b) Find the eigenvalues (stretches)  $\lambda_1$  and  $\lambda_2$  and the associated eigenvectors  $\mathbf{N}_1$  and  $\mathbf{N}_2$ . *Partial answer:*  $\lambda_1 = 2.2714$ ,  $\hat{\mathbf{N}}_1 = \{0.8385 \ 0.5449\}^T$ .
- (c) Use the polar decomposition to determine the symmetric stretch tensor  $\mathbf{U}$  and rotation tensor  $\mathbf{R}$ .
- 9.3 Determine the displacements and strains in the  $(x_1, x_2)$  system for the bodies shown in Figure P9.3.
- 9.4 Determine the displacements and strains in the  $(x_1, x_2)$  system for the bodies shown in Figure P9.4.

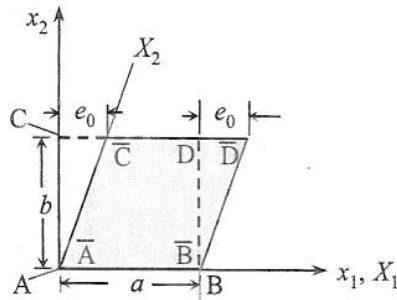


Figure P9.3

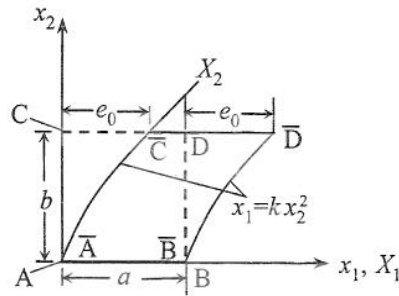


Figure P9.4

- 9.5 Consider the infinitesimal tetrahedron in Cartesian coordinates shown in Figure P9.5. If  $-\mathbf{t}_1, -\mathbf{t}_2, -\mathbf{t}_3$ , and  $\mathbf{t}$  denote the stress vectors in the outward directions on the faces of the infinitesimal tetrahedron whose areas are  $\Delta s_1, \Delta s_2, \Delta s_3$ , and  $\Delta s$ , respectively, we have by Newton's second law for the mass inside the tetrahedron,

$$\mathbf{t}\Delta s - \mathbf{t}_1\Delta s_1 - \mathbf{t}_2\Delta s_2 - \mathbf{t}_3\Delta s_3 + \rho\Delta v\mathbf{f} = \rho\Delta v\mathbf{a} \quad (\text{a})$$

where  $\Delta v$  is the volume of the tetrahedron,  $\rho$  the density,  $\mathbf{f}$  the body force per unit mass, and  $\mathbf{a}$  the acceleration. Establish the Cauchy formula by writing

$$\mathbf{t}_i = \sigma_{i1}\hat{\mathbf{e}}_1 + \sigma_{i2}\hat{\mathbf{e}}_2 + \sigma_{i3}\hat{\mathbf{e}}_3 = \sigma_{ij}\hat{\mathbf{e}}_j \quad (\text{b})$$

$$\Delta s_1 = (\hat{\mathbf{n}} \cdot \hat{\mathbf{e}}_1)\Delta s, \quad \Delta s_2 = (\hat{\mathbf{n}} \cdot \hat{\mathbf{e}}_2)\Delta s, \quad \Delta s_3 = (\hat{\mathbf{n}} \cdot \hat{\mathbf{e}}_3)\Delta s \quad (\text{c})$$

$$\Delta v = \frac{\Delta h}{3}\Delta s \quad (\text{d})$$

where  $\Delta h$  is the perpendicular distance from the origin to the slant face.

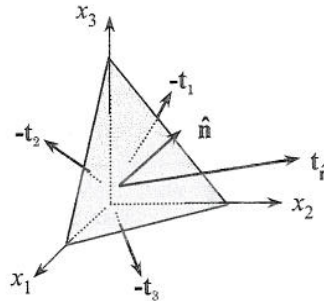


Figure P9.5

9.6 Establish the following relationships between area elements and volume elements of reference configuration and current configuration:

(a) *Nanson's formula*:  $\hat{\mathbf{n}} da = \mathbf{F}^{-T} \cdot \hat{\mathbf{N}} J dA$ .

(b)  $dv = J dV$ .

where  $dA$  and  $dV$  are area and volume elements, respectively, in the reference configuration and  $da$  and  $dv$  are area and volume elements, respectively, in the deformed configuration.

9.7 Let an arbitrary region in a continuous medium be denoted by  $v$  and the bounding closed surface of this region be continuous and denoted by  $s$ . Let each point on the bounding surface move with the velocity  $\mathbf{v}_s$ . It can be shown that the time derivative of the volume integral over some continuous function  $Q(\mathbf{x}, t)$  is given by

$$\frac{D}{Dt} \int_v Q(\mathbf{x}, t) dv \equiv \int_v \frac{\partial Q}{\partial t} dv + \oint_s Q \mathbf{v}_s \cdot \hat{\mathbf{n}} ds \quad (\text{a})$$

This expression for the differentiation of a volume integral with variable limits is sometimes known as the three-dimensional *Leibniz rule*. The material derivative operator  $D/Dt$  corresponds to changes with respect to a fixed mass, that is,  $\rho dv$  is constant with respect to this operator. Show formally by means of Leibniz's rule, the divergence theorem, and conservation of mass that

$$\frac{D}{Dt} \int_v \rho \phi dv \equiv \int_v \rho \frac{D\phi}{Dt} dv \quad (\text{b})$$

9.8 Newton's second law of motion applied to a continuum states that the rate of change of momentum following a material region of fixed mass is equal to the sum of all the forces on the region. When the forces are divided into surface forces and body forces, Newton's second law reads:

$$\frac{D}{Dt} \int_v \rho \mathbf{v} dv = \oint_s \hat{\mathbf{n}} \cdot \vec{\sigma} ds + \int_v \rho \mathbf{b} dv \quad (\text{a})$$

where  $\vec{\sigma}$  is the surface stress tensor,  $\mathbf{b}$  is the body force per unit mass,  $\rho$  is the mass density, and  $\mathbf{v}$  is the material velocity. Since the material particle mass  $\rho dv$  is constant with respect to the material time derivative  $D/Dt$ , make use of the divergence theorem and obtain the differential form of Newton's second law of motion for a continuum (see Chapter 7):

$$\rho \frac{D\mathbf{v}}{Dt} = \text{div } \vec{\sigma} + \rho \mathbf{b} \quad (\text{b})$$

9.9 Let  $e$  denote the thermodynamic internal energy per unit mass of a material. Then the equation of change for total energy of a material region can be written (see Chapter 7):

$$\frac{D}{Dt} \int_v \rho \left( e + \frac{v^2}{2} \right) dv = \oint_s \hat{\mathbf{n}} \cdot \vec{\sigma} \cdot \mathbf{v} ds + \int_v \rho \mathbf{b} \cdot \mathbf{v} dv - \oint_s \mathbf{q} \cdot \hat{\mathbf{n}} ds \quad (\text{a})$$

The first two terms on the right-hand side describe the rate of work done on the material region by the surface stresses and the body forces. The third integral describes the net *outflow* of heat from the region, causing a decrease of energy inside the region. The heat-flux vector  $\mathbf{q}$  describes the magnitude and direction of the flow of heat energy per unit time and per unit area.

By suitable operations obtain the differential form of the energy equation:

$$\rho \frac{D}{Dt} \left( e + \frac{v^2}{2} \right) = \text{div} \left( \vec{\sigma} \cdot \mathbf{v} \right) + \rho \mathbf{b} \cdot \mathbf{v} - \text{div} \mathbf{q} \quad (\text{b})$$

Subtract the contribution from kinetic energy and obtain

$$\rho \frac{De}{Dt} = \text{div} \left( \vec{\sigma} \cdot \mathbf{v} \right) - \mathbf{v} \cdot \text{div} \vec{\sigma} - \text{div} \mathbf{q} \quad (\text{c})$$

This is called the *thermodynamic form* of the energy equation for a continuum.

- 9.10 Determine the two-dimensional displacement field and the infinitesimal strain field for the simple shear of a rectangular block shown in the figure below. Determine the normal and shear strain in the diagonal line element of the rectangular block shown in Figure P9.10.

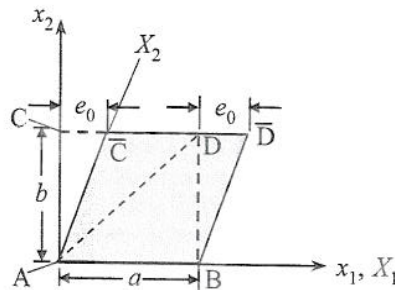


Figure P9.10

## References

1. Malvern, L. E., *Introduction to the Mechanics of a Continuous Medium*, Prentice-Hall, Englewood Cliffs, NJ (1969).
2. Hinton, E. (ed), *NAFEMS Introduction to Nonlinear Finite Element Analysis*, NAFEMS, Glasgow, UK (1992).
3. Bonet, J. and Wood, R. D., *Nonlinear Continuum Mechanics for Finite Element Analysis*, Cambridge University Press, New York (1997).
4. Bathe, K. J., *Finite Element Procedures*, Prentice-Hall, Englewood Cliffs, NJ (1996).
5. Reddy, J. N., *Energy Principles and Variational Methods in Applied Mechanics*, Second Edition, John Wiley, New York (2002).
6. Reddy, J. N. and Rasmussen, M. L., *Advanced Engineering Analysis*, John Wiley, New York, 1982; reprinted by Krieger, Melbourne, FL (1990).
7. Heyliger, P. R. and Reddy, J. N., "A Mixed Updated Lagrangian Formulation for Plane Elastic Bodies," *Journal of Composites Technology & Research*, **9**(4), 131-140 (1987).
8. Heyliger, P. R. and Reddy, J. N., "On a Mixed Finite Element Model for Large Deformation Analysis of Elastic Solids," *International Journal of Non-Linear Mechanics*, **23**(2), 131-145 (1988).
9. Roy, S. and Reddy, J. N., "Non-Linear Analysis of Adhesively Bonded Joints," *International Journal of Non-Linear Mechanics*, **23**(2), 97-112 (1988).
10. Reddy, J. N., *Mechanics of Laminated Composite Plates and Shells: Theory and Analysis*, 2nd edn, CRC Press, Boca Raton, FL (2004).

11. Horrigmoe, G. and Bergan, P. G., "Incremental Variational Principle and Finite Element Models for Nonlinear Problems," *Computer Methods in Applied Mechanics and Engineering*, **7**, 201-217 (1976).
12. Wunderlich, W., "Incremental Formulations for Geometrically Nonlinear Problems," in *Formulations and Algorithms in Finite Element Analysis*, K.J. Bathe, J.T. Oden, and W. Wunderlich (eds), 193-239, MIT Press, Boston, MA (1977).
13. Ramm, E., "A Plate/Shell Element for Large Deflections and Rotations," in *Formulations and Computational Algorithms in Finite Element Analysis*, K.J. Bathe, J. T. Oden, and W. Wunderlich (eds), MIT Press, Boston, MA (1977).
14. Bergan, P. G. and Soreide, T. H., "Solution of Large Displacement and Instability Problems Using the Current Stiffness Parameter," *Finite Elements in Nonlinear Mechanics*, 647-649, Tapir Press (1978).
15. Rao, K. P., "A Rectangular Laminated Anisotropic Shallow Thin Shell Finite Element," *Computer Methods in Applied Mechanics and Engineering*, **15**, 13-33 (1978).
16. Bathe, K. J. and Bolourchi, S., "A Geometric and Material Nonlinear Plate and Shell Element," *Computers and Structures*, **11**, 23-48 (1980).
17. Bathe, K. J. and Ho, L. W., "A Simple and Effective Element for Analysis of General Shell Structures," *Computers and Structures*, **13**, 673-681 (1981).
18. Crisfield, M. A., "A Fast Incremental/Iterative Solution Procedure That Handles Snap-Through," *Computers and Structures*, **13**, 55-62 (1981).
19. Chang, T. Y. and Sawamiphakdi, K., "Large Deformation Analysis of Laminated Shells By Finite Element Method," *Computers and Structures*, **13**, 331-340 (1981).
20. Kanok-Nukulchai, W., Taylor, R. L., and Hughes, T. J. R., "A Large Deformation Formulation for Shell Analysis by the Finite Element Method," *Computers and Structures*, **13**, 19-27 (1981).
21. Surana, K. S., "Geometrically Nonlinear Formulation for the Three Dimensional Solid-Shell Transition Finite Elements," *Computers and Structures*, **15**, 549-566 (1982).
22. Chao, W. C. and Reddy, J. N., "Analysis of Laminated Composite Shells Using a Degenerated 3-D Element," *International Journal for Numerical Methods in Engineering*, **20**, 1991-2007 (1984).
23. Stanley, G. M. and Felippa, C. A., "Computational Procedures for Postbuckling for Composite Shells," in *Finite Element Methods for Nonlinear Problems*, P. G. Bergan, K. J. Bathe, and W. Wunderlich (eds.), 359-385, Springer-Verlag, Berlin (1986).
24. Liao, C. L., Reddy, J. N., and Engelstad, S. P., "A Solid-Shell Transition Element for Geometrically Nonlinear Analysis of Laminated Composite Structures," *International Journal for Numerical Methods in Engineering*, **26**, 1843-1854 (1988).
25. Liao, C. L. and Reddy, J. N., "A Continuum-Based Stiffened Composite Shell Element for Geometrically Nonlinear Analysis," *AIAA Journal*, **27**(1), 95-101 (1989).
26. Liao, C. L. and Reddy, J. N., "Analysis of Anisotropic, Stiffened Composite Laminates Using a Continuum Shell Element," *Computers and Structures*, **34**(6), 805-815 (1990).
27. Scordelis, A. C. and Lo, K. S., "Computer Analysis of Cylindrical Shells," *ACI Journal*, **61**, 539-561 (1964).
28. Zienkiewicz, O. C., Taylor, R. L., and Too, J. M., "Reduced Integration Techniques in General Analysis of Plates and Shells," *International Journal for Numerical Methods in Engineering*, **3**, 275-290 (1971).
29. Zaghoul, S. A. and Kennedy, J. B., "Nonlinear Behavior of Symmetrically Laminated Plates," *Journal of Applied Mechanics*, **42**, 234-236 (1975).
30. Putcha, N. S. and Reddy, J. N., "A Refined Mixed Shear Flexible Finite Element for the Nonlinear Analysis of Laminated Plates," *Computers and Structures*, **22**, 529-538 (1986).

---

## Material Nonlinearities and Coupled Problems

---

### 10.1 Introduction

Recall that nonlinearities arise from two independent sources. (1) Nonlinearity due to changes in the geometry or position of the material particles of a continuum, which is called the *geometric nonlinearity*. (2) Nonlinearity due to the nonlinear material behavior, which is called *material nonlinearity*. In solid mechanics, the geometric nonlinearity arises from large strains and/or large rotations, and these enter the formulation through the strain-displacement relations as well as the equations of motion. In fluid mechanics and coupled fluid flow and heat transfer, the geometric nonlinearity arises as a result of the spatial (or Eulerian) description of motion, and they enter the equations of motion through material time derivative term. Material nonlinearity in all disciplines of engineering arise from nonlinear relationship between the kinetic and kinematic variables, for example, stress-strain relations, heat flux-temperature gradient relations, and so on. In general, material nonlinearities arise due to the material parameters (e.g. moduli, viscosity, conductivity, etc.) being functions of strains (or their rates), temperature, and other basic variables.

The finite element formulations presented in the previous chapters were largely based on geometric nonlinearity. However, the nonlinearity in the one- and two-dimensional field problems discussed in Chapters 3 and 5 could have come from either sources. In this chapter, material nonlinear formulations are given attention. This field is very broad and special books are devoted to various types of nonlinearities (e.g. plasticity, viscoelasticity, and non-Newtonian materials). The objective here is to briefly discuss nonlinear elastic and elastic-plastic material models for solids and power-law model for viscous incompressible fluids.

## 10.2 Nonlinear Elastic Problems

Materials for which the constitutive behavior is only a function of the current state of deformation are known as *elastic*. In the special case in which the work done by the stresses during a deformation is dependent only on the initial state and the current configuration, the material is called *hyperelastic*, that is, there exists a strain energy density function  $U_0(E_{ij})$  such that

$$S_{ij} = \frac{\partial U_0}{\partial E_{ij}} \quad (10.2.1)$$

where  $S_{ij}$  and  $E_{ij}$  are the components of the second Piola-Kirchhoff stress tensor and Green-Lagrange strain tensor, respectively. When  $U_0$  is a nonlinear function of the strains, the body is said to be nonlinearly elastic. A nonlinearly elastic material has the following features: (a)  $U_0$  is a nonlinear function of strains, (b) all of the deformation is recoverable on removal of loads causing the deformation, and (c) there is no loss of energy (i.e. loading and unloading is along the same stress-strain path; see Figure 10.2.1).

Here we consider a one-dimensional problem to discuss the finite element formulation of a nonlinear elastic material for the case of kinematically infinitesimal strains. Consider the nonlinear uniaxial stress-strain relation

$$\sigma_{xx} = E \mathcal{F}(\varepsilon_{xx}) \quad (10.2.2)$$

where  $\varepsilon_{xx}$  is the infinitesimal strain,  $E$  is a material constant, and  $\mathcal{F}$  is a nonlinear function of the strain.

The virtual work expression for the axial deformation of a bar made of a nonlinear elastic material is

$$\begin{aligned} 0 &= \int_A \int_{x_a}^{x_b} \sigma_{xx} \delta \varepsilon_{xx} \, dx dA - \int_{x_a}^{x_b} f \delta u \, dx - P_1^e \delta u(x_a) - P_2^e \delta u(x_b) \\ &= \int_{x_a}^{x_b} [EA \mathcal{F}(\varepsilon_{xx}) \delta \varepsilon_{xx} - f \delta u] \, dx - P_1^e \delta u(x_a) - P_2^e \delta u(x_b) \end{aligned} \quad (10.2.3)$$

The residual vector for the finite element model is

$$R_i^e = \int_{x_a}^{x_b} \left[ EA \mathcal{F}(\varepsilon_{xx}) \frac{d\psi_i^e}{dx} - f \psi_i^e \right] dx - P_i^e \quad (10.2.4)$$

and the tangent stiffness matrix is

$$K_{ij}^e = \frac{\partial R_i^e}{\partial u_j^e} = EA \int_{x_a}^{x_b} \frac{\partial \mathcal{F}}{\partial \varepsilon_{xx}} \frac{\partial \varepsilon_{xx}}{\partial u_j^e} \frac{d\psi_i^e}{dx} \, dx = EA \int_{x_a}^{x_b} \left( \frac{\partial \mathcal{F}}{\partial \varepsilon_{xx}} \right) \frac{d\psi_i^e}{dx} \frac{d\psi_j^e}{dx} \, dx \quad (10.2.5)$$

where small strain assumption is used in arriving at the last step.

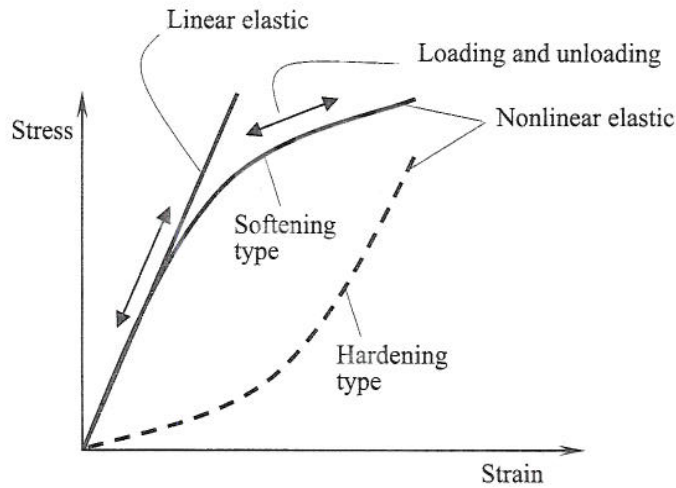


Figure 10.2.1 A nonlinear elastic stress-strain curve.

An example of the nonlinear elastic response is provided by Romberg-Osgood model

$$\mathcal{F}(\varepsilon_{xx}) = (\varepsilon_{xx})^n, \quad \frac{\partial \mathcal{F}}{\partial \varepsilon_{xx}} = n(\varepsilon_{xx})^{n-1} \quad (10.2.6)$$

where  $n > 0$  is a material parameter. The value of  $n = 1$  yields the linear elastic case. This discussion can be extended to multi-axial case, where  $\mathcal{F} = \mathcal{F}(\varepsilon_{ij})$ .

## 10.3 Small Deformation Theory of Plasticity

### 10.3.1 Introduction

Plasticity refers to non-recoverable deformation and non-unique stress paths in contrast to nonlinear elasticity, where the entire load-deflection path is unique and the strains are recovered on load removal. The mathematical theory of plasticity is of a phenomenological nature on the macroscopic scale, and the objective of the theory is to provide a theoretical description of the relationship between stress and strain for a material that exhibits an elasto-plastic response. The plastic behavior is characterized by irreversibility of stress paths and the development of permanent (i.e. non-recoverable) deformation (or strain), known as *yielding* (or plastic flow).

If uniaxial behavior of a material is considered, a nonlinear stress-strain relationship on loading alone does not determine if nonlinear elastic or plastic behavior is exhibited. Unloading part of the curve determines if it is elastic or plastic [see Figure 10.3.1(a) and (b)]; the elastic material follows the same path in loading and unloading, while the plastic material shows a *history-dependent* path unloading.

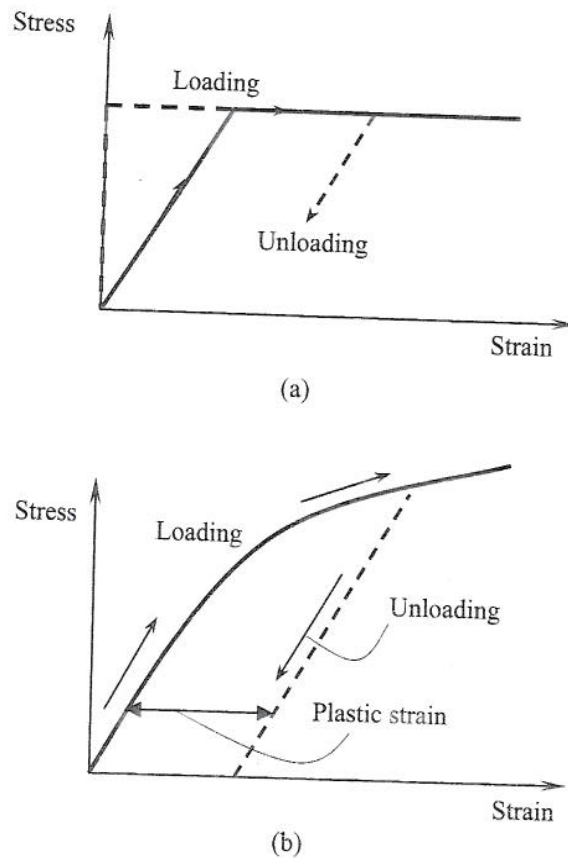


Figure 10.3.1 Stress-strain behavior of (a) ideal plasticity, and (b) strain-hardening plasticity.

The theory of plasticity deals with an analytical description of the stress-strain relations of a deformed body after a part or all of the body has yielded. The stress-strain relations must contain:

1. The elastic stress-strain relations.
2. The stress condition (or *yield criterion*) which indicates onset of yielding.
3. The stress-strain or stress-strain increment relations after the onset of plastic flow.

### 10.3.2 Ideal Plasticity

Many materials exhibit an ideal plastic (or elastic-perfectly-plastic) behavior, as shown in Figure 10.3.1(a). In this case, there exists a limiting stress, called *yield stress*, denoted by  $\sigma_Y$ , at which the strains are indeterminate. For all



stresses below the yield stress, a linear (or nonlinear) stress-strain relation is assumed:

$$\begin{aligned}\sigma_{ij} < \sigma_Y & \text{ linear elastic behavior} \\ \sigma_{ij} \geq \sigma_Y & \text{ plastic deformation (not recoverable)}\end{aligned}\quad (10.3.1)$$

### 10.3.3 Strain Hardening Plasticity

A hardening plastic material model provides a refinement of the ideal plastic material model. In this model, it is assumed that the yield stress depends on some parameter  $\kappa$  (e.g. plastic strain  $\varepsilon^p$ ), called the *hardening parameter*. The general yield criterion is expressed in the form

$$F(\sigma_{ij}, \kappa) = 0 \quad (10.3.2)$$

This yield criterion can be viewed as a surface in the stress space, with the position of the surface dependent on the instantaneous value of the hardening parameter  $\kappa$ . Since any yield criterion should be independent of the orientation of the coordinate system used,  $F$  should be a function of the stress invariants only. Experimental observations indicate that plastic deformation in metals is independent of hydrostatic pressure. Therefore,  $F$  must be a function of the stress invariants of the deviatoric stress tensor  $\sigma'$ :

$$F(J'_2, J'_3, \kappa) = 0, \quad J'_2 = \frac{1}{2}\sigma'_{ij}\sigma'_{ij}, \quad J'_3 = \frac{1}{3}\sigma'_{ij}\sigma'_{jk}\sigma'_{ki} \quad (10.3.3)$$

Two of the most commonly used yield criteria are given next.

*The Tresca yield criterion*

$$F = 2\bar{\sigma} \cos \theta - Y(\kappa) = 0, \quad \bar{\sigma} = \sqrt{J'_2} \quad (10.3.4)$$

*The Huber-von Mises yield criterion*

$$F = \sqrt{3J'_2} - Y(\kappa) = 0 \quad (10.3.5)$$

where  $Y$  is the yield stress from uniaxial tests,  $\theta$  is the angle between the line of pure shear and the principal stress  $\sigma_1$ , and  $\bar{\sigma} = \sqrt{J'_2}$  is called the *effective stress*.

After initial yielding, the stress level at which further plastic deformation occurs may be dependent on the current degree of plastic straining, known as *strain hardening*. Thus, the yield surface will vary (i.e. expand) at each stage of plastic deformation. When the yield surface is independent of the degree of plasticity, the material is said to be ideally (or perfectly) plastic.

If the subsequent yield surfaces are a uniform expansion of the original yield surface, the hardening model is said to be *isotropic*. On the other hand, if the subsequent yield surfaces preserve their shape and orientation but translate in the stress space, *kinematic hardening* is said to take place.

Consider the uniaxial stress-strain curve shown in Figure 10.3.2. The behavior is initially linear elastic with slope  $E$  (Young's modulus) until onset of yielding at the uniaxial yield stress  $\sigma_Y$ . Thereafter, the material response is elasto-plastic with the local tangent to the curve,  $E_T$ , called the elasto-plastic tangent modulus, continually changing.

At some stress level  $\sigma$  in the plastic range, if the load is increased to induce a stress of  $d\sigma$ , it results in a corresponding strain  $d\varepsilon$ . This increment of strain contains two parts: elastic  $d\varepsilon^e$  (recoverable) and plastic  $d\varepsilon^p$  (non-recoverable):

$$d\varepsilon = d\varepsilon^e + d\varepsilon^p, \quad d\varepsilon^e = \frac{d\sigma}{E}, \quad \frac{d\sigma}{d\varepsilon} = E_T \quad (10.3.6)$$

The strain-hardening parameter,  $H$ , is defined by

$$H = \frac{d\sigma}{d\varepsilon^p} = \frac{\frac{d\sigma}{d\varepsilon}}{1 - \frac{d\varepsilon^e}{d\varepsilon}} = \frac{E_T}{1 - \frac{E_T}{E}} \quad (10.3.7)$$

The element stiffness for the linear elastic portion is, say  $[K^e]$ :

$$[K^e] = \int_{x_a}^{x_b} [B]^T [D^e] [B] dx \quad (10.3.8)$$

where  $[D_e]$  is the linear elasticity matrix ( $D^e = E$  for the uniaxial case). When the element deforms plastically,  $[D^e]$  reflects the decreased stiffness. This is computed, for uniaxial material behavior, by the following procedure: The

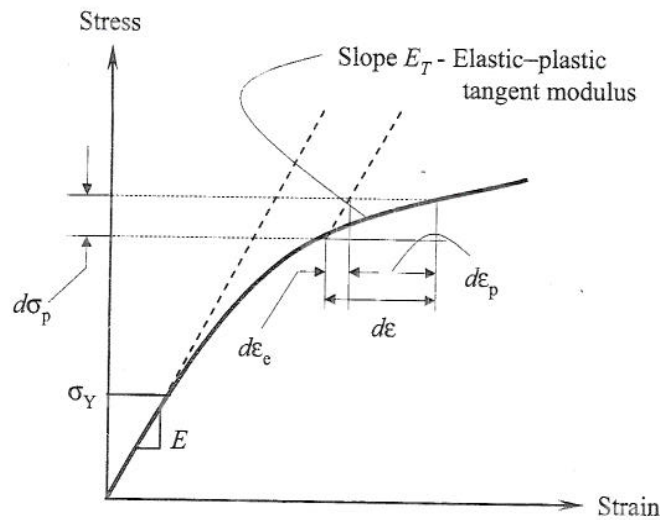


Figure 10.3.2 A strain hardening plastic behavior for the uniaxial case.

increment in load  $dF$  causes an incremental displacement  $du$

$$du = h_e d\varepsilon_{xx} = h_e (d\varepsilon^e + d\varepsilon^p), \quad dF = Ad\sigma = A_e H d\varepsilon^p \quad (10.3.9)$$

where  $h_e$  is the length and  $A_e$  the area of cross-section of the element. The effective stiffness is

$$E^{ep} = \frac{dF}{du} = \frac{A_e H d\varepsilon^p}{h_e (d\varepsilon^e + d\varepsilon^p)} = \frac{EA_e}{h_e} \left[ 1 - \frac{E}{(E + H)} \right] \quad (10.3.10)$$

The element stiffness for plastic range becomes,

$$[K^{ep}] = \int_{x_a}^{x_b} [B]^T [D^{ep}] [B] dx \quad (10.3.11)$$

where  $[D^{ep}]$  is the material stiffness in the plastic range. For uniaxial case  $D^{ep} = E^{ep}$ .

Equation (10.3.8) is valid when  $\sigma < \sigma_Y$  and Eq. (10.3.11) is valid for  $\sigma > \sigma_Y$ . Note that  $d\sigma = \sigma - \sigma_Y$  when  $\sigma > \sigma_Y$ .

### 10.3.4 Elastic-Plastic Analysis of a Bar

Here we present a detailed computational procedure for the analysis of an elasto-plastic problem. The procedure is described via a one-dimensional elasto-plastic bar problem. We shall consider a linear strain-hardening material subjected to an increasing uniaxial load.

#### Update of stresses

At a load-step number  $r$  where the deformation is elastic, the stress in a typical element with the strain increment  $\Delta\varepsilon^r$  can be readily updated as

$$\sigma_i^r = \sigma_i^{(r-1)} + E_i \Delta\varepsilon^r \quad (10.3.12)$$

where  $E_i$  is the elastic modulus of element  $i$ . This linear elastic behavior will continue up till a point where the resulting strain increment will initiate plastic yielding of the material. Now the updating of the stress in the element is not as straightforward as given in Eq. (10.3.12), and it can get complicated when the deformation is partly elastic and partly elasto-plastic, as shown from Points  $A$  to  $B$  in the stress-strain curve of Figure 10.3.3.

To update the stress state from Points  $A$  to  $B$ , one can first assume that the deformation is elastic and compute the corresponding elastic stress, commonly referred to as the *elastic stress predictor*. Using Eq. (10.3.12), the elastic stress predictor  $\sigma_e$  can be calculated as

$$\sigma_{ei} = \sigma_i^{(r-1)} + E_i \Delta\varepsilon_i^r \quad (10.3.13)$$

Computing the elastic stress predictor brings the stress state from Point *A* to *A'*. A correction is made to transfer the stress state back to the elasto-plastic state at Point *B*. We introduce a correction factor *R* (see Figure 10.3.3)

$$R = \frac{\sigma_{ei} - \sigma_y}{\sigma_{ei} - \sigma_i^{(r-1)}} \tag{10.3.14}$$

so that the stress at point *B* can be written as

$$\sigma_i^r = \sigma_i^{(r-1)} + [(1 - R)E_i + RE_T] \Delta \epsilon_i^r \tag{10.3.15}$$

Here  $E_T$  denotes the elastic-plastic tangent modulus, which is related to the elastic modulus  $E$  and strain-hardening parameter  $H$  by Eq. (10.3.7). In the case where the element has already yielded in previous load steps, as illustrated by point *C* in Figure 10.3.3, the approach of determining the elastic stress predictor and making correction to the stress state at point *D* still applies with  $R = 1$  in Eq. (10.3.15):

$$\sigma_i^r = \sigma_i^{(r-1)} + E_T \Delta \epsilon_i^r \tag{10.3.16}$$

**Update of plastic strain**

The extent of plastic flow in a deformed material can be readily characterized by the measure of plastic strain. To determine the plastic strain in an element at point *B* of Figure 10.3.3, it will be useful to rewrite Eq. (10.3.15) as

$$\sigma_i^r = \sigma_Y + E_T(R \Delta \epsilon_i^r) \equiv \sigma_Y + \Delta \sigma_i^r \tag{10.3.17}$$

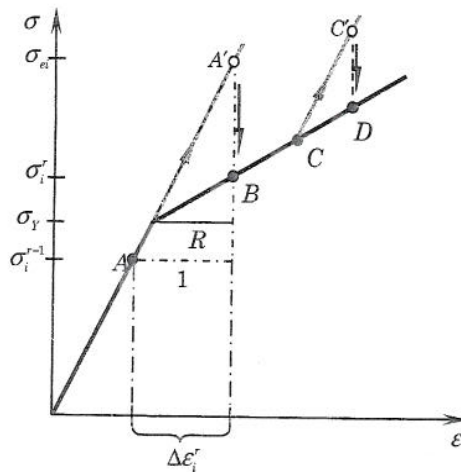


Figure 10.3.3 Transition of elastic to elasto-plastic behavior.

Equation (10.3.17) can be interpreted as that adjusts the stress state at point  $A$  to the yield stress before predicting the elastic stress and its correction. This will allow one to isolate the stress component  $\Delta\sigma_i^r$  and strain  $R\epsilon_i^r$  that are involved in the plastic flow. With Eq. (10.3.6), the plastic strain increment is

$$\Delta\epsilon_{pi}^r = R\Delta\epsilon_i^r - \frac{\Delta\sigma_i^r}{E_i} = \left(1 - \frac{E_T}{E_i}\right) R\Delta\epsilon_i^r \quad (10.3.18)$$

Equation (10.3.18) can also be used for elements that have already yielded in previous load steps by setting  $R = 1$ .

#### Update of yield stress limit

Besides assessing the extent of plastic deformation, the measure of the plastic strain will become especially crucial for strain-hardening materials where the yield limit is a function of the plastic strain. A plot of yield limit against the plastic strain for a typical linear strain-hardening material is shown in Figure 10.3.4. Once the plastic strain occurs, the yield limit will be modified and updated as

$$\sigma_{yi}^r = \sigma_Y + H \Delta\epsilon_{pi}^r \quad (10.3.19)$$

#### Identification of deformation modes

The updated yield limit will come in handy when one is to check the type of deformation an element is undergoing. Once the correct type of deformation is identified, the stress and strain values can then be updated according to Eqs. (10.3.15) and (10.3.18). There are four types of deformation:

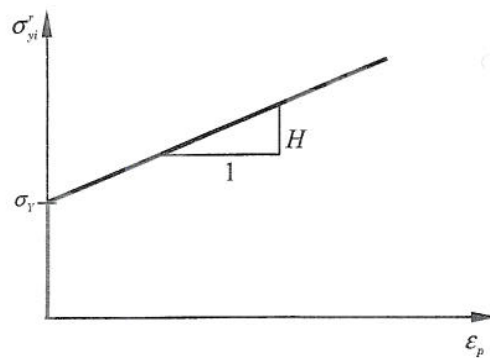


Figure 10.3.4 Stress-strain behavior of a strain-hardening material.



- (a) *Elastic Loading*: (an element that has not yielded previously continues to deform elastically)

$$|\sigma_i^{r-1}| < |\sigma_{yi}^{r-1}| \quad \text{and} \quad |\sigma_{ei}| < |\sigma_{yi}^{r-1}| \quad (10.3.20a)$$

- (b) *Elastic-Plastic Loading*: (an element that has not yielded previously will deform elasto-plastically)

$$|\sigma_i^{r-1}| < |\sigma_{yi}^{r-1}| \quad \text{and} \quad |\sigma_{ei}| > |\sigma_{yi}^{r-1}| \quad (10.3.20b)$$

- (c) *Plastic Loading*: (an element that previously yielded will continue to deform plastically)

$$|\sigma_i^{r-1}| > |\sigma_{yi}^{r-1}| \quad \text{and} \quad |\sigma_{ei}| > |\sigma_{yi}^{r-1}| \quad (10.3.20c)$$

- (d) *Elastic Unloading*: (an element previously yielded is now unloading elastically)

$$|\sigma_i^{r-1}| > |\sigma_{yi}^{r-1}| \quad \text{and} \quad |\sigma_{ei}| < |\sigma_{yi}^{r-1}| \quad (10.3.20d)$$

### Force equilibrium

Since the displacement finite element model is based on the principle of virtual displacements, the solution satisfies the equilibrium equations, provided the deformation is linearly elastic. However, in the finite element analysis of elasto-plastic problems equilibrium equations may not be satisfied during the period when stresses are adjusted to account for plastic strains. Adjustments must be made to achieve equilibrium at each step by redistributing the forces neighboring elements.

For example, consider a node  $N$  at the interface of element  $i$  that has yielded and the adjacent element  $i + 1$  that is still elastic (see Figure 10.3.5). At this node, the force equilibrium will be violated during the analysis because the force in element  $i$  is limited such that the stress in the element does not exceed the yield stress. The difference between the force calculated using the elastic analysis and the plastic force must now be taken up by all other elastic elements in the mesh. Thus to restore equilibrium of forces, a force correction must be made at the node  $N$ :

$$\Delta F = F_i - F_{i+1} - F_N \quad (10.3.21)$$

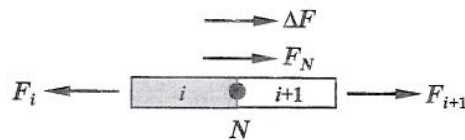


Figure 10.3.5 Force equilibrium at node  $N$ .

However, to preserve the finite element equations of the original problem (to retain the same forces in other unaffected elements), the force correction cannot be imposed as a nodal force. Instead, the force correction may be applied as a nodal displacement

$$\Delta u_N^c = \frac{\Delta F L_i}{E_T A_i} \quad (10.3.22)$$

where  $L_i$  and  $A_i$  are the length and cross-sectional area of element  $i$ . This correction procedure will continue until force equilibrium at all nodes is restored, within an acceptable error of tolerance.

Figure 10.3.6 contains the flow chart of various steps in the elasto-plastic analysis of a typical problem. A subroutine that updates stresses and plastic strains is also given in Box 10.3.1.

### A numerical example

Consider a bar of length 5 m that is fixed at one end and is subjected to a uniform body force  $f$ . The material properties of the bar are taken as

$$E = 10^4 \text{ N/m}^2, \quad A = 1 \text{ m}^2, \quad \sigma_y = 5 \text{ N/m}^2, \quad H = 10^3 \text{ N/m}^2$$

The bar is discretized using a mesh of five linear elements. The elasto-plastic iterative scheme discussed in this section was implemented and the results are presented in Tables 10.3.1 and 10.3.2. At the start of the analysis when elements are still elastic, a nominal body force of 0.005 N/m was imposed to find the maximum stress induced in the elements. The critical load  $F_{cr}$  for the first element to yield was computed from this maximum element stress and is imposed in the next load-step:

$$f_{cr} = \frac{\sigma_Y f}{\max|\sigma_i|} \quad (10.3.23)$$

Here  $i$  is the element number and  $N$  is the total number of unyielded elements. In the new load-step where  $f$  is 1.1111 N/m, the computed results reveal that the first element (element 1 in this example) had just yielded; up to this point, the analysis is still elastic. Then another nominal body force of 0.005 N/m is added to calculate the critical load for the next element to yield. The stiffness of the yielded Element 1 is reduced in this load-step and the results in Table 10.3.2 indicate a violation of force equilibrium at the nodes connecting the yielded element, except for the node that is fixed. Corrections to the nodal displacements were made until equilibrium was satisfied at all nodes. Only then, the critical load for the next element to yield could be calculated and the same procedure is repeated until all elements yield.

Reaction forces at the fixed end of the bar against the free-end displacements are plotted in Figure 10.3.7, together with the results from

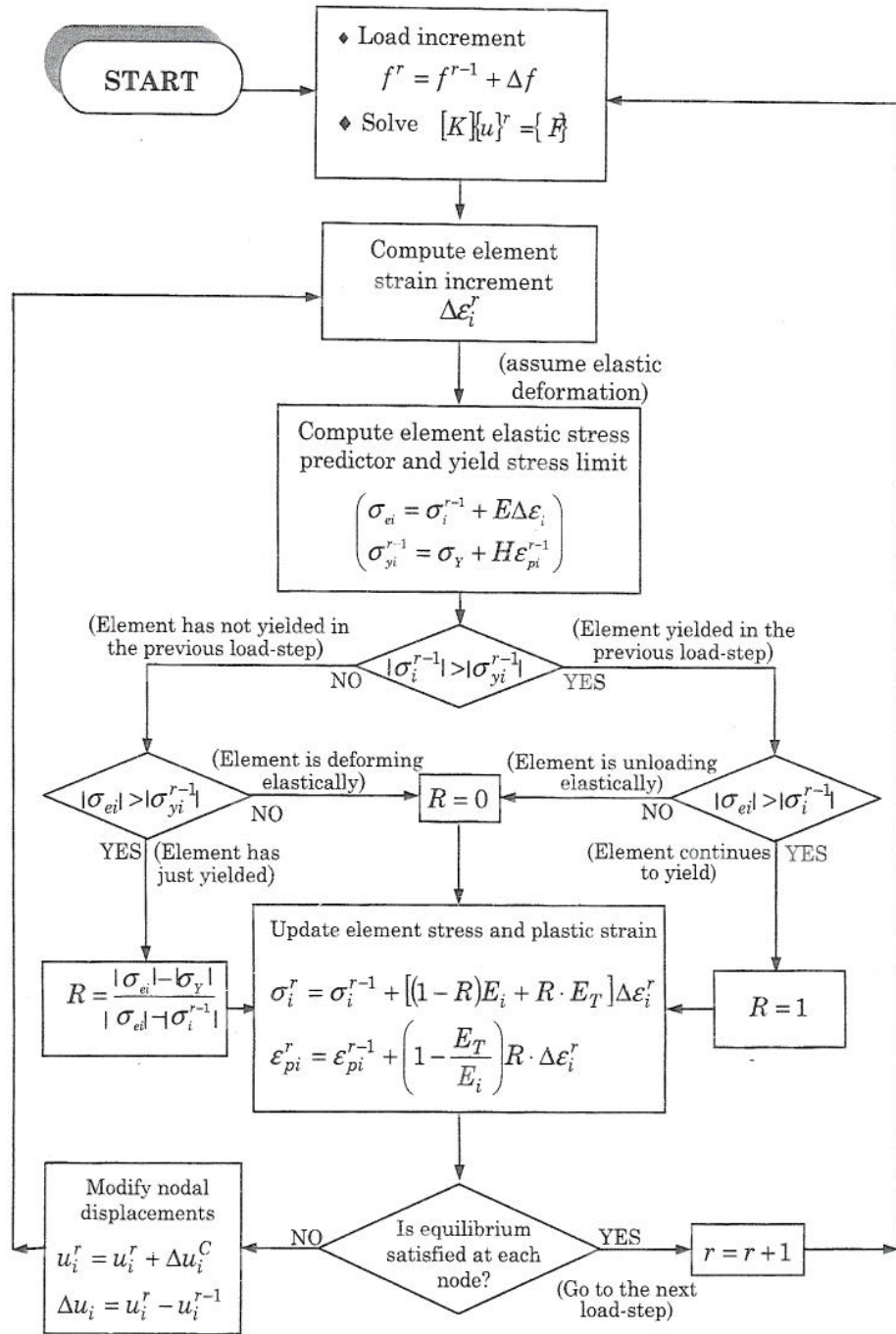


Figure 10.3.6 Flow chart for elasto-plastic analysis of a bar.



**Box 10.3.1** Fortran statements for the subroutine to calculate the stress and plastic strain of a bar element.

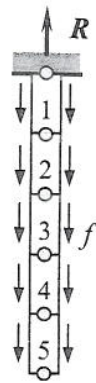
```

SUBROUTINE STRESS(N,MXELM,NDF,NPE,IELEM,ELSIG,PSTRAIN)
C
C -----
C The subroutine evaluates the stress at the center of the element and then update
C the stress and plastic strain against the yield criteria.
C SIGMA    ... Updated elastic stress      YOUNG ... Elastic modulus
C TYIELD   ... Current yield limit        TYOUNG... Elasto-plastic tangent modulus
C ELSIG(N) ... Elastic stress of element N  YSTRESS... Yield stress
C PSTRAIN(N)... Plastic strain of element N  HP      ... Strain hardening parameter
C -----
      Definition of global and local variables and common blocks
C Compute the total strain increment at the center of element
      H = ELX(NPE) - ELX(1)
      CALL SHP1D (H,IELEM,NPE,0.D0)
      UX=0.D0
      DO K=1,NPE
         UX=UX+EPV((K-1)*NDF+1)*GDSF(K)
      ENDDO
C Update the elastic stress and current yield limit
      SIGMA = ELSIG(N)+YOUNG*UX
      IF(ELSIG(N).GT.0.0)TYIELD=YSTRESS+HP*PSTRAIN(N)
      IF(ELSIG(N).LE.0.0)TYIELD=-YSTRESS+HP*PSTRAIN(N)
C Check the updated elastic stress for yielding
      IF (ABS(ELSIG(N)) .GT. ABS(TYIELD)) THEN
         IF (ABS(SIGMA) .GT. ABS(ELSIG(N))) THEN
            R = 1.D0
         ELSE
            R = 0.D0
         ENDIF
      ELSE
         IF (ABS(SIGMA) .GT. ABS(TYIELD)) THEN
            R = (ABS(SIGMA)-ABS(TYIELD))/(ABS(SIGMA)-ABS(ELSIG(N)))
         ELSE
            R = 0.D0
         ENDIF
      ENDIF
C Correct the elastic stress and calculate the plastic strain
      ELSIG(N)= ELSIG(N)+((1.D0-R)*YOUNG+R*TYOUNG)*UX
      PSTRAIN(N)= PSTRAIN(N)+(R/(1.D0+HP/YOUNG))*UX
      RETURN
      END

```

Table 10.3.1 Nodal displacements for various load steps.

Body force $f$	Node no.	Nodal displacement*
0.0050	2	$2.2500 \times 10^{-6}$
	3	$4.0000 \times 10^{-6}$
	4	$5.2500 \times 10^{-6}$
	5	$6.0000 \times 10^{-6}$
	6	$6.2500 \times 10^{-6}$
1.1111	2	$5.0000 \times 10^{-4}$
	3	$8.8889 \times 10^{-4}$
	4	$1.1667 \times 10^{-3}$
	5	$1.3333 \times 10^{-3}$
	6	$1.3889 \times 10^{-3}$
1.1161	2	$5.2475 \times 10^{-4}$ ( $5.2475 \times 10^{-4}$ )
	3	$9.1539 \times 10^{-4}$ ( $9.1539 \times 10^{-4}$ )
	4	$1.1944 \times 10^{-3}$ ( $1.1944 \times 10^{-3}$ )
	5	$1.3618 \times 10^{-3}$ ( $1.3618 \times 10^{-3}$ )
	6	$1.4176 \times 10^{-3}$ ( $1.4176 \times 10^{-3}$ )
10.0050	2	$4.9525 \times 10^{-2}$ ( $4.4525 \times 10^{-2}$ )
	3	$8.8044 \times 10^{-2}$ ( $7.8044 \times 10^{-2}$ )
	4	$1.1556 \times 10^{-1}$ ( $1.0056 \times 10^{-1}$ )
	5	$1.3207 \times 10^{-1}$ ( $1.1207 \times 10^{-1}$ )
	6	$1.3257 \times 10^{-1}$ ( $1.1257 \times 10^{-1}$ )



\* Values in parenthesis are corrected to satisfy force equilibrium at each node.

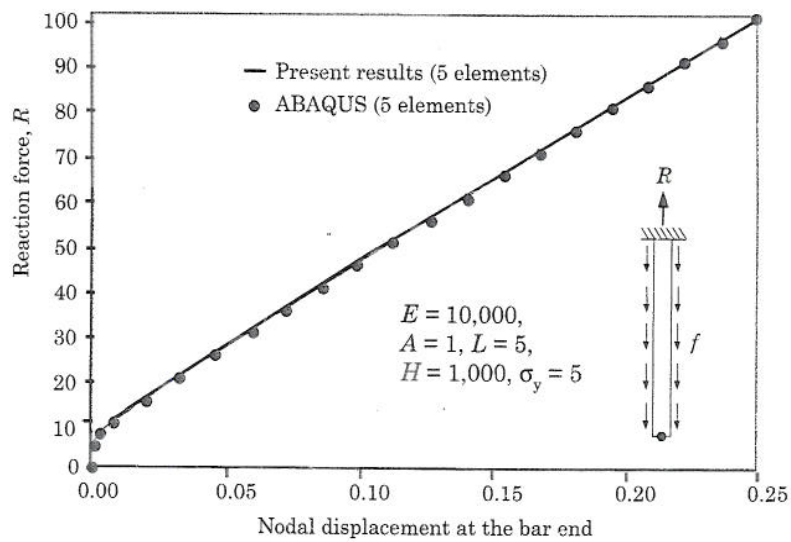


Figure 10.3.7 Reaction forces versus nodal displacements at bar end.

Table 10.3.2 Element stresses and strains for various load steps.

Body force $f$	Element number	Total strain $\epsilon$	Plastic strain $\epsilon_p$	Bar force $ F  = \sigma A$
0.0050	1	$2.2500 \times 10^{-6}$	0	0.0225
	2	$1.7500 \times 10^{-6}$	0	0.0175
	3	$1.2500 \times 10^{-6}$	0	0.0125
	4	$0.7500 \times 10^{-6}$	0	0.0075
	5	$0.2500 \times 10^{-6}$	0	0.0025
1.1111	1*	$5.0000 \times 10^{-4}$	0	5.0000
	2	$3.8889 \times 10^{-4}$	0	3.8889
	3	$2.7778 \times 10^{-4}$	0	2.7778
	4	$1.6667 \times 10^{-4}$	0	1.6667
	5	$0.5556 \times 10^{-4}$	0	0.5556
1.1161	1	$5.5248 \times 10^{-4}$	$4.5680 \times 10^{-3}$	9.5680
	2	$3.9064 \times 10^{-4}$	0	3.9064
	3	$2.7903 \times 10^{-4}$	0	2.7903
	4	$1.6742 \times 10^{-4}$	0	1.6742
	5	$0.5581 \times 10^{-4}$	0	0.5581
Corrected to satisfy force equilibrium	1	$5.2475 \times 10^{-4}$	$0.2250 \times 10^{-4}$	5.0225
	2	$3.9064 \times 10^{-4}$	0	3.9064
	3	$2.7903 \times 10^{-4}$	0	2.7903
	4	$1.6742 \times 10^{-4}$	0	1.6742
	5	$0.5581 \times 10^{-4}$	0	0.5581
...	...	...	...	...
10.0050	1	$4.9525 \times 10^{-2}$	$4.4568 \times 10^{-2}$	49.5680
	2	$3.8519 \times 10^{-2}$	$3.4563 \times 10^{-2}$	39.5630
	3	$2.7514 \times 10^{-2}$	$2.4558 \times 10^{-2}$	29.5580
	4	$1.6508 \times 10^{-2}$	$1.4553 \times 10^{-2}$	19.5530
	5	$0.5503 \times 10^{-2}$	$0.4548 \times 10^{-2}$	9.5480
Corrected to satisfy force equilibrium	1	$4.4525 \times 10^{-2}$	$4.0023 \times 10^{-2}$	45.0225
	2	$3.3519 \times 10^{-2}$	$3.0018 \times 10^{-2}$	35.0175
	3	$2.2514 \times 10^{-2}$	$2.0013 \times 10^{-2}$	25.0125
	4	$1.1508 \times 10^{-2}$	$1.0008 \times 10^{-2}$	15.0075
	5	$5.0275 \times 10^{-4}$	$0.0025 \times 10^{-4}$	5.0025

\* Element just yielded at that load step.

the commercial finite element software ABAQUS. There is a very good agreement with the solutions generated by the iterative scheme discussed and those obtained with ABAQUS. A 20-element mesh also produced results identical to those in Figure 10.3.7; the results are also verified using ABAQUS. Figure 10.3.8 contains the true stress-strain diagram of Element 1, where one may note that the elasto-plastic material curve is recovered.

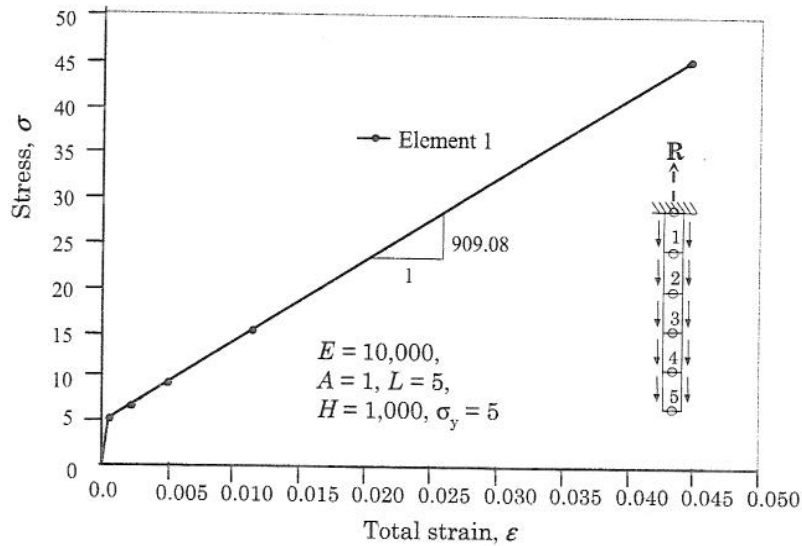


Figure 10.3.8 True stress-strain curve of Element 1.

## 10.4 Non-Newtonian Fluids

### 10.4.1 Introduction

Some of the most challenging and important areas currently under investigation in computational fluid mechanics concern flows of non-Newtonian fluids. A non-Newtonian fluid is defined to be the one whose constitutive behavior is nonlinear (i.e., stresses are nonlinear functions of strain rates). Such fluids may or may not have memory of past deformation (i.e. viscoelastic or not). Practical examples of such fluids are multigrade oils, liquid detergents, paints, and printing inks. Polymer solutions and polymer melts also fall within this category. All such flows are extremely important in forming processes of various kinds applied to metals, plastics, or glass.

Numerical approaches used for analyzing flows of non-Newtonian fluids differ very little from the ones used for Newtonian fluids. When the shear viscosity is a function of the rate of deformation tensor (i.e., for so-called power-law fluids), the equation of motion can still be written explicitly in terms of velocity components. For such fluids, the same formulations as those of the Newtonian fluids can be used. For example, the pressure-velocity and penalty finite element models discussed in Chapter 7 can be used for power-law fluids. The constitutive equations of a viscoelastic fluid can be described in terms of the *extra stress* components and are given in terms of either differential equations or as integral equations. In a differential constitutive model, the extra stress components and their derivatives are related to the

velocity components and their derivatives [6–9]. The computational models of viscoelastic fluids obeying a differential model require us to treat stress components as independent variables along with the velocity components and pressure.

Most existing works in the finite-element analysis of viscoelastic fluids have considered different types of Maxwell/Oldroyd models, in which both viscosity and relaxation time are constants. The analyses were based on mixed formulations in which the velocities, pressure, and stresses are treated as nodal variables. An important class of fluids, which are characterized by shear viscosity and elasticity require additional study from numerical simulation point of view. The viscoelastic effects along with memory effects of such fluids can be studied using the White–Metzner model [7].

The objective of this section is to study penalty finite element models of power-law and viscoelastic White–Metzner type fluids. As a part of this discussion, we present finite element models of equations governing flows of viscous incompressible fluids through axisymmetric geometries. Therefore, first we rewrite the conservation of mass and momentum in the cylindrical coordinate system.

#### 10.4.2 Governing Equations in Cylindrical Coordinates

Equations (7.3.1)–(7.3.3) can be expressed in a cylindrical coordinate system,  $(r, \theta, z)$ , by writing all vectors and tensors, including the del operator, in terms of components in a cylindrical coordinate system. For example, the del operator and the material time derivative operators in the cylindrical coordinate system are given by

$$\nabla = \hat{\mathbf{e}}_r \frac{\partial}{\partial r} + \hat{\mathbf{e}}_\theta \frac{1}{r} \frac{\partial}{\partial \theta} + \hat{\mathbf{e}}_z \frac{\partial}{\partial z} \quad (10.4.1)$$

$$\frac{D}{Dt} = \frac{\partial}{\partial t} + v_r \frac{\partial}{\partial r} + \frac{v_\theta}{r} \frac{\partial}{\partial \theta} + v_z \frac{\partial}{\partial z} \quad (10.4.2)$$

where  $(\hat{\mathbf{e}}_r, \hat{\mathbf{e}}_\theta, \hat{\mathbf{e}}_z)$  are the unit basis vectors and  $(v_r, v_\theta, v_z)$  are the velocity components in the  $r$ ,  $\theta$ , and  $z$  directions, respectively. Note that the basis vector  $\hat{\mathbf{e}}_z$  is constant while the vectors  $\hat{\mathbf{e}}_r$  and  $\hat{\mathbf{e}}_\theta$  depend on the angular coordinate  $\theta$ . Thus the derivatives of the basis vectors  $\hat{\mathbf{e}}_r$  and  $\hat{\mathbf{e}}_\theta$  with respect to the coordinates  $r$  and  $z$  are zero, and the derivatives with respect to  $\theta$  are given by

$$\frac{\partial \hat{\mathbf{e}}_r}{\partial \theta} = \hat{\mathbf{e}}_\theta; \quad \frac{\partial \hat{\mathbf{e}}_\theta}{\partial \theta} = -\hat{\mathbf{e}}_r \quad (10.4.3)$$

The components of the strain rate tensor  $\mathbf{D}$  in Eq. (7.2.13) and constitutive relations (7.2.11) and (7.2.15) take the form

$$D_{rr} = \frac{\partial v_r}{\partial r}; \quad D_{\theta\theta} = \frac{1}{r} \frac{\partial v_\theta}{\partial \theta} + \frac{v_r}{r}$$

$$D_{zz} = \frac{\partial v_z}{\partial z}; \quad 2D_{r\theta} = \frac{\partial v_\theta}{\partial r} - \frac{v_\theta}{r} + \frac{1}{r} \frac{\partial v_r}{\partial \theta} \quad (10.4.4)$$

$$2D_{\theta z} = \frac{1}{r} \frac{\partial v_z}{\partial \theta} + \frac{\partial v_\theta}{\partial z}; \quad 2D_{zr} = \frac{\partial v_r}{\partial z} + \frac{\partial v_z}{\partial r}$$

$$\sigma_{rr} = -P + 2\mu D_{rr}; \quad \sigma_{\theta\theta} = -P + 2\mu D_{\theta\theta}; \quad \sigma_{zz} = -P + 2\mu D_{zz}$$

$$\sigma_{r\theta} = 2\mu D_{r\theta}; \quad \sigma_{\theta z} = 2\mu D_{\theta z}; \quad \sigma_{zr} = 2\mu D_{zr} \quad (10.4.5)$$

The governing equations (7.3.1)–(7.3.3) expressed in the cylindrical coordinate system are

$$\frac{1}{r} \frac{\partial}{\partial r}(rv_r) + \frac{1}{r} \frac{\partial v_\theta}{\partial \theta} + \frac{\partial v_z}{\partial z} = 0 \quad (10.4.6)$$

$$\rho \left( \frac{Dv_r}{Dt} - \frac{v_\theta^2}{r} \right) = \rho f_r + \frac{1}{r} \left[ \frac{\partial(r\sigma_{rr})}{\partial r} + \frac{\partial\sigma_{r\theta}}{\partial \theta} + \frac{\partial(r\sigma_{zr})}{\partial z} \right] - \frac{\sigma_{\theta\theta}}{r} \quad (10.4.7a)$$

$$\rho \left( \frac{Dv_\theta}{Dt} + \frac{v_r v_\theta}{r} \right) = \rho f_\theta + \frac{1}{r} \left[ \frac{\partial(r\sigma_{r\theta})}{\partial r} + \frac{\partial\sigma_{\theta\theta}}{\partial \theta} + \frac{\partial(r\sigma_{\theta z})}{\partial z} \right] + \frac{\sigma_{r\theta}}{r} \quad (10.4.7b)$$

$$\rho \left( \frac{Dv_z}{Dt} \right) = \rho f_z + \frac{1}{r} \left[ \frac{\partial(r\sigma_{zr})}{\partial r} + \frac{\partial\sigma_{z\theta}}{\partial \theta} + \frac{\partial(r\sigma_{zz})}{\partial z} \right] \quad (10.4.7c)$$

$$\rho C_s \frac{DT}{Dt} = \frac{1}{r} \frac{\partial}{\partial r} \left( rk_{rr} \frac{\partial T}{\partial r} \right) + \frac{1}{r^2} \frac{\partial}{\partial \theta} \left( k_{\theta\theta} \frac{\partial T}{\partial \theta} \right) + \frac{\partial}{\partial z} \left( k_{zz} \frac{\partial T}{\partial z} \right) + \Phi + Q \quad (10.4.8)$$

where the stress components are known in terms of the velocity components *via* equations (10.4.4) and (10.4.5). The viscous dissipation  $\Phi$  is given by

$$\Phi = 2\mu (D_{rr}^2 + D_{\theta\theta}^2 + D_{zz}^2) + 4\mu (D_{r\theta}^2 + D_{rz}^2 + D_{z\theta}^2) \quad (10.4.9)$$

and the material time derivative becomes

$$\frac{D}{Dt} = \frac{\partial}{\partial t} + v_r \frac{\partial}{\partial r} + \frac{v_\theta}{r} \frac{\partial}{\partial \theta} + v_z \frac{\partial}{\partial z} \quad (10.4.10)$$

Note that the time derivative of a vector (or tensor) in a rotating reference frame is given by (see Reddy and Rasmussen [5], pp. 69–74)

$$\left[ \frac{D(\cdot)}{Dt} \right]_{nonrot} = \left[ \frac{D(\cdot)}{Dt} \right]_{rot} + \omega \times (\cdot) \quad (10.4.11)$$

where  $\omega = \frac{d\theta}{dt} \hat{e}_z = \frac{v_\theta}{r} \hat{e}_z$  is the angular velocity vector of the rotating frame of reference. Therefore, we have

$$\begin{aligned} \left( \frac{D\mathbf{v}}{Dt} \right)_{nonrot} &= \left( \frac{D\mathbf{v}}{Dt} \right)_{rot} + \left( \frac{v_\theta}{r} \hat{e}_z \right) \times \mathbf{v} \\ &= \hat{e}_r \left( \frac{Dv_r}{Dt} - v_\theta \frac{v_\theta}{r} \right) + \hat{e}_\theta \left( \frac{Dv_\theta}{Dt} + v_r \frac{v_\theta}{r} \right) + \hat{e}_z \frac{Dv_z}{Dt} \end{aligned} \quad (10.4.12)$$

Equation (10.4.11) could be used in conjunction with (10.4.7a-c) to provide a description of fluid motion in a rotating cylindrical coordinate system.

For axisymmetric conditions (i.e. all variables are independent of  $\theta$ , and  $f_\theta = v_\theta = 0$ ), the governing equations are simplified to

$$\frac{1}{r} \frac{\partial}{\partial r} (rv_r) + \frac{\partial v_z}{\partial z} = 0 \quad (10.4.13)$$

$$\rho \left( \frac{\partial v_r}{\partial t} + v_r \frac{\partial v_r}{\partial r} + v_z \frac{\partial v_r}{\partial z} \right) = \rho f_r + \frac{1}{r} \frac{\partial (r\sigma_{rr})}{\partial r} + \frac{\partial \sigma_{zr}}{\partial z} - \frac{\sigma_{\theta\theta}}{r} \quad (10.4.14a)$$

$$\rho \left( \frac{\partial v_z}{\partial t} + v_r \frac{\partial v_z}{\partial r} + v_z \frac{\partial v_z}{\partial z} \right) = \rho f_z + \frac{1}{r} \frac{\partial (r\sigma_{zr})}{\partial r} + \frac{\partial \sigma_{zz}}{\partial z} \quad (10.4.14b)$$

$$\rho C_s \left( \frac{\partial T}{\partial t} + v_r \frac{\partial T}{\partial r} + v_z \frac{\partial T}{\partial z} \right) = \frac{1}{r} \frac{\partial}{\partial r} \left( rk_{rr} \frac{\partial T}{\partial r} \right) + \frac{\partial}{\partial z} \left( k_{zz} \frac{\partial T}{\partial z} \right) + \Phi + Q \quad (10.4.15)$$

### 10.4.3 Power-Law Fluids

Many fluids used in industrial applications are characterized by so-called power-law constitutive behavior. Power-law fluids exhibit nonlinear material behavior according to the relation

$$\sigma = \tau - P\mathbf{I}, \quad \tau = 2\mu(I_2)\mathbf{D} \quad (10.4.16)$$

$$\mu = \mu_0 (I_2)^{\frac{(n-1)}{2}} \quad (10.4.17a)$$

$$I_2 = \frac{1}{2} D_{ij} D_{ij} \quad (\text{sum on } i \text{ and } j) \quad (10.4.17b)$$

where  $\tau$  is the viscous part of the stress tensor  $\sigma$ ,  $\mathbf{I}$  is the unit tensor,  $I_2$  is the second invariant of  $\mathbf{D}$ , and parameters  $\mu_0$  and  $n$  characterize the fluid (determined experimentally). For many non-Newtonian fluids, the viscosity  $\mu$  decreases with increasing shear rate. These are called *shear thinning fluids* and have the power law index  $n < 1$ . Fluids with power law index  $n > 1$  are called *shear-thickening fluids*. For such fluids,  $\mu$  increases with increasing shear rate. For  $n = 1$ , Eq. (10.4.17a) gives the Newtonian relation ( $\mu = \mu_0$ , constant). The power-law constitutive relation in (10.4.16) makes the problem nonlinear for  $n \neq 1$ , even for the case where the convective term  $\mathbf{v} \cdot \nabla \mathbf{v}$  is negligible.

To illustrate how the power-law constitutive equation affects the finite element equations, we consider steady, isothermal, axisymmetric flows of viscous incompressible fluids. Assuming negligible viscous dissipation and body forces, The governing equations (10.4.13)–(10.4.15) can be expressed

in terms of the velocity components  $(v_r, v_z)$  as

$$\frac{1}{r} \frac{\partial}{\partial r} (r v_r) + \frac{\partial v_z}{\partial z} = 0 \quad (10.4.18)$$

$$\rho \left( v_r \frac{\partial v_r}{\partial r} + v_z \frac{\partial v_r}{\partial z} \right) = \frac{1}{r} \frac{\partial}{\partial r} \left( 2\mu r \frac{\partial v_r}{\partial r} \right) + \frac{\partial}{\partial z} \left[ \mu \left( \frac{\partial v_r}{\partial z} + \frac{\partial v_z}{\partial r} \right) \right] - 2\mu \frac{v_r}{r^2} - \frac{\partial P}{\partial r} \quad (10.4.19)$$

$$\rho \left( v_r \frac{\partial v_z}{\partial r} + v_z \frac{\partial v_z}{\partial z} \right) = \frac{1}{r} \frac{\partial}{\partial r} \left[ \mu r \left( \frac{\partial v_r}{\partial z} + \frac{\partial v_z}{\partial r} \right) \right] + \frac{\partial}{\partial z} \left( 2\mu \frac{\partial v_z}{\partial z} \right) - \frac{\partial P}{\partial z} \quad (10.4.20)$$

The penalty-finite element model of Eqs. (10.4.18)–(10.4.20) is straightforward. After replacing  $P$  in Eqs. (10.4.19) and (10.4.20) with

$$P = -\gamma_p \left( \frac{\partial v_r}{\partial r} + \frac{v_r}{r} + \frac{\partial v_z}{\partial z} \right) \quad (10.4.21)$$

one may construct their weak forms and go on to develop the finite element model [note that Eq. (10.4.18) is no longer used]. The value of the penalty parameter  $\gamma_p$  that is most suitable for this class problems must be determined by conducting numerical experiments with some benchmark problems. The finite element model has the form

$$[\mathbf{C}(\mathbf{v}) + \mathbf{K}(\mu) + \mathbf{K}_p]\{\mathbf{v}\} = \{\mathbf{F}\} \quad \text{or} \quad [\hat{\mathbf{K}}(\mathbf{v})]\{\mathbf{v}\} = \{\mathbf{F}\} \quad (10.4.22)$$

where  $[\mathbf{C}]$ ,  $[\mathbf{K}]$ , and  $[\mathbf{K}_p]$  are the convective, diffusive, and penalty contributions to the coefficient matrix. Note that  $[\mathbf{C}]$  and  $[\mathbf{K}]$  both depend on the unknown velocity field.

The direct iteration scheme for this case is given by

$$[\hat{\mathbf{K}}(\{\mathbf{v}\}^{(r-1)})]\{\mathbf{v}\}^r = \{\mathbf{F}\} \quad (10.4.23)$$

where  $[\hat{\mathbf{K}}]$  is evaluated using the viscosity  $\mu = \mu(D_{ij})$  computed according to Eq. (10.4.17a) at the  $r$ th iteration. It would be more appropriate to compute  $\mu$  at the Gauss points of the element and use it in the evaluation of  $\hat{K}_{ij}$ , than to assume  $\mu$  is element-wise constant. For example, consider the element coefficients  $K_{ij}^{11}$  in the diffusion/viscous portion of the coefficient matrix:

$$K_{ij}^{11} = \int_{\Omega^e} \left( 2\mu \frac{\partial \psi_i}{\partial x} \frac{\partial \psi_j}{\partial x} + \mu \frac{\partial \psi_i}{\partial y} \frac{\partial \psi_j}{\partial y} \right) dx dy \quad (10.4.24)$$



For numerical evaluation of  $K_{ij}^{11}$  we use the Gauss quadrature rule

$$K_{ij}^{11} = \sum_{I,J=1}^{NGP} AMU(I, J) * [2.0 * GDSF(1, i) * GDSF(1, j) + GDSF(2, i) * GDSF(2, j)] * CONST \quad (10.4.25)$$

where  $AMU(I, J)$  is the value of  $\mu$  at the  $(I, J)$ th Gauss point. Obviously,  $AMU(I, J)$  must be evaluated using Eq. (10.4.17a) prior to using it in Eq. (10.4.25).

#### 10.4.4 White-Metzner Fluids

The general constitutive equation for fluids dominated by shear viscosity is given by (see [7-9])

$$\tau + \lambda \left\{ \frac{\partial \tau}{\partial t} + \mathbf{v} \cdot \nabla \tau - [(\nabla \mathbf{v})^T \cdot \tau + \tau \cdot (\nabla \mathbf{v})] \right\} = 2\eta \mathbf{D} \quad (10.4.26)$$

where  $\lambda$  is the relaxation time,  $\eta$  is the shear viscosity of the fluid, and  $\mathbf{D}$  is the rate of deformation tensor.

To characterize the White-Metzner fluid, it is necessary to know the viscosity curve as a function of shear rate and the first normal stress difference. The extra stress tensor  $\tau$  is separated into purely viscous part  $\tau^2$  and viscoelastic part  $\tau^1$ :

$$\tau = \tau^1 + \tau^2 \quad (10.4.27)$$

$$\tau^1 + \lambda \left\{ \frac{\partial \tau^1}{\partial t} + \mathbf{v} \cdot \nabla \tau^1 - [(\nabla \mathbf{v})^T \cdot \tau^1 + \tau^1 \cdot (\nabla \mathbf{v})] \right\} = 2\eta_1 \mathbf{D} \quad (10.4.28)$$

$$\tau^2 = 2\eta_2 \mathbf{D} \quad (10.4.29)$$

and  $\eta_1$  and  $\eta_2$  can be defined as the fractions of the shear viscosity  $\eta$ . The fluid which obeys Eq. (10.4.27) is characterized by  $\eta_1, \eta_2$ , and  $\lambda$ , which are the functions of rate of deformation tensor,  $\mathbf{D}$ .

Here, the relaxation time  $\lambda$  is assumed to depend on the shear rate  $\gamma$  according to

$$\lambda(\gamma) = a + b(\log \gamma) + c(\log \gamma)^2, \quad \gamma = \sqrt{4I_2} \quad (10.4.30)$$

All constants in Eq. (10.4.30) are evaluated by curve fitting data of polymeric melts (see [16]). Also,  $\eta$  is assumed to be of the particular form

$$\eta = \eta(I_2), \quad I_2 = \frac{1}{2} D_{ij} D_{ij} \quad (10.4.31)$$

Although Eq. (10.4.31) gives the general functional form for the viscosity function, experimental observation and a theoretical basis must be used to provide a specific model for non-Newtonian viscosities. A variety of models can be used to calculate viscosity. Here, the power law model in Eq. (10.4.17a) is used (replace  $\mu$  with  $\eta$ ).

In view of Eq. (10.4.27), the equation of motion (in the absence of body forces) for the White-Metzner viscoelastic fluids can be written as

$$\nabla \cdot (\tau^1 + 2\eta_2 \mathbf{D}) - \nabla P = \rho \left( \frac{\partial \mathbf{v}}{\partial t} + \mathbf{v} \cdot \nabla \mathbf{v} \right) \quad (10.4.32)$$

For simplicity, we drop the superscript 1 from  $\tau^1$  in Eq. (10.4.32) as well as in Eq. (10.4.28). Equations (10.4.32) and (10.4.28), together with the continuity equation  $\nabla \cdot \mathbf{v} = 0$ , represent the system of governing equations for the White-Metzner fluids. The viscosity  $\eta_1$  is calculated using Eq. (10.4.28) and  $\lambda$  from Eq. (10.4.30). Viscosity  $\eta_2$  is often taken as a function of  $\eta_1$ . Note that the power-law constitutive equation can be obtained as a special case from Eq. (10.4.28).

For axisymmetric flows of White-Metzner fluids, the governing equations are given by

$$\frac{\partial u}{\partial r} + \frac{u}{r} + \frac{\partial w}{\partial z} = 0 \quad (10.4.33)$$

$$\begin{aligned} \frac{\partial}{\partial r} \left( \tau_{rr} + 2\eta_2 \frac{\partial u}{\partial r} \right) + \frac{1}{r} \left( \tau_{rr} + 2\eta_2 \frac{\partial u}{\partial r} - \tau_{\theta\theta} - 2\eta_2 \frac{u}{r} \right) \\ + \frac{\partial}{\partial r} \left[ \tau_{rz} + \eta_2 \left( \frac{\partial u}{\partial z} + \frac{\partial w}{\partial r} \right) \right] - \frac{\partial P}{\partial r} = \rho \left( \frac{\partial u}{\partial t} + u \frac{\partial u}{\partial r} + w \frac{\partial u}{\partial z} \right) \end{aligned} \quad (10.4.34)$$

$$\begin{aligned} \frac{\partial}{\partial r} \left[ \tau_{rz} + \eta_2 \left( \frac{\partial u}{\partial z} + \frac{\partial w}{\partial r} \right) \right] + \frac{1}{r} \left[ \tau_{rs} + \eta_2 \left( \frac{\partial u}{\partial z} + \frac{\partial w}{\partial r} \right) \right] \\ + \frac{\partial}{\partial z} \left( \tau_{zz} + 2\eta_2 \frac{\partial w}{\partial z} \right) - \frac{\partial P}{\partial z} = \rho \left( \frac{\partial w}{\partial t} + u \frac{\partial w}{\partial r} + w \frac{\partial w}{\partial z} \right) \end{aligned} \quad (10.4.35)$$

$$\tau_{rr} + \lambda \left[ \frac{\partial \tau_{rr}}{\partial t} + u \frac{\partial \tau_{rr}}{\partial r} + w \frac{\partial \tau_{rr}}{\partial z} - 2 \left( \frac{\partial u}{\partial r} \tau_{rr} + \frac{\partial u}{\partial z} \tau_{rz} \right) \right] = 2\eta_1 \frac{\partial u}{\partial r} \quad (10.4.36a)$$

$$\tau_{zz} + \lambda \left[ \frac{\partial \tau_{zz}}{\partial t} + u \frac{\partial \tau_{zz}}{\partial r} + w \frac{\partial \tau_{zz}}{\partial z} - 2 \left( \frac{\partial w}{\partial z} \tau_{zz} + \frac{\partial w}{\partial r} \tau_{rz} \right) \right] = 2\eta_1 \frac{\partial w}{\partial z} \quad (10.4.36b)$$

$$\begin{aligned} \tau_{rz} + \lambda \left[ \frac{\partial \tau_{rz}}{\partial t} + u \frac{\partial \tau_{rz}}{\partial r} + w \frac{\partial \tau_{rz}}{\partial z} - 2 \left( \frac{\partial u}{\partial r} \tau_{rz} + \frac{\partial w}{\partial z} \tau_{rz} + \frac{\partial u}{\partial z} \tau_{zz} + \frac{\partial w}{\partial r} \tau_{rr} \right) \right] \\ = \eta_1 \left( \frac{\partial w}{\partial r} + \frac{\partial u}{\partial z} \right) \end{aligned} \quad (10.4.36c)$$

$$\tau_{\theta\theta} + \lambda \left[ \frac{\partial \tau_{\theta\theta}}{\partial t} + u \frac{\partial \tau_{\theta\theta}}{\partial r} + w \frac{\partial \tau_{\theta\theta}}{\partial z} - 2 \frac{u}{r} \tau_{\theta\theta} \right] = 2\eta_1 \frac{u}{r} \quad (10.4.36d)$$

where  $v_r = u$  and  $v_z = w$  denote the velocity components in the radial and axial directions, respectively.

The (mixed) penalty-finite element model of the above equations can be developed by constructing the weak forms of Eqs. (10.4.34)–(10.4.36) [after replacing the pressure with Eq. (10.4.21)] and interpolating velocities ( $u, w$ ) and extra stress components ( $\tau_{rr}, \tau_{\theta\theta}, \tau_{zz}, \tau_{rz}$ ) as follows (with equal interpolation of all variables):

$$\begin{aligned} u(r, z, t) &= \sum_{j=1}^N u_j(t) \psi_j(r, z), & w(r, z, t) &= \sum_{j=1}^N w_j(t) \psi_j(r, z) \\ \tau_{rr}(r, z, t) &= \sum_{j=1}^L \tau_{rr}^j(t) \psi_j(r, z), & \tau_{zz}(r, z, t) &= \sum_{j=1}^L \tau_{zz}^j(t) \psi_j(r, z) \\ \tau_{rz}(r, z, t) &= \sum_{j=1}^L \tau_{rz}^j(t) \psi_j(r, z), & \tau_{\theta\theta}(r, z, t) &= \sum_{j=1}^L \tau_{\theta\theta}^j(t) \psi_j(r, z) \end{aligned} \quad (10.4.37)$$

where,  $(u_j, w_j)$  are the nodal velocities,  $(\tau_{rr}^j, \tau_{zz}^j, \tau_{rz}^j, \tau_{\theta\theta}^j)$  are the nodal extra stress components, and  $\psi_j$  are the Lagrange interpolation functions. The finite element model has the general form

$$[M^e] \{\dot{\Delta}^e\} + [K^e] \{\Delta^e\} = \{F^e\} \quad (10.4.38)$$

where

$$\{\Delta^e\} = \begin{Bmatrix} \{u\} \\ \{w\} \\ \{\tau_{rr}\} \\ \{\tau_{zz}\} \\ \{\tau_{rz}\} \\ \{\tau_{\theta\theta}\} \end{Bmatrix} \quad (10.4.39)$$

The nonzero coefficient matrices are listed below.

$$\begin{aligned} K_{ij}^{11} &= \int_{\Omega^e} \left[ \rho \psi_i \left( \bar{u} \frac{\partial \psi_j}{\partial r} + \bar{w} \frac{\partial \psi_j}{\partial z} \right) + \eta_2 \left( 2 \frac{\partial \psi_i}{\partial r} \frac{\partial \psi_j}{\partial r} + \frac{\partial \psi_i}{\partial z} \frac{\partial \psi_j}{\partial z} + \frac{\psi_i \psi_j}{r^2} \right) \right] r dr dz \\ &\quad + \gamma_p \int_{\Omega^e} \left( \frac{\partial \psi_i}{\partial r} + \frac{1}{r} \psi_i \right) \left( \frac{\partial \psi_j}{\partial r} + \frac{1}{r} \psi_j \right) r dr dz \\ K_{ij}^{12} &= \int_{\Omega^e} \left( \eta_2 \frac{\partial \psi_i}{\partial z} \frac{\partial \psi_j}{\partial r} \right) r dr dz + \gamma_p \int_{\Omega^e} \left( \frac{\partial \psi_i}{\partial r} + \frac{1}{r} \psi_i \right) \frac{\partial \psi_j}{\partial z} r dr dz \\ K_{ij}^{13} &= \int_{\Omega^e} \frac{\partial \psi_i}{\partial r} \psi_j r dr dz, & K_{ij}^{31} &= -2 \int_{\Omega^e} \eta_2 \psi_i \frac{\partial \psi_j}{\partial r} r dr dz \\ K_{ij}^{21} &= \int_{\Omega^e} \left( \eta_2 \frac{\partial \psi_i}{\partial r} \frac{\partial \psi_j}{\partial z} \right) r dr dz + \gamma_p \int_{\Omega^e} \left( \frac{\partial \psi_j}{\partial r} + \frac{1}{r} \psi_j \right) \frac{\partial \psi_i}{\partial z} r dr dz \\ K_{ij}^{22} &= \int_{\Omega^e} \left[ \rho \psi_i \left( \bar{u} \frac{\partial \psi_j}{\partial r} + \bar{w} \frac{\partial \psi_j}{\partial z} \right) + \eta_2 \left( \frac{\partial \psi_i}{\partial r} \frac{\partial \psi_j}{\partial r} + 2 \frac{\partial \psi_i}{\partial z} \frac{\partial \psi_j}{\partial z} \right) \right] r dr dz \\ &\quad + \gamma_p \int_{\Omega^e} \frac{\partial \psi_i}{\partial z} \frac{\partial \psi_j}{\partial z} r dr dz \end{aligned}$$

$$\begin{aligned}
K_{ij}^{24} &= \int_{\Omega^e} \frac{\partial \psi_i}{\partial z} \psi_j r dr dz, & K_{ij}^{25} &= \int_{\Omega^e} \frac{\partial \psi_i}{\partial r} \psi_j r dr dz \\
K_{ij}^{33} &= \int_{\Omega^e} \left\{ \psi_i \psi_j + \lambda \left[ \psi_i \left( \bar{u} \frac{\partial \psi_j}{\partial r} + \bar{w} \frac{\partial \psi_j}{\partial z} \right) - 2 \psi_i \left( \frac{\partial \bar{u}}{\partial r} \psi_j \right) \right] \right\} r dr dz \\
K_{ij}^{35} &= 2 \int_{\Omega^e} \lambda \frac{\partial u}{\partial z} \psi_i \psi_j r dr dz, & K_{ij}^{42} &= -2 \int_{\Omega^e} \eta_2 \psi_i \frac{\partial \psi_j}{\partial z} r dr dz \\
K_{ij}^{44} &= \int_{\Omega^e} \left\{ \psi_i \psi_j + \lambda \left[ \psi_i \left( \bar{u} \frac{\partial \psi_j}{\partial r} + \bar{w} \frac{\partial \psi_j}{\partial z} \right) - 2 \frac{\partial \bar{w}}{\partial z} \psi_i \psi_j \right] \right\} r dr dz \\
K_{ij}^{45} &= -2 \int_{\Omega^e} \lambda \frac{\partial \bar{w}}{\partial r} \psi_i \psi_j r dr dz, & K_{ij}^{51} &= -2 \int_{\Omega^e} \eta_1 \psi_i \frac{\partial \psi_j}{\partial z} r dr dz \\
K_{ij}^{52} &= -2 \int_{\Omega^e} \eta_1 \psi_i \frac{\partial \psi_j}{\partial r} r dr dz, & K_{ij}^{53} &= -2 \int_{\Omega^e} \lambda \frac{\partial \bar{w}}{\partial r} \psi_i \psi_j r dr dz \\
K_{ij}^{54} &= -2 \int_{\Omega^e} \lambda \frac{\partial \bar{u}}{\partial z} \psi_i \psi_j r dr dz, & K_{ij}^{61} &= -2 \int_{\Omega^e} \eta_1 \psi_i \frac{\psi_j}{r} r dr dz \\
K_{ij}^{55} &= \int_{\Omega^e} 2 \left\{ \psi_i \psi_j + \lambda \left( \bar{u} \frac{\psi_j}{\partial r} + \bar{w} \frac{\partial \psi_j}{\partial z} \right) - \left( \frac{\partial \bar{u}}{\partial r} + \frac{\partial \bar{w}}{\partial z} \right) \psi_i \psi_j \right\} r dr dz \\
K_{ij}^{66} &= \int_{\Omega^e} \left\{ \psi_i \psi_j + \lambda \left[ \psi_i \left( \bar{u} \frac{\partial \psi_j}{\partial r} + \bar{w} \frac{\partial \psi_j}{\partial z} \right) - 2 \frac{\bar{u}}{r} \psi_i \psi_j \right] \right\} r dr dz \\
M_{ij}^{11} &= \int_{\Omega^e} \rho \psi_i \psi_j r dr dz, & M_{ij}^{22} &= \int_{\Omega^e} \rho \psi_i \psi_j r dr dz \\
M_{ij}^{33} &= \int_{\Omega^e} \lambda \psi_i \psi_j r dr dz, & M_{ij}^{44} &= \int_{\Omega^e} \lambda \psi_i \psi_j r dr dz \\
M_{ij}^{55} &= \int_{\Omega^e} \lambda \psi_i \psi_j r dr dz, & M_{ij}^{66} &= \int_{\Omega^e} \lambda \psi_i \psi_j r dr dz
\end{aligned} \tag{10.4.40}$$

Bar over  $u$  and  $w$  indicate that they are to be calculated using values from the previous iteration.

For viscoelastic fluids, specification of velocities is insufficient on account of fluid memory. If the boundary of the domain contains an entry region, then fully developed flow conditions may be assumed. All extra stress components must be specified as essential boundary conditions along the entry region. Failing to do so may lead to the propagation of errors throughout the flow domain when relaxation time  $\lambda$  becomes large.

### 10.4.5 Numerical Examples

Consider the steady flow of a power-law fluid in a uniform pipe ( $R = 1$ ,  $L = 6$ ,  $w_0 = 10$ ,  $n = 0.2$ ,  $\mu_0 = 1.0$ , and  $\gamma_p = 10^8$ ). The geometry and boundary conditions of the computational domain are shown in Figure 10.4.1. Three different meshes shown in Figure 10.4.2 are used. The finite element results obtained using the velocity finite element model in Eq. (10.4.22) along with

the analytical results for the axial velocities as a function of the radial distance are presented in Table 10.4.1.

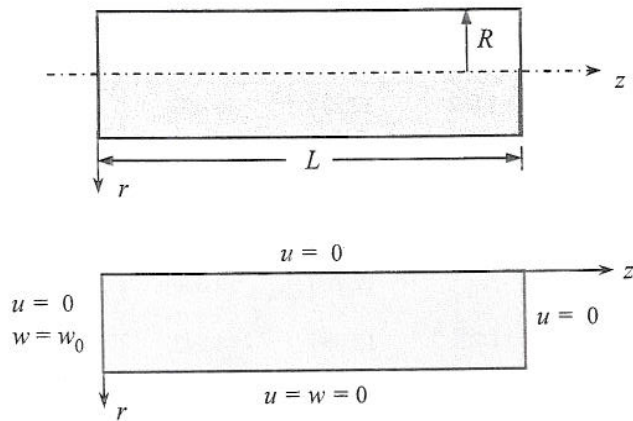


Figure 10.4.1 Geometry and boundary conditions for flow through a pipe.

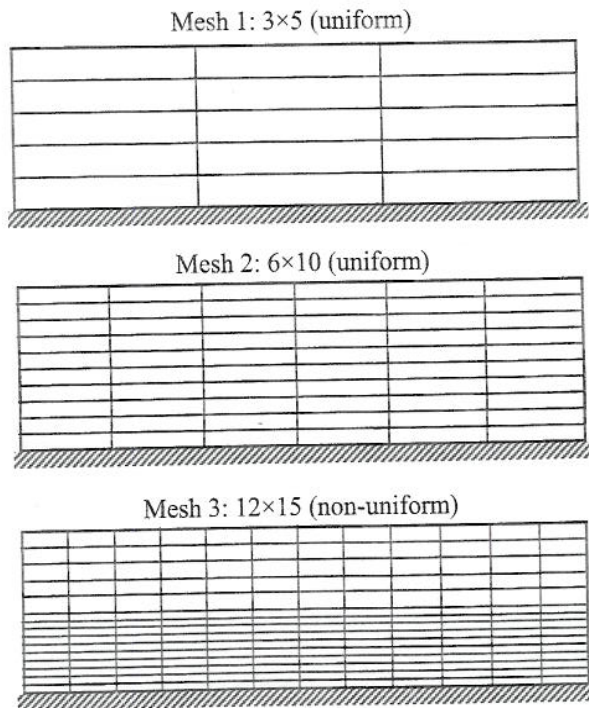


Figure 10.4.2 Three different meshes used for the pipe flow.

**Table 10.4.1** A comparison of the velocity field  $w(r, 6)$  for the flow of a power-law fluid in a pipe ( $R = 1$ ,  $L = 6$ ,  $w_0 = 10$ ,  $n = 0.2$ ,  $\mu_0 = 1.0$ , and  $\gamma_p = 10^8$ ).

$r$	Velocity, $w(r, 6)$			
	Mesh 1	Mesh2	Mesh 3	Analytical*
0.00	11.894	12.833	13.402	13.333
0.05	—	—	—	13.333
0.10	—	12.832	13.401	13.333
0.15	—	—	—	13.333
0.20	11.865	12.826	13.395	13.332
0.25	—	—	—	13.330
0.30	—	12.795	13.360	13.324
0.35	—	—	—	13.309
0.40	11.721	12.686	13.243	13.279
0.45	—	—	—	13.223
0.50	—	12.401	12.940	13.125
0.55	—	—	12.679	12.964
0.60	10.852	11.783	12.305	12.711
0.65	—	—	11.787	12.328
0.70	—	10.610	11.086	11.765
0.75	—	—	10.156	10.960
0.80	7.916	8.563	8.946	9.838
0.85	—	—	7.396	8.305
0.90	—	5.133	5.451	6.248
0.95	—	—	2.993	3.532
1.00	0.000	0.000	0.000	0.000

$$* w(r, 6) = w_0 \left( \frac{3n+1}{n+1} \right) \left[ 1 - \left( \frac{r}{R} \right)^{1+\frac{1}{n}} \right].$$

Next, the same problem (with  $R = 1$  and  $L = 5$ ) is studied with the mixed finite element model in Eq. (10.4.38). Both power-law ( $n = 0.25$ ,  $\eta_0 = 10^4$ ,  $\eta_2 = 0$ ) and White-Metzner ( $n = 0.25$ ,  $\eta_0 = 10^4$ ,  $\eta_2 = 0$ ,  $a = 0.435$ ,  $b = -0.453$ ,  $c = 0.1388$ ) fluids are analyzed. A uniform mesh of  $10 \times 6$  bilinear elements is used. In addition to the velocity boundary conditions shown in Figure 10.4.1, the stresses are specified to be zero at the entrance. The penalty parameter is taken to be  $\gamma_p = 10^8 \eta_0$ .

Figures 10.4.3 and 10.4.4 contain plots of the axial velocity profiles at  $z = 2.0$  and  $z = 5.0$ , respectively. We note that the velocity profiles obtained with the velocity model (VM) in Eq. (10.4.22) and mixed model (MM) in Eq. (10.4.38) are essentially the same when stress boundary conditions are not imposed. The stress boundary conditions (which can be imposed point-wise only in the mixed model) do have an effect: specification of the stresses at the inlet increases the centerline velocity for both power-law fluids as well as

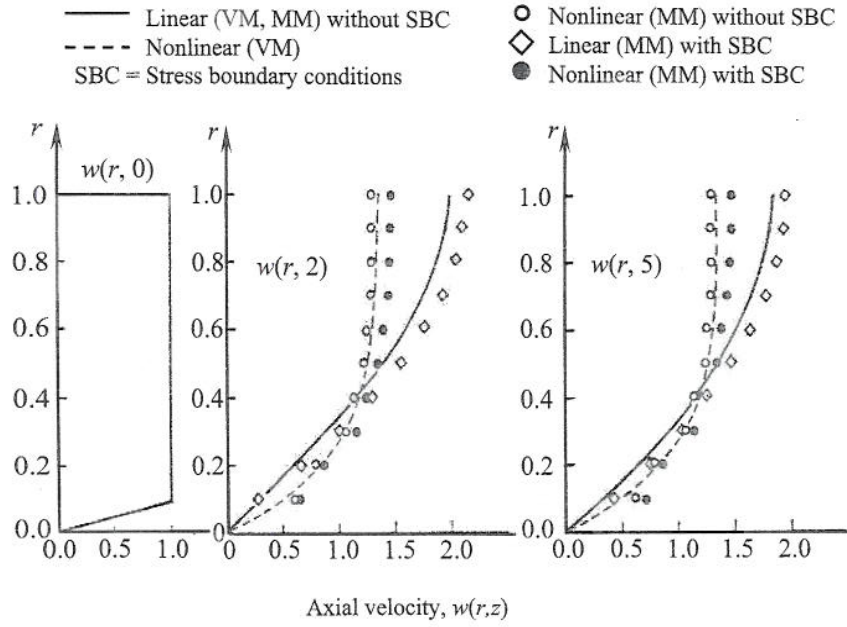


Figure 10.4.3 Axial velocity profiles for the flow of power-law fluid through a pipe.

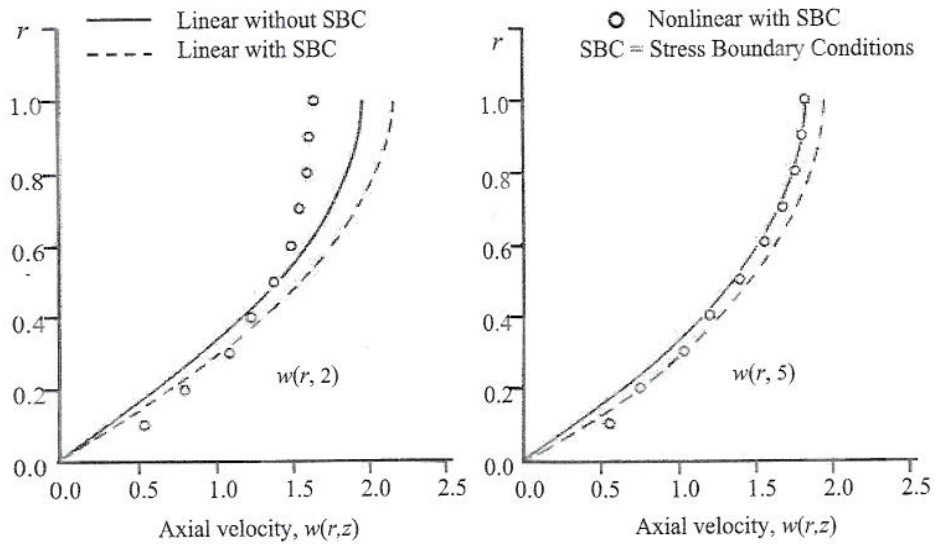


Figure 10.4.4 Axial velocity profiles for the flow of White-Metzner fluid through a pipe.

White-Metzner fluids. If the stress boundary conditions are not imposed, the mixed model for the White-Metzner fluid does not yield converged solution. Figure 10.4.5 shows the effect of the penalty parameter on the velocity field. The results are self-explanatory.

**Table 10.4.2** Effect of the convective terms on the velocity field for the flow of a power-law fluid in a pipe ( $R = 1, L = 5, w_0 = 10, n = 0.2,$  and  $10 \times 6Q4$  mesh).

$r$	Velocity, $w(r, 5)$			
	Newtonian	Non-Newtonian		
		$Re = 0$	$Re = 10^2$	$Re = 10^3$
0.0	1.8358	1.3357	1.1312	1.0267
0.1	1.8001	1.3355	1.1302	1.0265
0.2	1.7398	1.3338	1.1289	1.0266
0.3	1.6461	1.3271	1.1270	1.0268
0.4	1.5186	1.3081	1.1241	1.0271
0.5	1.3578	1.2657	1.1197	1.0275
0.6	1.1651	1.1849	1.1097	1.0274
0.7	0.9397	1.0468	1.0799	1.0265
0.8	0.6712	0.8273	0.9809	1.0209
0.9	0.3079	0.4795	0.6709	0.8967
1.0	0.0000	0.0000	0.0000	0.0000

\*  $Re = \frac{\rho w_0 R}{\eta_0}$ .

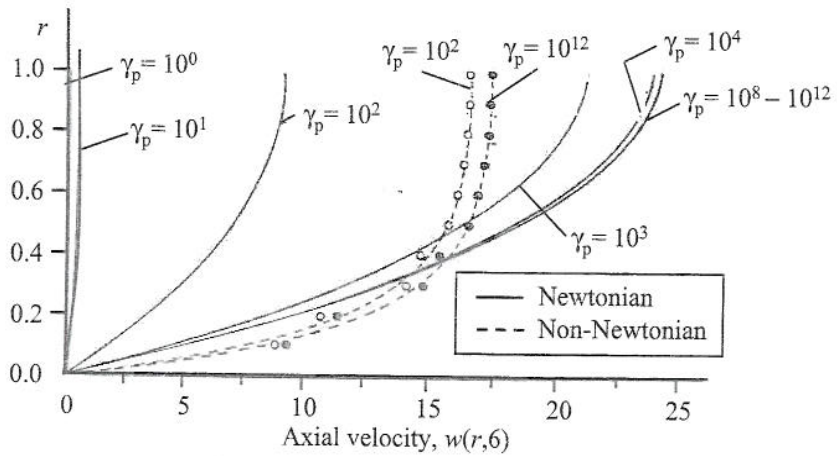


**Figure 10.4.5** The effect of the penalty parameter on the flow of a power-law fluid.



The effect of the convective terms on the velocity field is also investigated for the power-law fluid ( $n = 0.25$ ,  $\eta_0 = 10^4$ ,  $\eta_2 = 0$ ,  $R = 1$ ,  $L = 5$ , and  $w_0 = 1$ ) using the velocity model in Eq. (10.4.22). The results are presented in Table 10.4.2. The effect is to flatten the velocity profile from a parabolic one. Figure 10.4.6 shows the axial velocity profile for flow through a plane channel ( $a = 6$ ,  $b = 1$ ,  $n = 0.2$ ,  $\eta_0 = \eta_1 = 1$ ). The results are in good agreement with those in [9].

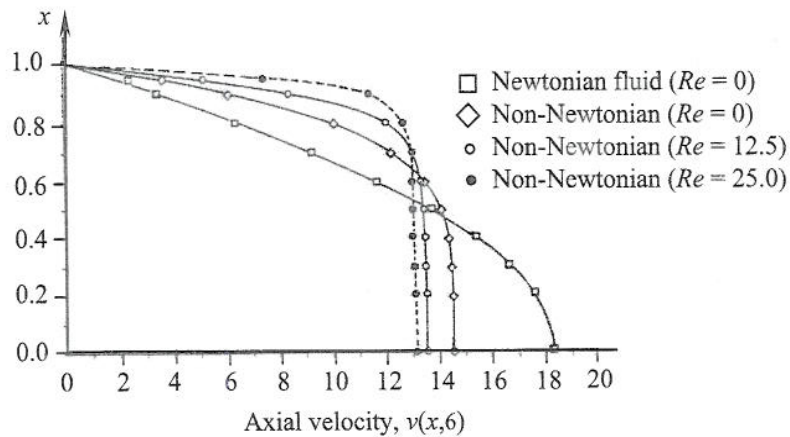


Figure 10.4.6 Axial velocity profiles for flow of power-law fluid through a plane channel.

## 10.5 Coupled Fluid Flow and Heat Transfer

### 10.5.1 Finite Element Models

There exist many engineering systems where the fluid flow is affected by the heat transfer to or from the system and vice versa. Convective cooling of a heated body (like in an internal combustion engine) is a generic example of the coupling. In such cases, we solve the governing equations of fluid flow (i.e. the Navier–Stokes equations and continuity equation) as well as the heat transfer (i.e. the energy equation), as discussed in Section 7.3. The energy equation is given by [see Eq. (7.3.3)]

$$\rho C \left[ \left( u \frac{\partial T}{\partial x} + v \frac{\partial T}{\partial y} \right) + \frac{\partial T}{\partial t} \right] = \frac{\partial}{\partial x} \left( k_{11} \frac{\partial T}{\partial x} \right) + \frac{\partial}{\partial y} \left( k_{22} \frac{\partial T}{\partial y} \right) + \Phi + q \quad (10.5.1)$$

where  $C$  is specific heat,  $\Phi$  is the dissipation energy

$$\Phi = \sigma_{ij} \varepsilon_{ij} \quad (10.5.2)$$

and  $q$  is internal heat generation.

The finite element model of the energy equation is given by

$$[C^e]\{\dot{T}^e\} + [H^e]\{T^e\} = \{Q^e\} \quad (10.5.3)$$

where

$$\begin{aligned} H_{ij}^e &= \rho C \int_{\Omega^e} \psi_i^{(2)} \left( u \frac{\partial \psi_j^{(2)}}{\partial x} + v \frac{\partial \psi_j^{(2)}}{\partial y} \right) dx dy \\ &\quad + \int_{\Omega^e} \left( k_{11} \frac{\partial \psi_i^{(2)}}{\partial x} \frac{\partial \psi_j^{(2)}}{\partial x} + k_{22} \frac{\partial \psi_i^{(2)}}{\partial y} \frac{\partial \psi_j^{(2)}}{\partial y} \right) dx dy \\ C_{ij}^e &= \rho C \int_{\Omega^e} \psi_i^{(2)} \psi_j^{(2)} dx dy \\ Q_i^e &= \int_{\Omega^e} \psi_i^{(2)} (q + \Phi) dx dy + \oint_{\Gamma^e} q_n \psi_i^{(2)} ds \end{aligned} \quad (10.5.4)$$

$u$  and  $v$  being the velocity components (that couple to the fluid flow problem), and  $\psi_i^{(2)}$  the Lagrange interpolation functions used to interpolate the temperature field.

Equation (10.5.3) must be solved along with the flow equations

$$[M^e]\{\dot{\Delta}^e\} + [K^e]\{\Delta^e\} = \{F^e\} \quad (10.5.5)$$

developed earlier (see Chapters 7 and 8). Both equations, Eqs. (10.5.3) and (10.5.5), must be solved iteratively, using the latest velocity field and temperature field to compute the coefficient matrices. It should be noted that fluid flow equations are coupled to the heat transfer equation through the body force terms  $f_x$  and  $f_y$  in the Navier–Stokes equations. For buoyancy-driven flows, the body force in the direction of the gravity is a function of the temperature, that is,  $f_y = -\rho g \beta (T - T_0)$  if the  $y$ -axis is taken vertically up. Thus, the momentum equations are fully coupled with the energy equation.

The following strategy is found suitable for the convective heat transfer problems. Solve the energy equation (10.5.3) with an assumed velocity field (say, zero). Then use the assumed velocity and temperature fields in (10.5.5) and solve for the new velocity field. The initial guess of the velocity field can be either the linear (Stokes) solution (or the solution of a problem at lower Rayleigh number when solving for high Rayleigh number flows). The Rayleigh number  $Ra$  and Prandtl number  $Pr$  (characteristic numbers used in convective heat transfer) are defined by

$$Ra = \frac{\beta g L^3 \Delta T}{\kappa \nu}, \quad \nu = \frac{\mu}{\rho}, \quad \kappa = \frac{k}{\rho c_p}, \quad Pr = \frac{\nu}{\kappa}$$

where  $g$  is acceleration due to gravity,  $\beta$  is thermal expansion coefficient,  $L$  the characteristic dimension of the flow region,  $\Delta T$  the temperature difference between hot and cold walls,  $\rho$  the density,  $\mu$  the viscosity,  $k$  the conductivity, and  $c_p$  is the specific heat at constant pressure.

### 10.5.2 Numerical Examples

Here we include couple of sample problems, taken from Reddy and Gartling [15], to illustrate the ideas presented above.

#### *Heated cavity*

Consider a closed square cavity filled with a viscous incompressible fluid. The top and bottom faces of the cavity are assumed to be insulated while the vertical faces subjected to different temperatures, as shown in Figure 10.5.1(a). A typical  $16 \times 16$  mesh of eight-node quadratic elements is shown in Figure 10.5.1(b).

This problem was solved using the earliest versions of NACHOS code [24], which is based on velocity–pressure (mixed) formulation and used the direct iteration (Picard) scheme. More recent solutions have been obtained using Newton's method for the combined equation set equivalent to (10.5.3) and (10.5.5). The streamline and isotherm plots are shown in Figures 10.5.2 and 10.5.3 for Rayleigh numbers of  $Ra = 10^4$  and  $10^6$ , respectively ( $Pr = \nu/\kappa = 0.71$ ). For the lower Rayleigh number, the flow is relatively weak and the thermal field is only slightly perturbed from a conduction solution. At the higher Rayleigh number, the flow field develops a considerable structure while the thermal field becomes vertically stratified in the core of the cavity with high heat flux regions along the vertical boundaries [24].

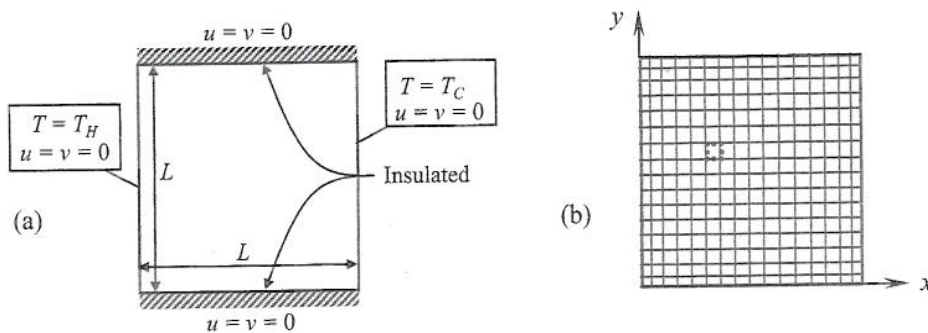


**Figure 10.5.1** (a) Geometry of a heated square cavity. (b) A typical finite element mesh.

*Solar receiver*

Figure 10.5.4 shows a cross section of an annular solar receiver tube surrounded by an eccentrically located glass envelope. The inner tube carries a heat transfer fluid that is heated by a flux that varies with position around the tube. The incident flux is due to solar energy being concentrated on the tube by a parabolic trough collector. The glass envelope provides a shield to reduce the forced convection (wind) heat loss from the collector tube [15, 24].

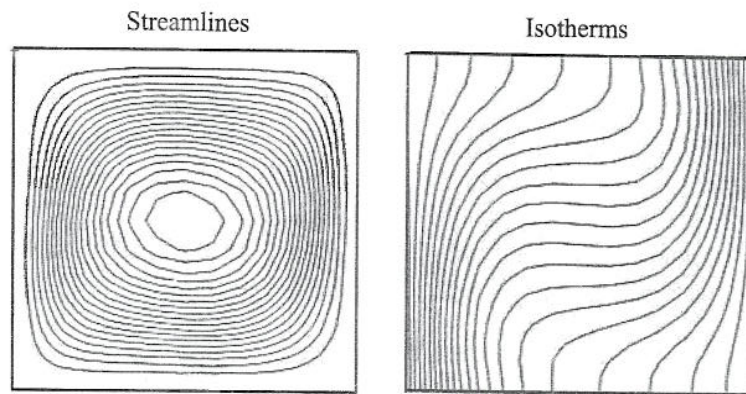


**Figure 10.5.2** Streamlines and isotherms for natural convection in a square cavity filled with viscous fluid ( $Ra = 10^4$ ,  $Pr = 0.71$ ).

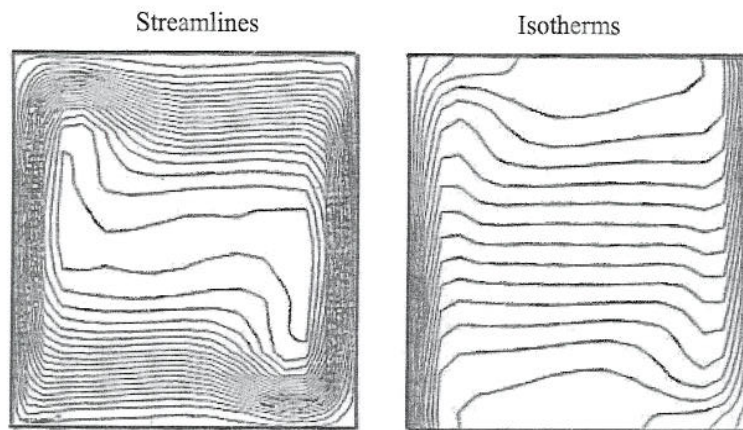


**Figure 10.5.3** Streamlines and isotherms for natural convection in a square cavity filled with viscous fluid ( $Ra = 10^6$ ,  $Pr = 0.71$ ).

Figures 10.5.5–10.5.7 contain streamline and isotherm plots for an air-filled annulus for various temperature and geometric configurations. The flow pattern and heat flux distribution are quite sensitive to variations in these parameters even though the Rayleigh number is the same for all cases [15, 24].

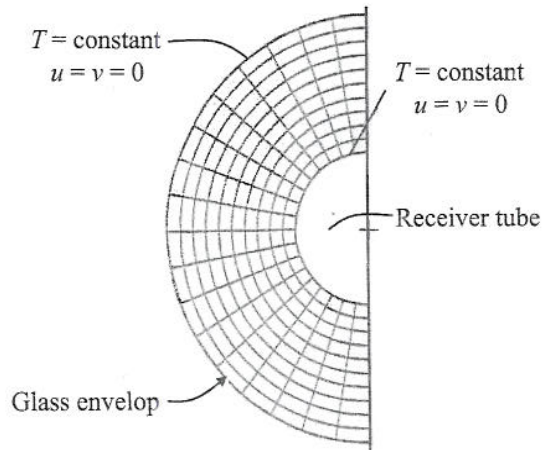


Figure 10.5.4 Mesh and boundary conditions for the annular solar receiver.

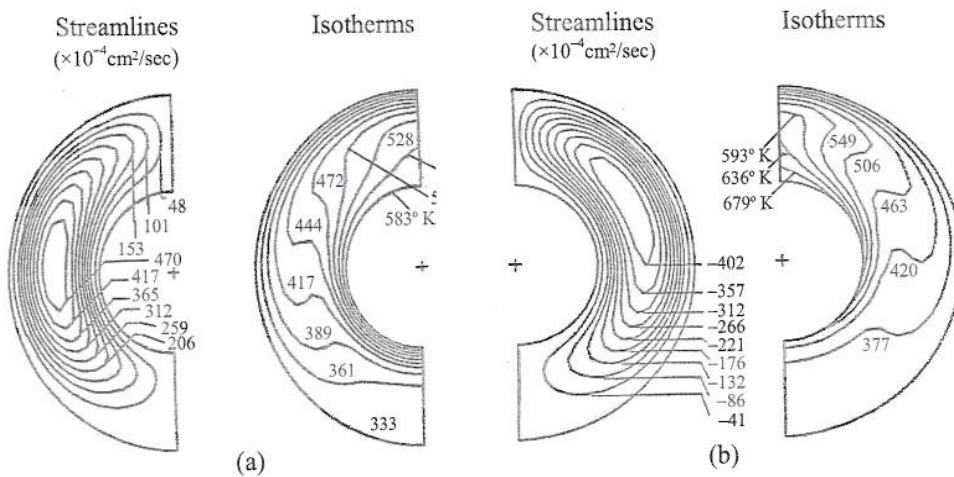


Figure 10.5.5 Plots of streamlines and isotherms for the solar receiver. (a) uniform wall temperature,  $Ra = 1.2 \times 10^4$ . (b) asymmetric wall temperature, hot on top ( $Ra = 1.2 \times 10^4$ ).

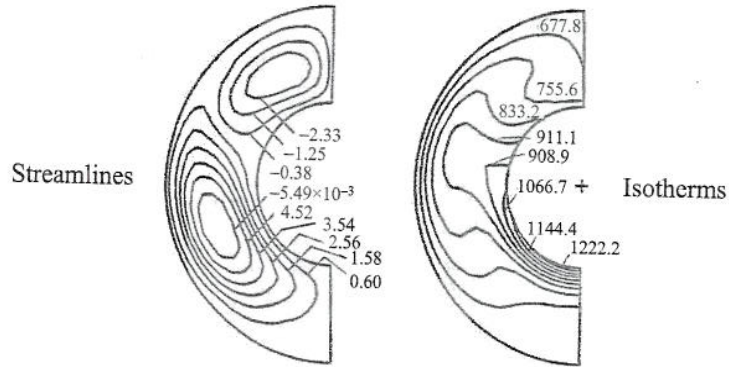


Figure 10.5.6 Plots of streamlines and isotherms for the solar receiver; uniform wall temperature, *hot on bottom* ( $Ra = 1.2 \times 10^4$ ).

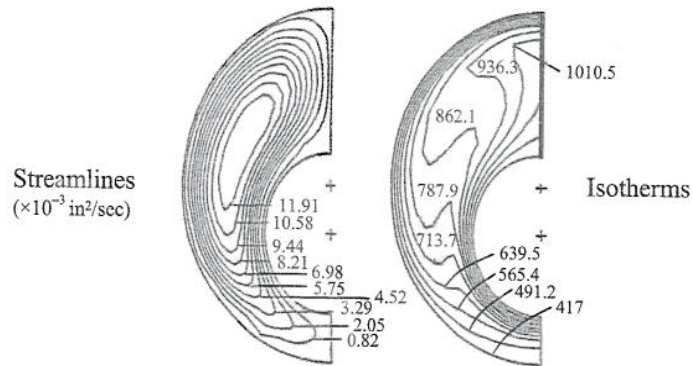


Figure 10.5.7 Plots of streamlines and isotherms for the solar receiver; uniform wall temperature, *eccentric geometry* ( $Ra = 1.2 \times 10^4$ ).

Additional details on the formulation as well as applications of coupled heat transfer and fluid flow can be found in [17-24] (in particular, see [23,24] and Chapter 5 of the book by Reddy and Gartling [15] and reference therein).

## References

1. Hill, R., *The Mathematical Theory of Plasticity*, Oxford University Press, Oxford, U.K., 1950.
2. Johnson, W. and Mellor, P. B., *Engineering Plasticity*, John Wiley, New York (1983).
3. Owen, D. R. J. and Hinton, E., *Finite Elements in Plasticity: Theory and Practice*, Pineridge Press, UK (1980) (see pp. 26-29 for one-dimensional bar problems; pp. 129-148 for one-dimensional Timoshenko beams; pp. 215-281 for two-dimensional problems).
4. Zienkiewicz, O. C. and Taylor, R. L., *The Finite Element Method*, 4th edn, Vol. 2: *Solid and Fluid Mechanics, Dynamics and Non-Linearity*, McGraw-Hill, London, UK (1989) (see Chapter 7).
5. Reddy, J. N. and Rasmussen, M. L., *Advanced Engineering Analysis*, John Wiley, New York (1982); reprinted by Krieger Publishing, Melbourne, FL (1991).
6. Phan Thien, N. and Tanner, R. I., "A New Constitutive Equation Derived From Network Theory," *Journal of Non-Newtonian Fluid Mechanics*, **2**, 353-365 (1977).
7. White, J. L. and Metzner, A. B., "Development of Constitutive Equations for Polymeric Melts and Solutions," *Journal of Applied Polymer Science*, **7**, 1867-1889 (1963).
8. Crochet, M. J. and Walters, K., "Numerical Methods in Non-Newtonian Fluid Mechanics," *Annual Review of Fluid Mechanics*, **15**, 241-260 (1983).
9. Crochet, M. J., Davies, A. R., and Walters, K., *Numerical Simulation of Non-Newtonian Flow*, Elsevier, Amsterdam, The Netherlands (1984).
10. Gartling, D. K. and Phan Thien, N., "A Numerical Simulation of a Plastic Fluid in a Parallel-Plate Plastometer," *Journal of Non-Newtonian Fluid Mechanics*, **14**, 347-360 (1984).
11. Reddy, J. N. and Padhye, V. A., "A Penalty Finite Element Model for Axisymmetric Flows of Non-Newtonian Fluids," *Numerical Methods for Partial Differential Equations*, **4**, 33-56 (1988).
12. Iga, M. and Reddy, J. N., "Penalty Finite Element Analysis of Free Surface Flows of Power-Law Fluids," *International Journal of Non-Linear Mechanics*, **24**(5), 383-399 (1989).
13. Reddy, M. P. and Reddy, J. N., "Finite Element Analysis of Flows of Non-Newtonian Fluids in Three-Dimensional Enclosures," *International Journal of Non-Linear Mechanics*, **27**(1), 9-26 (1992).
14. Reddy, M. P. and Reddy, J. N., "Numerical Simulation of Forming Processes Using a Coupled Fluid Flow and Heat Transfer Model," *International Journal for Numerical Methods in Engineering*, **35**, 807-833 (1992).
15. Reddy, J. N. and Gartling, D. K., *The Finite Element Method in Heat Transfer and Fluid Dynamics*, Second Edition, CRC Press, Boca Raton, FL (2001).
16. Coleman, C. J., "A Finite Element Routine for Analyzing Non-Newtonian Fluids, Part 1," *Journal of Non-Newtonian Fluid Mechanics*, **7**, 289-301 (1980).
17. Gartling, D. K., "Convective Heat Transfer Analysis by the Finite Element Method," *Computer Methods in Applied Mechanics and Engineering*, **12**, 365-382 (1977).
18. Marshall, R. S., Heinrich, J. C., and Zienkiewicz, O. C., "Natural Convection in a Square Enclosure by a Finite Element, Penalty Function Method, Using Primitive Fluid Variables," *Numerical Heat Transfer*, **1**, 315-330 (1978).
19. Reddy, J. N. and Satake, A., "A Comparison of Various Finite Element Models of Natural Convection in Enclosures," *Journal of Heat Transfer*, **102**, 659-666 (1980).

20. Reddy, J. N., "Penalty-Finite-Element Analysis of 3-D Navier-Stokes Equations," *Computer Methods in Applied Mechanics and Engineering*, **35**, 87-106 (1982).
21. de Vahl Davis, G. and Jones, I. P., "Natural Convection in a Square Cavity: A Comparison Exercise," *International Journal for Numerical Methods in Fluids*, **3**, 227-248 (1983).
22. Dhaubhadel, M., Telionis, D., and Reddy, J. N., "Finite Element Analysis of Fluid Flow and Heat Transfer for Staggered Bundle of Cylinders in Cross Flow," *International Journal for Numerical Methods in Fluids*, **7**, 1325-1342 (1987).
23. Pelletier, D. H., Reddy, J. N., and Schetz, J. A., "Some Recent Developments and Trends in Finite Element Computational Natural Convection," in *Annual Review of Numerical Fluid Mechanics and Heat Transfer*, Vol. 2, C. L. Tien and T. C. Chawla (eds.), Hemisphere, New York, 39-85 (1989).
24. Gartling, D. K., "Convective Heat Transfer Analysis by the Finite Element Method," *Computer Methods in Applied Mechanics and Engineering*, **12**, 365-382 (1977).



---

## Appendix A1

# Solution Procedures for Linear Algebraic Equations

---

### A1.1 Introduction

All finite element equations, after assembly and imposition of boundary (and initial) conditions, can be expressed as a set of linear algebraic equations that must be solved. In general, the finite element equations are of the form

$$[A]\{X\} = \{B\} \quad (\text{A1.1.1})$$

where  $[A]$  is the coefficient matrix resulting from the assembly of element matrices,  $\{X\}$  column of unknowns (typically nodal values), and  $\{B\}$  is the known column vector. In the finite element method,  $[A]$  is a banded sparse matrix that may be either symmetric or unsymmetric depending on the characteristics of the governing differential equation(s) describing the physical problem, and possibly the nonlinear solution method used (see Appendix A2).

A banded matrix is one in which all elements beyond a diagonal parallel to the main diagonal are zero. The maximum number of non-zero diagonals above or below the main diagonal plus 1 (to account for the main diagonal) is called *half bandwidth* (NHBW) of the matrix [see Figure A1.1.1(a)]. When the matrix is symmetric, it is sufficient to store elements in upper or lower half bandwidth of the matrix  $[A]$  [see Figure A1.1.1(b)] and write solvers to take note of the fact  $a_{ij} = a_{ji}$  for all rows  $i$  and columns  $j$  of the matrix. When the matrix is not symmetric, one must store all elements in the full bandwidth ( $2*\text{NHBW}-1$ ) of the matrix. Here we include the Fortran subroutines of a symmetric banded equation solver (SYMSOLVR) and unsymmetric banded equation solver (UNSYMSLV).

A linear set of algebraic equations can be solved by either a direct or iterative method. Direct methods, like the Gauss elimination method, provide the solution after a fixed number of steps and are less sensitive to the



The limitations on CPU time and storage requirements preclude the use of direct solvers for complex problems with more than a quarter million equations, and iterative methods are found to be more efficient in that they require less storage and CPU time. Iterative methods are approximate and only converged solutions will be close to the true solution. In iterative methods, the global matrix formation may be avoided. The major operation in iterative methods is the matrix-vector multiplication as compared to the matrix reduction (by elementary operations) in direct methods. A significant advantage of iterative methods is that a given set of equations can be divided into as many subsets of equations as there are processors and calculations can be performed in parallel on the array of processors. However, convergence characteristics of iterative methods depend on the condition number of the system of linear equations, and a suitable preconditioner is a must to achieve convergence.

Following this introduction, a brief review of some methods for the solution of linear algebraic equations is presented. For additional details, the reader may consult [2-4].

## A1.2 Direct Methods

### A1.2.1 Preliminary Comments

*Direct methods* are those in which simultaneous linear algebraic equations are solved "exactly" (within the computational round-off error) by successive elimination of variables and back substitution. The Gauss elimination method is a fixed-step technique [2-8], and frontal [5] and skyline [6] solution methods are examples of direct solution methods that use the Gauss elimination technique efficiently. The direct methods are the most commonly used techniques when the number of equations involved is not too large. The number of elementary operations for Gauss elimination is of the order  $n^3/3 + O(n^2)$ , where  $n$  denotes the number of unknowns.

The *frontal* solution procedure [5] is faster than most direct solvers; it requires less core space as long as active variables can be kept in the core, and it allows for partial pivoting. An additional advantage is that no specific node numbering scheme is needed, though a judicious element numbering helps to minimize the front width.

Due to the fact that the approximation functions are defined only within an element, the coefficient matrix in the finite element method is banded; that is,  $a_{ij} = 0$  for  $j > i + n_b$ , where  $n_b$  is the half bandwidth of the matrix  $[A]$ . This greatly reduces the number of operations in solving the equations, if we make note of the fact that elements outside the bandwidth are zero. Of course, the bandwidth size depends on the global node numbering. The skyline technique is one in which bandedness of the finite element equations is exploited by storing the row number  $m_j$  of the first nonzero element in column  $j$ . The

variables  $m_i, i = 1, 2, \dots, n$ , define the skyline of the matrix. For additional details see Bathe [6].

Here, we include the Fortran subroutines of a symmetric banded equation solver (SYMSOLVR) and unsymmetric banded equation solver (UNSYMSLV) that are used in most of the calculations presented in this book [7].

### A1.2.2 Symmetric Solver

In the case of symmetric solver the global coefficient matrix  $[A] \equiv [GLK]$  is stored in symmetric banded form ( $NEQ \times NHBW$ ), where  $NEQ$  is the number of global equations and  $NHBW$  is the half bandwidth. Fortran statements for the assembly of element coefficient matrices  $[ELK]$  and element source vector  $\{ELF\}$  for the symmetric case are included in Box A1.2.1. Note that the global source vector is stored in array  $\{GLF\}$ . After Gauss elimination is completed in SYMSOLVR (see Box A1.2.2), the solution is returned in array  $\{GF\}$ .

**Box A1.2.1** Fortran statements for the calculation of the half bandwidth and assembly of element coefficient matrices.

```

DO 140 N=1,NEM
  DO 110 I=1,NPE
    NI=NOD(N,I)
    ELU(I)=GAMA*GP2(NI)+(1.0-GAMA)*GP1(NI)
110  ELX(I)=GLX(NI)
    CALL ELEKMF(IEL,NPE,NONLIN,F0)
    DO 130 I=1,NPE
      NR=(NOD(N,I)-1)*NDF
      DO 130 II=1,NDF
        NR=NR+1
        L=(I-1)*NDF+II
        GLF(NR)=GLF(NR)+ELF(L)
      DO 120 J=1,NPE
        NCL=(NOD(N,J)-1)*NDF
        DO 120 JJ=1,NDF
          M=(J-1)*NDF+JJ
          NC=NCL-NR+JJ+1
          IF(NC.GT.0)THEN
            GLK(NR,NC)=GLK(NR,NC)+ELK(L,M)
          ENDIF
        CONTINUE
      CONTINUE
    CONTINUE
  CONTINUE

```

GAMA = Acceleration parameter,  $\rho$   
 [see Eq. (3.4.5)]  
 GP2 = Solution from the  $(r - 2)$  iteration  
 GP1 = Solution from  $(r - 1)$  iteration

**Box A1.2.2** Subroutine for solution of banded *symmetric* equations.

```

SUBROUTINE SYMSOLVR(NRM,NCM,NEQNS,NBW,BAND,RHS,IRES)
C
C The subroutine solves a banded, symmetric, system of algebraic equations [BAND]{U} = {RHS}
C using the Gauss elimination method: The coefficient matrix is input as BAND(NEQNS,NBW) and
C the column vector is input as RHS(NEQNS), where NEQNS is the actual number of equations and
C NBW is the half band width. The true dimensions of the matrix [BAND] in the calling program, are
C NRM by NCM. When IRES is greater than zero, the right hand elimination is skipped.
C
IMPLICIT REAL*8(A-H,O-Z)
DIMENSION BAND(NRM,NCM),RHS(NRM)
MEQNS=NEQNS-1
IF(IRES.LE.0) THEN
  DO 30 NPIV=1,MEQNS
    NPIVOT=NPIV+1
    LSTSUB=NPIV+NBW-1
    IF(LSTSUB.GT.NEQNS) THEN
      LSTSUB=NEQNS
    ENDIF
    DO 20 NROW=NPIVOT,LSTSUB
      NCOL=NROW-NPIV+1
      FACTOR=BAND(NPIV,NCOL)/BAND(NPIV,1)
      DO 10 NCOL=NROW,LSTSUB
        ICOL=NCOL-NROW+1
        JCOL=NCOL-NPIV+1
10    BAND(NROW,ICOL)=BAND(NROW,ICOL)-FACTOR*BAND(NPIV,JCOL)
20    RHS(NROW)=RHS(NROW)-FACTOR*RHS(NPIV)
30    CONTINUE
  ELSE
40    DO 60 NPIV=1,MEQNS
      NPIVOT=NPIV+1
      LSTSUB=NPIV+NBW-1
      IF(LSTSUB.GT.NEQNS) THEN
        LSTSUB=NEQNS
      ENDIF
      DO 50 NROW=NPIVOT,LSTSUB
        NCOL=NROW-NPIV+1
        FACTOR=BAND(NPIV,NCOL)/BAND(NPIV,1)
50    RHS(NROW)=RHS(NROW)-FACTOR*RHS(NPIV)
60    CONTINUE
  ENDIF
C
C Back substitution
C
  DO 90 IJK=2,NEQNS
    NPIV=NEQNS-IJK+2
    RHS(NPIV)=RHS(NPIV)/BAND(NPIV,1)
    LSTSUB=NPIV-NBW+1
    IF(LSTSUB.LT.1) THEN
      LSTSUB=1
      Continued in the inset
    ENDIF
  ENDIF
  NPIVOT=NPIV-1
  DO 80 JKI=LSTSUB,NPIVOT
    NROW=NPIVOT-JKI+LSTSUB
    NCOL=NPIV-NROW+1
    FACTOR=BAND(NROW,NCOL)
80    RHS(NROW)=RHS(NROW)-
      FACTOR*RHS(NPIV)
90    CONTINUE
    RHS(1)=RHS(1)/BAND(1,1)
  RETURN
  END

```

### A1.2.3 Unsymmetric Solver

In the case of unsymmetric solver the matrix  $[GLK]$  is stored in full bandwidth form ( $NEQ \times NBW$ ), where  $NEQ$  is the number of global equations and  $NBW = 2 * NHBW$  is twice the half bandwidth. Since there is an additional column in  $NBW$ , we use it to store the global source vector; that is,  $GLF(I) \rightarrow GLK(I, NBW)$ . Fortran statements for the assembly of element matrices for the unsymmetric case are included in Box A1.2.3. After Gauss elimination is completed in UNSYMSLV (see Box A1.2.4), the solution is returned in the last column of the coefficient matrix  $\{GLK(I, NBW)\}$ .

**Box A1.2.3** Fortran statements for assembly of the element matrices and source vector into a banded *unsymmetric* global matrix.

```

DO 140 N=1,NEM
  DO 110 I=1,NPE
    NI=NOD(N,I)
    ELU(I)=GAMA*GP2(NI)+(1.0-GAMA)*GP1(NI)
110   ELX(I)=GLX(NI)
      CALL ELEKMF(IEL,NPE,NONLIN,F0)
      DO 130 I=1,NPE
        NR=(NOD(N,I)-1)*NDF
        DO 130 II=1,NDF
          NR=NR+1
          L=(I-1)*NDF+II
          GLK(NR,NBW)=GLK(NR,NBW)+ELF(L)
          DO 120 J=1,NPE
            NCL=(NOD(N,J)-1)*NDF
            DO 120 JJ=1,NDF
              M=(J-1)*NDF+JJ
              NC=NCL-NR+JJ+NHBW
              IF(NC.GT.0)THEN
                GLK(NR,NC)=GLK(NR,NC)+ELK(L,M)
              ENDIF
            CONTINUE
          CONTINUE
        CONTINUE
      CONTINUE
140  CONTINUE

```

## A1.3 Iterative Methods

### A1.3.1 General Comments

Among the various iterative methods that are available in the literature, the Conjugate Gradient (CG) method [9] is most widely used because it is a finite step method (i.e., apart from round-off errors, the solution is achieved in a fixed number of iterations) and it can be used to determine the inverse. However, the number of iterations required depends on the condition number of the coefficient matrix. The convergence of the conjugate gradient method, and iterative methods in general, can be improved by preconditioning and/or scaling the equations [10-12].



The limitations on storage can be overcome by solving the equations at the element level, that is, use the Gauss-Seidel iteration idea for the set of variables associated with the element. This approach avoids assembly of element matrices to form the global coefficient matrix. This idea of using the element-by-element data structure of the coefficient matrix was first pointed out by Fox and Stanton [13] and Fried [14-16]. The phrase *element-by-element* refers to a particular data structure for finite element techniques wherein information is stored and maintained at the element level rather than assembled into a global data structure. In this method the matrix-vector multiplications are carried out at the element level and the assembly is carried out on the resultant vector. This idea proves to be very attractive when solving large problems, because the matrix-vector multiplication can be done in parallel on a series of processors. Another advantage of this method is that the resultant savings in storage, compared to direct solvers, allows solution of large problems on small computers.

For iterative solution methods, the advantages of the element-by-element data structure over assembling the global coefficient matrix are

1. the need for formation and storage of a global matrix is eliminated, and therefore the total storage and computational costs are low,
2. the amount of storage is independent of the node numbering and mesh topology and depends on the number and type of elements in the mesh, and
3. the element-by-element solution algorithms can be vectorized for efficient use on supercomputers.

The major disadvantage of the element-by-element data structure is the limited number of preconditioners that can be formulated from the unassembled matrices. This becomes of critical importance when the linear system is not well-conditioned as in the mixed method, incompressible flow model. A review of the literature on element-by-element algorithms can be found in [17], and the methods have been investigated by numerous investigators [18-32].

### A1.3.2 Solution Algorithms

In this section, we review three iterative solvers from [17] that are applicable to nonsymmetric, positive definite equation systems that are typical of isothermal flow algorithms. The three iterative solution schemes used here are the Biorthogonal Conjugate Gradient method (BCG) [11], the Lanczos ORTHORES [11], and the GMRES [31].

The conjugate gradient method for solving a system of equations can be interpreted as the search for the minimum of the energy  $E$  of the system. The energy of the system is a minimum when the residual vector



$\mathbf{r} = \tilde{\mathbf{F}} - \tilde{\mathbf{K}}\mathbf{U}^*$  vanishes. The algorithm for the biorthogonal conjugate gradient method (also known as two-term form of the steepest descent method, Lanczos/ORTHOMIN) for unsymmetric systems of equations [11,17] is given in Table A1.3.1, and the steps involved in the Lanczos ORTHORES solution algorithm [11,17] are given in Table A1.3.2.

The third iterative solver uses the GMRES solution algorithm. For an approximate solution of the form  $\bar{\mathbf{U}}_0 + \mathbf{z}$ , where  $\bar{\mathbf{U}}_0$  is the initial guess vector and  $\mathbf{z}$  is a member of the Krylov space  $\mathcal{K}$  of dimension  $k$ , the GMRES algorithm determines the vector  $\mathbf{z}$  such that  $\|\tilde{\mathbf{F}} - \tilde{\mathbf{K}}(\bar{\mathbf{U}}_0 + \mathbf{z})\|$  is minimized, where  $\|\cdot\|$  denotes the  $L_2$ -norm. The Krylov space is given by  $\mathcal{K} = \text{span}\{\bar{\mathbf{U}}_0, \tilde{\mathbf{K}}\bar{\mathbf{U}}_0, \tilde{\mathbf{K}}^2\bar{\mathbf{U}}_0, \dots, \tilde{\mathbf{K}}^{k-1}\bar{\mathbf{U}}_0\}$ . Therefore, when solving large systems of equations, as the value of  $k$  increases, the amount of storage required also increases. This drawback can be overcome by employing the GMRES algorithm iteratively by using a smaller value for  $k$  and restarting the algorithm after every  $k$  steps. The restart version of the GMRES algorithm [31,17] is explained in Table A1.3.3.

The presence of a penalty matrix in the global coefficient matrix of the penalty model spoils the condition number. This results in slow convergence when using iterative solvers. However, the convergence of the iterative solvers can be improved by preconditioning the system. In [17], the system of equations is transformed using diagonal scaling matrix (Jacobi/diagonal preconditioning). Accordingly,

$$\tilde{\mathbf{K}}\mathbf{U}^* = \tilde{\mathbf{F}} \text{ becomes } \bar{\mathbf{K}}\bar{\mathbf{U}} = \bar{\mathbf{F}} \quad (\text{A1.3.1})$$

$$\bar{\mathbf{K}} = \mathbf{W}^{-1/2}\tilde{\mathbf{K}}\mathbf{W}^{-1/2}; \bar{\mathbf{U}} = \mathbf{W}^{1/2}\mathbf{U}^*; \bar{\mathbf{F}} = \mathbf{W}^{-1/2}\tilde{\mathbf{F}} \quad (\text{A1.3.2})$$

where  $W_{ii} = \tilde{K}_{ii}^{-1}$  is a diagonal matrix. During the matrix multiplication, the element-by-element data structure is exploited and the multiplications are carried out at the element level and the residuals are then assembled to form the global vector. The diagonal terms are always positive because of the viscous and penalty terms.

## References

1. Carey, G. F. and Oden, J. T., *Finite Elements: Computational Aspects*, Prentice Hall, Englewood Cliffs, NJ (1984).
2. Atkinson, K. E., *An Introduction to Numerical Analysis*, John Wiley, New York (1978).
3. Carnahan, B., Luther, H. A., and Wilkes, J. O., *Applied Numerical Methods*, John Wiley, New York (1969).
4. Fadeev, D. K. and Fadeeva, V. N., *Computational Methods of Linear Algebra*, Freeman, San Francisco, CA (1963).
5. Hood, P., "Frontal Solution Program for Unsymmetric Matrices," *International Journal for Numerical Methods in Engineering*, **10**, 379-399 (1976); also see **10**, 1055 (1976) for a correction.

**Table A1.3.1** Steps involved in using biorthogonal conjugate gradient method (Lanczos/ORTHOMIN solver).

Repeat the following steps for each nonlinear iteration:

I. *Initial Calculations*

- (1) Form the element stiffness matrix  $\tilde{\mathbf{K}}^e$  and force vector  $\tilde{\mathbf{F}}^e$ .
- (2) Apply essential and/or natural boundary conditions, and modify  $\tilde{\mathbf{K}}^e$  and  $\tilde{\mathbf{F}}^e$ .
- (3) Store the element matrices in  $\bar{\mathbf{A}}$  (whose dimensions are nem, neleq, neleq)\*.
- (4) Store the inverse of the diagonal terms of the global system in  $\mathbf{W}$  ( $W_{ii} = \sum_{e=1}^{\text{nem}} \tilde{K}_{ii}^{-1}$ ).
- (5) Assemble the global force vector.

II. *Preconditioning*

Form the preconditioned system of equations

$$\bar{\mathbf{K}}\bar{\mathbf{U}} = \bar{\mathbf{F}}; \quad \bar{\mathbf{K}} = \mathbf{W}^{-1/2}\tilde{\mathbf{K}}\mathbf{W}^{-1/2}, \quad \bar{\mathbf{U}} = \mathbf{W}^{1/2}\mathbf{U}^*, \quad \bar{\mathbf{F}} = \mathbf{W}^{-1/2}\tilde{\mathbf{F}}$$

III. *Lanczos ORTHOMIN Algorithm*

- (1) For known initial solution vector  $\bar{\mathbf{U}}^0$ , compute:

$$\mathbf{r}^0 = \bar{\mathbf{F}} - \bar{\mathbf{K}}\bar{\mathbf{U}}^0, \quad \mathbf{P}^0 = \mathbf{r}^0, \quad \tilde{\mathbf{r}}^0 = \tilde{\mathbf{P}}^0 = \mathbf{r}^0,$$

$$\alpha_0 = 0, \quad \lambda_0 = \frac{(\mathbf{r}^0, \tilde{\mathbf{r}}^0)}{(\bar{\mathbf{K}}\mathbf{P}^0, \tilde{\mathbf{r}}^0)}, \quad \bar{\mathbf{U}}^1 = \bar{\mathbf{U}}^0 + \lambda_0\mathbf{P}^0$$

- (2) For each ORTHOMIN iteration  $m = 1, 2, 3, \dots$ , compute  $[(a, b) = \sum a_i b_i]$ :

$$\lambda_m = \frac{(\mathbf{r}^m, \tilde{\mathbf{r}}^m)}{(\bar{\mathbf{K}}\mathbf{P}^m, \tilde{\mathbf{r}}^m)}, \quad \alpha_m = \frac{(\mathbf{r}^m, \tilde{\mathbf{r}}^m)}{(\mathbf{r}^{m-1}, \tilde{\mathbf{r}}^{m-1})},$$

$$\mathbf{P}^m = \mathbf{r}^m + \alpha_m\mathbf{P}^{m-1}, \quad \tilde{\mathbf{P}}^m = \tilde{\mathbf{r}}^m + \alpha_m\tilde{\mathbf{P}}^{m-1},$$

$$\mathbf{r}^{m+1} = \mathbf{r}^m - \lambda_m\bar{\mathbf{K}}\mathbf{P}^m, \quad \tilde{\mathbf{r}}^{m+1} = \tilde{\mathbf{r}}^m - \lambda_m\bar{\mathbf{K}}^T\tilde{\mathbf{P}}^{m-1},$$

$$\bar{\mathbf{U}}^{m+1} = \bar{\mathbf{U}}^m + \lambda_m\mathbf{P}^m$$

- (3) Convergence criterion  $\|\bar{\mathbf{U}}^{m+1}\|/\|\mathbf{r}^0\| \leq 10^{-6}$
- (4) If convergence criterion is satisfied  $\bar{\mathbf{U}}^* = \mathbf{W}^{-1/2}\bar{\mathbf{U}}^{m+1}$

\* nem = number of elements in the finite element mesh, neleq = number of element equations.

**Table A1.3.2** Steps involved in using Lanczos/ORTHORES solver.

Repeat the following steps for each nonlinear iteration:

I. *Initial Calculations*

- (1) Form the element stiffness matrix  $\tilde{\mathbf{K}}^e$  and force vector  $\tilde{\mathbf{F}}^e$ .
- (2) Apply the boundary conditions, and modify  $\tilde{\mathbf{K}}^e$  and  $\tilde{\mathbf{F}}^e$ .
- (3) Store the element matrices in  $\bar{\mathbf{A}}$  (whose dimensions are  $n_{em}$ ,  $n_{e\ell q}$ ,  $n_{e\ell q}$ ).
- (4) Store inverse of the diagonal terms of the global system in  $\mathbf{W}$

$$W_{ii} = \sum_{e=1}^{n_{em}} \tilde{K}_{ii}^{-1}$$

- (5) Assemble the global force vector.

II. *Preconditioning:*

Form the preconditioned system of equations

$$\bar{\mathbf{K}}\bar{\mathbf{U}} = \bar{\mathbf{F}}, \quad \bar{\mathbf{K}} = \mathbf{W}^{-1/2}\tilde{\mathbf{K}}\mathbf{W}^{-1/2}, \quad \bar{\mathbf{U}} = \mathbf{W}^{1/2}\tilde{\mathbf{U}}, \quad \bar{\mathbf{F}} = \mathbf{W}^{-1/2}\tilde{\mathbf{F}}$$

III. *Lanczos ORTHORES Algorithm*

- (1) For known initial solution vector  $\bar{\mathbf{U}}^0$ , compute:

$$\mathbf{r}^0 = \bar{\mathbf{F}} - \bar{\mathbf{K}}\bar{\mathbf{U}}^0$$

- (2) For each ORTHORES iteration  $m = 0, 1, 2, \dots$ , compute ( $\tilde{\mathbf{r}} = \mathbf{r}_0, \lambda^0 = 0$ ):

$$\lambda^{m+1} = \frac{(\mathbf{r}^m, \tilde{\mathbf{r}}^m)}{(\bar{\mathbf{K}}\mathbf{r}^m, \tilde{\mathbf{r}}^m)}$$

$$\beta^{m+1} = \begin{cases} 1 & ; \text{if } m = 0 \\ \left[ 1 - \frac{\lambda^{m+1}}{\lambda^m} \frac{(\mathbf{r}^m, \tilde{\mathbf{r}}^m)}{(\mathbf{r}^{m-1}, \tilde{\mathbf{r}}^{m-1})} \frac{1}{\beta^m} \right]^{-1} & ; \text{if } m \geq 1 \end{cases}$$

$$\mathbf{r}^{m+1} = \beta^{m+1}(\mathbf{r}^m - \lambda^{m+1}\bar{\mathbf{K}}\mathbf{r}^m) + (1 - \beta^{m+1})\mathbf{r}^{m-1}$$

$$\tilde{\mathbf{r}}^{m+1} = \beta^{m+1}(\tilde{\mathbf{r}}^m - \lambda^{m+1}\bar{\mathbf{K}}\tilde{\mathbf{r}}^m) + (1 - \beta^{m+1})\tilde{\mathbf{r}}^{m-1}$$

$$\bar{\mathbf{U}}^{m+1} = \beta^{m+1}(\bar{\mathbf{U}}^m + \lambda^{m+1}\mathbf{r}^m) + (1 - \beta^{m+1})\bar{\mathbf{U}}^{m-1}$$

- (3) Check convergence

$$\|\bar{\mathbf{U}}^{m+1}\|/\|\mathbf{r}^0\| \leq 10^{-6}$$

- (4) If convergence criterion is satisfied, set

$$\mathbf{U}^* = \mathbf{W}^{-1/2}\bar{\mathbf{U}}^{m+1}$$

Table A1.3.3 Steps involved in using the GMRES solver.

Repeat the following steps for each nonlinear iteration:

I. *Initial Calculations*

- (1) Form the element stiffness matrix  $\tilde{\mathbf{K}}^e$  and force vector  $\tilde{\mathbf{F}}^e$ .
- (2) Apply the boundary conditions, and modify  $\tilde{\mathbf{K}}^e$  and  $\tilde{\mathbf{F}}^e$ .
- (3) Store the element matrices in  $\bar{\mathbf{A}}$  (whose dimensions are nem, neleq, neleq).
- (4) Store inverse of the diagonal terms of the global system in  $\mathbf{W}$ :  $W_{ii} = \sum_{e=1}^{\text{nem}} \tilde{K}_{ii}^{-1}$
- (5) Assemble the global force vector.

II. *Preconditioning*: Form the preconditioned system of equations

$$\bar{\mathbf{K}}\bar{\mathbf{U}} = \bar{\mathbf{F}}, \quad \bar{\mathbf{K}} = \mathbf{W}^{-1/2}\tilde{\mathbf{K}}\mathbf{W}^{-1/2}, \quad \bar{\mathbf{U}} = \mathbf{W}^{1/2}\tilde{\mathbf{U}}, \quad \bar{\mathbf{F}} = \mathbf{W}^{-1/2}\tilde{\mathbf{F}}$$

III. *GMRES Algorithm*

- (1) *Start* Choose  $\bar{\mathbf{U}}^0$  and compute

$$\mathbf{r}^0 = \bar{\mathbf{F}} - \bar{\mathbf{K}}\bar{\mathbf{U}}^0, \text{ and}$$

$$\mathbf{v}^1 = \bar{\mathbf{U}}^0 / \|\bar{\mathbf{U}}^0\|$$

- (2) *Iterate*: For  $j = 1, 2, \dots, k$  do:

$$h_{i,j} = (\bar{\mathbf{K}}\mathbf{v}_j, \mathbf{v}_i), \quad i = 1, 2, \dots, j,$$

$$\hat{\mathbf{v}}_{j+1} = \bar{\mathbf{K}}\mathbf{v}_j - \sum_{i=1}^j h_{i,j}\mathbf{v}_i,$$

$$h_{j+1,j} = \|\hat{\mathbf{v}}_{j+1}\|, \text{ and}$$

$$\mathbf{v}_{j+1} = \hat{\mathbf{v}}_{j+1}/h_{j+1,j}$$

- (3) *Form the approximate solution*

$$\bar{\mathbf{U}}^k = \bar{\mathbf{U}}^0 + \mathbf{V}\mathbf{y}, \text{ where } \mathbf{y} \text{ minimizes}$$

$$\|\mathbf{e} - \bar{\mathbf{H}}\mathbf{y}\|, \mathbf{y} \in \mathbf{R}^k.$$

- (4) *Restart*

$$\text{Compute } \mathbf{r}^k = \bar{\mathbf{F}} - \bar{\mathbf{K}}\bar{\mathbf{U}}^k;$$

check convergence; if satisfied stop; otherwise, compute

$$\bar{\mathbf{U}}^0 := \bar{\mathbf{U}}^k, \mathbf{v}_1 := \bar{\mathbf{U}}^k / \|\bar{\mathbf{U}}^k\|, \text{ and go to step 2.}$$

- (5) Convergence criterion  $\|\bar{\mathbf{U}}^{m+1}\|/\|\mathbf{r}^0\| \leq 10^{-6}$

- (6) If convergence criterion is satisfied  $\mathbf{U}^* = \mathbf{W}^{-1/2}\bar{\mathbf{U}}$

where  $\mathbf{V}$  is a  $N \times k$  matrix whose columns are 1-2 orthonormal basis vectors  $\{\mathbf{v}_1, \mathbf{v}_2, \dots, \mathbf{v}_k\}$ ,  $\mathbf{e} = \{\|\bar{\mathbf{U}}^0\|, 0, \dots, 0\}$ , and  $\bar{\mathbf{H}}$  is the upper  $k \times k$  Hessenberg matrix whose entries are the scalars  $h_{i,j}$ . When using the restart version of the GMRES algorithm, the total number of iteration  $m$  can be computed from the number of restarts and the dimension of  $k$ .

6. Bathe, K. J., *Finite Element Procedures*, Prentice Hall, Englewood Cliffs, New Jersey (1998).
7. Reddy, J. N., *An Introduction to the Finite Element Method*, 2nd edn, McGraw-Hill, New York (1993).
8. Reddy, J. N. and Gartling, D. K., *The Finite Element Method in Heat Transfer and Fluid Dynamics*, CRC Press, Boca Raton, FL (1994); 2nd edn (2000).
9. Hestenes, M. R. and Stiefel, E. L., "Methods of Conjugate Gradients for Solving Linear Systems," *National Bureau of Standards Journal of Research*, **49**, 409-436 (1952).
10. Golub, G. H. and Van Loan, C. F., *Matrix Computations*, 2nd edn, The Johns Hopkins University Press, Baltimore, MD (1989).
11. Jea, K. C. and Young, D. M., "On the Simplification of Generalized Conjugate-Gradient Methods for Nonsymmetrizable Linear Systems," *Linear Algebra Applications*, **52**, 399-417 (1983).
12. Evans, D. J., "Use of Preconditioning in Iterative Methods for Solving Linear Equations with Symmetric Positive Definite Matrices," *Computer Journal*, **4**, 73-78 (1961).
13. Fox, R. L. and Stanton, E. L., "Developments in Structural Analysis by Direct Energy Minimization," *AIAA Journal*, **6**, 1036-1042 (1968).
14. Fried, I., "Gradient Methods for Finite Element Eigenproblems," *AIAA Journal*, **7**, 739-741 (1969).
15. Fried, I., "More on Generalized Iterative Methods in Finite Element Analysis," *AIAA Journal*, **7**, 565-567 (1969).
16. Fried, I., "A Gradient Computational Procedure for the Solution of Large Problems Arising from the Finite Element Discretization Method," *International Journal for Numerical Methods in Engineering*, **2**, 477-494 (1970).
17. Reddy, M. P., Reddy, J. N., and Akay, H. U., "Penalty Finite Element Analysis of Incompressible Flows Using Element by Element Solution Algorithms," *Computer Methods in Applied Mechanics and Engineering*, **100**, 169-205 (1992).
18. Wathen, A. J., "An Analysis of Some Element-by-Element Techniques," *Computer Methods in Applied Mechanics and Engineering*, **74**, 271-287 (1989).
19. Hughes, T. J. R., Levit, I., and Winget, J., "An Element-by-Element Implicit Algorithm for Heat Conduction," *Journal of the Engineering Mechanics Division, ASCE*, **109**(2), 576-585 (1983).
20. Winget, J. M. and Hughes, T. J. R., "Solution Algorithms for Nonlinear Transient Heat Conduction Analysis Employing Element-by-Element Iterative Strategies," *Computer Methods in Applied Mechanics and Engineering*, **52**, 711-815 (1985).
21. Carey, G. F. and Jiang, B., "Element-by-Element Linear and Nonlinear Solution Schemes," *Communications in Applied Numerical Methods*, **2**, 145-153 (1986).
22. Hayes, J. L. and Devloo, P., "An Element-by-Element Block Iterative Method for Large Non-Linear Problems," in *Innovative Methods for Nonlinear Behavior*, W. K. Liu et al. (eds.), Pineridge Press, Swansea, UK, 51-62 (1985).
23. Buratynski, E. K., "An Element-by-Element Method for Heat Conduction CAE Including Composite Problems," *International Journal for Numerical Methods in Engineering*, **26**, 199-215 (1988).
24. Levit, I., "Element By Element Solvers of Order N," *Computers & Structures*, **27**(3), 357-360 (1987).
25. de La Bourdinnaye, A., "The Element-by-Element Method as a Preconditioner for Linear Systems Coming from Finite Element Models," *International Journal of Supercomputer Applications*, **3**, 60-68 (1989).

26. Prakhya, K. V. G., "Some Conjugate Gradient Methods for Symmetric and Nonsymmetric Systems," *Communications in Applied Numerical Methods*, **4**, 531-539 (1988).
27. Carey, G. F., Barragy, E., R. Mclay, and Sharma, M., "Element-by-Element Vector and Parallel Computations," *Communications in Applied Numerical Methods*, **4**, 299-307 (1988).
28. Hayes, L. J. and Devloo, P., "A Vectorized Version of a Sparse Matrix-Vector Multiplication," *International Journal for Numerical Methods in Engineering*, **23**, 1043-1056 (1986).
29. Shakib, F., Hughes, T. J. R., and Johan, Z., "A Multi-Element Group Preconditioned GMRES Algorithm for Nonsymmetric Systems Arising in Finite Element Analysis," *Computer Methods in Applied Mechanics and Engineering*, **75**, 415-456 (1989).
30. Tezduyar, T. E. and Liou, J., "Grouped Element-By-Element Iteration Schemes for Incompressible Flow Computations," *Computational Physics Communications*, **53**, 441-453 (1989).
31. Saad, Y. and Schultz, M. H., "GMRES: A Generalized Minimal Residual Algorithm for Solving Nonsymmetric Linear Systems," *SIAM Journal of Scientific and Statistical Computations*, **7**(3), 856-869 (1986).
32. Mitchell, J. A. and Reddy, J. N., "A Multilevel Hierarchical Preconditioner for Thin Elastic Solids," *International Journal for Numerical Methods in Engineering*, **43**, 1383-1400 (1998).

---

## Appendix A2

# Solution Procedures for Nonlinear Algebraic Equations

---

### A2.1 Introduction

Finite element formulations of nonlinear differential equations lead to nonlinear algebraic equations for each element of the finite element mesh. The element equation is of the form,

$$[K^e(\{u^e\})]\{u^e\} = \{F^e\} \quad (\text{A2.1.1})$$

where

$$\begin{aligned} [K^e] & - \text{element coefficient matrix (or "stiffness" matrix), which} \\ & \text{depends on the solution vector } \{u^e\}, \\ \{u^e\} & - \text{column vector of element nodal values, and} \\ \{F^e\} & - \text{column vector of element nodal "forces".} \end{aligned} \quad (\text{A2.1.2})$$

When  $[K^e]$  is independent of  $\{u^e\}$ , the matrix coefficients can be evaluated for all elements, and the assembled equations can be solved for the global nodal values  $\{u\}$  after imposing boundary conditions. When  $[K^e]$  depends on the unknown solution vector  $\{u^e\}$ , the matrix coefficients cannot be evaluated. If we can find an approximation to  $\{u^e\}$ , say  $\{u^e\}^1$ , then  $[K^e(\{u^e\}^1)]$  can be evaluated and assembled. This amounts to linearizing the nonlinear equations, Eq. (A2.1.1). Then a next approximation to the solution can be obtained by solving the assembled equations,

$$\{u\}^2 = [K(\{u\}^1)]^{-1}\{F\} \quad (\text{A2.1.3})$$

This procedure can be repeated until the approximate solution comes close to the actual solution in some measure. Such a procedure is called an iterative procedure.

Here we discuss the following commonly used iterative procedures:

1. The Picard Iteration (or Direct Iteration) Method
2. The Newton–Raphson Iteration Method
3. The Riks Method

The details of these methods are discussed next, with the aid of a single nonlinear equation. For a more complete presentation of these methods, the reader may consult the references at the end of this appendix.

Consider the nonlinear equation,

$$K(u) \cdot u = F \quad \text{or} \quad R(u) = 0 \quad (\text{A2.1.4})$$

where  $u$  is the solution to be determined,  $K(u)$  is a known function of  $u$ ,  $F$  is the known ‘force’, and  $R$  is the residual

$$R(u) = K(u) \cdot u - F \quad (\text{A2.1.5})$$

A plot of the equilibrium path,  $R(u, F) = 0$ , is shown in Figure A2.1.1. For any value  $u_1$ ,  $K(u_1)$  denotes the secant of the curve at  $u = u_1$ , and  $(\frac{\partial R}{\partial u})|_{u_1}$  denotes the tangent of the curve at  $u = u_1$ .

## A2.2 Picard Iteration Method

In the Picard iteration, also known as the *direct iteration* method, we begin with an initial guess for  $u$ , say  $u^{(0)}$ , ( $u^{(0)} = 0$  in Figure A2.1.1) and determine a first approximation to  $u$  by solving the equation

$$u^{(1)} = (K(u^{(0)}))^{-1} F \quad (\text{A2.2.1})$$

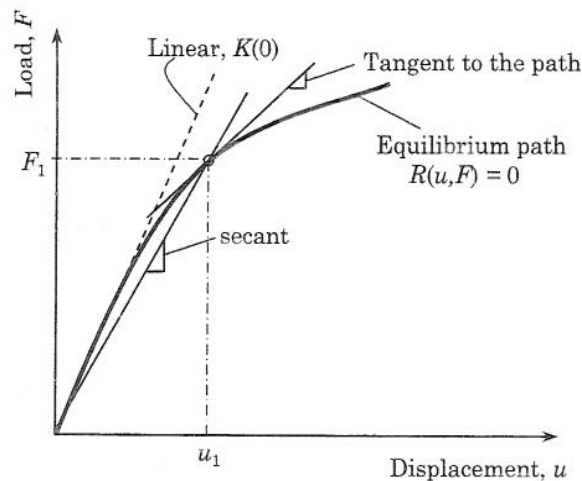


Figure A2.1.1 Typical force–displacement curve.



$u^{(1)} \neq u$ , and a second approximation for  $u$  is sought by using the last approximation to evaluate  $K$

$$u^{(2)} = \left( K(u^{(1)}) \right)^{-1} F \quad (\text{A2.2.2})$$

This procedure is continued until the difference between two consecutive approximations of  $u$  differ by a preselected value. Thus, the algorithm and criterion for convergence may be written as

$$\text{Algorithm} \quad u^{(r)} = \left( K(u^{(r-1)}) \right)^{-1} F \quad (\text{A2.2.3})$$

$$\text{Convergence Criterion} \quad \sqrt{\frac{(u^{(r)} - u^{(r-1)})^2}{(u^{(r)})^2}} < \epsilon \quad (\text{A2.2.4})$$

where  $\epsilon$  denotes the *convergence tolerance* and  $r$  denotes the iteration number.

A geometric interpretation of the procedure described above is illustrated in Figure A2.2.1(a) for an initial guess of  $u^{(0)} = 0$ . At the beginning of iteration  $r$ , the secant of the curve  $R(u) = 0$  is found at the point  $u = u^{(r-1)}$  and the solution  $u^{(r)}$  is computed using Eq. (A2.2.3). Figure A2.2.1(a) shows the convergence to the true solution  $u_c$ , whereas Figure A2.2.1(b) shows a possible divergence of the algorithm. Thus, the success of the algorithm depends on the nature of the nonlinear curve  $R(u) = 0$ , the initial guess, and the load increment.

In the direct iteration method discussed above, the secant is evaluated at each iteration and inverted to obtain the next approximate solution. This can be computationally very expensive when the number of algebraic equations to be solved is large, that is, when  $K$  is a matrix and  $[K]^{-1}$  is its inverse. When  $K$  has a linear portion, and in most problems of interest to us it does, an *alternative direct iteration* algorithm can be formulated. Let

$$K(u) = K_L + K_N(u) \quad (\text{A2.2.5})$$

where  $K_L$  and  $K_N(u)$  are the linear and nonlinear parts of  $K$ . Note that  $K_L$  is the slope at  $u = 0$  of the curve  $R(u) = 0$ . Then we can write

$$u^{(r)} = (K_L)^{-1} [F - K_N(u^{(r-1)}) \cdot u^{(r-1)}] \quad (\text{A2.2.6})$$

This scheme involves evaluating the nonlinear part  $K_N$  at each iteration, which is computationally less expensive when compared to evaluating  $[K(u^{r-1})]$  and inverting it. The inversion of  $K_L$  is required only once, and it should be saved for subsequent use. The criterion in Eq. (A2.2.4) can be used to check for convergence.

Geometrically, the alternative direct iteration algorithm uses the initial slope, that is, slope at the origin of the curve for *all* iterations, while updating the *effective force*

$$\hat{F} \equiv F - K_N(u^{(r-1)}) \cdot u^{(r-1)}$$

at each iteration (see Figure A2.2.2). The rate of convergence of this algorithm, if at all it converges, is slower than that in Eq. (A2.2.3).

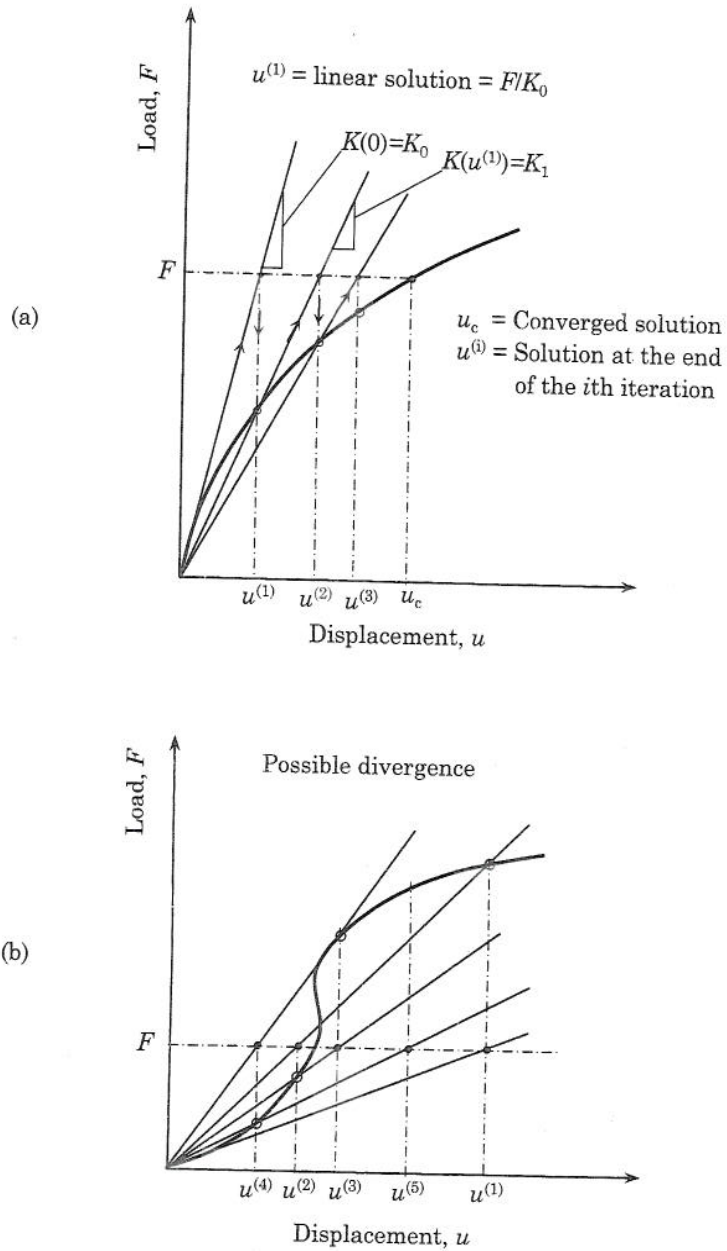


Figure A2.2.1 Direct iteration scheme. (a) Case of convergence. (b) Case of divergence.



$K^e(\{\bar{u}^e\})$ , where  $\{\bar{u}^e\} = \gamma\{u^e\}^{(r-2)} + (1 - \gamma)\{u^e\}^{(r-1)}$ , and  $0 \leq \gamma \leq 1$  is called the *relaxation* or *acceleration parameter*. In this case Eqs. (A2.2.7) and (A2.2.8) take the form,

$$\text{Algorithm 1} \quad \{u\}^r = [K(\{\bar{u}\})]^{-1}\{F\} \quad (\text{A2.2.12})$$

$$\text{Algorithm 2} \quad \{u\}^r = [K_L]^{-1}(\{F\} - [K_{NL}(\{\bar{u}\})]\{\bar{u}\}) \quad (\text{A2.2.13})$$

$$\{\bar{u}\} = \gamma\{u\}^{(r-2)} + (1 - \gamma)\{u\}^{(r-1)} \quad (\text{A2.2.14})$$

The actual value of  $\gamma$  varies from problem to problem.

The computational algorithm of the direct iteration is summarized below. At each load level follow the steps:

1. Compute element matrices  $[K^e]$  and  $\{F^e\}$  (for transient problems,  $[K^e]$  and  $\{F^e\}$  are to be replaced by  $[\hat{K}^e]$  and  $\{\hat{F}^e\}$ ) using the solution  $\{u\}^{(r-1)}$  from the previous iteration (of current load and/or time). For the first iteration of the subsequent load steps, use  $\{u_c\}$ , the converged solution of the last load step. For the first load step use  $\{u_c\} = 0$ , provided  $[K^e]^{-1}$  exists, to compute the linear solution.
2. Assemble the element matrices  $[K^e]$  and  $\{F^e\}$  (or  $[\hat{K}^e]$  and  $\{\hat{F}^e\}$ ).
3. Apply the boundary conditions on the assembled set of equations.
4. Solve the assembled equations.
5. Check for convergence using Eq. (A2.2.9).
- 6a. If the convergence criterion is satisfied, increase the load to next level, initialize the counter on iterations, and repeat Steps 1-5.
- 6b. If the convergence criterion is not satisfied, check if the maximum number of allowable iterations is exceeded. If yes, terminate the computation printing a message to that effect. If the number of iterations did not exceed the maximum allowed, update  $\{u\}^{(r-1)}$  and  $\{u\}^{(r)}$  and repeat Steps 1-5.

### A2.3 Newton-Raphson Iteration Method

Suppose that we know solution of Eq. (A2.1.1) at  $(r - 1)$ st iteration and interested in seeking solution at the  $r$ th iteration. We expand  $R(u)$  about the known solution  $u^{(r-1)}$  in Taylor's series,

$$R(u) = R(u^{(r-1)}) + \left(\frac{\partial R}{\partial u}\right)\Big|_{u^{(r-1)}} \cdot \delta u + \frac{1}{2} \left(\frac{\partial^2 R}{\partial u^2}\right)\Big|_{u^{(r-1)}} \cdot (\delta u)^2 + \dots = 0 \quad (\text{A2.3.1})$$

where  $\delta u$  is the increment,

$$\delta u^{(r)} = u^{(r)} - u^{(r-1)} \quad (\text{A2.3.2})$$

Assuming that the second- and higher-order terms in  $\delta u$  are negligible, we can write Eq. (A2.3.1) as

$$\begin{aligned}\delta u^{(r)} &= -\left(K_T(u^{(r-1)})\right)^{-1} \cdot R(u^{(r-1)}) \\ &= \left(K_T(u^{(r-1)})\right)^{-1} \left(F - K(u^{(r-1)}) \cdot u^{(r-1)}\right)\end{aligned}\quad (\text{A2.3.2})$$

where  $K_T$  is the slope (tangent) of the curve  $R(u)$  at  $u^{(r-1)}$ :

$$K_T = \left. \frac{\partial R}{\partial u} \right|_{u^{(r-1)}} \quad (\text{A2.3.3})$$

The residual or *imbalance force*,  $R(u^{(r-1)})$  is gradually reduced to zero if the procedure converges. Equation (A2.3.2) gives the increment of  $u$  at the  $r$ th iteration so that the total solution is

$$u^{(r)} = u^{(r-1)} + \delta u^{(r)} \quad (\text{A2.3.4})$$

The iteration is continued until a convergence criterion, say Eq. (A2.2.4), is satisfied. Other convergence criteria include checking the magnitude of the imbalance force.

A geometrical interpretation of the Newton-Raphson procedure is shown in Figure A2.3.1(a). For most problems, the method has faster convergence characteristics. Figure A2.3.1(b) illustrates possible divergence of the iterative procedure for certain problems.

The Newton-Raphson method requires that the tangent  $K_T$  be computed at each iteration. This can be very expensive when many degrees of freedom are involved. A *modified Newton-Raphson technique* involves, for a fixed load step, either keeping  $K_T$  fixed while updating the imbalance force at each iteration (see Figure A2.3.2) or updating  $K_T$  only at each preselected number of iterations while updating the imbalance force at each iteration. There are several other modifications of the procedure.

The Newton-Raphson and modified Newton-Raphson procedures take the following forms when applied to the assembly of element equations (A2.3.2):

*Newton-Raphson Procedure*

$$\{\delta U\} = -[K_T]^{-1}\{R\} \quad (\text{A2.3.5})$$

*Modified Newton-Raphson Procedure*

$$\{\delta U\} = -[\bar{K}_T]^{-1}\{\bar{R}\} \quad (\text{A2.3.6})$$

where  $[K_T]$  is the *tangent matrix*

$$[K_T] = \left. \frac{\partial \{R\}}{\partial \{U\}} \right|_{\{U\}^{r-1}} \quad \text{or} \quad (K_T)_{ij} = \frac{\partial R_i}{\partial U_j} = K_{ij} + \sum_{k=1}^n \frac{\partial K_{ik}}{\partial U_j} U_k \quad (\text{A2.3.7a})$$

and

$$\{R\} = [K(\{U\}^{(r-1)})]\{U\}^{(r-1)} - \{F\} \quad (\text{A2.3.7b})$$

$$[\bar{K}_T] = [K_T(\{\bar{U}\})], \quad [\bar{K}] = [K(\{\bar{U}\})] \quad (\text{A2.3.8})$$

and  $\{\bar{U}\}$  is the solution at the beginning of the current load step, and

$$\{\bar{U}\}^{(r)} = \{U\}^{(r-1)} + \{\delta U\}^{(r)} \quad (\text{A2.3.9})$$

The relaxation procedure described in Eq. (A2.3.9) can be used to accelerate convergence for certain nonlinear problems.

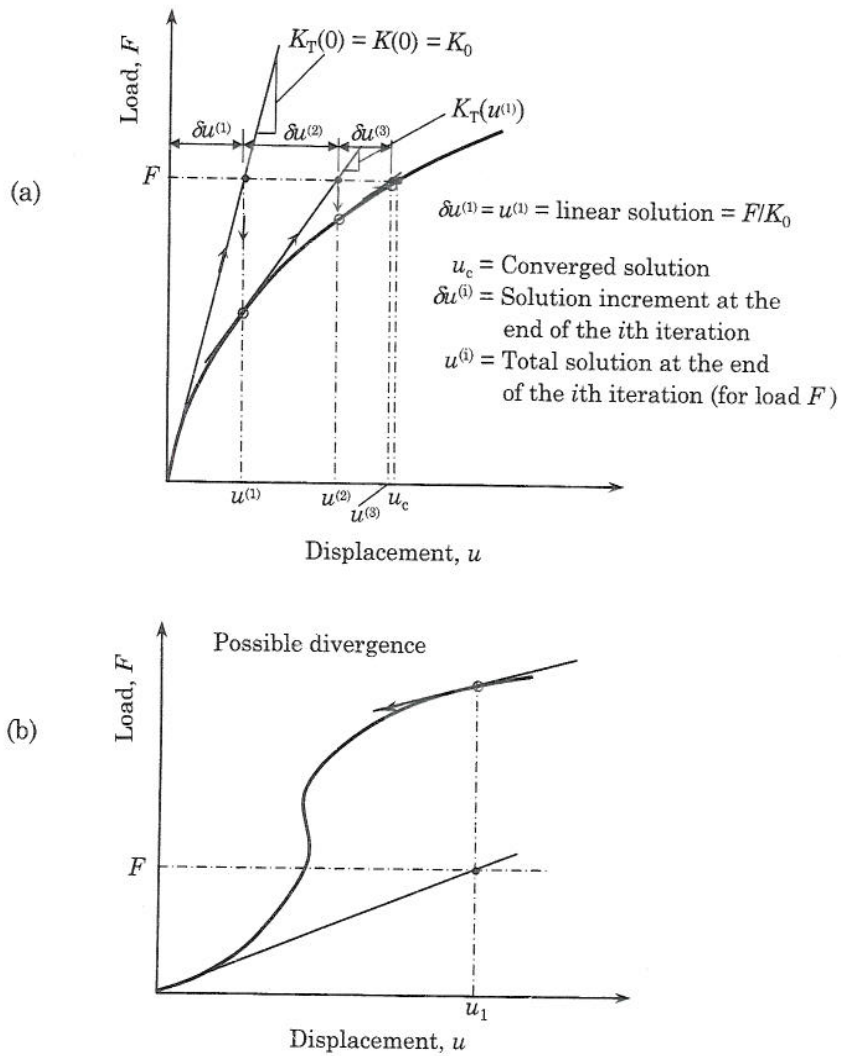


Figure A2.3.1 The Newton-Raphson scheme. (a) A case of convergence. (b) A case of divergence.

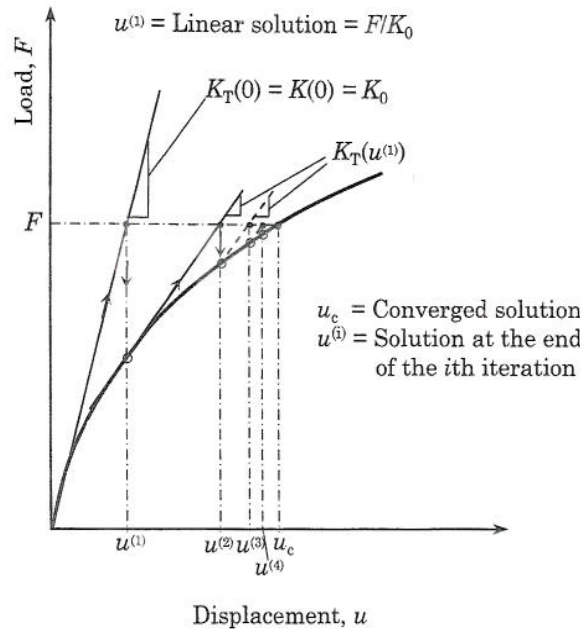


Figure A2.3.2 Modified Newton-Raphson scheme.

Since only the increment of the solution is computed in each iteration of the Newton-Raphson iteration, the incremental equations in (A2.3.5) and (A2.3.6) are subject to homogeneous form of specified essential boundary conditions of the problem. Thus after the first iteration of the first load step, any specified non-zero values of  $\{U\}$  should be set to zero so that in the subsequent iterations and loads,  $\{\delta u\}$  is subjected to homogeneous boundary conditions.

For each load step, the following computations are required for the Newton-Raphson or modified Newton-Raphson procedure:

1. Evaluate element matrices  $[K^e]$  and  $\{F^e\}$  (or  $[\hat{K}^e]$  and  $\{\hat{F}^e\}$  for the transient problems), and compute  $[K_T^e]$  and  $\{R^e\}$  using Eqs. (A2.3.7a,b) for an element.
2. Assemble element matrices  $[K_T^e]$  and  $\{R^e\}$ ; for the modified Newton-Raphson iteration procedure, save either assembled  $[K_T]$  or its inverse for use in subsequent iterations.
3. Apply the boundary conditions on the assembled set of equations.  
*Note:* Set the specified boundary conditions on  $\{U\}$  to zero after Step 3 in the first iteration of the first load step.
4. Solve the assembled equations.
5. Update the solution vector using Eq. (A2.3.9).

6. Check for convergence.
- 7a. If the convergence criterion is satisfied, increase the load, initialize the iteration counter, and repeat Steps 1–6. For the modified Newton–Raphson iteration, compute  $\{F^e\} - [\bar{K}]\{U^e\}^{(r-1)}$  in Step 1 and go to Step 2.
- 7b. If the convergence criterion is not satisfied, check if the maximum number of iterations allowed is exceeded. If it is, terminate the computation by printing a message. If the maximum allowable number of iterations is not exceeded, go to Step 1.

In order to reduce the number of operations per iteration, in the modified Newton–Raphson method the same system matrices are used for several iterations. These matrices are updated only at the beginning of each load step or only when the convergence rate becomes poor. The modified Newton–Raphson method may require more iterations to reach a new equilibrium point.

#### A2.4 Riks and Modified Riks Schemes

The Newton–Raphson method and its modifications are often used to trace nonlinear solution paths. However, the Newton–Raphson method fails to trace the nonlinear equilibrium path through the limit point (see Figure A2.4.1), because in the vicinity of a limit point the tangent matrix  $[K_T]$  becomes singular, and the iteration procedure diverges. Riks [1] and Wempner [2] suggested a procedure to predict the nonlinear equilibrium path through limit points. The method provides the Newton–Raphson method and its modifications with a technique to control progress along the equilibrium path. The theoretical development of this method and its modification can be found in [3–6]. In the modified Riks method (see [3–6]) the load increment for each load step is considered to be an unknown (see [3]) and solved as a part of the solution.

The basic idea of the Riks technique can be described for a single nonlinear equation as follows (see Figure A2.4.2): The length  $\Delta s$  of the tangent to the current equilibrium point is prescribed, and the new point is found as the intersection of the *normal to the tangent* with the equilibrium path [see Figure A2.4.2(a)]. Then iteration is performed along the normal toward the new equilibrium point, as illustrated in Figure A2.4.2(a). Crisfield [4] suggested using a circular arc in place of the normal [see Figure A2.4.2(b)]. The center of the circle is at the current equilibrium point and  $\Delta s$  is its radius. For multidimensional problems the normal and circular arcs become a plane and sphere, respectively, Crisfield [4] updated the tangent stiffness matrix only at the beginning of each load increment (i.e. modified Newton–Raphson method). In the present study we describe the modified Riks method due to Crisfield [4].



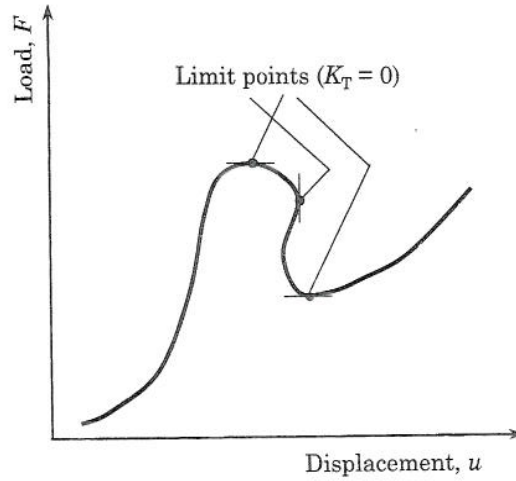


Figure A2.4.1 Load-deflection curve with limit points.

We wish to solve Eq. (A2.1.4) for  $u$  as a function of the source term  $F$ . If  $F$  is independent of the geometry, we can write it as

$$F = \lambda \bar{F} \quad (\text{A2.4.1})$$

where  $\lambda$  is a scalar, called *load parameter*, which is considered as an unknown parameter. Equation (A2.1.5) becomes

$$R = K(u) \cdot u - \lambda \bar{F} \quad (\text{A2.4.2})$$

Now suppose that the solution  $(u_n^{(r-1)}, \lambda_n^{(r-1)})$  at  $(r-1)$ st iteration of the  $n$ th load step is known and we wish to determine the solution  $(u_n^{(r)}, \lambda_n^{(r)})$  at the  $r$ th iteration. Expanding  $R$ , which is now a function of  $\lambda$  and  $u$ , in Taylor's series about the known solution, we have,

$$\begin{aligned} R(u_n^{(r)}, \lambda_n^{(r)}) &= R(u_n^{(r-1)}, \lambda_n^{(r-1)}) + \left(\frac{\partial R}{\partial \lambda}\right)^{(r-1)} \delta \lambda_n^{(r)} + \left(\frac{\partial R}{\partial u}\right)^{(r-1)} \delta u_n^{(r)} + \dots \\ &= 0 \end{aligned}$$

Omitting the higher-order terms involving the increments  $\delta \lambda_n^{(r)}$  and  $\delta u_n^{(r)}$ , we obtain

$$0 = R_n^{(r-1)} - \bar{F} \cdot \delta \lambda_n^{(r)} + (K_T)^{(r-1)} \cdot \delta u_n^{(r)} \quad (\text{A2.4.3})$$

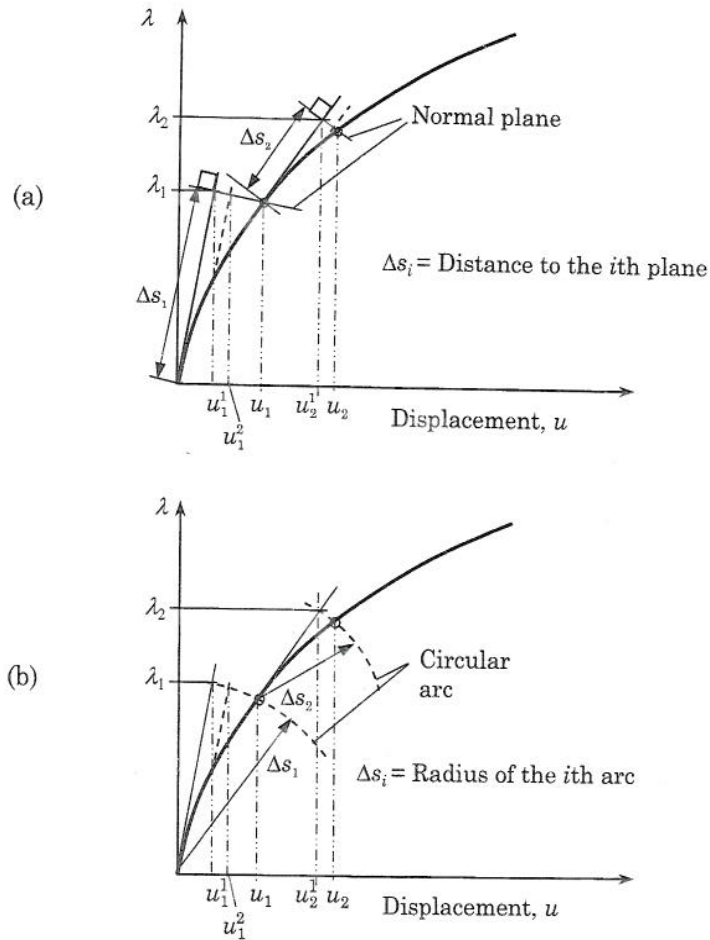


Figure A2.4.2 The Riks scheme. (a) Normal plane method. (b) Circular arc method.

where  $K_T = \partial R / \partial u$  is the tangent matrix [see Eq. (A2.3.3)]. The incremental solution at the current iteration of the  $n$ th load step is given by

$$\begin{aligned} \delta u_n^{(r)} &= -K_T^{-1} (R_n^{(r-1)} - \bar{F}) \cdot \delta \lambda_n^{(r)} \\ &\equiv \delta \bar{u}_n^{(r)} + \delta \lambda_n^{(r)} \cdot \delta \hat{u}_n \end{aligned} \quad (\text{A2.4.4a})$$

where  $\delta u_n^{(r)}$  is the usual increment in displacement due to known out-of-balance force vector  $R_n^{(r-1)}$  with known  $\lambda_n^{(r-1)}$  and  $K_T$  is the tangent at the beginning of the current load increment (i.e. Modified Newton-Raphson method is used)

$$\delta \bar{u}_n^{(r)} = -K_T^{-1} R_n^{(r-1)} \quad (\text{A2.4.4b})$$

and  $\delta\hat{u}_n$  is the tangential solution (see Figure A2.4.3)

$$\delta\hat{u}_n = K_T^{-1}\bar{F} \tag{A2.4.4c}$$

Note that  $K_T$  is evaluated using the converged solution  $u_{n-1}$  of the last load step,

$$K_T = \left(\frac{\partial R}{\partial u}\right)\Big|_{u=u_{n-1}} = K(u_{n-1}) + \left(\frac{\partial K}{\partial u}\right)\Big|_{u=u_{n-1}} \cdot u_{n-1} \tag{A2.4.5}$$

and  $\delta\hat{u}_n$  is computed at the beginning of each load step.

The solution at the  $r$ th iteration of the current load step is given by

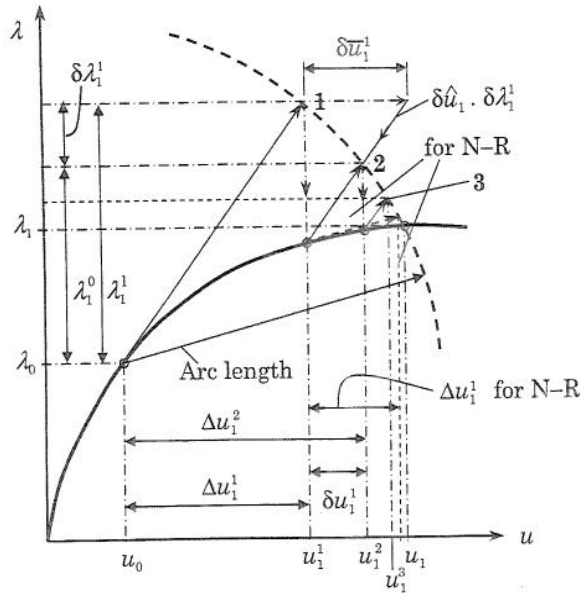
$$u_n = u_{n-1} + \Delta u_n^{(r)} \tag{A2.4.6a}$$

$$\Delta u_n^{(r)} = \Delta u_n^{(r-1)} + \delta u_n^{(r)}, \quad \lambda_n^{(r)} = \lambda_n^{(r-1)} + \delta\lambda_n^{(r)} \tag{A2.4.6b}$$

For the very first iteration of the first load step, we assume  $u = u_0$ , and a value for the incremental load parameter  $\delta\lambda_1^0$ , and solve the equation

$$\delta\hat{u}_1 = (K_T)^{-1}\bar{F} \tag{A2.4.7}$$

and compute  $\delta u_1^{(0)} = \delta\lambda_1^0 \cdot \delta\hat{u}_1$ .



A2.4.3 Modified Riks scheme.

Select the arc length  $\Delta s$  to be the length of the vector

$$(\Delta s)^2 = \Delta u_n^{(r)} \cdot \Delta u_n^{(r)} \quad (\text{A2.4.8})$$

Substituting for  $\Delta u_n^{(r)}$  from Eqs. (A2.4.6b) [and  $\delta u_n^{(r)}$  from Eq. (A2.4.4a)] we obtain the following quadratic equation for the increment in the load parameter,  $\delta \lambda_n^{(r)}$ :

$$a_1[\delta \lambda_n^{(r)}]^2 + 2a_2[\delta \lambda_n^{(r)}] + a_3 = 0 \quad (\text{A2.4.9a})$$

where

$$\begin{aligned} a_1 &= \delta \hat{u}_n \cdot \delta \hat{u}_n \\ a_2 &= (\Delta u_n^{(r-1)} + \delta \bar{u}_n^{(r)}) \cdot \delta \hat{u}_n \\ a_3 &= (\Delta u_n^{(r-1)} + \delta \bar{u}_n^{(r)}) \cdot (\Delta u_n^{(r-1)} + \delta \bar{u}_n^{(r)}) - (\Delta s)^2 \end{aligned} \quad (\text{A2.4.9b})$$

Let us denote the roots of this quadratic equation as  $\delta \lambda_{n1}^{(r)}$  and  $\delta \lambda_{n2}^{(r)}$ . To avoid "tracing back" the equilibrium path (i.e. going back on the known equilibrium path), we require the angle between the incremental solution vectors at two consecutive iterations,  $\Delta u_n^{(r-1)}$  and  $\Delta u_n^{(r)}$ , be positive. Corresponding to the two roots,  $\delta \lambda_{n1}^{(r)}$  and  $\delta \lambda_{n2}^{(r)}$ , there correspond to two values of  $\Delta u_n^{(r)}$ , denoted  $\Delta u_{n1}^{(r)}$  and  $\Delta u_{n2}^{(r)}$ . The root that gives the positive angle is the one we select from  $(\delta \lambda_{n1}^{(r)}, \delta \lambda_{n2}^{(r)})$ . The "angle" is defined to be product of the vector  $\Delta u_n^{(r-1)}$  and  $\Delta u_n^{(r)}$ . Then we check to see which one of the following two products is positive:

$$\Delta u_n^{(r-1)} \cdot \Delta u_{n1}^{(r)} \text{ and } \Delta u_n^{(r-1)} \cdot \Delta u_{n2}^{(r)} \quad (\text{A2.4.10a})$$

If both roots are positive, then we select the ones closest to the linear solution,

$$\delta \lambda_n^{(r)} = -\frac{a_3}{2a_2} \quad (\text{A2.4.10b})$$

The first arc length  $\Delta s$  is computed using Eqs. (A2.4.7) and (A2.4.8):

$$\Delta s = \delta \lambda_1^0 \sqrt{\delta \hat{u}_1 \cdot \delta \hat{u}_1} \quad (\text{A2.4.11})$$

To control the number of iterations taken to converge in the subsequent load increments,  $\delta s$  can be scaled,

$$\Delta s_n = \Delta s_{n-1} \cdot \frac{I_d}{I_0} \quad (\text{A2.4.12})$$

where  $\Delta s_{n-1}$  is the arc length used in the last iteration of the  $(n-1)$ st load step,  $I_d$  is the number of desired iterations (usually  $< 5$ ) and  $I_0$  is the number of iterations required for convergence in the previous step. Equation

(A2.4.12) will automatically give small arc lengths in the areas of the most severe nonlinearity and longer lengths when the response is linear or nearly linear. To avoid convergence of the solution at a higher equilibrium path, maximum arc lengths should be specified.

For all load steps after the first, the initial incremental load parameter  $\delta\lambda_n^{(0)}$  is calculated from

$$\delta\lambda_n^{(0)} = \pm \Delta s_n \cdot [\delta\hat{u}_n \cdot \delta\hat{u}_n]^{-\frac{1}{2}} \quad (\text{A2.4.13})$$

The plus sign is for continuing the load increment in the same direction as the previous load step and the negative sign is to reverse the load step. The sign follows that of the previous increment unless the value of determinant of the tangent matrix has changed in sign.

The modified Riks procedure described above for a single equation can be extended to the finite element equations in (A2.1.1). We introduce a load parameter  $\lambda$  as an additional dependent variable,

$$\{F\} = \lambda\{\bar{F}\} \quad (\text{A2.4.14})$$

In writing Eq. (A2.4.14), loads are assumed to be independent of the deformation. The assembled equations associated with Eq. (A2.1.1) become

$$\{R(\{U\}, \lambda)\} = [K]\{U\} - \lambda\{\bar{F}\} = 0 \quad (\text{A2.4.15})$$

The residual vector  $\{R\}$  is now considered as a function of both  $\{U\}$  and  $\lambda$ .

Now suppose that the solution  $(\{U\}_n^{(r-1)}, \lambda_n^{(r-1)})$  at the  $(r-1)$ st iteration of the  $n$ th load step is known. Expanding  $\{R\}$  in Taylor's series about  $(\{U\}_n^{(r-1)}, \lambda_n^{(r-1)})$ , we have

$$R_i = R_i(\{U\}_n^{(r-1)}, \lambda_n^{(r-1)}) + \left(\frac{\partial R_i}{\partial \lambda}\right)_{U_j^{r-1}, \lambda_n^{r-1}} \cdot \delta\lambda^{(r)} - \left(\frac{\partial R_i}{\partial U_j}\right)_{U_j^{r-1}, \lambda_n^{r-1}} \delta U_j^{(r)} + \dots$$

where the subscript 'n' is omitted for brevity. Omitting second- and higher-order terms involving  $\delta\lambda^{(r)}$  and  $\delta U_j^{(r)}$ , we can write

$$\{0\} = \{R\}^{(r-1)} - \delta\lambda_n^{(r)} \cdot \{\bar{F}\} + [K_T]\{\delta U\}^{(r)}$$

or

$$\{\delta U\}_n^{(r)} = -[K_T]^{-1}\{R\}^{(r-1)} + \delta\lambda_n^{(r)}[K_T]^{-1}\{\bar{F}\} \quad (\text{A2.4.16a})$$

$$\equiv \{\delta\bar{U}\}_n^{(r)} + \delta\lambda_n^{(r)}\{\delta\hat{U}\}_n \quad (\text{A2.4.16b})$$

where  $\{F\}$  is the load vector,  $\{R\}_n^{(r-1)}$  the unbalanced force vector at iteration  $(r-1)$ ,

$$\{\delta\bar{U}\}_n^{(r)} = -[K_T]^{-1}\{R\}_n^{(r-1)}, \quad (\text{A2.4.17a})$$

and  $\delta\lambda_n^{(r)}$  the load increment [given by Eq. (A2.4.10)], and

$$\{\delta\hat{U}\}_n = [K_T]^{-1}\{\bar{F}\} \quad (\text{A2.4.17b})$$

For the first iteration of any load step,  $\delta\lambda_n^{(0)}$  is computed from [see Eq. (A2.4.13)]:

$$\delta\lambda_n^{(0)} = \pm\Delta s_n(\{\delta\hat{U}\}_n^T\{\delta\hat{U}\}_n)^{-1/2} \quad (\text{A2.4.18})$$

where [see Eq. (A2.4.12)]

$$(\Delta\hat{s})_n = (\Delta\hat{s})_n \cdot I_d/I_0 \quad (\text{A2.4.19a})$$

and  $(\Delta\hat{s})_n$  is the arc length computed using the relation

$$(\Delta\hat{s})_n = \sqrt{\{\Delta U\}_{n-1}^T\{\Delta U\}_{n-1}} \quad (\text{A2.4.19b})$$

$\{\Delta U\}_{n-1}$  being the converged solution increment of the previous load step.

For the first iteration of the first load step, we use:

$$\Delta s = \delta\lambda_1^0 \sqrt{\{\delta\hat{U}\}_1^T \cdot \{\delta\hat{U}\}_1} \quad (\text{A2.4.20a})$$

$$\{\delta\hat{U}\}_1 = [K_T]^{-1}\{\bar{F}\}, \quad [K_T] = [K_T(\{U_0\})] \quad (\text{A2.4.20b})$$

where  $\delta\lambda_1^0$  is an assumed load increment and  $\{U_0\}$  is an assumed solution vector (often we assume  $\delta\lambda_1^0 = 1$  and  $\{U_0\} = \{0\}$ ).

The solution increment is updated using

$$\{\Delta U\}_n^r = \{\Delta U\}_n^{(r-1)} + \{\delta U\}_n^{(r)} \quad (\text{A2.4.21})$$

and the total solution at the current load step is given by

$$\{U\}_n = \{U\}_{n-1} + \{\Delta U\}_n^{(r)} \quad (\text{A2.4.22})$$

The constants in Eq. (A2.4.9b) are computed using

$$\begin{aligned} a_1 &= \{\delta\hat{U}\}_n^T\{\delta\hat{U}\}_n \\ a_2 &= (\{\Delta U\}_n^{(r-1)} + \{\delta\bar{U}\}_n^{(r)})^T\{\delta\hat{U}\}_n \\ a_3 &= (\{\Delta U\}_n^{(r-1)} + \{\delta\bar{U}\}_n^{(r)})^T(\{\Delta U\}_n^{(r-1)} + \{\delta\bar{U}\}_n^{(r)}) - (\Delta s)_n^2 \end{aligned} \quad (\text{A2.4.23})$$

The computational algorithm of the modified Riks method is summarized next.

**First iteration of first load step**

- (i) Choose a load increment  $\delta\lambda_1^0$  (say,  $\delta\lambda_1^0 = 1$ ) and solution vector  $\{U\}_0$  (say,  $\{U\}_0 = \{0\}$ ).  
 (ii) Form element matrices  $[K_T^e]$  and

$$\{R^e\} = [K^e]\{U^e\}_0 - \{F^e\}$$

- (iii) Assemble element matrices.  
 (iv) Apply the boundary conditions.  
 (v) Solve for  $\{\delta\hat{U}\}_1$  and  $\{\delta\bar{U}\}_1^{(1)}$  using Eqs. (A2.4.17a,b).  
 (vi) Compute the solution increment [see Eqs. (A2.4.16) and (A2.4.21)] and update the solution

$$\begin{aligned}\{\delta U\}_1^{(1)} &= \{\delta\bar{U}\}_1^{(1)} + \delta\lambda_1^0\{\delta\hat{U}\}_1; & \{\Delta U\}_1^{(1)} &= \{\delta U\}_1^{(1)} \\ \{U\}_1 &= \{U\}_0 + \{\delta U\}_1^{(1)}\end{aligned}$$

- (vii) Update the load increment  $\lambda_1^{(1)} = \delta\lambda_1^0$ .  
 (viii) Compute the arc length [see Eq. (A2.4.20a)]

$$\Delta s = \delta\lambda_0 \sqrt{\{\delta\hat{U}\}_1^T \{\delta\hat{U}\}_1}$$

- (ix) Go to Step 9.

**First iteration of any load step except the first**

1. Calculate the system matrices  $[K^e]$ ,  $[K_T^e]$  and  $\{F^e\}$ .
2. Assemble the element matrices.
3. Apply the boundary conditions.
4. Compute the tangential solution

$$\{\delta\hat{U}\}_{n-1} = [K_T]^{-1}\{\bar{F}\}$$

5. Compute the initial incremental load parameter  $\delta\lambda_n^{(0)}$  by Eq. (A2.4.18):

$$\delta\lambda_n^{(0)} = \pm(\Delta s)_n [\{\delta\hat{U}\}_n^T \cdot \{\delta\hat{U}\}_n]^{-1/2} \quad (\text{A2.4.24})$$

6. Compute the incremental solution using Eq. (A2.4.17a):

$$\{\bar{U}\}_n^{(r)} = -[K_T]^{-1}\{R\}_n^{(0)}$$

7. Update the total solution vector and load parameter:

$$\begin{aligned}\{\delta U\}_n^{(1)} &= \{\delta\bar{U}\}_n^{(1)} + \delta\lambda_n^{(0)}\{\delta\hat{U}\}_n^{(1)} \\ \{U\}_n &= \{U\}_{n-1} + \{\delta U\}_n^{(1)} \\ \lambda_n^{(1)} &= \lambda_n^{(0)} + \delta\lambda_n^{(0)}, & \{\Delta U\}_n^{(1)} &= \{\delta U\}_n^{(1)}\end{aligned} \quad (\text{A2.4.25})$$

8. Check for convergence [see Eq. (A2.4.28)]. If convergence is achieved, go to step 15 below. If not, continue with the 2nd iteration by going to step 9.

The  $r$ th iteration of any load step ( $r = 2, 3, \dots$ )

9. Update the external load vector

$$\{F\}^{(r-1)} = \lambda_n^{(r-1)} \{\bar{F}\} \quad (\text{A2.4.26})$$

10. Update the system matrices (skip forming of  $[K_T]$  for modified Newton-Raphson iteration).
11. Solve for  $\{\delta\bar{U}\}_n^{(r)}$  and  $\{\delta\hat{U}\}_n$  from the two sets of equations in (A2.4.17a,b); for the modified Newton-Raphson method Eq. (A2.4.17b) need not be resolved.
12. Compute the incremental load parameter  $\delta\lambda [= \delta\lambda_n^{(r)}]$  from the following quadratic equation:

$$a_1(\delta\lambda)^2 + 2a_2\delta\lambda + a_3 = 0$$

$$\begin{aligned} a_1 &= \{\delta\hat{U}\}_n^T \cdot \{\delta\hat{U}\}_n \\ a_2 &= (\{\delta\bar{U}\}_n^{(r)} + \{\Delta U\}_n^{(r-1)})^T \cdot \{\delta\hat{U}\}_n \\ a_3 &= (\{\delta\bar{U}\}_n^{(r)} + \{\Delta U\}_n^{(r-1)})^T \cdot (\{\delta\bar{U}\}_n^{(r)} + \{\Delta U\}_n^{(r-1)}) - (\Delta s)^2 \end{aligned}$$

and  $\Delta s$  is the arc length of the current load step. Two solutions  $\delta\lambda_1$  and  $\delta\lambda_2$  of this quadratic equation are used to compute two corresponding vectors  $\{\Delta U\}_{n1}^{(r)}$  and  $\{\Delta U\}_{n2}^{(r)}$ . The  $\delta\lambda$  that gives positive value to the product  $\{\Delta U\}_{n1}^{(r-1)} \cdot \{\Delta U\}_{n1}^{(r)}$  is selected. If both  $\delta\lambda_1$  and  $\delta\lambda_2$  give positive values of the product, we use the one giving the smallest value of  $(-a_3/a_2)$ .

13. Compute the correction to the solution vector

$$\{\delta U\}_n^{(r)} = \{\delta\bar{U}\}_n^{(r)} + \delta\lambda \cdot \{\delta\hat{U}\}_n,$$

and update the incremental solution vector, the total solution vector and the load parameter:

$$\begin{aligned} \{\Delta U\}_n^{(r)} &= \{\Delta U\}_n^{(r-1)} + \{\delta U\}_n^{(r)} \\ \{U\}_n &= \{U\}_{n-1} + \{\Delta U\}_n^{(r)} \\ \lambda_n^{(r)} &= \lambda_n^{(r-1)} + \delta\lambda_n^{(r)} \end{aligned} \quad (\text{A2.4.27})$$

14. Repeat steps 9–13 until the following convergence criterion is satisfied:

$$\left[ \frac{(\{U\}_n^{(r)} - \{U\}_n^{(r-1)})^T \cdot (\{U\}_n^{(r)} - \{U\}_n^{(r-1)})}{(\{U\}_n^{(r)})^T \{U\}_n^{(r)}} \right]^{\frac{1}{2}} < \epsilon \quad (\text{A2.4.28})$$

15. Adjust the arc length for the subsequent load steps by [see Eq. (A2.4.9a)]  $\Delta s = \Delta\hat{s}(I_d/I_0)$ .

16. Start a new load step by returning to Step 1.



## References

1. Riks, E., "The Application of Newton's Method to the Problem of Elastic Stability," *Journal of Applied Mechanics*, **39**, 1060-1066 (1972).
2. Wempner, G. A., "Discrete Approximations Related to Nonlinear Theories of Solids," *International Journal of Solids and Structures*, **7**, 1581-1599 (1971).
3. Batoz, J. L. and Dhatt, G., "Incremental Displacement Algorithms for Non-linear Problems," *International Journal for Numerical Methods in Engineering*, **14**, 1262-1267 (1979).
4. Crisfield, M. A., "A Fast Incremental/Iterative Solution Procedure that Handles 'Snap-Through'," *Computers and Structures*, **13**, 55-62 (1981).
5. Bergan, P. G., Horrigmoe, G., Krakeland, B., and Soreide, T. H., "Solution Techniques for Non-linear Finite Element Problems," *International Journal for Numerical Methods in Engineering*, **12**, 1677-1696 (1978).
6. Padovan, J. and Tovichakchaikul, S., "Self-Adaptive Predictor-Corrector Algorithms for Static Nonlinear Structural Analysis," *Computers & Structures*, **15**, 365-377 (1982).
7. Newton, I., "De analysis per aequationes infinitas (1690)," in *The Mathematical Papers of Isaac Newton, Vol. 11 (1667-1670)*, D. T. Whiteside (ed.), Cambridge University Press, Cambridge, UK, 207-247 (1968).
8. Raphson, J., "Analysis Aequationum universalis seu ad aequationes algebraicas resolendas methodus generalis et expedita, ex nove infinitarum serierum doctrina deducta ac demonstrata," London (1690) (original in British Library, London).
9. Cajori, F., "Historical Note on the Newton-Raphson Method of Approximation," *American Mathematical Monthly*, **18**, 29-32 (1911).
10. Bicanic, N. and Johnson, K. H., "Who was '-Raphson'?" *International Journal for Numerical Methods in Engineering*, 148-152 (1979).

---

## Subject Index

---

- Acceleration of convergence, 65  
 Acceleration parameter, 66, 101, 107, 444  
 $\alpha$ -family of approximation, 289, 296  
 Algorithm, 441, 443, 444  
 Almansi-Hamel strain tensor, 332, 333, 353  
 Alternative direct iteration algorithm, 441  
 Amplification matrix, 295  
 Area coordinates, 37  
 Assembly of element, 33, 251  
 Axial force, 91, 112
- Backward difference method, 290, 291, 293, 307  
 Basis vectors, 405  
 BCIZ triangle, 161  
 Beam:  
   bending of, 88  
   Euler-Bernoulli theory of, 88  
   Timoshenko theory of, 110  
 Bilinear form, 17, 28, 241, 270  
 Biorthogonal Conjugate Gradient method, 432  
 Boundary conditions:  
   Dirichlet, 16  
   essential, 16, 76  
   force, 92  
   mixed, 79  
   natural, 16, 79, 92  
   Neumann, 16  
   of fluids, 234  
 Boussinesq approximation, 233
- $C^1$ -Continuity, 155  
 Cauchy-Green deformation tensor, 331, 332  
 Cauchy strain tensor, 332  
 Cauchy stress, 334  
 Central difference method, 290, 292  
 Clamped, 107, 121, 151, 167, 192, 195, 209, 212, 217, 220  
 Classical beam theory, 88  
 Classical plate theory (CPT):  
   assumptions of, 141  
   boundary conditions, 149  
   displacement field, 142  
   equations of motion, 148  
   finite element model of, 153  
   strains, 142  
 Codazzi conditions, 197  
 Coefficients:  
   of thermal expansion, 152  
 Collocation method, 274  
 Computational mechanics, 1  
 Conditionally stable, 295  
 Configuration, 328, 337, 338, 339  
 Conforming element, 161  
 Conjugate gradient method, 274, 277, 280, 430  
 Consistent mass matrix, 292  
 Consistent penalty model, 245, 246  
 Constant-average-acceleration method, 293, 309, 312, 371  
 Constitutive relations, 405  
 Continuity equation, 231, 242  
 Continuum formulation, 87  
 Convergence criterion, 441, 443

- Convergence tolerance, 441  
 CPT, *see*: Classical plate theory  
 Crank-Nicolson scheme, 291, 307, 312  
 Cylindrical coordinate system, 405  
 Cylindrical shell, 209, 212
- Deformation gradient tensor, 330  
 Direct iteration, 65, 77, 98, 107, 121, 131, 408, 440  
 Direct methods, 427  
 Displacement finite element model, 157  
 Doubly-curved shell, 196, 210  
   displacement field, 204  
   equations of motion, 205  
   finite element model of, 206, 207  
   strains, 204  
   stress resultants, 203
- Eigenvalue problem, 289  
 Eigenvalues, 334  
 Elasticity tensor, 346  
 Elastic-perfectly-plastic, 392  
 Elasto-plastic tangent modulus, 394  
 Element-by-element, 432  
 Energetically-conjugate, 336  
 Engineering constants, 376  
 Equations of equilibrium,  
   Euler-Bernoulli beam theory, 91  
   Timoshenko beam theory, 113  
 Essential boundary condition, 76  
   *see* Boundary conditions  
 Euler strain tensor, 332, 343  
 Euler-Bernoulli beam theory, 88  
   displacement field of, 88  
 Euler-Bernoulli hypotheses, 88  
 Euler-Lagrange equations, 112, 176  
 Eulerian description, 230  
 Euler's explicit method, 4  
 Explicit scheme, 288  
 Extensional stiffnesses, 94, 153
- Finger tensor, 332  
 Finite difference method, 5  
 Finite element, 5, 13  
 Finite element mesh, 25  
 Finite element method, 5, 290
- Finite element model of:  
   beams (EBT), 95  
   beams (TBT), 113  
   heat transfer, 297, 418  
   isotropic, Newtonian, viscous,  
     incompressible fluids, 235  
   plates (CPT), 153  
   plates (FSDT), 177  
   power law fluids, 407, 411
- First-order shear deformation theory:  
   displacement field, 173  
   equations of motion, 177  
   finite element model of, 177, 179  
   generalized displacement, 173  
   strains, 174
- First law of thermodynamics, 232  
 First Piola-Kirchhoff stress, 335  
 Fixed edge, 151  
 Flow over a backward-facing step, 277  
 Flow past a circular cylinder, 278  
 Fluid mechanics, 229  
 Force boundary condition, 92  
 Forward difference scheme, 4, 290, 291  
 Fourier's heat conduction law, 233  
 Free-body diagram, 17  
 Free edge, 151  
 Frontal solution, 427  
 FSDT, *see*: First-order shear  
   deformation theory  
 Full integration, 104, 116, 118, 120, 168
- Galerkin's method, 15, 291, 293  
 Gauss elimination method, 427  
 Gauss points, 45, 135, 185, 251  
 Gauss quadrature, 45, 102, 116, 118, 135  
 Gauss weights, 45, 135, 251  
 Gauss-Legendre quadrature, 44  
 Generalized nodal displacements, 90  
 Generalized nodal forces, 89  
 Geometric nonlinearity, 7, 389  
 Global coordinates, 30, 130, 133  
 GMRES, 432  
 Governing Equations:  
   of Newtonian, viscous,  
     incompressible fluids, 235  
   of non-Newtonian fluids, 406  
 Green-Lagrange incremental strain, 341

- Green-Lagrange strain tensor,  
201, 331, 333, 340, 390
- h*-refinement, 218
- Half bandwidth, 425
- Hamilton's principle, 369
- Hardening, 8
- Heated cavity, 419
- Heat flux, 233
- Hermite cubic interpolation  
functions, 95
- Hinged, 119, 219
- Homogeneous motion, 331
- Hydrostatic pressure, 233
- Hyperelastic material, 346, 390
- Ideal plastic, 392
- Imbalance force, 445
- Implicit scheme, 288
- Incompressibility condition, 231
- Incompressible flow, 229
- Infinitesimal strain tensor, 341, 343
- Initial conditions, 288, 292
- Initial-value problem, 3
- Interpolation property, 19, 30
- Inviscid fluid, 229
- Isoparametric formulation, 42
- Iterative method, 274, 430
- Jacobian, 44, 134, 331, 340
- Jacobian matrix, 43, 134, 251
- Kinetic hardening, 394
- Kirchhoff assumptions, 141
- Kirchhoff free-edge condition, 150
- Kirchhoff stress increment tensor, 344
- Kovaszny flow, 275
- Ladyzhenskaya-Babuska-Brezzi (LBB)  
condition, 248
- Lagrange interpolation, 30, 32, 38,  
114, 130, 155, 179, 207, 411, 418
- Higher-order, 20
- Linear, 19, 95
- Quadratic, 20
- Lagrange multiplier method, 241
- Lagrangian description, 230, 328
- Lamé constants, 199, 233
- Laminar flow, 230
- Lanczos orthores, 433
- Least squares finite element model,  
267, 269, 272, 299, 315
- Least squares functional, 271, 272,  
275, 277, 299, 318
- Linear acceleration method, 293
- Linear element, 23
- Linear form, 17, 28, 241, 270
- Linear rectangular element, 32
- Linear triangular element, 30
- Linearly independent, 15
- Local coordinates, 133
- Locking, 274
- membrane, 102, 117
- shear, 115, 184
- Load increments, 100, 106, 108, 119, 172,  
361
- Master element, 36, 41
- Material coordinates, 328
- Material description, 230, 328
- Material nonlinearity, 7, 389
- Material stiffnesses, 376
- Material strain rate tensor, 336
- Mathematical model, 1
- Matrix,
- coefficient, 23
- stiffness, 23, 358
- tangent stiffness, 358
- Membrane locking, *see* Locking
- Metric, 197
- Mindlin plate theory, 181
- Mixed finite element model, 237, 246,  
254, 274
- Moment, 91
- Natural boundary condition, 16, 79,  
92
- Navier-Stokes equation, 230, 232
- Newmark's integration scheme, 293,  
296, 371
- Newton-Raphson iteration scheme,  
68, 78, 98, 107, 121, 131, 157,  
189, 439, 444
- modified, 70, 445

- Newtonian fluid, 229, 233  
 Newton's iteration procedure, 68  
 Nodal degrees of freedom, 23  
 Nodes, 6, 26  
     global, 33  
 Nonconforming element, 161  
 Nonlinear analysis of:  
     Euler-Bernoulli beams, 88  
     Timoshenko beams, 110  
 Non-Newtonian fluid, 229, 404  
 Numerical integration, 40  
 Numerical simulation, 3  
     *p*-refinement, 21  
 Parabolic equations, 289  
 Penalty finite element model, 237,  
     241, 246, 405  
 Penalty parameters, 243, 247, 256,  
     261  
 Picard iteration, 65, 440  
 Pinned, 107, 121  
 Plane stress, 365  
 Plane stress-reduced stiffnesses, 152,  
     376  
 Plastic flow, 391  
 Plasticity, 391  
 Power-law fluid, 404, 407  
 Primary variables, 16, 27, 62, 112,  
     150, 177, 206, 235  
 Primitive variables, 235  
 Principal radii of curvature, 197  
 Principle of:  
     conservation of angular  
         momentum, 232  
     conservation of energy, 232  
     conservation of linear momentum,  
         232  
     conservation of mass, 231, 340  
     minimum total potential energy, 18  
     virtual displacements, 89, 111, 145,  
         174, 347, 369  
     virtual work, 349, 352  
 Quadratic element, 23  
 Rate of deformation gradient tensor,  
     336  
 Rectangular elements, 38  
 Reduced integration, 102, 104, 118, 120,  
     168, 212, 214, 249, 254, 274, 377  
 Reduced integration penalty model,  
     244  
 Relaxation, 443  
 Residual, 15  
 Riks, 440, 448  
 Riks-Wempner method, 378  
     modified, 381  
 Romberg-Osgood model, 391  
 Rotation tensor, 334  
 Sanders' shell theory, 196, 205  
 Second Piola-Kirchhoff stress, 335,  
     390  
 Secondary variables, 16, 27, 62, 112,  
     150, 177, 206, 235  
 Serendipity elements, 39  
 Shallow cylindrical panel, 217, 219  
 Shear correction coefficient, 111, 175  
 Shear correction factors, 203  
 Shear force, 112, 203  
 Shear locking, *see* Locking  
 Shear thickening fluids, 407  
 Shear thinning fluids, 407  
 Simply supported, 151, 167, 169, 185,  
     189, 210, 312, 378, 381  
 Skyline technique, 427  
 Softening, 9  
 Solar receiver, 420  
 Space-time coupled formulation, 321  
 Spatial approximation, 287  
 Spatial description, 230, 329  
 Specific heat, 236  
 Stability, 295, 296  
 Stiffnesses:  
     bending, 94, 153  
     extensional, 94, 153  
     extensional-bending, 94  
 Stokes flow, 230, 241, 269  
 Strain-displacement relations, 143  
     nonlinear, 88  
 Strain energy, 89, 174  
 Strain energy density, 390  
 Strain hardening, 393, 394  
 Strain rate tensor, 232, 405  
 Stream function, 237

- Stress,
  - Cauchy, 334
  - deviatoric, 393
  - invariants, 393
  - tensor, 232
  - vector, 334
- Stretch tensor, 334
- Subparametric formulation, 42
- Superconvergent element, 95
- Superparametric formulation, 42
- Tangent matrix, 69, 131, 445
- Tangent stiffness matrix, 98, 117, 157, 182, 390
- Theorem of Rodrigues, 197
- Thermal coefficients of expansion, 153
- Thermal stress resultant, 153
- Timoshenko beam theory, 110
  - displacement field of, 110
  - finite element model of, 113
- Tolerance, 65, 108, 119, 169, 189, 192
- Total Lagrangian description, 338
- Total Lagrangian formulaion, 348, 353
- Transverse force, 2, 175
- Tresca yield criterion, 393
- Triangular elements, 37
- Turbulent flow, 230
- Unconditionally stable, 295
- Updated Green-Lagrange strain tensor, 342
- Updated Kirchhoff stress increment tensor, 344
- Updated Kirchhoff stress tensor, 344
- Updated Lagrangian description, 338
- Updated Lagrangian formulation, 350, 360
- Validation, 12
- Variational problem, 17, 241, 242, 270
- Vectors, 23
- Velocity gradient tensor, 335
- Velocity-Pressure model, 237
- Velocity-Pressure-Velocity model, 299
- Velocity-Pressure-Vorticity model, 299
- Verification, 11
- Viscoelastic fluid, 404
- Viscosity, 229
- Viscous incompressible fluid, 407
- Viscous stress tensor, 233
  - von Kármán nonlinearity, 300
  - von Kármán strains, 89, 144, 174
  - von Mises yield criterion, 393
- Vorticity, 237, 271
- Weak form, 16, 26, 62, 128, 239
- Weak forms for:
  - Doubly-curved shell, 206
  - Euler-Bernoulli beam, 89
  - heat transfer, 297
  - plates (CPT), 147
  - plates (FSDT), 174, 300
  - steady Stokes flow, 241
  - Timoshenko beam, 111
- Weight functions, 15
- Weighted-integral, 15
- Weingarten-Gauss relations, 197
- White-Metzner model, 409
- Yield criterion, 392
- Yield stress, 392
- Yielding, 391